Neuroprotective and anti-inflammatory potentials of rutin in an in vitro model of Alzheimer's disease

Halimatu HASSAN

School of Pharmacy and Bioengineering

Keele University

Thesis submitted for the degree of Doctor of Philosophy

June, 2024

Table of Contents

Table of Figures

Table of Tables

MITIGATION STATEMENT

My research has been significantly impacted by numerous factors, which have hindered me from achieving many of the objectives I intended to carry out. These factors include the COVID-19 pandemic, health issues, the loss of loved ones, and caring responsibilities. Being a laboratory-based research, my work has been severely affected due to the COVID-19 pandemic. The institute where I conduct my research was closed for approximately 6 months during the first lockdown, preventing me from accessing the laboratory. Additionally, during the second lockdown, I faced another period of about 3 months where laboratory access was unavailable. These interruptions have had a substantial impact on my research progress.

Furthermore, my personal circumstances have also contributed to the challenges I faced. I fell ill twice during my research, and I experienced immense grief due to the loss of my only sister and my biological daughter. These tragic events significantly affected my mental well-being, leading to stress and depression that further hindered my research progress. Additionally, I have significant caring responsibilities for my children, which require my attention and time.

Initially, my plan was to conduct research on rat microglia to study anti-inflammation. However, due to the circumstances and challenges I encountered, I had to modify my approach. Instead, I focused on studying microglia cell line Bv2 cells. Moreover, my original plans included evaluating other mechanisms of action of rutin, such as studying antioxidant enzymes like GPX, SOD, and CAT. Unfortunately, due to the disruption of laboratory access, I was unable to carry out these evaluations as planned.

Despite these setbacks, I have made the best effort to adapt to the circumstances and continue my research to the best of my abilities. I remain committed to the advancement of my research and will explore alternative strategies to overcome the challenges I have faced.

ABSTRACT

Alzheimer's disease (AD) is the most common form of dementia, affecting around 26 million people worldwide, with an expected four-fold increase by 2050. It is characterized by cognitive and mental deficits and is caused by the accumulation of toxic amyloid beta (Aβ) and neurofibrillary tangles in the brain, leading to neurotoxicity, oxidative stress, and neuro-inflammation. Recent research has identified a molecular link between ischemia/hypoxia and the processing of amyloid precursor protein (APP) in AD. Brain regions of AD patients show reduced cerebral blood flow, which activates β&γ secretases involved in Aβ production. Hypoxia-inducible factor (HIF) is stabilized in response to hypoxia, and its role in AD pathogenesis is not yet fully understood.

The neuro-inflammation triggered by Aβ deposition is an important component of AD and can contribute to neurodegeneration. The aging population and the significant burden on the healthcare system necessitate the development of new diagnostic, preventive, and treatment strategies for AD. Currently, only symptomatic therapies are available, highlighting the urgent need for novel approaches. Flavonoids, a class of therapeutic molecules, have shown promise in AD treatment. Rutin, a naturally occurring flavonoid glycoside found in various foods and fruits, possesses antioxidant, anti-inflammatory, and cytoprotective properties. However, its specific effects on microglial activation and inflammatory responses in AD are not well understood.

In this study, primary neuron, PC12 cell and BV2 models were used to investigate the neuroprotective and anti-inflammatory potential of rutin in AD. We examined the effects of rutin on Aβ-induced neurotoxicity, apoptosis, reactive oxygen species (ROS), and lipid peroxidation in normoxia and hypoxic conditions. Result revealed that rutin increased cell viability and reduced cell apoptosis in primary neuron, PC12 cell in both conditions. Furthermore, rutin decreased

reactive oxygen species (ROS), and lipid peroxidation triggered by Aβ in both normoxic and hypoxic conditions. In Oder understand neuro-inflammation, BV-2 microglial cells were treated with lipopolysaccharide (LPS) to induce inflammation. Rutin was co-administered with LPS, and its effects on inflammatory cytokine expression and nitric oxide levels were assessed. Rutin was found to decrease the production of pro-inflammatory cytokines and shift microglial activation from the M1 to the M2 phenotype, indicating a reduction in microglia-related neuro-inflammation.

In conclusion, Aβ-induced neurotoxicity, apoptosis, ROS, lipid peroxidation and oxidative damage in primary neurons and PC12 cells, which can be exacerbated by hypoxia, but rutin demonstrates protective effects by reducing the effects. Rutin also attenuates microglial activation and neuro-inflammation. These findings suggest that rutin may have therapeutic potential for AD treatment, due to its antioxidant properties and potential role in HIF stabilization. However, further research is needed to better understand AD pathogenesis and conduct preclinical testing of rutin as a potential treatment. Additional studies are necessary to improve the bioavailability of rutin and investigate its protective effects in AD, which could provide a foundation for future clinical trials.

ACKNOWLEDGMENTS

PUBLICATIONS AND CONFERENCES

Publications

Hassan, H. and Chen, R, 2021. Hypoxia in Alzheimer's disease: effects of hypoxia inducible factors. *Neural Regeneration Research*, 16(2); 310-311.

CHEN, R., HASSAN, H., RAWLINSON, C. and MORGAN, DM, 2021. Pharmacological properties of rutin and its potential uses for Alzheimer's disease. *Journal of Experimental stroke and translational Medicine, JESTM* (2021), 13(2), 1-12.

Conferences

Hassan, H., Chen, R.and Morgan, DM, 2019. Neuroprotection by rutin in an invitro model of Alzheimer disease, *Institute of science and technology in medicine Keele University, United Kingdom, early Careers symposium*, 23rd May 2019.

Hassan, H., Chen, R.and Morgan, DM, 2020. Rutin protects rat Pheouchromocytoma (PC12) cells from $A\beta_{25-35}$ toxicity in both normoxia and hypoxia conditions. The virtual congress on Brain Health Innovation and technology, BrainHIT2020, 12-13 October 2020.

LIST OF ABBREVIATIONS

7-AAD	7-amino-actinomycin D
Aβ	Amyloid beta
AChE	Acetylcholinesterase enzymes
AD	Alzheimer's disease
AMPA	α-amino-3-hydroxy-5-methyl-4-isoxazolepropionic acid
ATP	Adenosine triphosphate
Bax	Bcl-2-associated-X
Bcl-2	B-cell lymphoma 2
BBB	Blood-brain barrier
BHT	Butylated hydroxytoluene
BSA	Bovine serum albumin
Ca^{2+}	Calcium ion
CBF	Cerebral blood flow
CBP	CREB-binding
CCK8	Cell counting kit 8
cDNA	Complementary deoxyribonucleic acid
Cdk5	Cyclin dependent kinase 5
DAPI	4'6-diamidino-2-phenylindole dihydrochloride

DCFDA	Dichlorofluorescin diacetate
DMEM	Dulbecco's Modified Eagles's Medium
DMSO	Dimethyl sulfoxide
FACS	Fluorescence-activated cell sorting
GLUT1	Glucose transporters
GSH	Glutathione
GSK3b	Glycogen synthase kinase 3b
GSSG	Gluthathione disulphide
GPx	Glutathione peroxidase
HIF-1α	Hypoxia inducible factors
Hx	Hypoxia
IL-6	Interleukin 6
Interleukin-1β	Interleukin IL-1β
IgG	Immunoglobulin G
LD50	Median lethal dose
LDH	Lactose dehydrogenase
LOAD	Late onset Azheimer's disease
MDA	Malondialdehyde

MIP-1a	Macrophage inflammatory protein 1a
MTT	3-(4, 5-dimethylthiazol-2-yl)-2, 5-diphenyltetrazolium bromide
NFT	Neurofibrillary tangles
NMDA	N-methyl-D-Aspartate
nNOS	Neuronal nitric-oxide synthase
NO	Nitric oxide
NT	Neurotransmitter
NX	Nomoxia
PBS	Phosphate buffer saline
PC12	Pheochromocytoma cells
PDL	Poly-D-lysine
PHD	Prolyl hydroxylase
PI3K / Akt	phosphatidylinositol-3 kinase / protein kinase B
PMSF	Phenylmethylsulfonyl fluoride
PS	Penicillin / Streptomycin
PS	Phosphatidylserine
qRT-PCR	Quantitative real-time polymerase chain reaction
RIPA	Radio-immuno precipitation assay
RT	Reverse transcriptase

ROS	Reacting oxygen species
SOD	Superoxide dismutase
TBA	Thiobarbituric acids
TBS	Tris-buffered saline
TBS-T	Tris buffered saline – Tween
TNFa	Tumour necrosis factor alpha
TGF-β	Transforming growth factor-β
ThT	Thioflavin T assay.
Tuj1	Class III beta tubulin

Chapter 1

INTRODUCTION

1.1. Overview of Alzheimer's disease

Alzheimer's disease (AD) is a progressive neurodegenerative disease and the most common type of dementia. Currently, approximately 44 million people worldwide suffer from dementia, with AD accounting for about 60% of dementia cases (~26 million people) (Winblad, 2016; Brookmeyer et al., 2018). With the aging population, the prevalence of AD is expected to increase, affecting approximately 106.8 million people worldwide by 2050, representing a fourfold increase (Eteghad et al., 2014; Brookmeyer et al., 2018). In the United States, it is estimated that 6.08 million Americans had clinical AD or mild cognitive impairment due to AD in 2017, a number projected to reach 15 million by 2060 (Brookmeyer et al., 2017). In the UK, approximately 800,000 people were living with dementia, and 62% of these cases were caused by AD, with a predicted increase to over 2 million by 2051 (Alzheimer's Society, 2015). It is alarming to note that approximately one person develops dementia every 3 minutes (Alzheimer's Society, 2015).

AD can manifest as either late-onset (sporadic) or early-onset (familial) cases. Late-onset AD, affecting individuals over the age of 65, accounts for 95% of all AD cases (Singh, 2006). Familial AD, responsible for 5% of cases, can cause symptoms to appear as early as 30 years of age, with an inherited dominant gene accelerating the disease progression (Shen & Kelleher, 2007). AD patients experience cognitive and mental deficits, including memory loss, confusion, and disturbances in personality and intellect. As a progressive neurodegenerative disease, AD symptoms worsen over time and typically present in three main stages. Early symptoms include

1

recent event memory loss, difficulty remembering object names, and repetitive questioning or conversations. In the middle stage, symptoms progress to increased confusion and disorientation, delusions, and repetitive behavior. As the disease advances, end-stage symptoms include difficulty swallowing, significant weight loss, and mobility issues (Alzheimer's Association, 2017).

AD is characterized by the progressive loss of neurons and synapses in specific anatomical regions. Cortical atrophy, diffused proportionately throughout the cerebral hemispheres rather than being prominent in specific lobes or one side of the brain, is a significant characteristic of the AD brain (Vinters, 2015). Currently, the definitive diagnosis of AD is confirmed through autopsy or brain biopsy. In clinical practice, the diagnosis is typically based on the patient's history and findings from the Mental Status Examination (Mosconi, 2010). Symptomatic therapies, including cholinesterase inhibitors and N-methyl-D-aspartate (NMDA) antagonists, are the current treatment options for AD. Psychotropic medications are often prescribed to manage secondary symptoms such as depression, agitation, and sleep disorders (Madhusoodanan et al., 2007). While these treatments aim to slow disease progression and improve the quality of life, they do not target the underlying cause, and a definitive cure for AD is yet to be found (Alzheimer's Association, 2017).

In recent years, there has been a shift towards providing care for AD patients in home settings rather than medical facilities. The percentage of Alzheimer's decedents who died in medical facilities decreased from 14.7% in 1999 to 6.6% in 2014, while the percentage of those who died at home increased from 13.9% in 1999 to 24.9% in 2014 (Brookmeyer, 2017). AD is the sixth leading cause of death in the United States, accounting for 3.6% of all deaths in 2014.

Economically, AD poses a significant public health problem. The total payments for healthcare and long-term care for individuals with AD or other dementias in the United States reached an estimated $259 billion in 2017. By 2050, these costs could rise as high as $1.1 trillion (Alzheimer's

Association, 2017). In the UK, the cost of dementia was 23 billion pounds in 2013 (Alzheimer's Society, 2013). Low-income countries accounted for less than 1% of the worldwide costs (but 14% of the prevalence of dementia), middle-income countries accounted for 10% of the costs (but 40% of the prevalence of dementia), and high-income countries accounted for 89% of the costs (but 46% of the prevalence of dementia). The discrepancy is due to the significantly lower cost per person in lower-income countries, with costs of US$868 in low-income countries, US$3,109 in lower-middle-income countries, US$6,827 in upper-middle-income countries, and US$32,865 in high-income countries (Wimo, 2013). In high-income countries, informal care (45%) and formal social care (40%) contribute to the major costs, while the proportionate contribution of direct medical costs (15%) is lower. In low-income and lower-middle-income countries, direct social care costs are minimal, and the predominant costs are associated with informal care provided by families (Wimo, 2013).

1.2. Historical Background of AD

The disease is named after German psychiatrist and pathologist Alois Alzheimer, who first described it in 1906 (Hippius and Neundorfer, 2003). In 1901, Dr. Alzheimer observed a 51-year-old patient named Mrs. Auguste Deter at the Frankfurt Asylum. She exhibited symptoms such as loss of short-term memory, disorientation, aggression, and paranoia. The patient passed away four years after Dr. Alzheimer left Heidelberg. Dr. Alzheimer obtained the patient's brain and medical records and conducted a brain biopsy to examine the correlation between the medical records and the patient's symptoms. He discovered distinct plaques and neurofibrillary tangles in the brain histology. On November 3rd, 1906, Dr. Alzheimer reported "a peculiar severe disease process of the cerebral cortex" at the 37th Meeting of South-West German Psychiatrists held in Tübingen. He described the patient's symptoms, including progressive cognitive disorder, local neurological

symptoms, hallucinations, delusions, and psychological and social disability. He also presented histological observations, such as senile plaques, neurofibrillary tangles, and atherosclerotic alterations. However, this report received a poor reception from academia from the beginning (Hippius and Neundörfer, 2003). One of his colleagues, Emil Kraepelin, first named the disease "Alzheimer's Disease" in the eighth edition of his book Psychiatrie in 1910 (Hippius and Neundörfer, 2003). At that time, the name of the disease indicated "presenile dementia," but its meaning was later expanded to include "senile dementia," which is the more common type of dementia (Müller, 2013).

Following the invention of the electron microscope in 1931 and the development of cognitive measurement scales in 1968, progress has been made in understanding the neurogenetics and pathophysiology of AD (Maurer & Maurer, 2003). In 1984, researchers identified "a novel cerebrovascular amyloid protein" known as beta-amyloid (Aβ), which is the chief component of Alzheimer's brain plaques and a prime suspect in triggering nerve cell damage (Glenner and Wong, 1984). In 1986, researchers discovered that the tau protein is a key component of tangles, which are the second pathological hallmark of AD and another prime suspect in nerve cell degeneration (Wippold, 2008; Alberto, 2011). In 1987, the first gene associated with the inherited forms of AD was identified. This gene, located on chromosome 21, codes for amyloid precursor protein (APP) (Goldgaber, 1987; Kang, 1987; Tanzi, 1987a, 1988). In 1993, the first Alzheimer's risk factor gene was identified. APOE-e4, a form of the apolipoprotein (APOE) gene on chromosome 19, was recognized as the first gene that increases the risk for AD but does not determine its occurrence (Strittmatter, 1993). In the past 20 years, significant discoveries have been made regarding the mechanisms through which altered amyloid, phosphorylated tau, inflammation, oxidative stress, and hormonal changes contribute to neuronal degeneration in AD.

1.3. Pathology and Pathogenesis of AD

Although the exact aetiology of the disease is not known, AD has distinguishing pathological characteristics, including neurofibrillary tangles, granulovascular bodies, and argentophilic plaques that consist predominantly of amyloid proteins (Alzheimer's.org.uk, 2014). In the brains of AD patients, there is an accumulation of amyloid-beta (Aβ) in the extracellular matrix (Radu, 2013), and there is aggregation of neurofibrillary tangles consisting of hyperphosphorylated tau protein (a microtubule-associated protein) in neuronal cell bodies (Robert, 2009). The formation of neurofibrillary tangles in nerve cells and the deposition of Aβ plaques cause disruption of normal cell architecture and nerve damage, resulting in cell death in the cerebral cortex, which is associated with cognitive function and memory (Turner, 2014).

Neuroinflammation plays a significant role in the pathogenesis of AD, as there is a significant upregulation of inflammatory mediators such as macrophage inflammatory protein-α (MIP-1α), transforming growth factor-β (TGF-β), Interleukin-1β (IL-1β), IL-6, IL-8, and tumor necrosis factor-α (TNFα) in the brains of AD patients (Paduraria, 2013). Post-mortem studies have shown that the blood-brain barrier (BBB) is compromised, and proteins such as albumin, immunoglobulin, fibrinogen, and thrombin accumulate in the cortex and hippocampus (Montagne, 2015). Brain imaging studies also reveal the accumulation of iron and microbleeding in AD, primarily in the hippocampus (Montagne, 2015). Furthermore, there is a decrease in the metabolic rate of glucose in the brains of AD patients due to downregulation of glucose transporters GLUT1 and GLUT3. This results in neurodegeneration through downregulation of O-linked-N-acetylglucosaminylation (O-GlcNAcylation) and hyperphosphorylation of tau in AD (Kalaria, 1999; Liu, 2008).

1.3.1. Amyloid plaques

Senile amyloid plaques are formed by the extracellular nonvascular accumulation of Aβ40 and Aβ42 peptides, which result from the abnormal processing of amyloid precursor protein (APP) by β- and γ-secretases and an imbalance in the generation and clearance pathways (Alzheimer's, 1995; Kumar and Singh, 2015). APP is an integral membrane protein expressed in many tissues, particularly in the synapses of neurons. It has been implicated as a regulator of synaptic formation and repair (Priller, 2006), anterograde neuronal transport (Turner, 2003), and iron export (Duce, 2010).

Human APP can be processed through two alternative pathways: amyloidogenic and nonamyloidogenic (Figure 1.1). In the nonamyloidogenic pathway, APP is first cleaved by α-secretase, releasing soluble APPα (sAPPα) and leaving an 83-amino-acid C-terminal fragment (C83). This cleavage is increased by neuronal activity and the activation of muscarinic acetylcholine receptors (Haass, 1995). Further processing involves intramembrane cleavage of the α- and β-C-terminal fragments by γ-secretase, liberating the P3 and A4 peptides, respectively (Kahle and De Strooper, 2003; Iwatsubo T, 2004). The A4 peptides, also known as Aβ peptides, fold into beta-pleated sheet structures that are highly fibrillogenic. They bind congophilic dyes and exhibit birefringence upon exposure to polarizing light, characteristic of amyloid (Sipe and Cohen, 2000). Antibodies targeting Aβ peptides have shown their involvement in the early formation of amyloid plaques, which may not be detected with congophilic dyes (Rozemuller, 1989).

The amyloidogenic processing of APP involves sequential cleavages by β- and γ-secretases at the N and C termini of Aβ, respectively (Figure 1.1) (Joshi and Wang, 2015). The 99-amino-acid C-terminal fragment (C99) generated by β-secretase cleavage can be internalized and further processed by γ-secretase at multiple sites, leading to the production of cleavage fragments ranging

from 43 to 51 amino acids. These fragments are further cleaved to generate the main final forms of Aβ: the 40-amino-acid Aβ40 and the 42-amino-acid Aβ42, which predominantly constitute amyloid plaques in AD (Olsson, 2014; Takami, 2009). Aβ42 is particularly fibrillogenic and associated with the pathology of AD (Masters, 2015).

The cleavage of C99 by γ-secretase also liberates an APP intracellular domain (AICD), which can translocate to the nucleus and potentially regulate gene expression, including the induction of apoptotic genes. Additionally, the cleavage of APP/C99 by caspases produces a neurotoxic peptide (C31) (Lu, 2000). The β-site APP cleaving enzyme is abundant in neurons, which may accelerate the amyloidogenic processing pathway in the brain and impair neuronal survival.
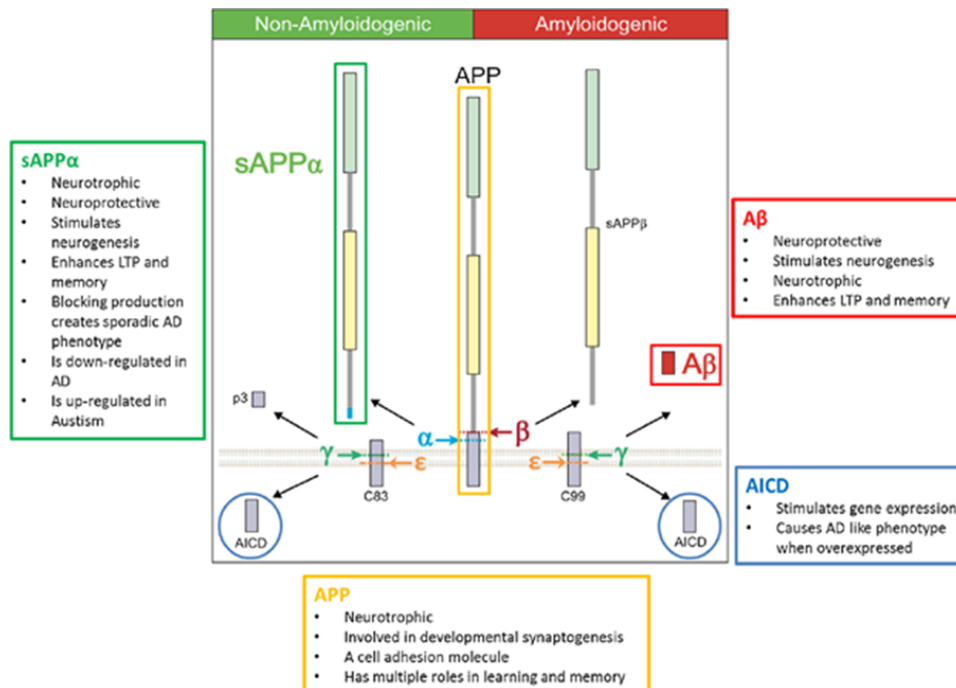
Figure 1.1 Cleavage of APP and Physiological roles of APP and APP Fragments. Amyloid precursor protein (APP) can be cleaved through two mutually exclusive pathways. Different fragments resulting from APP processing, including Aβ, can have multiple roles in normal brain physiology, as shown in the boxes. In the amyloidogenic pathway, APP is cleaved by β-secretase

(beta-site APP cleaving enzyme 1, BACE1) and γ-secretase enzymes (PSEN1 is the catalytic core of the multiprotein γ-secretase complex). The initial β-secretase cleavage produces a large soluble extracellular domain, secreted amyloid precursor protein-β (sAPPβ). The remaining membrane-bound C99 fragment is then subjected to multiple sequential γ-secretase cleavages. These cleavages begin near the inner membrane at the γ-secretase cleavage site epsilon (ε-site), generating the APP intracellular domain (AICD). Subsequent γ-secretase cleavages trim the remaining membrane-bound component to produce different-length Aβ peptides, including Aβ43, Aβ42, Aβ40, and Aβ38. (Joshi and Wang, 2015).

In the non-amyloidogenic pathway, APP is consecutively processed by α- and γ-secretases to produce secreted amyloid precursor protein α (sAPPα), p3 (which is Aβ17-40/42), and AICD. The major α-secretase enzyme is A Disintegrin and metalloproteinase domain-containing protein 10 (ADAM10). The cleavage via amyloidogenic and non-amyloidogenic pathways depends on the cellular localization of cleavage enzymes and full-length APP, which are expressed and trafficked in specific subcellular locations (Morris et al., 2015).
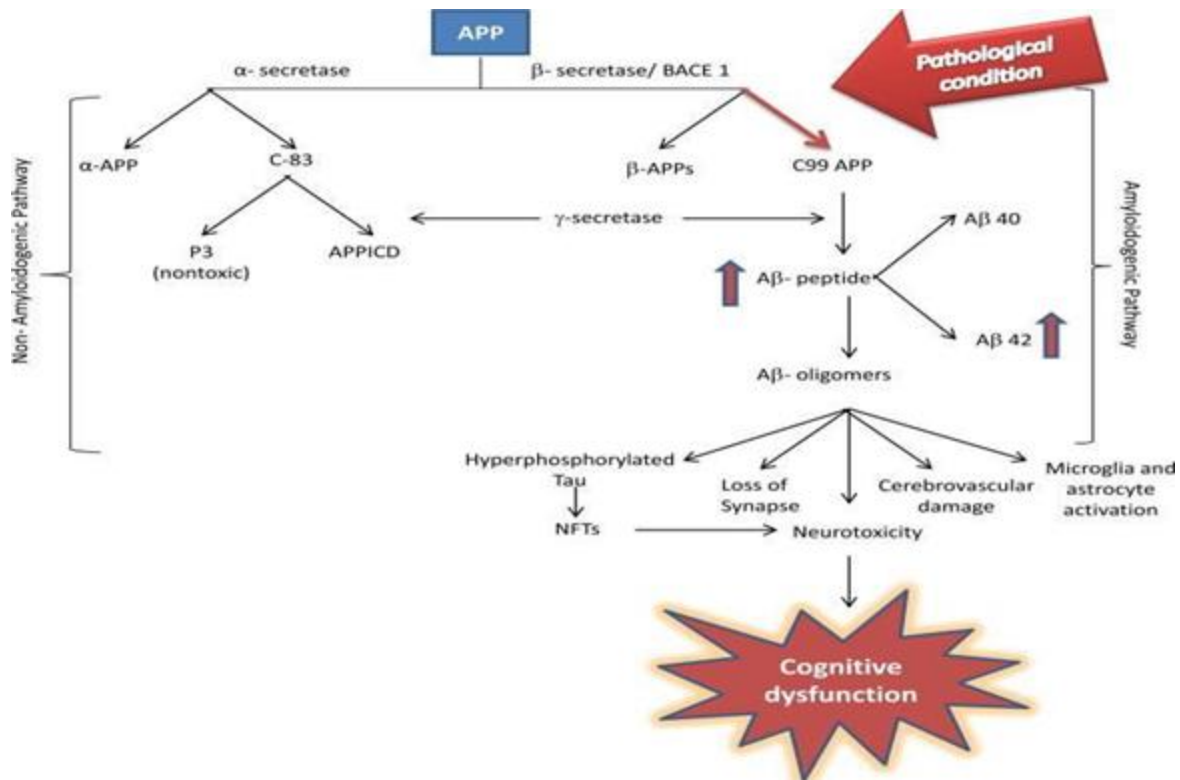
Figure 1.2 Diagrammatic presentation of APP processing pathway. APP is cleaved by α, β, and γ secretases. In the non-amyloidogenic pathway, α-secretase cleaves APP to form soluble sAPPα and non-toxic p3. In the amyloidogenic pathway, Aβ peptides are formed via APP cleavage by β and γ secretases. Aβ40 and Aβ42 form oligomers that result in neuronal toxicity and cell death (Kumar et al., 2015).

The two types of amyloid plaques most observed in AD are diffuse plaques and dense core plaques (Figure 1.3) (Thal et al., 2006; Serrano-Pozo et al., 2011). Diffuse plaques are formed in the neuropil and are weakly stained by thioflavin S and other amyloid binding dyes (e.g., Congo red). They lack argyrophilia on Bodian silver stains and do not show distinct accumulation of activated microglia and reactive astrocytes. In contrast, dense core plaques have dense reticular or radiating compact dense amyloid and are intensely positive with thioflavin S fluorescent microscopy and Congo red, indicating that they contain more fibrillogenic forms of Aβ (Thal et al., 2006).

Additionally, a subset of dense core plaques has neuritic elements, as shown in Fig. 1.3c and d. Dense core neuritic plaques are also accompanied by synaptic loss, activated microglia, and reactive astrocytes (Thal et al., 2006). On the other hand, diffuse plaques can be observed in advanced AD, even though they lack neuritic components. The diffuse plaques are positive with Aβ immunohistochemistry and contain filamentous Aβ at the ultrastructural level, but it is uncertain whether diffuse plaques are a part of pathological aging or an early stage in the maturation of neuritic Aβ plaques (Thal et al., 2006).
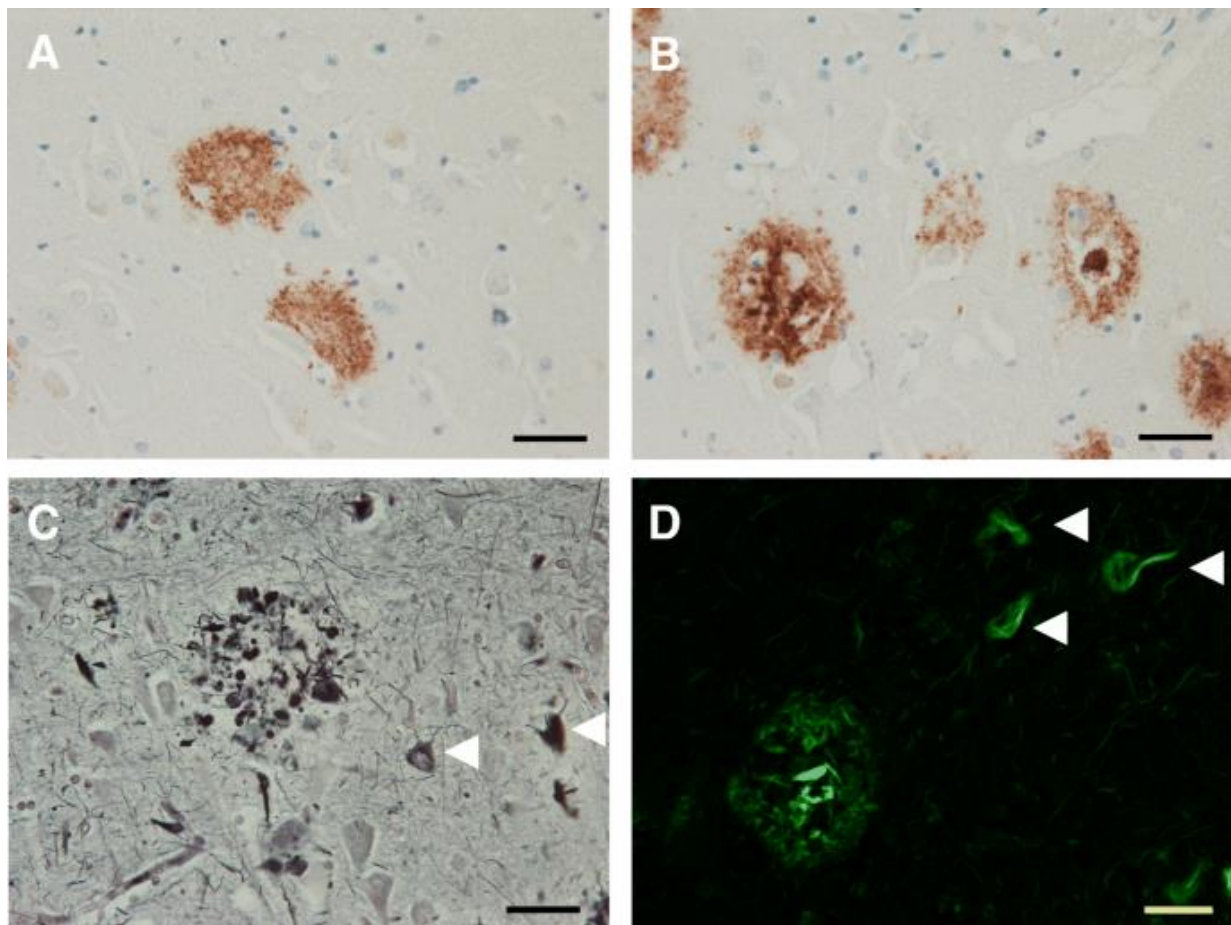
Figure 1.3 Alzheimer's Senile Plaques. Immunohistochemistry of affected Alzheimer's tissues using antibodies directed against Aβ peptides demonstrates the presence of both diffuse (a) and dense core (b) senile plaques. These dense core plaques are often associated with neuritic elements that

can stain filamentous tau and correlate with disease severity. Neuritic AD plaques are readily

observed using Bielchowsky silver staining (c) or Thioflavin S staining (d). These stains can also

label neurofibrillary tangles, as shown by the arrowheads. The scale bars are 40 μm (Serrano-

Pozo et al., 2011), (Thal et al., 2006).

Neuritic plaques contain activated microglia and reactive astrocytes, and their processes intermingle with neuritic elements in the plaque periphery. Some of the dystrophic neurites related to neuritic plaques contain tau filaments, which have a paired helical filament morphology as observed with electron microscopy (Serrano-Pozo et al., 2011). These are termed "type 1" dystrophic neurites, and it is proposed that they occur in regions receiving input from neurons bearing neurofibrillary tangles in their soma (Thal et al., 2006). These dystrophic neurites are heterogeneous in nature. Additionally, some dystrophic neurites contain neurofilament proteins, suggesting cytoskeletal changes in the neurodegenerative process (Dickson and Vickers, 2001). Recent studies have revealed that exogenous Aβ fibrils lead to cell death and disruption of membrane integrity in a cell culture model (Han et al., 2017). Understanding the links between amyloid-driven neuritic pathology, more widespread tau neuronal and thread pathology, as well as neuronal loss, remains an area of active research (Kalaria, 1999; Liu et al., 2008).
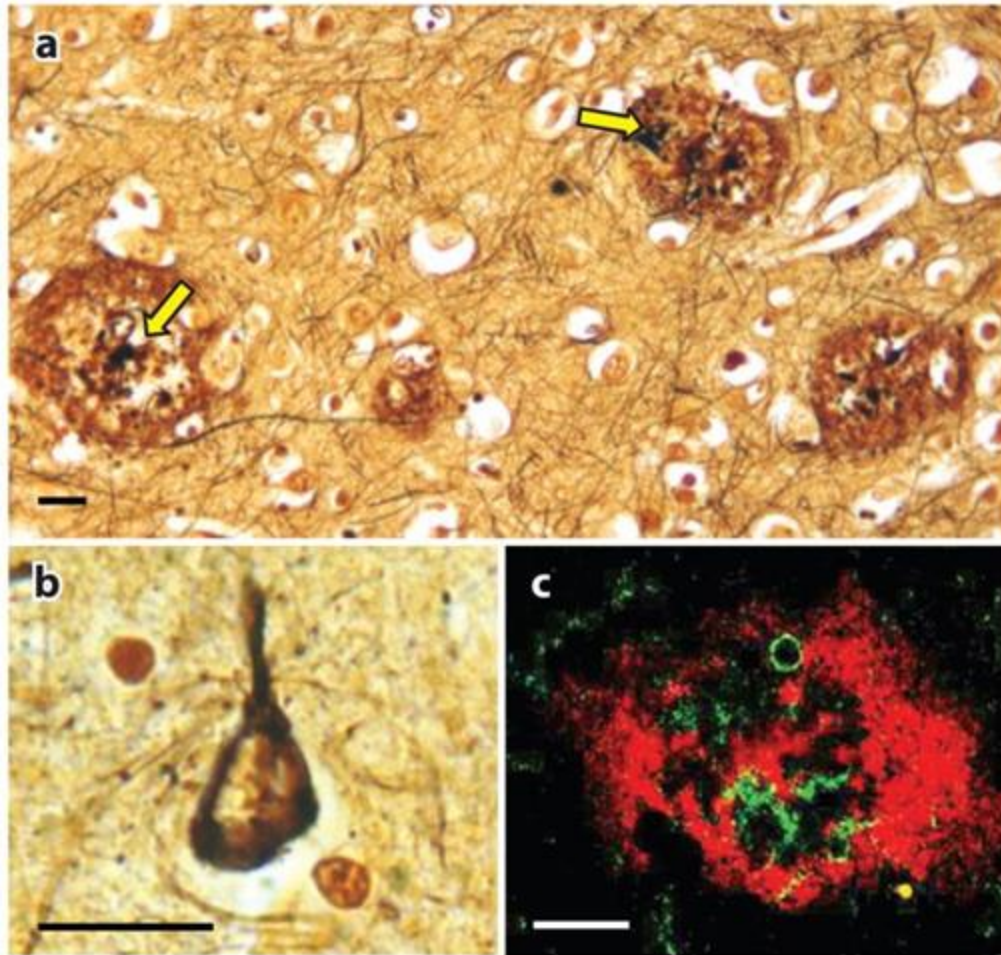
Figure 1.4. Pathology of Alzheimer's disease. Brain sections from a patient with dementia are stained with silver, revealing neuritic plaques in panel 'a' and a neurofibrillary tangle in panel 'b'. The plaques in panel 'a' consist of an amorphous reddish protein (Aβ) with dystrophic neurites (indicated by yellow arrows and dark black material). (c) Aβ plaque stained with an anti-Aβ antibody (red) shows infiltrating microglia stained with an IBA1 antibody (green). Each line represents 40 microns. (Richard et al., 2011).

1.3.2. Neurofibrillary tangles (NFTs)

Neurofibrillary tangles (NFTs) are comprised of the microtubule-associated protein tau, in the form of filamentous aggregates. Tau proteins are a group of six highly soluble protein isoforms

produced by alternative splicing from the microtubule-associated protein tau (MAPT) gene (Goedert et al., 1988; 1989). Tau protein is found in neurons and plays a crucial role in stabilizing internal microtubules. Under normal conditions, tau is a phosphoprotein, with isoform expression and phosphorylation levels regulated during development. Normal brain tau contains 2-3 moles of phosphate per mole of the protein (Kopke et al., 1993; Iqbal et al., 2010), which is optimal for its interaction with tubulin and the promotion of microtubule assembly.

In the disease state, tau has been found to be abnormally hyperphosphorylated, resulting in significantly higher phosphate content than normal tau due to phosphorylation at new sites on the protein (Kopke et al., 1993). Hyperphosphorylation of tau can inhibit microtubule assembly and disrupt preassembled microtubules in vitro (Alonso et al., 2001). Under pathological conditions, tau has also been shown to be present in dendrites and impair synaptic function (Hoover et al., 2010). More recently, it has been proposed that tau acts as a prion-like protein in disease transmission (Alonso et al., 2018). Hyperphosphorylation of tau impairs its biological activity, and in the brains of individuals with Alzheimer's disease (AD), tau is three to four-fold more hyperphosphorylated than in the normal adult brain. In this hyperphosphorylated state, tau polymerizes into paired helical filaments (PHF) admixed with straight filaments (SF), forming neurofibrillary tangles. The abnormally hyperphosphorylated tau in AD brain is distinguished from transiently hyperphosphorylated tau by its ability (1) to sequester normal tau, MAP1, and MAP2 and disrupt microtubules, and (2) to self-assemble into PHF/SF. The cytosolic abnormally hyperphosphorylated tau, due to oligomerization, unlike normal tau, can sediment, and upon self-assembly into PHF/SF, it loses its ability to sequester normal microtubule-associated proteins (MAPs). Truncated forms of tau present in the AD brain also promote self-assembly. The tau polymerized into neurofibrillary tangles is apparently inert and does not bind to tubulin or promote

microtubule assembly (Alonso et al., 2006; Iqbal et al., 1994; Khatoon et al., 1995). Up to 40% of the abnormally hyperphosphorylated tau in the AD brain is present in the cytosol and not polymerized into paired helical filaments/neurofibrillary tangles (Kopke et al., 1993; Iqbal et al., 1986; Bancher et al., 1989). The cytosolic abnormally hyperphosphorylated tau (AD P-tau) in AD does not bind to tubulin and promote microtubule assembly but instead inhibits assembly and disrupts microtubules, as described in Fig. 1.5 (Alonso et al., 1994; Li et al., 2007; Wang et al., 1993). This toxic property of pathological tau involves the sequestration of normal tau by the diseased protein (Alonso et al., 1994; Alonso et al., 1996). AD P-tau also sequesters the other two major neuronal microtubule-associated proteins, MAP1 A/B and MAP2 (Alonso et al., 1997). The toxic behavior of AD P-tau appears to be solely due to its abnormal hyperphosphorylation because dephosphorylation of diseased tau converts it into a normal-like protein (Alonso et al., 1994; Li et al., 2007; Wang et al., 1996).

Normal and Pathological Taus
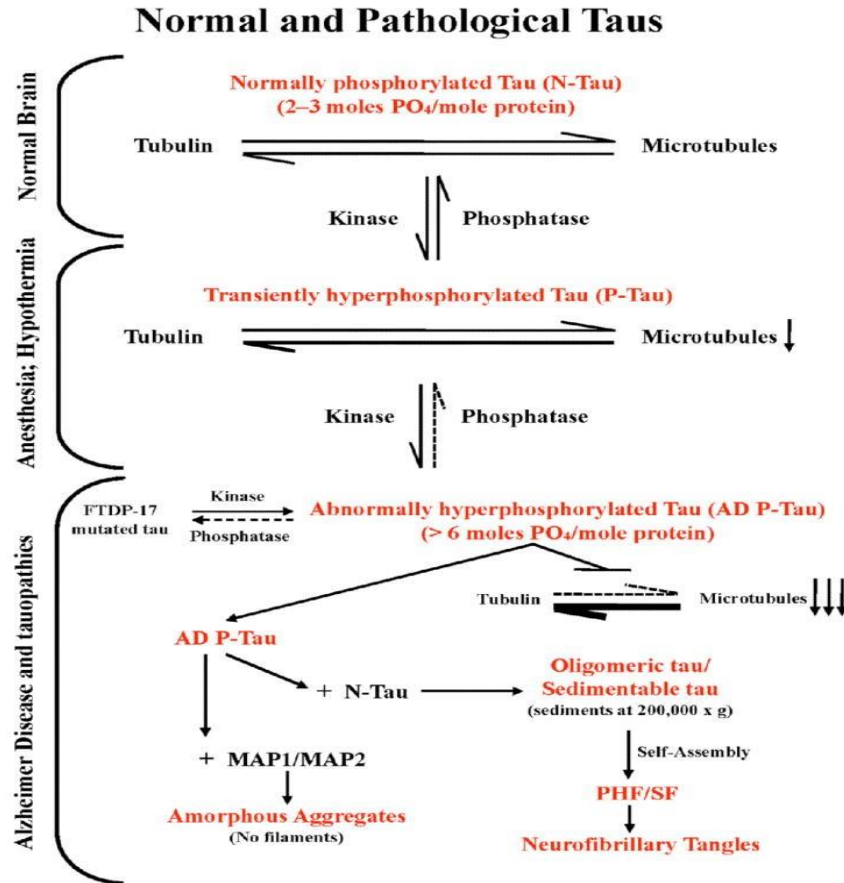
Figure 1.5. A diagrammatic representation of various pathological states of tau originating from normal brain tau and associated loss of normal and gain of toxic functions. Normal brain tau, which has a stoichiometry of 2–3 moles phosphate/mole of the protein, stimulates the assembly of tubulin and stabilizes the structure of microtubules. During development, anesthesia, and hypothermia, such as during hibernation, tau undergoes transient hyperphosphorylation. During development, the level of brain tubulin is >4 mg/ml, the critical concentration required for self-assembly into microtubules, and the role of tau for this function is less critical. However, hyperphosphorylation of tau during anesthesia and hypothermia leads to a decrease in the microtubule network and its associated functions (Alonso et al., 1994; Li et al., 2007; Wang et al., 1993).

In the AD brain, an imbalance between phosphorylation and dephosphorylation, apparently caused by a decrease in protein phosphatase-2A activity, leads to abnormal hyperphosphorylation of tau. This abnormal hyperphosphorylated tau (AD P-tau) sequesters normal microtubule-associated proteins (MAPs) from microtubules, causing inhibition and disruption of microtubules. Additionally, the binding of AD P-tau to MAP1 or MAP2 results in the formation of amorphous aggregates, while binding to normal tau forms oligomers. Unlike normal tau, which is highly soluble, the tau oligomers formed with AD P-tau can be sedimented at 200,000 × g and self-assemble into paired helical filaments (PHF)/straight filaments (SF) in the form of neurofibrillary tangles (Kopke et al., 1993; Iqbal et al., 2010).

The abnormal hyperphosphorylation of tau makes it resistant to proteolysis by the calcium-activated neutral protease, and turnover of hyperphosphorylated tau is several-fold slower than that of normal tau. Consequently, tau levels are significantly increased in AD brains compared to normal brains. The fact that tangle-bearing neurons seem to survive for many years and that the decrease in microtubule density in AD brain is unrelated to PHF accumulation suggests a self-defense role of tangle formation. Using an inducible transgenic mouse model expressing human four-repeat tau with the P301L mutation, it was revealed that cognitive deficiencies correlated with the appearance of soluble hyperphosphorylated tau. When tau expression was turned off in this model, there was no clearance of polymerized tau, soluble phosphotau decreased, and there was an improvement in cognition, suggesting that polymerized tau alone was not sufficient to cause cognitive decline or neuronal cell death (Santacruz et al. 2005). Research have demonstrated

widespread neurodegeneration in human tau transgenic mice, but PHF-containing neurons appeared "healthy" in terms of nuclear morphology, suggesting that the polymerization of hyperphosphorylated tau into fibrils was likely neuroprotective (Andorfer et al. 2005). Thus, these studies collectively demonstrate the pivotal involvement of abnormal hyperphosphorylation in neurofibrillary degeneration and the disruptive properties of cytosolic abnormally hyperphosphorylated tau to the microtubule network, while AD P-tau polymer remains inert. The loss of normal tau function (stabilization and maintenance of microtubules), combined with a toxic gain of function, could compromise axonal transport, and contribute to synaptic degeneration. Accumulation of tau oligomers alone at synapses, instead of neurofibrillary tangles, has been shown to cause synaptic malfunction. This occurs through a process called tau seeding, in which tau oligomers can propagate their pathology to healthy neighboring neurons by crossing synapses. Understanding the influence of inflammation on extracellular tau proteins will provide a better understanding of the inflammatory process in tau pathology. (Guerrezo-munoz et al., 2015).

1.4.1. The Amyloid Cascade Hypothesis in AD

The amyloid cascade hypothesis, proposed by Hardy and Allsop in 1991, suggests that a mutation causes the cleavage of amyloid precursor protein (APP) by β- and γ-secretases, resulting in the production of amyloid-beta (Aβ) (Hardy and Higgins, 1992). Aβ is a sticky fragment that tends to aggregate and form plaques. These plaques are believed to contribute to the degeneration of hippocampal cells and the formation of neurofibrillary tangles (NFTs). In a 25-year review of the hypothesis, Selkoe and Hardy (2016) expanded upon the original hypothesis by proposing that the mutation of the ApoE4 gene could be one of the probable causes for the accumulation of Aβ. They suggest that ApoE4 is associated with reduced clearance of Aβ from the brain, thereby leading to the onset of the disease.
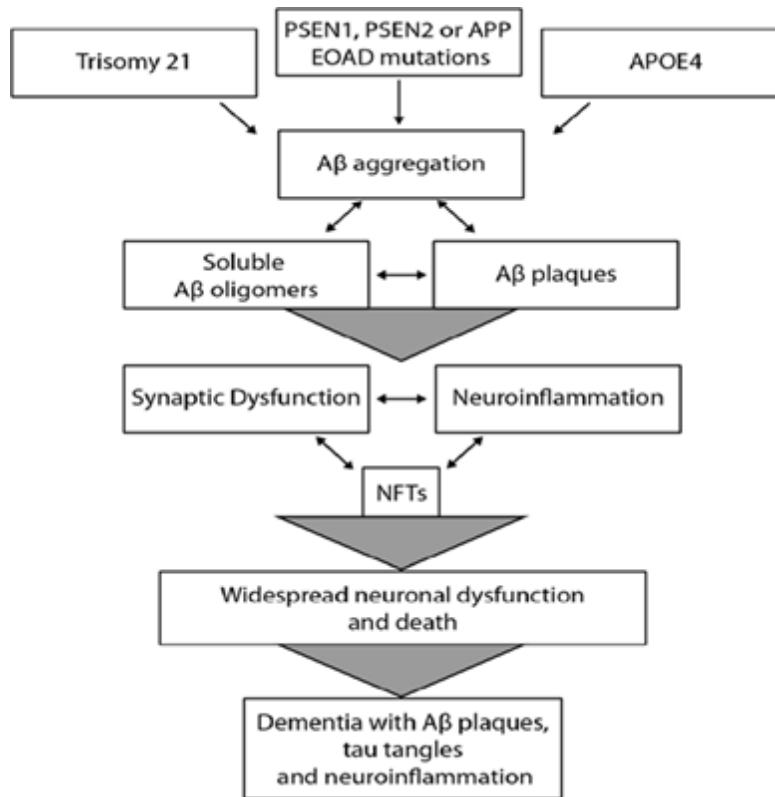
Figure 1.6. The Amyloid Hypothesis. The amyloid hypothesis proposes that the aggregation of amyloid-beta (Aβ) triggers a cascade of events that leads to Alzheimer's disease (AD). Familial mutations in PSEN1, PSEN2, or APP are associated with early-onset AD (EOAD), and these genetic risk factors are believed to affect the cleavage of Aβ from APP, resulting in its oligomerization and the formation of Aβ plaques. As shown above, Individuals with trisomy 21 (Down Syndrome), who have an extra copy of APP, also experience EOAD (Morris, 2015).

The strongest genetic risk factor for late-onset AD (LOAD) is the presence of at least one APOE4 allele. The exact triggers for Aβ accumulation in LOAD are still unclear, but it is suggested that various contributing factors, such as reduced Aβ clearance due to APOE genotype, may play a role. The oligomerization of Aβ is proposed to initiate a cascade involving the formation of neurofibrillary tangles (NFTs) composed of hyperphosphorylated tau, synapse loss, neuron death, and widespread neuroinflammation, particularly in brain regions associated with learning and

18

memory, such as the hippocampus. As the burden of amyloid increases, the progressive loss of synapses and neurons is thought to lead to dementia (Morris, 2015).

Putative evidence in support of the hypothesis: The Aβ hypothesis is supported by compelling evidence for the origins of AD. Studies involving APP, PS1, PS2, and APOE have provided substantial support for the hypothesis, as depicted in Figure 1.6. Mutations in APP, PS1, and PS2 are associated with EOAD, while APOE4 mutations are linked to LOAD. Familial mutations in PSEN1, PSEN2, or APP are postulated to affect the cleavage of Aβ from APP, leading to its oligomerization and eventual plaque formation. Individuals with trisomy 21 (Down Syndrome), who have an extra copy of APP, also suffer from EOAD (Figure 1.6).

The discovery that transgenic mice expressing familial human APP and PSEN mutations recapitulate many, though not all, features of the human disease (Games et al., 1995) further solidified the connection between aberrant Aβ production and the AD phenotype. This finding firmly linked the field to the amyloid hypothesis for subsequent decades. The conclusions of these studies were based on the unquestioned assumption that Aβ, rather than altered expression of APP or its products, causes AD pathology. This assumption was rooted in the fact that Aβ is a key component of plaques and exerts neurotoxic effects on healthy cells (Pike et al., 1995). Additionally, the hyperphosphorylation of tau, which is believed to occur downstream of Aβ, was recognized as a critical mediator of Aβ-induced neurotoxicity (Ittner and Gotz, 2011), placing Aβ at the top of the pathological cascade in AD. The strongest genetic risk factor for LOAD is the presence of at least one APOE4 allele. The triggers for Aβ accumulation in LOAD remain unclear, but it is suggested that multiple contributing factors, including reduced Aβ clearance due to APOE genotype, may be involved.

In general, the risk genes identified for LOAD have subtle effects and do not directly associate with the APP gene or its processing enzymes. The well-known genetic link to LOAD is the APOE4 allele (Jonsson et al., 2012). APOE is responsible for the clearance of Aβ fragments (Corbin et al., 2013). Among the four isoforms, APOE1, APOE2, and APOE3 exhibit normal Aβ clearance in wild-type mice, while the presence of the inherited ApoE4 allele reduces Aβ clearance (Singh et al., 2006). Although the ApoE4 allele provides convincing evidence for Aβ accumulation, there is no evidence that it directly causes AD; rather, the polymorphism in ApoE4 accelerates the development of AD. Evidence from the PDAPP transgenic mouse models (AD mouse model) demonstrated that APOE1 regulates Aβ clearance, with the effectiveness gradually decreasing in APOE2, APOE3, and APOE4 genes. Therefore, there is sufficient evidence to suggest that APOE genes play a significant role in AD, supporting the Aβ cascade hypothesis (Reitz, 2012).

Recently, another strong risk gene for LOAD, a variant of the triggering receptor expressed on myeloid cells 2 gene (TREM2), has been identified, implicating excessive innate immunity in Alzheimer's pathogenesis (Jonsson et al., 2012). While these two mutations have been investigated, many more suspected genes have been associated with LOAD, as shown in Table 1.1. Most of these genetic risk factors have been interpreted in the context of the amyloid hypothesis due to their modulatory effects.

Table 1.1 Suspected Genes Associated with LOAD (Samantha et al., 2014)

Chromosome Position	Gene
1q32	CR1
6p12	CD2AP
7q22.1	ZCWPW1

11p11	CELF1
2q37.1	INPP5D
6p21.1	TREM2
7q34	EPHA1
11q12.1	MS4A6A
2q14	BIN1
6p21.3	HLA-DRB1
8p21.1	PTK2B
11q14	PICALM
5q14.3	MEF2C
7p14.1	NME8
8p21-p12	CLU
11q23.2-q24.2	SORL1
14q22.1	FERMT2
19p13.3	ABCA7
19q13.2	APOE
20q13.31	CASS4
14q32.12	SLC24A4/RIN3
19q13.2	PLD3
19q13.3	CD33
21q21.3	APP

Putative Evidence against the Hypothesis: Despite considerable evidence supporting the amyloid cascade hypothesis, there are some controversies against the hypothesis. The amyloid

cascade hypothesis suggests that Aβ derived from APP is the initial trigger in AD, resulting in neuronal cell death and dementia. However, studies have examined increased expression of APP pathologically like patients with AD in patients who suffer from head trauma (Reitz, 2012). This evidence suggests that increased expression of APP is due to neuronal injury, resulting in increased Aβ production. Therefore, this challenges the hypothesis that states that Aβ is the initial trigger for AD, indicating that AD pathogenesis is due to neurodegeneration.

Furthermore, neurofibrillary tangles (NFTs) are a hallmark of AD, formed because of Aβ causing aggregation of phosphorylated tau filaments into NFTs. NFTs have also been shown to increase due to head injury, like the way APP is overexpressed in head trauma (Reitz, 2012). This suggests that NFTs are not the cause of AD but rather a response to neuronal injury. Studies conducted in rats suggested that the formation of Aβ and NFTs may be reactive, as rats injected with toxins showed APP induction in hippocampal neurons (Reitz, 2012). This evidence suggests that an increase in APP may be due to the loss of nerves in the cortex, thus serving as an intermediate step to NFT formation.

Furthermore, although Aβ plaques and NFTs are considered the hallmarks of AD, studies examining the brains of a large number of patients with AD found that the origin of NFTs appeared first in a different part of the brain (limbic system) compared to where Aβ plaques initially appeared (cortical regions), and the spread of these pathologies differs as the disease progresses (Pimplikar, 2009). This suggests that the formation of Aβ plaques and NFTs may not be directly connected or that the relationship between the two is unclear. Additionally, studies have found that the level of Aβ plaque load does not directly correlate with the extent of dementia in AD patients, and some patients with severely impaired memory showed no plaques at all upon post-mortem analysis (Pimplikar, 2009). Neuroimaging has also shown the presence of plaques in cognitively

normal individuals (Pimplikar, 2009), indicating that plaques do not necessarily result in dementia seen in AD.

In the amyloid hypothesis, the origin of Aβ depositions in AD remains unclear but is fundamental to the pathology of AD (Assema et al., 2012). While genetic mutations are linked to excessive Aβ production in familial early-onset AD, most late-onset AD cases may be due to inadequate clearance of Aβ from the brain rather than increased production (Cirrito et al., 2005).

Zenaro et al. (2015) suggest that Aβ is not the main cause of AD, as Aβ plaques can be found in the brains of elderly patients without AD. The article argues that factors such as the activation of microglial cells contribute to the pathogenesis of AD. Microglial cells are part of the cerebral immune system and respond to pathological changes in the brain. The repeated activation of microglial cells may contribute to the loss of blood-brain barrier (BBB) integrity and the progression of AD (Wake et al., 2011).

Munoz and Feldman (2000) suggest that in patients with mild dementia, the density of Aβ plaques does not linearly correlate with the severity of cognitive dysfunction. They propose that aging is a major risk factor for AD development, as increased oxidative damage to proteins and membrane lipids, along with a decrease in antioxidant enzyme function, may play a role in AD development. The argument that Aβ plaques develop in the aging brain regardless of the presence of AD has been a major counterargument against the amyloid cascade hypothesis. However, in a 25-year review of the hypothesis, Selkoe and Hardy (2016) addressed this argument and proposed that while the amyloid cascade is important in AD, it may not be the primary driver of the disease beyond a certain point. Once AD progresses beyond the mild stage, the anti-amyloid approach may no longer be effective. Smith et al. (2017) emphasize that preventing amyloid accumulation

could slow or stop AD progression and suggest that research should focus on finding a cure for the disease rather than proving a theory.

1.4.2. Amyloid β Toxicity

According to the amyloid cascade hypothesis, APP is normally cleaved by α-secretase, but in aberrant processing, it is cleaved by β- and γ-secretases, resulting in an imbalance between the production and clearance of Aβ peptide (Kumar et al., 2015). This leads to the aggregation of Aβ peptide into soluble oligomers and the formation of insoluble fibrils with a beta-sheet conformation, which are eventually deposited in diffuse senile plaques (Kumar et al., 2015).

Recent studies have shown that Aβ42 oligomers are produced by the cooperative activities of both neurons and associated astrocytes (Dal Pra et al., 2015). These Aβ42 oligomers induce oxidative damage and promote tau hyperphosphorylation, resulting in toxic effects on synapses and mitochondria. During the late stage, Aβ42 plaques attract microglia (Kumar et al., 2015). The activation of microglia leads to the production and release of proinflammatory cytokines, including IL-1β, TNF-α, and IFN-γ. These cytokines stimulate the nearby astrocytes and neurons to produce more Aβ42 oligomers, thereby activating more Aβ42 production and dispersal (Dal Pra et al., 2014). Aβ oligomers also lead to the destruction of oligodendroglia (Antanitus, 1998). Oligodendroglia is particularly susceptible to oxidative stress caused by Aβ oligomers due to their low content of reduced glutathione (GSH) and high concentration of iron, which impairs their ability to scavenge oxygen radicals (Galimberti et al., 2013).

Neurotoxicity: Aβ lies at the heart of the amyloid cascade hypothesis, and its amyloid fibrillar form is the primary component of amyloid plaques found in the brains of AD patients. Aβ toxicity is responsible for various pathological aspects of AD, including neuroinflammation, neurofibrillary tangles, and oxidative damage as shown in figure 1.7 (Richard et al., 2011). Earlier

research on tissue culture has shown that exposure to Aβ fibrils leads to cell death within 24 hours due to the toxicity of Aβ on neurons, and this cell death may be attributed to apoptosis triggered by the oxidative effects of Aβ (Deshpande et al., 2006). There is controversy regarding the form of Aβ that is toxic to neurons, with evidence suggesting picomolar toxicity of oligomeric assemblies, possibly in the form of dimers, as well as multimeric pore-like complexes of Aβ monomers (Shankar et al., 2008). There is also evidence indicating differences in the relative toxicities of intracellular and extracellular Aβ, as intracellular injection of Aβ42 results in neuronal death and intracellular Aβ is seen in early AD (Laferla et al., 2007).
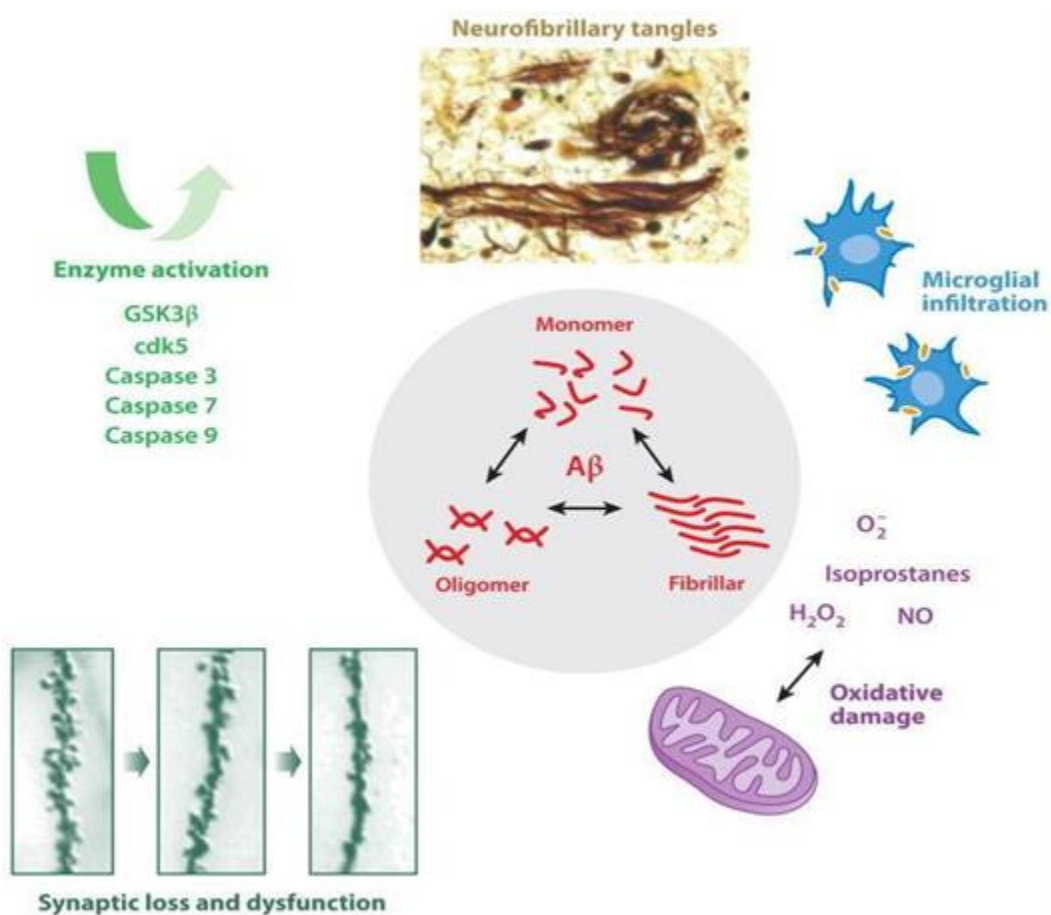
Figure 1.7. Amyloid Beta Toxicity in Neurons. An equilibrium between several species of extracellular and intracellular Aβ, including monomeric, oligomeric, and fibrillar forms, causes

toxicity through several mechanisms, including microglial infiltration, the generation of reactive

oxygen species, and synaptic damage. Neurofibrillary tangles are generated by Aβ-induced tau

phosphorylation and cleavage. Enzymes activated directly by extracellular Aβ include GSK3β,

Cdk5, and multiple caspases, which activate tau cleavage and phosphorylation among their many

harmful effects (Richard et al., 2011).

The interaction of Aβ with different neurotransmitter receptors is considered one of the most significant pathological events in the origin of AD, particularly in synaptic dysfunction associated with cognition. It has been reported that Aβ decreases the activation of α-amino-3-hydroxy-5-methyl-isoxazolepropionic acid (AMPA) receptors and reduces their amount at the postsynaptic level. This occurs through several mechanisms: (a) Aβ increases the activity of Caspase 3, which proteolytically acts on the AMPA receptor; (b) Aβ inhibits the auto-phosphorylation of Ca2+/Calmodulin II-dependent protein kinase (CaMKII), which phosphorylates the AMPA receptor; (c) Aβ directly phosphorylates the GluR2 subunit, promoting the endocytosis of the receptor; (d) Aβ induces the endocytosis of AMPA receptors; (e) Aβ stimulates extra synaptic NMDA receptors, potentially coupled with the p38 MAPK pathway; and (f) signaling pathways activated through Aβ-induced inflammation may also converge on the activation of p38 mitogen-activated protein kinase (MARK) (Gasparini and Dityatev, 2008). Aβ has a significantly higher affinity for α7-nicotinic receptors compared to αβ 1–40, and it has been proposed that this binding plays a significant role in the internalization and accumulation of Aβ in cholinergic neurons. Blocking α7 receptors has been shown to successfully prevent the internalization and accumulation of Aβ 1–42. The presence of α7-nicotinic receptors in neurons that predominantly accumulate Aβ 1–42 suggests that this receptor may contribute to the selective cellular toxicity of Aβ in the brain of AD patients (Oddo et al., 2005). Palop and Mucke (2010) suggested that Aβ reduces excitatory

transmission across synapses by decreasing glutamatergic synaptic transmission, leading to synaptic loss over time. Increased Aβ levels result in an inhibitory effect on neuronal excitability through a negative feedback loop, leading to a decline in neurological function. Aβ aggregation leads to synaptic degeneration, as depicted in Figure 1.7. These distinct pathological features are found in the neocortex, hippocampus, and other subcortical regions, which are essential for cognitive function. The presence of such lesions in the brain also serves as diagnostic markers for predicting the progression of AD (Eteghad et al., 2014).

Oxidative Damage: Aβ possesses metal-binding sites, particularly for Cu2+, in its first 15 amino acids, constituted by histidines 6, 13, and 14, and the tyrosine at position 10 (Kontush et al., 2001). Aβ can reduce Cu2+ and Fe3+ to their more affinity-favorable forms, Cu+ and Fe2+, respectively. This enables molecular oxygen to react with reduced metals, generating superoxide anion, which combines with hydrogen atoms to form hydrogen peroxide. Hydrogen peroxide can then react with another reduced metallic ion, leading to the production of hydroxyl radicals via the Fenton reaction. Radicals of Aβ can extract protons from neighboring lipids or proteins, generating lipid peroxides and carbonyls, respectively (Smith et al., 2007). The role of metals in Aβ's toxicity has been demonstrated in experiments where the withdrawal of metals from the reaction medium or the use of deferoxamine significantly reduced Aβ toxicity levels in cellular cultures (Hureau and Faller, 2009).

Aβ has been found in various intracellular membranous structures, including the endoplasmic reticulum, Golgi system, lysosomes, endosomes, and the mitochondria's inner membrane or matrix (Wang et al., 2007). However, the origin of mitochondrial Aβ is still uncertain. While APP is believed to be in the mitochondrial outer membrane, enzymes with β-secretase activity have not been found at the mitochondrial inner membrane, and only the γ-secretase class of enzyme has

been observed. This suggests two possibilities: either the products of β-secretases are transported to the mitochondria from other cellular sources, where their proteolysis by γ-secretases takes place, or Aβ peptides are generated at a separate site and subsequently transported inside the mitochondria. A tight temporal and sequential relationship exists between the accumulation of mitochondrial Aβ and its dysfunction (Wang et al., 2007). In vitro studies have shown that exposure of mitochondria to Aβ leads to a decrease in respiratory states and the activity of cytochrome c oxidase and other enzymes in the Krebs cycle. Other studies have demonstrated that, in the presence of calcium, Aβ can create transition pores in the mitochondrial membrane, resulting in the release of cytochrome C and the initiation of pro-apoptotic signaling pathways. Aβ can directly inhibit the generation of mitochondrial ATP and affect the proper functioning of the α-subunit of ATP synthase (Schmidt et al., 2008). Additionally, research has revealed that subtoxic and chronic administration of Aβ inhibits the transport of nuclear proteins to the mitochondria, leading to impairment in membrane potential and the production of ROS (Sirk et al., 2007). Enzymes such as NADPH oxidase, xanthine oxidase, and A2 phospholipases (both cytosolic and calcium-dependent forms) have also been implicated in mitochondrial dysfunction and ROS production caused by Aβ. Pharmacological blockade of these enzymes significantly reduces ROS production and mitochondrial dysfunction induced by Aβ (Wang et al., 2007).

Neuroinflammation: The early accumulation of Aβ in the brain can lead to brain cell pathology through inflammation, including complement activation, microgliosis, increased cytokine expression, astrocytosis, and acute phase protein response. The immune response in the brain following Aβ deposition results in the accumulation of inflammatory mediators, including free radicals, IL-1, IL-6, TNFα, and microglial activation (Verdile et al., 2004).

Calcium Dysregulation: It is well established that cellular exposure to Aβ leads to an increase in intracellular calcium, which is associated with cell damage and death (Arispe et al., 2007). However, the mechanism by which this increase in intracellular calcium occurs is not well understood. Various Aβ-activated receptors and channels have been implicated, but it is also known that Aβ can directly interact with the lipid components of the cell membrane, forming pores or ionic channels that ease calcium entry into the cell. The presence of Aβ-formed pores or ionic channels has been shown by specific blockade, resulting in a significant reduction in both calcium entry and neuronal damage (Arispe et al., 2007).

1.5. Neuroinflammation in AD

Neuroinflammation is a complex response to brain injury involving the activation of glia, the release of inflammatory mediators such as cytokines and chemokines, and the generation of ROS (Dejan et al., 2017). Inflammatory responses in the brain are associated with increased levels of prostaglandins (PGs), particularly PGE2. PGE2 signaling is mediated by interactions with four distinct G-protein-coupled receptors, EP1, EP2, EP3, and EP4, which are differentially expressed on neuronal and glial cells throughout the CNS. Elevated PGE2 and inflammatory mediators are also characteristic of the aging brain. An increased state of neuroinflammation renders the aged brain more susceptible to the disruptive effects of both intrinsic and extrinsic factors, such as infection, diseases, toxicants, or stress (Dejan et al., 2017). Neuroinflammation is an immune response in neurodegenerative diseases involving the activation of microglia and astroglia, which under normal physiology have phagocytic functions. In AD, microglia secrete proinflammatory cytokines, prostaglandins, ROS, and NOS, which result in chronic stress and, over a prolonged period, neuronal death (Rossi, 2015). Neuroinflammation associated with AD can be inhibited by nonsteroidal anti-inflammatory drugs (NSAIDs) through maintaining Ca2+ homeostasis, targeting

γ-secretase, Rho-GTPases, and PPAR (Nicola Kakis et al., 2008). Several NSAIDs like ibuprofen, indomethacin, and flurbiprofen have been found to decrease Aβ (1-42) peptides both in in vivo and in vitro models through the inhibition of cyclooxygenase (COX) enzymes (Miguel-Alvarez et al., 2015).

Inflammatory cytokines regulate the immune response and participate in crosstalk between immune cells and other cell types (Miller et al., 2013; Xie et al., 2014). NF-κB is a transcription complex that plays a key role in cytokine-mediated inflammatory reactions (Chen et al., 2014b; Kang et al., 2015; Zhang et al., 2015). NF-κB induces the transcription of numerous inflammatory cytokines during the early stage, including TNF-α, IL-1β, and IL-6, thereby increasing the inflammatory response (Shin et al., 2011; Du et al., 2013).

Rutin has been found to be useful in hypoxic, glutamate, and oxidative stress (Pu et al., 2007). In a rat model of sporadic dementia of Alzheimer's type, rutin reduced neuroinflammation (Javed et al., 2012), and in dexamethasone-treated mice, it exhibited neuroprotective effects (Tongjaroenbuangam et al., 2011). Rutin has been shown to attenuate streptozotocin-induced inflammation by decreasing the activity of glial fibrillary acidic protein, IL-8, COX-2, inducible nitric oxide synthase (iNOS), and NF-κB, thereby preventing gross anatomical changes in the rat hippocampus. This effect could be useful in averting cognitive deficits and proves to be beneficial in the treatment of sporadic dementia of Alzheimer's type (Javed et al., 2012). Rutin treatment also reduced the levels of NF-κB, p65, TNF-α, IL-1β, and IL-6 in a rat spinal cord injury model, indicating its anti-inflammatory properties (Paniagua-Torija et al., 2015). Studies have shown that rutin decreases TNF-α and IL-1β generation in microglia (Wang et al., 2012; Zong et al., 2012). Furthermore, rutin has been reported to exert an anti-inflammatory effect in irradiated rats with cerebral ischemia/reperfusion injury (Abd-El-Fattah et al., 2010).

Neuroinflammation is described as the activation of the resident immune cells in the CNS (Robert et al., 2004). These activated immune cells include the tissue-resident microphages of the CNS called microglia (Ginhoux et al., 2010). These microglia fight infections and repair tissue damage (Disabato et al., 2016). The microglia can often resolve the situation on their own without cytokine release during minor infections or minor tissue damage. But in more serious situations, the microglia will secrete cytokines to attract help from blood-borne immune cells (Disabato et al., 2016). While this initially starts as a normal brain response to regain normal functioning, neuroinflammation can persist longer than usual and predisposes to malfunction.

It is proposed that inflammation can be induced by Aβ peptide plaques and NFTs (the pathological hallmarks of AD) or fragments of degenerated neurons (Akiyama et al., 2000; Chiroma et al., 2018). These pathological variations stimulate glial cells to release pro-inflammatory cytokines (e.g., TNF-α, IL-1β, IL-6) and inflammation reactive proteins (e.g., C-reactive protein (CRP)). The increased levels of CRP and pro-inflammatory cytokines then act either through autocrine or paracrine pathways, or both, to stimulate glial cells for additional production of p-tau, Aβ42, and pro-inflammatory molecules. Therefore, a positively self-supporting arrangement is formed in which inflammatory mediators perform a double role by stimulating glial cells and activating molecular pathways causing neurodegeneration.

Senile plaques are associated with activated microglia cells, reactive astrocytes, immunoreaction with antibodies (against CRP, TNF-α, IL-6, IL-1), and complement proteins (Akiyama et al., 2000; Chiroma et al., 2018). TNF-α, IL-6, and IL-1 have the capability to induce the synthesis of Aβ42 and phosphorylation of tau protein, while p-tau and Aβ42 can cause the production of TNF-α, IL-6, and IL-1 by glial cells (Gosselin et al., 2007; Chiroma et al., 2018).
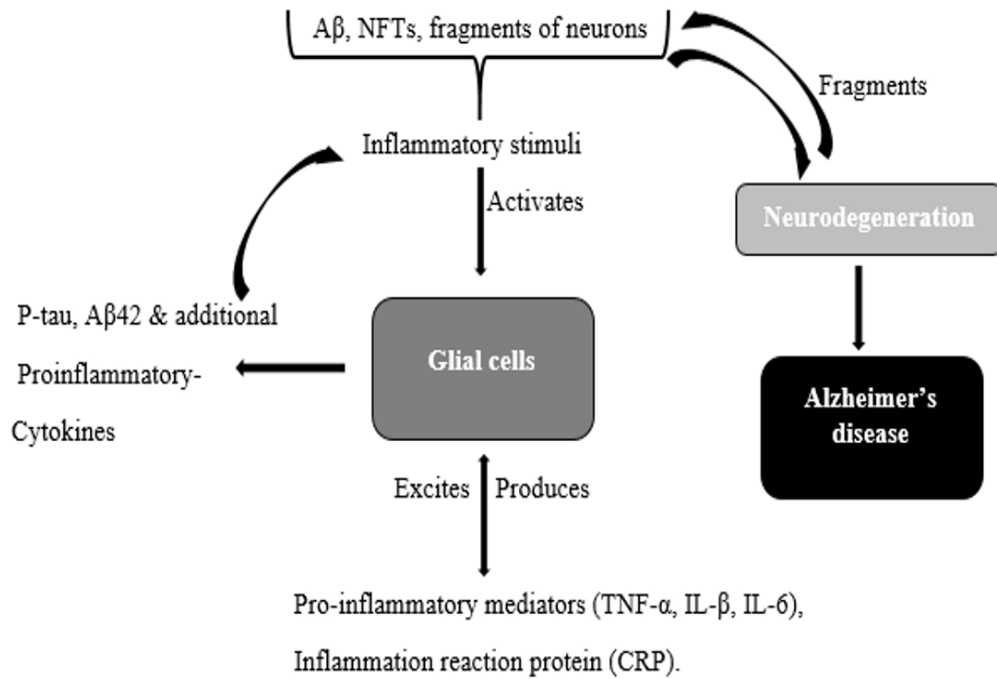
Figure 1.8. Inflammatory Hypothesis of AD

Inflammatory stimuli, such as Aβ, NFTs, and fragments of neurons, activate glial cells, leading to the production of pro-inflammatory mediators and inflammatory reaction proteins. These products further stimulate glial cells, promoting the production of P-tau, Aβ42, and additional pro-inflammatory cytokines, thereby maintaining a cycle of inflammation. This cycle contributes to neurodegeneration and other AD pathologies (Akiyama et al., 2000).

Oxidative and nitrosative stress generate an excess of oxygen and nitrogen molecules in tissues, causing tissue damage and leading to neuroinflammation. Excessive stress or previous injury can make an individual's toll-like receptors (TLRs) more sensitive, resulting in the release of inflammatory molecules in response to an immune stressor (Girate et al., 2013). TLRs are proteins that play a role in the innate immune system and are expressed on sentinel cells such as macrophages and microglia (Jiajun et al., 2014). Chemicals called damage-associated molecular

patterns (DAMPs) can trigger the release of more inflammatory molecules, some of which activate the TLRs (Morris et al., 2015).

1.5.1. Role of Neuroinflammation on Aβ Pathology in AD

Inflammation occurs in pathologically vulnerable areas of the AD brain, while regions with less AD pathology, such as the cerebellum, experience less frequent or absent inflammation (Akiyama et al., 2000; Chiroma et al., 2018). Inflammatory mediators are upregulated in response to inflammation within the brain (Akiyama et al., 2000; Chiroma et al., 2018) (Figure 1.9). Transgenic animals exhibiting inflammatory cytokines show significant pathological changes, including demyelination, neurodegeneration, gliosis, and activation of astrocytes and microglia. Clinical trials using anti-inflammatory drugs have reported that these drugs can slow the progression or delay the onset of AD (Akiyama et al., 2000; Chiroma et al., 2018).

In the development of AD, the production of Aβ and reduced clearance of Aβ play significant roles. Impairment in the clearance of Aβ in the brain has been observed in AD. In the early stages of the disease, microglia can promote the clearance of Aβ and prevent pathological progression. However, persistent microglial activation can lead to the release of cytotoxic molecules (e.g., RNS, ROS, chemokines, complement proteins, and pro-inflammatory cytokines), which can increase Aβ production and reduce its clearance rate. This occurs through the dysregulation of astrocytes and microglia, decreased expression of Aβ-degrading enzymes, and loss of structural and functional integrity of the blood-brain barrier (Brandenburg 2010; Yany et al., 2011).

1.5.2. Role of Neuroinflammation on Tau Pathology in AD

The role of inflammation in aggravating tau pathology was first observed in vitro studies using primary microglia cells stimulated by lipopolysaccharide (LPS) or Aβ before being cultured with primary neocortical neurons (Li et al., 2003). These studies showed that the secretion of IL-1β (a

pro-inflammatory cytokine) by microglial stimulation leads to elevated tau phosphorylation through the activation of p38-mitogen-activated protein kinases (MAPK). This finding was further confirmed in vivo using a 3xTg model exhibiting both amyloid and tau pathologies

(Oddo et al., 2003). Chronic administration of LPS activated tau phosphorylation at several phosphorylation sites associated with pre- and post-tau tangle pathology in 3xTg mice at early and advanced stages (Kitazawa et al., 2005; Chiroma et al., 2018). Microglial activation and subsequent release of IL-1β were involved in the stimulation of glycogen synthase kinase-3β (GSK-3β) or cyclin-dependent kinase-5 (CDK-5) (SY et al., 2011). Chronic overexpression of TNF-α, another pro-inflammatory cytokine, led to an increase in the pre-tangle-associated pT231 epitope (Janelsins et al., 2008).

On the other hand, overexpression of interferon-γ (IFNγ), a pro-inflammatory cytokine prominently related to viral infections, led to dephosphorylation of tau at pre-tangle phosphorylation positions (Mastrangelo et al., 2009). These studies suggest that the stimulation or inhibition of tau pathology aggravation depends on the type of pro-inflammatory cytokines or immunological stressors present. Additionally, there is evidence that chronic administration of nonsteroidal anti-inflammatory drugs (NSAIDs) such as r-flurbiprofen or ibuprofen can cause tau dephosphorylation despite poor brain penetration, indicating that basal peripheral inflammation contributes to the progression of tau pathology (Barron et al., 2017).

Tau phosphorylation plays an important role in triggering a pathological cascade of events that eventually leads to the formation of NFTs. Studies have shown an increase in tau aggregation after chronic administration of LPS in the 3xTg model, whereas acute LPS treatment in the rTG510 model resulted in increased tau phosphorylation without affecting tau aggregation (SY, 2011).

Pro-inflammatory cytokines significantly induce tau phosphorylation, but it is unclear whether this leads to the formation of tau aggregates. Furthermore, evidence suggests that inflammation plays an important role in tau pathology through the induction of microglial phagocytosis of tau oligomers, potentially inhibiting the spread of tau pathology. While most research on tau protein comes from preclinical studies, it is important to conduct clinical studies to examine the role of inflammation in tau pathology (Guerrezo-munoz et al., 2015).
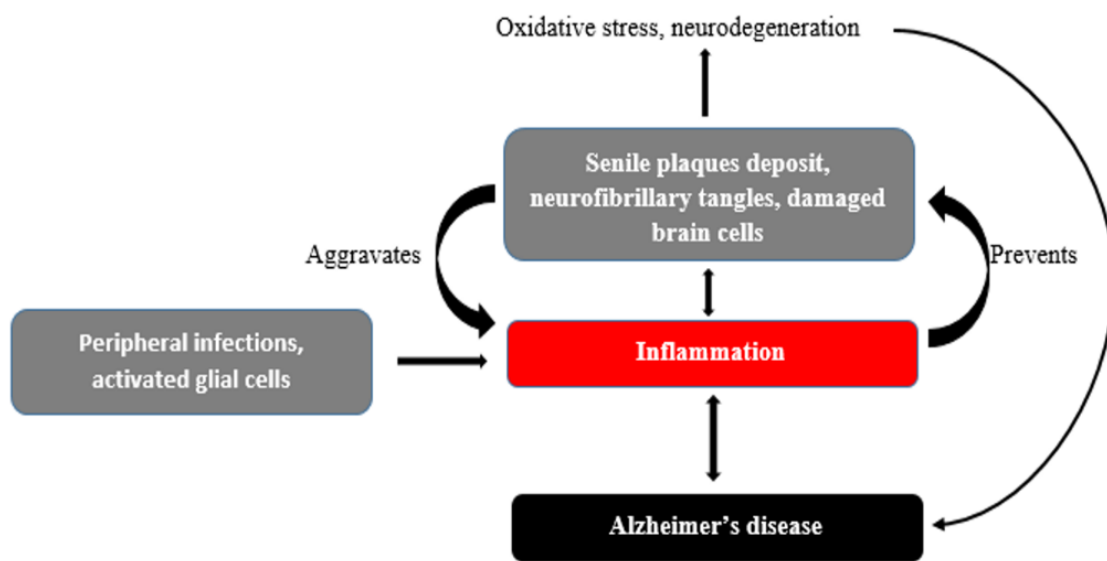
Figure 1.9 Mechanisms involved in the role of inflammation in AD. Senile plaque deposits, neurofibrillary tangles, damaged brain cells, peripheral infections, and activated glial cells can lead to brain changes present in AD, such as neurodegeneration, neuroinflammation, and oxidative stress. When the neurotoxic insults are mild, the inflammation serves as a defensive mechanism. However, when the insults are high, the inflammation is aggravated, which, in turn, increases neurodegeneration and AD pathology (Akiyama et al., 2000).

1.5.3. Systemic Inflammation and AD

Evidence from epidemiological and translational research suggests that inflammation from outside the CNS (i.e., systemic inflammation) may promote neurodegenerative and Alzheimer's-specific pathology within the brain. Studies have revealed that individuals with AD and mild cognitive impairment have higher levels of proinflammatory cytokines, cytokine receptors, and other inflammatory markers (e.g., IL-6, soluble TNFα receptor-1 (sTNFα-R1), and CRP) within the blood. These findings raise questions about whether systemic inflammation plays a mechanistic, compensatory, or associative role in dementia pathogenesis. Large cohort studies have found that individuals with higher levels of inflammatory proteins in the blood during midlife (decades before the typical age of dementia symptom onset) were at an increased risk for cognitive decline leading to aging (Walker et al., 2019). Additionally, elevations in inflammatory proteins during midlife have been associated with smaller brain volumes and abnormal white matter microstructural integrity during aging (Walker et al., 2017). These findings provide significant insight into the temporal relationship between inflammation and adverse neurocognitive outcomes and suggest that systemic inflammation occurring at an early age before the onset of dementia may promote the progression of cognitive decline and neurodegenerative processes.

Research has found that systemic inflammation can exert a downstream effect on brain structure and function via an immune-brain axis. Circulating inflammatory proteins in the blood can communicate with the CNS through multiple neural and humoral pathways, including via afferent vagus nerve signaling, transcytosis of cytokines through blood-vessel walls into circumventricular organs, and receptor-mediated transcytosis of cytokines across the blood-brain barrier (Figure 1.10). Regardless of the mechanism, inflammation outside of the CNS is believed to increase inflammatory signaling within the CNS, promoting the activation of microglia and astrocytes and

their transition to a reactive proinflammatory phenotype (M1 and A1, respectively) (Cunningham and Hennessy, 2015). Although transient inflammatory activation of neural immune cells is thought to be beneficial for the clearance of pathogenic proteins, prolonged M1 and A1 activation is believed to stimulate neurodegenerative processes and potentiate aspects of AD pathology. Specifically, activated M1 and A1 glial cells can promote synaptic loss through complement-mediated phagocytosis of synapses, exacerbate tau pathology through the upregulation of kinases that hyperphosphorylate tau and lead to its misfolding, and produce proinflammatory cytokines that can induce neuronal and glial cell death via apoptosis and inflammasome activation.
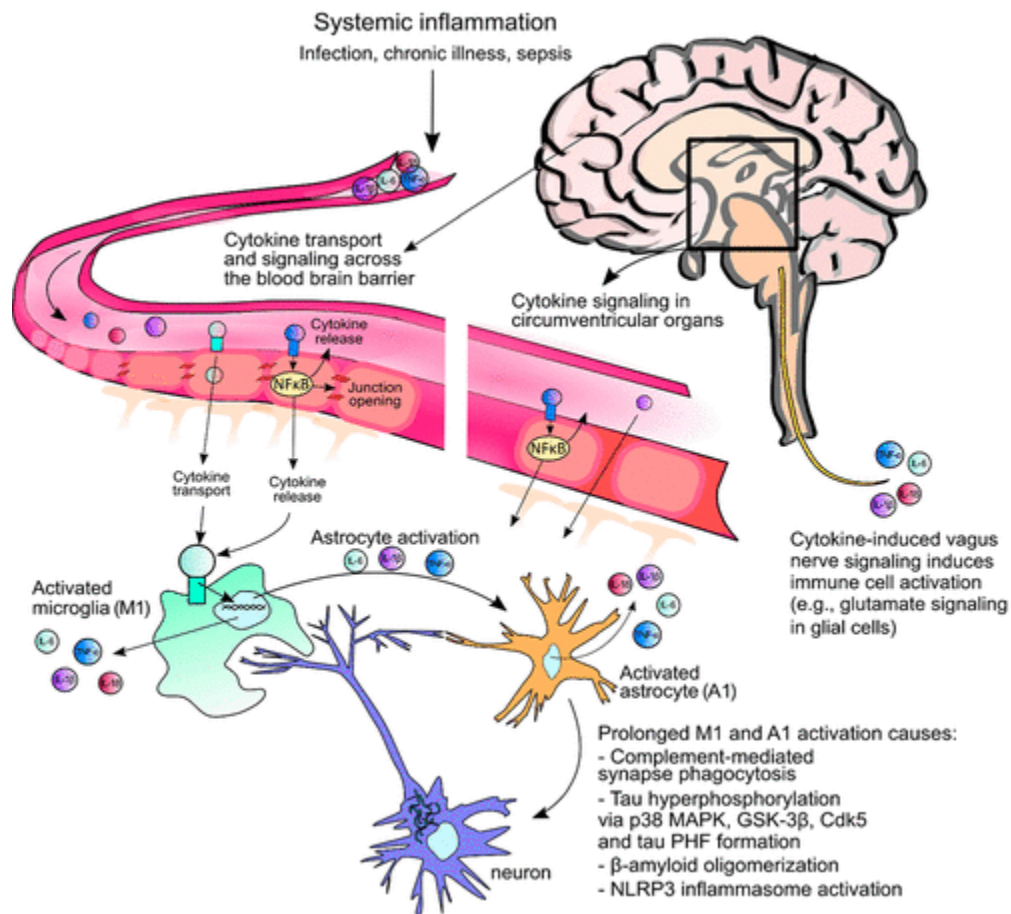
Figure 1.10 Systemic inflammation, neuroinflammation, and Alzheimer's-specific pathways.

Systemic inflammation, caused by events such as infection, chronic illness, and sepsis, is marked by increased circulating proinflammatory cytokines (e.g., IL-1β, IL-6, TNF-α, and IL-18). These cytokines may signal the central nervous system by crossing the blood-brain barrier, signaling across the glial barrier in circumventricular organs such as the area postrema, and stimulating the vagus nerve to induce signaling within the brain. These cytokines can bind to receptors on endothelial cells and cause a signaling cascade in three directions: cytokine release into the bloodstream, opening of tight junctions between endothelial cells, and cytokine release into the brain. Proinflammatory cytokines and endotoxins in the periphery can also stimulate the vagus nerve, which communicates through the medullary reticular formation, locus coeruleus, and hypothalamus to stimulate the hypothalamic-pituitary-adrenal (HPA) axis. Vagus-nerve-regulated glutamatergic stimulation of neural immune cells also induces the release of proinflammatory cytokines and chemokines in the central nervous system, activating microglia and astrocytes to release proinflammatory cytokines (Cunningham and Hennessy, 2015).

Prolonged inflammatory activation of microglia and astrocytes is believed to promote neurodegeneration and Alzheimer's-related pathologies by way of complement-mediated synaptic phagocytosis by microglia, upregulation of kinases that contribute to tau hyperphosphorylation, β-amyloid oligomerization, and NLRP3 inflammasome activation. IL, interleukin; p38 MAPK, p38-mitogen-activated protein kinase; GSK-3β, glycogen synthase kinase 3β; NFκB, nuclear factor kappa-light-chain-enhancer of activated B cells; PHF, paired helical filaments (Cunningham and Hennessy, 2015).

An important pathway by which inflammation promotes AD is by altering the abundance of metabolites derived from the degradation of the essential amino acid tryptophan, collectively called "kynurenines." This degradation generates a range of bioactive intermediate metabolites,

including kynurenic acid (KA), 3-hydroxykynurenine (3HK), 3-hydroxyanthranilic acid (3HA), and quinolinic acid (QA), which can directly target neurotransmitter receptors, affect redox processes, and modulate the activity of immune cells (Schwarcz et al., 2012). Extrahepatic degradation of tryptophan is controlled by the ubiquitously expressed indoleamine 2,3-dioxygenases (IDO) 1 and 2. The activity of IDO is low under basal conditions but is dramatically increased in immune cells by stimuli such as proinflammatory cytokines (e.g., IL-6 and IFN γ), thus providing a direct connection between elevated levels of inflammation and the production of potentially deleterious kynurenines that can alter brain physiology. Persistent IDO activation by cytokines has been shown to lead to the overproduction of the neurotoxic and cytotoxic metabolites 3HK, 3HA, and QA (Cunningham and Hennessy, 2015). 3HK and 3HA generate free radicals through autoxidation and interactions with metals. QA can also generate free radicals and is an NMDA receptor agonist, which can induce excitotoxicity by increasing glutamate release. QA also increases the phosphorylation of several proteins, including tau, which plays a central role in AD (Cunningham and Hennessy, 2015). The levels of IDO in the brain are low compared to the rest of the body. However, tryptophan, KA, and 3HK can also cross the blood-brain barrier, making peripheral production of these metabolites by immune cells a major contributor to the levels of these metabolites in the brain, where they can be metabolized by glial cells and infiltrating macrophages into downstream metabolites such as QA. This is important because under conditions of increased, persistent inflammatory activation, concentrations of harmful kynurenines rise in the blood and can then cause local concentrations in the brain to increase to levels toxic to neuronal and glial cells.

1.6. Hypoxia in AD

Over 95% of AD patients are LOAD, who are the elderly. These patients often have reduced cerebral blood flow that leads to chronic hypoxia. In the AD process, hypoxia enhances a shift in APP processing toward the amyloidogenic pathway and downregulates the function of α-secretase (Lall et al., 2019; Hassan and Chen, 2021). Hypoxia inhibits the expression and activity of an amyloid-degrading peptidase called 'neprilysin' in cortical neurons of rats, increasing the accumulation of Aβ peptides in the affected regions (Lall et al., 2019). It has been shown that hypoxia interacts with Aβ peptide, aggravating neuronal death. There is an increased vulnerability of hippocampal neurons to Aβ peptide toxicity during hypoxia. Calcium dyshomeostasis is a fundamental mechanism in AD pathogenesis. Aβ interaction with the plasma membrane leads to elevated cytoplasmic Ca2+ concentrations and enhances neuron excitation. Chronic hypoxia enhances Ca2+ entry and mitochondrial Ca2+ content, potentiates posttranscriptional trafficking of L-type Ca2+ channels. Both hypoxia and Aβ can trigger the activation of microglia, leading to a maladaptive neuroinflammatory response (Lall et al., 2019).

Cells respond to hypoxia by stabilizing hypoxia-inducible factor (HIF), a key transcription factor regulating oxygen homeostasis. The levels of HIF in cells are directly regulated by four oxygen-sensitive hydroxylases: three prolyl hydroxylases (PHD1-3) and one asparaginyl hydroxylase, factor inhibiting HIF (Chen et al., 2018). Both oxygen and 2-oxoglutarate are substrates of these enzymes, while iron and ascorbate are cofactors. In a normal oxygen environment, HIF hydroxylase is active and degrades the HIF-α subunit. However, in a reduced oxygen environment where oxygen is absent as a substrate, the HIF hydroxylases become inactive, resulting in the accumulation of the HIF-α subunit. The stabilized HIF-α subunit binds to the HIF-β subunit, forming the HIF molecule (Figure 1.11). The stabilization of HIF upregulates the expression of

hundreds of HIF-targeted genes that help cells and tissues survive in hypoxia, as well as a number of apoptotic genes, such as Bax and BNIP3 (Figure 1.11). HIF-1α is ubiquitously expressed and appears to be the most active isoform during short periods (2–24 hours) of intense hypoxia or anoxia (<0.1% O2) in some cell lines. HIF-2α is more tissue-specific and is emerging as a distinct entity in target gene induction in vascular endothelial cells. It is known as an endothelium-specific HIF-α isoform. HIF-2α is active under mild or physiological hypoxia and continues to be active even after 48–72 hours of hypoxia. HIF-2α shares 48% amino acid homology with HIF-1α and binds to similar promoter sites but differs in the cofactors it recruits. HIF-1 and HIF-2 have largely overlapping but also some non-redundant functions. In some contexts, HIF-1α plays a key role in the initial response to hypoxia, whereas HIF-2α drives the hypoxic response during chronic hypoxic exposure.
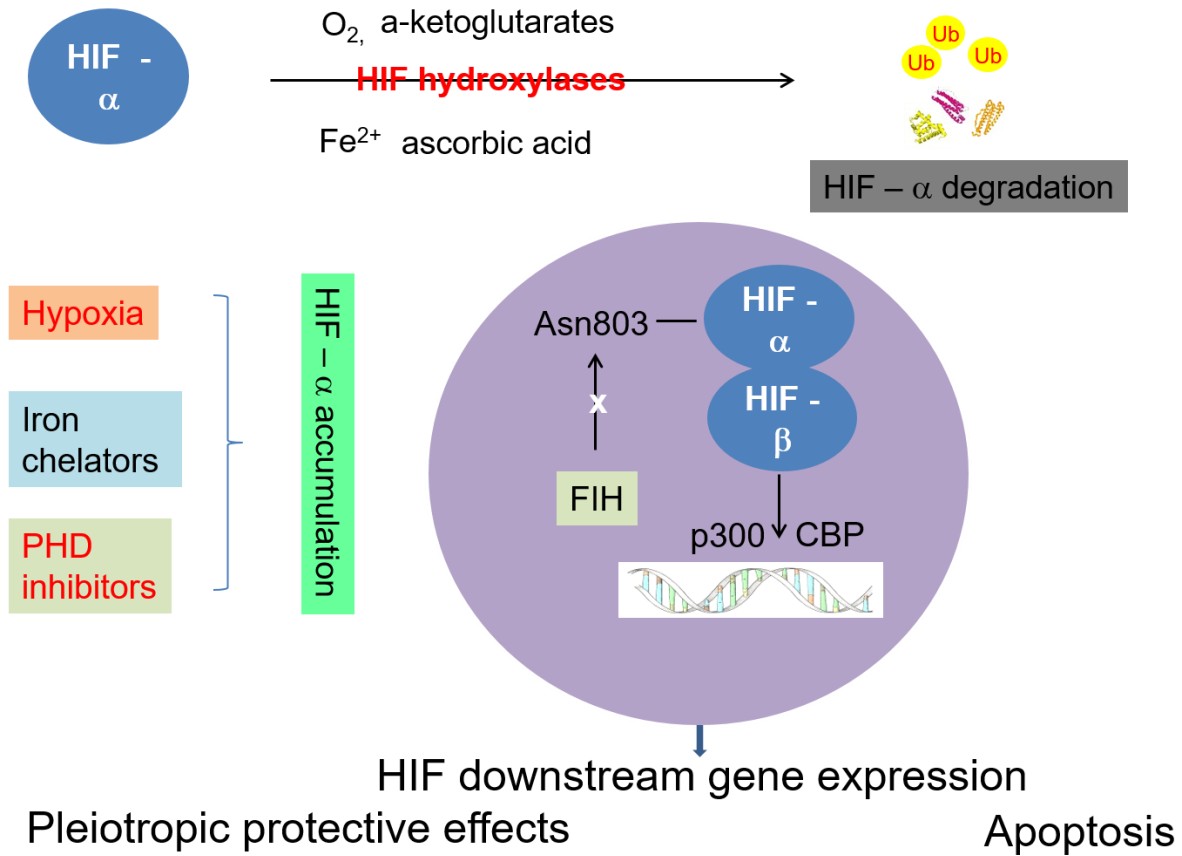
Figure 1.11 Schematic diagram describing the hypoxia-inducible factor pathway. Hypoxia-inducible factor (HIF), a key mediator of oxygen homeostasis, generates numerous pleiotropic protective effects under hypoxia but also participates in apoptosis. Hypoxia mimetic agents, including iron chelators and HIF prolyl hydroxylase (PHD) inhibitors, can remove reactive oxygen species (ROS) and reduce neuroinflammation, in addition to activating HIF. Pharmacological stabilization of HIF can be neuroprotective and explored as an adjunctive therapy for chronic ischemic/hypoxic diseases (Lall et al., 2019); (Hassan and Chen, 2021)..

Sequence analysis and gel shift studies have revealed that HIF-1 binds to the β-secretase 1 (BACE1) promoter. Overexpression of HIF-1α in neuronal cells increases BACE1 mRNA and protein levels, while down-regulation of HIF-1α reduces the levels of BACE1. It has also been

observed that HIF-1 binds to the promoter of anterior pharynx-defective phenotype (APH-1), upregulating its expression and leading to an increase in γ-cleavage of amyloid precursor protein and Notch. HIF-1 also binds to the gene promoter of neprilysin and suppresses its transcription (Lall et al., 2019).

On the other hand, HIF-1 has been proposed as a neuroprotective factor that can suppress neuronal cell death caused by hypoxia or oxidative stress and protect against Aβ peptide toxicity (Zheng et al., 2015; Ashok et al., 2017; Merelli et al., 2018). Recombinant adeno-associated virus vector expressing the human HIF-1α gene (recombinant adeno-associated virus-HIF-1α) inhibits neuronal apoptosis of the hippocampus induced by Aβ peptides. HIF-1 increases glycolysis and the hexose monophosphate shunt, maintains the mitochondrial membrane potential and cytosolic accumulation of cytochrome C, thereby inactivating caspase-9 and caspase-3, and preventing neuronal death in the AD brain. Oxidative damage caused by Aβ peptide induces mitochondrial dysfunction, which is a major characteristic of neuronal apoptosis.

Additional pathological features of AD include astrocyte activation and reduced glucose metabolism in some selected brain areas. Maintenance of HIF-1α levels reverses Aβ peptide-induced glial activation and glycolytic changes, mediating a neuroprotective response to Aβ peptide by maintaining metabolic integrity. HIF-1 is the major transcription factor that increases capillary network density and improves blood circulation in living tissue by regulating protein expression, such as erythropoietin, glucose transporter 1 and 3, and vascular endothelial growth factor. Erythropoietin is able to block Aβ-generated neuronal apoptosis, while glucose transporter 1 and 3 increase glucose transport into brain nerve cells. All in all, HIF-1 participates in hypoxia-induced adaptive reactions to restore cellular homeostasis and postpone the progression of AD (Figure 1.11).

43

A group of agents that can upregulate HIF levels in normoxia are termed hypoxia mimetic agents, as shown in Figure 1.11 (Chen et al., 2018). These agents include HIF hydroxylase inhibitors and iron chelators. Inhibition of HIF hydroxylase not only exerts pleiotropic neuroprotective effects as a consequence of HIF induction but also has antioxidant and anti-inflammatory effects (Figure 1.11). HIF hydroxylase inhibition, which engages multiple downstream effector pathways, is a promising therapeutic intervention that can challenge the heterogeneity in AD pathophysiology present in humans. Because HIF hydroxylase inhibition leverages endogenous adaptive programs, the breadth of the response will not lead to an increased likelihood of toxicity. It is important to emphasize that HIF hydroxylase inhibition does not equal HIF activation. HIFs are only one of several growing substrates known to modulate via HIF hydroxylase (Chen et al., 2018). There are no studies applying PHD inhibitors for AD treatment. Li et al. (2018) applied FG4592 for the treatment of Parkinson's disease both in vitro and in vivo. FG4592, a HIF PHD inhibitor, is currently used for anemia treatment in patients with chronic kidney disease. Li et al. (2018) concluded that FG4592 could potentially be used for treating Parkinson's disease by improving neuronal mitochondrial function under oxidative stress.

Iron chelation has been widely studied to treat neurodegenerative diseases, including AD and Parkinson's disease, as iron accumulation is common in aging and neurodegenerative diseases (Devos et al., 2020). Abnormal iron metabolism generates hydroxyl radicals through the Fenton reaction, triggers oxidative stress reactions, causes lipid peroxidation, damages cell proteins and DNA, and ultimately leads to cell death. Iron promotes Aβ aggregation and induces aggregation of hyperphosphorylated tau. Iron chelators have the potential to activate HIF in addition to iron chelation. The neuroprotective effects of iron chelators act against the generation of free radicals derived from iron but could also be due to upregulation of the hypoxia rescue genes via HIF

stabilization (Merelli et al., 2018) (Hassan and Chen, 2021). The amount of HIF can be adjusted with doses of hypoxia mimetic agents, and the specific activation of HIF-1 or HIF-2 can be achieved (Chen et al., 2018). Carefully monitoring the activation of HIF-1 and HIF-2 by some novel iron chelators will help translate iron chelation therapy for neurodegenerative diseases, including AD.

1.7. Current Pharmacological Treatment

Current pharmacological treatments aim to improve symptoms of dementia and delay further deterioration. There are four drugs licensed for the treatment of AD (Table 1.2). The three AChE inhibitors—donepezil, galantamine, and rivastigmine—are recommended by the National Institute for Health and Clinical Excellence (NICE) for the treatment of mild to moderate dementia in AD. AChE inhibitors alleviate the symptoms of AD by enhancing acetylcholine signaling and exerting anti-inflammatory effects. They reduce the level of free radicals and amyloid toxicity while also decreasing the release of cytokines from activated microglia (Tabet, 2006).

Memantine, a glutamate receptor antagonist, is recommended for patients with moderate to severe AD who are intolerant to AChE inhibitors. By blocking NMDA receptors, memantine counteracts the elevated glutamate levels in the AD brain, preventing overstimulation of NMDA receptors and the subsequent influx of calcium (Turner, 2014).

Table 1.2 Summary of AD Drugs

Drug Name	Drug Type and Use	How It Works	References
Namenda® (memantine)	NMDA antagonist prescribed for	Blocks the toxic effects associated	(Turner, 2014); (Wang et al., 2017)

	symptoms of moderate to severe AD	with excess glutamate and regulates glutamate activation.	
Razadyne® (galantamine)	Cholinesterase inhibitor prescribed for symptoms of mild to moderate AD	Prevents the breakdown of acetylcholine and stimulates nicotinic receptors to release more acetylcholine in the brain.	(Tabet, 2006); (Chlerrito et al., 2017); (Yiannopoulou et al., 2013)
Exelon® (rivastigmine)	Cholinesterase inhibitor prescribed for symptoms of mild to moderate AD	Prevents the breakdown of acetylcholine and butyrylcholine in the brain.	(Tabet, 2006); (Yiannopoulou et al., 2013); (Chlerrito et al., 2017)
Aricept®	Cholinesterase inhibitor	Prevents the breakdown of	(Yiannopoulou et al., 2013); (Tabet, 2006); (Chlerrito et al., 2017)

		acetylcholine in the brain.	

Current AD treatments such as AChE inhibitors and NMDA receptor antagonists can only improve cognition and memory but do not inhibit the progression of the disease (Liao et al., 2015). Therefore, the development of new treatments is essential for AD, considering their antioxidant activities, neuroprotective effects, inhibitory activities of AChE, self-induced Aβ1-42 aggregation, as well as permeability of the BBB (Liao et al., 2015).

1.8. New Research on the Treatment of AD

In recent years, targeting the amyloid cascade has emerged as an attractive strategy to discover novel therapeutic options. Two common approaches used to prevent Aβ accumulation in the brain include the development of β-secretase inhibitors and direct inhibitors of Aβ aggregation (Mohamed et al., 2016). Many studies focus on the prevention of Aβ neuritic plaque formation and ameliorating pathological changes in the brain. These include:

1. Regulation of Aβ homeostasis in the brain endothelium

2. Gene therapy controlling low-density lipoprotein receptor-related protein 1 (LRP1) expression

3. Aβ immunotherapy

4. High doses of vitamin C supplementation

5. Use of angiotensin-converting enzyme (ACE) inhibitors and angiotensin receptor blockers (ARBs)

6. Use of the diabetes drug liraglutide

7. Dietary supplementation with omega-3 fatty acids.

1.8.1. Neuronal Target of Aβ

The anti-amyloid approach targets several aspects of APP metabolism to reduce Aβ toxicity. Researchers have focused on reducing Aβ production using β and γ-secretase inhibitors and activators of α-secretase to enhance Aβ clearance.

1.8.1.1. α-secretase activators

ADAM10, when moderately expressed in APP mouse models, has been found to reduce levels of Aβ and prevent its deposition as plaques (Lichtenthaler et al., 2011). This is because α-secretase activity arises in the middle of the Aβ domain of APP, producing a large sAPPα neuroprotective fragment (Lichtenthaler et al., 2011). However, the use of ADAM10 to increase levels of α-secretase has been avoided by researchers due to its tumorigenic potential (Jacobsen et al., 2010). Selegiline, which is used to slow the progression of AD, has been shown to increase α-secretase activity via protein trafficking-related mechanisms (Yang et al., 2009). Curcumin-based modified compounds (e.g., curcumin-valine, curcumin-isoleucine) have been found to be α-secretase activators, promoting α-secretase activity and ADAM10 immunoreactivity (Narasingappa et al., 2012). This has led to the discovery of natural α-secretase-inducing compounds such as ginsenoside and those contained in the leaves of Ginkgo biloba, which regulate non-amyloidogenic APP-processing pathways (Zhang et al., 2012). The naturally occurring compound triptolide has also been found to inhibit the processing of amyloidogenic APP (Wang et al., 2014). All these natural compounds were found to reduce $A\beta_{42}$, $A\beta_{25}$, and $A\beta_{25\text{-}35}$ (Kaur et al., 2015).

1.8.1.2. β-secretase inhibitors

BACE1 is the primary target for research as its inhibition effectively blocks Aβ production (Roberts, 2001). BACE1 inhibitors have shown inhibition of BBB permeability and robust Aβ reduction in vitro (Robert, 2011). Human clinical trials are investigating several Aβ secretase inhibitors, including AZD3293, MK-8931, E2609, and HPP854. Studies of β-secretase inhibitors AZD3293, CT5-21166, and MK-8931 are investigating their ability to reduce β40 and Aβ42 levels (Selkoe & Schenk, 2003).

Over the past two decades, many potent BACE inhibitors have been developed, but only a few have entered clinical trials. Selectivity over other aspartic proteases (BACE2, pepsin, renin, cathepsin D, and cathepsin E) and blood-brain barrier (BBB) permeability are major challenges. Phase I clinical trials on BACE1 inhibitors, including CTS-21166 and MK-8931, have shown promise in reducing plasma Aβ levels and CSF Aβ reduction, respectively. However, MK-8931 did not demonstrate clinical benefit in cognition and subsequent phase III trials were discontinued (Egan et al., 2018; Merck, 2018). Other BACE1 inhibitors, including LY2886721, AZD3839, atabecestat, and lanabecestat, also revealed poor results in late-stage clinical trials.

Curcumin, asiaticoside, and tryptoline are among the first naturally occurring compounds that inhibit Aβ aggregation by inhibiting BACE1 in both in vitro and in vivo studies. These compounds have been found to reduce Aβ40 and Aβ42 levels and induce α-secretase (Cole et al., 2007). While β-secretase inhibitors show promise in reducing Aβ levels in AD, they do not improve cognitive functions in AD patients. Further research is needed to understand their functions and adverse effects in AD patients.

1.8.1.3. γ-Secretase inhibitors

Diverse classes of γ-secretase inhibitors and modulators have been used over the last decade and have been shown to modulate or reduce the level of Aβ (Li et al., 2000). However, most of them are associated with toxicity. Inhibition of γ-secretase represents an excellent strategy for the inhibition of Aβ generation, although it has been shown to cleave a wide range of important substrates. One of these substrates is Notch, which is a cell surface signaling receptor essential for cell development, differentiation, and tumor suppression (Sorensen and Conner, 2010). SCH 97466, an arylsulfonamide series, was tested as a γ-secretase inhibitor, but it resulted in sufficient Notch signaling without downregulating Aβ levels (Mangialasche et al., 2010). Researchers then sought to develop notch-sparing inhibitors of the arylsulfonamide series like avagacestat but experienced notch-related problems similar to those seen with semagacestat (Coric et al., 2012). Clinical studies investigating ELND006, a notch-sparing compound, were stopped because of liver toxicity. In contrast, CHF-5074 and NIC5-15 are γ-secretase inhibitors that have been found to reduce Aβ levels in AD. NIC5-15 is currently being investigated in a phase II clinical trial, but the development of CHF-5074 was terminated due to adverse effects (Ross et al., 2013).

1.8.2. Inhibition of tau hyperphosphorylation

Tau phosphorylation plays a role in microtubule stabilization in axons. Hyperphosphorylation of tau leads to the formation of paired helical fragments, which form neurofibrillary tangles. This leads to a loss of microtubule binding capacity, resulting in neuronal death (West and Bhugra, 2015). Therefore, neuroprotective strategies aim to inhibit the phosphorylation of tau protein and stabilize microtubules (Shefet-Carasso and Benhar, 2015). In recent years, immunomodulation has been chosen as the best option for effective clearance of tau aggregation (Jaume et al., 2015).

Increased expression of active forms of various kinases like CDK5, GSK3β, Fyn, JNK, P38, ERK1, and ERK2 contribute to the increased phosphorylation of tau in neurofibrillary tangles (Berk et al., 2014). As a result, significant research has been devoted to the development of kinase inhibitors as an effective strategy. SP600125, a JNK inhibitor, exerts beneficial effects on cognition and neurodegeneration in an APP/PS1 transgenic mouse model (Zhou et al., 2015). Pathological activation of CDK5 occurs due to an increase in intracellular calcium in AD, which results in hyperphosphorylation of tau and neuronal death (Comins et al., 2006). Therefore, CDK5 inhibitors like roscovitine and flavopiridol have shown neuroprotective activity in in vitro and in vivo studies (Delatorre et al., 2012). Inhibitors of GSK3β are at the most advanced stage of clinical development in AD. Tideglusib, an inhibitor of GSK3β that has completed phase II trials, was discontinued because it showed no clinical efficacy (Lovestone et al., 2015). Phosphatase activation has been considered another therapeutic approach. Protein phosphatase 2 (PP2A) Agonists are under development, and sodium selenite (VELO15) is currently in phase II trials. Experimental studies have shown that VELO15 administration to rodents shows significant cognitive enhancement, and sodium selenate reduces tau phosphorylation (Janet Van Eersel et al., 2010).

Derivatives of methylene blue dye inhibit the formation of tau and amyloid aggregation, improve mitochondrial electron transport chain efficacy, reduce oxidative stress, prevent mitochondrial damage, and modulate autophagy (Hochgrafe et al., 2015). Several clinical trials are currently underway, including NCT01626391, NCT01689233, NCT01689246, and NCT0166378, to evaluate the efficacy of these therapies in AD (Hochgrafe et al., 2015).

Microtubule stabilizers will yield similar results to inhibitors of tau hyperphosphorylation. TPI 287, a derivative of taxane, stabilizes microtubules by binding to tubulin and has been considered

a possible therapy for AD. The clinical trial NCT01966666 will evaluate the safety, pharmacokinetic properties, and tolerability of TPI-287 in AD. Epothilone D is a microtubule-stabilizing compound that decreases tau neuropathology, hippocampal neuronal loss, and axonal dystrophy and improves axonal transport. However, drug development for AD was stopped after an unsuccessful clinical trial (Shemesh et al., 2011). Experimental studies have shown that a soluble form of tau is the most toxic (Zhang et al., 2012). Therefore, future therapeutic strategies should target soluble forms of tau.

1.8.3. Neuroprotection via the cholinergic system

Neurodegenerative diseases have been associated with alterations in neurotransmitters. Alzheimer's disease (AD) involves the degeneration of cholinergic neurons and the loss of cholinergic signals to the hippocampus and neocortex. Studies have revealed a decrease in choline acetyltransferase, acetylcholine release, and a reduction in nicotinic and muscarinic receptors in the cerebral cortex and hippocampus of postmortem AD brains (Ada et al., 2014). Acetylcholinesterase (AChE) inhibitors act by increasing acetylcholine bioavailability at synapses (Wallace and Bertrand, 2013). Although AChE inhibitors do not reverse the pathogenesis of AD or decrease its progression, their use in combination therapy should not be excluded. Ladostigil (TO3326) is a reversible inhibitor of AChE and an irreversible inhibitor of brain monoamine oxidases A and B; it improves extrapyramidal symptoms and provides an antidepressant effect (Weinreb et al., 2011). It is an antiapoptotic, antioxidant, anti-inflammatory, and neuroprotective agent. Phase II clinical trials with ladostigil, registered as NCT01429623 and NCT01354691, are currently underway (Weinreb et al., 2011).

Between 2011 and 2012, Avraham Pharmaceuticals evaluated a six-month course of ladostigil with ever-increasing doses of up to 80 mg twice daily in a Phase 2 study involving 201 individuals

with mild to moderate Alzheimer's disease. This trial did not meet its primary endpoint of change on the ADAS-cog11, and further development for Alzheimer's disease was terminated (Schneider et al., 2019).

In January 2012, the company initiated a second Phase 2 study to evaluate a lower dose of ladostigil for its ability to delay progression from mild cognitive impairment (MCI) to AD. This trial enrolled 210 patients with a clinical diagnosis of MCI. It compared a three-year course of 10 mg of ladostigil once daily to placebo, with the primary outcome being the conversion from MCI to AD as determined by a clinical dementia rating (CDR) of 1 or greater. In September 2016, the company disclosed that ladostigil also did not meet its primary endpoint in this trial but showed a trend in the direction of a treatment benefit. Treatment benefits were reported on MRI and select cognitive tests, and the results were formally published in Neurology (Schneider et al., 2019).

1.8.4. Neuroprotection by targeting oxidative stress

An imbalance between reactive oxygen species (ROS) and existing antioxidants results in oxidative stress. This leads to Aβ aggregation into insoluble plaques, which increases the generation of reactive ROS. ROS attack key molecules such as enzymes, DNA, membranes, and lipids, leading to cell death. Natural antioxidants such as flavonoids, vitamins (E, C, and carotenoids), phytochemicals, and synthetic compounds provide protection in AD. A phase III trial combining vitamin E and memantine has been conducted, and a phase III trial of vitamin E and selenium is currently ongoing (NCT00040378). Antioxidant compounds like rutin and carotenoids have shown neuroprotective effects in experimental AD models (Javed et al., 2012).

High-dose vitamin C supplementation is a promising treatment for AD. It is well tolerated and rarely causes gastrointestinal disturbances (Martindale, 2005). An earlier study showed that a short course of vitamin C treatment did not attenuate the neuropathological features of AD, such as Aβ

plaque accumulation, oxidative stress, and acetylcholinesterase (AChE) activity (Harrison et al., 2010). However, as pointed out by Kook et al. (2014), mice can synthesize their own vitamin C, which might mask the effect of supplementation. To address this, Kook et al. genetically modified mice in which no vitamin C is produced endogenously, and the significant changes in the results were solely due to the administration of ascorbic acid. The modified AD mouse model mimics the condition in humans and confirms the direct effect of vitamin C. Continuous supplementation of high-dose ascorbic acid improves the Aβ burden in the cortex and hippocampus by 57.9% and 40.3%, respectively (Kook et al., 2014). Although the dose in humans has not been well defined, taking vitamin C supplements for the prophylaxis of AD in addition to a healthy, balanced diet is still beneficial.

1.8.5. Anti-inflammatory therapy

Neuroinflammation is an immune response in neurodegenerative diseases that involves the activation of microglia and astroglia, which normally have phagocytic functions. In Alzheimer's disease (AD), microglia secrete proinflammatory cytokines, prostaglandins, reactive oxygen species (ROS), and nitric oxide synthase (NOS), leading to chronic stress and neuronal death over a prolonged period (Rossi, 2015). Neuroinflammation associated with AD can be inhibited by nonsteroidal anti-inflammatory drugs (NSAIDs) through the maintenance of Ca2+ homeostasis and the targeting of γ-secretase, Rho-GTPases, and PPAR (Nicola Kakis et al., 2008). Several NSAIDs, such as ibuprofen, indomethacin, and flurbiprofen, have been found to decrease Aβ (1-42) peptides in both in vivo and in vitro models by inhibiting cyclooxygenase (COX) enzymes (Miguel-Alvarez et al., 2015). However, both ibuprofen and tarenflurbil have shown no efficacy for the treatment of AD in clinical trials (Pasqualetti et al., 2009). CHF5074, which is not a COX inhibitor, has been found to inhibit Aβ (1-42) by blocking γ-secretase in in vitro models (Ross et

al., 2013). Research indicates that CHF5074 modulates microglia by reducing amyloid burden and microglia activation (Imbimbo et al., 2013). Treatment with CHF5074 in patients improves several cognitive measures and reduces inflammatory marker levels in phase II trials (Rossi et al., 2013).

1.8.6. Targeting Mitochondrial Dysfunctions

Aβ accumulation inhibits mitochondrial import channels, leading to decreased complex activity and increased ROS production (Cottrell et al., 2002). Lipoic acid in combination with vitamin E and C decreases oxidative stress. Combination therapy of lipoic acid and omega-3 fatty acids is in phase I/II trials (NCT01780974, NCT0158941) (Shinto et al., 2014). α-lipoic acid (ALA), also known as thioctic acid, is an organosulfur component produced by plants, animals, and humans, and it possesses various pharmacological properties (Brufani, 2014; Salehi et al., 2019). It has high antioxidant potential and is widely used as a racemic drug for diabetic polyneuropathy-associated pain and paresthesia. Naturally, ALA is located in mitochondria, where it is used as a cofactor for pyruvate dehydrogenase (PDH) and α-ketoglutarate dehydrogenase complexes (Singh and Jialal, 2008; Maglione et al., 2015). Despite its various potentials, ALA's therapeutic efficacy is relatively low due to its pharmacokinetic profile. It has a short half-life and bioavailability (about 30%) triggered by its hepatic degradation, reduced solubility, and instability in the stomach. However, the use of various innovative formulations has greatly improved ALA bioavailability (Singh and Jialal, 2008; Maglione et al., 2015; Salehi et al., 2019).

1.9. Model currently used to study Alzheimer's disease

There are experimental models used to study AD that are necessary for interpreting the major mechanisms of AD and evaluating novel therapeutics. Usually, in vitro and in vivo models (e.g., cell and rodent models, respectively) are used before conducting clinical trials on human patients (Li et al., 2016; Blaikie et al., 2022). Ex vivo models (e.g., rodent brain slices) and in silico models,

which are more recently used (e.g., virtual ligand screening), have been established to assist in demonstrating AD.

1.9.1. In vitro models of AD

In vitro models of AD study the pathological changes at a cellular level (see Table 1.3). These models can be performed under controlled environmental conditions and have simpler maintenance, lower cost, and easier handling compared to in vivo models (Li et al., 2016; Blaikie et al., 2022). Studies can also be conducted within a shorter time, and the pharmacodynamics of the experiments can be evaluated (Arantes et al., 2013; Blaikie et al., 2022). However, due to the simplicity of this model, reliable pharmacokinetic data cannot be generated, although initial toxicity studies can be carried out (Blaikie et al., 2022).

Therefore, in order to understand the mechanisms underlying the development and treatment of AD, an ideal in vitro model is required that can mimic the progression of AD, including the degeneration of neurons and the formation of amyloid plaques and neurofibrillary tangles. This includes primary culture and stem cell lines. To create an ideal in vitro AD model, cell lines such as primary culture cell lines derived from rodents, cells derived from cancer cells such as neuroblastoma and pheochromocytoma cells, are used. Induced pluripotent stem cells (iPSCs) are also explored by either taking skin cells from Down syndrome patients or by transfecting cells with genes associated with AD (PSEN1, PSEN2, or APP) (Zheng, 2006).

Neuroblastoma: Human neuroblastoma (SH-SY5Y) has been used to generate an in vitro model for AD and other neurodegenerative diseases by guiding the SH-SY5Y cells into neuronal lineage using several differentiating factors. This is particularly significant when exploring the role of microtubule and tau function in AD (Zheng, 2006). These cells possess synaptic structures, functional axonal vesicle transport, and express neuro-specific proteins, including nuclear protein

NeuN, neuron-specific class III β-tubulin, and synaptic protein Sv2 (Agholme, 2010). Immortal rat hippocampal cell lines are generated from the embryonic rat hippocampus to provide cell lines derived from a known brain region that express phenotypes of particular subsets of cells, unlike cancer cell lines. The cells are immortalized by retroviral-mediated oncogene transduction using tsA58 and U19tsa alleles of the simian virus 40 large tumor antigen (Eves, 1992; Carolindah, 2013). This cell line has distinct features of conditional proliferation and the ability to differentiate into neurons after ceasing division. They are significant for understanding the pathogenesis of AD since hippocampal neurons are responsible for cognition and memory (Agholme, 2010).

Human induced pluripotent stem cells (iPSCs) are also used as an AD model, established using primary human fibroblast cells isolated from patients with familial Alzheimer's disease (FAD) (Yagi, 2011). These cells are reprogrammed using OCT4, SOX2, KLF4, LIN28, and NANOG transcription factors to induce pluripotent stem cells (iPSCs). From the iPSCs, two clones are established by retroviral transduction using presenilin1 mutations A246E (PS1-2 iPSC and PS1-4 iPSC) and with PS2 mutations, N141I (PS2-1 iPSC and PS2-2 iPSC). FAD patient-specific iPSCs go through neural differentiation to model AD pathogenesis in vitro, aiming to determine the effect of presenilin mutations during neural differentiation. An increased ratio of Aβ42 to Aβ40 in iPSCs with mutated PS1 and PS2 was detected compared to non-AD control iPSCs. The increased Aβ42 secretion by living human neurons derived from AD patients supports the amyloid cascade pathogenesis. These cells were tested for their suitability in drug screening using γ-secretase inhibitor and modulator. The outcomes revealed that Aβ secretion was inhibited and modulated as expected by adding agents against γ-secretase. Therefore, living human neurons from patients (FAD-iPSC-derived neurons) are suitable for drug development and testing new drugs (Yagi, 2011). Another in vitro human cellular model for AD pathogenesis derived from Down syndrome

(a disease that results from trisomy 21) patients has been reported (Shi, 2012). Down syndrome patients were chosen because the disease has a high incidence of AD due to the triplication of APP in chromosome 21, resulting in autosomal dominant EOAD (Selkoe, 2008). This model was created by differentiating iPSC lines and ES cell lines derived from patients with Down syndrome into cortical neurons. The differentiated cortical neurons from Down syndrome ES cells (DS-ES cells) and the control exhibit no differences in the expression and localization of full-length APP protein. Both DS-ES cell and DS-iPS cell-derived cortical neurons show the same distribution of intracellular and extracellular aggregates of Aβ42 peptides. Late stages of AD pathogenesis are also represented by the presence of hyperphosphorylated Tau protein in the dendrites and cell bodies of DS-iPSC-derived cortical neurons. This model is appropriate for understanding the pathogenesis of AD in Down syndrome patients at early and late stages. It can also be used as a good model for drug screening as the disease is progressive, and the two hallmarks of AD are observed over time, thus recapitulating AD pathogenesis in humans (Carolindah, 2013). Table 1.3. Summary of common in vitro models of AD, including the pathological significance of each model to AD, the studies that can be conducted, and the advantages and disadvantages of the models.

Table 1.3 Summary of common in vitro models of AD

Model	Pathological Relevance to AD	Phenotype & Assessments	Advantages	Disadvantages	References

2D Cell Culture	HBMEC (Human brain microvascular endothelial cell)	Barrier property s like BBB	Study drug delivery	• Inexpensive •Well-established • Simple to manipulate and analyse •Mass of comparative literature •Easy to control environment	•Not representative of real environments •Response to stimuli not reflective of actual case • Usually only one cell type; lack of interaction and contribution of different cell types • Often cancer-derived, with a multitude of genetic changes	(Bachmeier et al., 2010
	BCEC (Brain capillary endothelial cell)	Retain BBB characteristics	Study drug delivery Study Aβ effect on BBB			(Burkhart et al., 2015) (Gali et al., 2019)
	RBE4 (Rat brain endothelial cell)	Retain BBB properties Express BACE-1 and APP	Study BACE-1 activity and APP processing Study drug delivery			(Brambilla et al., 2015) (Roux and Couraud 2005)
	SH-SY5Y (Human neuroblastoma cell).	Neuron model Can be differentiat	Study neurotoxicity Study AD			(de Madeiros et al., 2019)

	ed into cholinergic phenotype Express tau	mechanisms and pathways including Aβ and oxidative stress			(Chang and Teng 2015
SK-N-MC (Human neuroepithelioma cell).	Cholinergic-like neuron model	Study AD mechanisms including Aβ			(Kuo and Tsao 2017)
PC-12 (Rat pheochromocytoma cell).	Neuron model	Study AD mechanisms and pathways including Aβ and oxidative stress			(Yang et al., 2017)
HEK293 (Human embryonic	Express tau	Study tauopathy			(Houck et al., 2016)

	kidney cell 293).					
	7W CHO (7W Chinese hamster ovary cell).	Express APP	Study Aβ pathway			(Myre et al., 2009)
	BV-2 (Murine microglial cell).	Inflammati on model	Study inflammat ory pathways			(Bing et al., 2020)
iPSCs	Neurons, astrocytes, microglia, etc	Differentia ted into different cell types	Study AD mechanis ms	•Compare cell types of interest from healthy vs AD patients	•Genetic diversity between individuals • Genomic instability	(Penny et al., 2020) (Li et al., 2020)
3D Cell Cultu re	Derived from cell lines or iPSCs	Can contain multiple cell types Cellular environme nt may be	Study AD mechanis ms	• iPSCs from AD patients better represent AD pathology •3D conditions	•Reproducib ility issues • More complex, but still not entirely	(Choi et al., 2016) (Marrazz o et al., 2019)

		more similar to that of organs		better reflect *in vivo* environments	representative of *in vivo*	

1.9.2 In vivo models of AD

Both transgenic and non-transgenic animal models of AD have been developed to mimic the pathological changes related to the human disease. Generally, mammalian models such as mice and rats are used for the studies of AD, although non-mammals including C. elegans (Caenorhabditis elegans) and fruit flies (Drosophila melanogaster) are also used and highly beneficial as they are subject to less stringent ethical standards and have lower costs (Alzheimer's Association, 2019) (Table 1.4). Overall, animal models allow profound studies of the pathogenesis of AD and can reproduce the main hallmarks of the disease (Chierrito et al., 2017; Blaikie et al., 2022). Compared to cell models, animal models are also essential for safe assessments of novel therapeutics as their multifaceted systems provide a better replication of human pharmacokinetics and thus enhance the prediction of toxicity. However, the complexity of animal models leads to a lack of control over experimental conditions (Arantes-Rodrigues et al., 2013). Additionally, transgenic models are inadequate in accurately revealing the human condition because sporadic AD is linked with age rather than genetic mutations (Van Dam and De Deyn, 2011). With mounting evidence indicating the multifactorial nature of AD, disease models with only a single cause are unable to reproduce the complete human pathology. Strict ethical standards and higher costs are also associated with animal models compared to in vitro models. Table 1.4. Summary of

common in vivo models of AD, including the pathological significance of each model to AD, the studies that can be done, and the advantages and disadvantages of the models.

Table 1.4 Summary of common in vivo models of AD

Model		Pathological Relevance to AD	Phenotype & Assessments	Advantages	Disadvantages	References
Transgenic	*C. elegans*	$A\beta$- or tau-expressing models e.g. CL4176: $A\beta_{1-42}$ in muscle cells CL2355: $A\beta_{1-42}$ in neurons	Study AD mechanisms, including paralysis and uncoordinated motility	•Simple genetic manipulation •Short lifespan •Several orthologues of human AD-related genes and pathways	• Expression in muscle •Simple nervous system; lack of defined brain •Basic measures for	(Link, 1995)

				• Low cost	cognitive decline	
Zebra fish	Express APP or tau e.g. APPsw: Aβ deposition hTAU-P301L: tau hyper-phosphorylation and aggregation	Study APP processing and other AD pathways	• Share the same major organs/tissues with humans •Similar genetic structure to humans •Cheap to maintain •Large quantity of eggs with short generation time	•Genetic manipulation is more challenging •Require strictly controlled environmental variables •Basic measures for cognitive decline	(Paquet et al., 2009)

| | *Drosophila* | Transgenic expression of APP or tau e.g. UAS-Aβ42: Aβ in retinal neurons UAS-tau: tau aggregation | Study Aβ and tau toxicity | •Short lifespan

• Low cost

•Orthologues of AD-related genes and some functional conservation of proteins | •Brain anatomy and major organs differ substantially from humans

•Basic measures for cognitive decline

• Unable to conserve permanently as frozen stocks | (Crowther et al., 2005) |

	Rat	APP, tau, PSEN1, and combination transgenic models e.g. TgF344-AD: Aβ aggregation APP + PS1: Aβ aggregation	Study AD mechanisms including Aβ, tau and inflammatory pathways	•Brain surgery easier as brains are larger than mice •Easier to handle compared to mice	• Model of FAD rather than more common SAD • Difficult to reproduce complete AD pathology	(Gong et al., 2006)
	Mouse	APP, tau, PSEN1, and combination transgenic models e.g. 5xFAD: Aβ aggregation	Study AD mechanisms including Aβ, tau and inflammatory pathways	•Technically easier to inject DNA into embryos than rats •Ease of breeding and	• Difficult to reproduce complete AD pathology • NFT do not develop	(Games et al., 1995)

				relatively low maintenanc e costs	without tau mutations which do not occur in human AD	
Chemically/mecha nically induced	Rodents (mouse, rat)	Induce cholinergic hypofuncti on, memory dysfunction , brain inflammati on e.g. AlCl$_3$: Aβ and tau aggregation	Study AD changes not directly related to APP/tau	• Rapid and easy to attain •Specific neurotrans mitter pathway explored	• Can lack hallmarks of AD (Aβ plaques and NFTs)	(Xiao et al., 2011)
Spontaneous	Dog	Progressive Aβ pathology e.g.	Study age-related Aβ aggregati	•Share several key molecular	•Late-onset of disease compared	(Cummi ngs et al., 1993)

		aged canine: Aβ aggregation	on and oxidative stress	pathways of human AD • Model of more common, sporadic form of AD	to transgenic models • High costs • Strict ethical considerations	
	Rodents (mouse, rat)	Accelerated aging and APP overproduction e.g. SAMP8: Aβ in brain	Study AD hallmarks in old age	•Assessable behaviours •Age-related cognitive decline	•Longer period of pathology development than transgenic models	(Yagi et al., 1988)
	Non-human primates	Develop Aβ and tau aggregates, and brain atrophy e.g.	Study AD pathology in model most	•Similar brain anatomy to humans		

Model			Phenotype	Ref
		aged vervet: Aβ plaques and tau	relevant to human	•Close genetic proximity		

Generally, the most popular in vivo models for AD are rodents, specifically mice and rats. These models are frequently used due to their relatively lower maintenance costs and their suitability for genetic breeding and manipulation. Moreover, the nervous systems of rodents are similar to those of humans, and their behaviors are complex, allowing for the study of AD-relevant cognitive impairments in these models. Various methods, including transgenic, chemically/mechanically induced, and spontaneous approaches, can be used to induce an AD-like disease state in these models (Blaikie et al., 2022). However, no single model can fully replicate the complex pathology of human AD. Table 1.5 provides a summary of the common AD rodent models, along with the corresponding phenotype of each model relevant to AD.

Table 1.5 Common rodent models for AD

Model			Phenotype	Ref
Transgenic	3xTg	PSEN1 M146V, APP KM670/671NL (Swedish), MAPT P301L (mouse Thy1.2 promoter)	Aβ plaques, tau tangles, synaptic plasticity deficit, cognitive impairment, learning and memory deficits	(Oddo et al., 2003)

	5xFAD	APP KM670/671NL (Swedish), APP I716V (Florida), APP V717I (London), PSEN1 M146L (A > C), PSEN1 L286V (mouse Thy1 promoter)	Aβ plaques, neuronal loss, synaptic loss and plasticity deficit, cognitive impairment, impaired spatial memory, learning and memory deficits, impaired social recognition, motor impairments	(Oakley et al., 2006)
	APOE-KO	ApoE knockout	High serum cholesterol, Aβ plaques, tau tangles, potential cognitive impairment	(Piedrahita et al., 1992)
	APP/PS1	APP V717I (London), PSEN1	Aβ plaques, neuron and synaptic loss,	(Anantharaman et al., 2006)

		A246E (mouse Thy1 promoter)	cognitive impairment, spatial learning and memory deficits	
	J2O	APP KM670/671NL (Swedish), APP V717F (Indiana) (human PDGF-β promoter)	Aβ plaques, neuron loss, synaptic loss and plasticity deficit, cognitive impairment, spatial learning and memory deficits	(Games et al., 1995)
	Tg2576	APP KM670/671NL (Swedish) (hamster PrP promoter)	Aβ plaques, synaptic loss and plasticity deficit, cognitive impairment, spatial learning and working memory deficits	(Hsiao et al., 1996)

Induced	AlCl₃	Aluminium chloride	$A\beta$ plaques and tau tangles, cholinergic deficit, cognitive impairment, spatial learning and memory deficits	(Erasmus et al., 1993)
	HFCD	High fat-cholesterol diet	$A\beta$ plaques, high serum cholesterol, inflammation, cognitive impairment, memory and behavioural deficits	(Thirumangalakudi et al., 2008)
	OKA	Okadaic acid	Tau tangles, inflammation, neuron loss, cognitive impairment, memory deficits	(Zhang and Simpkins 2010)

	SCO	Scopolamine	Aβ plaques, tau tangles, cholinergic deficit, cognitive impairment, learning and memory and behaviour deficits	(Flood and Cherkin 1986)
	STZ	Streptozotocin	Aβ plaques, tau tangles, neuron loss, reduced glucose uptake, cholinergic deficit, cognitive impairment, spatial learning and working memory deficits	(Salkovic-Petrisic et al., 2006).
	TBI	Traumatic brain injury	Aβ plaques, inflammation, neuron loss, cognitive	(Dixon et al., 1999).

			impairment, learning and memory deficits	
Spontaneous	Age	Aging	Inflammation, synaptic plasticity deficit, cognitive impairment, memory deficit	(Dunnett et al., 1988).
	KKAy	Diabetic type 2	Aβ plaques, tau tangles, inflammation, cognitive impairment, spatial learning and memory deficits	(Iwatsuka et al., 1970).
	SAMP8	Senescence accelerated mouse-prone 8	Aβ plaques, tau tangles, inflammation, cognitive impairment,	(Takeda et al., 1997).

Task		Cognitive test	Description	Ref
			learning and memory deficits	

Several experiments are conducted in rodents to assess the disease state of the animals, determine the phenotypic relevance to human AD, and screen potential therapeutics. Behavioral tests that investigate the cognitive function of rodents are commonly used in AD experiments, as they are crucial for studying the major symptom of AD, which is memory impairment. Table 1.6 below provides an overview of the common behavioral tests employed in AD studies using rodent models.

Table 1.6 Common rodent behavioural tests for AD

Task		Cognitive test	Description	Ref
Contextual memory	Fear conditioning	Reference memory, hippocampal-dependent associative learning	Animal is exposed to aversive stimulus (mild shock) associated with a conditioned stimulus (tone). Freezing response associated with tone alone is measured	(Fanselow 1980).

	Passive-avoidance learning	Reference memory, associative learning	Animal learns to avoid mild aversive stimulus associated with entering desired compartment (darkness)	(van der Poel 1967)
Spatial memory	Morris water maze	Reference memory, working memory, hippocampal spatial memory	Animal must find stable platform in circular pool based on prior learned visual clues	(Morris et al., 1982)
	Radial arm (water) maze	Reference memory, working memory, spatial memory	Animal placed in maze with several arms radiating from central platform and must guide themselves towards food reward (in water, maze is submerged and	(Olton, and Samuelson 1976)

			escape platform used in place of food reward)	
	Barnes maze	Reference memory, working memory	Animal placed on circular platform with several holes around circumference and must find escape box accessed through one of the holes	(Barnes 1979)
Working memory	Y-maze/T-maze	Reference memory, working memory	Animal placed in 3-arm maze and alternations (explorations of each arm) are recorded	(Blodgett and McCutchan 1947).
	Object recognition	Learning and recognition memory	Animal given different objects to explore then positions of objects are	(Ennaceur and Delacour 1988).

			changed and some novel objects introduced to test recognition	

The most widely used mouse models for AD are the 3xTg and the 5xFAD models, which develop Aβ plaques at 6 months and 2 months, respectively (Chierrito et al., 2017). The 3xTg mice overexpress transgenic APP and tau and exhibit a progressive onset of symptoms, while the 5xFAD model overexpresses transgenic APP and develops a significantly more severe and rapid-onset disease with severe amyloid pathology (Russo-Savage et al., 2020). The 3xTg model is considered a more appropriate model for age-related sporadic AD (SAD), while the 5xFAD mice are mainly used to model familial AD (FAD). Several behavioral tests listed in Table 1.6 are used to study 3xTg mice treated with an anti-Aβ antibody, including the Morris water maze and the object recognition test. The Morris water maze showed progress in spatial memory in treated mice, and the object recognition test revealed improvement in recognition memory. However, no significant progress was observed in exploratory behavior or anxiety, which was attributed to reduced clearance of Aβ in the amygdala compared to other brain regions. Although the amygdala remained the most affected region with Aβ even after treatment, explaining the improvement in hippocampal-dependent tasks but not those related to the amygdala.

1.9.3. Ex vivo models of AD

Ex vivo models combine the benefits of both in vitro and in vivo systems by directly investigating intact affected tissues while controlling the extracellular environment (Brai et al., 2017). Generally, primary cell and tissue cultures and brain slices from genetically modified AD rodents

are used as ex vivo models (Kniewallner et al., 2018); (Blaikie et al., 2022). Primary cells provide better representations of in vivo conditions compared to cell lines and do not involve the high costs of animal experiments. However, primary cells often lack stability between donors and are dependent on sub-culturing conditions. For example, a co-culture of astrocytes and neurons derived from a triple-transgenic murine model of AD was used in a study to investigate cell physiology and the effects of drug treatments at a cellular level. The study found that palmitoylethanolamide (PEA) exerted protective effects against neurodegeneration by neutralizing reactive astrogliosis. Another study tested the neuroprotective effects of vanillin, using primary tissue culture of rat brain tissue treated with vanillin and subjected to Fe^{2+}-induced neurotoxicity. This model allowed the investigation of the therapeutic effects of vanillin in a system that represents in vivo conditions, revealing its ability to ameliorate oxidative imbalance, dysregulated metabolic pathways, elevate ATPase activity, and inhibit cholinergic enzymatic activities. Brain slices from mice can also be studied ex vivo to observe the effects of stress and/or drug treatments on each cell and tissue type (Kniewallner et al., 2018).

1.9.4. In silico AD model

In recent years, in silico methods have been used for modeling AD and drug development due to their lack of ethical considerations and relatively low costs. These methods are employed for designing and screening new drugs against protein targets and to help elucidate disease mechanisms (Hassan et al., 2018). In silico methods are typically used in conjunction with traditional in vitro experiments to validate the results. Drug design using in silico modeling can predict pharmacokinetics and target affinity, enabling the screening of large collections of potential ligands to identify leads with the greatest predicted target affinity (Tewari et al., 2018). Hence, large collections of potential ligands can be screened to identify leads with the greatest predicted

target affinity which can then be synthesised and tested. This reduces costs and time because only a selected number of ligands need to be synthesised following the virtual ligand screening. Possible improvements on the ligand structure to optimise affinity for the target can also be recommended using *in silico* modelling (Cruz-Vicente et al., 2021); (Blaikie et al., 2022). Ligand binding interactions can be enhanced by side chain either added or removed based on the size of the active site on the target In addition, based on the properties of residues within the active site, substituents can be altered on the ligand structure to form interactions with these areas (e.g. whether hydrophobic or hydrophilic substituents). A classical example of disease modelling (Anastasio 2011) demonstrated that cerebrovascular disease can contribute to amyloid dysregulation which can result to the progression of AD. By modelling the numerous elements which are related with the amyloid regulatory pathway, it was possible to identify alternative therapeutic targets, and hence recommend potential treatments. Further development of the model, predictions on the response to pharmacological interventions can be achieved, and also demonstrate the potential for oestrogen to significantly reduce amyloid levels. Recent model from (Madrasi et al., 2021); (Blaikie et al., 2022). Based on quantitative systems pharmacology (QSR) was developed to rationalise the lack of clinical efficacy of amyloid-modulating therapeutics. With the rising availability of artificial intelligence (AI) and machine learning, these techniques have been applied recently to AD research in several capacities, e.g determining individual risk of AD, drug development, and in efforts to decipher the cause of AD. AI is capable of processing large datasets and analysing it with a greater degree of accuracy, though, this relies significantly on the quality of the data input. A machine learning diagnostic platform to detect AD by analysing retinal images was reported (Wisely et al., 2020). AI was applied to identify potential candidates for repurposing as AD therapeutics by studying differentially expressed genes in association to disease

progression (Rodriguez et al., 2021), and recommending potential treatments which have an affinity for the identified targets. In spite of the clear benefits of AI including rapid processing and low error compared to human methods, these techniques remain tremendously costly to implement which currently limits their application and regular use.

The generation of brain organoids from iPSCs is another experimental model of AD that is expected to be increasingly employed in the future. Brain organoids allow the study of brain development, mechanisms of neurological and neurodegenerative disorders, and screening of therapeutic compounds (Lee et al., 2017); (Shou et al., 2020). By using patient-derived iPSCs, personalized therapeutic strategies can be developed, and novel insights into molecular and genetic disease mechanisms can be discovered. However, challenges exist with the use of brain organoids, including technical difficulties in culturing these models and lack of reproducibility. Efforts are being made to enhance their physiological relevance by incorporating immune and vascular systems (Chen et al., 2021). Currently, brain organoids cannot fully simulate the pathological features of the disease observed in humans, but ongoing research aims to improve their fidelity. Brain organoids have the potential to bridge the translational gap between animal models and clinical trials.

1.9.5. General advantages and disadvantages of current AD models

Experimental models are necessary for toxicity studies before human trials. Recently, two mammalian species are considered least essential for preclinical toxicity studies. Any toxic effects are typically established in initial in vitro and in vivo studies, and efforts are made to minimize these adverse effects before mammalian and human testing (Mesiti et al., 2019); (Blaikie et al., 2022). These studies provide important information about the estimated safe and tolerable dosage ranges, as well as the pharmacokinetic profile of the drug. In vitro models are useful for

establishing the mechanisms that generate the hallmarks of AD (Li et al., 2016). In vivo models provide insights into the complex pathogenesis of AD and replicate the progressive nature of the disease observed in patients. However, none of the current experimental models can fully mimic the complexity of the disease as seen in human patients. The poor translation of positive preclinical results to patient trial outcomes is attributed to the lack of accurate disease modeling (Li et al., 2016); (Blaikie et al., 2022). Therefore, ongoing research aims to develop experimental models that better represent AD development. Furthermore, the use of multiple AD models in preclinical studies, replicating diverse features of the disease, is becoming a common practice to obtain more reliable indications of potential effects in humans. Although an accurate representation of the human condition during AD is currently unattainable, the significance of experimental modeling cannot be underestimated in advancing our knowledge of AD progression and testing novel therapies.

1.10. In vitro hypoxia model

In vitro, oxygen pressures can be modified, and hypoxia can be induced using different procedures. The most common method is the use of hypoxia chambers, which are filled with a gas mixture containing a specific amount of oxygen (usually around 1-2% O2) (Croes et al., 2015); (Rinderknecht et al., 2021). Alternative methods have also been developed to induce hypoxia, including:

(i) Pericellular oxygen concentrations in conventional cell culture can be determined by the cellular oxygen consumption rate and the rate of oxygen diffusion, which is influenced by the height of the culture medium (Camp and Capitano, 2007). By increasing the height of the culture medium, the pO2 can be reduced.

(ii) Oxygen levels can be enzymatically reduced using glucose oxidase (GOX), which consumes oxygen within the culture medium. By adding catalase (CAT), the produced H2O2 can be converted to H2O, thereby consuming 1/2 O2 per cycle (Mueller et al., 2009).

(iii) Hypoxia mimetics such as cobalt chloride (CoCl2) or desferrioxamine can chemically stabilize HIF-1α without affecting oxygen pressure. Hypoxia mimetics are generally classified into iron chelators, iron competitors, and 2-oxoglutarate (2OG) analogs. CoCl2, by competing with iron ions, can inhibit the prolyl hydroxylases (PHDs) responsible for HIF-1α hydroxylation, thereby enabling its stabilization.

The different methods for inducing hypoxia in vitro are summarized in Figure 1.12.
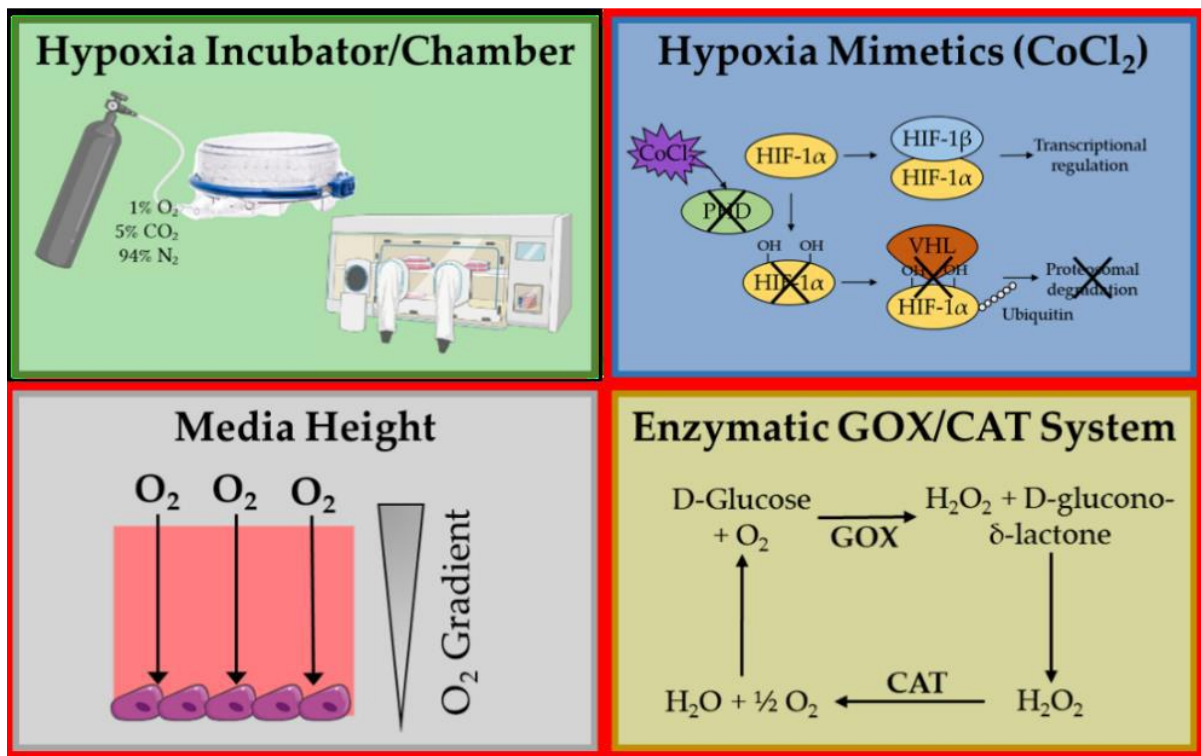
Figure 1.12 Methods for hypoxia induction in vitro. In comparison to the widely used hypoxia chambers, all tested methods are much cheaper and easier to use. The enzymatic system leads to a similar induction of the cellular hypoxia response whereas CoCl2 just resembles some hypoxia

features and the increase of medium height induces more a physiological oxygen concentration than a real hypoxia. When considering some basic limitations of the three used systems they provide a good alternative to the hypoxia chamber. For all three cell culture systems the enzymatic system showed the strongest hypoxic response and provided an easy set-up. (Mueller et al., 2007); (Rinderknecht et al., 2021).

Abbreviations CoCl2 - cobalt chloride, PHD - prolyl hydroxylase domain proteins, HIF-1 - hypoxia-inducible factor 1, VHL - Von Hippel–Lindau E3 Ligase, GOX - glucose oxidase, CAT - catalase.

1.10.1. Comparison of hypoxia induction using different systems in adherent cells, monocytic (suspension) cells, and in vitro 3D systems.

Most in vitro research utilizes hypoxia chambers as the standard procedure to induce hypoxia by reducing the oxygen concentration in the culture environment (from 18% to 1-5%), resulting in a decrease in pericellular oxygen tension. However, the use of hypoxia chambers or incubators has several disadvantages. One major constraint is that the environmental oxygen concentration may not accurately reflect the oxygen concentration at the cellular level (Pavlacky and Polak, 2020); (Rinderknecht et al., 2021). Alternative methods to induce or mimic hypoxia without reducing the environmental oxygen concentration have been developed, offering the advantage of not requiring special equipment. Increasing the height of the culture medium reduces the partial oxygen pressure at the cellular site, primarily driven by the cells' oxygen consumption. CoCl2 has long been recognized as a strong inducer of HIF-1α in cellular systems, mimicking the cellular response to hypoxia to a certain degree. The glucose oxidase/catalase system reduces oxygen in cultures through enzymatic consumption (Mueller et al., 2007); (Rinderknecht et al., 2021).

1.10.1.1. Advantages and disadvantages of hypoxia induction systems and a comparison with the hypoxia chamber

Table 1.7 summarizes the advantages and disadvantages of the three different hypoxia induction systems and compares them with the hypoxia chamber. Increased media heights do not appear to induce HIF-1α and do not show an effect on monocytic cells and in vitro 3D cultures. In contrast, CoCl2 and the enzymatic system induce stabilization of HIF-1α protein in cell culture systems. Chemical induction of hypoxia with CoCl2 results in HIF-1α stabilization in 2D cell cultures, and to a lesser extent in monocytic (suspension) cells, but it does not significantly induce cytokine expression. This indicates the need for "real hypoxia." It is suggested that a higher concentration of CoCl2 may be necessary in monocytic suspension cells (Guo et al., 2006), which is in line with the 3D culture system.

Research shows that the enzymatic system was most effective in inducing reactions to hypoxia in osteogenic cells (2D culture), monocytic cells (suspension culture), and in vitro 3D cultures. Hypoxia-associated induction of chemokines in 2D and monocytic cells was observed in in vitro experiments (Kim et al., 2016); (Sierra-Filardi et al., 2014). Functional reactions in in vitro 3D cultures (VEGFA, RUNX2) were similar to those obtained in an equine fracture hematoma model using a hypoxia chamber, as well as in patient and in vivo data (Hoff et al., 2017). Additionally, all cytokines were strongly induced by GOX/CAT and by increased media heights in 2D cultures, compared to only stabilizing HIF-1α with CoCl2. Chemical and enzymatic hypoxia inducers can also affect cell functions in addition to inducing hypoxia. Cobalt chloride has been shown to induce cellular apoptosis in a hypoxia-independent manner when supplemented in higher doses (Muñoz-Sánchez and Chánez-Cárdenas, 2018). Properly establishing ratios between catalase and glucose oxidase is necessary in the enzymatic system, as an imbalance between the two enzymes can result

in excessive generation of H2O2, leading to further stimulation of inflammatory conditions (Owegi et al., 2010); (Rinderknecht et al., 2021). The enzymatic system also requires regular medium changes due to reduced functionality of the enzymes over time. The induction of VEGFA in the control conditions in the in vitro hematomas 3D indicates that hypoxia is internally induced in the 3D structure, as found in other 3D structures (Qin et al., 2013). Uneven oxygen delivery is a common problem in nonvascularized 3D cultures, which also occurs when working with hypoxia chambers (Funamoto et al., 2012). Therefore, in 3D structures, chemical inducers or the enzymatic system are better options than increasing the medium height or reducing environmental oxygen.

Combining two hypoxia induction methods can lead to promising results. Research has shown the use of a hypoxic environment (1% O2) in combination with the alternative chemical prolyl hydroxylase inhibitor DFO (desferrioxamine) to stimulate the hypoxic response, as it was not strong enough with either the hypoxic environment or the chemical inducer alone (Pfeiffenberger et al., 2020). Additionally, elevated medium heights alone are not enough to induce strong hypoxia; they can be used to support other hypoxia induction methods. Combining increased medium height with reduced environmental oxygen increases the reduction in pericellular oxygen levels (Oze et al., 2012). Furthermore, a combination of medium height and CoCl2 effectively induces chemokine expression in osteogenic 2D cells, allowing for the induction of "real hypoxia" in combination with a strong HIF-1α response. Another factor to consider when choosing a method for hypoxia induction is the possibility of intermittent hypoxia (preconditioning/hypoxia with reoxygenation phases). Intermittent hypoxia has been shown to be more effective in inducing inflammation in monocytic cells, and preconditioning to moderate hypoxia improves tissue regeneration and tolerance to stronger hypoxic conditions (Rybnikova and Samoilov, 2015); (Rinderknecht et al., 2021). Theoretically, intermittent hypoxia induction is possible with all

methods. For hypoxia chambers and increased medium heights, intermittent hypoxia needs to be tightly controlled by oxygen measurements, as the change in pericellular oxygen concentrations is relatively slow. For all other induction methods, (partial) changes in the medium are needed, allowing for a fast onset of hypoxia, with the enzymatic system having the advantage of hypoxia onset in less than two minutes (Baumann et al., 2008).

Table 1.7 Overview of different in vitro hypoxia induction methods

	Medium Height	Cobalt Chloride	GOX/CAT 1	Hypoxia Chamber
Assay principle	Lowered local oxygen concentration due to reduced gas exchange	Blocking of HIF-1_ degradation	Consumption of (all) oxygen by enzymatic system	Lowered environ Mental oxygen concentration
Lowered oxygen concentration	yes	no	yes	yes
Approx. induction time (53)	Up to several hours	Immediate stabilization	~20 to 60 min (22)	~4 to 24 h
Ability to monitor pO2	Yes	No	Yes	Yes
2D Culture	Yes	Yes	Yes	Yes

Suspension Culture	No	Yes	Yes	Yes
3D Culture	Limited	Yes	Yes	Yes
Animal models	No	Yes	No data available	Yes
Advantages	Easy	Easy	"Real" hypoxia	most natural system
		easy		
Disadvantages	Slow induction of hypoxia (no Sharp drop in pO2) High amounts of medium needed Inter-plate differences Problems in 3D-cultures	only mimicking of hypoxia Chemical needs to be added can be toxic	enzymatic homeostasis can be disturbed side products of enzymatic reaction	much equipment needed Slow onset of hypoxia Limited space in incubator
Costs for 100 96-well plates 3	RPMI+5% FCS: _ 58£ Depending on medium costs (x1.7 of normal medium costs at 5.4 mm	_ 41£	_ 4.50£ (getting less with more plates because GOX is cheaper than CAT)	Depending on chamber system and gas Gas: _ 100£ Chamber: 1300£ –>25,000£
Literature	Camp and Capitano, 2007	Al Okail et al. 2010	Mueller et al. 2009	

In comparison to the widely used hypoxia chambers, all the tested methods are also cheaper and easier to use (Table 1.7). The enzymatic system leads to a similar induction of cellular hypoxia response, while CoCl2 resembles some hypoxic features, and an increase in medium height

induces more physiological oxygen concentration than true hypoxia. Considering the basic limitations of the systems, they are a good alternative to the hypoxia chamber.

1.10.2. Effects of pericellular pO2 control on hypoxia signaling in vitro

There is a need to modify experimental conditions of in vitro hypoxia to better mimic those in living patients. These modifications include the upregulation of HIF-1α, nuclear factor-kappa B (NF-kB), reactive oxygen species (ROS), and the decreased availability of nitric oxide, which are all influenced by oxygen concentration. HIF-1α expression, in particular, increases exponentially as oxygen tension decreases. Using gas-permeable plates that allow for close control of pericellular pO2 cycles for intermittent hypoxia has revealed significant variations in the effects of different pO2 levels on the expression of HIF and NF-kB. This confirms the conflicting results obtained in several studies that employed different models of hypoxia induction to explore their influence on HIF mechanisms (Polak et al., 2015); (Pavlacky and Polak, 2020).

1.10.2.1. Sustained Hypoxia

The influence of pericellular pO2 measurement is evident in tumor hypoxia. In vitro hypoxia has been used to investigate the effect of oxygenation dynamics on breast cancer radiosensitivity, and continuous measurement of pericellular pO2 has shown a diminished response to hypoxia (Edin et al., 2012). In vitro hypoxia models have also been employed to study the accumulation of hypoxia-inducible molecules in tumors, suggesting their potential use in drug testing. Microfluidic chips that create pO2 gradients and induce multiple oxygenation states have been developed for this purpose (Wang et al., 2013).

In vitro hypoxia can also be studied to reveal the molecular mechanisms underlying ischemia/reperfusion injury in neurons and cardiomyocytes. Perfused models of cardiomyocytes

subjected to abrupt anoxia and reperfusion have been used to study the opening of mitochondrial permeability transition pores, which play a role in cell death during ischemia-reperfusion injury (Panel et al., 2017). Additionally, a steady perfusion-based microfluidic system has been developed to continuously monitor the effects of hypoxia on the electrophysiological properties of cardiomyocytes.

1.10.2.2. Intermittent Hypoxia

Precise pO2 control is also important for modeling intermittent hypoxia (IH). In vitro models using gas-permeable dishes and mimicking the pathophysiology of obstructive sleep apnea (OSA) have shown agreement with animal models and patient observations, including changes in NF-kB modulation (Murphy et al., 2017). Similarly, culturing adipocytes in clinically relevant IH conditions with pericellular pO2 monitoring has revealed the accumulation of triglycerides, linking obesity and OSA. Consistent results have been obtained when other cell types were subjected to IH protocols with defined pO2 levels in vitro, matching the gene expression profiles found in OSA patients, and suggesting the role of inflammation in the disease's pathophysiology (Chuang et al., 2014).

Monitoring pericellular pO2 levels has revealed the central role of HIF-1α in the molecular response to IH in various cell types. This molecule has been found to be upregulated in skin vasculature of OSA patients, as well as in the aortas of mice and human cultures of coronary artery endothelial cells where IH was maintained by gas bubbling in the medium (Kaczmarek et al., 2013). In addition, a protective mechanism of pancreatic cells exposed to IH and hyperglycemia, based on ROS reduction, has been discovered in both in vivo and in vitro studies (Li et al., 2018). Various hypoxic modalities have been studied using gas-permeable culture dishes to create an amyocardial ischemia model.

Disadvantages of Conventional Systems

Differences in the results regarding the role of hypoxia in cell cultures can be attributed to various variables, such as using different cell types. Incorporating the native pO2 of the tissue type and its temporal development in the disease being studied into the in vitro model could reduce result variability. However, many recent publications on in vitro hypoxia still use simplified models that do not consider the difference between headspace and pericellular O2 tensions. These studies cover various areas of hypoxic research but lack pericellular O2 measurements, making it difficult to determine if there is a higher concentration of oxygen in the control group and by what margin. This complicates result interpretation, especially for cell cultures that are sensitive to ischemic hypoxic injury, such as cardiomyocytes, neurons, kidney cells, and endothelial cells with high oxygen consumption rates. Furthermore, some studies fail to provide information about the height of the medium overlay above the adherent cell culture, introducing another unknown variable that could affect the results and reproducibility. Additionally, some studies only employ chemical insults to mimic hypoxia. Consequently, some studies argue against the merit of cell cultures in hypoxia research, while others suggest that the results obtained from these models are in line with in vivo studies. This emphasizes the significance of maintaining strict conditions for in vitro hypoxia, characterizing the experimental setup in detail, including pericellular pO2 values, and ensuring adequate pO2 equilibration time in the case of intermittent hypoxia (Pavlacky and Polak, 2020).

1.11. 3D CELL CULTURES

Introducing the element of three-dimensionality to cell cultures, which is an intrinsic characteristic of all multicellular organisms, can improve the potential of in vitro models to recapitulate the in vivo environment (Duval et al., 2017). This also applies to conditions in which hypoxia plays a

vital role, including cancer, as the 3D structure has been found to play an integral part in tumor biology (Tanner et al., 2012). While some models only employ single cell type spheroids, more complex platforms that replicate physiological interactions found in vivo include multiple cell types in a 3D structure, such as cancer stromal or endothelial cells (Magdeldin et al., 2017). Similarly, 3D cell culture has been used to study the effect of hypoxia from an ischemic perspective in various cell types, including cardiomyocytes (Sepuri et al., 2017), astrocytes (Chaitanya et al., 2014), endothelial cells (Gammella et al., 2013), and hypoxia related to pulmonary fibrosis in fetal lung fibroblasts (Sucre et al., 2017). Additionally, the effects of both continuous hypoxia and IH on vascular sprouting have been discovered in endothelial cells (Alhawarat et al., 2019). Hypoxic 3D tissue structures encompassing retinal astrocytes and endothelial cells provide a useful drug-screening device, outperforming standard 2D co-cultures (Beharr et al., 2017).

With the propagation of experiments conducted in 3D cell cultures, consideration of pericellular pO2 is necessary, particularly because the element of three-dimensionality and variable thickness of cellular structures bring additional irregularities that impede gas diffusion, resulting in the formation of oxygen concentration gradients (McMurtrey, 2016). Several novel approaches have been developed to tackle the challenges of pO2 in 3D tissue structures. Oxygen-sensing microelectrodes have been employed to measure pericellular oxygen gradients in thicker hydrogel-based tissues (Lewis et al., 2017). However, this approach has disadvantages such as its invasive nature, time demands, and technical challenges requiring repetitive calibrations and measurements in various spots inside the tissue, leading to a motivated search for alternative approaches.

A number of fluorescence quenching probes have been tested, which infiltrate through cells (Dmitriev et al., 2015) or are incorporated into microbeads dispersed in a 3D hydrogel (Figure 1.13A) (Lesher-Pérez et al., 2017), and then visualized using confocal microscope imaging. This

enables the formation of a dense network of pO2 reporter points throughout the 3D cell culture block. Semi-quantitative approaches to the assessment of pericellular pO2 in 3D cultures include mathematical models (McMurtrey, 2016) and probes (e.g., Hypoxyprobe) (Gomes et al., 2016), or the incorporation of paramagnetic particles into cellular spheroids with subsequent electron paramagnetic resonance-based detection (Langan et al., 2016).

A unique characteristic of 3D cell culture systems is the probability of actively inducing a controlled oxygen gradient across the model based on experimental needs. These gradients can be induced by perfusion with an oxygen scavenger in the medium (Lam et al., 2018), by positioning the culture between two micro-channel circuits perfused with gas, each with a different oxygen level (Figure 1.13B) (Oppegard and Eddington, 2013), or by incorporating an oxygen-consuming reaction of specific hydrogel materials, either encapsulating (Figure 1.13C) (Lewis et al., 2017) or being in close proximity to the cells (Figure 1.13D) (Li et al., 2016), thus regulating the pericellular oxygen levels.
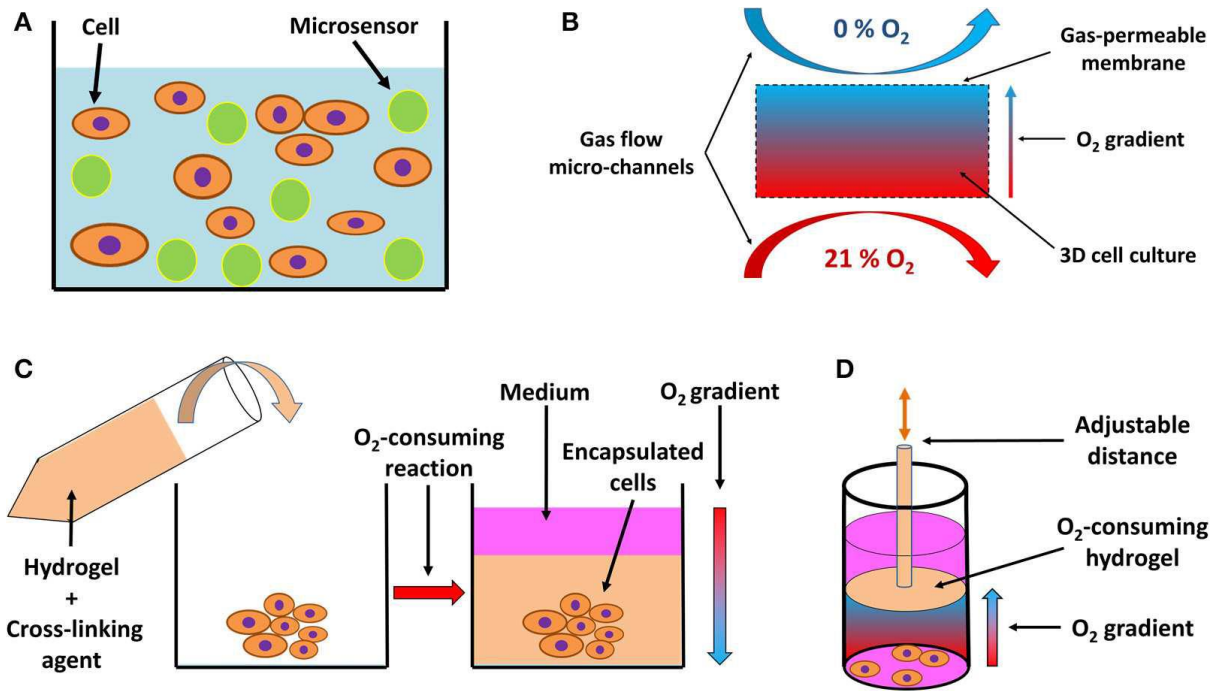
Figure 1.13 Schematic drawing of systems for 3D in vitro hypoxia

(1.13A) Fluorescent sensor-laden microbeads incorporated into a 3D hydrogel with cells, serving as a pO2 reporter throughout the 3D system (Lesher-Pérez et al., 2017).

(1.13B) 3D culture positioned between two gas perfusion microchannels, which are in contact with the culture via a gas-permeable membrane, allowing for an oxygen gradient to be formed across the culture between an oxygen-rich and oxygen-poor environment (Oppegard and Eddington, 2013).

(1.13C) Encapsulation of a 3D cell culture or explanted tissue by an oxygen-consuming hydrogel, creating a hypoxic environment. The oxygen consumption is a result of the cross-linking reaction and hydrogel formation, resulting in an oxygen gradient from the top layer of the culture to deeper, more oxygen-deprived regions (Lewis et al., 2017).

(1.13D) Preformed oxygen-consuming hydrogel immersed in a 3D culture creates a hypoxic environment with an oxygen gradient toward the hydrogel. The gradient and the level of hypoxia can be adjusted by moving the hydrogel across the culture on a mobile pillar (Li et al., 2016).

1.12. RUTIN

1.12.1. Overview of Rutin

Flavonoids, a group of natural antioxidants, are found in fruits, vegetables, roots, grains, bark, flowers, stems, wine, and tea (Panche et al., 2016). The most common native flavonoid is rutin, which is found in a wide variety of plants (>70 plant species) and plant-based products (Chua, 2013; Ola et al., 2015). Rutin is also called rutoside, quercetin-3-O-rutinoside, vitamin P, and sophorin. These names originate from the Latin name for the rue plants (Ruta graveolens), from which it was first isolated in the 19th century. Rue plants have the highest rutin content (86.6 mg/g dw), followed by buckwheat flowers (53.5 mg/g dw) (Sofic, 2010). Buckwheat has been cultivated as a source of rutin for herbal drug preparation in the United States since the mid-20th century, and nowadays buckwheat plants (Fagopyrum spp.) are considered a major dietary source of rutin (Chua, 2013).

Chemically, rutin, 2-(3,4-dihydroxyphenyl)-5,7-dihydroxy-3-[α-L-rhamnopyranosyl-(1→6)-β-D-glucopyranosyloxy]-4H-chromen-4-one, is a glycoside composed of the flavonolic aglycone quercetin along with the disaccharide rutinose (Figure 1.12). It appears as an odorless yellow crystalline powder that is practically insoluble in water and partially soluble in alcohol (Cao,

2010). Living organisms are unable to synthesize rutin, so it can only be ingested through plant products.
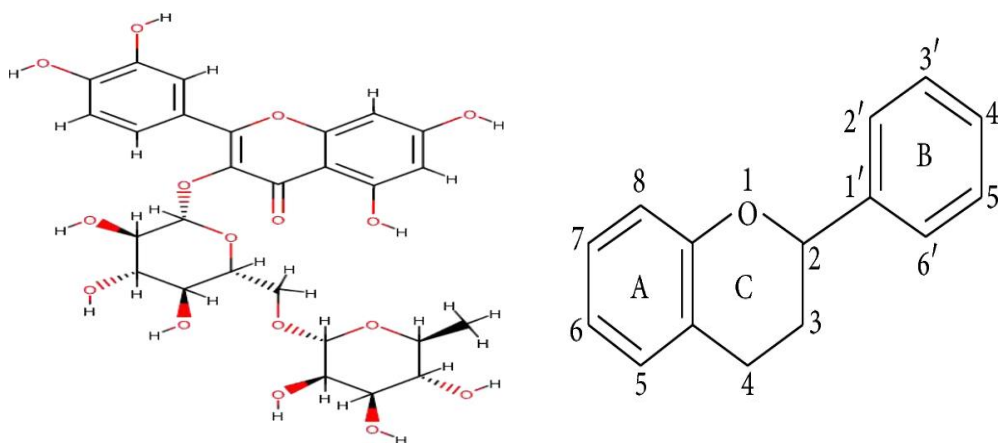
Figure 1.14 Chemical structure of rutin. Rutin (rutoside, quercetin-3-O-rutinoside) is 2-(3,4-dihydroxyphenyl)-5,7-dihydroxy-3-[α-L-rhamnopyranosyl-(1→6)-β-D-glucopyranosyloxy]-4H-chromen-4-one and is classified as a polyphenolic flavonoid (Cao, 2010).

Rutin has several pharmacological and biological effects, such as anti-inflammatory, antioxidant, antihypertensive, antiapoptotic, antiautophagic, and neuroprotective activities (Caglayan, 2019). It has various protective effects in vitro as well as in vivo against oxidative stress and lipid peroxidation (Alhoshani, 2017). Rutin attenuates oxidative stress, decreases in vitro production of nitric oxide (NO) and proinflammatory cytokines, inhibits Aβ aggregation and cytotoxicity (Wang, 2012). Additionally, this bioflavonoid could protect kidneys against ischemia-reperfusion-induced injury (Korkmaz and Kolankaya, 2013), ameliorate oxidative stress and preserve hepatic and renal function after exposure to cadmium and ethanol (Abarikwu, 2017), alleviate cisplatin-induced nephrotoxicity in rats (Alhoshani, 2017), and attenuate gentamicin-induced renal damage by decreasing oxidative stress, inflammation, autophagy, and apoptosis in rodents (Kandemir, 2015). Rutin has also been proposed for the treatment of AD (Habtemariam S, 2016; Khan, 2020).

1.12.2. The Bioavailability and Blood-Brain Barrier (BBB) Penetration of Rutin

1.12.2.1 The Bioavailability of Rutin

The bioavailability of rutin has been extensively studied, particularly its aglycon quercetin (Manach et al., 2005; de Oliveira et al., 2016). Numerous research studies have investigated the bioavailability and bio-efficacy of polyphenols in humans, including 14 studies specifically on quercetin and its glycosides. These studies have revealed that quercetin glucosides are more efficiently absorbed than quercetin, while rutin (rhamnoglucoside) is absorbed at a slower rate. The increased plasma levels of quercetin observed after administering glycoside forms of quercetin, as opposed to its aglycone form, and the dependence of quercetin disposition on the sugar moiety (Graefe et al., 2001) have been attributed to the metabolism of rutin in the large intestine. Recent studies have proposed mechanisms involving the mucus layer in the bioavailability of flavonoid glycosides (Gonzales et al., 2016). Soluble flavonoid glycosides can penetrate the mucus layer to reach the epithelium. Upon contact with the brush border, β-glucosidases cleave off the glucose moiety, releasing the aglycone, which can then passively diffuse through the cells. Rutin, which contains rhamnose, remains intact in the small intestines and is transported to the large intestines, where it is either fermented by intestinal bacteria or acted upon by secreted bacterial rhamnosidase to release the aglycone. Additionally, rutin aglycone quercetin reaches the epithelia, where phase I and phase II metabolism occur (Gonzales et al., 2016). The combination of rutin's resistance to first-pass metabolism and its secretion into the lumen may enhance therapeutic efficacy in the ileum and colon (Mascaraque et al., 2015; de Oliveira et al., 2016). However, experimental proof is still required for the theory of absorption in the large intestine, as some studies have shown that rutin is resistant to hydrolysis by gut microbiota and Bifidobacterium. Conversely, several investigations have demonstrated that both

rutin and quercetin are absorbed in the small intestine, possibly via the SGLT-1 transporter. However, quercetin undergoes rapid metabolism, leading to reduced bioavailability, while rutin is relatively spared from glucuronidation and primarily absorbed in its non-metabolized form (Mascaraque et al., 2015; de Oliveira et al., 2016). The involvement of active transporters in the transport of flavonoid glycosides remains unclear, and further research is necessary to understand this mechanism. Overall, the poor water solubility of rutin results in a low concentration gradient between the gut and blood vessel, leading to inadequate transport of rutin.

To increase the solubility and oral bioavailability of rutin, various delivery formulations have been developed (Mauludin et al., 2009). However, additional studies are needed to achieve efficient and safe use of rutin in oral pharmaceutical preparations. Lipinski's rule of five is a commonly used method to evaluate the "drug-likeness" of a compound. It states that compounds are more likely to have poor absorption or permeability if they have more than five hydrogen-bond donors, a molecular mass exceeding 500, a calculated log P greater than 5, or a sum of nitrogen and oxygen atoms in the molecule greater than 10. Rutin has more than five hydrogen bond donors and more than 10 hydrogen bond acceptors and does not comply with Lipinski's rule of five (Zhang and Wilkinson, 2007). However, according to Zhang and Wilkinson, the "rule of five" has been somewhat exaggerated, as only 51% of all FDA-approved small-molecule drugs are administered orally and comply with this rule. Data suggests that the bioavailability of rutin varies significantly depending on food matrices (Masoodi and Alhamdan, 2010; Tenore et al., 2013; de Oliveira et al., 2016), including other micronutrients and macronutrients present in consumed foods, which can affect the metabolism of quercetin and its glycoside forms. Furthermore, the pharmacokinetics of rutin/quercetin differ significantly in different animal models (Gohlke et al., 2013).

1.12.2.2 The Blood-Brain Barrier (BBB) Penetration of Flavonoid (Rutin)

Exchange between blood and interstitial fluid does not occur in the capillaries of the brain, which have developed to limit the movement of molecules and cells between the blood and the brain. This significant feature provides a natural defense for the brain against toxic substances circulating in the blood. Cell adhesion molecules play a role in forming tight junctions between endothelial cells, providing an important protective function in limiting the movement of substances into the brain (Palmer 2010). Additionally, the BBB plays a vital role in supplying essential nutrients, drugs, hormones to the brain, and eliminating toxic metabolites from the brain. The BBB consists of three cell types: endothelial cells, astrocytes, and pericytes. Endothelial cells in the BBB form a discrete boundary between two different physiological environments, and the movement of chemicals through this barrier indicates passage through a biological membrane (McNamara and Leggas 2009; Faria et al., 2012).

There are three main routes by which a compound can cross biological membranes. First, it can pass through a purely passive process if it is small, lipid-soluble, nonionized, and there is a concentration gradient between the two sides of the membrane (principle of Fick's law) (Lehman-McKeeman, 2008. This passive process does not require energy expenditure. Second, carrier-mediated transport involves one or more transporters and can be saturable and specific. This type of transport can be uniport (transport of a single molecule), symport (transport of two or more different molecules or ions in the same direction), or antiport (transport of two or more different molecules or ions in opposite directions). Third, specialized transport includes endocytosis, which can occur with or without interaction with membrane receptors and is more likely for larger molecules and proteins (Taft 2009). Various transporters of different classes have been described in relation to the BBB (Uchida et al., 2011; Faria et al., 2012). Since BBB cells have tight junctions

99

and no fenestrations, transport systems are vital not only for the movement of nutrients, vitamins, drugs, and xenobiotics but also for actively limiting the passage of potential harmful substances into the brain.

The mechanisms by which flavonoids are transported across the BBB and whether other dietary components can affect their access to the central nervous system (CNS) are still not clear. Some experimental evidence suggests that α-tocopherol promotes the transport of quercetin and rutin across the BBB, potentially by modulating P-glycoprotein action and/or impairing the phosphorylation/dephosphorylation mechanism that controls the influx of metabolites (Maciej et al., 2015; Faria et al., 2012). Chronic administration of flavonoid rutin has been shown not to induce pro-oxidant or cytotoxic side effects on the hippocampus, indicating that dietary factors like α-tocopherol can modulate the uptake of flavonoids into the CNS and enhance their neuroprotective potential (Faria et al., 2012).

Various *in vitro* cellular models of BBB have been used to study flavonoid transfer across the BBB. For example, ECV304 (representing the peripheral side of the BBB) co-cultured with C6 glioma cells (representing the CNS side), bEND5 and RBE4 have been the most common cellular models of BBB (Youdim et al., 2003). Using this approach, various flavonoids of diverse sub-classes (flavanones rutin) were observed to access and transverse the endothelial cells layer. Additionally, the main flavonoid metabolites in the circulation, glucuronides and O-methylated derivatives are also integrated into these cells. In addition to accumulating these flavonoid metabolites, it appeared that these cells were capable of deconjugating glucuronide derivatives liberating aglycone forms which can then be capable of entering glial cells and thus the brain (Ishisaka et al., 2011). Using RBE4 cells, flavan-3-ols, flavonols and anthocyanins have been shown to be able to transverse cells in a time-dependent manner, with quercetin showing the least

100

transport efficiency (Faria et al., 2010). In another study, the isomers (+)-catechin and (−)-epicatechin were found to cross the BBB layer, with, a significant difference between the transport of these two isomers reported (Youdim et al., 2003). This suggest the involvement of a stereo-selective process for flavanol passage across BBB which can due to differences in their efflux out of cells. In addition, the hCMEC/D3 cell line, an immortalized human cerebral micro-vessel endothelial cell line, have also been utilized as a BBB model. Using this model, the transport of flavan-3-ols along with their metabolism to glucuronides were detected, similar to earlier observations with RBE4 cells (Faria et al., 2011). Additionally, synthesized O-methylated flavan-3-ols (Gonzalez-Manzano et al., 2009) were found to traverse these cells more efficiently compared to the parent compounds in the same model (Faria et al., 2011). In addition to cellular models, *in situ* models of the BBB have also been utalised to evaluate flavonoid access to the brain. Thus, the permeability of radiolabelled quercetin rutin and naringenin was tested in an *in situ* rat model of perfusion, and both quercetin, rutin and naringenin were found to be localized in all 7 regions of the brain to different degrees following perfusion of the carotid artery (Youdim et al., 2004). Quercetin and rutin showed a lower permeability than naringenin, which was assumed to be correlated with its lower lipophilicity or because naringenin did not seem to be a substrate for P-gp unlike quercetin.

1.12.3. Other Flavonoid and rational of using Rutin for this study

Table 1.8: Classification, structure, and food sources of some dietary flavonoids.

Class	Flavonoid	Dietary source	References
Flavanol			

	(+)-Catechin	Tea	(Lopez, et al., 2001)
	(−)-Epicatechin		
	Epigallocatechin		
	Chrysin, apigenin		
	red pepper, and tomato skin		
Flavone ,	Rutin, luteolin, and luteolin glucosides	Fruit skins, red wine buckwheat, red pepper and tomato skin	(Stewart et al.,2000)
Flavonol	Kaempferol, quercetin, myricetin, and tamarixetin	Onion, red wine, olive oil, berries, and grapefruit.	(Stewart et al.,2000)
Flavanone	Naringin, naringenin, taxifolin, and hesperidin	Citrus fruits, grapefruits, lemons, and oranges	(Miyake et al., 2000)
Isoflavone	Genistin, daidzin	Soyabean	(Reinli and Block 1996)
Anthocyanidin	Apigenidin, cyaniding	Cherry, easberry, and strawberry	(Hertog et al.,1992)

Flavonoids possess many pharmacological functions, which include:

1. Antioxidant Activity:

The antioxidant mechanism of action of flavonoids can involve several processes, such as suppressing the formation of reactive oxygen species (ROS) by inhibiting enzymes or chelating trace elements involved in free radical generation, scavenging ROS, and upregulating or protecting

antioxidant defenses (Mishra et al., 2013). Some flavonoids can combine radical scavenging activity with the ability to interact with enzyme functions, inhibiting enzymes involved in ROS generation, such as microsomal monooxygenase and glutathione peroxidase. Flavonoids also protect lipids against oxidative damage through various mechanisms. They can chelate metal ions (such as iron and copper), which inhibits free radical generation (Mishra et al., 2013). For example, quercetin is known for its iron-chelating and iron-stabilizing properties, while epicatechin and rutin are strong radical scavengers and inhibitors of lipid peroxidation in vitro.

2. Hepatoprotective Activity:

Several flavonoids, including catechin, apigenin, quercetin, naringenin, rutin, and venoruton, have been found to exhibit hepatoprotective activities (Zhu et al., 2012). In conditions such as diabetes, which can lead to hepatic manifestations, the expression of glutamate-cysteine ligase catalytic subunit (Gclc), glutathione levels, and ROS levels are reported to be decreased in the liver of diabetic mice. Anthocyanins, a type of flavonoid, have been shown to have a preventive effect against various diseases. Cyanidin-3-O-β-glucoside (C3G), an anthocyanin, increases hepatic Gclc expression by elevating cAMP levels to activate protein kinase A (PKA). This activation, in turn, upregulates cAMP response element-binding protein (CREB) phosphorylation, promoting CREB-DNA binding and increasing Gclc transcription. Increased Gclc expression results in decreased hepatic ROS levels and proapoptotic signaling (Zhu et al., 2012).

3. Antibacterial Activity:

Flavonoids have been demonstrated to have antimicrobial effects against a wide range of microorganisms in vitro. Plant extracts rich in flavonoids from diverse species have been shown to exhibit antibacterial activity (Pandey et al., 2010). Several flavonoids, including apigenin,

galangin, flavone and flavonol glycosides, isoflavones, flavanones, and chalcones, have potent antibacterial activity. Naringenin and sophoraflavanone G, for example, exhibit intensive antibacterial activity against methicillin-resistant Staphylococcus aureus (MRSA) and streptococci. The antibacterial effects of flavonoids may be due to the alteration of membrane fluidity in hydrophilic and hydrophobic regions, suggesting that these compounds can reduce the fluidity of outer and inner layers of bacterial membranes (Tsuchiya and Iinuma, 2000).

4. Anti-Inflammatory Activity:

Certain flavonoids have been found to significantly affect the function of the immune system and inflammatory cells, exhibiting anti-inflammatory and analgesic effects. Flavonoids such as hesperidin, apigenin, luteolin, and quercetin possess anti-inflammatory properties. Flavonoids can specifically influence the function of enzyme systems involved in the generation of inflammatory processes, particularly tyrosine and serine-threonine protein kinases (Hunter, 1995). Numerous flavonoids have been shown to inhibit platelet adhesion, aggregation, and secretion at concentrations of 1-10 mM. The effect of flavonoids on platelets has been associated with the inhibition of arachidonic acid metabolism (Hunter, 1995).

5. Anticancer Activity:

Dietary factors, including flavonoids, play a vital role in the prevention of cancers. Flavonoids found in fruits and vegetables have been identified as cancer chemopreventive agents (Mishra et al., 2013). The consumption of onions and/or apples, major sources of the flavonol quercetin, has been inversely associated with the incidence of prostate, lung, stomach, and breast cancer. Additionally, moderate wine consumption has been linked to a lower risk of developing lung, endometrial, esophageal, stomach, and colon cancer (Koen et al., 2005). Flavonoids exert their

anticancer effects through various mechanisms, including the downregulation of mutant p53 protein, cell cycle arrest, and tyrosine kinase inhibition, inhibition of heat shock proteins, estrogen receptor binding capacity, and inhibition of Ras protein expression.

Rationale for Choosing Rutin in This Study:

Rutin is a flavonoid glycoside found in citrus plants. It is known for its neuroprotective effects, likely due to its antioxidant and anti-inflammatory properties. Rutin protects cell membranes by increasing their rigidity through interactions with phospholipids, thereby preventing oxidative damage (Mostafa, 2017).

Studies have shown that rutin decreases β-amyloid plaque aggregation, nitric oxide production, pro-inflammatory cytokines, cytotoxicity, and oxidative stress in vitro. In addition, it has been reported to have neuroprotective effects on Alzheimer's disease transgenic mice in vivo. These effects include attenuating memory deficits, increasing antioxidant parameters such as reduced glutathione and superoxide dismutase, decreasing lipid peroxidation levels (indicated by malondialdehyde), and reducing brain interleukin-1β and interleukin-6 levels (Xu et al., 2014).

Rutin inhibits amyloid beta (Aβ) aggregates and processing in Alzheimer's disease (Habtemariam, 2016; Mostaf et al., 2019). It has been reported that the use of plant-derived bioactive components like rutin can ameliorate various neurodegenerative diseases. The mechanism of action is attributed to the amelioration of antioxidant enzymes, the reduction of pro-inflammatory cytokines, anti-apoptotic effects, restoration of mitochondrial complex enzyme activity, and activation of the MAPK cascade, thus promoting neuronal survival (Enogieru et al., 2018).

Furthermore, rutin plays a vital role in decreasing $A\beta_{25-35}$ fibril formation and accumulation in vitro, thereby reducing neurotoxicity (Jiménez-Aliaga et al., 2011; Mostaf et al., 2019). It has also

been shown to inhibit Aβ aggregation and cytotoxicity and prevent mitochondrial damage. Rutin decreases the production of pro-inflammatory cytokines such as TNF-α and interleukin-1 in vitro, while increasing the levels of catalase, superoxide dismutase enzymes, and reduced glutathione (Wang et al., 2012).

Administration of Congo red/rutin magnetic nanoparticles intravenously in transgenic mice has resulted in the amelioration of neurologic changes and a decrease in memory deficits in the brain (Hu et al., 2015). Additionally, rutin has been found to reduce oligomeric Aβ, IL-1, and IL-6 levels in the brains of transgenic mice (Xu et al., 2014). In a dose-dependent manner, rutin improves recognition against scopolamine-induced memory deficits in an Alzheimer's model without affecting locomotor activity (Ramalingayya et al., 2016). Rutin has also been shown to improve cognition and attenuate inflammation in an Alzheimer's model, reducing the expression of IL-8, COX-2 enzyme, NF-κB, and inducible iNOS, as well as ameliorating hippocampal histological abnormalities (Javed et al., 2012). Furthermore, rutin inhibits scopolamine-induced amnesia without affecting zebrafish locomotor activity in a zebrafish model of Alzheimer's (Richetti et al., 2011).

The mechanisms of action of rutin involve inhibiting aggregation and cytotoxicity of Aβ, reducing oxidative stress induced by Aβ, and lowering Aβ42 levels. Polyphenol compounds, including rutin, exhibit inhibitory effects on Aβ42 aggregation by binding hydrophobic β-sheet channels with their aromatic structure and disrupting Aβ hydrogen bonding through the action of hydroxyl groups as electron donors. Rutin, with its aromatic core and polyhydroxyl groups, likely functions through these mechanisms (Porat, 2006; Porzoor, 2015; Velandera, 2017; Phan, 2019; Pu, 2007). Rutin also reduces Aβ42-induced cytotoxicity by interacting with Aβ to modify the structure of Aβ oligomers and inhibit their cytotoxicity. It has been shown to decrease $Aβ_{25-35}$ fibril formation and

106

accumulation in vitro, thereby reducing neurotoxicity (Jiménez-Aliaga et al., 2011; Xu et al., 2014).

Considering the extensive evidence on the beneficial effects of rutin, such as its ability to inhibit Aβ aggregation, reduce inflammation and oxidative stress, and improve cognitive function, rutin appears to be a promising candidate for this study.

Neuroinflammation is a complex response to brain injury involving the activation of glia, release of inflammatory mediators such as cytokines and chemokines, and generation of reactive oxygen species (ROS) (DiSabato et al., 2016). Inflammatory responses in the brain are associated with increased levels of prostaglandins (PGs), particularly PGE2. Elevated PGE2 and inflammatory mediators are also characteristic of the aging brain. An increased state of neuroinflammation renders the aged brain more susceptible to the disruptive effects of both intrinsic and extrinsic factors such as infection, diseases, toxicants, or stress (DiSabato et al., 2016).

In Alzheimer's disease (AD), microglia secrete proinflammatory cytokines, PGs, ROS, and NOS, which result in chronic stress and, over a prolonged period, neuronal death (Calsolaro and Edison, 2016; Rawlinson et al., 2020). Rutin administration has been observed to reduce "neuroinflammation" in a rat model of AD (Javed et al., 2012) and exhibit neuroprotective effects in dexamethasone-treated mice (Tongjaroenbuangam et al., 2011). Studies have shown that rutin decreases the generation of TNF-α and IL-1β in microglia (Wang et al., 2012). Additionally, research has reported the inhibition of Aβ aggregation and cytotoxicity by rutin, prevention of mitochondrial damage, reduction of pro-inflammatory cytokine production (TNF-α and IL-1), and increased levels of catalase (CAT) and superoxide dismutase (SOD) enzymes (Wang et al., 2012).

Sodium rutin has been found to attenuate neuroinflammation, enhance microglia-mediated Aβ clearance, ameliorate synaptic plasticity impairment, and reverse spatial learning and memory deficits in two mouse models of AD (Pan et al., 2019). Rutin exerts its neuroprotective potential by interacting with critical protein and lipid kinase signaling cascades in the brain, such as PI3K/Akt, protein kinase C, and MAPK, resulting in the inhibition of apoptosis triggered by Aβ and promoting neuronal survival and synaptic plasticity. It also has beneficial effects on the vascular system, leading to changes in cerebrovascular blood flow through angiogenesis and neurogenesis (Xu et al., 2014).

Research has shown that oral administration of rutin may protect the CA3 region of the hippocampus in rats and impact their behavior, decreasing memory impairment due to trimethyltin toxicity (Koda et al., 2008, 2009). Rutin has exhibited an antidepressant-like effect, partially through its neuroprotective effect on the hippocampus by acting on NMDA receptors (Anjomshoa et al., 2020). Rutin pre-treatment has been found to reduce infarct size and neurological deficits in rats after middle cerebral artery occlusion and protect the antioxidant content of enzymes in the brain (Khan et al., 2009; AbdEl-fatah et al., 2010). It has also protected against the neurodegenerative effects of prion accumulation by increasing the production of neurotrophic factors and inhibiting apoptotic pathway activation (Aldhabi et al., 2015). Rutin has shown potential anticonvulsant and antioxidant activities against oxidative stress in kainic acid-induced seizure in mice (Nassiri-Asl et al., 2013).

Furthermore, rutin has been found to attenuate age-related memory deficits in mice (Kishore, 200 5), improve learning and memory in normal, aged, and experimentally-induced amnesic mice, possibly through its potent antioxidant action (Kishore and Singh, 2005). Rutin has protected against spatial memory impairment induced by trimethyltin and synaptophysin in the hippocampus

108

(Zhang et al., 2014), as well as in AD transgenic mice (Xu et al., 2014). It significantly attenuated memory deficits in AD transgenic mice, decreased oligomer Aβ levels, increased SOD activity and GSH/GSSG ratio, reduced GSSG and MDA levels, downregulated microgliosis and astrocytosis, and decreased IL-Iβ and IL-6 levels in the brain (Xu et al., 2014). Rutin has also improved memory and behavior in open field tests, elevated plus and Y-mazes tests, possibly due to its reduction in neuro-apoptosis (Man et al., 2015). It prevented cognitive deficits and morphological changes in the hippocampus, attenuated lipid peroxidation, COX-2, GFAP, IL-8, iNOS, and NFκB in a rat model of sporadic dementia (Javed et al., 2012). Additionally, it prevented memory deficits and ameliorated oxidative stress, apoptosis, and neurite growth in a rat model for cognitive dysfunction (Ramalingayya et al., 2017). Rutin has been found to inhibit apoptosis by decreasing oxidative stress, Bax/Bcl-2, caspase-3 and -9, and c-Jun and p38 phosphorylation in a dopaminergic cell model (Park et al., 2015).

Rational of using Rutin for this study:

Rutin has been selected for this study due to its high ability to cross the blood-brain barrier (BBB). Many drugs used for the treatment of neurodegenerative diseases struggle to cross the BBB (HABTEMARIAM, 2016). Research has revealed that rutin can modify both the cognitive and behavioral symptoms associated with neurodegenerative diseases by crossing the BBB and acting as an antioxidant in neuronal cells and an anti-inflammatory drug. Despite its poor water solubility and low bioavailability, rutin has demonstrated the ability to cross the BBB. Studies have shown that the peak plasma concentration (Cmax) of rutin was 262.85 ± 6.15 ng/ml after oral administration of a dose of 35 mg rutin to rabbits (Ramaswamy et al., 2017), and its concentration in serum was approximately 300 ng/ml after 2 hours of oral administration with 100 mg/kg rutin to mice (Pan et al., 2019). After intravenous administration of a dose of 10 mg/kg to rats, the Cmax

of rutin in plasma and brain homogenate was 1511.24 ± 46.92 ng/ml and 111.57 ± 12.01 ng/ml, respectively (Ahmad et al., 2016; Xiao-ying et al., 2021).

Various strategies have been developed to improve the solubility and bioavailability of rutin to prolong its clinical application. The sodium salt of rutin, for example, has been found to be highly water-soluble with increased bioavailability and the ability to cross the BBB (Pan et al., 2019; Xiao-ying et al., 2021). Rutin has been shown to cross the BBB and reach cerebrospinal fluid (CSF) concentrations high enough to neutralize pathological tau. Therefore, rutin is believed to exert direct effects on tau pathology in the brain.

Moreover, flavonoids, including rutin, can undergo rapid metabolism, which can be overcome by methoxylation to improve their intestinal absorption, bioavailability, and stability (Mostafa et al., 2018). Loading rutin extracted from Calendula officinalis L. flowers onto a novel nanoparticle-lipid polymer hybrid has demonstrated efficacy in targeting rutin delivery to the brain. These nanoparticles are biocompatible and bioavailable, as confirmed by a hemolysis test, thereby opening up possibilities for the formulation of novel neuro-pharmaceuticals for brain targeting using natural products (Ishak et al., 2017).

In addition to its ability to cross the BBB, rutin has been found to possess antioxidant and anti-inflammatory properties, which are important in AD pathogenesis. Oxidative stress and neuroinflammation are key features of AD, and the use of antioxidants and anti-inflammatory agents has been proposed as a potential therapeutic strategy (Nabavi et al., 2015). Rutin has demonstrated the ability to reduce oxidative stress and inflammation in animal models of AD, thereby exerting a neuroprotective effect. It has also shown other potential neuroprotective effects, such as improving cognitive function and reducing amyloid-beta accumulation, which are significant pathological features of AD (Liu et al., 2016).

Furthermore, rutin exhibits low toxicity and is generally safe for human consumption, making it an attractive candidate for further study in Alzheimer's disease. While other flavonoids have also been studied for their potential therapeutic effects in AD, rutin's unique combination of neuroprotective, antioxidant, and anti-inflammatory properties, as well as its ability to cross the BBB and low toxicity, make it a promising candidate for further research in this field.

1.12.4. Pharmacological properties of rutin

1.12.4.1. Rutin as an antioxidant

Reactive oxygen species (ROS) are highly reactive chemicals formed from O2 and are by-products of the normal metabolism of oxygen. ROS are mainly produced in the mitochondria but can also be generated in other organelles (Balaban, 2005). ROS include free radicals (superoxide, O−2), hydroxyl radicals (OH), or non-radicals (hydrogen peroxide, H2O2). OH has been recognized as the most reactive form of ROS, primarily responsible for the toxic effects of ROS, while O−2 is proposed to play a vital role in ROS production (Bolisetty and Jaimes, 2013).

Cells possess defense mechanisms, including small-molecule antioxidants and antioxidant enzymes, to reduce cellular levels of ROS (Gandhi, 2012). Superoxide dismutases (SOD) convert O−2 into the more stable form of H2O2. H2O2 can generate OH, a highly reactive hydroxyl radical, which can be further reduced by catalase (CAT), glutathione peroxidase (GPX), and other peroxidases to form H2O and O2 (Patten, 2010). The cellular antioxidant glutathione (GSH) is involved in two types of reactions. First, GSH, in its reduced form, non-enzymatically reacts with O−2 and OH to eliminate ROS (Gandhi, 2012). GSH serves as the electron donor for the reduction of peroxides in the GPX reaction. When GSH reacts with ROS, it is oxidized (GSSG) and forms glutathione disulfide, the final product of GPX reactions. GSH can then be restored from glutathione disulfide through a reaction with glutathione reductase, transferring electrons from

NADPH to glutathione disulfide (Dringen, 2003). Several studies have indicated that GSH plays a role in inhibiting DNA damage and apoptotic cell death following oxidative stress (Song and Zou, 2015). Therefore, cellular antioxidants and antioxidant enzymes work together to inhibit ROS accumulation in cells. Dysregulation of their functions indicates altered oxidative states, which may result in cell death (Song and Zou, 2015).

Several mechanisms have been found to be responsible for the antioxidant activities of rutin in both in vitro and in vivo models. It has been revealed that rutin's chemical structure allows it to scavenge ROS directly. It is also alleged to increase the production of GSH, and the cellular oxidative defense systems are believed to be upregulated through increased expression of various antioxidant enzymes such as CAT and SOD (Al-Enazi, 2014). Additionally, rutin inhibits xanthine oxidase, which is involved in ROS generation (Kostić et al., 2015). It also scavenges ROS by donating hydrogen atoms to superoxide anions, peroxy radicals, and hydroxyl radicals (Caglayan, 2019). Research has shown that rutin effectively reduces the level of malondialdehyde (MDA) while increasing CAT, GPX, SOD, GSH, and Nrf2 levels in colistin-induced neurotoxicity (Xu et al., 2014). Rutin inhibits enhanced activity of xanthine and NADPH oxidases, the primary cellular enzymes responsible for the generation of superoxide radicals. Due to its polyphenolic structure, rutin can scavenge free radicals and chelate transition metal ions, which participate in

Fenton reactions to generate reactive hydroxyl radicals (Ghiasi, 2012; Nassiri-Asl, 2013). The main functional groups in the rutin molecule are the hydroxyl groups at positions 5 and 7 of the A ring, as well as the double bond in the C ring of the quercetin-polyphenolic component, and these are responsible for its antioxidant activity (Cos et al., 1998). Additionally, research has shown that rutin can inhibit the overproduction of oxygen radicals by neutrophils under pathological conditions such as rheumatoid arthritis or cancer (Ostrakhovitch and Afanas'ev, 2001). Rutin

112

facilitates the degradation of peroxides, including lipid peroxides, by regulating the level of GSH and effectively protects phospholipids from peroxidation. Some in vivo studies have revealed that rutin treatment significantly attenuates the decrease in the levels and activities of GSH and GSH-dependent enzymes (GSH-Px and GSSG-R) in several rat models of disease (Javed, 2012). Furthermore, rutin-facilitated regulation of the redox balance in fibroblasts prevents the decrease in nonenzymatic antioxidants, including vitamins E and C, after UV irradiation (Gegotek, 2016). Rutin's antioxidant properties allow it to reduce oxidative stress in almost all in vitro and in vivo studies, as evidenced by reduced reactive oxygen species (ROS) production, nicotinamide adenine dinucleotide phosphate (NADPH) oxidase (NOX) activity, and oxidative products such as MDA and thiobarbituric acid reactive substances (TBARS), in addition to increased antioxidant status, such as superoxide dismutase, glutathione, glutathione peroxidase, and catalase, in various cardiovascular disease models (Geetha et al., 2017; Huang et al., 2017; Imam et al., 2017; Li et al., 2013; Panchal et al., 2011; Saklani et al., 2016; Singh et al., 2015; Xianchu et al., 2018). Rutin significantly reduces cisplatin-induced oxidative stress by inhibiting lipid peroxidation and increasing antioxidant activity (Aksu et al., 2017).

1.12.4.2. Rutin as an antiapoptotic agent

Cell proliferation and elimination are essential for maintaining physiological homeostasis in organisms (Galluzzi, 2012). The process of cell death, including programmed cell death and necrosis, plays a crucial role in various physiological processes such as pathogenesis, metamorphosis, embryogenesis, and tissue turnover (Hakem and Harrington, 2005). Programmed cell death, also known as apoptosis, involves a regulated process of cell suicide in response to specific signals (Alberts, 2002). Apoptosis is controlled by a range of extracellular and intracellular signals that are absorbed from the cell environment and within the cell itself (LeBlanc, 2003). It is

characterized by distinct morphological features, helps maintain tissue homeostasis, and regulates the appropriate number of cells in multicellular organisms by eliminating unwanted cells (Giorgi, 2008). Various endogenous tissue-specific agents and exogenous cell-damaging agents can initiate programmed cell death under critical physiological conditions (Neuman, 2011). Exogenous factors that activate programmed cell death include physical agents (radiation, physical trauma, and chemotherapeutic drugs) and infectious agents (viruses and bacterial toxins) that can act on most cell types (Neuman, 2011).

Mitogen-activated protein kinase (MAPK) is involved in the signal transduction pathways of apoptosis (Pereira, 2013), and its levels indicate whether the cell survives or undergoes apoptosis, as they reflect cellular damage (Yamaoka, 2012; Nafees, 2015). The expression of MAPK is upregulated during apoptosis in neurons and glial cells after spinal cord injury (SCI) (Lee, 2010; Ha, 2011). Additionally, MAPK expression can contribute to the inflammatory response (Breton-Romero and Lamas, 2013). Inactive p38 MAPK is predominantly distributed in the cytoplasm and translocates to the nucleus upon activation to regulate gene expression through the phosphorylation of transcription factors (Tang, 2013; Chen, 2014). Extracellular stimuli, such as inflammatory cytokines, induce the phosphorylation and activation of p38 MAPK through a kinase cascade (Zhu, 2013; Park, 2015). Activated p38 MAPK induces the expression of enzymes such as COX and iNOS, as well as numerous inflammatory-related molecules, thereby promoting the inflammatory response (Breton-Romero and Lamas, 2013).

Research has shown that rutin protects against liver and lung injury through its antioxidative and anti-inflammatory actions, as well as by modulating the MAPK pathway (Pan, 2014; Yeh, 2014). Rutin has been found to reduce p38 MAPK expression in a spinal cord injury (SCI) model, suggesting its potential to protect spinal cord cells by lowering the expression of pro-apoptotic

proteins (Hong-liang, 2017). Furthermore, rutin has been shown to protect human dopaminergic cells against rotenone-induced injury by inhibiting the p38 MAPK signaling pathway (Park, 2014). It has also exhibited anti-inflammatory effects, potentially attributed to its suppression of p38 MAPK in UVB-irradiated mouse skin (Choi, 2014). Rutin has been found to decrease the activities of caspase-9 and caspase-3, which are key factors in the neuroprotective action of rutin on spinal cord cells. This observation aligns with previous reports indicating that rutin alleviates cell death by inhibiting caspase-3 activity in dopaminergic and hippocampal neurons (Na, 2014; Song, 2014). Rutin protects spinal cord cells by reducing oxidative stress and inflammation, and by decreasing the expression of pro-apoptotic proteins through the inhibition of the p38 MAPK pathway (Hong-liang et al., 2017). Moreover, it significantly protects fibroblasts from UV-induced apoptosis, particularly in response to UVA, by reducing caspase activation and cytochrome c release, while increasing Bcl-2 expression (Agnieszka, 2017). These findings also suggest that the observed inhibition of HO-1 expression may modulate the cell survival mediated by rutin. Additionally, rutin pretreatment has been shown to significantly attenuate H2O2-induced apoptosis in HUVEC cells (Agnieszka, 2017). The antiapoptotic effects of rutin may synergize with its ability to protect DNA from oxidative damage, as demonstrated in ischemia-induced rat brains (Agnieszka, 2017). Additionally, treatment with rutin has been shown to reduce the expression of p53, a protein involved in activating DNA repair mechanisms and inducing apoptosis in response to DNA damage (Agnieszka, 2017). Rutin administration has been found to attenuate "ischemic neural apoptosis" by suppressing p53 expression and lipid peroxidation, while increasing the activity of endogenous antioxidant defense enzymes (Khan, 2009). In another study investigating the effect of rutin on Sevoflurane and Propofol-induced neurotoxicity, the results indicated that rutin exhibited neuroprotective potential, as it improved memory and behavior in tests such as the open

field test, elevated plus maze, and Y-maze. This effect may be attributed to the reduction in neuroapoptosis (Yi-Gang, 2015).

Rutin has also been shown to protect against the neurodegenerative effects of prion accumulation by increasing the production of neurotrophic factors and inhibiting the activation of apoptotic pathways in neuronal cells. These findings suggest that rutin may have clinical benefits for prion diseases and other neurodegenerative disorders (Na, 2014).

Apoptosis of hair follicular cells is a leading cause of hair follicle degeneration. In a particular study, apoptosis of human follicular dermal papilla cells was observed after treatment with staurosporine, but this effect was completely reversed by exposure to rutin, spermidine, and zeaxanthin. The expression of anti-apoptotic molecules such as Bcl-2 and MAP-kinases, as well as their phosphorylated forms, was preserved, indicating the potential use of rutin in preventing apoptosis of hair follicular cells, a leading cause of baldness (Carelli, 2012).

Caspase-dependent apoptotic cell death occurs due to the inactivation of survival pathways, such as the PI3K/Akt pathway (GómezSintes, 2016; Snigdha, 2012). Rutin inhibits intrinsic apoptosis by binding to the proapoptotic proteins Bax and Bcl-2 homologous antagonist/killer (Bak) (Khodapasand, 2015; Lindqvist, 2014). Studies have revealed that rutin reduces apoptotic cells in ischemic-reperfusion-induced apoptosis models, both in vivo and in vitro, as well as in doxorubicin- and pirarubicin-induced cardiotoxicity, by suppressing the protein expressions of caspase-3, -7, and -9 (Jeong, 2009; Kim, 2010; Lin, 2018). The reduction of caspase proteins by rutin is associated with an increase in Bcl-2 expression and a decrease in Bax expression (Ma, 2017; Wang, 2018). This suggests that rutin may prevent apoptosis via the Bcl-2-regulated apoptotic pathway, but the exact mechanisms by which rutin modulates Bcl-2, Bax, and caspase proteins are still not well understood.

116

1.12.4.3. Rutin as an Antiautophagic Agent

Autophagy is a process that involves the release of cellular waste materials, such as impaired proteins and organelles, by autophagosomes, which are then delivered to lysosomes for degradation into reusable monomers, such as amino acids (Li, 2018). The kinase mammalian target of rapamycin (mTOR), located on the lysosomal membrane, plays a key role in the autophagy process (Dunlop & Tee, 2014; Schirone, 2017). The activation of upstream pathways of mTOR, including the phosphatidylinositol-3 kinase (PI3K)/Akt/mTOR pathway or adenosine monophosphate-activated protein kinase (AMPK)/mTOR pathway, can inhibit autophagic response (Pires, 2017). In the absence of growth factors, phosphorylation of the protein kinase Akt is diminished, leading to the induction of autophagy (Li, 2016).

The direct link between rutin and mTOR remains unclear due to a lack of studies demonstrating the effects of rutin on mTOR, PI3K, and AMPK. However, numerous studies have shown that rutin can enhance the phosphorylation of Akt in diabetic cardiomyopathy, drug-induced cardiotoxicity, and myocardial ischemic reperfusion injury in animal models. For example, in a study where rutin was administered at a dose of 100 mg/kg orally for a week before doxorubicin induction and concurrently for 11 weeks with doxorubicin injection in rats, rutin inhibited the downregulation of Akt phosphorylation induced by doxorubicin (Ma, 2017). In a diabetic cardiomyopathy-induced cardiac dysfunction model, the administration of rutin at a dose of 60 mg/kg for 6 weeks significantly increased the phosphorylation of Akt in diabetic ApoE knockout mice compared to the untreated diabetic group (Huang, 2017). Another study revealed that rutin isolated from Lonicera japonica increased Akt phosphorylation in H_2O_2-mediated injury in H9c2 cells. The activation of Akt by rutin was associated with a reduction in the protein expressions of microtubule-associated protein light chain 3 (LC3), Atg5, and p62, and this pattern of expressions

was observed in both in vivo and in vitro models (Ma, 2017). These findings suggest that rutin may act directly on cells as a parent compound or after undergoing metabolism in vivo.

1.12.4.4. Rutin as an Anti-inflammatory Agent

The anti-inflammatory effect of rutin can be explained by its inhibition of some important enzymes involved in inflammation. Rutin has been found to alleviate oxidative stress and inflammation induced by reactive oxygen species (ROS) in rats by targeting p38-MAPK, i-NOS, NFκB, COX-2, TNF-α, and IL-6 (Nafees, 2015). It has also been shown to decrease brain damage and improve neurological dysfunctions through its anti-inflammatory properties (Hao, 2016). Rutin has been observed to inhibit the release of high mobility group box 1 (HMGB1) and downregulate HMGB1-dependent inflammatory responses in human endothelial cells, as well as inhibit HMGB1-mediated hyperpermeability and leukocyte migration in mice (Yoo, 2014). HMGB1 is a protein that acts as a late mediator of severe vascular inflammatory conditions. Furthermore, treatment with rutin has resulted in reduced release of HMGB1 induced by cecal ligation and puncture, as well as reduced sepsis-related mortality, indicating its potential as a therapeutic agent for severe vascular inflammatory diseases through inhibition of the HMGB1 signaling pathway (Yoo, 2014).

Rutin has been shown to reduce the levels of NFκB and the products of its transcriptional activity, such as TNF-α, in UV-irradiated fibroblasts (Banu, 2009). Studies have revealed that rutin suppresses the phosphorylation of NFκB by inhibiting MAPK in lung tissue and decreases the expression and cytoplasmic relocation of NFκB (Yeh, 2014). Rutin has been found to inhibit the activity of cyclooxygenases, important enzymes in the inflammatory process, and suppress the expression of COX-2 and iNOS, via the suppression of p38/MAPK, in UVB-irradiated mouse skin, exerting anti-inflammatory effects (Choi, 2014). It has also been shown to suppress p38 levels (Sancho, 2003). The inhibition of NFκB activity may be associated with decreases in fibroblast

endocannabinoid levels (Sancho, 2003). Current research has revealed that rutin exerts a therapeutic effect against hepatic fibrosis by modulating liver inflammation. Rutin regulates liver inflammation and fibrogenesis by targeting TLR4 and P2X7r pathways, which are crucial pathways in the immune and inflammatory response (Hou, 2020). TLR4 controls the rate of hepatic inflammation and plays a distinctive role in hepatocyte homeostasis. Rutin ameliorated hepatic fibrosis and inflammation by suppressing TLR4 and its upstream or downstream related signals, which are crucial for extracellular matrix metabolism and anti-inflammation. Therefore, TLR4 can be considered a valuable target for rutin in the regulation of chronic liver diseases (Hou, 2020). P2X7r is highly expressed in immune and inflammatory systems and promotes inflammasome formation upon activation. Activated P2X7r promotes NLRP3-dependent mature IL-1β secretion and participates in pro-inflammatory events (Giuliani, 2017; Miller, 2011; Quan, 2018).

In carfilzomib-induced cardiotoxicity models, pretreatment with rutin at doses of 20 and 40 mg/kg in rats leads to a significant downregulation of NF-κB mRNA expression by increasing its inhibitory protein, IκB-α (Imam, 2017). This downregulation further reduces the expression of various pro-inflammatory cytokines, such as IL-6, CRP, and TNF-α (Dong, 2010). In diabetes, elevated levels of IL-6, CRP, and TNF-α are commonly observed (Mirza, 2012). In diabetic cardiomyopathic rats, oral administration of rutin at a dose of 50 mg/kg/day for 24 days after diabetic induction reduces the expression of TNF-α and CRP levels (Saklani, 2016). Pre-treatment with rutin at a dose of 100 mg/kg/day for 8 days in a sepsis-induced cardiac injury model in mice also demonstrates a reduction in TNF-α and IL-6 levels and cardiac inflammation area (Xianchu, 2018). Rutin has been found to potently inhibit the release of proinflammatory TNF-α and IL-1β from monocytes (Yuandani, 2017). Overall, rutin is believed to directly scavenge free radicals by

119

chelating metal iron ions, thereby reducing oxidative stress and inflammation and ultimately attenuating the remodeling process. However, detailed information regarding the molecular mechanism and sequence of events by which rutin mitigates the cardiac remodeling process through its antioxidant and anti-inflammatory effects is still lacking.

1.12.4.5. Neuroprotection of Rutin

Flavonoids are believed to exert their neuroprotective potential by interacting with critical protein and lipid kinase signaling cascades in the brain, leading to the inhibition of apoptosis triggered by neurotoxic species and promoting neuronal survival and synaptic plasticity. Rutin, as a flavonoid, also exhibits neuroprotective effects through its beneficial effects on the vascular system, which can cause changes in cerebrovascular blood flow capable of inducing angiogenesis, neurogenesis, and alterations in neuronal morphology. Through these mechanisms, the consumption of flavonoid-rich foods has the ability to limit neurodegeneration and reverse age-related dementia cases. Given the interest in developing new drugs to enhance brain functions, flavonoids like rutin may serve as important precursor molecules to be explored in the development of a new generation of brain-enhancing drugs (Xu, 2014).

Research has shown that oral administration of rutin can protect the CA3 region of the hippocampus in rats and have an impact on their behavior, reducing memory impairment associated with trimethyltin toxicity in a water maze (Koda, 2002). Rutin pretreatment reduces infarct size and neurological deficits in rats after middle cerebral artery occlusion and preserves the antioxidant content of enzymes in the brain (Khan, 2009). Rutin administration also protects the brain tissue of male Wistar rats from cerebral ischemia (AbdEl-fatah, 2010). Rutin attenuates age-related memory deficits in mice (Kishore, 2005). It improves learning and memory in normal, aged, and experimentally-induced amnesic mice, possibly through its potent antioxidant action

(Kishore and Singh, 2005). Rutin protects against spatial memory impairment induced by trimethyltin and preserves synaptophysin levels (Zhang, 2014). Studies have revealed that rutin improves spatial memory in AD transgenic mice by decreasing Aβ oligomer levels and attenuating oxidative stress and neuroinflammation. It significantly attenuates memory deficits in AD transgenic mice, decreases oligomeric Aβ levels, increases SOD activity and the GSH/GSSG ratio, reduces GSSG and MDA levels, downregulates microgliosis and astrocytosis, and decreases IL-1β and IL-6 levels in the brain. These findings indicate that rutin is a promising agent for AD treatment due to its antioxidant, anti-inflammatory, and Aβ oligomer-reducing activities (Xu, 2014). Rutin protects against the neurodegenerative effects of prion accumulation by increasing the production of neurotrophic factors and inhibiting the apoptotic pathway activation. This suggests that rutin may have clinical benefits for prion diseases and other neurodegenerative disorders (Aldhabi, 2014).

Rutin has shown therapeutic potential for the treatment of neurodegenerative diseases associated with oxidative stress (Park, 2014). It can be effective in reducing neurotoxicity, and its neuroprotective effect may be mediated through its antioxidant activity (Motamedshariaty, 2014). Rutin has also demonstrated potential anticonvulsant and antioxidant activities against oxidative stress in kainic acid-induced seizures in mice (Marjan Nassiri-Asl, 2013). Rutin has neuroprotective abilities and has been shown to improve memory and behavior in open field tests, elevated plus and Y-mazes tests. This improvement may be attributed to the reduction in neuroapoptosis (Man, 2015). Rutin has been found to improve memory, decrease oligomeric β-amyloid levels, lipid peroxidation, IL-1β and IL-6 levels, increase antioxidant enzymes and GSH levels in an Alzheimer's disease mouse model (Xu, 2014). Rutin prevents cognitive deficits and morphological changes in the hippocampus, attenuates lipid peroxidation, COX-2, GFAP, IL-8,

iNOS, and NFκB in a rat model of sporadic dementia (Javed, 2012). It also prevents memory deficits, ameliorates oxidative stress, apoptosis, and neurite growth in a rat model of cognitive dysfunction (Ramalingayya, 2017).

1.13. Aims and Objectives of the Study

AD is a progressive, degenerative, and terminal disease. Identifying a natural product with the ability to combat AD pathology would help reduce disease progression.

The general aim of the study is to characterize the neuroprotective and anti-inflammatory potentials of rutin in an in vitro model of AD and to determine the mechanisms of action. Additionally, we will investigate the pharmacological properties of rutin under hypoxic conditions in a cellular model of AD.

The objectives of the study are as follows:

A. To investigate the dose-related toxicity of $A\beta_{25\text{-}35}$ on PC12 cells and primary rat neurons in both hypoxic and normoxic conditions.

B. To characterize the neuroprotective effects of rutin against $A\beta_{25\text{-}35}$-induced toxicity in PC12 cells and primary rat neurons under both hypoxic and normoxic conditions.

C. To determine the anti-inflammatory effects of rutin against LPS-induced inflammation in BV2 cells.

Chapter 2

MATERIALS AND METHODS

2.1. Materials

Rat adrenal pheochromocytoma (PC12) cells, Dulbecco's Modified Eagle's Medium (DMEM) containing high glucose (4.5 g/L), Dulbecco's Phosphate-buffered saline (PBS), fetal bovine serum (FBS), inactivated horse serum (HS), penicillin and streptomycin (10,000 units/mL & 10,000 µg/mL), Trypan Blue, poly-D-lysine (PDL) (50x), dimethyloxalylglycine (DMOG), dimethyl sulfoxide (DMSO), 3-(4,5-dimethylthiazol-2-yl)-2,5-diphenyltetrazolium bromide (MTT), 4-DL-dithiothreitol (DTT), trypsin (50x), Amyloid beta $_{25\text{-}35}$, rutin, phenyl-methyl-sulfonyl fluoride (PMSF), and protease inhibitor cocktail were from Sigma-Aldrich (St Louis, MO, USA).

Laemmli buffer (4x), 4-15% Mini-PROTEAN TGX Precast polyacrylamide gel, skimmed milk, Precision Plus Protein Dual Color Standard, Trans-Blot SD Semi-Dry Electrophoretic transfer cell were from Bio-Rad (Hertfordshire, UK). Amersham™ Protran® Premium nitrocellulose blotting membranes were from VWR (Leicestershire, UK). RIPA (radioimmunoprecipitation assay) buffer (10x) was from New England Biolabs Ltd (Hertfordshire, UK). Rabbit polyclonal antibody to β-actin was from Abcam (Cambridge, UK), mouse polyclonal antibody to HIF-1α was from Novus Biologics (Abingdon, UK), goat anti-rabbit IgG HRP affinity, and goat polyclonal anti-mouse IgG HRP affinity were from Dako, BD Transduction Laboratories, Agilent (Cheshire, UK). Pierce BCA protein assay kit, Pierce ECL western blotting substrates, and Techne PROPLATE 48 were from ThermoFisher Scientific (Loughborough, UK). The non-radioactive cytotoxicity assay kits were from Promega (Southampton, UK). Mouse TNFα DuoSet ELISA kits were purchased from R&D Systems (Minneapolis, MN). Both DCFDA cellular ROS detection assay kit and lipid peroxidation (MDA) assay kit were from Abcam (Cambridge, UK). Plastic materials for cell

cultures including pipettes, T25 cell culture vessel, 96-, 24-, and 12-well plates were from Greiner Bio-One (Gloucestershire, UK). Guava cell dispersal reagent, Guava nexin kit, Guava instrument cleaning fluid, Guava Easy check kit, and 0.22 μm syringe filter were obtained from Merck Millipore, USA.

2.2. Cell Culture

2.2.1 Ethical Permissions

All animals used in the experiments were euthanized under Schedule 1 according to the Animals Scientific Procedures Act (1986) (ASPA). The work is exempted from the need for Animal Welfare and Ethical Review Board (AWERB) approval under the ASPA and all subsequent amendments under both UK and European Law. All animals used in this study were treated in accordance with ASPA guidelines.

2.2.2 PC12 Cell Culture

PC12 cells are derived from rat pheochromocytoma of the rat adrenal medulla. They were first cultured by Greene and Tischler in 1976. PC12 cells were used because they are easy to culture, have an enormous amount of background information, and are readily available. PC12 cells are commonly used and suitable for early studies to perform various assays and determine the underlying mechanisms (Holloway and Gavins, 2016; Sommer, 2017). They have been used in several disease models such as Parkinson's disease, Huntington's disease, Alzheimer's disease, and stroke (Holloway and Gavins, 2016).

Thawing and Freezing PC12 Cells

PC12 cells were obtained from Sigma-Aldrich, UK (Cat # 88022401) in a frozen state in cryopreservation media containing 10% DMSO and stored at -80°C. As shown in Figure 2.1, the cryovials were quickly thawed in a 37°C water bath. The cells were then transferred into a 15 mL Falcon tube containing 10 mL of "complete" PC12 cell media [high-glucose DMEM (Dulbecco's Modified Eagle's Media with 4,500 mg/ml glucose, L-glutamine and sodium bicarbonate, without pyruvate) supplemented with 5% FBS, 5% HS, and 1% PS] and mixed well by pipetting (trituration). The cells were then centrifuged at 100 rcf (relative centrifugal force) for 5 minutes. The supernatant was discarded, the cells were resuspended in fresh complete media, and the cell suspension was transferred into a T25 flask (passage 1: P1). The PC12 cells were incubated at 37°C in a humidified atmosphere of 5% CO_2 in air and examined every day. The culture media (approximately two-thirds) was renewed every 2-3 days until confluency. Upon confluency, the cells were passaged. The cell suspension was transferred into a 15 mL Falcon tube and centrifuged at 100 rcf for 5 minutes. Two-thirds of the media was discarded, and fresh media (approximately 10 mL) was added. The cell suspension was transferred into 4 x T25 flasks (P2). Upon confluency, following the same procedure, the cells were further passaged. Confluent cultures at P3 were frozen (procedure detailed below) or used for experiments. The PC12 cells were used for experiments up to a maximum of P8.
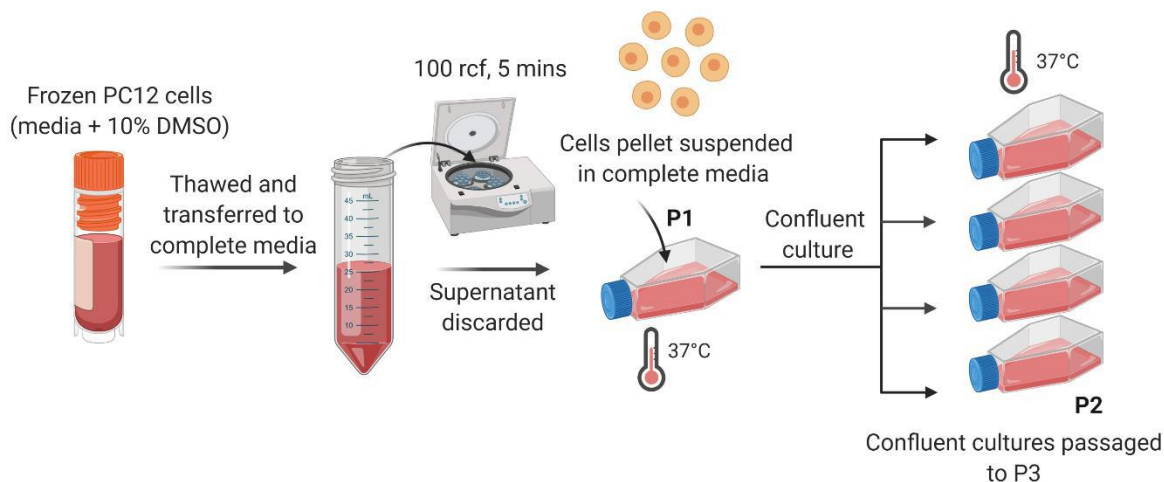
Figure 2.1 Diagrammatic representation of thawing and culturing PC12 cells. Frozen PC12 cells were thawed and transferred to 10 mL of complete media. The cell suspension was centrifuged at 100 rcf for 5 minutes, the supernatant was discarded, and cells were resuspended in 10 mL of complete media. The cell suspension was then transferred into a T25 flask. The cells were maintained in a standard incubator with a humidified atmosphere containing 5% CO2 at 37°C. The cells were examined daily, and two-thirds of the media was renewed every 2-3 days. Upon confluency, the cells were passaged (Singh et al., 2021).

To freeze the PC12 cells for future use: The cell suspension was centrifuged at 100 rcf for 5 minutes. Cryopreservation media containing 10% sterile DMSO in complete media was prepared. DMSO is a cytoprotectant added to prevent the formation of intracellular and extracellular crystals during freezing. The cell pellet was suspended in the cryopreservation media (approximately 1 x 106 cells in 1.5 mL). The suspension was triturated in cryovials and placed in a freezing container. The container was frozen at -20°C for 2 hours, followed by -80°C overnight, and then transferred into a liquid nitrogen cylinder for long-term storage.

Seeding/plating for experiments: PC12 cells were seeded (1.2 x 106 cells in 5 mL of complete medium) in uncoated T25 flasks for protein/RNA extraction, flow cytometry, and trypan blue exclusion assays. For MTT and LDH assays, poly-D-lysine (PDL) coated 96-well plates received 1.2 x 104 cells per well (100 μL).

2.2.3. Poly-D-lysine (PDL) coating

Plastic surfaces coated with PDL possess a net positive charge that is preferred by certain cells, such as neurons and glial cells, for attachment, growth, and differentiation. It also facilitates cell binding, which is essential for certain cell-based assays (Holloway and Gavins, 2016). PDL (0.1 mg/mL) was used to coat cell culture plates/flasks. A sufficient amount of the PDL solution was added to cover the cell culture plates/flasks (1 mL per 25 cm2 area) and incubated overnight (maximum time). The solution was then aspirated, and the plates/flasks were washed three times with D-PBS. Subsequently, the plates/flasks were allowed to air dry for approximately 6 hours before introducing cells.

2.2.4. Cell passage

When the cells reached about 80% confluence, they were sub-cultured. They were transferred to a centrifuge tube and centrifuged at 100 g for 3 minutes. The supernatant was carefully removed, and the cell pellet was re-suspended with 1 mL of complete growth medium and then brought up to a final volume of 15 mL in a T75 flask.

$$1 \; x \; 25^2 cm \; flask \; \xrightarrow[split \; 1:3]{} 1x75^2 cm \; flask \; OR \; 3x25^2 cm \; flasks$$

Cells were exposed to two different conditions: normoxic conditions, which involved incubation at 21% O2, 5% CO2, and 37°C in a 95% humidity incubator, and hypoxic conditions, which were

induced within an airtight hypoxia chamber (Ruskin Invivo2 400, RS Biotech, Irvine, UK) with 0.3% O2.

For all experiments, cell counting was performed using a Neubauer chamber. Once the cells reached 80% confluence, 20 µL of the cell suspension was mixed with 20 µL of 0.4% Trypan Blue in an Eppendorf tube. The mixture was then transferred onto the haemocytometer grid. The actual cell count was determined by counting the total number of cells within four haemocytometer grids, dividing the count by 4, and multiplying it by a factor of 2 to adjust for the trypan blue dilution factor. The percentage viability of the cells was subsequently measured.

$$Actual\ cell\ count\ in\ sample = \frac{Totsl\ cell\ count}{2} x10^4/mL$$

$$Percentage\ viability = \frac{Live\ cell\ count}{Total\ cell\ count} x10^4/mL$$
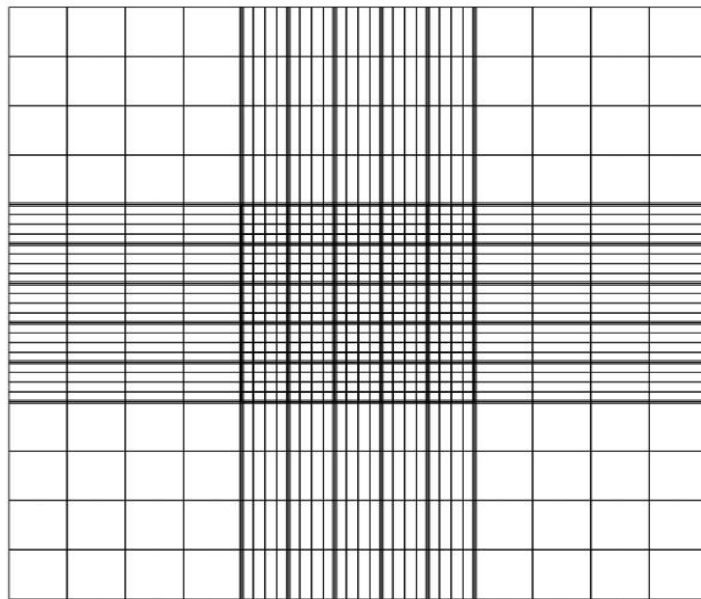
Figure 2.2 Neubauer Chamber. The viable cells were counted in each large square and the actual cell count was determined by counting the total number of cells within four haemocytometer grids

and dividing by 4, and multiplying it by a factor of 2 for adjustment of the trypan blue dilution
factor (Singh et al., 2021).

2.2.5. Primary Rat Cortical Neuronal Cultures

Rat embryos E17-18 were removed from time-mated Sprague-Dawley pregnant rats. The rat embryos were then placed in ice-cold Hank's Balanced Salt Solution (HBSS) in a petri dish. The embryos were removed from their placental sac, and each embryo underwent decapitation at the head/neck junction. The head was placed in ice-cold HBSS in a new petri dish. The embryonic brains were removed from the head cavity. The cortices were collected while the brainstem, cerebellar tissue, meninges, and the hippocampus (darker, C-shaped region) were discarded. The cortices were placed in a fresh Petri dish containing ice-cold HBSS and then dissociated in another fresh Petri dish (containing 1 mL of cold Neurobasal media) using a scalpel.

A 15 mL falcon tube was prepared with 1 mL of Neurobasal media containing 0.05% trypsin and 100 μg/mL deoxyribonuclease (DNAse), which was warmed for approximately 15 minutes at 37 °C. The minced cortices were transferred into the falcon tube and triturated using a pipette (20-30 times). The mixture was then incubated for 15 minutes at 37 °C. Afterward, 6 mL of pre-heated (37 °C) Neurobasal media containing 10% FBS was added to inactivate the trypsin. The cortices were further triturated (20-30 times). The suspension was centrifuged at 200 rcf for 5 minutes, and the supernatant was discarded. Then, 10 mL of "complete" Neurobasal media (Neurobasal media supplemented with 2% B27 serum-free supplement, 2mM L-glutamine, and 1% PS) was added. The suspension was sieved through a 70μm cell strainer. The cells were counted using a Neubauer chamber.

The cells were plated onto PDL-coated plates at densities of 1.5 x 10^6 cells in 5 mL (T25 flasks for protein/RNA extraction), 3 x 10^4 cells / 100 μL (96-well plates for MTT/LDH assay), and 1.5 x 10^5 cells / 300 μL (24-well plates for immunofluorescence (IF) staining). They were then placed in a standard incubator with a humidified atmosphere containing 5% CO2 at 37 °C (Figure 2.3). The cultures were examined, and a 50% media change with fresh media was performed on DIV1. Thereafter, the 50% media change was performed every 2-3 days until confluency. Typically, experiments were performed at DIV 9-14.
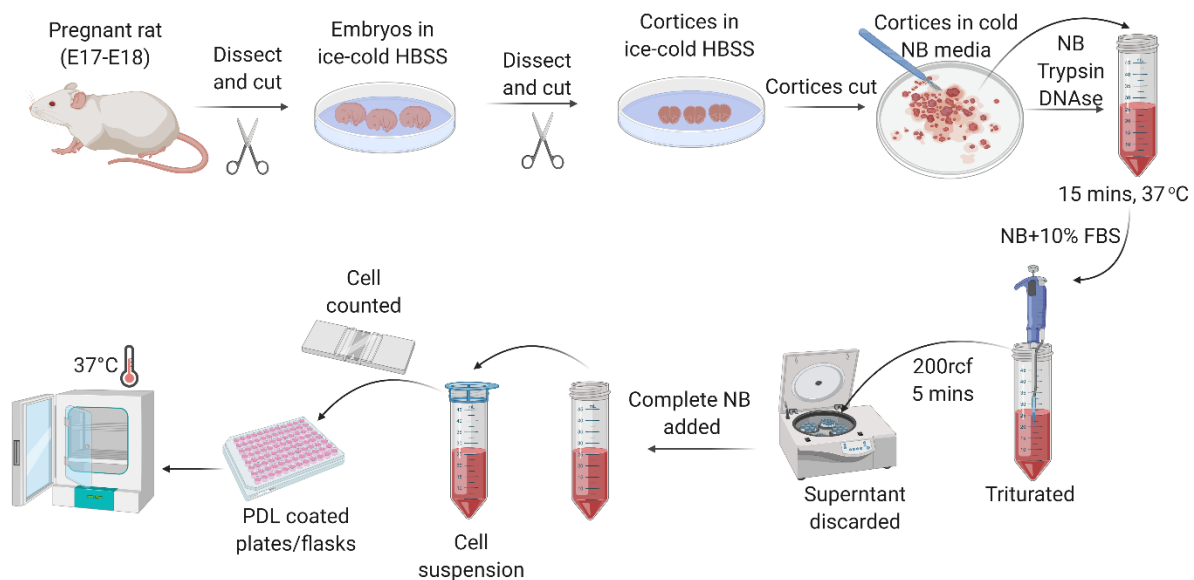
Figure 2.3. Primary Rat Cortical Neuronal Culture. Cortices were obtained from E17-18 pregnant rats. The cortices were enzymatically digested, triturated, and centrifuged. The supernatant was removed, and complete Neurobasal (NB) media were added. The cell suspension was sieved through a 70μm cell strainer, and the cells were counted and transferred into PDL-coated plates and flasks. The cultures were maintained in a standard incubator with a humidified atmosphere containing 5% CO2 at 37 °C (Singh et al., 2021).

2.2.5.1: Determination of Neuron Purity in Primary Culture and Contamination by Other Brain-Derived Cells

Genetic and epigenetic variability between cell lines, as well as differences in investigator techniques, cell culture conditions, and differentiation protocols, often result in imperfect neural progenitor cell (NPC) differentiation, which subsequently affects the purity and quality of subsequent neuronal cultures (Topol et al., 2015). A typical example is the contamination of differentiated NPC cultures by neural crest cells (NCCs) during rosette selection, a developmental stage similar to the formation of neuroepithelial cells within the neural tube (Wilson and Stice, 2006; Bowles et al., 2019). NCCs, also known as mesenchymal stem cells, are characterized by the presence of the cell surface marker CD271 (nerve growth factor receptor; NGFR) (Alvarez et al., 2015). NCCs are multipotent cells capable of differentiating into various brain-related lineages, such as Schwann cells in peripheral nerves (Woodhoo and Sommer, 2008), enteric neurons, bone, and muscle cells, but they cannot differentiate into central nervous system (CNS) neurons. Consequently, during neuronal differentiation from NPCs, infiltrating NCCs will continue to proliferate and contaminate the neuronal culture with an undefined non-neuronal cell type. As NPC passage number increases, NCCs will persistently proliferate and may render the NPC population unsuitable for neuronal differentiation. Glial differentiation has commonly been reported to increase in higher passages of NPC cultures (Paavilaine et al., 2018).

The cell surface marker CD133 (Promonin 1) has been described as a characteristic of NPCs (Yuan et al., 2011). Cells expressing CD133 are positive for other common NPC markers, such as Nestin and OCT4. Additionally, CD133 has been confirmed as an effective cell surface marker for isolating NPCs from human brain tissue using fluorescence-activated cell sorting (FACS), indicating that the expression of this marker is a useful characteristic for defining NPCs.

The presence of CD271+ and CD133- cells in NPC cultures significantly affects the quality and purity of neuronal cultures after differentiation. Contamination of neuronal cultures with non-neuronal cells poses challenges in analyzing cell-autonomous neuronal phenotypes and introduces unwanted noise in data collection and analysis. Moreover, NPC lines from different individuals and genetic backgrounds are likely to contain varying proportions of CD271+/CD133- cells, resulting in significantly different populations of neurons and high variability in sample purity and quality. To improve the quality of NPCs, it is necessary to initiate neuronal differentiation protocols from a consistent pool of NPCs across cell lines, leading to a more homogeneous population of resulting neurons and increased consistency across differentiations.

Minimizing the number of CD271+/CD133- cells in NPC cultures is crucial to achieving this goal. One approach is to use NPC cultures with very low passage numbers (P < 3-4), although this may not always be practical. Instead, FACS has been successfully utilized to select for CD271-/CD133+ cells, enabling the use of NPC cultures for more than 50 passages (Cheng et al., 2018; Bowles et al., 2019). The first method of using early passage cultures is effective in experienced hands, but it limits the use of each cell line to a short period of time, restricts expansion potential, and necessitates repeated NPC differentiation from iPSCs. In contrast, while the FACS method is highly successful in purifying NPC cultures, it is a labor-intensive, expensive, and time-consuming technique that yields a very low number of live cells. Moreover, there is a potential for contamination and prolonged recovery times due to slow proliferation rates (Muratore et al., 2014).

Magnetic cell sorting (MACS) method can also be employed to enrich NPC cultures for CD271-/CD133+ cells. This method is simple, inexpensive, and time-efficient, and has demonstrated similar efficiency to FACS while achieving a higher yield of live cells and inducing less sorting-

associated cellular stress. Studies have shown that MACS leads to much purer neuronal cultures after differentiation compared to unsorted cell lines, and the protocol can be used in both early (P < 5) and late (P > 10) passage cultures to maintain clean NPC populations. Therefore, MACS is established as a cheaper, more efficient, and convenient method for sorting NPCs than FACS, and its inclusion in standard NPC-neuron differentiation protocols significantly improves the longevity of NPC cell lines, as well as the quality and stability of resulting neuronal populations.

In general, several techniques can be used to determine neuron purity in primary culture and detect contamination by other brain-derived cells. Some commonly used procedures include:

- Immunocytochemistry: This technique involves using specific antibodies that target proteins expressed on the surface of different cell types. By staining the cells with these antibodies, neurons can be distinguished from other brain-derived cells such as astrocytes or microglia. For example, antibodies against the neuronal marker MAP2 (microtubule-associated protein 2) can be used to specifically identify neurons in a mixed culture (Zhang and Firestein, 2019).

- Fluorescence-activated cell sorting (FACS): FACS is a flow cytometry-based technique that separates different cell types based on their physical and chemical properties. Cells can be sorted into different populations based on their fluorescence intensity by labeling them with fluorescent markers. For example, neurons can be labeled with a fluorescent dye such as NeuN (neuronal nuclei) and sorted from other brain-derived cells (Guez-Barber et al., 2012).

- RNA sequencing: RNA sequencing can be used to determine the gene expression profile of a mixed culture. Different cell types can be identified based on their specific gene expression patterns by analyzing the transcriptome of individual cells. For example,

neurons can be identified by their expression of specific neuronal genes such as Tubb3 (tubulin beta-3 chain), while astrocytes can be identified by their expression of GFAP (glial fibrillary acidic protein) (Darmanis et al., 2017).

- Simple Shaking Method: This method involves purifying immature neurons from differentiating neural stem cell progeny. The shaking purification technique allows for easy, low-cost, efficient, and large-scale separation of immature neurons from dNSC progeny, benefiting both basic and clinical applications (Azari et al., 2014).

- Electrophysiology: Electrophysiology techniques such as patch-clamp recordings can be used to measure distinct electrical properties of neurons. In contrast, glial cells are generally electrically inactive. Hence, electrophysiology can be used to evaluate the purity of neuronal cultures (Gage et al., 1995).

- Morphological assessment: Neurons have distinct morphologies, such as long processes and a round or triangular cell body, while glial cells have more flattened cell bodies and shorter processes. Therefore, visual inspection of cells under a microscope can be used to evaluate the purity of neuronal cultures (Brewer et al., 1993).

- Gene expression analysis: Gene expression analysis can also be used to evaluate the purity of neurons in primary cultures. This method involves analyzing the expression of genes specific to neurons, such as NSE or Synapsin, using techniques like quantitative PCR or microarray analysis. The purity of neurons can then be determined by examining the expression of these genes in the culture. Recent research studies have used gene expression analysis to assess the purity of human induced pluripotent stem cell-derived neuron cultures (Li et al., 2019).

2.2.6. Hypoxia chamber

Source 1: www.eppendorf.com/co2-incubators

Figure 2.4. Hypoxia chamber. Hypoxia/hyperoxia incubators are used for experiments that require oxygen levels below that of the ambient atmosphere. As oxygen levels regulate many metabolic functions in cells, hypoxia incubators allow reproducible and precise control of O2 gas within the chamber, usually by varying the level of nitrogen. However, not all incubators can control extremely low (less than 1%) oxygen levels. Hypoxia incubators with built-in imaging systems and plate readers are available and are used for cancer cell research, metabolic disease research, and investigations of cellular growth factors (Lechpammer et al., 2018).

An in vitro hypoxia chamber incubator is a specialized laboratory instrument used to culture and study cells under controlled oxygen conditions. This equipment is designed to mimic the physiological oxygen levels in various tissues, allowing researchers to study how cells behave and respond to hypoxic conditions. It is commonly used in cell culture experiments where the cells are

exposed to varying levels of oxygen to simulate certain pathological or physiological conditions in vivo, such as tumor hypoxia, ischemia, or chronic lung disease (Chan and Loscalzo, 2010).

Hypoxia is a condition where there is a deficiency of oxygen in tissues, which can occur in various disease states, such as cancer, heart disease, and stroke. By simulating hypoxia in the laboratory, researchers can study the cellular responses and molecular mechanisms that occur in these conditions (Bhandari and Deem, 2018).

The in vitro hypoxia chamber incubator works by controlling the concentration of oxygen in the chamber. The hypoxia chamber typically consists of a sealed chamber with controlled oxygen concentrations ranging from atmospheric (21%) down to as low as 0.1%. The chamber is designed to maintain a stable and consistent oxygen concentration throughout the culture period, typically ranging from a few hours to several days. The chamber's gas mixture is regulated by a gas controller or sensor system that maintains the desired oxygen level by supplying the chamber with precise amounts of gas mixtures, usually nitrogen or carbon dioxide, to reduce the concentration of oxygen (Lechpammer et al., 2018).

There are various types of in vitro hypoxia chamber incubators available on the market, each with unique features and specifications. Some popular models include the ProOx C21 Hypoxia Chamber Incubator from BioSpherix, the H35 Hypoxystation from Don Whitley Scientific, and the Hypoxia Chamber H2000 from Invivo2. These chambers are typically equipped with temperature and humidity control, as well as CO_2 and O_2 sensors to monitor and maintain the oxygen concentration within the chamber (Lechpammer et al., 2018).

The chamber incubator is equipped with temperature and humidity control to maintain optimal conditions for cell culture, including heating elements and water reservoirs. These elements

maintain a stable temperature and humidity inside the chamber, essential for maintaining optimal conditions for cell growth.

Additionally, the hypoxia chamber incubator may have specialized features, such as integrated culture plates, microscope access ports, or advanced imaging systems to monitor cell growth and behavior (Lechpammer et al., 2018).

Overall, the in vitro hypoxia chamber incubator provides researchers with a sophisticated and controlled environment to study cell behavior in hypoxic conditions, which can help uncover mechanisms of disease and enable the development of new therapeutic strategies.

In addition to studying cellular responses to hypoxia, the in vitro hypoxia chamber incubator can also be used for a wide range of research applications, including stem cell research, tissue engineering, drug discovery, and cancer research.

Source 2: www.eppendorf.com/co2-incubators

Figure 2.5 Hypoxystation. Hypoxystation is the only hypoxic chamber purpose-built for physiological cell culture research. It is specifically designed to create normoxic, hypoxic, and anoxic conditions within a controlled and sustained workstation environment. This hypoxic

137

incubator is ideal for research requiring the ability to accurately control oxygen, carbon dioxide, temperature, and humidity. With such accurate control and the ability to manipulate cells in situ without altering the incubation environment, research into cell biology can be performed over a comprehensive range of oxygen tensions with precision (www.eppendorf.com/co2-incubators).

The touchscreen interface allows you to monitor all settings and eliminates the need for other dials, switches, and gauges. The transfer airlock provides effective cell ware transfer to and from the chamber. An optional removable front design allows for the setup of larger equipment needed inside the chamber. The ergonomic glove ports for gloved or bare hand working make the Hypoxystation comfortable for in situ manipulations.

This hypoxia workstation has been designed in conjunction with cell biology researchers to ensure ultimate performance combined with user comfort, convenience, and reliability. It has two sleeved ports on a removable (standard) front and one instant access port, and it has sufficient space to accommodate a variety of equipment inside the chamber while still providing a generous working and hypoxic incubation area (www.eppendorf.com/co2-incubators).

2.2.6.1. How the desired oxygen percentage was achieved in cells and verified

Achieving and verifying the desired oxygen percentage in a cell hypoxia chamber typically involves the following steps:

1. Calibration of the hypoxia chamber: Before the experiment, the hypoxia chamber was calibrated to ensure that it is functioning correctly and can maintain the desired oxygen percentage. This involves testing the oxygen sensors, checking the seals of the chamber, and verifying the flow rates of the gas mixtures.

2. Gas mixing: The gas mixture required to achieve the desired oxygen percentage is prepared using a gas mixer. This usually involves mixing nitrogen gas (which is used to decrease the oxygen concentration) with air or a gas mixture containing a higher oxygen concentration.

3. Oxygen control: After the gas mixture was prepared, it was circulated into the hypoxia chamber to displace the oxygen-rich air inside. The oxygen concentration inside the chamber was then monitored using

4. Oxygen sensor, and adjustments were made to the gas flow rates to maintain the desired oxygen percentage.

5. Verification: To verify that the desired oxygen percentage has been achieved and is being maintained, the oxygen concentration inside the chamber is monitored continuously during the experiment using an oxygen sensor. This ensures that any changes in oxygen concentration are detected and corrected in real-time.

In order to achieve the desired oxygen percentage of 0.3% in the hypoxia chamber in our study, we controlled the flow of gases into the chamber using precision gas flow meters and regulators. The chamber was first purged with a gas mixture containing a lower oxygen concentration, typically below 0.3%, until the desired level was reached. The chamber was then maintained at this oxygen level by adjusting the flow rates of the gas mixture containing oxygen and other gases, such as nitrogen and carbon dioxide.

The hypoxia chamber is also equipped with sensors to monitor and maintain the oxygen level within the chamber. These sensors measure the oxygen concentration and send feedback to the gas flow regulators, which adjust the flow rates accordingly to maintain the desired oxygen percentage of 0.3%.

In addition to precise gas flow control, the chambers are often sealed and insulated to prevent oxygen leaks or fluctuations from external sources. This helps to maintain the desired oxygen level within the chamber and ensure the accuracy and reproducibility of experiments conducted in hypoxic conditions.

2.2.6.2. Rationale for the hypoxia used in this study

Hypoxia, characterized by low oxygen concentration, has been suggested as a potential contributor to Alzheimer's disease (AD) pathology. AD brains often exhibit areas of hypoxia due to impaired blood flow, leading to cognitive decline and neuronal damage. In AD patients, particularly those with late-onset AD (LOAD) who are elderly, reduced cerebral blood flow can result in chronic hypoxia. Hypoxia has been shown to enhance the shift in amyloid precursor protein (APP) processing toward the amyloidogenic pathway and down-regulate the function of α-secretase, promoting the accumulation of amyloid-beta (Aβ) peptides, a hallmark of AD (Lall, 2019; Hassan and Chen, 2021).

Studies have demonstrated that hypoxia inhibits the expression and activity of neprilysin, an amyloid-degrading enzyme, leading to increased Aβ peptide accumulation (Lall, 2019). Hypoxia also exacerbates the neurotoxic effects of Aβ peptides, increasing the vulnerability of hippocampal neurons and contributing to neuronal death. Calcium dyshomeostasis, which is a fundamental mechanism in AD pathogenesis, is further exacerbated by the interaction between Aβ and the plasma membrane during hypoxia, resulting in elevated cytoplasmic calcium concentrations and neuronal excitability. Chronic hypoxia enhances calcium entry and mitochondrial calcium content, potentiating the posttranscriptional trafficking of L-type calcium channels. Additionally, both hypoxia and Aβ can activate microglia, leading to a maladaptive neuroinflammatory response (Lall, 2019).

Therefore, this study was conducted using hypoxia to gain valuable insights into the mechanisms underlying AD pathology. Hypoxia is commonly employed in such studies to mimic the hypoxic conditions observed in AD brains. By subjecting neurons and PC12 cells to hypoxia, we investigated the effects of oxygen deprivation on cellular function and the development of AD pathology. Hypoxia has been shown to increase the production of beta-amyloid, the accumulation of tau protein, and activate various signaling pathways involved in inflammation, oxidative stress, and cell death, all of which are implicated in AD pathogenesis. Exploring these pathways under hypoxic conditions in vitro can aid in identifying potential targets for drug development and therapeutic interventions for AD.

In summary, the use of hypoxia in this research provides a valuable tool for investigating the mechanisms underlying AD and identifying potential therapeutic targets.

2.2.7. BV2 Microglia cells

BV-2 cells are an immortal cell line frequently used as a substitute for primary microglia in pharmacological studies. They are derived from raf/myc-immortalized murine neonatal microglia and offer advantages such as cost-effectiveness and faster experimental turnaround compared to primary microglia (Henn, 2009; Lund, 2005). BV-2 cells express NADPH oxidase, which is associated with microglial-induced neuronal damage, making them a suitable model for studying microglial behavior (Wu, 2006; Yang, 2007). BV-2 cells closely resemble primary microglia in terms of cytokine secretion, which is an important aspect of this experiment (Lund, 2005).

BV2 cells were cultured in 75 cm2 tissue culture flasks using DMEM supplemented with 10% FBS, 100 IU/mL penicillin, and 100 µg/mL streptomycin. The cells were maintained in a humidified incubator at 37°C with 5% CO_2. When the cultures reached approximately 80% confluence, they were split. To split the cultures, the cells were washed twice with 5 mL Hanks

buffered saline solution (HBSS) at room temperature and then incubated with trypsin/EDTA until detachment. Trypsin action was stopped by adding 10 mL of growth medium to prevent cellular damage. The cells were then centrifuged at 100 x g for 5 minutes to harvest them. The cell pellet was resuspended in fresh growth medium and seeded into 96-well plates with 200 µL of growth medium in each well, at a density of 0.01 x 106 cells.

2.3. Drugs preparation

2.3.1. Rutin preparation

Rutin, a bioflavonoid antioxidant, was purchased from Sigma. It was initially dissolved in DMSO and subsequently diluted in the appropriate culture medium for treatment at the indicated concentrations. Rutin (100 µM) was co-administered with $A\beta_{25-35}$, and for the vehicle control group, a final concentration of 1% DMSO was used. The effect of rutin on $A\beta$ and $A\beta$ plus hypoxia ($A\beta$/hypoxia)-induced toxicity and apoptosis in PC12 cells and neurons was investigated. Cells were cultured in normoxia (21% O_2) and hypoxia (0.3% O_2). Rutin was co-administered with $A\beta$ in cells for 24 hours.

2.3.2 $A\beta_{25-35}$ Preparation

$A\beta_{25-35}$ (molecular formula: $C45H81N13014S$, molecular weight: 1060.27 Da), the most toxic peptide fragment derived from the amyloid precursor protein, was dissolved in deionized distilled water at a concentration of 1 mM. It was then allowed to aggregate and become toxic at 37°C for 4 days.

142

2.3.2.1. Validation/Normalized Aβ aggregation and determination of toxicity

Amyloid beta (Aβ) aggregates are important biomarkers for neurodegenerative diseases, such as Alzheimer's disease. Several techniques can be used to validate or normalize Aβ aggregation and determine its toxicity, which include:

- Thioflavin T (ThT) Assay: ThT is a fluorescent dye that specifically binds to Aβ aggregates. The ThT assay can detect Aβ aggregates and determine their relative levels. This method has been used in numerous studies to validate Aβ aggregation (Manno et al., 2020).

- Atomic Force Microscopy (AFM): AFM is a powerful imaging technique used to visualize and measure the size and shape of Aβ aggregates. AFM can also determine the toxicity of Aβ aggregates by measuring their mechanical properties, such as stiffness, and their interaction with cell membranes (Raman et al., 2013).

- Cell Viability Assays: Cell viability assays can assess the toxicity of Aβ aggregates on cultured cells. For example, the MTT assay measures mitochondrial activity, which is indicative of cell viability. This method has been used to demonstrate the toxic effects of Aβ aggregates on neuronal cells (Guntert et al., 2006).

- Immunohistochemistry: Immunohistochemistry can validate Aβ aggregation in brain tissue samples from animal models or human patients. This method involves staining brain tissue with antibodies that specifically bind to Aβ aggregates, which can then be visualized using microscopy (Wirths et al., 2004).

A combination of these methods can provide a comprehensive analysis of Aβ aggregation and toxicity. In this study, the normalization and determination of Aβ aggregation and toxicity were performed as follows:

Aβ$_{25-35}$ was prepared as a 1 mM stock in sterile ddH2O and incubated for 4 days at 37ºC to induce aggregation and toxicity (Lou, 2011; Xian, 2016). During days 1-3, there was no significant aggregation, but aggregation and toxicity were achieved on day 4. The Aβ$_{25-35}$ solution was then stored in the refrigerator at 4ºC for future use.

To confirm Aβ$_{25-35}$ aggregation, a Thioflavin T (ThT) fluorescence assay was performed to detect fibril formation. ThT assays measure changes in fluorescence using microscopy or spectroscopy. Spectroscopy assays monitor fibrillization over time, and although differences in binding have been observed, the size remains the same.

The Thioflavin T (ThT) fluorescence assay monitored fibrillization over time using a Tecan Infinite microplate reader. The results showed increased ThT binding in the Aβ$_{25-35}$ treated group compared to the control, which was statistically significant. Additionally, the toxicity of Aβ$_{25-35}$ was assessed using MTT and LDH release assays.

2.3.2.2. Determination of Aβ$_{25-35}$ toxicity

Following treatment, the toxicity of Aβ$_{25-35}$ was assessed using MTT and LDH release assays. Cell viability and cytotoxicity were evaluated using the MTT and LDH release assays, respectively. Cells were seeded on PDL pre-coated 96-well plates at a density of 1.2 x 104 cells/well and cultured in "complete" medium for 24 hours. The medium was then removed, the cells were washed twice with fresh medium, and fresh medium was added.

2.3.2.3. Quality control and storage of Aβ$_{25-35}$ aggregates

To ensure quality control and proper storage of Aβ$_{25-35}$ aggregates, the following steps were taken:

144

Quality Control: The quality of $A\beta_{25-35}$ aggregates can be checked using techniques such as circular dichroism (CD), transmission electron microscopy (TEM), or Thioflavin T (ThT) assay. These techniques confirm the formation of beta-sheet structures and the presence of fibrils (Saeedi et al., 2016). In this study, the quality control of $A\beta_{25-35}$ aggregates was evaluated using the Thioflavin T (ThT) assay.

Storage: Proper storage conditions are critical for maintaining the quality and stability of $A\beta_{25-35}$ aggregates. $A\beta_{25-35}$ aggregates can be stored as lyophilized powders at -20°C or lower temperatures (Saeedi et al., 2016). In this study, $A\beta_{25-35}$ was stored at -20°C, and to prevent protein degradation and aggregation, the samples were aliquoted to avoid repeated freeze-thaw cycles. After the formation of $A\beta_{25-35}$ aggregates, they were stored at 4°C.

Avoid Contamination: It is important to avoid contamination during the preparation and handling of $A\beta_{25-35}$ aggregates. Sterile techniques were employed, ensuring that all equipment and solutions were properly cleaned and sterilized. When working with $A\beta_{25-35}$ aggregates, appropriate safety precautions were taken, as the peptide can form toxic oligomers and fibrils. The work was conducted inside a fume hood, and appropriate personal protective equipment, such as gloves, lab coats, and safety goggles, were worn.

Record-Keeping: Accurate record-keeping of the preparation date, concentration, and storage conditions of $A\beta_{25-35}$ aggregates was maintained. This information can be helpful for future experiments and ensures that the aggregates are of good quality.

Use of Appropriate Controls: In the experiments using $A\beta_{25-35}$ aggregates, appropriate controls were used, including negative controls to account for non-specific binding or other experimental artifacts. This helps ensure that the observed effects are due to the $A\beta_{25-35}$ aggregates and not some

other factor. Proper quality control and storage of Aβ$_{25-35}$ aggregates ensure their quality and contribute to reliable and reproducible results in experiments.

2.3.2.4 Thioflavin T (ThT) Spectroscopic Assay

Thioflavin T (ThT) is a benzothiazole salt obtained through the methylation of dehydrothiotoluidine with methanol in the presence of hydrochloric acid. ThT is used as a dye to visualize and quantify the presence or fibrillization of misfolded protein aggregates or amyloid. The Thioflavin T (ThT) Assay measures changes in fluorescence intensity of ThT upon binding to amyloid fibrils. The enhanced fluorescence can be observed using fluorescence microscopy or spectroscopy. The spectroscopic assay is typically used to monitor fibrillization over time. The ThT stock solution is prepared by adding 8 mg of ThT to 10 mL of phosphate buffer (10 mM phosphate, 150 mM NaCl, pH 7.0), which is then filtered through a 0.2 µm syringe filter. The stock solution is stored in the dark and remains stable for about one week. The stock solution is diluted in phosphate buffer (1 mL of ThT stock to 50 mL of buffer) to generate the working solution. The fluorescence intensity of 1 mL of the working solution is measured by exciting at 450 nm and measuring emission at 482 nm over time. A small aliquot (5–10 µL) of untreated protein solution is added to the cuvette, stirred for 1 minute, and the intensity is measured over time. This serves as the control sample. Steps 3–4 are repeated with 5–10 µL of the aggregated protein solution. An intensity measurement above that of the control sample indicates the presence of amyloid fibrils. Fluorescence is measured using a 96-well black plate and a Tecan microplate reader with excitation at 450 nm and emission at 482 nm. Each reading represents the average of three values determined by a time scan after subtracting the fluorescence contribution from the control solution. Each assay is performed in triplicate.

2.4 Assessment of Cell Viability

After treatment, cell viability and cytotoxicity were assessed using the MTT assay and LDH release assay, respectively. Cells were seeded on poly-D-lysine (PDL) pre-coated 96-well plates at a density of 1.2×104 cells/well and cultured in complete medium for 24 hours. The medium was then removed, and the cells were washed twice with the medium before replacing it with fresh medium.

2.4.1 MTT Assays

Cell viability was evaluated by means of a standard colorimetric assay that measures the mitochondrial reductase-catalyzed reduction of yellow MTT to a purple formazan product. Mitochondrial activity was assessed by a standard colorimetric assay for mitochondrial succinate dehydrogenase which catalysed reduction of yellow MTT (3-(4, 5-dimethylthiazol-2-yl)-2, 5-diphenyltetrazolium bromide, a tetrazole) to a purple formazan product. The amount of colour formed is proportional to the sum of viable or metabolically active cells. Initially, MTT solution was prepared by dissolving 5 mg of MTT concentrate in 1 mL of D-PBS in the dark. 10 μL of the 5 mg/mL MTT solution diluted in Dulbecco's medium was added to the culture medium (final concentration, 0.5 mg/mL) at about four hours (4hrs) before the completion of the incubation period,. All samples were then incubated at 37°C under the treatment conditions. At the end of the treatment, the culture supernatant was aspirated, and the surviving cells were solubilized in 50 μL of DMSO and incubated for an additional 10 minutes at 37°C. The optical density (OD) value of each well was determined by measuring absorbance at 540 nm using a Tecan Infinite M200 PRO microplate reader (Tecan Group Ltd, Reading, UK). The absorbance reading of the DMSO background was subtracted from all sample absorbance readings, and the viability of cells for each treatment group was calculated based on Equation 1.

$$Cell\ viability = \frac{OD\ value(Experimental\ group)}{OD\ value(Control\ group)} \times 100\% \tag{1}$$

The viability of control cells in the complete medium was considered 100% viable, and the OD value of the control group was used to normalize the treatment samples. The results are expressed as the percentage of cells capable of reducing MTT.

2.4.2. LDH Release Assay

Lactate dehydrogenase (LDH) assay measures the LDH release in the culture media. LDH is a stable cytoplasmic enzyme present in all cells and catalyse the interconversion of lactate and pyruvate. When the plasma membrane of the cell is damaged, intracellular LDH is rapidly released into the culture supernatant. The LDH released is measured with an enzymatic assay, which results in the conversion of tetrazolium salt, iodonitrotetrazolium (INT) into a red formazan product in the presence of diaphorase. The amount of colour formed is proportional to the number of lysed cells. A non-radioactive cytotoxicity assay kit was used in this study, to evaluate the LDH, and the reagent containing tetrazolium salts was prepared by mixing 12 mL of assay buffer with substrate mix in the dark. After treatment, 50 µL of each sample media was transferred to an unused 96-well flat bottom plate, after which, 50 µL of the prepared reagent was added. The mixture was incubated at room temperature for 30 minutes, protected from light. After 30 minutes, 50 µL of stop solution was added to each well and mixed. Maximum LDH release control was generated by adding 10 µL 10x lysis solution to wells containing control cells, 45 minutes before adding the reagent mixture. Thereafter, the amounts of formazan dye formed were assessed by measuring the absorbance with a microplate reader at 490 nm. % LDH release was quantified using the equation below

$$Percent\ Cytotoxicity\ (\%) = 100 \times \frac{Experimental\ LDH\ Release}{Maximum\ LDH\ Release} \tag{2}$$

The data are presented as the mean percentage of LDH release from the maximum control.

2.5. Measurement of NO Production (Griess Assay)

The Griess assay is a commonly used method for measuring the production of nitric oxide (NO) in biological samples. To measure NO production using the Griess assay, the cell culture is treated with Griess reagent, which contains sulfanilamide and N-(1-naphthyl) ethylenediamine dihydrochloride (NED). The assay is based on the reaction between nitrite (NO_2-) and sulfanilamide under acidic conditions to form a diazonium salt. This diazonium salt can then react with NED to form a pink azo dye, which can be quantified using a spectrophotometer. The amount of nitrite in the sample is calculated based on a standard curve generated using known concentrations of sodium nitrite. The Griess assay is a simple and inexpensive method for measuring NO production, widely used in both basic research and clinical settings. However, it is important to note that the assay measures nitrite, a stable metabolite of NO, rather than NO itself. Therefore, other methods such as electron paramagnetic resonance (EPR) spectroscopy or fluorescent probes may be used to directly measure NO production. The Griess reagent was utilized to measure nitrate in the culture media. A sodium nitrate standard (1.56-100 μM) was added in a volume of 50 μL to generate a standard curve. Then, 50 μL of Griess reagent (1% sulfanilamide, 0.1% naphtylethylenediamine dihydrochloride in 2% phosphoric acid) was added to each well, including both the standard and experimental samples. The plate was incubated for 15 minutes at room temperature, and the absorbance was measured at 540 nm using a plate reader. Unknown concentrations were determined by linear regression analysis of the standard curve.

2.6. Hoechst-33342 Staining

Hoechst 33258 is a fluorescent dye commonly used for DNA staining in microscopy. Nuclear condensation can be observed using DNA-binding dyes like Hoechst 33258 or 4', 6-diamidino-2-

phenylindole (DAPI) under a conventional fluorescent microscope that emits light at ∼350 nm and transmits light at ∼460 nm. Hoechst stains are a family of fluorescent dyes used for labeling DNA in fluorescence microscopy. This dye is excited by ultraviolet light at around 350 nm and emits blue/cyan fluorescence light with a maximum emission at 461 nm. Hoechst stains can be used on live or fixed cells and are often an alternative to other nucleic acid stains like DAPI. Hoechst 33258 preferentially binds to adenine-thymine (A-T) regions of DNA, allowing it to observe nuclear condensation and distinguish apoptotic cells from healthy and necrotic cells. A 24-well plate containing 12 mm round coverslips coated with PDL was seeded with 2x105 cells/well in 500 μL of DMEM. The cells were then treated and fixed in 4% paraformaldehyde (PFA) for 15 minutes at room temperature, followed by washing with PBS. Hoechst stock solution (10 mg/mL) was diluted (1:2000) and added to the coverslips. The cells were incubated for 10 minutes at 37°C. The staining solution was removed, and the coverslips were washed with Dulbecco's phosphate-buffered saline (DPBS). Finally, the coverslips were mounted onto microscopic slides using Vectashield without DAPI. Images were obtained using an EVOS FL inverted microscope (Thermofisher, UK).

2.6.1. Quantification of Hoechst-33342 Staining

ImageJ software was employed to quantify the fluorescence intensity from Hoechst 33258-stained images. The following steps were followed:

1. Open the Hoechst-stained image in ImageJ.

2. Convert the image to 8-bit format by navigating to Image > Type > 8-bit.

3. Threshold the image by going to Image > Adjust > Threshold. Adjust the threshold until only the nuclei are selected.

4. Utilize the 'Analyze Particles' function by going to Analyze > Analyze Particles. Set the size range to select the nuclei and select 'Show Outlines' to verify if all the nuclei are selected.

5. Once all the nuclei are selected, the 'Analyze Particles' function will generate results with information on each nucleus.

6. To obtain the total fluorescence intensity of the nuclei, sum up the integrated density values from the results.

2.7. Flow Cytometry to Detect Apoptosis

The Guava Nexin Kit, which includes Annexin V and 7-amino-actinomycin D (7-AAD) double stain, was utilized to evaluate early apoptosis in cells. Annexin V is a calcium-dependent phospholipid-binding protein that specifically binds to phosphatidylserine (PS), a membrane component normally located on the inner face of the cell membrane. During early apoptosis, PS molecules are translocated to the outer surface of the cell membrane, where Annexin V can bind to them. On the other hand, 7-AAD is a dye that cannot penetrate viable cells but can enter dead or damaged cells. It binds to double-stranded DNA by intercalating between base pairs in G-C-rich regions. After cell treatment, 100 μL of cell suspension was transferred to a 1.5 mL microcentrifuge tube. To disrupt cell clusters, 50 μL of 0.8x Guava cell dispersal reagent was added to the tube and incubated for 20 minutes at 37°C. The cell suspension was then microcentrifuged for 5 minutes (14500g), and the culture media was removed. Next, 100 μL of DMEM and 100 μL of Guava Nexin reagent were added to the sample, which was then stained for 20 minutes at room temperature. The stained sample was acquired using a Guava easyCyte flow cytometer, and the data were analyzed using Guava analysis software. A total of 10,000 events within the gate were acquired for each sample, and three samples were acquired per condition.

The data were expressed as percentages of cells in each quadrant. Viable cells (Annexin V and 7-AAD negative cells) were located in the lower left quadrant, early apoptotic cells (Annexin V positive and 7-AAD negative cells) were located in the lower right quadrant, and necrotic/late apoptotic cells (Annexin V and 7-AAD positive cells) were located in the upper right quadrant.
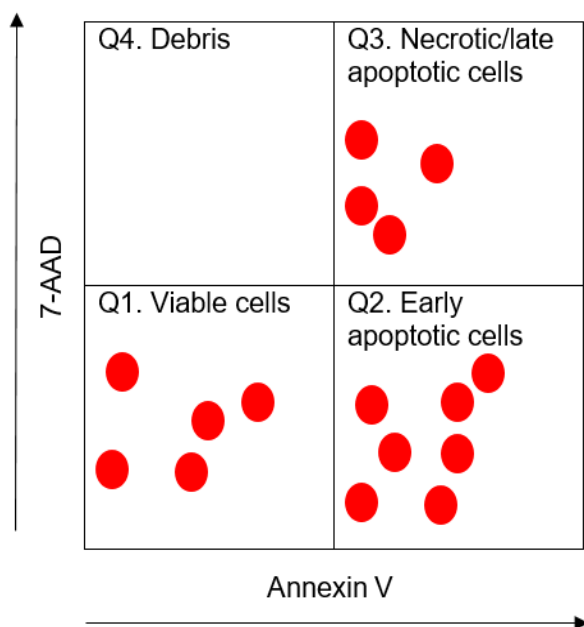
Figure 2.6 Schematic of Data Acquired by Flow Cytometry Using Annexin V/7-AAD Double Staining. The acquired data from flow cytometry were expressed as percentages of cells in each quadrant. Viable cells (Annexin V and 7-AAD negative cells) were represented in the lower left quadrant, early apoptotic cells (Annexin V positive and 7-AAD negative cells) were represented in the lower right quadrant, and necrotic/late apoptotic cells (Annexin V and 7-AAD positive cells) were represented in the upper right quadrant (Chen 2016; Vermes et al., 2000).

2.8. Measurement of Reactive Oxygen Species (ROS)

Intracellular oxidant production in PC12 cells was measured using a DCFDA cellular ROS detection assay kit (ABCam, ab113851). DCFDA, 2'7'-dichlorofluorescin diacetate, is a

fluorogenic dye that detects hydroxyl, peroxyl, and other ROS activity within the cell. After entering the cell, DCFDA is deacetylated by cellular esterases, resulting in a non-fluorescent compound. This compound is later oxidized by ROS into 2'7'-dichlorofluorescin (DCF), a highly fluorescent compound that can be detected by fluorescence spectroscopy with maximum excitation and emission spectra of 495nm and 529nm, respectively.

PC12 cells were seeded in a dark, clear bottom 96-well microplate with 25,000 cells per well and incubated overnight. The cells were then washed with 1x buffer and incubated with 25 μM DCFDA for 45 minutes at 37°C. Subsequently, the cells were washed with PBS and treated with water, $A\beta_{25-35}$ (30 μM), $A\beta_{25-35}$ (30 μM) + 1% DMSO, $A\beta_{25-35}$ (30 μM) + Rutin (50, 100, 200 μM) for 6 hours. After two washes with PBS, DCF fluorescence was measured using a Hitachi F-2000 Spectrofluorimeter (excitation: 485nm; emission: 535nm). The change was determined as a percentage of the control after subtracting the background.

2.9. Measurement of Malondialdehyde (MDA)

MDA, an index of lipid peroxidation, was measured using a commercial kit (ABCam, ab118970) based on the thiobarbituric acid (TBA) method. This kit detects free MDA, which forms adduct with TBA. If MDA is bound to collagen or other proteins, it will not be detected unless released. However, the acid treatment in the assay precipitates all proteins, so most of the MDA present in the sample should be free, allowing for the detection of total MDA.

PC12 cells cultured in T25 flasks were treated with water, $A\beta_{25-35}$ (30 μM), $A\beta_{25-35}$ (30 μM) + 1% DMSO, $A\beta_{25-35}$ (30 μM) + Rutin (50, 100, 200 μM) for 24 hours. The cells were then washed twice with PBS and homogenized with 303 μL of lysis solution (300 μL of MDA lysis buffer with 3 μL BHT [100x]) using a Dounce homogenizer (10-50 passes) on ice. BHT (butylated hydroxytoluene) was added to stop further sample peroxidation during processing. The homogenate was centrifuged

at 13,000g for 10 minutes to remove insoluble material. The supernatant was collected and mixed with 600 μL of TBA. The mixture was incubated at 95°C for 60 minutes and cooled to room temperature. Then, 200 μL of supernatant (containing MDA-TBA adduct) was transferred to a 96-well microplate. The plate was read at 532 nm using a Tecan Infinite M200 PRO microplate reader.

2.10. Mouse TNFα ELISA

The levels of TNFα in BV-2 cell culture media were determined using a mouse TNF-α DuoSet ELISA kit following the manufacturer's instructions. The capture antibody was coated onto a 96-well plate overnight at room temperature. The plate was then blocked with 300 μL of Reagent Diluent for 1 hour. Samples or standards diluted in Reagent Diluent (100 μL) were incubated for 2 hours. After three washes, 100 μL of the detection antibody was added and incubated for 2 hours. Following another three washes, 100 μL of Streptavidin-HRP was added and incubated for 20 minutes, protected from direct light. After three final washes, 100 μL of Substrate Solution was added and incubated for 20 minutes, protected from direct light. Then, 50 μL of Stop Solution was added, and the plate was read using a microplate reader set to 450 nm, with a reference reading at 540 nm to correct for optical imperfections in the plate. The TNFα concentrations were computed using standard curves derived from purified TNFα in the ELISA Kit.

2.11. Protein Extraction and Western Immunoblotting

2.11.1. Protein Extraction

PC12 cells were seeded into PDL-pre-coated T25 flasks at a density of 7×10^5 cells/ml in complete DMEM and grown to approximately 80% confluence at 37°C. After the indicated treatments, cells were washed twice with PBS to remove residual media. Cell extraction buffer was prepared on ice, containing 5 mL of 1x RIPA (radio-immune precipitation assay) buffer, 1 mM PMSF (50 μL), and 250 μL of protease inhibitor cocktail. Then, 130 μL of the cell extraction buffer was added to

each flask and mixed on orbital shakers for 15 minutes. The cells were scraped, sonicated (3 cycles of 10 seconds pulse with 5 seconds intervals), and centrifuged at 14,500g for 10 minutes. The supernatant was collected.

2.11.2. Protein Quantification

The protein concentration was determined using the Pierce BCA protein assay kit (Thermofisher, Loughborough, UK) according to the manufacturer's instructions. The Microplate Procedure was followed, using the dilution scheme for the microplate procedure for preparation of standards and working reagent. The working reagent was prepared by mixing 50 parts of BCA Reagent A with BCA Reagent B. Then, 25 µL of each sample was pipetted into a microplate well. 200 µL of the working reagent was added to each well, and the plate was thoroughly mixed on a plate shaker for 30 seconds. The plate was covered and incubated at 37°C for 30 minutes. After cooling to room temperature, the absorbance was measured at 562 nm on a plate reader. The average 562 nm absorbance measurement of the blank standard replicates was subtracted from the 562 nm measurements of all other individual sample replicates. A standard curve was prepared by plotting the average blank-corrected 562 nm measurement for each BSA standard against its concentration in µg/mL. The standard curve was then used to determine the protein concentration of each unknown sample as shown below.
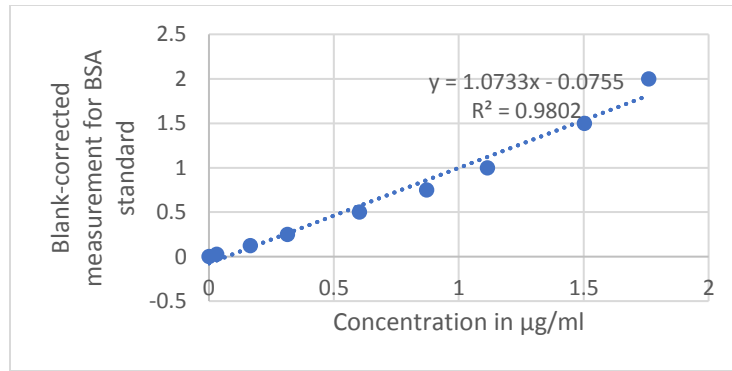
Figure 2.7 Standard curve indicating measurement for BSA standard. Standard curve for determination of the protein concentration of each unknown sample, prepared by plotting the average blank-corrected 562 nm measurement for each BSA standard against its concentration in µg/mL.

2.11.3. Western Immunoblotting

Samples were prepared by mixing 10 µL of 4x Laemmli buffer with the sample (30 µL) before denaturation at 100°C for 5 minutes. 4-15% Mini-PROTEAN TGX Precast polyacrylamide gels were then assembled within the Bio-Rad Mini-PROTEAN Tetra System and immersed in running buffer. Molecular weight standards (20 µL) and equal quantities of protein samples (20 µg/lane) were separated by SDS-polyacrylamide gel electrophoresis on the gel at 100V until the samples reached the gel end. Fractionated proteins were transferred and electroblotted to pre-treated 0.45 µm PVDF membranes under semi-dry conditions (Trans-Blot Cell, Bio-Rad, USA) at 11V for one hour. The membrane was blocked with 5% (fat-free) skimmed milk powder in PBS for one hour at room temperature to block non-specific binding sites (with agitation). The membrane was incubated with primary antibodies, anti-HIF-1α antibody (1:500 dilution) in 1% skimmed milk solution overnight at 4°C. The immunoblots were washed with TBST 3 times and incubated with the secondary antibody (anti-rabbit IgG HRP-conjugated antibody, 1:1000) for 1 hour at room

temperature. Membranes were washed extensively with TBS-T prior to development using an ECL solution (Thermofisher, U.K.) and imaged (FluorChem Western Blot imaging).

The blots were then stripped by mild stripping buffer and re-probed with rabbit polyclonal anti-β-actin (1:500) followed by the secondary antibody anti-rabbit IgG HRP-conjugated antibody (1:1000). The band densities were quantified by densitometric analysis using Image J software (Image J, NIH, Bethesda, USA) and were normalized to β-actin.

2.12. Measurement of gene expression by RT-qPCR

RNA extraction

Cells were split into 6-well plates and cultured overnight. Then, cells were treated with LPS (100 ng/mL), Amyloid-β $_{25-35}$ (30 μM), and/or rutin (100 μM) in triplicate for 24 hours. The RNA was extracted using either the column method (with the RNeasy Plus Mini Kit) or the TRIZOL method.

i.   Column method

The complete procedure for RNA (ribonucleic acid) extraction, conversion to cDNA (complementary deoxyribonucleic acid), and qRT-PCR (quantitative real-time polymerase chain reaction) using the column method is presented in Figure 2.5. RNA was extracted from cells using the RNeasy Plus Mini Kit. The cell pellet was harvested by transferring the cell suspension to a 15 mL falcon tube and centrifuging it (5 minutes, 100 rcf). Fixed cells were trypsinized (TrypLE) before centrifugation. Afterward, the supernatant was discarded, and 600 μL of RLT plus containing 40 μM dithiothreitol (DTT) was added to lyse the cell pellet and mixed thoroughly by pipetting. DTT is a reducing agent used to deactivate ribonuclease (RNase). The homogenized lysate was then transferred to the supplied generic DNA (gDNA) Eliminator spin column and centrifuged at 8000g for 30 seconds. The column was discarded, and the flow-through was mixed with an equal volume of 70% ethanol (which aids RNA precipitation). The sample was transferred

to the RNeasy spin column (700 µL at a time) and centrifuged (8000g for 15 seconds). The RNA pellets were washed with RW1 buffer (700 µL, 8000g for 15 seconds) and twice with RPE buffer (500 µL, 8000g for 15 seconds, then 8000g for 1 minute). The resulting RNA pellets were eluted in 50 µL of nuclease-free water, and the concentration was measured on the NanoDrop 1000 Spectrophotometer. The quality of the RNA samples was assessed using the 260/280 and 260/230 absorbance measurements.
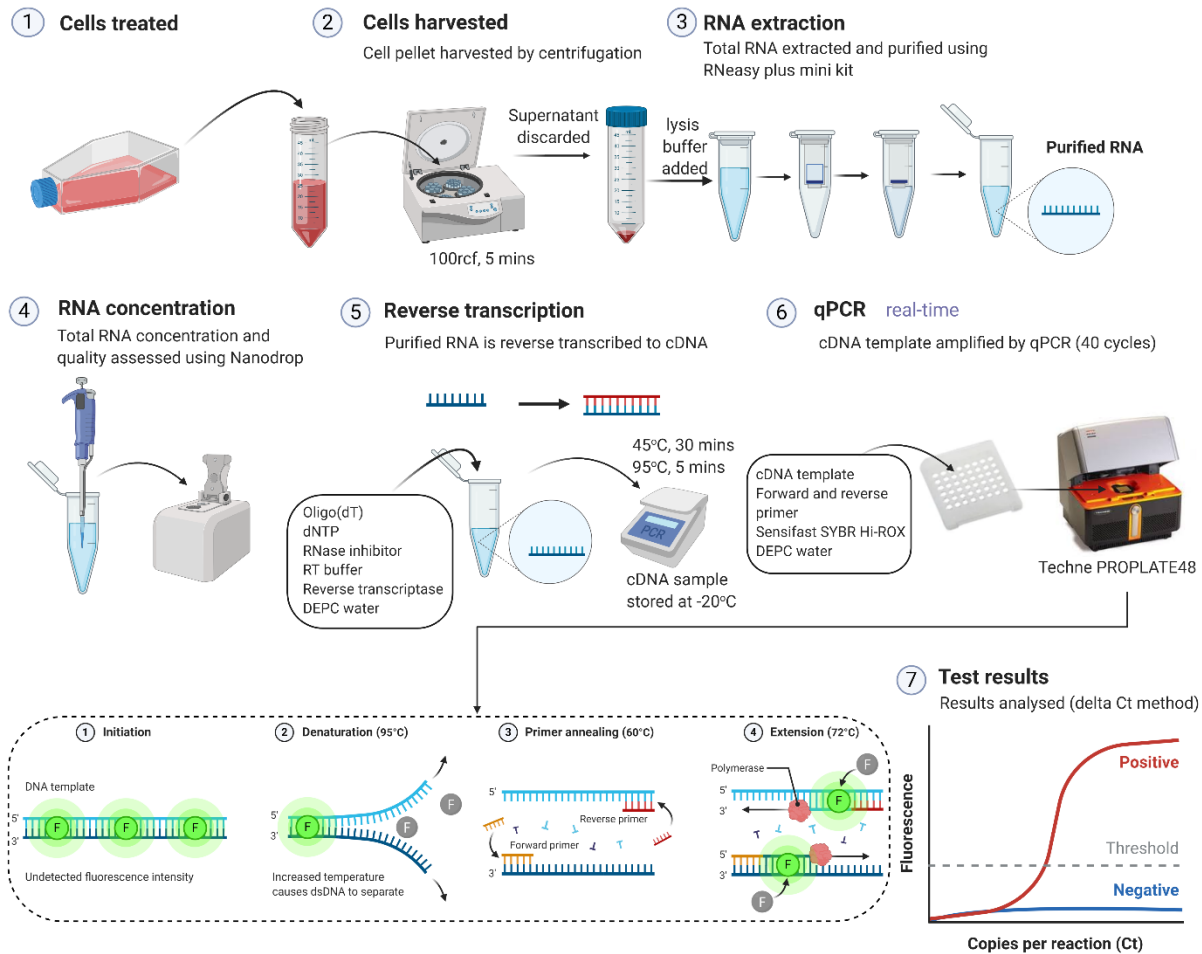
Figure 2.8 Procedure for determining gene expression through qRT-PCR. Total RNA was obtained using the RNeasy Plus Mini Kit, and the RNA quality and quantity were measured using a

NanoDrop. The RNA was converted into cDNA using the Tetro cDNA synthesis kit and quantified using qRT-PCR. The data obtained were analyzed using the delta Ct method (Singh et al., 2021).

ii.   TRIZOL method

The culture medium was removed, and cells were washed twice with 2 mL of ice-cold PBS. Then, 1 mL of TRIZOL reagent was added to lyse the cells. The cells were removed by scraping and trituration with a 1 mL pipette and transferred into 1.5 mL centrifuge tubes. Next, 0.2 mL of chloroform was added, vortex-mixed for 20 seconds, and then centrifuged (12,500 x g, 4°C, 15 minutes). The aqueous top layer was carefully removed and placed in a fresh tube. Then, 0.5 mL of isopropanol was added, vortex-mixed, and centrifuged (12,500 x g, 4°C, 10 minutes). The supernatant was removed (taking care not to disturb the white RNA pellets), and the RNA pellets were washed with 1 mL of 75% ethanol in each tube. The tubes were vortex-mixed and then centrifuged (7,500 x g, 5 minutes, 4°C), and the supernatant was discarded. The ethanol wash step was repeated once more, and then the pellet was allowed to air-dry for 5 minutes. Subsequently, 20 μL of RNAse- and DNAse-free water was added. The RNA concentration and purity were determined using Nanodrop spectrophotometry. The RNA concentration was measured by absorbance at 260 nm (A260) and was considered pure if the A260:A280 ratio was above 1.8 and the A260:A230 ratio was above 2.

iii.   Comparison of RNA yield between TRIZOL and column method of RNA extraction.

RNA was isolated from BV-2 cells using both the column and TRIZOL methods. TRIZOL, which is used for isolating both small and large RNA molecules, resulted in a higher yield of RNA compared to the column method. However, the column method was found to be easier and cleaner than the TRIZOL method (Table 2.1).

Table 2.1 Comparison of RNA yield between triazole and spin column methods

Samples	Triazole method			Column method		
	RNA (μg/ml)	260 :280 nm	260 : 230 nm	RNA (μg/ml)	260 :280 nm	260 : 230 nm
No1 C1	61.728	1.906	2.431	8.648	1.912	1.784
No1 C2	61.392	1.910	2.413	29.171	1.97	1.796
No1 C1	69.268	1.923	2.407	27.58	1.968	1.949
No1 C2	51.150	1.912	2.22	27.648	1.989	2.209
No1 C1	126.96	1.724	2.401	37.234	1.964	1.931
No1 C2	62.062	1.912	2.398	6.227	1.841	0.835

Table 2.1. Comparison of RNA yield between TRIZOL and column method of RNA extractions. TRIZOL is used for isolating both small and large RNA molecules, resulting in a higher yield of RNA compared to the column method. However, the column method is much easier and cleaner than the TRIZOL method.

cDNA generation

cDNA was generated from RNA using the Bio-Rad iScript cDNA synthesis kit. Fifteen microliters of RNA (specify the concentration if available) was incubated with 4 μL of 5x iScript Reaction Mix and 1 μL of iScript reverse transcriptase. The mixture was placed into a thermocycler following the reaction protocol: priming (5 minutes, 25°C); reverse transcription (20 minutes, 46°C); inactivation of reverse transcriptase (1 minute, 95°C) and then held at 4°C.

Real-time quantitative PCR (RT-qPCR)

RT-qPCR was used to investigate changes in gene expression, with Actin serving as a reference gene. The RT-qPCR was carried out with a 5 µL reaction volume (2.5 µL of 2x SensiFAST SYBR Hi-ROX Mix; 0.2 µL of 10 µM primer mix for both forward and reverse primers; 2.3 µL of cDNA) using the Techne Prime Pro 48 RT-qPCR system following the protocol. An initial activation step was performed for 2 minutes at 95°C, followed by 40 cycles of a 3-step cycling program consisting of 95°C for 5 seconds, 60°C for 10 seconds, and 72°C for 15 seconds. The primer sequences are described in Table 2.2.

Table 2.2 The primer sequences

IL-6:
F′, 5'CCA CTT CAC AAG TCG GAG GC, and R′, GGA GAG CAT TGG AAA TTG GGG T-3'
iNOS
(F) 5'□-GAACTGTAGCACAGCACAGGAAAT-3' and (R) 5' CGTACCGGATGAGCTGTGAAT-3'
TNF-α
(F) 5'-GCAACTGCTGCACGAAATC-3' (R) 5'-CTGCTTGTCCTCTGCCCAC-3'

This table presents the list of primers used for qRT-PCR studies along with their forward (FW) and reverse (RV) sequences.

After qPCR, the melt curves were assessed, and if concordant, those results were excluded from further analysis. Suitable reactions were then used to calculate the initial cDNA levels using the $2^{-\Delta\Delta Cq}$ method (Livak & Schmittgen, 2001). Changes in the gene of interest (GOI) expression were calculated relative to the average expression of three reference genes, as recommended by the MIQE guidelines (Bustin, 2009). For each sample, the Actin and TNFa, TGFβ, IL6, and NOS2 primers were used to measure whether a pre-set, quantifiable level of fluorescence was achieved in each of the samples' replicative cycles (e.g., $\Delta Cq = CqNOS2 - CqActin$). The relative abundance of cDNA in each sample was calculated from ΔCq, considering that each cycle leads to a twofold cDNA increase, resulting in increased fluorescence. The mean difference between control and treated samples ($\Delta\Delta Cq = \Delta Cqtreated - \Delta Cqcontrol$) was then calculated to determine the fold change ($2^{-\Delta\Delta Cq}$). This method generates data that exhibit a logarithmic normal distribution, which is suitable for graphical representation but cannot be statistically compared, except for identifying increases or decreases. Therefore, data analysis should be performed on $\Delta\Delta Cq$ data instead. The fold change can be calculated using the following equation:

$\Delta Cq = Cq$ (target gene) $- Cq$ (average of three reference genes)

$\Delta\Delta Cq = \Delta Cq$ (treated) $- \Delta Cq$ (untreated)

Fold change $= 2^{-\Delta\Delta Cq}$

2.13. Immunocytofluorescence

2.13.1 Quantification of Immunocytofluorescence Images

Immunofluorescence (IF) has emerged as an important method for biomedical research. With the development of antibodies targeted against specific proteins, IF is commonly used as a complementary tool for molecular profiling of tissue samples. This technique is valuable for

diagnostic purposes, such as subtyping diseases (e.g., tumors, inflammatory diseases, autoimmune disorders), as well as for evaluating the results of various experimental procedures in basic biomedical research. However, there are additional demands on IF/IHC-based research of human tissue samples, driven by the increasing complexity of molecular regulatory networks revealed through experiments on knockout animals, functional studies, and high-output analyses based on tissue homogenates (genome and proteome sequencing) (Huss and Coupland, 2020).

To determine the significance of a specific protein in cellular or tissue processes, it is necessary to quantify the staining in terms of "How much?" and "Where in the cell/tissue?" it is present, rather than simply observing the presence or absence of the signal (or staining) of that protein in the sample of interest. While the molecular function of a protein is determined by its biochemical properties, the cellular/tissue function of the protein is influenced by its spatial relationship with other proteins present in the same cellular/tissue compartment. These proteins may belong to a well-defined functional group and/or participate in interconnected regulatory pathways (Tummers and Thesleff, 2009; Roko Duplancic1 and Darko, 2021). IF signals possess three key properties:

i. Expression pattern: The expression pattern can be nuclear or nonnuclear (cytoplasmic, cell surface).
ii. Expression domain: The area occupied by the IF signal.
iii. Spatial gradient: How the IF signal is distributed within the cell/tissue based on the variation of its overall intensity.

Currently, there are software tools available for quantifying all these properties. While conventional computer-assisted scoring systems can quantify the expression patterns and expression domains of stained proteins, they often fail to quantify the spatial gradients of IF signals. This is not a major issue when quantifying protein markers expressed in well-defined cell

163

compartments (such as cell nuclei) or when their expression is localized to specific tissue structures that can be analyzed within smaller Regions-Of-Interest (ROIs) defined by the investigator (Riber-Hansen et al., 2012). However, the quantification of IF signals from ubiquitously expressed markers with non-nuclear expression patterns requires a different approach. This is primarily due to their typically large expression domains (which, in conventional approaches, would require selecting an increasing number of ROIs) and the fact that their spatial gradients are highly significant indicators of biological function (Rozario and DeSimone, 2010).

In summary, several methods can be used for the quantification of immunofluorescence images, including:

- Image analysis software: Various software tools, such as ImageJ, CellProfiler, and Fiji, are available for analyzing immunofluorescence images. These tools enable users to measure fluorescence intensity, analyze spatial patterns of fluorescence distribution, and perform colocalization analysis, among other features (Schindelin et al., 2015).

- Thresholding: This method involves setting a fluorescence intensity threshold to distinguish between positive and negative signals. It can be used to quantify the proportion of cells or regions with positive fluorescence signals (Peng and Thorn, 2017).

- Region of interest (ROI) analysis: ROI analysis entails selecting a specific area within the image and measuring fluorescence intensity within that area. This method is useful for quantifying the intensity of specific subcellular structures, such as the nucleus or cytoplasm (Carpenter et al., 2006).

- Automated image analysis: This approach utilizes machine learning algorithms to automatically identify and quantify immunofluorescence signals. It is particularly useful for high-throughput analysis of large datasets (Holtmaat et al., 2009).

164

- Colocalization analysis: Colocalization analysis involves examining the spatial relationship between two or more fluorophores within the image. This technique can quantify the degree of overlap between different markers and provide information about protein-protein interactions and subcellular localization (Costes et al., 2004).

2.13.2 Quantification of Tuj1+ Staining of Nuclei

Tuj1 staining is commonly used as a marker for neuronal cells. To quantify Tuj1 staining, we measured the proportion of cells that displayed positive staining for Tuj1. We first counted the total number of cells in the sample and then evaluated the number of cells that showed positive staining for Tuj1.

The sample was fixed and permeabilized, followed by incubation with an antibody against Tuj1. Images of the stained cells were acquired using an imaging system. To create a binary image, we applied a threshold to the images, where Tuj1-positive cells appeared as white and negative cells appeared as black. We then counted the number of Tuj1-positive cells by identifying cells that displayed the characteristic Tuj1 staining pattern, such as staining of neuronal axons. The total number of cells in the sample was also counted.

The percentage of Tuj1-positive cells was calculated by dividing the number of Tuj1-positive cells by the total number of cells and multiplying by 100. For example, we counted 200 cells and found that 132 of them were Tuj1-positive, the calculation would be as follows:

(132/200) x 100 = 66%

Therefore, we determined that 66% of the cells in the sample were positive for Tuj1 staining. Consequently, if 66% of the cells in a culture exhibit Tuj1 positivity, it indicates that 66% of the cells in the culture are neurons.

The remaining 34% of cells in the cultures may consist of other cell types, such as glial cells or non-neuronal cells. To detect and identify specific cell types, further analysis, staining, or cell sorting techniques may be required to characterize them. For instance, specific staining for glial cells or other neuronal markers can be employed to determine the proportion of each cell type in the culture. Microscopy can be used to count the number of cells stained with specific markers and calculate the percentage of each cell type. Neuronal markers like NeuN or MAP2 could be utilized to determine whether the Tuj1-negative cells are also neurons or if they belong to a different cell type. Alternatively, flow cytometry can be employed to analyze and quantify different cell types in a culture based on their specific markers.

Additional staining or cell sorting techniques may be necessary to further characterize the cell population.

2.13.3 Immunocytofluorescence Methodology

Primary neurons were grown on coverslips (1.5 x 105 cells) and subjected to the required treatments. After treatment, the coverslips were washed with PBS. Subsequently, 300 μL of 4% paraformaldehyde (PFA) was added to the coverslips and incubated for 20 minutes at room temperature on an orbital shaker. PFA serves as a fixative agent that reacts with the primary amines on proteins, forming cross-links known as methylene bridges. The PFA solution was then aspirated, and the coverslips were washed three times with PBS.

To permeabilize the cell membranes, 0.5% Triton X-100 in PBS was applied to the coverslips for 15 minutes at room temperature, followed by three washes with PBS. Non-specific binding sites were blocked by incubating the coverslips in a solution of 3% BSA in 0.1% PBS-Tween for 1 hour. After blocking, the blocking solution was aspirated. The primary antibody, Mouse monoclonal anti-Tubulin β3 (clone Tuj1) (Biolegend, USA, Cat # 801201), was prepared in 1%

BSA in 0.1% PBS-Tween. The antibody solution was added to the coverslips, including a negative control well without the primary antibody, and incubated overnight at 4°C.

Following the incubation with the primary antibody, the cells were washed three times with PBS and then incubated with the corresponding fluorescein isothiocyanate (FITC)-conjugated secondary antibody. The secondary antibody solution, prepared in 1% BSA in 0.1% PBS-Tween at a dilution factor of 1:200, was applied to the coverslips and incubated for 3 hours at room temperature. Subsequently, the cells were washed three times with PBS.

To mount the coverslips onto microscopic slides, Vectashield with DAPI (4',6-diamidino-2-phenylindole) was used. Finally, images were captured using the Nikon Eclipse 80i fluorescence microscope with a Hamamatsu digital camera, utilizing NIS-Element BR 3.22.14 software.

Primary antibody	Dilution factor
Mouse monoclonal anti-Tubulin β 3 (clone Tuj1) (Biolegend, USA, Cat # 801201)	1:1000
Rabbit polyclonal anti-GFAP (glial fibrillary acidic protein) (Agilent (DAKO), UK**, Cat # Z0334)**	1:500
Rabbit polyclonal anti-Map2 (microtubule-associated protein 2) (Abcam, UK, Cat # ab5392)	1:1000

2.14. Data Analysis

The data were presented as the mean value ± standard error of the mean (S.E.M). To ensure accuracy and consistency of the data, experiments using the 96-well plate reader were performed with 3-8 well replicates in each plate. The experiments were replicated at least three times. The normality of the data was assessed using the D'Agostino & Pearson normality test. In cases where the data were not normally distributed, the non-parametric Kruskal-Wallis test was performed for analysis of multiple groups (three or more datasets). For data with a normal distribution, unpaired two-tailed t-tests were used for comparisons of a single dataset against a control, and one-way ANOVA with Tukey's multiple comparison post-hoc test was used for comparisons of multiple groups against a time-matched control group. GraphPad PRISM 7 for Windows version 7.04 (GraphPad Software, Inc., CA, USA) was used for the analysis. A value of $P < 0.05$ was considered statistically significant, while a value of $P < 0.01$ was considered statistically highly significant.

Statistical analysis of the summary of the dose-response curve (half-maximal effective concentration (IC50/EC50) and maximum dose response) represents the behavior of the curve. The curves were generated from semilogarithmic plots, and the parameters derived from these curves were log-normally distributed (Kenakin 2014).

The IC50/EC50 values were calculated using GraphPad Prism software, which automatically generates these values using the following equation:

$$Y = Bottom + (Top-Bottom)/(1+10^{((LogEC50-X)\ *Hillslope)})$$

Chapter 3

RUTIN PROTECTS RAT PHEOCHROMOCYTOMA (PC12 CELLS) FROM Aβ$_{25-35}$ TOXICITY IN BOTH NORMOXIC AND HYPOXIC CONDITIONS

3.1. INTRODUCTION

The Aβ peptide is recognized as a peptide that aggregates and deposits in the brain tissue of AD patients, leading to the formation of senile or amyloid plaques. These neuritic plaques are the main pathological hallmark of AD. Aβ is a 4.2 kDa short peptide consisting of 40–42 amino acids, generated from the intracellular cleavage of the amyloid precursor protein (APP) by the sequential action of two proteolytic enzymes, beta- (β-) secretase and gamma- (γ-) secretase. The prevalent species are the 40- and 42-amino acid residue peptides, Aβ1–40 and Aβ1–42, with the latter being less abundant but more toxic (Benilova, 2012). Shorter variants of Aβ resulting from truncation by various proteases have also been found in the human brain. Among these variants, the 11-amino acid residue peptide Aβ$_{25-35}$ (GSNKGAIIGLM) is highly cytotoxic and has been extensively studied to understand the mechanism of Aβ action and modulation of its toxicity (Millucci, 2010; Daluz, 2017; Song, 2018). The Aβ$_{25-35}$ segment of Aβ plays a significant role in the aggregation and cytotoxicity of the peptide (Peters, 2016). Similar cytotoxic effects, including DNA damage, transcription dysregulation, and apoptosis, have been reported for Aβ$_{25-35}$ and Aβ$_{1-42}$, suggesting that these peptides may share a common mechanism of toxicity (Cardinal, 2012). Furthermore, studies on Aβ$_{25-35}$-membrane interactions indicate that the peptide can bind to membranes, insert into them, and form ion-conducting pores (Discala, 2014; Kandel, 2017; Smith, 2018).

In addition to the deposition of extracellular amyloid-β plaques and intracellular tau protein tangles, which are hallmark features of AD pathology, there are many functional disturbances in synapses and mitochondria, vascular disorders, and aberrant changes in microglia and astrocytes

(Querfurth and LaFerla, 2010; De Strooper and Karran, 2016). The molecular link between ischemia/hypoxia and APP processing has only recently been established.

There are many hypotheses regarding the pathogenesis of AD, including the amyloid cascade (Selkoe, 1991), tau hyperphosphorylation (Frost *et al*., 2009), neurotransmitters, and oxidative stress (Butterfield *et al*., 2019). However, the underlying causes and ideal treatment plans remain elusive. Currently, only a few drugs are available that merely improve symptoms, primarily targeting Aβ and tau, but do not delay the progression of the disease. Researchers are beginning to explore new theories of AD pathogenesis from different perspectives, including gamma oscillations, prion transmission, cerebral vasoconstriction, the growth hormone secretagogue receptor 1α (GHSR1α)-mediated mechanism, and infection. Discoveries in these areas may provide insights into the pathological mechanisms of AD and lead to the development of potential effective treatment strategies.

Among the hallmarks of AD pathology, such as the deposition of extracellular amyloid-β plaques and intracellular tau protein tangles, along with various functional disturbances in synapses, mitochondria, vascular disorders, and aberrant changes in microglia and astrocytes (Querfurth and LaFerla, 2010; De Strooper and Karran, 2016), the molecular link between ischemia/hypoxia and amyloid precursor protein (APP) processing has only recently been established. The development of neuroimaging techniques has revealed that many brain regions predisposed to AD pathology exhibit a significant decline in cerebral blood flow even at the stage of mild cognitive impairment preceding AD diagnosis. Non-invasive studies consistently support the histopathological observations showing widespread cerebral amyloid angiopathy (CAA) in the hippocampus and many regions of the cerebral cortex in AD patients (Attems et al., 2004; Jeynes and Provias, 2006). This brain hypoperfusion reduces oxygen and glucose delivery, thereby inducing local hypoxia,

which in turn stimulates Aβ production in both endothelial cells and neighboring neurons, leading to the generation of CAA (Pluta et al., 2013a, b; Belyaev et al., 2010; Dela Torre, 2000). It has been reported that sporadic AD could be initiated by ischemic episodes that activate APP processing and increase Aβ production (Belyaev *et al*., 2010). There is convincing evidence that hypoxia-inducible factor-1α (HIF-1α) activates both β and γ secretases, augmenting APP processing and Aβ production in hypoxia (Belyaev *et al*., 2010).

In this chapter, the responses of PC12 cells to Aβ aggregates were evaluated in terms of cell viability, apoptosis, ROS formation, and lipid peroxidation. These studies aimed to establish a suitable in vitro model of AD and investigate the neuroprotective effect of rutin (a bioflavonoid glycoside) on Aβ toxicity under normoxic and hypoxic conditions. The study aims to characterize the effects of hypoxia on Aβ-induced neurotoxicity in PC12 cells and evaluate the neuroprotective potential of rutin on Aβ toxicity in normoxic and hypoxic conditions.

The main objectives of the study include: studying the dose-related $Aβ_{25-35}$-induced toxicity of PC12 cells under hypoxic and normoxic conditions and characterizing the neuroprotective effects of rutin on $Aβ_{25-35}$-induced toxicity of PC12 cells under hypoxic and normoxic conditions.

Rationale for the conducted studies:

The challenges posed by an aging population and the significant financial impact on the healthcare system necessitate the development of novel diagnostic, preventive, and treatment strategies for dementia, particularly AD. Currently, autopsy or brain biopsy is the only definitive means of diagnosis. In clinical practice, the diagnosis is typically based on medical history and findings from the Mental Status Examination (Mosconi et al., 2010). Symptomatic therapies are the only available treatment strategies for AD. Current pharmacological treatments aim to improve

dementia symptoms and delay further deterioration (Tabet et al., 2006). In the UK, there are four drugs licensed for the treatment of AD. The three acetylcholinesterase (AChE) inhibitors, namely donepezil, galantamine, and rivastigmine, recommended by the National Institute for Health and Clinical Excellence (NICE), are used to treat mild to moderate dementia in AD. AChE inhibitors alleviate AD symptoms by augmenting acetylcholine signaling, exerting anti-inflammatory effects by decreasing the level of free radicals and amyloid toxicity, and reducing cytokine release from activated microglia (Tabet *et al*., 2006).

Memantine, which is a glutamate receptor antagonist, is recommended for patients with moderate to severe AD. Blocking the NMDA receptors antagonizes the elevated glutamate levels in the AD brain, inhibiting overstimulation of NMDA receptors and calcium influx (Turner et al., 2014). These treatments can only improve cognition and memory but do not inhibit the progression of the disease (Liao et al., 2015). Therefore, the development of new treatments is essential for AD, considering the antioxidant activities, neuroprotective effects, and inhibitory activities of AChE and self-induced Aβ1-42 aggregation (Liao et al., 2015). Hence, there is a need to identify a new treatment strategy for the cure of the disease.

Rutin is a naturally occurring flavonoid glycoside found in many foods and fruits, and it has numerous pharmacological effects such as antioxidant, anti-inflammatory, and cytoprotective functions. Rutin can inhibit aggregation and cytotoxicity of Aβ, inhibit mitochondrial damage, and decrease the production of ROS (Wang, 2012). Several studies have demonstrated that rutin can interfere with the aggregation and toxicity of Aβ, inhibit oxidative stress induced by Aβ, reduce Aβ42 levels in mutant human APP overexpressing cells, and reduce senile plaques in the brains of APP transgenic mice (Jimenez-Aliaga, 2011; Xu, 2014; Yu, 2015). Research investigating the blood-brain barrier (BBB) penetration of rutin in vivo using a rat model revealed that after

172

intravenous administration, rutin was able to penetrate the BBB and accumulate in the brain. The brain-to-plasma concentration ratio of rutin was 0.42, indicating moderate BBB penetration (Kim et al., 2014). Thus, rutin may serve as a novel drug for the treatment of AD due to its ability to scavenge free radicals and inhibit oxidative stress.

In addition, by subjecting neurons and PC12 cells to hypoxia, we investigated the effects of oxygen deprivation on cellular function and the development of AD pathology because studies have shown that hypoxia can increase the production of beta-amyloid and promote the accumulation of tau protein, which are also associated with the disease. Additionally, hypoxia can activate a variety of signaling pathways in cells, including those involved in inflammation, oxidative stress, and cell death, all of which are implicated in AD pathogenesis. By studying these pathways in vitro under hypoxic conditions, we can identify potential targets for drug development and therapeutic interventions for AD.

Furthermore, current research on AD treatment is conducted in normoxia, which does not truly reflect AD pathogenesis. Therefore, this study was conducted using hypoxia to provide valuable insights into the mechanisms underlying AD pathology. Hypoxia is often used in these studies as a means of imitating the hypoxic conditions observed in AD brains. Hence, the use of hypoxia in this research provides a useful tool for investigating the mechanisms underlying the disease and identifying potential therapeutic targets.

3.2. MATERIALS AND METHODS

PC12 cells were cultured according to the procedures described in Section 2.1.

3.2.1. Treatment

Confluent PC12 cells were used for the experiments. The complete media (100%) was aspirated, and the cells were washed twice with media prior to the experiments. $A\beta_{25-35}$ was prepared in aggregation form and applied to the cells. Cell viability and cytotoxicity were determined by MTT and LDH assays, respectively. Once the EC50 was determined, a single dose of $A\beta_{25-35}$ aggregates was used for the toxicity study and rutin treatment study. Rutin was initially dissolved in DMSO and subsequently diluted in the appropriate culture medium to the indicated concentrations. Rutin (100 μM) was co-administered with $A\beta_{25-35}$, and for the vehicle control group, a final concentration of 1% DMSO was used throughout. We investigated the effect of rutin on $A\beta_{25-35}$ and $A\beta_{25-35}$ plus hypoxia (0.3% O2) induced toxicity and apoptosis in PC12 cells. PC12 cells were treated under normoxia and hypoxia conditions for a duration of 24 hours.

Treatment for determination of EC50:

The treatment is divided into two groups: Group A (normoxia) and Group B (hypoxia).

Group A (normoxia):

Group 1: Negative control (H2O)

Group 3: Graded doses of $A\beta_{25-35}$ (3-70 μM)

The cells were plated in a 96-well plate. Experiments involving the use of the 96-well plate were performed with 3-8 well replicates per plate. The experiments were replicated at least three times. After the treatment, the cells were immediately incubated in a standard incubator with a humidified atmosphere containing 21% O2 and 5% CO2 at 37°C for 24 hours.

Group B (hypoxia):

Group 1: Negative control (H_2O)

Group 3: Graded doses of Aβ25-35 (3-70 μM)

The cells were plated in a 96-well plate. Experiments involving the use of the 96-well plate were performed with 3-8 well replicates per plate. The experiments were replicated at least three times. After the treatment, the cells were immediately incubated in a purpose-built INVIVO2 400 humidified hypoxia workstation (0.3% O2, 5% CO2, 94% N2) at 37°C. The media in filter-capped flasks was placed within the hypoxia workstation for 24 hours before use to deplete oxygen. After 24 hours of treatment in both conditions, cell viability and cytotoxicity were evaluated using MTT and LDH assays, respectively.

Treatments for viability and cytotoxicity studies in normoxic and hypoxic conditions:

The treatment is divided into two groups: Group A (normoxia) and Group B (hypoxia).

Group A (normoxia):

Group 1: Negative control (H_2O)

Group 2: Negative control (1% DMSO + H_2O)

Group 3: 30 μM Aβ25-35

Group 4: 30 μM Aβ25-35 + 1% DMSO

Group 5: Rutin 100 μM + 30 μM Aβ25-35

Group 6: Rutin + H_2O

The cells were plated in a 96-well plate. Experiments involving the use of the 96-well plate were performed with 3-8 well replicates per plate. The experiments were replicated at least three times. After the treatment, the cells were immediately incubated in a standard incubator with a humidified atmosphere containing 21% O2 and 5% CO2 at 37°C for 24 hours.

Group B (hypoxia):

Group 1: Negative control (H2O)

Group 2: Negative control (1% DMSO + H2O)

Group 3: 30 μM Aβ$_{25-35}$

Group 4: 30 μM Aβ$_{25-35}$ + 1% DMSO

Group 5: Rutin 100 μM + 30 μM Aβ$_{25-35}$

Group 6: Rutin + H2O

The cells were plated in a 96-well plate. Experiments involving the use of the 96-well plate were performed with 3-8 well replicates per plate. The experiments were replicated at least three times. After the treatment, the cells were immediately incubated in a purpose-built INVIVO2 400 humidified hypoxia workstation (0.3% O2, 5% CO2, 94% N2) at 37°C. The media in filter-capped flasks was placed within the hypoxia workstation for 24 hours before use to deplete oxygen.

After 24 hours of treatment in both conditions, cell viability and cytotoxicity were evaluated using MTT and LDH assays, respectively.

Treatments for determination of apoptosis of PC12 cells in normoxic and hypoxic conditions:

The treatment is divided into two groups: Group A (normoxia) and Group B (hypoxia).

Group A (normoxia):

Group 1: Negative control (1% DMSO + H_2O)

Group 2: 30 μM $A\beta_{25-35}$ + 1% DMSO

Group 3: Rutin 100 μM + 30 μM $A\beta_{25-35}$

The cells were plated in T25 flasks. After the treatment, the cells were immediately incubated in a standard incubator with a humidified atmosphere containing 21% O_2 and 5% CO_2 at 37°C for 24 hours.

Group B (hypoxia):

Group 1: Negative control (1% DMSO + H_2O)

Group 2: 30 μM $A\beta_{25-35}$ + 1% DMSO

Group 3: Rutin 100 μM + 30 μM $A\beta_{25-35}$

The cells were plated in T25 flasks. After the treatment, the cells were immediately incubated in a purpose-built INVIVO2 400 humidified hypoxia workstation (0.3% O_2, 5% CO_2, 94% N_2) at 37°C. The media in filter-capped flasks was placed within the hypoxia workstation for 24 hours before use to deplete oxygen.

After 24 hours of treatment in both conditions, the evaluation of ROS, annexin V and 7-AAD, determination of cell apoptosis by Hoechst 33258 staining, Tuj1 and DAPI stained nuclei immunofluorescence images, and determination of lipid peroxide were carried out in both conditions. Two treatment conditions, normoxia (Nx) and hypoxia (Hx), were used in the study. For normoxia (Nx), the cells were placed in a standard incubator with a humidified atmosphere containing 5% CO_2 at 37°C.

3.2.2. Timeline of PC12 cell treatment.
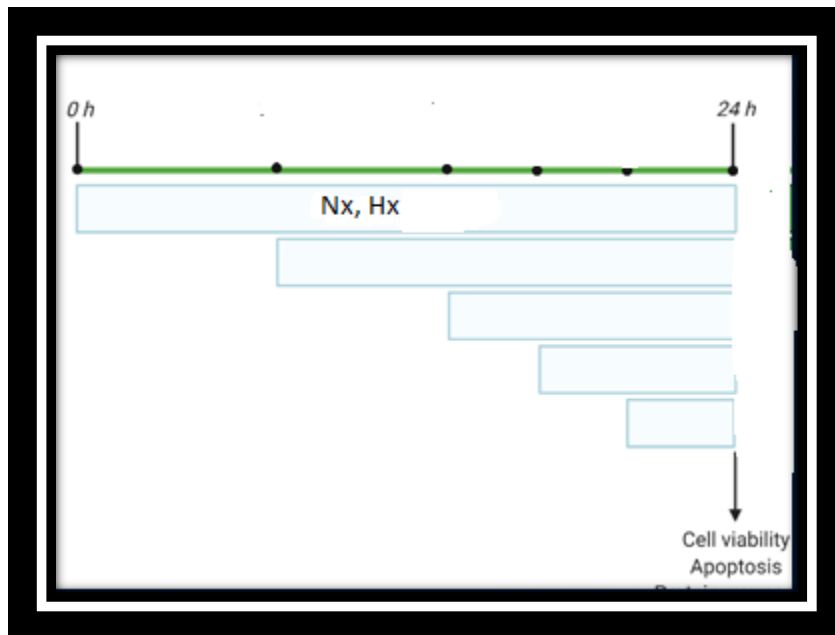
Figure 3.1 Timeline of PC12 cell treatment. PC12 cell cultures were established, and the onset of treatment was indicated as 0 hours [normoxia (Nx), hypoxia (Hx)] for a duration of 24 hours. All conditions were initiated simultaneously to ensure the experiments were completed together.

3.2.3. Experimental timeline for the hypoxia condition

Two treatment conditions, Normoxia (Nx) and hypoxia (Hx), were used in the study. For normoxia (Nx), the cells were placed in a standard incubator with a humidified atmosphere containing 21% O_2 and 5% CO_2 at 37°C. For hypoxia (Hx), the cells were placed in a purpose-built INVIVO2 400 humidified hypoxia workstation (0.3% O_2, 5% CO_2, 94% N_2) at 37°C. The media in filter-capped flasks was placed within the hypoxia workstation for 24 hours before use to deplete oxygen. We investigated the effects of Aβ and Aβ plus hypoxia and also evaluated the effect of rutin on Aβ and Aβ plus hypoxia (Aβ/hypoxia)-induced toxicity and apoptosis in PC12 cells and neurons for 24 hours. Rutin was co-administered with Aβ in both cell types for 24 hours.
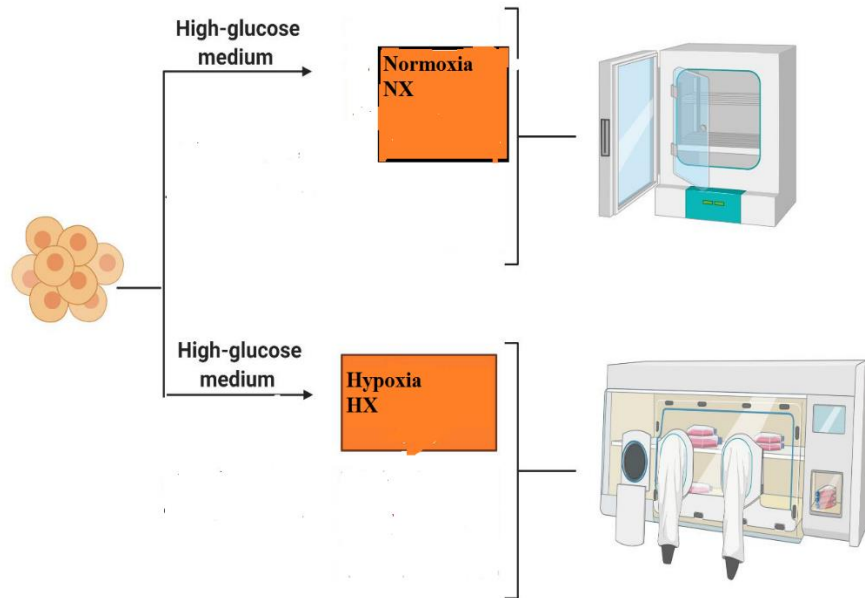
Figure 3.2 Illustration of the different treatment conditions i.e., the procedure for applying Normoxia (Nx) and hypoxia (hx) to the cells. For normoxia (Nx), the cells were placed in a standard incubator using a humidified atmosphere containing 21% O2 and 5% CO2 at 37°C for 24hrs. For hypoxia (Hx), the cells were placed in a purpose-built INVIVO2 400 humidified hypoxia workstation (0.3% O2, 5% CO2, 94% N2) at 37°C for 24 hours to deplete oxygen (Singh et al., 2021).

3.2.4. Data analysis

In this study, "n" represents the number of experiments performed on cells derived from separate flasks (different streams of cultured cells). For each biological replicate, at least three technical replicates were performed. In experiments using 96-well plates, at least eight well replicates were performed on each plate. The dataset obtained for each treatment condition was independent of other conditions (i.e., independent sampling; one rat, one number). The data obtained from each biological replicate were averaged. The data were represented as mean ± standard deviation (S.D.). Normality of the data was tested using the Anderson-Darling normality test. For normally

distributed data, one-way or two-way ANOVA with Tukey's post hoc analysis was performed. For data that were not normally distributed, the non-parametric Kruskal-Wallis test was used. PRISM version 8 (GraphPad Software Inc., CA, USA) for Windows version 10 was used for all data analysis. Values of $p < 0.05$ were considered statistically significant.

3.3. RESULTS

3.3.1. A$\beta_{25\text{-}35}$ Preparation

A$\beta_{25\text{-}35}$ was prepared as a 1 mM stock solution in sterile ddH2O and incubated for 4 days at 37ºC to induce aggregation and toxicity (Lou, 2011; Xian, 2016). No significant aggregation was observed on days 1-3, but aggregation and toxicity were achieved on day 4. Cell viability and cytotoxicity were evaluated using MTT and LDH release assays, respectively. The aggregated A$\beta_{25\text{-}35}$ was then stored at 4ºC in the refrigerator for future use. The aggregation and toxicity were not altered when stored at 4ºC for several weeks. Cell viability and cytotoxicity were still determined using MTT and LDH release assays with the aggregated A$\beta_{25\text{-}35}$ stored at 4ºC.

To confirm A$\beta_{25\text{-}35}$ aggregation, a Thioflavin T (ThT) fluorescence assay was performed to confirm fibril formation. ThT assays measure changes in fluorescence microscopy or fluorescent spectroscopy. The spectroscopy assays monitor fibrillization over time, and although differences in binding have been observed, the size remains the same.

The Thioflavin T (ThT) fluorescence assay monitored fibrillization over time using fluorescent spectroscopy with a Tecan Infinite microplate reader. The results showed increased ThT binding in the A$\beta_{25\text{--}35}$ treated group compared to the control, which was statistically significant (Figure 3.3).
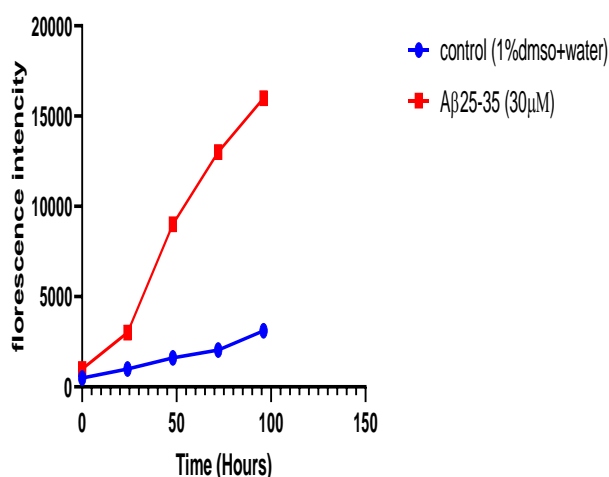
Figure 3.3. Confirmation of Aβ₂₅₋₃₅ aggregation. Aβ₂₅₋₃₅ (30 μM) aggregation was monitored by ThT fluorescence. Fluorescence intensity was measured at an excitation wavelength of 450 nm and an emission wavelength of 482 nm. There is statistical significant increased in ThT binding in Aβ₂₅₋₃₅ treated group compared to the control (1% DMSO +H₂O). The asterisks (*** indicate high significance (P<0.001) of the variable doses of Aβ₂₅₋₃₅ compared to the control group

3.3.2 Effects of Aβ₂₅₋₃₅ aggregate on PC12 cells under normoxia and hypoxia conditions.

3.3.2.1. Effects of Aβ₂₅₋₃₅ on PC12 cell viability (MTT assay) under normoxia and hypoxia, and determination of IC50

In Figure 3.4, PC12 cells were exposed to different concentrations of Aβ₂₅₋₃₅ (ranging from 0 to 70 μM) for 24 hours under normoxia and hypoxia conditions, and their viability was assessed using MTT assays. Treatment of PC12 cells with Aβ₂₅₋₃₅ for 24 hours under normoxia conditions resulted in a significant decrease in MTT activity (Figure 3.4A). There was a statistically significant decrease in MTT activity between the control group and the treatment groups with varying concentrations of Aβ₂₅₋₃₅ (P<0.001, n=5). The mean values for different concentrations were as follows: 3 μM (mean=71.85 ± 2.99), 5 μM (mean=70.34 ± 1.69), 10 μM (mean=68.97 ± 2.58), 20

181

µM (mean=58.29 ± 3.24), 30 µM (mean=37.24 ± 4.94), 40 µM (mean=32.59 ± 5.48), 50 µM (mean=25.03 ± 3.38), 60 µM (mean=19.67 ± 2.97), and 70 µM (mean=14.77 ± 4.12), Figure 3.4 A(i). The IC50 value was calculated as 30,44µM based on the relationship between cell viability measured by MTT activity and doses of $A\beta_{25\text{-}35}$ concentrations, Figure 3.4A (ii).

Treatment of PC12 cells with $A\beta_{25\text{-}35}$ for 24 hours under hypoxia conditions resulted in a significant decrease in MTT activity (Figure 3.4B). There was a statistically significant decrease in MTT activity between the control group and the treatment group of PC12 cells with varying concentrations of $A\beta_{25\text{-}35}$ ($P<0.001$, n=5). The decrease in MTT activity was higher compared to normoxia conditions. The mean values for different concentrations were as follows: 3 µM (mean=69.41 ± 3.39), 5 µM (mean=67.94 ± 2.03), 10 µM (mean=61.98 ± 4.49), 20 µM (mean=55.50 ± 2.08), 30 µM (mean=48.40 ± 3.39), 40 µM (mean=33.40 ± 3.40), 50 µM (mean=25.50 ± 1.08), 60 µM (mean=17.50 ± 4.01), and 70 µM (mean=10.70 ± 3.16) (Figure 3.4B(i). Figure 3.4B (ii) illustrates the percent viability of $A\beta_{25\text{-}35}$-induced PC12 cells (MTT assays) under hypoxia. The relationship between cell viability measured by MTT activity and doses of $A\beta_{25\text{-}35}$ is shown.
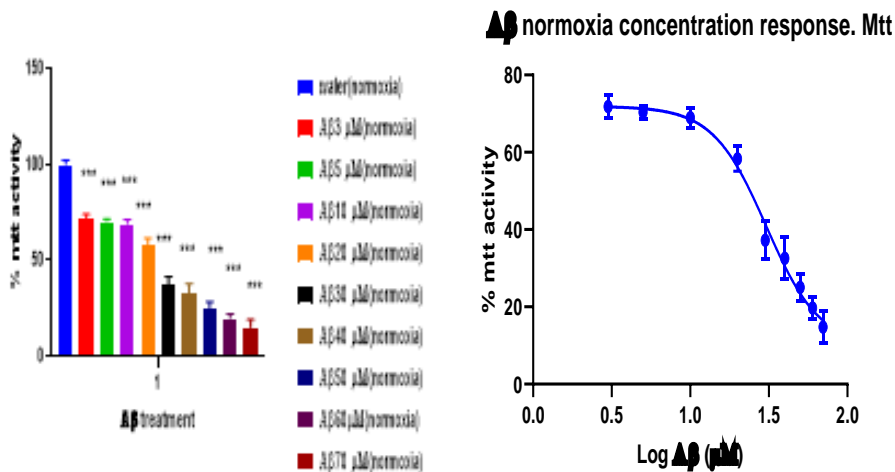
| Figure 3.4A (i) | Figure 3.4A (ii) |
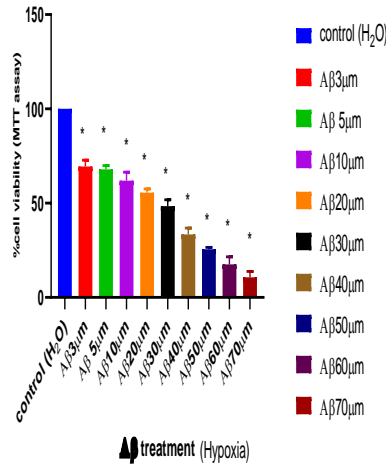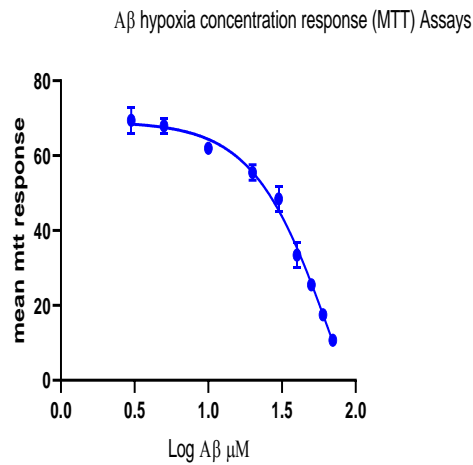
Figure 3.4B (i)   **Figure 3.4B (ii)**

Figure 3.4. Percentage viability (MTT assays) induced by Aβ₂₅₋₃₅ on PC12 cells under normoxic and hypoxic conditions. Figure 3.4A shows percentage of cell viability (MTT assays) by Aβ₂₅₋₃₅ on PC12 cells under normoxia. There is a statistically significant decrease in MTT activity between the treatment groups at 3 μM, 5 μM, 10 μM, 20 μM, 30 μM, 40 μM, 50 μM, 60 μM, and 70 μM of Aβ₂₅₋₃₅ for 24 hours (P<0.001) compared to the control group (n=5). The asterisks (*** indicate high significance (P<0.001) of the variable doses of Aβ₂₅₋₃₅ compared to the control group in normoxia (Figure 3.4A (i). Figure 3.4A (ii): Percent of cell viability of Aβ₂₅₋₃₅-induced PC12 cells (MTT assays) in normoxia. Relationship between cell viability measured by MTT activity and doses of Aβ₂₅₋₃₅ concentration in μM/mL. Figure 3.4B: Percentage viability (MTT assays) by Aβ₂₅₋₃₅ on PC12 cells under hypoxia. There is a statistically significant decrease in MTT activity between the treatment groups at 3 μM, 5 μM, 10 μM, 20 μM, 30 μM, 40 μM, 50 μM, 60 μM, and 70 μM of Aβ₂₅₋₃₅ for 24 hours (P<0.001) compared to the control group (n=6). The asterisk (*) represents significance (P<0.001) of variable doses of Aβ₂₅₋₃₅ compared to the control group in hypoxia (Figure 3.4B (i). The decrease in MTT activity is higher compared to that in normoxia.

Figure 3.4B (ii): Percent viability of Aβ$_{25-35}$-induced PC12 cells (MTT assays) in hypoxia. Relationship between cell viability measured by MTT activity and doses of Aβ$_{25-35}$ concentration.

3.3.2.2. Effects of Aβ$_{25-35}$ on PC12 cell cytotoxicity (LDH assay) in normoxia and hypoxia, and determination of EC50

Figure 3.5 represents Aβ$_{25-35}$-induced LDH release on PC12 cells in normoxia and hypoxia for 24 hours. There is a statistically significant increase in LDH activity of PC12 cells in normoxia between the treatment groups at 10 μM, 20 μM, 30 μM, 40 μM, 50 μM, 60 μM, and 70 μM of Aβ$_{25-35}$ for 24 hours (P<0.001) compared to the control group (n=5) (Figure 3.5A). The mean values for the treatment groups were as follows: 10 μM (mean=18.77 ± 3.28), 20 μM (mean=23.60 ± 5.00), 30 μM (mean=35.03 ± 2.20), 40 μM (mean=49.26 ± 3.21), 50 μM (mean=55.29 ± 2.10), 60 μM (mean=63.29 ± 3.13), and 70 μM (mean=68.28 ± 1.68) (Figure 3.5A (i). Percent cytotoxicity of Aβ$_{25-35}$-induced PC12 cells (LDH assays) in normoxia. Relationship between cell cytotoxicity measured by LDH activity and doses of Aβ$_{25-35}$ concentration. The EC50 was found to be 35.70 μM (Figure 3.5A (ii).

Aβ$_{25-35}$ induced LDH release in PC12 cells under hypoxia for 24 hours, and there is a higher increase in toxicity compared to normoxia (Figure 3.5B). Figure 3.5B (i) and 3.5B (ii) shows the percentage of cell cytotoxicity (LDH assays) of Aβ$_{25-35}$ on PC12 cells under hypoxia. There is a statistically significant increase in LDH activity between the treatment groups at 10 μM, 20 μM, 30 μM, 40 μM, 50 μM, 60 μM, and 70 μM of Aβ$_{25-35}$ for 24 hours (P<0.001) compared to the control group (n=5). The mean values for the treatment groups were as follows: 10 μM (mean=31.11 ± 1.87), 20 μM (mean=35.16 ± 2.65), 30 μM (mean=61.08 ± 1.67), 40 μM (mean=66.13 ± 1.73), 50 μM (mean=79.65 ± 2.43), 60 μM (mean=85.65 ± 1.22), and 70 μM (mean=91.65 ± 0.01). The increase in toxicity is higher in hypoxia (P<0.001) compared to the

control group (n=5) 3.5B (i). 3.5B (ii) shows Percent cytotoxicity of $A\beta_{25-35}$-induced PC12 cells (LDH assays) in hypoxia. Relationship between cell cytotoxicity measured by LDH activity and doses of $A\beta_{25-35}$ concentration.
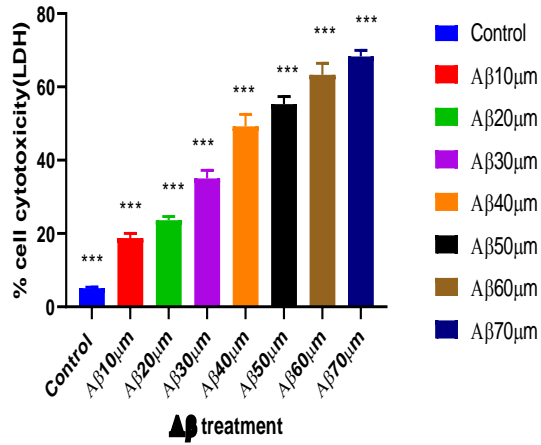
Figure 3.5 A (i)
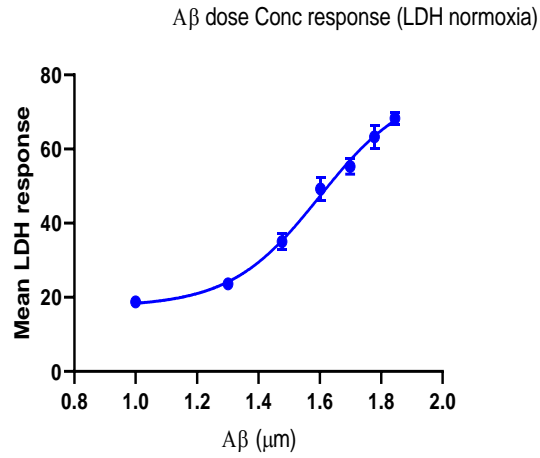
Figure 3.5 A(ii)
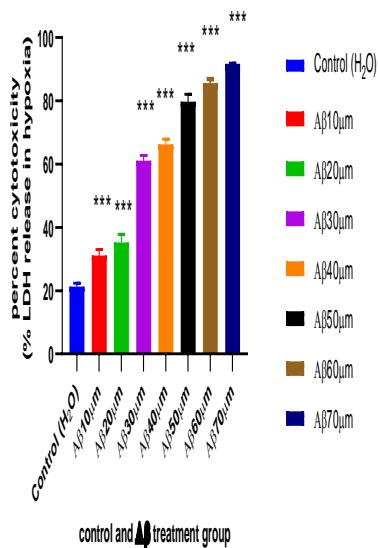
Figure 3.5 B (i)
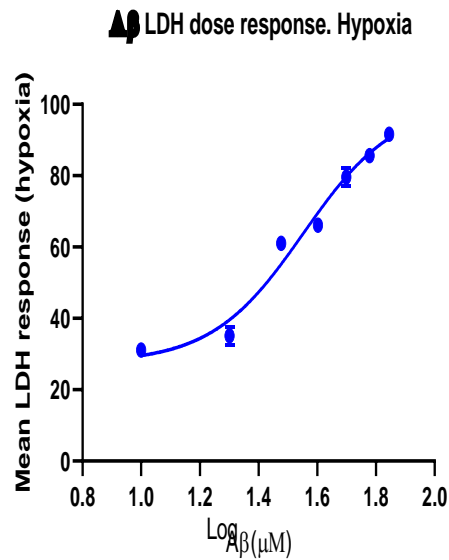
Figure 3.5 B (ii)

Figure 3.5 Percentage of cell cytotoxicity (LDH assays) induced by $A\beta_{25-35}$ on PC12 cells in normoxia and hypoxia. In Figure 3.5A(i), there is a statistically significant increase in LDH activity of PC12 cells in normoxia between the treatment groups at 10 μM, 20 μM, 30 μM, 40 μM,

50 μM, 60 μM, and 70 μM of Aβ25-35 for 24 hours (P<0.001) compared to the control group (n=5). The asterisks (*** in the figure) represent significant differences (P<0.001) between the variable doses of Aβ25-35 and the control group in normoxia. Figure 3.5A (ii) shows the relationship between cell cytotoxicity measured by LDH assays in normoxia and the doses of Aβ25-35 concentration. Figure 3.5B (i) shows the percentage of cell cytotoxicity (LDH assays) induced by Aβ25-35 on PC12 cells in hypoxia. There is a statistically significant increase in LDH activity between the treatment groups at 10 μM, 20 μM, 30 μM, 40 μM, 50 μM, 60 μM, and 70 μM of Aβ25-35 for 24 hours compared to the control group (n=5). The increase in toxicity is higher than that in normoxia (P<0.001). The asterisks (*** in the figure) represent significant differences (P<0.001) between the variable doses of Aβ25-35 and the control group in hypoxia. Figure 3.5B (ii) shows the relationship between cell cytotoxicity measured by LDH assays in hypoxia and the doses of Aβ25-35 concentration.

3.3.2.3. Confirmation of hypoxia (0.3% O2) treatment with HIF-1 accumulation in PC12 cells by western blotting

After determining the IC50, a concentration of 30 μM was used for the remaining experiments in PC12 cells. The cells were treated with 30 μM Aβ25-35 aggregates for 24 hours under both normoxia and hypoxia conditions (0.3% O2). The hypoxia treatment was confirmed by observing HIF-1 accumulation in the cells, as demonstrated in the western blotting experiment shown in Figure 3.6. In Figure 3.6A, the images represent HIF-1 alpha levels in PC12 cells, while Figure 3.6B presents the data in the form of a bar chart.
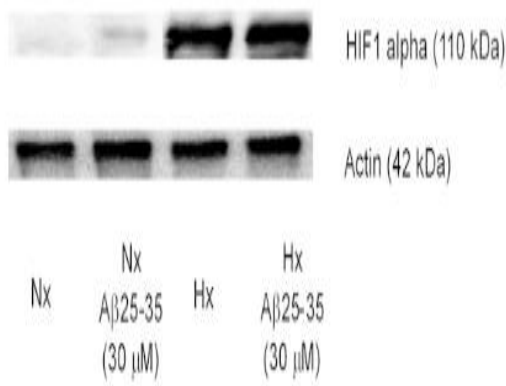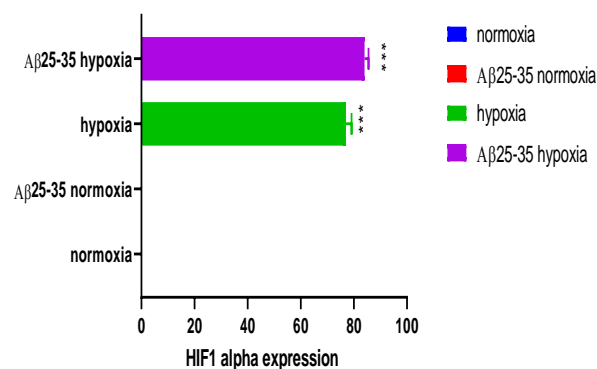
Figure 3. 6A   **Figure 3. 6B**

Figure 3.6. HIF activation in PC12 cells under hypoxia (0.3% O2). Figure 3.6A represents western blotting images of HIF1 alpha in PC12 cells under normoxia (Nx) conditions with and without Aβ25-35 aggregates, as well as under hypoxia (Hx) conditions with and without Aβ25-35 aggregates. Figure 3.6B shows a graph representing HIF1 alpha expression. No HIF1 alpha accumulation was observed in normoxia, while significant accumulation of HIF1 alpha was observed in PC12 cells under hypoxia conditions with and without Aβ25-35 aggregates. The asterisk (*) indicates significant difference of hypoxic group with and without Aβ25-35 aggregates (p < 0.05), when compared to control in normoxia with and without Aβ25-35 aggregates respectively.

3.3.2.4. Comparing the MTT activity and LDH release of Aβ25-35 (30 μM) under Normoxia and Hypoxia for 24 hours

As shown in Figure 3.7, PC12 cells were exposed to 30 μM of Aβ25-35 for 24 hours under normoxia and hypoxia conditions, and their viability and cytotoxicity were assessed using MTT and LDH assays. Treatment of PC12 cells with 30 μM Aβ25-35 for 24 hours under normoxia conditions resulted in a significant decrease in MTT activity (Figure 3.7A) (P<0.001) (n=5). Treatment of

187

PC12 cells with 30 μM Aβ$_{25-35}$ for 24 hours under hypoxia conditions also resulted in a significant decrease in MTT activity (Figure 3.7A), and the decrease was greater compared to that observed under normoxia conditions, with a mean value of 57.09 ± 2.98 in normoxia and 34.94 ± 3.03 in hypoxia.

Similarly, treatment of PC12 cells with 30 μM Aβ$_{25-35}$ for 24 hours under normoxia conditions resulted in a significant increase in LDH release (Figure 3.7B) (P<0.001) (n=5). Treatment of PC12 cells with 30 μM Aβ$_{25-35}$ for 24 hours under hypoxia conditions also resulted in a significant increase in LDH activity (Figure 3.7B), and the increase was higher compared to that observed under normoxia conditions, with a mean value of 35.41 ± 2.39 in normoxia and 61.94 ± 1.03 in hypoxia.
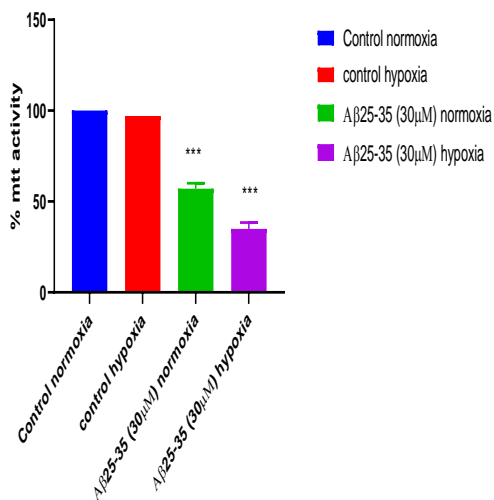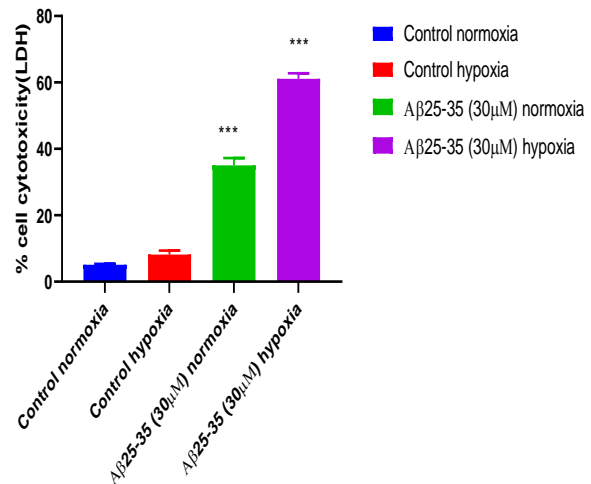
Figure 3.7A   Figure 3.7B

Figure 3.7. Comparing percentage cell viability (MTT assays) and cytotoxicity induced by Aβ$_{25-35}$ on PC12 cells under normoxic and hypoxic conditions. In figure 3.7A, there was a statistically significant decrease in MTT activity in the treatment group (30 μM Aβ$_{25-35}$) compared to the

control group (Figure 3.7A) (P<0.001) (n=5). The asterisks (***) represent a highly significant difference (p<0.001) of the treatment group (30 μM Aβ25-35) in both normoxia and hypoxia compared to the control group. Treatment of PC12 cells with Aβ25-35 for 24 hours in both normoxia and hypoxia resulted in a significant decrease in MTT activity. Similarly, treatment of PC12 cells with Aβ25-35 for 24 hours under normoxia conditions resulted in a significant increase in LDH release (Figure 3.7B) (P<0.001) (n=5). Treatment of PC12 cells with Aβ25-35 for 24 hours under hypoxia conditions resulted in a significant increase in LDH activity (Figure 3.7B). The asterisks (***) represent a highly significant difference (p<0.001) between the treatment group (30 μM Aβ25-35) in both normoxia and hypoxia compared to the control group.

3.3.2.5. Aβ25-35 induces PC12 cell apoptosis in both normoxia and hypoxia

Flow cytometry analysis using Annexin V/7-AAD double staining was performed to assess the level of apoptosis in both normoxia and hypoxia (Figure 3.8). Cells in the lower left quadrant represent viable cells, cells in the lower right quadrant represent early apoptosis, and cells in the upper right quadrant represent late apoptosis/necrosis. As shown in Figure 3.8C, a significant number of cells were undergoing early apoptosis after 24 hours of treatment with 30 μM Aβ25-35 in normoxia. In Figure 3.8D, the number of cells undergoing apoptosis was higher in hypoxia compared to normoxia. Figure 3.8E represents a graph showing the mean ± SE (n=3) for all the measurements. Figure 3.8A and 3.8B represent the control groups under normoxia and hypoxia, respectively.
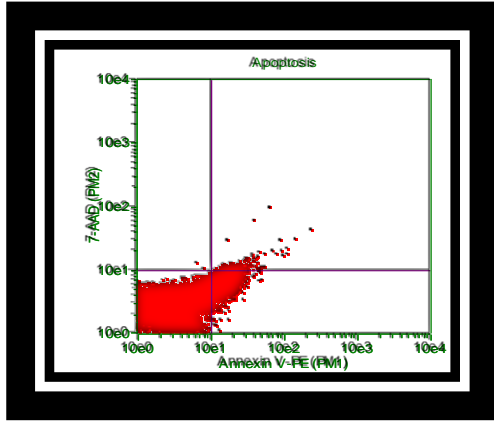
Figure 3.8A
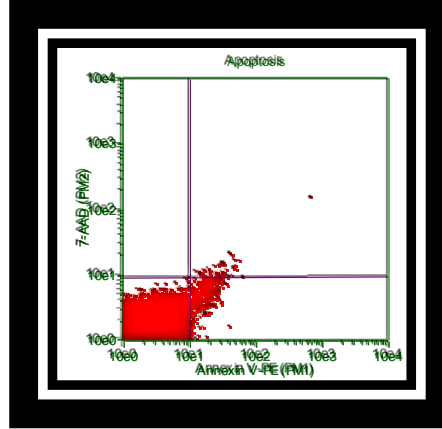
Figure 3.8B
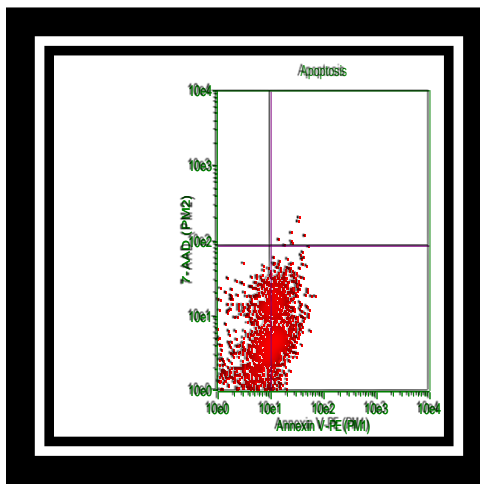
Figure 3.8C
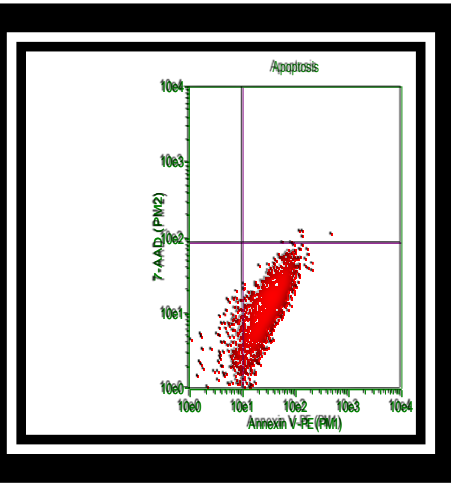
Figure 3.8D
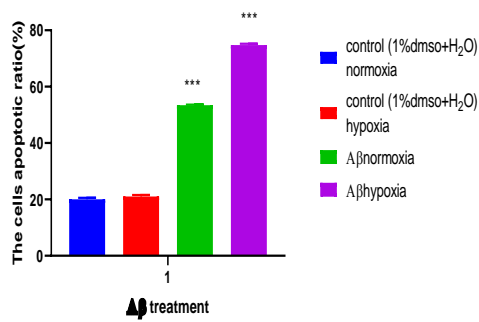
Figure 3.8E

Figure 3.8 . FACS analysis (Annexin V/7-AAD) of PC12 cells exposed to: 3.8A) control (1%

DMSO + water) in normoxia, 3.8B) control (1% DMSO + water) in hypoxia, 3.8C) 30 μM Aβ$_{25\text{-}35}$

for 24 hours in normoxia, and 3.8D) 30 μM Aβ$_{25\text{-}35}$ for 24 hours in hypoxia. Cells in each quadrant

were analyzed using FLOWJO software. Cells in the lower left quadrant represent viable cells, cells in the lower right quadrant represent early apoptosis, and cells in the upper right quadrant represent late apoptosis/necrosis. The mean ± SE (n=3) for all the measurements are shown in the graph, 3.8E. The asterisks (*** indicate high significance (P<0.001) between (30 μM Aβ$_{25-35}$) in normoxia and hypoxia group, compared to their respective control (water + 1% DMSO) in both normoxia and hypoxia.

3.3.2.6. Aβ$_{25-35}$ increases ROS levels in PC12 cells under both normoxia and hypoxia

As shown in Figure 3.9, ROS generation was measured by DCFDA flow cytometry. PC12 cells were exposed to: (Figure 3.9A) control (1% DMSO + water) in normoxia conditions, (Figure 3.9B) control (1% DMSO + water) in hypoxia conditions, (Figure 3.9C) 30 μM Aβ$_{25-35}$ for 24 hours in normoxia, and (Figure 3.9D) 30 μM Aβ$_{25-35}$ for 24 hours in hypoxia. The mean ± SE (n=3) for all the measurements is shown in the graph, Figure 3.9E. Results were analyzed by flow cytometry. Forward scatter represents the (DCFDA) ROS level, and side scatter represents the size of the cells. In normoxia conditions, the ROS level significantly increased in cells treated with 30 μM Aβ$_{25-35}$ compared to the control (mean = 25.72 ± 1.35). In hypoxia conditions, the ROS level significantly increased in cells treated with 30 μM Aβ$_{25-35}$ compared to the control (mean = 64.54 ± 0.82).
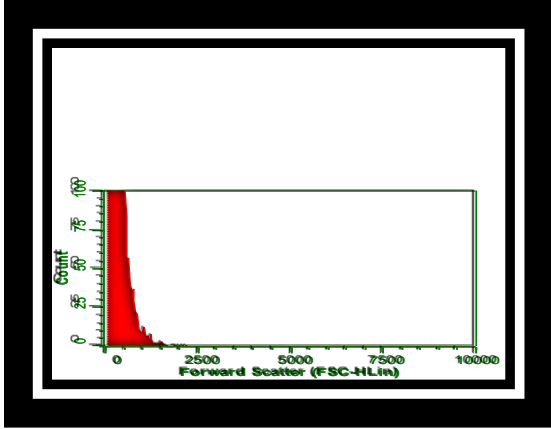
Figure 3.9A
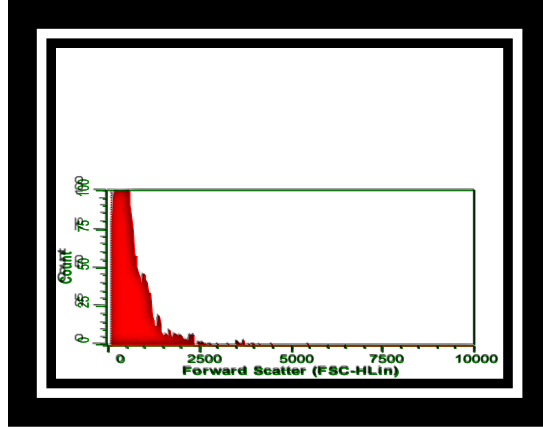
Figure 3.9B
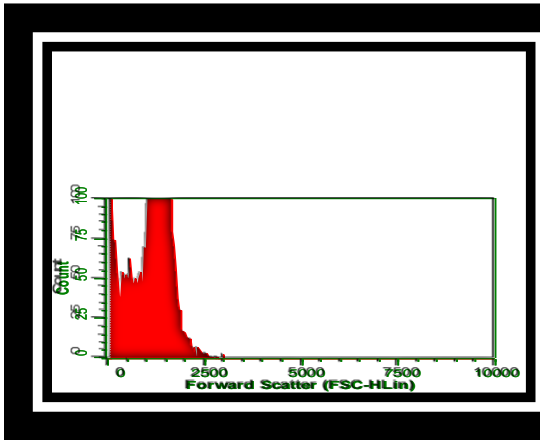
Figure 3.9C
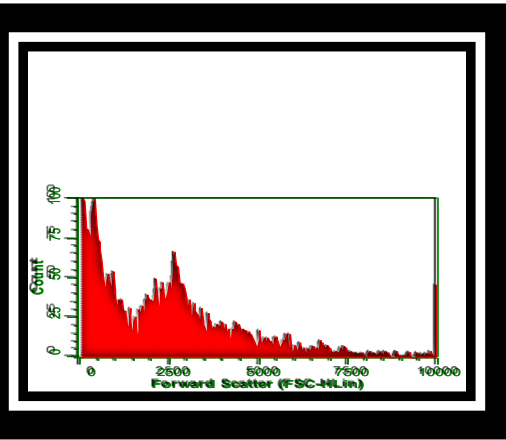
Figure 3.9D
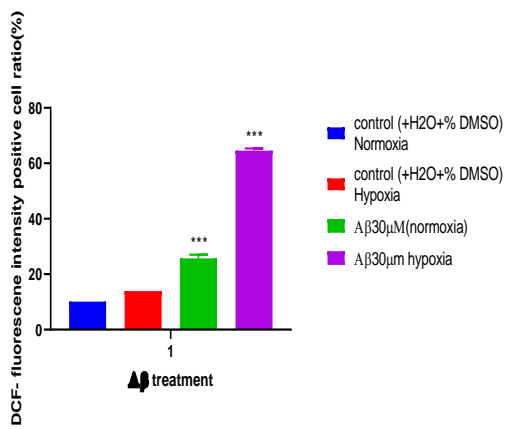
Figure 3.9E

Figure 3.9 .Effects of Aβ₂₅₋₃₅-induced ROS in PC12 cells under normoxic and hypoxic conditions.

ROS generation was measured by DCFDA flow cytometry. The level of ROS generation was

*calculated as follows: The level of ROS (%) = The percentage of DCF-positive cells. PC12 cells were exposed to: (Figure 3.9A) Control (water + 1% DMSO) in normoxia, (Figure 3.9B) Control (water + 1% DMSO) in hypoxia, (Figure 3.9C) 30 μM Aβ$_{25-35}$ for 24 hours in normoxia, and (Figure 3.9D) 30 μM Aβ$_{25-35}$ for 24 hours in hypoxia. The mean ± SE (n=3) for all the measurements are shown in the graph, Figure 3.9E. The ROS level significantly increases in cells treated with 30 μM Aβ$_{25-35}$ in normoxia and hypoxia compared to their control, and the ROS level is significantly higher in cells treated with 30 μM Aβ$_{25-35}$ in hypoxia compared to normoxia (P<0.001). The asterisks (*** indicate high significance difference (P<0.001) between (30 μM Aβ$_{25-35}$) in normoxia and hypoxia group, compared to their respective control (water + 1% DMSO) in both normoxia and hypoxia. Results were analyzed by flow cytometry. Forward scatter represents the (DCFDA) ROS level, and side scatter represents the size of the cells.*

3.3.2.7. Aβ$_{25-35}$ induces PC12 cell membrane peroxidation in both normoxic and hypoxic conditions.

Polyunsaturated fatty acids are attacked by free radicals, resulting in structural damage to the cell membrane and the generation of MDA, which is considered a marker of lipid peroxidation. PC12 cells were treated with Aβ$_{25-35}$ in both normoxia and hypoxia for 24 hours. Cell lysates were mixed with thiobarbituric acid (TBA) and allowed to react at a temperature of 95-100ºC for 60 minutes. MDA reacted with TBA, forming the MDA-TBA adduct, which was measured colorimetrically at 532 nm using a microplate reader. From the results shown in Figure 3.10, in normoxia conditions, the MDA level significantly increased in cells treated with 30 μM Aβ$_{25-35}$ compared to the control (mean = 0.100 ± 0.07). In hypoxia conditions, the MDA level significantly increased in cells treated with 30 μM Aβ$_{25-35}$ compared to the control (mean = 0.135 ± 0.005), and the level of MDA is higher than that in the normoxia condition.
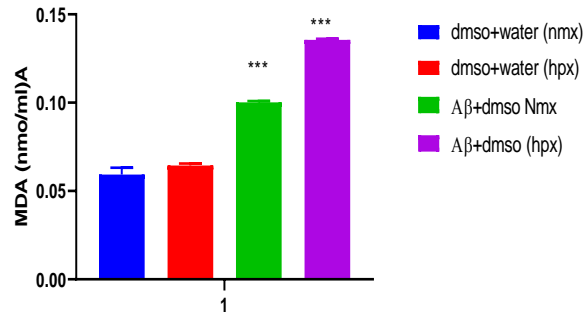
Figure 3.10. Effects of Aβ$_{25-35}$ treatment on lipid peroxidation of PC12 cells under normoxic and hypoxic conditions. Data are presented as mean ± SEM (n=3). *** P<0.001 vs. control group. Aβ$_{25-35}$ treatment of PC12 cells for 24 hours in normoxia significantly increases the MDA level compared to the control (P<0.001, n=3). Aβ$_{25-35}$ treatment of PC12 cells for 24 hours in hypoxia also significantly increases the MDA level compared to the control (P<0.001, n=3). *** represents a highly significant difference (P<0.001) between (30 μM Aβ$_{25-35}$) in normoxia or hypoxia compared to their respective control groups. The increase in MDA is higher than that in the normoxia condition.

3.3.3. Effects of rutin on Aβ$_{25-35}$-induced PC12 cells in both normoxia and hypoxia conditions.

3.3.3.1. Effects of rutin treatment on PC12 cell viability (24 hours) in normoxia and determination of IC50.

The effect of rutin on PC12 cells was determined by treating them with different concentrations of rutin for 24 hours. PC12 cells were incubated with various concentrations of rutin (7.813 μM, 15.625 μM, 31.25 μM, 62.5 μM, 125 μM, 250 μM, 500 μM, 1000 μM) for 24 hours (Figure 3.11). The MTT assay was used to determine cell viability. The results showed a stable cell viability as the dose of rutin increased, and the IC50 was determined to be 108.42 μM. This implies that rutin is safe to use.
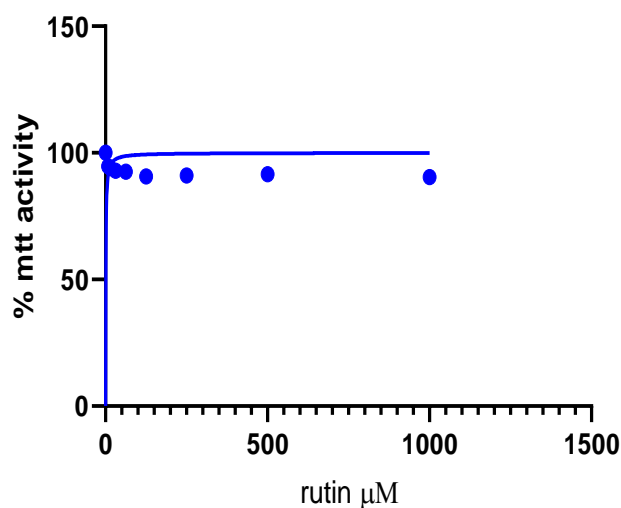
Figure 3.11. Effects of different doses of rutin on PC12 cells. Cell viability was measured using the MTT assay. The graph shows a stable cell viability as the dose of rutin increases up to approximately 1000 μM. The IC50 of rutin after a 24-hour treatment is determined to be 108.42 μM.

3.3.3.2. Effects of rutin (100 μM) on PC12 cell viability induced by Aβ$_{25-35}$ aggregates (30 μM) in both normoxia and hypoxia conditions.

After determining the IC50 of rutin, a concentration of 100 μM (approximately 1x EC50) was used for the remaining experiments involving rutin on PC12 cells. The effects of rutin on PC12 cells exposed to Aβ$_{25-35}$ aggregates (30 μM) under both normoxia and hypoxia conditions were examined by treating PC12 cells with 100 μM rutin in combination with 30 μM Aβ$_{25-35}$ for 24 hours. Figure 3.12A shows the effects of rutin co-treatment with Aβ$_{25-35}$ on the toxicity of PC12 cells under normoxia conditions. PC12 cells were incubated with 100 μM rutin and 30 μM Aβ$_{25-35}$ in combination for 24 hours. The MTT assay was used to assess cell viability. The results showed a statistically significant decrease in cell viability compared to the control group (control values) with 30 μM Aβ$_{25-35}$ (mean = 33.292 ± 1.43). There was also a statistically significant decrease in

cell viability compared to the control group (control values) with 30 μM Aβ$_{25-35}$ (+1% DMSO) (mean = 39.430 ± 2.80). However, the rutin at 100 μM showed a statistically significant increase in MTT activity (mean = 57.935 ± 6.29) compared to the 30 μM Aβ$_{25-35}$ (+1% DMSO) treatment group (mean = 39.430 ± 2.80).

Figure 3.12B shows the effects of rutin co-treatment with Aβ$_{25-35}$ on the toxicity of PC12 cells under hypoxia conditions. PC12 cells were incubated with 100 μM rutin and 30 μM Aβ$_{25-35}$ in combination for 24 hours. The MTT assay was used to assess cell viability. The results showed a significant decrease in cell viability compared to the control group with 30 μM Aβ$_{25-35}$ (mean = 20.903 ± 3.57). There was also a statistically significant decrease in cell viability compared to the control group (control values) with 30 μM Aβ$_{25-35}$ (+1% DMSO) (mean = 27.124 ± 5.750). However, the rutin at 100 μM showed a statistically significant increase in MTT activity (mean = 79.258 ± 7.12) compared to the 30 μM Aβ$_{25-35}$ (+1% DMSO) treatment group (mean = 27.124 ± 5.750).
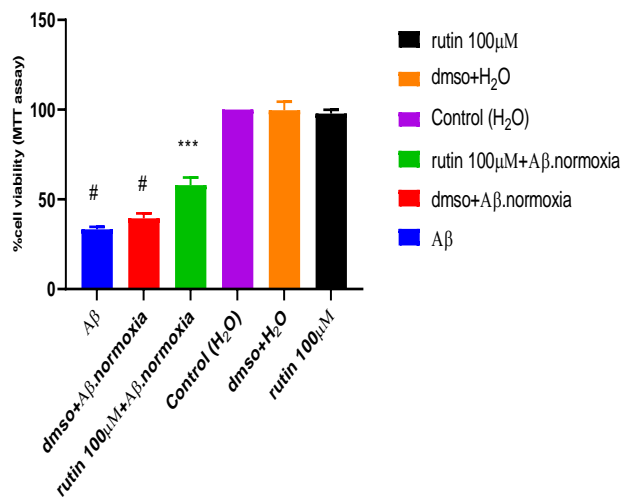
Figure 3.12A
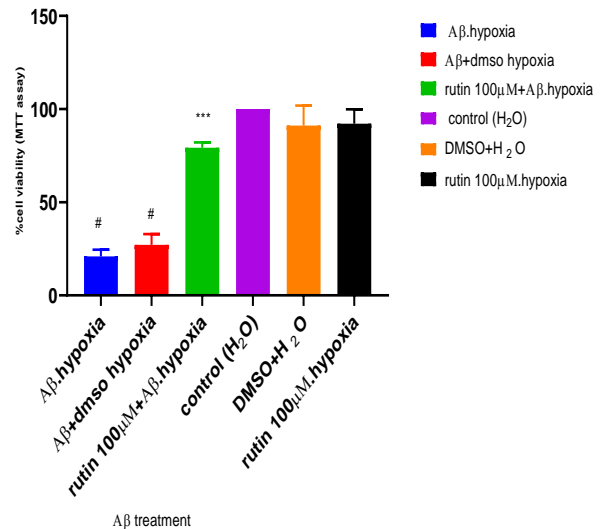
Figure 3.12B

Figure 3.12. Effects of rutin on Aβ25-35-induced cytotoxicity (MTT assays) in PC12 cells under normoxic and hypoxic conditions. Figure 3.12A shows effects of rutin on Aβ25-35-induced cytotoxicity in PC12 cells under normoxia. Cell viability was assessed using the MTT assay. The results showed a significant decrease in cell viability between (30 μM Aβ25-35) compared to the control group, (# indicates the significant difference, p<0.001). There was also a statistically significant decrease in cell viability between 30 μM Aβ25-35 treatment group compared to the control group (+1% DMSO) (# indicates the significant difference, p<0.001). However, treatment with rutin at 100 μM significantly reduced the loss of cell viability (P<0.001). *** represents a highly significant difference (, p<0.001) between the rutin treatment group (100 μM with 30 μM Aβ25-35) and the 30 μM Aβ25-35 treatment group under normoxic conditions. Figure 3.12B shows effects of rutin on Aβ25-35-induced cytotoxicity on PC12 cells under hypoxic conditions. Results showed a significant decrease in PC12 cell viability between 30 μM Aβ25-35 compared to the control group, (# indicates the significant difference, p<0.001). There was also a statistically significant decrease in PC12 cell viability between 30 μM Aβ25-35 treatment group compared to

the control group (+1% DMSO) (# indicates the significant difference, p<0.001). However,

treatment with rutin at 100 μM significantly increased MTT activity when co-administered with

$A\beta_{25-35}$ under hypoxic conditions (p<0.0001). *** represents a significant difference (p<0.001)

between the rutin treatment group (100 μM with 30 μM $A\beta_{25-35}$) and the 30 μM $A\beta_{25-35}$ treatment

group under hypoxic conditions.

3.3.3.3. Effects of rutin against $A\beta_{25-35}$-induced apoptosis of PC12 cells in both normoxic and hypoxic conditions.

Flow cytometry analysis using Annexin V/7-AAD double staining was employed to evaluate the

level of apoptosis in both normoxia and hypoxia. The cells in the lower left quadrant represent

viable cells, while the cells in the lower right quadrant represent early apoptosis, and those in the

upper right quadrant represent late apoptosis/necrosis. As shown in Figure 3.13B, a significant

number of cells underwent early apoptosis after 24 hours of treatment with 30 μM $A\beta_{25-35}$ under

normoxia. However, co-treatment with 30 μM $A\beta_{25-35}$ and rutin at 100 μM for 24 hours (Figure

3.13C) led to a significant reduction in the number of apoptotic/necrotic cells. In Figure 3.14B

under hypoxia, a higher number of cells exhibited apoptosis, with most cells shifting towards the

lower right quadrant. However, co-treatment with 30 μM $A\beta_{25-35}$ and rutin at 100 μM for 24 hours

(Figure 3.14C) resulted in a significant reduction in the number of apoptotic/necrotic cells.
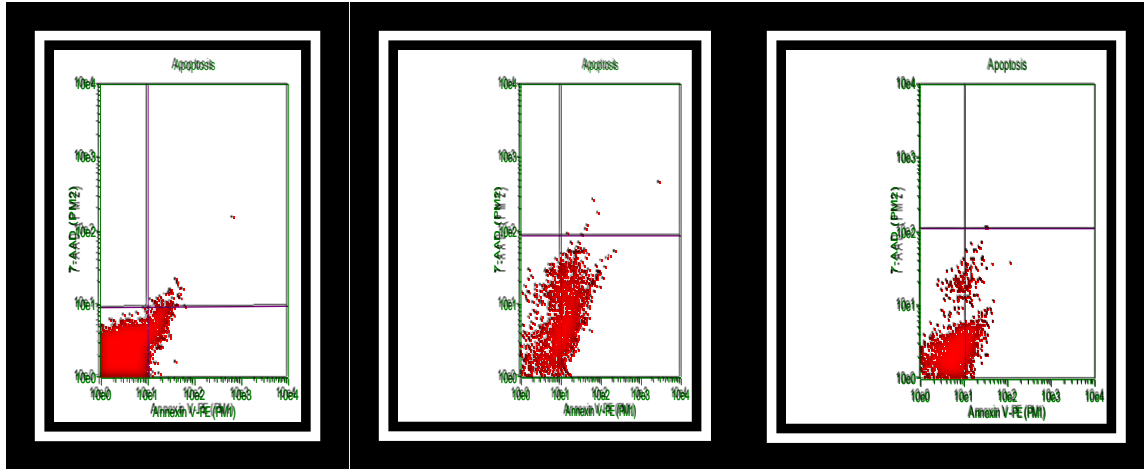
Figure 3.13A   Figure 3.13B   Figure 3.13C
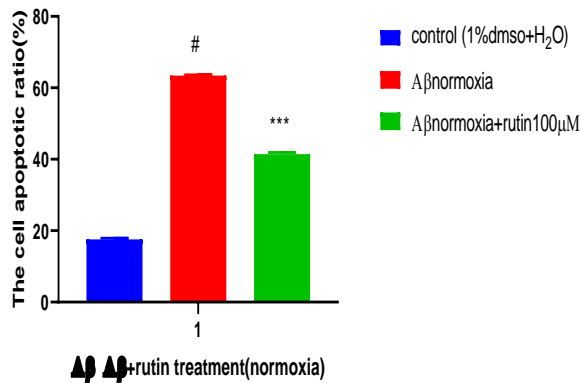
Figure 3.13D

Figure 3.13. FACS analysis (Annexin V/7-AAD) of PC12 cells exposed to Figure 3.13A, control (1%DMSO +water), Figure 3.13B, (30µM of Aβ25-35 for 24hrs normoxia), and Figure 3.13C, (30µM of Aβ25-35 + rutin 100 µM for 24hrs normoxia). The cells in each quadrant were analyzed using FLOWJO software. Cells in the lower left quadrant represent viable cells, cells in the lower right quadrant represent early apoptosis, and cells in the upper right quadrant represent late apoptosis/necrosis. The mean ± SE (n=3) for all measurements are shown in the graph, figure 3.13D. The # symbol indicates a significant difference (p<0.001) between the control group (1% DMSO + water) and 30 µM Aβ25-35 under normoxia. The *** symbol represents a highly

significant difference (p<0.001) between the rutin treatment group (100 μM with 30 μM Aβ$_{25-35}$)

and 30 μM Aβ$_{25-35}$ under normoxia.
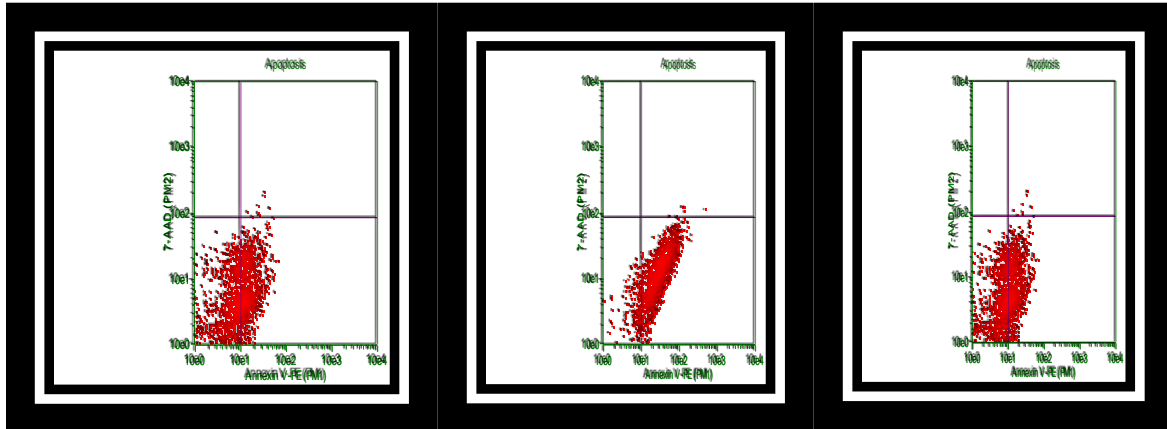
| Figure 3.14A | Figure 3.14B | Figure3.14C |
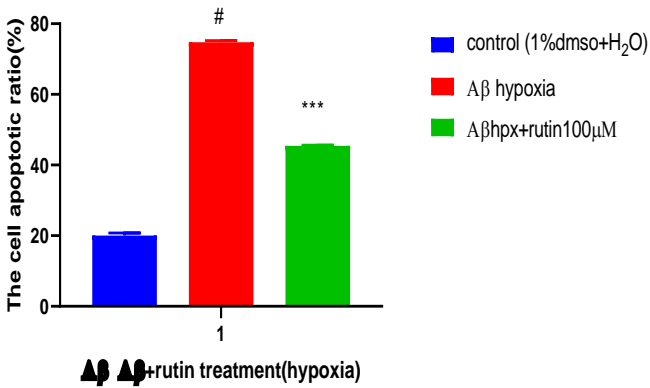
Figure 3.14D

Figure 3.14. FACS analysis (Annexin V/7-AAD) of PC12 cells exposed to Figure 3.14A: control

in hypoxia (1% DMSO + water), Figure 3.14B: 30 μM of Aβ$_{25-35}$ for 24 hours in hypoxia, and

Figure 3.14C: 30 μM Aβ$_{25-35}$ + rutin 100 μM for 24 hours in hypoxia. Cells in each quadrant were

analyzed using FLOWJO software. Cells in the lower left quadrant represent viable cells, cells in

the lower right quadrant represent early apoptosis, and cells in the upper right quadrant represent

late apoptosis/necrosis. The mean ± SE (n=3) for all measurements are shown in the graph (Figure 3.14D). # represents a significant difference (p<0.001) between the control group (1% DMSO + water) and 30 μM Aβ$_{25-35}$ in hypoxia. *** represents a highly significant difference (p<0.001) between the rutin treatment group (100 μM with 30 μM of Aβ$_{25-35}$) and 30 μM Aβ$_{25-35}$ in hypoxia.

3.3.3.4. Combining FACS analysis of both hypoxia and normoxia results of Figure 3.13 and 3.14 above
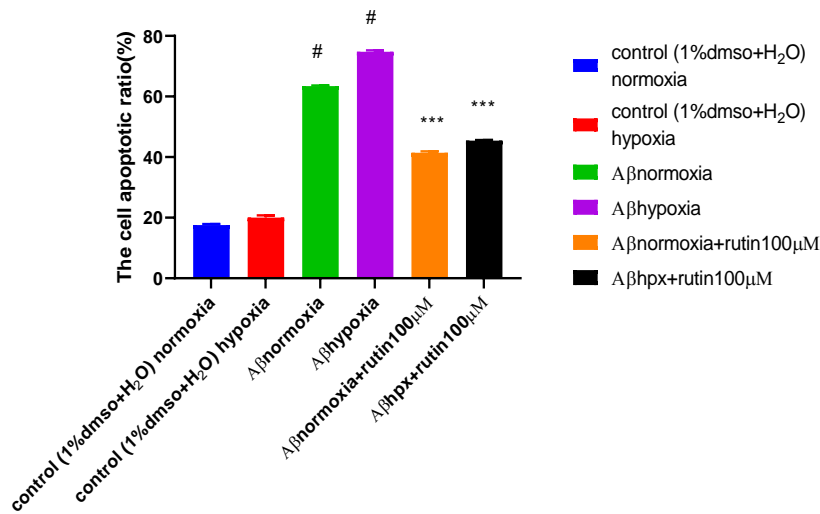
Figure 3.15. Effects of Rutin against Aβ$_{25-35}$ induced apoptosis of PC12 cells in normoxic and hypoxic conditions. As shown in Figure 3.15 above, a significant number of cells were undergoing early apoptosis at 24 hours of treatment with 30 μM Aβ$_{25-35}$ in normoxia. However, at 24 hours co-treatment of 30 μM Aβ$_{25-35}$ + rutin 100 μM, there was a significant reduction in the number of apoptotic/necrotic cells. # represents a significant difference (p<0.001) between 30 μM Aβ$_{25-35}$ (mean = 63.4147 ± 0.21) in normoxia compared to the control group (+1% DMSO). Rutin (100 μM) significantly reduces the number of apoptotic/necrotic cells, and *** represents a significant difference (p<0.001) between the rutin treatment group at (100 μM with 30 μM concentration of Aβ$_{25-35}$) (mean = 41.4486 ± 0.40) and 30 μM Aβ$_{25-35}$ in normoxia. In hypoxia, the number of

apoptotic cells was higher, indicating almost all the cells being apoptotic, shifting towards the lower right quadrant. However, at 24 hours co-treatment of 30 µM Aβ25-35 + rutin 100 µM, there was a significant reduction in the number of apoptotic/necrotic cells. # represents a significant difference (p<0.001) between 30 µM Aβ25-35 (mean = 74.7657 ±0.41) in hypoxia compared to the control group (+1% DMSO). Rutin (100 µM) significantly reduces the number of apoptotic/necrotic cells, and *** represents a significant difference (p<0.001) between the rutin treatment group at (100 µM with 30 µM concentration of Aβ25-35) (mean = 45.4213 ±0.22) and 30 µM Aβ25-35 in hypoxia.

3.3.3.5 Effects of Rutin on ROS Levels of PC12 Cells in Normoxic and Hypoxic Conditions

After treating PC12 cells with 30 µM Aβ25-35, 30 µM Aβ25-35 + 1% DMSO, and 30 µM Aβ25-35 + rutin 100 µM in both normoxic and hypoxic conditions, ROS generation was measured by DCFDA Flow cytometry. In normoxic conditions, the ROS level significantly increased in cells treated with 30 µM Aβ25-35 compared to the control (Figure 3.16B). However, cells treated with 30 µM Aβ25-35 + rutin 100 µM showed a significant decrease in ROS level compared to those treated with 30 µM Aβ25-35 alone (Figure 3.16C). In hypoxic conditions, the ROS level significantly increased in cells treated with 30 µM Aβ25-35 compared to the control, and the ROS level was higher than that in normoxia (Figure 3.17B). Cells treated with rutin 100 µM showed a significant decrease in ROS level compared to those treated with 30 µM Aβ25-35 in hypoxia (Figure 3.17C). The results revealed that treatment with rutin could inhibit the intracellular ROS accumulation induced by Aβ25-35 in PC12 cells in both normoxic and hypoxic conditions.
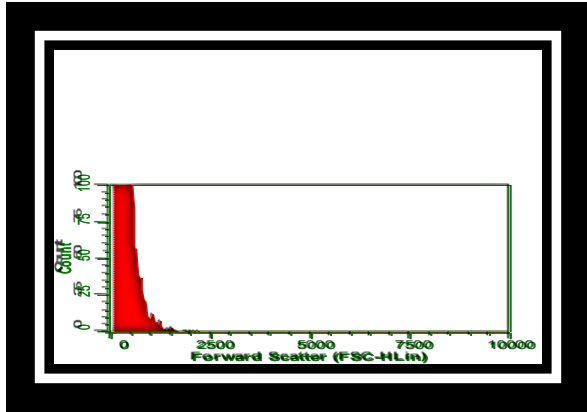
Figure 3.16A
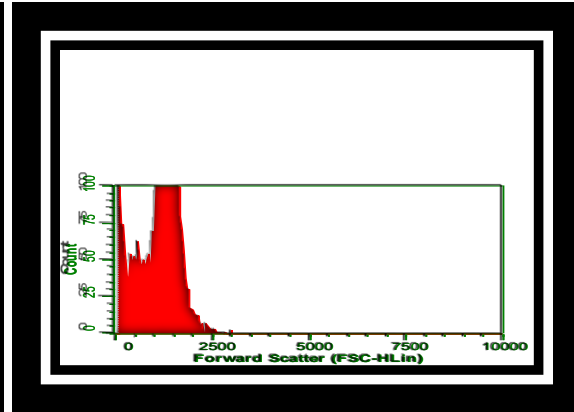
Figure 3.16B
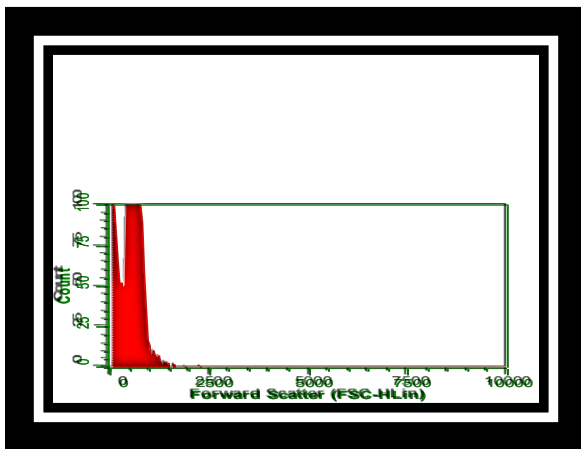
Figure 3.16C
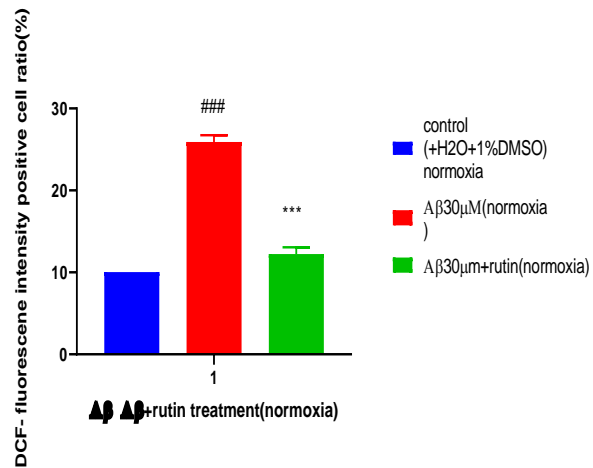
Figure 3.16D

Figure 3.16. Effects of rutin on Aβ$_{25-35}$ induced ROS levels in PC12 cells under normoxic conditions. ROS generation was measured by DCFDA Flow cytometry. PC12 cells were exposed to (Figure 3.16A): Control in normoxia, (Figure 3.16B): 30 μM Aβ$_{25-35}$ for 24 hours in normoxia, and (Figure 3.16C): 30 μM Aβ$_{25-35}$ + rutin 100 μM for 24 hours in normoxia. Figure 3.16D shows the mean ± SE (n=3) for all measurements displayed in the graph. Results were analyzed by flow cytometry, where forward scatter represents the (DCFDA) ROS level, and side scatter represents the size of the cells. In Figure 3.16B, the ROS level significantly increased in cells treated with

*Aβ₂₅₋₃₅ (30 μM) in normoxia compared to the control, with a mean of 25.921 ± 0.82. ### represents a significant difference (P<0.001) between the control group (1% DMSO + water) and 30 μM Aβ₂₅₋₃₅ in normoxia. In Figure 3.16C, cells treated with Aβ₂₅₋₃₅ + rutin 100 μM in normoxia showed a significant decrease in ROS level compared to Aβ₂₅₋₃₅ (30 μM) alone, with a mean of 12.243 ± 0.62, n=3. *** represents a significant difference (P<0.001) between the rutin treatment group at (100 μM with a 30 μM of Aβ₂₅₋₃₅) and 30 μM Aβ₂₅₋₃₅ alone in normoxia. Figure 3.16D displays the mean ± SE (n=3) for all measurements in the graph.*
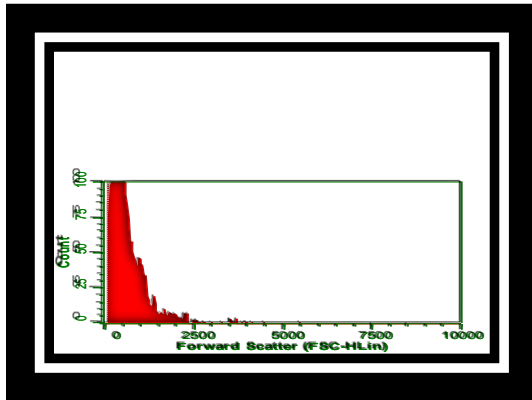
Figure 3.17A
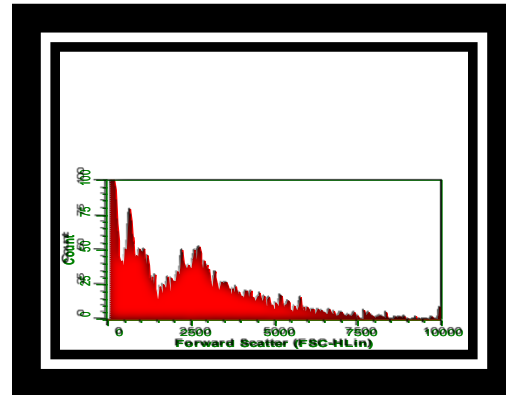
Figure 3.17B
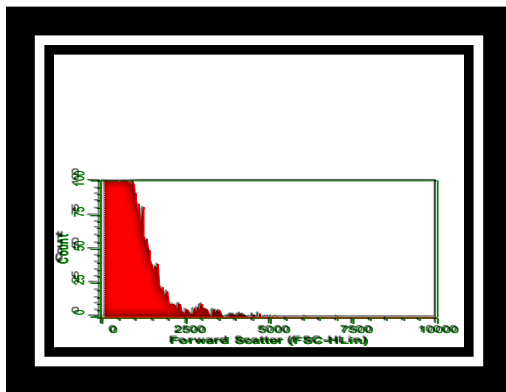
Figure 3.17C
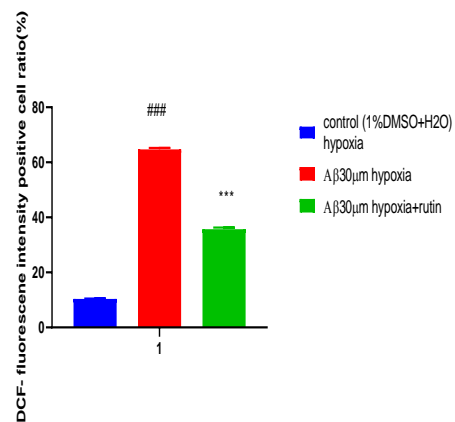
Figure 3.17D

Figure 3.17. Effects of rutin on Aβ$_{25-35}$ induced ROS levels in PC12 cells under hypoxic conditions. ROS generation was measured by DCFDA flow cytometry. PC12 cells were exposed to (Figure 3.17A): Control in hypoxia, (Figure 3.17B): 30 μM Aβ$_{25-35}$ for 24 hours in hypoxia, and (Figure 3.17C): 30 μM Aβ$_{25-35}$ + rutin 100 μM for 24 hours in hypoxia. Figure 3.17D shows the mean ± SE (n=3) for all measurements displayed in the graph. Results were analyzed by flow cytometry, where forward scatter represents the (DCFDA) ROS level, and side scatter represents the size of the cells. In Figure 3.17B, the ROS level significantly increased in cells treated with Aβ$_{25-35}$ (30 μM) in hypoxia compared to the control, with a mean of 64.703 ± 0.50. ### represents a significant difference (P<0.001) between the control group (1% DMSO + water) and 30 μM Aβ$_{25-35}$ in hypoxia. In Figure 3.17C, cells treated with Aβ$_{25-35}$ + rutin 100 μM in hypoxia showed a significant decrease in ROS level, P<0.001, with a mean of 35.667 ± 0.64. *** represents a significant difference (P<0.001) between the rutin treatment group at (100 μM plus a 30 μM of Aβ$_{25-35}$) and 30 μM Aβ$_{25-35}$ alone in hypoxia. In Figure 3.17D, the mean ± SE (n=3) for all measurements are shown in the graph.

3.3.3.6. Effects of Rutin on Malondialdehyde (MDA) Concentration in PC12 cells treated with Aβ$_{25-35}$ aggregates in normoxia and hypoxia

Polyunsaturated fatty acids are attacked by free radicals, resulting in structural damage to the cell membrane and the generation of MDA, which is considered a marker of lipid peroxidation. PC12 cells were treated with Aβ$_{25-35}$ with rutin co-treatment in normoxia and hypoxia for 24 hours. Cell lysates were mixed with thiobarbituric acid (TBA) and allowed to react at a temperature of 95-100ºC for 60 minutes. MDA reacted with TBA, forming the MDA-TBA adduct, which was measured colorimetrically at 532nm using a microplate reader.

From the results in Figure 3.18A, in normoxia conditions, the MDA level significantly increased in cells treated with 30 μM Aβ$_{25-35}$ compared to the control (mean = 0.100 ± 0.07). Cells treated with rutin 100 μM showed a significant decrease in MDA level compared to those treated with 30 μM Aβ$_{25-35}$ (mean = 0.071 ± 0.05).

In hypoxia conditions (Figure 3.18B), the MDA level significantly increased in cells treated with 30 μM Aβ$_{25-35}$ compared to the control (mean = 0.126 ± 0.01), and the level of MDA was higher than that in normoxia. Cells treated with rutin 100 μM showed a significant decrease in MDA level compared to those treated with 30 μM Aβ$_{25-35}$ in hypoxia, with a mean of 0.094 ± 0.001.
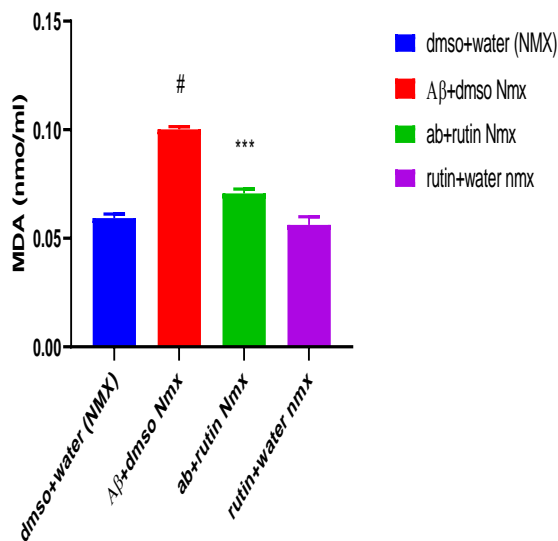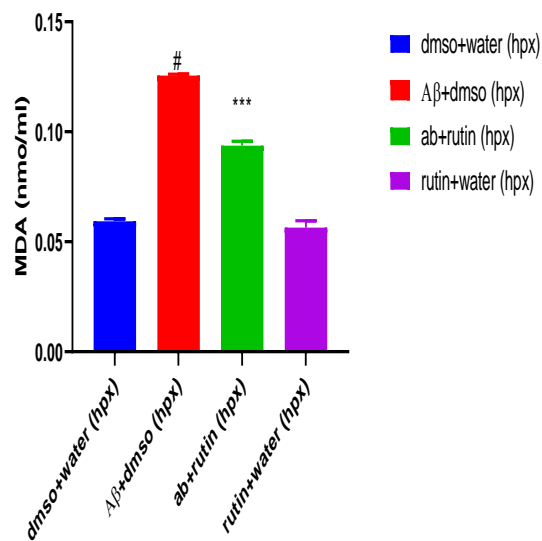
Figure 3.18A   Figure 3.18B

*Figure 3.18 . Effects of rutin treatment on lipid peroxidation caused by Aβ$_{25-35}$ on PC12 cells in normoxia. Figure 3.18A shows the effects of rutin treatment on lipid peroxidation caused by Aβ$_{25-35}$ on PC12 cells in normoxia. Data were presented as mean ± SEM (n=3). # represents significant difference P<0.001, between (30 μM Aβ$_{25-35}$) vs. the control group (1% DMSO + water) in normoxia. *** represents significant difference P<0.001, between rutin treatment group at (100*

206

μM plus 30 μM Aβ$_{25-35}$) vs. (Aβ$_{25-35}$ 30 μM + 1% DMSO). Treatment with rutin at 100 μM significantly decreased the MDA level compared to the Aβ$_{25-35}$ treatment group (P<0.001). *** represents a significant difference (P<0.001) between the rutin treatment group at 100 μM plus a 30 μM concentration of Aβ$_{25-35}$ and 30 μM Aβ$_{25-35}$ alone in normoxia. Figure 3.18B shows the effects of rutin treatment on lipid peroxidation caused by Aβ$_{25-35}$ on PC12 cells in hypoxia. Data were presented as mean ± SEM (n=3). # represents significant difference P<0.001, between (30 μM Aβ$_{25-35}$) vs. the control group (1% DMSO + water) in hypoxia. *** represents significant difference P<0.001, between rutin treatment group at (100 μM plus 30 μM Aβ$_{25-35}$) vs. Aβ$_{25-35}$ (30 μM) + 1% DMSO in hypoxia. Treatment with Aβ$_{25-35}$ for 24 hours in hypoxia significantly increased the MDA level compared to the control (P<0.001), and the increase is higher than that in normoxia. Treatment with rutin at 100 μM significantly decreased the MDA level compared to the Aβ$_{25-35}$ treatment group (P<0.001). *** represents a significant difference (P<0.001) between the rutin treatment group at (100 μM plus 30 μM of Aβ$_{25-35}$) and 30 μM Aβ$_{25-35}$ alone in hypoxia.

3.3 DISCUSSION

The Aβ peptide is a primary component of senile plaques and plays a vital role in neuronal and synaptic dysfunction during the progression of Alzheimer's disease (AD). During AD pathogenesis, Aβ monomers assemble into various unstable oligomeric species. Oligomeric Aβ further aggregates to form short, flexible, irregular protofibrils, which ultimately elongate into insoluble fibrillar assemblies with β-strand repeats oriented perpendicularly to the fiber axis (Walsh and Selkoe, 2007; Aleksić, 2017).

Several studies have shown that the aggregated form of Aβ$_{25\text{-}35}$ becomes toxic. Some experimental research reports have used deionized water to dissolve Aβ$_{25\text{-}35}$ or Aβ1-42, followed by incubation at 37 degrees Celsius for 3, 4, or 7 days (Xian et al., 2012, 2016; Li et al., 2008; Wang et al., 2012). In this research experiment, 1 mM stock of Aβ was dissolved in sterile water and incubated for 4 days at 37°C. Thioflavin T (ThT) fluorescence assay was performed to confirm Aβ$_{25\text{-}35}$ aggregation.

This study further evaluated the cytotoxicity of Aβ$_{25\text{-}35}$ on PC12 cells in both normoxic and hypoxic conditions, as well as its induction of apoptosis. The MTT assay, based on cellular nicotinamide adenine dinucleotide phosphate (NADPH)-dependent oxidoreductase activity, was used. Mitochondrial NADPH plays a crucial role in protecting against redox stress and cell death by maintaining the pool of reduced glutathione (GSH) and thioredoxin, which are imperative for the cellular antioxidant defense system (Bradshaw et al., 2019). Depletion of NADPH has been implicated in neurotoxicity and neurodegeneration (Bradshaw, 2019).

This study revealed a reduction in MTT activity of PC12 cells induced by Aβ$_{25\text{-}35}$ under normoxic conditions. This finding is consistent with previous studies by Abir et al. (2020), Balu et al. (2011), Yan-fang et al. (2013), and Yuna et al. (2017), which showed that exposure of cells to different

concentrations of Aβ$_{25-35}$ for 24 hours resulted in a concentration-dependent decrease in cell viability, indicating that Aβ$_{25-35}$ inhibits neuronal cell viability. The IC50 was also determined. Additionally, the reduction in MTT activity appeared to be more pronounced during hypoxic conditions, suggesting that PC12 cells are more susceptible to Aβ peptide toxicity during hypoxia. This is in line with the findings of Green and Peers (2001) and Webster (2006), which state that hippocampal neurons are more vulnerable to Aβ peptide toxicity during hypoxia, and chronic hypoxia enhances calcium ion (Ca^{2+}) entry and mitochondrial Ca^{2+} content, potentiates posttranscriptional trafficking of L-type Ca^{2+} channels, and creates transition pores in the mitochondrial membrane through which cytochrome C can be released, initiating pro-apoptotic signaling pathways.

The LDH enzyme is a soluble cytosolic enzyme present in eukaryotic cells and is released into the culture medium during cell death due to cell membrane rupture. In this study, the LDH assay showed a significant increase in LDH activity in Aβ$_{25-35}$ treated cells compared to the control, indicating that Aβ$_{25-35}$ is cytotoxic to PC12 cells. This suggests that Aβ in neuronal cells exhibits toxicity, which may be due to the interaction of iron with Aβ, leading to the generation of reactive oxygen species (ROS). This finding is consistent with the study by Merelli et al. (2018), which states that abnormal iron metabolism generates hydroxyl radicals through the Fenton reaction, triggers oxidative stress, and ultimately leads to cell death. Iron also promotes Aβ aggregation, and the interaction between iron and Aβ exhibits toxic effects. Furthermore, the increased cell toxicity was significantly amplified during hypoxia, indicating that hypoxia exacerbates Aβ peptide-induced neuronal death. This suggests that during hypoxia, the overexpression of HIF-1α binds to BACE1 mRNA and increases its expression. This is consistent with the findings of Sun et al. (2006) and Zhang et al. (2007), which show that hypoxia can alter amyloid precursor protein (APP)

processing, increase the activity of β- and γ-secretases, and significantly up-regulate BACE1 gene expression, resulting in increased β-, γ-secretase activity.

Oxidative stress increases with age through alterations in ROS generation or ROS elimination (Barja, 2004). The free radical hypothesis of aging suggests that the accumulation of ROS leads to damage of major cell components, including the nucleus, mitochondrial DNA, membranes, and cytoplasmic proteins (Harman, 2012). The imbalance between ROS generation and antioxidants has been termed oxidative stress and has been proposed as a cause of AD. The brain is particularly susceptible to oxidative stress due to its high consumption of oxygen, increased levels of polyunsaturated fatty acids, and low levels of antioxidants (Mattson, 2012). Oxidative stress and Aβ are closely related since Aβ aggregation induces oxidative stress in vivo and in vitro (Mattson, 2014; Zhu, 2004), and oxidants increase the production of Aβ (Murray, 2007; Tong, 2005). Transition metals, such as Cu (II), Zn (II), and Fe (III), enhance the neurotoxicity of Aβ through their reduction, which produces hydrogen peroxide (H2O2). Density functional theory calculations have revealed that the Aβ residue Tyr-10 is crucial for driving the catalytic generation of H2O2 by Aβ peptides in the presence of Cu (II). The phenoxy radical of Tyr-10, produced by the reaction with ROS, causes neurotoxicity and leads to the formation of dityrosine, which accelerates the aggregation of Aβ peptides (Barnham, 2004). Another important Aβ residue is Met-35; substitution of Met-35 with cysteine resulted in no protein oxidation in a C. elegans model. Additionally, inhibition of cytochrome c oxidase by Aβ42 involves the formation of a redox-active methionine radical (Crouch, 2006). Lipid peroxidation induced by Aβ peptides impairs the function of ATPases, glucose and glutamate transporters, and GTP-binding proteins due to covalent modification of the proteins by the aldehydic end products, such as 4-hydroxynonenal (HNE) (Mattson, 2004). Furthermore, Aβ peptides promote Ca2+ influx into neurons by inducing

membrane-associated oxidative stress, rendering neurons vulnerable to excitotoxicity and apoptosis (Bezprozvanny and Mattson, 2008). On the other hand, oxidative stress may also contribute to Aβ accumulation. Oxidant agents and oxidative products increase APP expression (Chen and Trombetta, 2004; Patil, 2006) as well as intracellular and secreted Aβ levels in neuronal and non-neuronal cells (Murray, 2007; Tong, 2005).

Several lines of evidence suggest that mitochondrial dysfunction is involved in AD pathogenesis (Abolhassani, 2017). Aβ accumulates in mitochondria in the AD brain, accompanied by altered mitochondrial structure, decreased mitochondrial respiratory function and ATP generation, impaired mitochondrial dynamics, and increased mitochondria-associated oxidative stress. Aβ has been detected in the mitochondria of AD patients and AD mouse models, and mitochondrial Aβ levels correlate with abnormalities in mitochondrial structure and function. Reduced mitochondria-associated energy metabolism has been observed in brain regions associated with amyloid plaques. Aβ also triggers abnormalities in mitochondrial dynamics, with aberrant changes observed in mitochondrial fusion and fission due to reduced energy production. Aβ exposure also results in the enrichment of proteins associated with increased mitochondrial fission and decreased mitochondrial fusion (Ebenezer, 2010; Wang, 2009).

It has been proposed that oxidative insults significantly contribute to AD pathogenesis (Butterfield, 2010). In AD, oxidative stress manifests early, supporting the notion that oxidative stress may drive Aβ-induced AD pathogenesis (Wang, 2014). Mitochondria are the primary source of intracellular ROS. Aβ peptides can induce ROS production from mitochondria, leading to the release of cytochrome c and apoptosis-inducing factor, thereby driving mitochondrial dysfunction, cell apoptosis, and neuronal loss (Moreira, 2010). Furthermore, a mitochondrial protein called appoptosin has been identified as a vital regulator for Aβ-induced neuronal cell death. In AD, the

211

expression of appoptosin is upregulated, activating the intrinsic caspase pathway. Remarkably, downregulation of appoptosin can protect against Aβ-induced neurotoxicity. Other mitochondrial proteins, such as amyloid-binding alcohol dehydrogenase and cyclophilin D, have also been shown to play a role in mitochondrial dysfunction (Du, 2008; Du, 2011).

From this experiment, ROS significantly increased in Aβ$_{25-35}$-induced PC12 cells in normoxia, indicating an increase in free radicals and oxidative damage. This finding agrees with the studies of Hong-Mei et al. (2017), Yue et al. (2018), Jordan et al. (2011), and Eri et al. (2020), which indicate that Aβ peptides can increase ROS generation and promote cell death through the mitochondrial pathway and/or death receptor pathway. Additionally, the results revealed a significant increase in ROS levels during hypoxic conditions. This suggests that mitochondria-derived ROS stabilize and activate HIF-1α during hypoxia. This finding agrees with Emerling et al. (2005) and Mylonis et al. (2006), which show that mitochondrial ROS can activate signaling pathways upstream of HIF-1, such as the extracellular signal-regulated mitogen-activated kinase (ERK) and p38 stress-activated MAPK pathways, leading to the phosphorylation and increased transcriptional activity of HIF-1α.

On the other hand, Annexin V (or Annexin A5) is a member of the annexin family of intracellular proteins that binds to phosphatidylserine (PS) in a calcium-dependent manner. PS is normally found on the intracellular leaflet of the plasma membrane in healthy cells, but during early apoptosis, membrane asymmetry is lost, and PS translocates to the external leaflet, where it binds to annexin V. Fluorochrome-labeled Annexin V can be used to specifically target and identify apoptotic cells. However, Annexin V binding alone cannot differentiate between apoptotic and necrotic cells. To distinguish between necrotic and apoptotic cells, a 7-amino-actinomycin D (7-AAD) solution is used. Early apoptotic cells exclude 7-AAD, while late-stage apoptotic cells stain

positively due to the passage of these dyes into the nucleus, where they bind to DNA. 7-AAD has a high DNA binding constant and is efficiently excluded by intact cells, making it useful for DNA analysis and discriminating dead cells during flow cytometric analysis. When excited by 488 laser light, 7-AAD fluorescence is detected in the red range of the spectrum (650 nm long-pass filter).

The use of flow cytometry provides rapid analysis of multiple characteristics of single cells, including cell size, cytoplasmic complexity, DNA or RNA content, and a wide range of membrane-bound and intracellular proteins. Flow cytometry can be used to detect and quantify the level of apoptosis in a population of cells at static points or in a time course. It allows the study of all aspects of apoptosis, from induction via surface receptors to late stages where DNA fragmentation occurs. In a flow cytometer, cells in suspension are drawn into a stream created by a surrounding sheath of isotonic fluid, enabling the cells to pass individually through an interrogation point. At the interrogation point, a beam of monochromatic light, usually from a laser, intersects the cells. Emitted light is given off in all directions and is collected via optics that isolate specific wavelength bands. The light signals are detected by photomultiplier tubes and digitized for computer analysis. Forward-scattered light represents cell size, while side-scattered light represents the complexity or granularity of the cells.

PC12 cells were used in Annexin V and 7-AAD double stain by flow cytometry to detect cellular apoptosis because PC12 cells are suspension cells that can easily move through the flow cytometer tube during the experiment. In Annexin V and 7-AAD double stain by flow cytometry, PC12 cells treated with $A\beta_{25-35}$ showed a significant level of early apoptosis. This indicates that $A\beta_{25-35}$ induced cellular apoptosis, which could be due to an increase in ROS, leading to oxidative damage to cellular proteins and DNA. This finding agrees with the studies of Yuna et al. (2018) and Pengjuan et al. (2015), which indicate that $A\beta$ treatment results in a sudden burst of ROS, leading

to cellular, protein, and DNA oxidative damage and subsequent apoptosis. The results also indicate that cells undergoing early apoptosis induced by Aβ_{25-35} are significantly increased during hypoxic conditions. This suggests that hypoxia may increase ROS levels by affecting mitochondrial membrane potential. This finding is in line with the studies of Bell et al. (2007), Klimova et al. (2008), which state that hypoxia increases ROS generation through electron transfer from ubisemiquinone to molecular oxygen at the Qo site of complex III of the mitochondrial transport chain.

There is significant evidence that oxidative stress induced by ROS overproduction, combined with the low antioxidative capacity of cells, plays an important role in AD. Lipid peroxidation resulting from excessive oxidative stress affects the function of nerve cells and leads to nitration of proteins and damage to nucleic acids. These combined negative effects ultimately lead to the functional impairment or loss of neurons. Lipid peroxidation is the main contributor to free radical-mediated damage to the neuronal membrane, and the secondary oxidation products, such as MDA and HNE, can cause further cellular damage. The presence of oxidized lipoprotein resulting from the presence of amyloid β is a primary hallmark of AD during disease progression.

This study evaluated MDA as a lipid peroxidation indicator to show the level of oxidative damage in Aβ_{25-35}-induced PC12 cells under both normoxia and hypoxia conditions. The results indicated a significant increase in MDA levels when PC12 cells were induced with Aβ_{25-35} in normoxia, suggesting Aβ_{25-35}-induced lipid peroxidation and the generation of free radical-mediated damage to the neuronal membrane, leading to oxidative stress. Abnormal iron metabolism can generate hydroxyl radicals through the Fenton reaction, triggering oxidative stress reactions, lipid peroxidation, and damage to cellular proteins and DNA, ultimately leading to cell death. This finding is consistent with the studies of Kunjathoor et al. (2004), Shao-wei et al. (2012), Peng-Xin

214

et al. (2014), and KASTHURI (2013). Furthermore, the lipid peroxidation induced by $A\beta_{25-35}$ was significantly higher in hypoxic conditions than in normoxia. This supports the notion that intracellular ROS paradoxically increase under hypoxia. This is in line with the findings of Chandel et al. (1998), Mansfield et al. (2004, 2005), Guzy et al. (2004), and Emerling et al. (2005), which state that mitochondria are the source of ROS involved in the hypoxic response and that ROS is necessary and sufficient to stabilize and activate HIF-1α, and mitochondrial ROS regulate HIF-1α stability during hypoxia.

It has been revealed that a history of stroke increases AD prevalence by approximately twofold in elderly patients (Schneider, 2003). The risk is higher when stroke is linked with atherosclerotic vascular risk factors (Jellinger, 2003). A common vascular component between the AD risk factors is hypoperfusion, and hypoxia is a direct consequence of hypoperfusion. Recently, it was revealed that hypoxia can modify APP processing, increasing the activity of β- and γ-secretases. Research indicated that hypoxia significantly up-regulates BACE1 gene expression, and this increases β-secretase activity (Sun, 2006). Additionally, it was revealed that hypoxia increases Aβ deposition and neuritic plaque formation, as well as memory deficit, in Swedish mutant APP transgenic mice. These findings provide a molecular mechanistic link of vascular factors with AD. It has been revealed that overexpression of HIF-1α in neuronal cells increases BACE1 mRNA and protein levels, while down-regulation of HIF-1α reduces the levels of BACE1 (Zhang, 2007). Hypoxic conditions were also shown to increase γ-secretase activity. HIF-1α binds to the anterior pharynx-defective phenotype (APH-1) promoter to up-regulate its expression. The activation of HIF-1α induced by hypoxia increases the expression of APH-1 mRNA and protein, resulting in an increased γ-cleavage of APP and Notch (Li, 2009). Furthermore, hypoxia has also been linked to neuronal and glial-cell calcium dysregulation through the formation of calcium-permeable pores,

dysregulated glutamate signaling, and intracellular calcium-store dysfunction. Hypoxia has also been strongly linked to neuroinflammation (Rahul, 2019). It has been confirmed by many research studies that hypoxia facilitates AD pathology (Shiota, 2013; Liu, 2015; Zhang, 2017). Research has shown that hypoxia may increase the level of ROS (Zhang and Le, 2010), Aβ production (Li, 2009), enhance tau phosphorylation (Gao, 2013), and induce neuroinflammation (Smith, 2013). The mitochondria-derived ROS can activate hypoxia-inducible factor-1α (HIF-1α) through different mechanisms, including post-translational modification (Bruick and McKnight, 2001), and p38 mitogen-activated protein kinase (Emerling, 2005). The levels of intracellular ROS unexpectedly increase in hypoxia (Guzy, 2005). It has been suggested that NADPH oxidase might be an important ROS-generating cellular oxygen sensor because it is expressed in tissues associated with systemic hypoxic responses (Marshal, 1996). On the other hand, it has been suggested that mitochondria are the source of ROS involved in the hypoxic response. The electron transport chain consists of five multiprotein complexes. Complexes I and II oxidize the energy-rich molecules NADH and FADH2, respectively, and transfer the electrons to ubiquinol, which carries them to complex III. Complex III then transports the electrons across the inner mitochondrial membrane to cytochrome c, which carries them to complex IV. Complex IV uses the electrons to reduce oxygen to water. Besides transporting the electrons, complexes I, II, and III generate ROS (Klimova and Chandel, 2008). It has now been established that hypoxia increases ROS through the transmission of electrons from ubisemiquinone to molecular oxygen at the Qo site of complex III of the mitochondrial transport chain (Bell, 2007). The mitochondria-derived ROS are both required and necessary to stabilize and activate HIF-1α. It has been confirmed that antioxidants reverse hypoxia-induced HIF-1α activation (Aminova, 2008). Antitumorigenic effects of antioxidants have been attributed to the inhibition of HIF-1α-dependent events (Gao,

2007). Furthermore, the addition of oxidants, such as H2O2, induces HIF-1α activity up-regulation in normoxia (Page, 2008). Mitochondrial ROS regulate HIF-1α stability on hypoxia through different mechanisms. These probably involve the PHDs, the oxidases involved in the post-translational modification that signals HIF-1α for degradation (Bruick and McKnight, 2001). Under hypoxic conditions, mitochondrial ROS can also activate signaling pathways upstream of HIF-1, such as the p38 stress-activated MAPK pathways. ERK2 phosphorylates HIF-1α in vitro and in vivo and increases its transcriptional activity (Mylonis, 2006). Under hypoxic conditions, regulation of HIF-1α stability is modified by the phosphatidylinositol 3 kinase (PI3K)-protein kinase B (PKB/Akt) signaling pathway (Shaw and Cantley, 2006). Several studies revealed that generation of ROS can activate this pathway and lead to the enhancement of HIF-1α in cancer cells (Zhou, 2007; Flu, 2007).

The increase in the aging population and the significant financial impact on the healthcare system necessitate the development of novel diagnostic, prevention, and treatment strategies for AD. Currently, symptomatic therapies are the only available treatment strategies for AD. Thus, there is an urgent need to identify a new treatment strategy for the cure of AD. Research has recognized flavonoids as a unique class of therapeutic molecules for the cure of AD.

Rutin is a naturally occurring flavonoid glycoside found in many foods and fruits, and it has numerous pharmacological functions such as antioxidant, anti-inflammatory, and cytoprotective properties. Several experimental studies have revealed that rutin has neuroprotective effects, possibly due to its antioxidant activities. Numerous mechanisms have been found to be responsible for the antioxidant activities of rutin in both in vitro and in vivo models. It has been revealed that its chemical structure can scavenge reactive oxygen species (ROS) directly. The main functional groups in the rutin molecule are the hydroxyl groups at positions 5 and 7 of the A ring, as well as

the double bond in the C ring of the quercetin-polyphenolic component, which are responsible for its antioxidant activity (Cos, 1998). It is also assumed to increase the production of GSH and upregulate cellular oxidative defense systems by increasing the expression of various antioxidant enzymes such as CAT and SOD (Al-Enazi MM, 2014). Additionally, rutin inhibits xanthine oxidase, which is involved in ROS generation (Kostić et al., 2015). It also scavenges ROS by donating hydrogen atoms to superoxide anions, peroxy radicals, and hydroxyl radicals (Caglayan, 2019). Research has revealed that rutin effectively reduces the level of malondialdehyde (MDA) while increasing CAT, GPX, SOD, GSH, and the nuclear factor erythroid 2–related factor 2 (Nrf2) levels in colistin-induced neurotoxicity (Xu et al., 2014). Rutin inhibits enhanced activity of xanthine and NADPH oxidase (NOX), which are the primary cellular enzymes responsible for the generation of superoxide radicals. It facilitates peroxide degradation, including lipid peroxides, by regulating the level of GSH and effectively protects phospholipids from peroxidation. Several in vivo studies have revealed that rutin treatment significantly attenuates the decrease in the levels and activities of GSH and GSH-dependent enzymes (GSH-Px and GSSG-R) in rats (Javed, 2012). In addition, rutin-facilitated regulation of the redox balance in fibroblasts prevents the decrease in non-enzymatic antioxidants, including vitamins E and C, after UV irradiation (Gegotek et al., 2016). Rutin significantly reduces cisplatin-induced oxidative stress by inhibiting lipid peroxidation and increasing antioxidant activity (Aksu et al., 2017). Collectively, rutin reduces ROS production, NOX activity, and oxidative products like MDA and thiobarbituric acid reactive substances, while increasing antioxidant status such as SOD, GSH, GPX, and CAT (Geetha et al., 2017; Huang et al., 2017; Imam et al., 2017; Panchal et al., 2011; Saklani et al., 2016; Singh et al., 2015; Liu et al., 2018).

This study investigated the effect of rutin on $A\beta_{25-35}$-induced toxicity and apoptosis of PC12 cells under both normoxia and hypoxia conditions. The MTT and LDH assays were used to determine cell viability and cytotoxicity, and the IC50 of rutin was also evaluated. The results showed stable cell viability as the dose of rutin increased, and the IC50 was approximately 108 μM, suggesting that rutin is safe to use. Therefore, in the experimental study, a concentration of 100 μM (approximately 1x EC50) was used for the remaining rutin experiments on PC12 cells. The study investigated whether rutin treatment could inhibit PC12 cell cytotoxicity after the induction of $A\beta_{25-35}$ in both normoxia and hypoxia conditions. The study further investigated whether rutin treatment could inhibit $A\beta_{25-35}$-induced apoptosis of PC12 cells in both normoxia and hypoxia conditions. Results revealed that rutin inhibits $A\beta_{25-35}$-induced cytotoxicity of PC12 cells in both normoxia and hypoxia. Rutin was found to significantly increase cell viability and decrease cell cytotoxicity in $A\beta_{25-35}$-induced PC12 cells under normoxia. This implies that rutin protects PC12 cells against $A\beta_{25-35}$-induced cytotoxicity by inhibiting cellular damage. The result is in line with the finding of Shao-wei (2012), which states that rutin is a multifunctional flavonoid that can inhibit $A\beta$ aggregation and cytotoxicity. Additionally, rutin significantly increased cell viability and reduced cell cytotoxicity in $A\beta_{25-35}$-induced PC12 cells under hypoxia conditions. Therefore, since HIF-1 has been shown to participate in hypoxia-induced adaptive reactions to restore cellular homeostasis, rutin, as an iron chelator, may activate HIF in addition to iron chelation. This implies that rutin may have pharmacological functions in HIF stabilization, which may serve as a neuroprotective mechanism and be explored as an adjunctive therapy for AD.

The mechanisms of apoptosis are highly complex, involving an energy-dependent cascade of molecular events. There are two linked apoptotic pathways: the extrinsic or death receptor pathway and the intrinsic or mitochondrial pathway, where molecules in one pathway can influence the

other (Igney and Krammer, 2002). There is an additional pathway that involves T-cell mediated cytotoxicity and perforin-granzyme-dependent killing of the cell. The perforin/granzyme pathway can induce apoptosis via granzyme B or granzyme A. The extrinsic, intrinsic, and granzyme B pathways converge on the same terminal or execution pathway, which starts with the cleavage of caspase-3 and results in DNA fragmentation, degradation of cytoskeletal and nuclear proteins, cross-linking of proteins, formation of apoptotic bodies, expression of ligands for phagocytic cell receptors, and finally uptake by phagocytic cells. Caspase-dependent apoptotic cell death occurs due to the inactivation of survival pathways, like the PI3K (phosphatidylinositol 3-kinase)/Akt (protein kinase B) pathway (GómezSintes, 2016; Snigdha, 2012).

Bcl-2 (B-cell lymphoma 2) inhibits intrinsic apoptosis by binding to the proapoptotic proteins Bax and Bcl-2 homologous antagonist/killer (Bak) (Khodapasand, 2015). The granzyme A pathway activates a parallel, caspase-independent cell death pathway via single-stranded DNA damage (Martinvalet, 2005).

Rutin has been shown to reduce p53 expression, a protein involved in the activation of DNA repair mechanisms and induction of apoptosis in response to DNA damage (Gegotek, 2019). Rutin administration has been found to attenuate "ischemic neural apoptosis" due to the suppression of p53 expression and lipid peroxidation, along with an increase in endogenous antioxidant defense enzymes (Khan, 2009). Another study showed that rutin exhibited neuroprotective potential due to the reduction in neuroapoptosis (Man, 2015). Rutin reduces apoptotic cells in ischemic-reperfusion-induced apoptosis in both in vivo and in vitro models, as well as in doxorubicin- and pirarubicin-induced cardiotoxicity, by suppressing caspase-3, -7, and -9 protein expressions (Jeong, 2009; Kim, 2010). Reduction of caspase proteins by rutin is related to an increase in Bcl-2 and a decrease in Bax proteins (Ma, 2017; Wang, 2018). This suggests that rutin may prevent

apoptosis via the Bcl-2-regulated apoptotic pathway, but the exact mechanisms by which rutin can modulate Bcl-2, Bax, and caspases proteins are still not understood.

This research further investigated the effect of rutin on $A\beta_{25-35}$-induced cellular apoptosis by annexin V and 7AAD double stain through flow cytometry analysis in both normoxia and hypoxia. The results revealed that the level of apoptosis was significantly reduced in normoxia, indicating that rutin can inhibit cellular apoptosis, possibly through a decrease in ROS levels and inhibition of cellular, protein, and DNA oxidative damage. Additionally, the results revealed that the level of apoptosis was also significantly reduced in hypoxia condition, implying that rutin, as an antioxidant, may reverse hypoxia-induced HIF-1α activation, suppressing neuronal cell death caused by hypoxia or oxidative stress, and also protect against Aβ peptide toxicity.

Free radicals attack polyunsaturated fatty acids, leading to the production of lipid peroxidation and resulting in membrane damage and the generation of MDA, which serves as a key indicator of lipid peroxidation induced by free radicals (Yang, 2012). Products of lipid peroxidation like 4-hydroxynonenal (HNE) are increased in the brain of AD patients (Arlt, 2002). Therefore, scavenging free radicals and increasing antioxidant enzyme activity can reduce oxidative damage.

The Lipid Peroxidation Assay Kit is a robust and sensitive kit for the detection of malondialdehyde (MDA) produced as an end product of lipid peroxidation. In this assay, free MDA present in the sample reacts with Thiobarbituric Acid (TBA) and generates an MDA-TBA adduct, which can easily be quantified colorimetrically (OD 532 nm) or fluorometrically (Ex/Em = 532/553 nm). It detects MDA levels as low as 0.1 nmol/well in the fluorometric MDA in the samples. This kit detects free MDA, which forms adduct with TBA. If bound to collagen or other proteins, it will not be detected unless released. The acid treatment in the assay, however, precipitates all proteins, so most of the MDA present in the sample should be free, and hence total MDA is detected.

From this experiment, rutin (a bioflavonoid antioxidant) significantly reduces ROS levels when compared with $A\beta_{25\text{-}35}$ treatment group in normoxia condition. This implies that rutin can scavenge free radicals, thereby protecting neuronal cells from oxidative damage, demonstrating its antioxidant potential. This is in line with the findings of Xiao, 2015; Karim, 2011; and Shao-wei, 2012. Additionally, it also significantly reduces ROS levels in hypoxia condition. This indicates that rutin may have the ability to chelate iron and stabilize HIF-1, which maintains the mitochondrial membrane potential and cytosolic accumulation of cytochrome C. This can inactivate caspase-9 and caspase-3, and thus prevent neuronal death in the AD brain, thereby inhibiting oxidative stress.

Additionally, MDA, a lipid peroxidation indicator, was measured to show the level of oxidative damage in both normoxic and hypoxic conditions. The results indicate that the level of MDA was significantly reduced when $A\beta_{25\text{-}35}$-induced PC12 cells were treated with rutin in normoxia, indicating its antioxidative effects. This is in line with the findings of Shao-wei, 2012, and Peng-Xin, 2014. The results also indicate that the level of MDA was significantly reduced when $A\beta_{25\text{-}35}$-induced PC12 cells were treated with rutin in hypoxia. This implies that rutin, as an iron chelator, has neuroprotective potential by inhibiting the generation of free radicals derived from iron, and may also upregulate the hypoxia rescue genes via HIF stabilization.

Conclusion

In conclusion, this research study discovered dose-dependent toxicity of $A\beta_{25\text{-}35}$ aggregates in PC12 cells. $A\beta_{25\text{-}35}$ aggregates induced apoptosis and increased the levels of ROS and lipid peroxidation in PC12 cells under normoxia conditions. Furthermore, the combined treatment of $A\beta_{25\text{-}35}$ aggregates and hypoxia significantly enhanced the toxic effects of $A\beta_{25\text{-}35}$ aggregates, possibly due to increased ROS during hypoxia.

Additionally, in both normoxia and hypoxia conditions, rutin was found to be neuroprotective against $A\beta_{25-35}$-induced cytotoxicity in PC12 cells. Rutin treatment significantly reduced $A\beta_{25-35}$-induced cell apoptosis, ROS levels, and lipid peroxidation, thereby inhibiting cellular damage. The results suggest that rutin attenuates or reverses $A\beta_{25-35}$-induced cytotoxicity and apoptosis in PC12 cells, potentially through scavenging of free radicals due to its antioxidant effects. Therefore, rutin may serve as a novel drug for the treatment of Alzheimer's disease, due to its ability to scavenge free radicals, inhibit oxidative stress, chelate iron, and its potential role in HIF stabilization.

Chapter 4

RUTIN PROTECTS PRIMARY NEURONS FROM Aβ$_{25-35}$ TOXICITY IN BOTH NORMOXIC AND HYPOXIC CONDITIONS

4.1. Introduction

Alzheimer's disease (AD) is the most common neurodegenerative disease, affecting approximately 26 million people worldwide (Brookmeyer et al., 2018). The pathogenesis of AD is believed to be triggered by the excessive accumulation of the toxic amyloid beta (Aβ) (Prasansuklab and Tencomnao, 2013). Recently, a molecular link between ischemia/hypoxia and amyloid precursor protein (APP) processing has been established (Salminen et al., 2017). Brain regions susceptible to AD pathology display a significant decline in cerebral blood flow during the phase of mild cognitive impairment that precedes AD diagnosis (Attems et al., 2004; Jeynes and Provias, 2006). In response to ischemia/hypoxia, the brain stabilizes hypoxia-inducible factor (HIF). However, there is compelling evidence that HIF-1α activates both β and γ secretases, thereby augmenting APP processing and Aβ production under hypoxic conditions. Nevertheless, there are few studies on the effects of hypoxia on Aβ-induced neurotoxicity. Furthermore, current research on AD treatment is primarily conducted under normoxic conditions, which does not fully reflect the AD pathogenesis.

Rutin is a naturally occurring flavonoid glycoside found in many foods and fruits, known for its pharmacological effects such as antioxidant, anti-inflammatory, and cytoprotective functions. Rutin is a common dietary flavonol glycoside composed of quercetin and disaccharide rutinose (Kreft et al., 1999). It is a bioflavonoid found in fruits, especially citrus fruits (e.g., orange, grapefruit, lime, and apple), as well as berries (e.g., mulberry, cranberries). Rutin is one of the primary flavonoids found in numerous multivitamin preparations and herbal remedies (Kreft et al.,

1999), and it is a constituent of over 130 registered medicinal preparations (Chua, 2013). Rutin exhibits several pharmacological properties, including reducing oxidative stress, preventing inflammation, cardiovascular and neuroprotective effects, and demonstrating anti-cancer and antidiabetic activities (Aldhabi et al., 2015; Riaz et al., 2018). Within the brain, rutin exerts numerous neuroprotective actions, such as protecting neurons against injury induced by neurotoxins, suppressing neuroinflammation, and potentially enhancing memory (Kamalakkannan et al., 2006). Rutin scavenges free radicals, inhibits superoxide radical production, and enhances the activity of antioxidant enzymes like glutathione peroxidase and reductase to maintain levels of reduced glutathione, a biological antioxidant (Kamalakkannan et al., 2006). Rutin has therapeutic potential for the treatment of neurodegenerative diseases associated with oxidative stress (Park et al., 2014; Motamedshariaty et al., 2014). It also possesses vaso- and cardioprotective properties (Kim et al., 2005; Riaz et al., 2018). Rutin may strengthen blood vessel walls, reduce capillary permeability, and improve blood concentration. Additionally, by having antiplatelet functions and decreasing the cytotoxicity of oxidized low-density lipoprotein cholesterol, rutin may reduce the risk of atherogenesis (Sheu et al., 2004).

The aim of this study is to characterize the effects of hypoxia on Aβ-induced neurotoxicity in primary neurons and evaluate the neuroprotective potential of rutin against Aβ toxicity under normoxic and hypoxic conditions. The main objectives of the study include:

1. Studying dose-related $A\beta_{25-35}$-induced toxicity in primary neurons under both hypoxic and normoxic conditions.

2. Characterizing the neuroprotective effects of rutin against $A\beta_{25-35}$-induced toxicity in primary neurons under both hypoxic and normoxic conditions.

4.2 MATERIAL AND METHOD

Primary rat cortical neurons were cultured according to the procedures described in Section 2.2.

4.2.1 Treatment

Confluent PC12 cells and primary neuronal cultures were used for experiments. The complete media (100%) was aspirated, and the cells were washed twice with media prior to experiments. $A\beta_{25-35}$ was prepared in an aggregated form and applied to the cells. Cell viability and cytotoxicity were determined by MTT and LDH assays, respectively. Once the EC50 was determined, a single dose of $A\beta_{25-35}$ aggregates was used for the study of toxicity mechanisms, as well as for the rutin treatment study.

Rutin was initially dissolved in DMSO and subsequently diluted in the appropriate culture medium to the indicated concentrations for treatment. For the vehicle control group, a final concentration of 1% DMSO was used throughout. We investigated the effect of rutin on $A\beta_{25-35}$ and $A\beta_{25-35}$ plus hypoxia (0.3% O2)-induced toxicity and apoptosis in primary rat neurons. Rutin (100 μM) was co-administered with $A\beta_{25-35}$ aggregates in the cells.

The treatment procedure is the same as that of PC12 cells, except for the graded doses of $A\beta_{25-35}$ used for viability and cytotoxicity studies below.

Treatment for determination of EC50:

The treatment is divided into two groups: Group A (normoxia) and Group B (hypoxia).

Group A (normoxia):

Group 1: Negative control (H2O)

Group 3: Graded doses of $A\beta_{25-35}$ (0.03-32 μM)

The cells were coated in a 96-well plate, with experiments involving 3-8 well replicates per plate. The experiments were replicated at least three times. After the treatment, the cells were immediately incubated in a standard incubator with a humidified atmosphere containing 21% O_2 and 5% CO_2 at 37ºC for 24 hours.

Group B (hypoxia):

Group 1: Negative control (H_2O)

Group 3: Graded doses of $A\beta_{25-35}$ (0.03-32 μM)

The cells were coated in a 96-well plate, with experiments involving 3-8 well replicates per plate. The experiments were replicated at least three times. After the treatment, the cells were immediately incubated in a purpose-built INVIVO2 400 humidified hypoxia workstation (0.3% O_2, 5% CO_2, 94% N_2) at 37ºC. The media in filter-capped flasks was placed within the hypoxia workstation for 24 hours before use to deplete oxygen.

After 24 hours of treatment in both conditions, the viability and cytotoxicity were evaluated by MTT and LDH assays, respectively.

4.2.2 Data analysis:

Studies performed with primary neuronal cultures, n represents studies performed on cells derived from different rats. For each biological replicate, at least three technical replicates were performed. In experiments employing 96-well plates, at least 8 well replicates were performed on each plate. The dataset obtained for each treatment condition was independent of other conditions (i.e., independent sampling; one rat, one number). The data obtained from each of the biological replicates were averaged. The data were represented as mean ± standard deviation (S.D.). The data were tested for normality using the Anderson-Darling normality test. For normally distributed data,

227

one-way or two-way ANOVA with Tukey's post hoc analysis was performed. For data that were not normally distributed, the non-parametric Kruskal-Wallis test was used. PRISM version 8 (Graph Software Inc, CA, USA) for Windows version 10 was used for all data analysis. Values of $p < 0.05$ were considered statistically significant.

4.3 RESULTS

4.3.1 Primary rat neuron culture

The primary rat neuron culture was characterized by immunofluorescence staining with Tuj1, a neuron-specific stain found in the cell bodies, dendrites, axons, and axonal terminals. A typical healthy culture (Figure 4.1) consisted of 65.84% ± 7.23% Tuj1+ nuclei. Healthy neurons exhibited numerous long axons (Tuj1 staining).
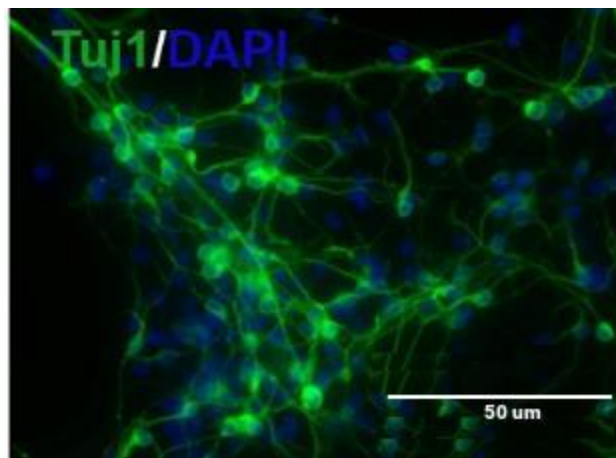
Figure 4.1 Fluorescence micrographs of a typical primary rat cortical neuronal culture. A representative double-merged micrograph of Tuj1 (FITC) and DAPI stained neuronal culture is shown. A healthy culture consists of neurons (Tuj1+) with numerous axons. A typical healthy culture consists of 65.84%±7.23% Tuj1+ nuclei.

4.3.2: Dose-dependent Aβ$_{25-35}$ on primary neurons in normoxia and hypoxia conditions

4.3.2.1: Dose-dependent Aβ$_{25-35}$ on primary neurons - (MTT assay) in normoxia and hypoxia, and IC50 determination

Different concentrations of Aβ$_{25-35}$, including 3 μM, 5 μM, 10 μM, 20 μM, 30 μM, 40 μM, and 50 μM, as well as 60 μM and 70 μM, were used for PC12 cells. However, in neurons, the concentration range of 50-70 μM induced high levels of neuronal toxicity. Therefore, a concentration range of (0-32 μM) was used to determine the IC50.

As shown in Figure 4.2, neuronal cells were exposed to different concentrations of Aβ$_{25-35}$ ranging from (0-32 μM) for 24 hours under normoxia and hypoxia conditions, and their viability was assessed using MTT assays. Treatment of neuronal cells with Aβ$_{25-35}$ for 24 hours under normoxia conditions resulted in a significant decrease in MTT activity (Figure 4.2A). There was a statistically significant decrease in MTT activity between the control group and the variable concentrations of Aβ$_{25-35}$ treatment groups in normoxia (P<0.001, n=5), figure 4.2A (i). Figure 4.2A (ii) represents cells treated with various Aβ$_{25-35}$ concentrations (0.03, 0.1, 0.3, 1, 3, 10, 32 μM) and quantified on a normalized response curve, which significantly decreased the MTT activity (p < 0.001). The mean top value was 78.89, the mean IC50 was 31.32 μM, and the mean LogIC50 was 1.497 μM.

Treatment of neuronal cells with Aβ$_{25-35}$ for 24 hours under hypoxia conditions resulted in a significant decrease in MTT activity, (figure 4.2B). There was a statistically significant decrease in MTT activity between the control group and the variable concentrations of Aβ$_{25-35}$ treatment groups, and the reduction in MTT activity was higher than that in normoxia (P<0.001, n=5), with the following mean values: 0.032 μM (mean=49.74±0.48), 0.1 μM (mean=47.85±0.38), 0.3 μM (mean=44.81±0.29), 1μM (mean=43.54±0.96), 3μM (mean=41.77±2.12), 10μM

(mean=38.25±1.78), and 32 μM (mean=28.61±0.93), Figure 4.2B(i). Neuronal cells treated with the various Aβ$_{25-35}$ concentrations (0.03, 0.1, 0.3, 1, 3, 10, 32 μM) were quantified on a normalized response curve, which significantly decreased the MTT activity (p < 0.001). The mean top value was 47.06, the mean IC50 was 16.27 μM, and the mean LogIC50 was 1.211 μM (Figure 4.2B (ii).
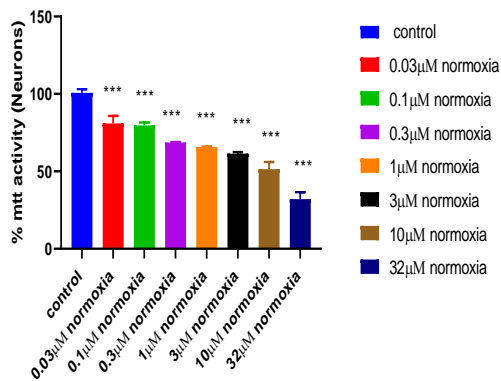
Figure 4.2A (i)
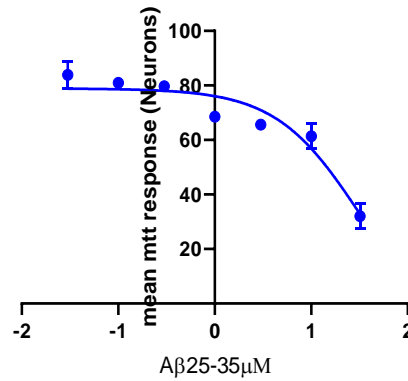
Figure 4.2A (ii)
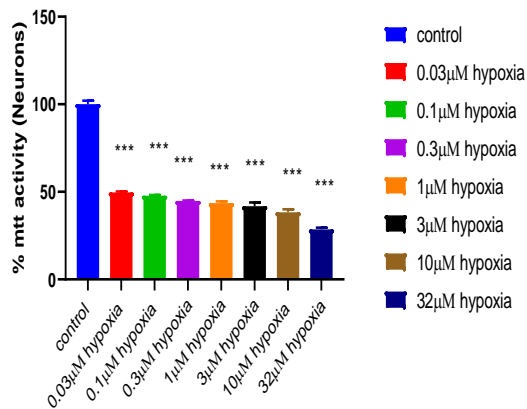
Figure 4.2 B (i)
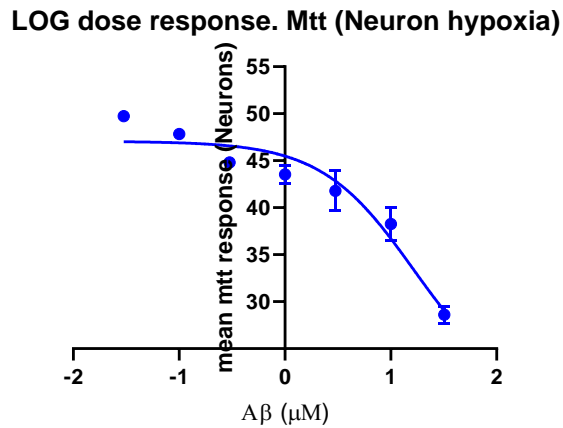
Figure 4.2 B (ii)

Figure 4.2 Percentage viability (MTT assays) induced by Aβ$_{25-35}$ on neurons in normoxic and hypoxic conditions. Figure 4.2A (i) shows effect of Aβ$_{25-35}$-induced toxicity on neuronal cell viability (MTT assays) in normoxia. There was a statistically significant decrease in MTT activity between the control group and the variable concentrations of Aβ$_{25-35}$ treatment groups (0.03, 0.1,

0.3, 1, 3, 10, 32 μM) (P<0.001, n=5). *** represents a significant difference (P<0.001) between the control group (H₂O) and the variable doses of Aβ₂₅₋₃₅ in normoxia. Figure 4.2A (ii) shows Neuronal cells treated with various Aβ₂₅₋₃₅ concentrations (0.03, 0.1, 0.3, 1, 3, 10, 32 μM) were quantified on a response curve, and there was a significant decrease in MTT activity (p < 0.001). Figure 4.2B indicates effect of Aβ₂₅₋₃₅-induced toxicity on primary neuron cell viability (MTT assays) in hypoxia. Figure 4.2B (i) indicates that there was a statistically significant decrease in MTT activity between the control group and the variable concentrations of Aβ₂₅₋₃₅ treatment groups (0.03, 0.1, 0.3, 1, 3, 10, 32 μM) (P<0.001, n=5). *** represents a significant difference (P<0.001) between the control group (H₂O) and the variable doses of Aβ₂₅₋₃₅ in hypoxia. Figure 4.2B (ii) shows neuronal cells treated with various Aβ₂₅₋₃₅ concentrations (0.03, 0.1, 0.3, 1, 3, 10, 32 μM) were quantified on a response curve, and there was a significant decrease in MTT activity (p < 0.001).

4.3.2.2: Dose-dependent Aβ₂₅₋₃₅ on primary neurons - (LDH assay) in normoxia and hypoxia, and IC50 determination.

As shown in Figure 4.3, neuronal cells were exposed to different concentrations of Aβ₂₅₋₃₅ ranging from (0-32 μM) for 24 hours in normoxia and hypoxia conditions, and their cytotoxicity was assessed using LDH assays. Aβ₂₅₋₃₅ induced LDH release on neurons in normoxia for 24 hours (figure 4.3A). There was a statistically significant increase in LDH activity of neuronal cells in normoxia at concentrations of Aβ₂₅₋₃₅ (0.3, 1, 3, 10, 32 μM) for 24 hours (P<0.001, n=5), (Figure 4.3A (i). This cells treated with various Aβ₂₅₋₃₅ concentrations (0.03, 0.1, 0.3, 1, 3, 10, 32 μM) in normoxia, were quantified on a response curve, and there was a significant increase in LDH activity (p < 0.001) with (Mean top value: 66.79, mean EC50: 11.86 μM, mean LogEC50: 1.074 μM), (figure 4.3A (ii).

Furthermore, Aβ$_{25-35}$ induced LDH release on neurons in hypoxia for 24 hours (figure 4.3B). There was a statistically significant increase in LDH activity of neuronal cells in hypoxia in the treatment group (10, 32 μM) of Aβ$_{25-35}$ for 24 hours (P<0.001), and LDH levels were higher than in normoxia, (figure 4.3B (i). This cells treated with the various Aβ$_{25-35}$ concentrations (0.03, 0.1, 0.3, 1, 3, 10, 32 μM) were quantified on a normalized response curve, and there was a significant increase in LDH activity (p < 0.001) with (Mean top value: 72.79, mean EC50: 0.618 μM, mean LogEC50: 0.618 μM - 0.208 μM, (Figure 4.3B (ii)).
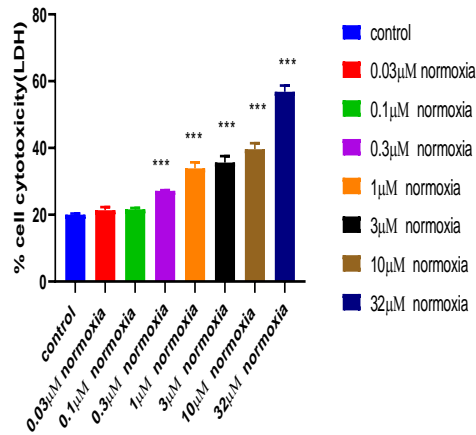
Figure 4.3A (i)
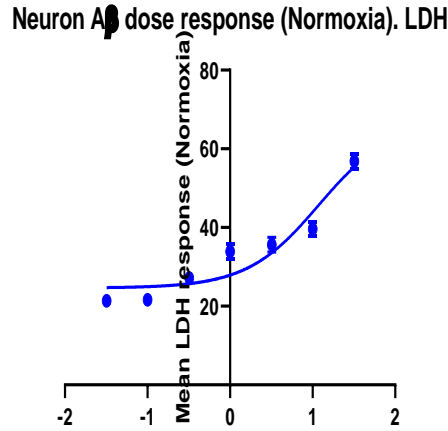
Figure 4.3A (ii)
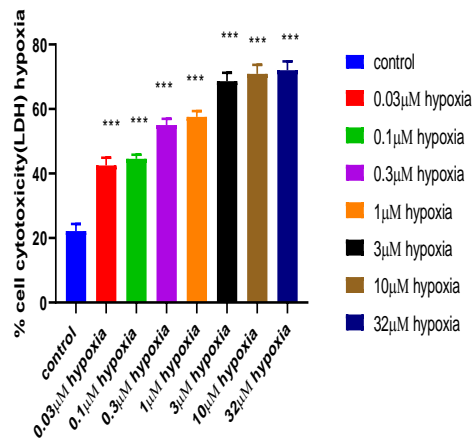
Figure 4.3B (i)
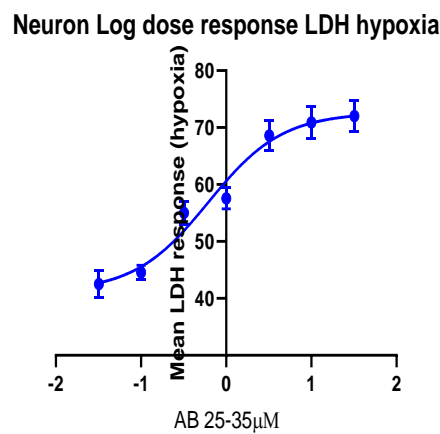
Figure 4.3B (ii)

Figure 4.3 Percentage cell cytotoxicity (LDH assays) induced by Aβ$_{25-35}$ on neurons in normoxia and hypoxia.There is a statistically significant increase in LDH activity of neurons in normoxia in the treatment group at concentrations of Aβ$_{25-35}$ (0.03, 0.1, 0.3, 1, 3, 10, 32 μM) for 24 hours (P<0.001). *** represents a significant difference (P<0.001) between the control group (H$_2$O) and the variable doses of Aβ$_{25-35}$ in normoxia, (Figure 4.3A (i). Neurons were treated with various Aβ$_{25-35}$ concentrations (0.03, 0.1, 0.3, 1, 3, 10, 32 μM) and quantified on a normalized response curve, showing a significant increase in LDH activity (p < 0.001), (Figure 4.3A (ii). There is a statistically significant increase in LDH activity of neuronal cells in hypoxia in the treatment group

at concentrations of Aβ$_{25-35}$ (0.03, 0.1, 0.3, 1, 3, 10, 32 μM) for 24 hours (P<0.001), and the increase is higher than that in normoxia. *** represents a significant difference (P<0.001) between the control group (H$_2$O) and the variable doses of Aβ$_{25-35}$ in hypoxia, (Figure 4.3B (i). Neurons treated with various Aβ$_{25-35}$ concentrations (0.03, 0.1, 0.3, 1, 3, 10, 32 μM) were quantified on a normalized response curve, showing a significant increase in LDH activity (p < 0.001), (Figure 4.3B (ii).

4.3.3: Effects of Aβ$_{25-35}$-induced apoptosis on neurons in both normoxia and hypoxia.

Hoechst 33258 staining was used to specifically stain the nuclei of the cells in order to distinguish the compact chromatin of apoptotic nuclei and sort cells based on their DNA content. It characterizes the degree of Aβ$_{25-35}$-induced cell apoptosis (Figure 4.4). Neurons treated with 30 μM of Aβ$_{25-35}$ in normoxia for 24 hours exhibited nuclei fragmentation (Figure 4.4C), and nucleus fragmentation was higher in hypoxia compared to normoxic conditions (Figure 4.4D).
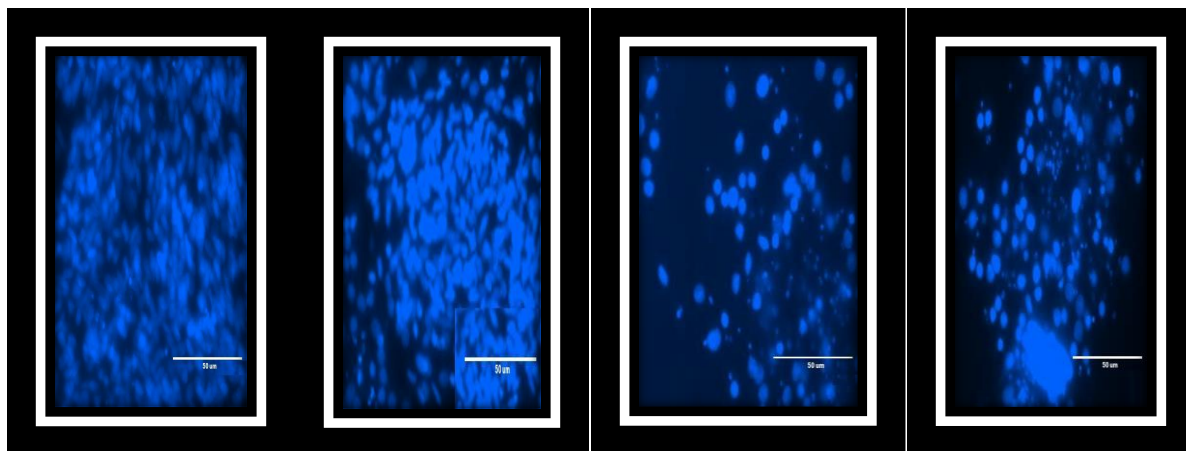
Figure 4.4A   **Figure 4.4B**   **Figure 4.4C**   **Figure 4.4D**
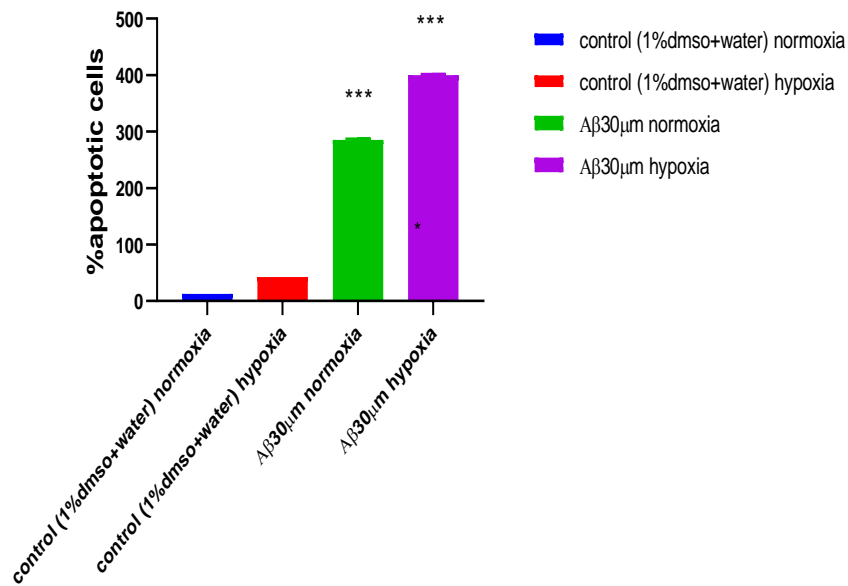
Figure 4.4E

Figure 4.4 Neuronal cells stained with Hoechst 33258. Morphological analysis of chromatin in (Figure 4.4A), control in normoxia, (Figure 4.4B), control in hypoxia, (Figure 4.4C), Aβ$_{25-35}$ treatment in normoxia, and (Figure 4.4D), Aβ$_{25-35}$ treatment in hypoxia. (Figure 4.4E), graph represents the percentage of apoptotic cells with nucleus fragmentation (n=3). *** represents a significant difference (P<0.01) between 30 μM of Aβ$_{25-35}$ and their respective controls in both normoxia and hypoxia conditions.

4.3.4. Immunofluorescence images of primary rat neurons after treatment in normoxia and hypoxia.

Figure 4.5 shows Immunofluorescence images of primary rat neurons after Aβ$_{25-35}$ treatment in normoxia and hypoxia. Tuj1 and DAPI staining of nuclei were used to assess cell morphology and functions. A healthy neuron consists of numerous long axons (Tuj1 staining) and bright nuclei (DAPI staining) in the control normoxia group (Figure 4.5 (Ai). Figure 4.5 (Aii) shows the control group in hypoxia. Neurons treated with 30 μM of Aβ$_{25-35}$ in normoxia for 24 hours becomes shorter

235

with fewer neurites and reduced cell densities compared to the control (Figure 4.5B). These effects are further enhanced in hypoxia conditions (Figure 4.5C).
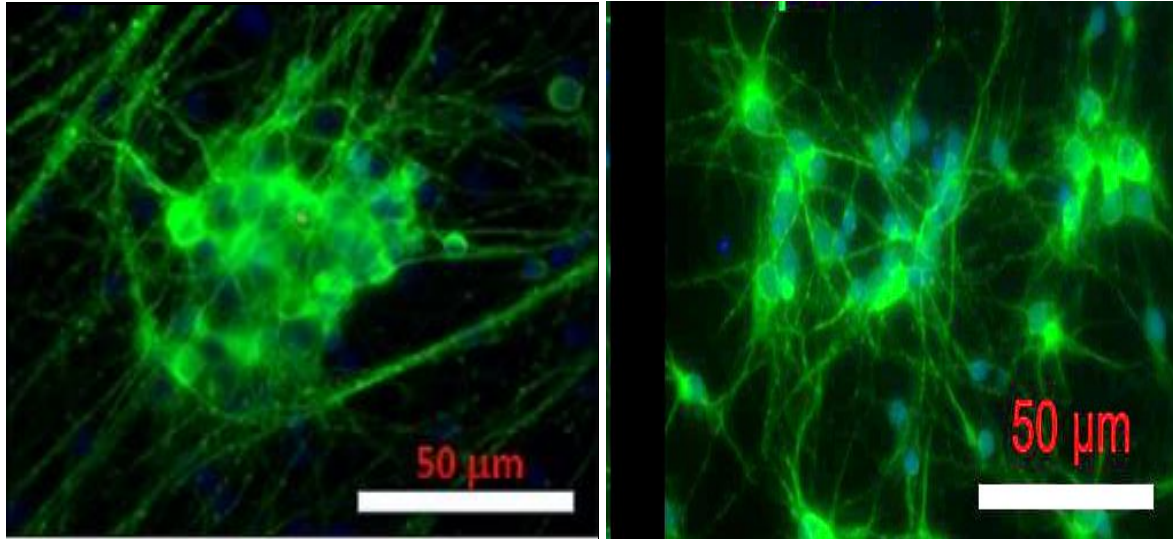
Figure 4.5 (Ai) Control normoxia   Figure 4.5 (Aii) Control hypoxia
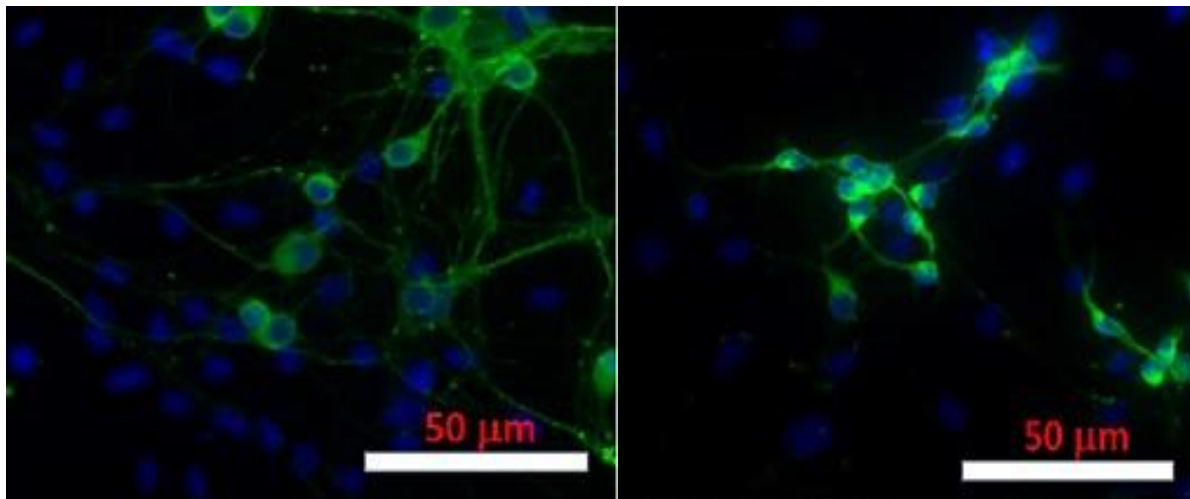
Figure 4.5 B. A$\beta_{25\text{-}35}$ (30μM) in normoxia   Figure 4.5 C. A$\beta_{25\text{-}35}$ (30μM) in hypoxia

Figure 4.5. Representative double-merged immunofluorescence images (FITC-labeled neuron-specific Tuj1 and DAPI-stained nuclei) of primary rat neurons following A$\beta_{25\text{-}35}$ treatment in normoxia and hypoxia conditions. Figure 4.5 (Ai): Control normoxia group. This shows a healthy neuron which consists of numerous long axons (Tuj1 staining) and bright nuclei (DAPI staining). Figure 4.5 (Aii): Control group in hypoxia. This shows a reduced healthy neuron consisting of

decreased long axons when compared with normoxia. In Figure 4.5B, neurons treated with 30 μM of Aβ25-35 in normoxia for 24 hours shows shorter and fewer neurites when compare with control in normoxia. Figure 4.5C depicts neurons treated with 30 μM of Aβ25-35 in hypoxia for 24 hours, exhibiting even significantly shorter and fewer neurites compared to control in hypoxia conditions.

4.3.5. Dose-dependent Aβ25-35 plus rutin (100 μM) on primary neurons in normoxia and hypoxia conditions.

4.3.5.1. Dose-dependent Aβ25-35 plus rutin (100 μM) on primary neurons - MTT assay in normoxia and hypoxia, with IC50 determined.

Neuronal cells were exposed to different concentrations of Aβ25-35 (ranging from 0 to 32 μM) plus rutin (100 μM) for 24 hours in both normoxia and hypoxia conditions. Cell viability was assessed using MTT assays. Treatment of neuronal cells with Aβ25-35 (ranging from 0 to 32 μM) plus rutin (100 μM) for 24 hours in normoxia resulted in a significant decrease in MTT activity at concentrations of 0.1, 0.3, 1, 3, 10, and 32 μM compared to the control (P<0.001, n=5) (Figure 4.6A). Figure 4.6B represents the quantification of different concentrations of Aβ25-35 (ranging from 0 to 32 μM) plus rutin (100 μM) for 24 hours in normoxia, showing a significant decrease in MTT activity (p < 0.001) and presenting the mean top value (91.76), mean IC50 (~6618 μM), and mean LogEC50 (~5.821 μM). Figure 4.6C illustrates the EC50 shift of Aβ25-35 (ranging from 0 to 32 μM) versus Aβ25-35 plus rutin treatment, indicating a shift of the curve to the right. Therefore, there is a significant increase in cell viability in the Aβ25-35 plus rutin (100 μM) treatment group compared to the Aβ25-35 (ranging from 0 to 32 μM) treatment group in normoxia.

Treatment of neuronal cells with Aβ25-35 (ranging from 0 to 32 μM) plus rutin (100 μM) for 24 hours in hypoxia resulted in a significant decrease in MTT activity at concentrations of 0.3, 1, 10, and 32 μM compared to the control (P<0.001, n=5) (Figure 4.7A). Figure 4.7B represents the

237

quantification of different concentrations of Aβ$_{25-35}$ (ranging from 0 to 32 μM) plus rutin (100 μM) for 24 hours in hypoxia, showing a significant decrease in MTT activity (p < 0.001) and presenting the mean top value (98.05), mean IC50 (~8869 μM), and mean LogEC50 (7.948 μM). Figure 4.7C illustrates the EC50 shift of Aβ$_{25-35}$ (ranging from 0 to 32 μM) versus Aβ$_{25-35}$ plus rutin treatment, indicating a shift of the curve to the right. Therefore, there is a significant increase in cell viability in the Aβ$_{25-35}$ plus rutin (100 μM) treatment group compared to the Aβ$_{25-35}$ (ranging from 0 to 32 μM) treatment group in hypoxia.
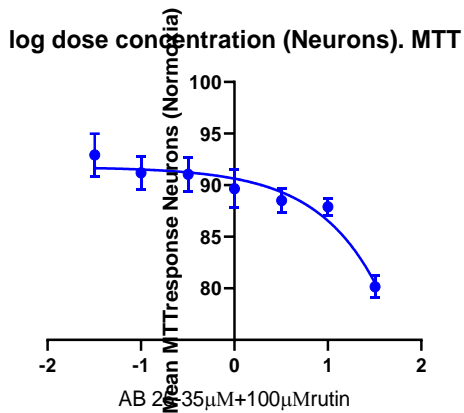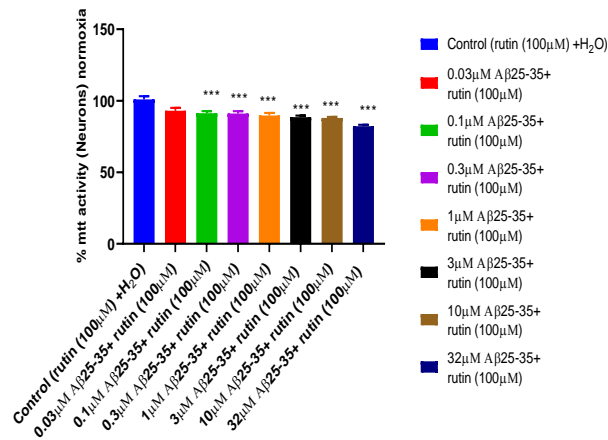
Figure 4.6(A)

Figure 4.6(B)
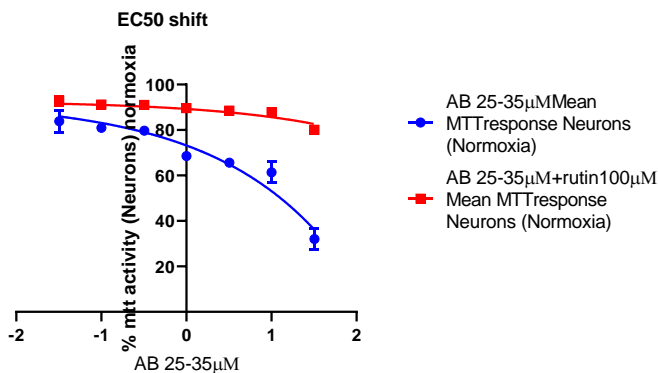
Figure 4.6(C)

Figure 4.6 Effects of rutin on Aβ$_{25-35}$-induced cytotoxicity in primary neuron cells under normoxia.

Neuronal cells were treated with various concentrations of Aβ$_{25-35}$ (0.03, 0.1, 0.3, 1, 3, 10, 32 μM)

+ rutin (100 μM) co-administration for 24 hours. Rutin (100 μM) + H₂O was considered 100%, and the data were normalized against that. *** represents a significant difference (P<0.001) between the control group (Rutin 100 μM + H₂O) and the variable concentrations of Aβ₂₅₋₃₅ (0-32 μM) plus rutin (100 μM) for 24 hours under normoxia. In Figure 4.6B, viability was evaluated using the MTT assay and quantified on a normalized response curve. Figure 4.6C indicates the EC50 shift of Aβ₂₅₋₃₅ (0-32 μM) versus Aβ₂₅₋₃₅ (0-32 μM) + rutin treatment group. There is a shift of the curve to the right.

Figure 4.7
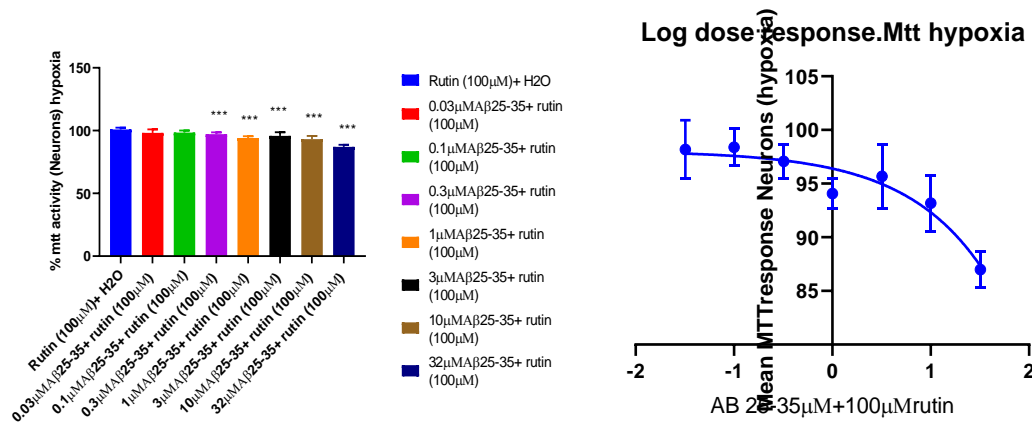
Figure 4.7A

Figure 4.7B

Figure 4.7 C

239
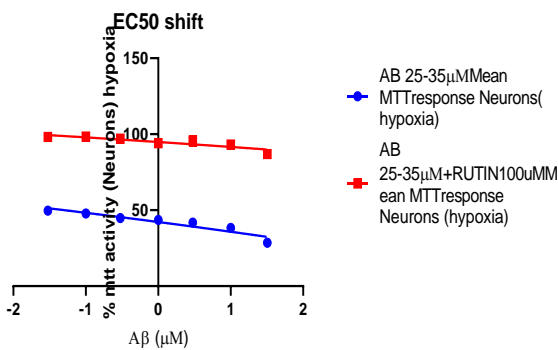
Figure 4.7 Effects of rutin on Aβ$_{25-35}$-induced cytotoxicity in primary neuron cells under hypoxia. Neuron cells were treated with Aβ$_{25-35}$ at various concentrations (0.03, 0.1, 0.3, 1, 3, 10, 32 μM) + rutin (100 μM) co-administration for 24 hours. Rutin (100 μM) + H$_2$O was considered 100%, and the data were normalized against that. *** represents a significant difference (P<0.001) between the control group (Rutin 100 μM + H$_2$O) and the variable doses of Aβ$_{25-35}$ in hypoxia. In Figure 4.7B, viability was evaluated using the MTT assay and quantified on a normalized response curve. Figure 4.7C indicates the EC50 shift of Aβ$_{25-35}$ (0-32 μM) versus Aβ$_{25-35}$ (0-32 μM) + rutin treatment group. There is a shift of the curve to the right.

4.3.5.2. Dose-dependent Aβ$_{25-35}$ + rutin (100 μM) on primary neurons (LDH assay) in normoxia and hypoxia, and EC50 determined.

Neuronal cells were exposed to different concentrations of Aβ$_{25-35}$ ranging from (0-32 μM) plus rutin (100 μM) for 24 hours under normoxia and hypoxia conditions, and their cytotoxicity was assessed by LDH assays. Treatment of neuronal cells with Aβ$_{25-35}$ ranging from (0-32 μM) plus rutin (100 μM) for 24 hours under normoxia conditions resulted in an increase in LDH activity as the dose of Aβ$_{25-35}$ increased (Figure 4.8A). Figure 4.8B represents different concentrations of Aβ$_{25-35}$ ranging from (0-32 μM) plus rutin (100 μM) for 24 hours in normoxia quantified on a normalized response curve (P < 0.001) (mean top value: 149, mean EC50: 318 μM, mean LogEC50: 9.50 μM). Figure 4.8C shows the EC50 shift of Aβ$_{25-35}$ (0-32 μM) versus Aβ$_{25-35}$ (0-32 μM) + rutin (100 μM). There is a shift of the curve to the left, indicating a significant decrease in cell cytotoxicity.

Treatment of neuronal cells with Aβ$_{25-35}$ ranging from (0-32 μM) plus rutin (100 μM) for 24 hours under hypoxia conditions resulted in an increase in LDH release as the dose of Aβ$_{25-35}$ increased (Figure 4.9A). Figure 4.9B represents different concentrations of Aβ$_{25-35}$ ranging from Aβ$_{25-35}$ (0-

32 μM) plus rutin (100 μM) for 24 hours in hypoxia, quantified on a normalized response curve (P < 0.001) (mean top value: 63.24, mean EC50: 101.8 μM, mean LogEC50: 2.008 μM). Figure 4.9C shows the EC50 shift of Aβ$_{25-35}$ (0-32 μM) versus Aβ$_{25-35}$ (0-32 μM) + rutin (100 μM) treatment group under hypoxia. There is a shift of the curve to the left, indicating a significant decrease in cell cytotoxicity.
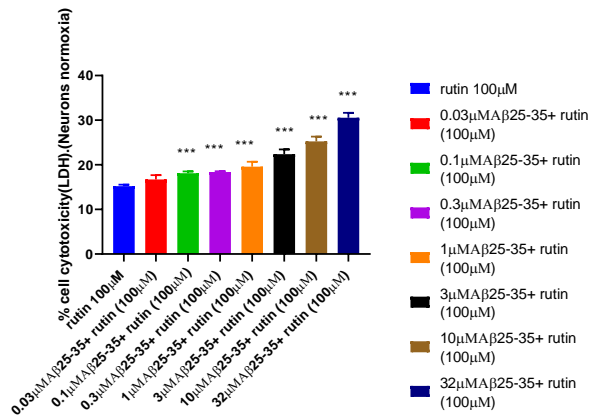
Figure 4.8A
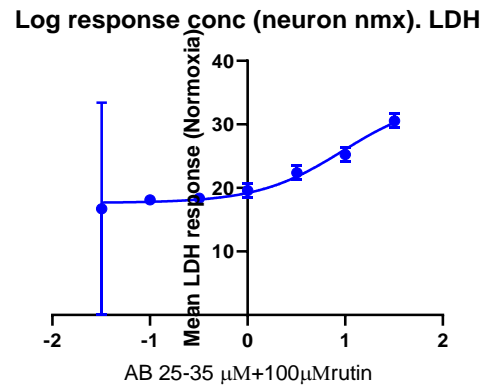
Figure 4.8B
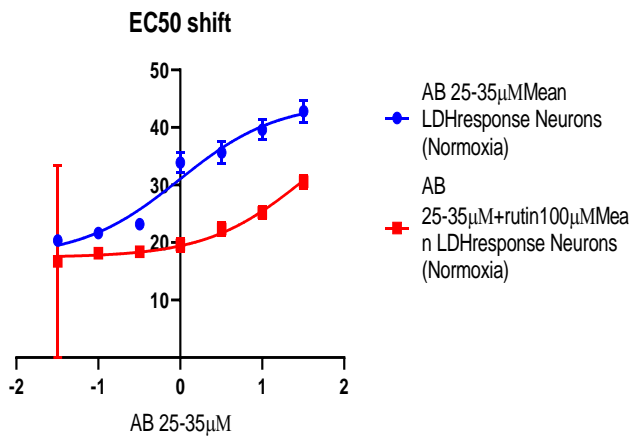
Figure 4.8C

Figure 4.8 Effects of rutin on Aβ$_{25-35}$-induced cytotoxicity of primary neuron cells in normoxia. Neuron cells were treated with Aβ at various concentrations (0.03, 0.1, 0.3, 1, 3, 10, 32 μM) + rutin (100 μM) co-administration for 24 hours. Rutin (100 μM) + H$_2$O was considered 100%, and the data were normalized against that. *** represents a significant difference (P < 0.001) between

241

the control group (Rutin 100 μM + H₂O) and the variable doses of Aβ₂₅₋₃₅ + Rutin 100 μM in

normoxia. In Figure 4.8B, cytotoxicity was evaluated using the LDH assay and quantified on a

normalized response curve. Figure 4.8C indicates the EC50 shift of Aβ₂₅₋₃₅ (0-32 μM) versus Aβ₂₅₋₃₅ (0-32 μM) + rutin treatment group. There is a shift of the curve to the left.
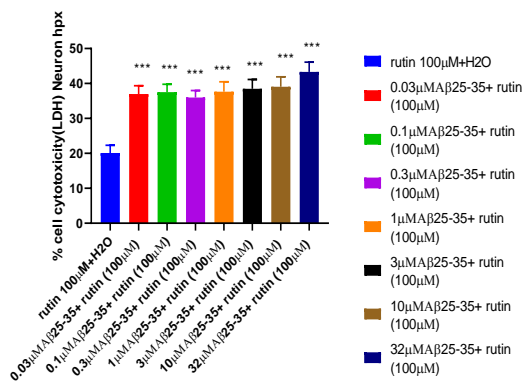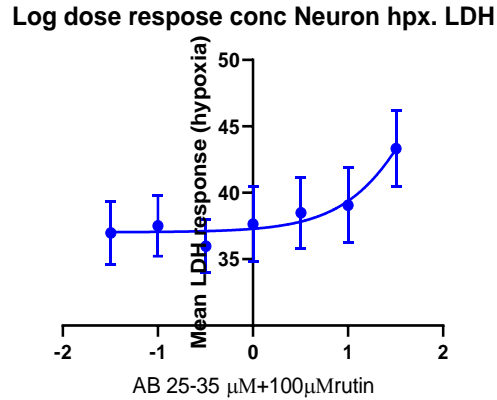
Figure 4.9A   Figure 4.9B
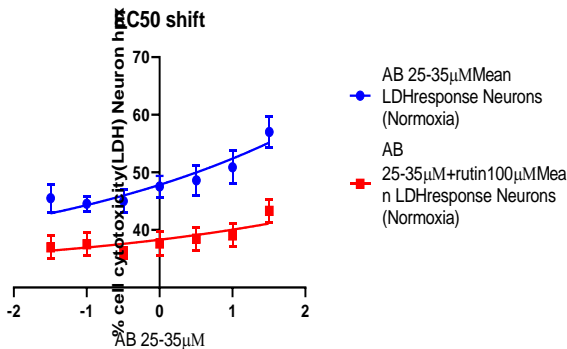
Figure 4.9C

Figure 4.9 Effects of rutin on Aβ₂₅₋₃₅-induced cytotoxicity of primary neuron cells in hypoxia.

Neuron cells were treated with Aβ at various concentrations (0.03, 0.1, 0.3, 1, 3, 10, 32 μM) +

rutin (100 μM) co-administration for 24 hours. Rutin (100 μM) + H₂O was considered 100%, and

the data were normalized against that. *** represents a significant difference (P < 0.001) between

the control group (Rutin 100 μM + H₂O) and the variable doses of Aβ₂₅₋₃₅ + Rutin 100 μM in

hypoxia. In Figure 4.9B, viability was evaluated using the LDH assay and quantified on a

normalized response curve. Figure 4.9C indicates the EC50 shift of Aβ$_{25-35}$ (0-32 μM) versus Aβ$_{25-35}$ (0-32 μM) + rutin treatment group. There is a shift of the curve to the left.

4.3.5.3. Combined analysis of the variable doses of Aβ$_{25-35}$ plus rutin (100 μM) on primary neurons - LDH assay in hypoxia and normoxia results (Figure 4.8 and 4.9) above
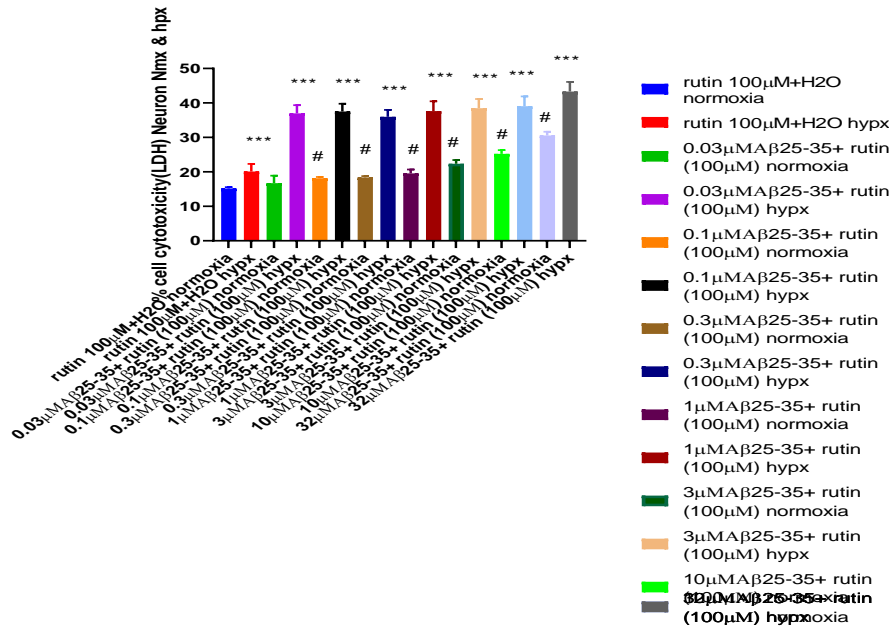
Figure 4.10 : Effects of rutin on variable doses of Aβ$_{25-35}$-induced cytotoxicity of primary neuron cells in normoxia and hypoxia. Neuron cells were treated with Aβ at various concentrations (0.03, 0.1, 0.3, 1, 3, 10, 32 μM) + rutin (100 μM) co-administration for 24 hours in both normoxia and hypoxia. Rutin (100 μM) + H$_2$O in normoxia and hypoxia were considered 100%, and the data were normalized against those, respectively. # represents a significant difference (P < 0.001) between the control group (Rutin 100 μM + H$_2$O) and the variable doses of Aβ$_{25-35}$ + Rutin 100 μM in normoxia. *** represents a significant difference (P < 0.001) between the control group (Rutin 100 μM + H$_2$O) and the variable doses of Aβ$_{25-35}$ + Rutin 100 μM in hypoxia.

4.3.6. Effects of Rutin against Aβ₂₅₋₃₅-induced apoptosis of primary neurons in normoxia and hypoxia.

4.3.6.1. Effects of Rutin against Aβ₂₅₋₃₅-induced apoptosis of primary neurons under normoxia conditions.

Hoechst 33258 staining was used to assess alterations in cellular morphology in order to characterize the degree of Aβ$_{25\text{-}35}$-induced cell apoptosis (Figure 4.11). Primary neurons treated with 30 μM of Aβ$_{25\text{-}35}$ in normoxia for 24 hours showed nuclei fragmentation (Figure 4.11B), while treatment with 100 μM rutin for 24 hours significantly reduced nuclei fragmentation (Figure 4.11C).
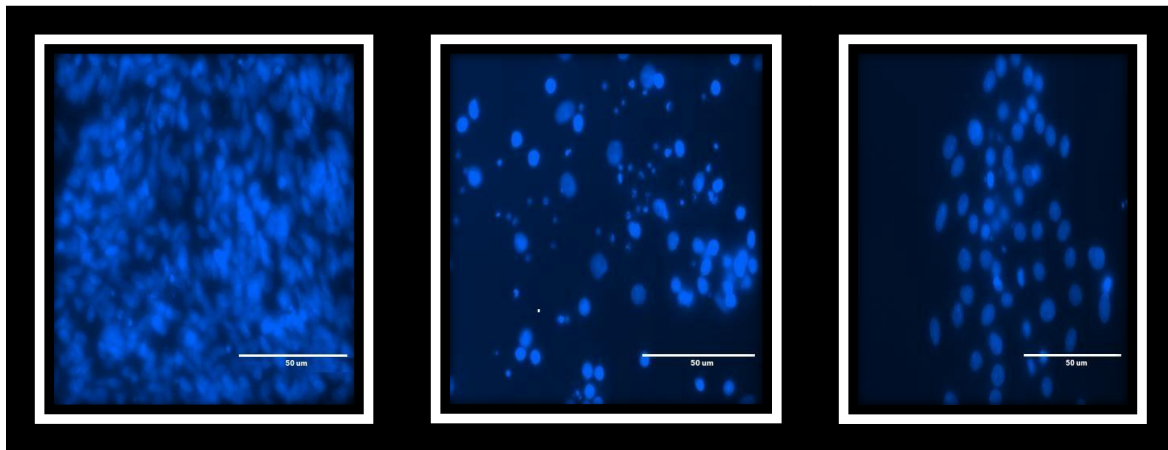
Figure 4.11A   Figure 4.11B   Figure 4.11C
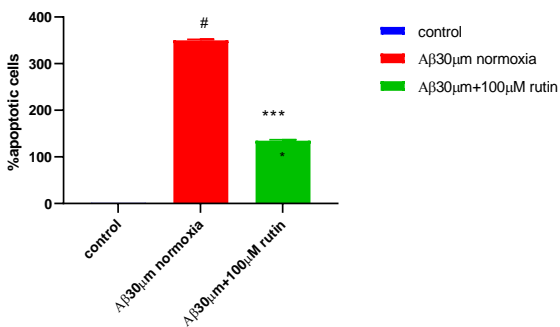
Figure 4.11D

Figure 4.11 Primary neurons stained with Hoechst 33258. Morphological analysis of chromatin in (Figure 4.11A) control, (Figure 4.11B) Aβ$_{25-35}$ treatment in normoxia, and (Figure 4.11C) Aβ$_{25-35}$ treatment plus rutin-treated cells. In Figure 4.11B, cells showed nuclei fragmentation following Aβ$_{25-35}$ treatment. Figure 4.11C shows that rutin treatment markedly reduced nuclei fragmentation. The graph represents the percentage of apoptotic cells, which had nuclei fragmentation (n=3). # represents a statistically significant difference (p < 0.01) between 30 μM Aβ$_{25-35}$ against the control (H$_2$O), and *** represents a significant difference (p < 0.001) between the rutin treatment group at 100 μM plus 30 μM concentration of Aβ$_{25-35}$ and 30 μM Aβ$_{25-35}$ alone in normoxia (Figure 4.11D).

4.3.6.2. Effects of Rutin against Aβ$_{25-35}$-induced apoptosis in primary neurons in hypoxia.

In Figure 4.12, primary neurons treated with 30 μM of Aβ$_{25-35}$ in hypoxia for 24 hours showed higher nuclei fragmentation compared to that in normoxia (Figure 4.12B). However, treatment with 100 μM rutin for 24 hours significantly reduced nuclei fragmentation (Figure 4.12C).
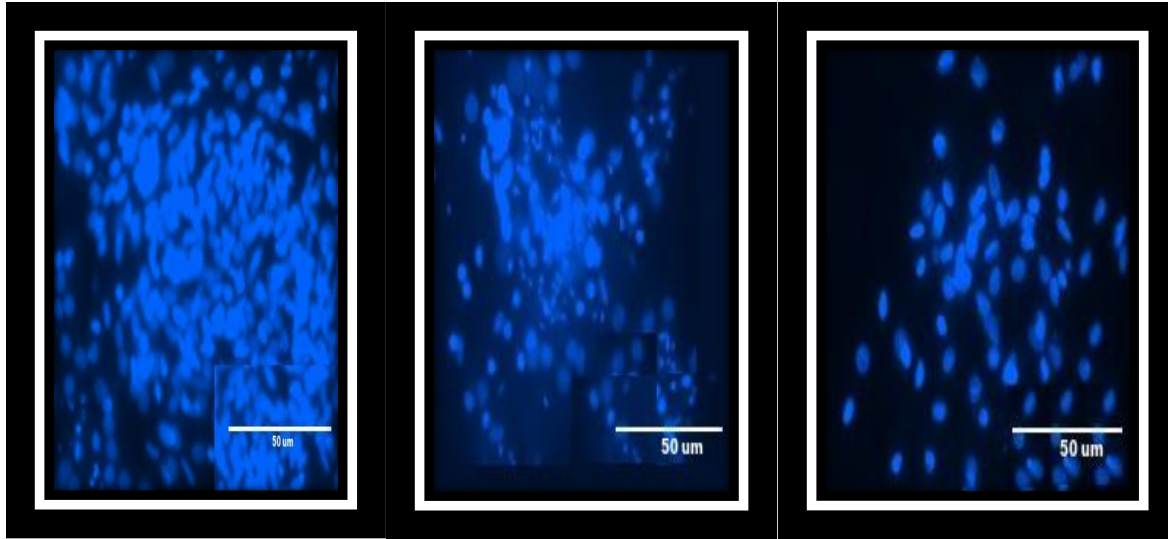
Figure 4.12A   Figure 4.12B   Figure 4.12C
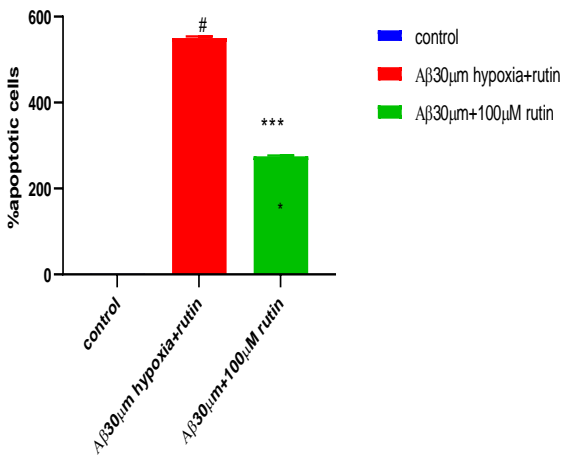
Figure 4.12D

Figure 4.12 Primary neurons stained with Hoechst 33258. Morphological analysis of chromatin in (Figure 4.12A) control, (Figure 4.12B) Aβ$_{25-35}$ treatment in hypoxia, and (Figure 4.12C) Aβ$_{25-35}$ treatment plus rutin-treated cells. In Figure 4.12B, cells showed nuclei fragmentation following Aβ$_{25-35}$ treatment in hypoxia. Figure 4.12C shows that rutin treatment markedly reduced the nuclei fragmentation. The graph represents the percentage of apoptotic cells, which had nuclei

fragmentation (n=3). # represents a statistically significant difference (p < 0.01) between 30 μM

Aβ$_{25-35}$ against the control (H$_2$O) group, and *** represents a significant difference (p < 0.001)

between the rutin treatment group at (100 μM plus 30 μM concentration of Aβ$_{25-35}$) and 30 μM

Aβ$_{25-35}$ alone in hypoxia (Figure 4.12D).

4.3.7. Immunofluorescence images of primary rat neurons treated with Aβ$_{25-35}$ and rutin in normoxia and hypoxia.

Double merged immunofluorescence (FITC-labeled neuron-specific Tuj1 and DAPI-stained nuclei) images of Tuj1 and DAPI staining of nuclei in primary rat neurons treated with Aβ$_{25-35}$ and rutin are shown in figure 4.13. Neurons became healthier with numerous, long axons (Tuj1 staining) and bright nuclei (DAPI staining) after co-treatment of 30 μM Aβ$_{25-35}$ with 100 μM rutin in both normoxia and hypoxia for 24 hours.
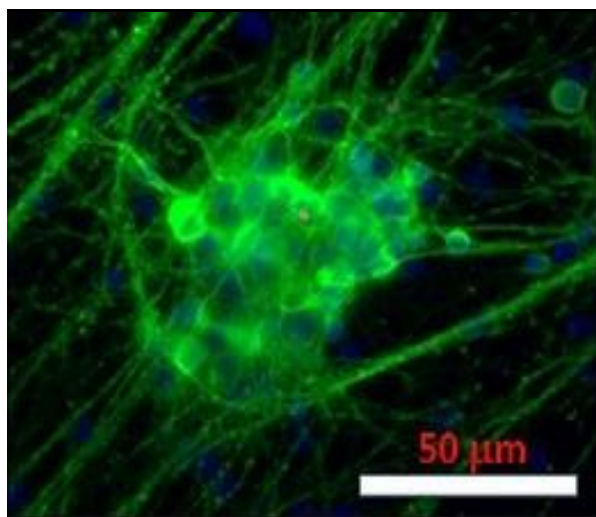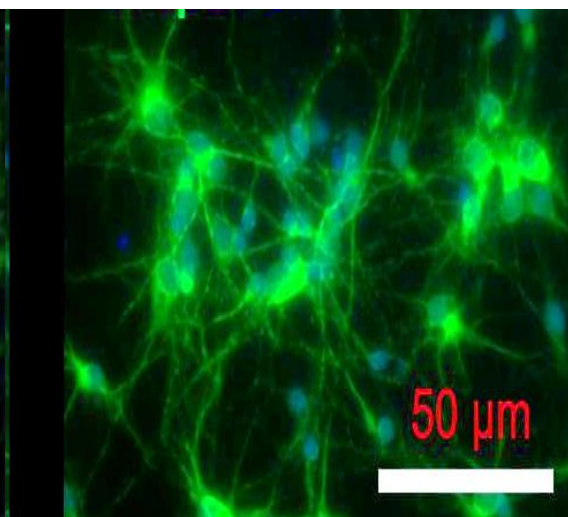
Figure 4.13A   Figure 4.13B
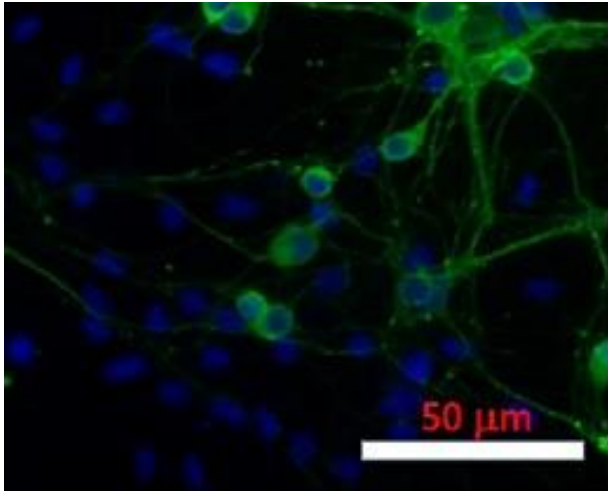
Figure 4.13**C**
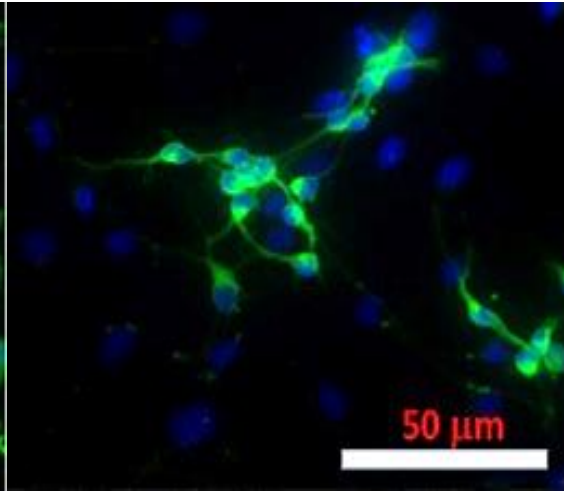
Figure 4.13**D**
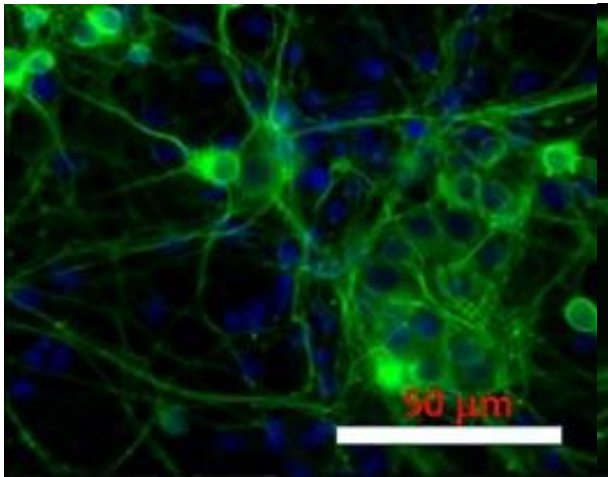
Figure 4.13**E**
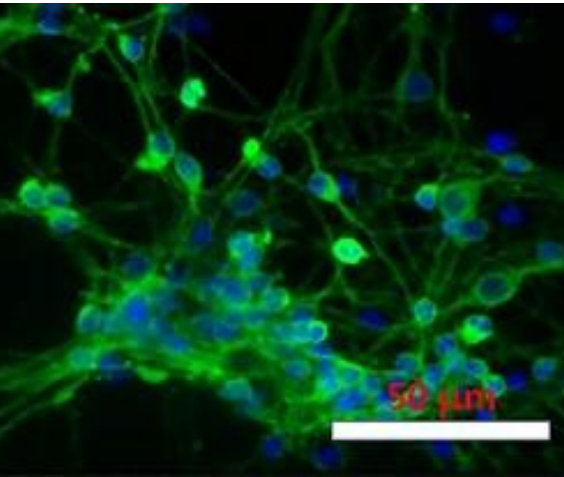
Figure 4.13**F**

Figure 4.13**G**

248
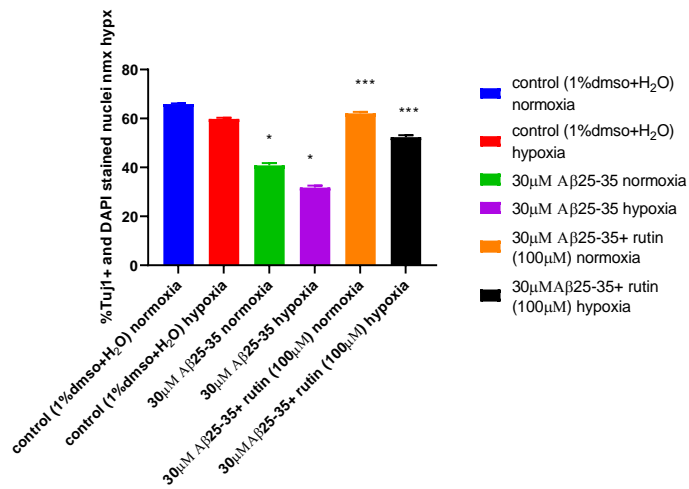
Figure 4.13. Representative double merged (FITC-labeled neuron-specific Tuj1 and DAPI-stained nuclei) immunofluorescence images of primary rat neurons following Aβ$_{25-35}$ plus rutin (100 μM) in normoxia and hypoxia conditions. Figure 4.13A and Figure 4.13B show healthier controls in normoxia and hypoxia, respectively. Figure 4.13C indicates neurons with significant shorter and fewer neurites after treatment with 30 μM Aβ$_{25-35}$ in normoxia for 24 hours when compared with control in normoxia. Figure 4.13D indicates neurons with significant shorter and fewer neurites after treatment with 30 μM Aβ$_{25-35}$ in hypoxia for 24 hours compared with control in hypoxia. Figure 4.13E shows significant healthier neurons with numerous, long axons (Tuj1 staining) and bright nuclei (DAPI staining) after co-treatment of 30 μM Aβ$_{25-35}$ with 100 μM rutin in normoxia for 24 hours, compared to the treatment group of 30 μM Aβ$_{25-35}$ in normoxia (Figure 4.13C). Figure 4.13F shows significant healthier neurons with numerous, long axons (Tuj1 staining) and bright nuclei (DAPI staining) after co-treatment of 30 μM Aβ$_{25-35}$ with 100 μM rutin in hypoxia for 24 hours, compared to the treatment group of 30 μM Aβ$_{25-35}$ alone in hypoxia (Figure 4.13D). Figure 4.13G represents the mean ± SE (n=3) for all the measurements shown in the graph. * represents a statistically significant difference (p < 0.01) between 30 μM Aβ$_{25-35}$ in normoxia and hypoxia against their respective control (1%DMSO + H$_2$O), and *** represents a significant difference (p < 0.001) between the rutin treatment group at (100 μM plus 30 μM concentration of Aβ$_{25-35}$) in both conditions and 30 μM Aβ$_{25-35}$ alone in both normoxia and hypoxia.

4.4 DISCUSSION

Alzheimer's disease (AD), which is a progressive neurodegenerative disease, is the most common type of dementia. Several hypotheses have been proposed for AD pathogenesis, including the amyloid cascade, tau hyperphosphorylation, neurotransmitters, and oxidative stress. However, the underlying causes and ideal treatment plans are still not fully understood. Currently, only a few

drugs are available that improve symptoms but do not delay the progression of the disease. New theories on the pathogenesis of AD from different perspectives are being discovered, such as gamma oscillations, prion transmission, cerebral vasoconstriction, growth hormone secretagogue receptor 1α (GHSR1α)-mediated mechanisms, and infection. Advances in these areas may help explain the pathological mechanisms of AD and lead to potential effective treatment strategies.

Among the hallmarks of AD pathology, such as the deposition of extracellular amyloid-β plaques and intracellular tau protein tangles, along with functional disturbances in synapses and mitochondria, vascular disorders, and aberrant changes in microglia and astrocytes, the molecular link between ischemia/hypoxia and amyloid precursor protein (APP) processing has only recently been established. Neuroimaging techniques have revealed that many brain regions predisposed to AD pathology exhibit a significant decline in cerebral blood flow, even at the stage of mild cognitive impairment preceding AD diagnosis. This brain hypoperfusion reduces oxygen and glucose delivery, leading to local hypoxia, which in turn stimulates Aβ production in endothelial cells and neighboring neurons, promoting the generation of cerebral amyloid angiopathy (CAA). It has been reported that sporadic AD could be initiated by ischemic episodes that activate APP processing and increase Aβ production. There is convincing evidence that hypoxia-inducible factor-1α (HIF-1α) activates both β and γ secretases, enhancing APP processing and Aβ production in hypoxia.

This study evaluated the cytotoxicity of primary neurons induced by $Aβ_{25-35}$ in normoxic and hypoxic conditions and also examined the apoptosis of primary neurons under these conditions. Findings revealed a reduction in MTT activity of primary neurons induced by $Aβ_{25-35}$ in normoxia, which is consistent with previous findings indicating that $Aβ_{25-35}$ inhibits neuronal cell viability in a concentration-dependent manner. The IC50 was also determined. Furthermore, the reduction in

MTT activity appeared to be more pronounced during hypoxic conditions, suggesting that primary neurons are more susceptible to Aβ peptide toxicity during hypoxia, in line with previous research showing increased vulnerability of hippocampal neurons to Aβ peptide toxicity during hypoxia.

Additionally, the LDH assay showed a significant increase in LDH activity between the control and Aβ$_{25-35}$ treated cells, indicating that Aβ$_{25-35}$ was cytotoxic to primary neurons. This suggests that Aβ exhibits toxicity in neurons, possibly due to the interaction between iron and Aβ, leading to toxic effects and generation of reactive oxygen species (ROS). Moreover, the increase in cell toxicity appeared to be significantly higher during hypoxia, indicating an interplay between hypoxia and Aβ peptide, exacerbating neuronal death. This can be attributed to the overexpression of HIF-1α, which binds to BACE1 mRNA and increases its expression. Hypoxia can also alter APP processing, increasing the activity of β and γ secretases, and significantly up-regulating BACE1 gene expression, resulting in increased β and γ secretase activity.

Oxidative stress, resulting from an imbalance between the generation of reactive oxygen species (ROS) and antioxidants, has been proposed as a cause of AD. The brain is particularly susceptible to oxidative stress due to its high oxygen consumption, elevated levels of polyunsaturated fatty acids, and low levels of antioxidants. Oxidative stress and Aβ are closely related, as Aβ aggregation induces oxidative stress both in vivo and in vitro.

Apoptosis, a form of programmed cell death, has been suggested as an important mechanism of neurodegeneration in AD pathogenesis, supported by evidence of apoptotic cell death in postmortem AD brains and cultured neurons incubated with Aβ peptides. Aβ peptide-triggered neuronal cell death may involve different pathways, including stress kinase activation, membrane receptor-mediated response, calcium imbalance, and oxidative stress, ultimately leading to the activation of caspases.

This study evaluated Aβ$_{25-35}$-induced apoptosis of primary neurons using Hoechst 33342 staining under both normoxic and hypoxic conditions. Cells undergoing apoptosis exhibit nuclear condensation and DNA fragmentation, which can be detected through Hoechst 33342 staining and fluorescence microscopy (Allen, 2020). The nuclei of healthy cells are generally spherical, with evenly distributed DNA. During apoptosis, the DNA becomes condensed, distinguishing it from necrosis. Nuclear condensation can be observed using DNA-binding dyes like Hoechst 33342 or 4', 6-diamidino-2-phenylindole (DAPI) under a conventional fluorescent microscope that emits light at ~350 nm and transmits light at ~460 nm. Hoechst stains are a family of fluorescent dyes used for labeling DNA in fluorescence microscopy. This dye is excited by ultraviolet light at around 350 nm and emits blue/cyan fluorescence light with a maximum emission at 461 nm. Hoechst stains can be used on live or fixed cells and are often an alternative to other nucleic acid stains like DAPI. The key difference is that Hoechst 33342, with an additional ethyl group, is more lipophilic and can readily cross intact cell membranes. It also appears to be less toxic than DAPI, ensuring higher cell viability. Hoechst 33342 preferentially binds to adenine-thymine (A-T) regions of DNA, allowing it to observe nuclear condensation and distinguish apoptotic cells from healthy and necrotic cells.

Primary neurons treated with Aβ$_{25-35}$ exhibit distinct nuclei fragmentation, indicating changes in cellular morphology and significant induction of apoptosis. This aligns with the findings of Zhi-kun (2012), which state that Aβ$_{25-35}$ can induce apoptosis in neurons. Moreover, primary neurons treated with Aβ$_{25-35}$ under hypoxic conditions show higher levels of nuclei fragmentation compared to normoxic conditions, suggesting increased cellular apoptosis. This indicates that Aβ$_{25-35}$ induces cellular apoptosis, which can be enhanced by the increased production of reactive oxygen species (ROS) during hypoxia, leading to oxidative damage of cellular components,

proteins, and DNA. This agrees with the findings of Yuna (2018) and Pengjuan (2015), which suggest that Aβ treatment leads to an abrupt increase in ROS levels, resulting in cellular, protein, and DNA oxidative damage and subsequent apoptosis.

Tuj1 is a tubulin protein specifically used during the differentiation of neuronal cell types (Lee, 1990). Tubulins are the main building blocks of microtubules, which are structural components of the cytoskeleton involved in cell structure maintenance, intracellular transport, and cell division. In immunohistochemical staining, Tuj1 is found in the cell bodies, dendrites, axons, and axon terminals of immature neurons. Tuj1 is particularly useful for detecting injury-related changes in the somatic cytoskeleton composition (Geisert, 1989). Immunofluorescence images of primary rat neurons, representative of double-merged (FITC-labeled neuron-specific Tuj1 and DAPI staining of nuclei), were evaluated to assess cellular morphology and functions. Neurons treated with $Aβ_{25-35}$ in normoxic conditions exhibited shortened length, fewer neurites, and reduced cell densities, which were further increased under hypoxic conditions. This suggests that $Aβ_{25-35}$ induces loss of cell structure and functions, resulting in cellular, protein, and DNA oxidative damage, ultimately leading to apoptosis.

It has been revealed that a history of stroke increases the prevalence of AD by approximately twofold in elderly patients (Schneider, 2003). The risk is higher when stroke is associated with atherosclerotic vascular risk factors (Jellinger, 2003). Hypoperfusion, a common vascular component among AD risk factors, leads to hypoxia. Recent findings indicate that hypoxia can modify amyloid precursor protein (APP) processing, increasing the activity of β- and γ-secretases. Hypoxia significantly upregulates BACE1 gene expression, thereby enhancing β-secretase activity (Sun, 2006). Hypoxia also promotes Aβ deposition, neuritic plaque formation, and memory deficits in Swedish mutant APP transgenic mice. These findings provide a molecular mechanistic

link between vascular factors and AD. Overexpression of HIF-1α in neuronal cells increases BACE1 mRNA and protein levels, while downregulation of HIF-1α reduces BACE1 levels (Zhang, 2007). Hypoxic conditions have also been shown to increase γ-secretase activity. HIF-1α binds to the anterior pharynx-defective phenotype (APH-1) promoter, upregulating APH-1 expression. Hypoxia-induced activation of HIF-1α increases APH-1 mRNA and protein expression, leading to increased γ-cleavage of APP and Notch (Li, 2009). Furthermore, hypoxia has been linked to dysregulation of neuronal and glial-cell calcium, dysregulated glutamate signaling, intracellular calcium store dysfunction, and neuroinflammation. Multiple research studies confirm the facilitation of AD pathology by hypoxia (Shiota, 2013; Liu, 2015; Zhang, 2017). Hypoxia has been shown to increase ROS levels (Zhang and Le, 2010), Aβ production (Li, 2009), enhance tau phosphorylation (Gao, 2013), and induce neuroinflammation (Smith, 2013). Mitochondria-derived ROS can activate HIF-1α through post-translational modification or p38 mitogen-activated protein kinase (MAPK) pathways. Intracellular ROS levels unexpectedly increase under hypoxic conditions (Guzy, 2005). NADPH oxidase has been suggested as an important ROS-generating oxygen sensor expressed in tissues associated with systemic hypoxic responses (Marshal, 1996). Alternatively, mitochondria have also been implicated as the source of ROS involved in the hypoxic response. The electron transport chain, consisting of five multiprotein complexes, generates ROS during the oxidation of NADH and FADH2 (derived from energy-rich molecules) and their transfer to ubiquinol. These complexes generate ROS while transporting electrons. Complexes I, II, and III are involved in ROS generation (Klimova and Chandel, 2008). It has been established that hypoxia increases ROS production through the transmission of electrons from ubisemiquinone to molecular oxygen at the Qo site of complex III in the mitochondrial transport chain (Bell, 2007). Mitochondria-derived ROS are required to stabilize

254

and activate HIF-1α. Antioxidants have been shown to reverse hypoxia-induced HIF-1α activation (Aminova, 2008). Antitumorigenic effects of antioxidants are attributed to the inhibition of HIF-1α-dependent events (Gao, 2007). Additionally, the addition of oxidants like H2O2 induces HIF-1α activity upregulation even in normoxic conditions (Page, 2008). Mitochondrial ROS regulates HIF-1α stability during hypoxia, possibly involving the phosphatidylinositol 3 kinase (PI3K)-protein kinase B (PKB/Akt) signaling pathway (Shaw and Cantley, 2006). Studies suggest that ROS generation can activate this pathway, leading to HIF-1α enhancement in cancer cells (Zhou, 2007; Flu, 2007).

Rutin is a common dietary flavonol glycoside composed of quercetin and the disaccharide rutinose. Rutin exhibits several pharmacological properties, such as reducing oxidative stress and preventing inflammation (Aldhabi et al., 2015; Riaz et al., 2018). It exerts numerous neuroprotective actions within the brain, including protecting neurons against injury induced by neurotoxins, suppressing neuroinflammation, and potentially enhancing memory. Rutin scavenges free radicals, inhibits superoxide radical production, and enhances the activity of antioxidant enzymes such as glutathione peroxidase and reductase to maintain the levels of reduced glutathione, which is a biological antioxidant (Kamalakkannan et al., 2006). Rutin has therapeutic potential for the treatment of neurodegenerative diseases associated with oxidative stress (Park et al., 2014; Motamedshariaty et al., 2014). Research has shown that rutin significantly attenuated memory deficit in AD transgenic mice, decreased oligomer Aβ levels, increased superoxide dismutase (SOD) activity and the glutathione (GSH)/glutathione disulfide (GSSG) ratio, reduced GSSG and malondialdehyde (MDA) levels, downregulated microgliosis and astrocytosis, and decreased IL-Iβ and IL-6 levels in the brain (Xu et al., 2014). This indicates that rutin is a

promising agent for AD treatment due to its antioxidant, anti-inflammatory, and Aβ oligomer-reducing activities (Xu et al., 2014).

This study investigated the effect of rutin on Aβ$_{25-35}$-induced toxicity and apoptosis in primary rat neurons under both normoxia and hypoxia conditions. MTT and LDH assays were used to determine cell viability and cytotoxicity, and the IC50 of rutin was also evaluated. The results showed stability of cell viability as the dose of rutin increased, and the IC50 was around 100 μM, indicating that rutin is safe to use. Therefore, a concentration of 100 μM was used for the remaining experiments involving rutin on primary neurons. The study investigated whether rutin treatment could inhibit primary neuron cytotoxicity after the induction of Aβ$_{25-35}$ under normoxia and hypoxia conditions. Results revealed that rutin inhibits Aβ$_{25-35}$-induced cytotoxicity in primary neurons under both normoxia and hypoxia. Rutin was found to significantly increase cell viability and decrease cell cytotoxicity in Aβ$_{25-35}$-induced primary neurons under normoxia. This implies that rutin protects neurons against Aβ$_{25-35}$-induced cytotoxicity by inhibiting cellular damage. The results are consistent with the findings of Shao-wei (2012), which states that rutin is a multifunctional flavonoid that can inhibit Aβ aggregation and cytotoxicity. Additionally, rutin significantly increased cell viability and reduced cell cytotoxicity in Aβ$_{25-35}$-induced primary neurons under hypoxia conditions. Thus, rutin may activate HIF, indicating its potential pharmacological function in HIF stabilization.

This research study further investigated the effect of rutin on Aβ$_{25-35}$-induced cellular apoptosis by Hoechst 33258 staining under both normoxia and hypoxia. The results revealed a significant reduction in the level of apoptosis in normoxia, suggesting that rutin can inhibit cellular apoptosis, possibly through a decrease in ROS and by inhibiting cellular, protein, and DNA oxidative damage. Additionally, the results revealed a significant reduction in the level of apoptosis under

hypoxia conditions, indicating that rutin, as an antioxidant, may reverse hypoxia-induced HIF-1α activation, suppress neuronal cell death caused by hypoxia or oxidative stress, and protect against Aβ peptide toxicity.

Immunofluorescence images using double merged (FITC-labeled neuron-specific Tuj1 and DAPI staining of nuclei) revealed healthier neurons with longer and more neurites when Aβ$_{25-35}$-induced neurons were treated with rutin under both normoxia and hypoxia conditions. This shows that rutin can inhibit the loss of cell structure and functions, further confirming the cytoprotective effects of rutin.

In conclusion, this study discovered dose-dependent Aβ$_{25-35}$ aggregates toxicity on primary neurons. Aβ$_{25-35}$ aggregates induced apoptosis in primary neurons under normoxia conditions. Furthermore, the combined treatment of Aβ$_{25-35}$ aggregates and hypoxia significantly enhanced toxicity and apoptosis, possibly due to an increase in ROS during hypoxia. Additionally, in both normoxia and hypoxia conditions, rutin was found to be neuroprotective against Aβ$_{25-35}$-induced cytotoxicity in primary neurons. Rutin treatment also significantly reduced Aβ$_{25-35}$-induced cell apoptosis, thus inhibiting cellular damage. This results indicate that rutin attenuates Aβ$_{25-35}$-induced cytotoxicity and apoptosis in primary neurons, possibly through its scavenging of free radicals and antioxidant effects. Therefore, rutin may serve as a novel drug for AD treatment, given its ability to scavenge free radicals, inhibit oxidative stress, chelate iron, and potentially stabilize HIF.

Chapter 5

RUTIN REDUCES THE INFLAMMATORY RESPONSE OF BV-2 MICROGLIA CELLS IN THE PRESENCE OF LPS IN ALZHEIMER'S DISEASE

5.1 INTRODUCTION

Inflammation is the response of tissues to chemical or mechanical injury and infection, often caused by various bacteria (Hu, 2013). It manifests with features such as swelling, redness, heat, and pain and is a crucial defense response against injury, tissue ischemia, autoimmune responses, or infectious agents. However, the inflammatory response can also cause significant damage to the individual. Lipopolysaccharide (LPS), a constituent of the outer membrane of gram-negative bacteria, triggers cellular responses that play critical roles in the pathogenesis of inflammatory responses (Wang, 2011). LPS induces an acute inflammatory response to pathogens and has been widely used to establish inflammatory models due to its ability to stimulate the release of inflammatory cytokines such as interleukin (IL)-8, IL-6, and IL-1β in various cell types (Zhou et al., 2016; Tong et al., 2019). Inflammation is a major contributing factor to the damage observed in autoimmune diseases, as it activates the production of inflammatory mediators like kinins, cyclooxygenases, and cytokines. LPS has been shown to promote the secretion of TNF-α and IL-6 in a dose-dependent manner. TNF-α is an early endogenous mediator of inflammation, and IL-6 is a major pro-inflammatory cytokine involved in the acute-phase response (Hu et al., 2013). These inflammatory factors can be used as markers to assess the degree of inflammation.

Alzheimer's disease (AD) is a degenerative, progressive, and terminal neurological disease. The neuro-pathogenesis of AD is believed to be triggered by the excessive accumulation of toxic beta-amyloid (Aβ), which leads to neurotoxicity, neuroinflammation, oxidative stress, and neuronal cell death (Prasansuklab and Tencomnao, 2013). Microglia, the resident immune cells in the brain,

normally remain in a resting state but become activated in response to pathogens, toxins, or cellular damage. Microglia-mediated neuroinflammation, characterized by excessive microglial activation and overproduction of pro-inflammatory cytokines and chemokines, is a significant component of AD. While it initially functions as a defense mechanism against Aβ deposition in the brain, it can also lead to neurodegeneration (Mosher and Wyss-Coray, 2014). Excessive activation of microglia not only releases inflammatory cytokines but also synthesizes and releases cytotoxic factors like nitric oxide and reactive oxygen species, causing significant neuronal cell damage (Mosher and Wyss-Coray, 2014). Inhibition of microglia-mediated inflammatory responses could have a potential therapeutic role in the treatment of AD. Additionally, Aβ inhibits long-term potentiation (LTP), a promising cellular mechanism for memory formation, and microglia are involved in this inhibition (Wang et al., 2014). Therefore, besides direct neuronal cell death, Aβ also induces neuronal cell death through neuroinflammation and inhibition of synaptic plasticity. Activated microglia release pro-inflammatory mediators, including nitric oxide (NO), inducible NO synthase (iNOS), interleukins (IL), tumor necrosis factor-alpha (TNF-α), and toxic free radicals, leading to progressive damage in neurodegenerative disorders, including Alzheimer's disease (Kim et al., 2004; Hyun Kang, 2014). In vitro studies have shown that microglia can be activated by lipopolysaccharide (LPS), which is used to study neuroinflammatory mechanisms (Kim et al., 2004; Hyun Kang, 2014). LPS-activated BV-2 microglia cells increase the production of immune-related cytotoxic factors and pro-inflammatory cytokines (Park et al., 2013). Therefore, agents that reduce microglial activation and their pro-inflammatory responses could be important therapeutic strategies for treating neuroinflammatory disorders. Given the existing literature supporting the role of microglial activation in neurodegenerative disorders, there is considerable interest in

identifying compounds from natural sources that can reduce or prevent neuroinflammation and could be beneficial in neurodegenerative diseases, including AD.

Rutin is a naturally occurring flavonoid glycoside found in many foods and fruits, and it possesses various pharmacological functions, including antioxidant, anti-inflammatory, and cytoprotective effects. It is a common dietary flavonol glycoside composed of quercetin and the disaccharide rutinose. Rutin is present in fruits such as oranges, grapefruits, limes, apples, berries (e.g., mulberries, cranberries), and is one of the primary flavonoids found in numerous multivitamin preparations and herbal remedies (Kreft, 1999; Chua, 2013). Rutin exhibits several pharmacological properties, including reducing oxidative stress, preventing inflammation, and exerting cardiovascular and neuroprotective effects (Aldhabi, 2015; Riaz, 2018). It attenuates oxidative stress, decreases the production of nitric oxide (NO) and pro-inflammatory cytokines in vitro, inhibits amyloid β (Aβ) aggregation and cytotoxicity (Wang et al., 2012). Rutin exerts numerous neuroprotective actions within the brain, including its ability to protect neurons against injury induced by neurotoxins, suppress neuroinflammation, and potentially enhance memory. It scavenges free radicals, inhibits superoxide radical production, and enhances the activity of antioxidant enzymes such as glutathione peroxidase and reductase to maintain reduced glutathione levels, which is a biological antioxidant (Kamalakkannan et al., 2006). Rutin has therapeutic potential for the treatment of neurodegenerative diseases associated with oxidative stress (Park et al., 2014; Motamedshariaty et al., 2014).

Xu et al. reported that rutin decreases β-amyloid plaque aggregation, nitric oxide production, pro-inflammatory cytokines, cytotoxicity, and oxidative stress in vitro. They also investigated its in vivo neuroprotective effects on Alzheimer's disease transgenic mice, observing attenuation of memory deficits, increased antioxidant parameters such as reduced glutathione and superoxide

dismutase, decreased lipid peroxidation levels (indicated by malondialdehyde), as well as decreased brain interleukin-1β and interleukin-6 levels (Xu et al., 2014). Habtemariam reported that rutin can modify both cognitive and behavioral symptoms associated with neurodegenerative diseases by crossing the blood-brain barrier and acting as an antioxidant in neuronal cells and an anti-inflammatory drug. It has also shown effects on amyloid beta (Aβ) aggregates and processing in Alzheimer's disease (Habtemariam, 2016). Enogieru et al. reported the use of plant-derived bioactive components like rutin in many neurodegenerative diseases. They attributed its mechanism of action to the amelioration of antioxidant enzymes, decrease in pro-inflammatory cytokines, anti-apoptotic effects, restoration of complex enzyme activity in mitochondria, and activation of the MAPK cascade, thereby aiding in neuronal survival (Enogieru et al., 2018). Jiménez-Aliaga et al. reported the effects of rutin in vitro in decreasing $Aβ_{25-35}$ fibril formation and accumulation, thus decreasing neurotoxicity (Jiménez-Aliaga et al., 2011), while Wang et al. reported the inhibition of Aβ aggregation and cytotoxicity by rutin, as well as the prevention of mitochondrial damage, reduction in the production of pro-inflammatory cytokines (TNF-α and IL-1) in vitro, and increased levels of catalase, superoxide dismutase enzymes, and reduced glutathione levels (Wang et al., 2012). Interestingly, the administration of (Congo red/rutin) magnetic nanoparticles intravenously in transgenic mice resulted in the amelioration of neurologic changes and a decrease in memory deficits in their brains (Hu et al., 2015). Additionally, Xu et al. showed that rutin reduced oligomeric Aβ, IL-1, and IL-6 levels in the brains of transgenic mice (Xu et al., 2014). Ramalingayya et al. reported that rutin improved recognition in a dose-dependent manner against scopolamine-induced memory deficits in an Alzheimer's model without any disturbance to locomotor activity (Ramalingayya et al., 2016). Javed et al. stated that rutin improved cognition and attenuated streptozotocin-induced inflammation in another Alzheimer's

model by decreasing the expression of IL-8, COX-2 enzyme, NF-κB, as well as inducible iNOS and ameliorating hippocampal histological abnormalities (Javed et al., 2012).

Symptomatic therapies are the only treatment strategy available for AD. The standard medical treatments include AChE inhibitors and a partial NMDA antagonist. Psychotropic medications are often used to treat secondary symptoms of AD, such as depression, agitation, and sleep disorders (Madhusoodanan, 2007). These treatments are aimed at slowing the advancement of the disease and improving the quality of life; however, they do not cure the disease (Alzheimer's Association, 2018). Therefore, there is an urgent need to identify new treatment strategies for the cure of AD.

The aim of this study is to evaluate the anti-inflammatory potential of rutin on BV2 microglia cells and determine the mechanisms of action.

5.2 Material and Methods

5.2.1 Immortal cell lines

BV-2 cells are an immortal cell line frequently used as a substitute for primary microglia (PM) in pharmacological studies. They originate from raf/myc-immortalized murine neonatal microglia and are cheaper and faster to work with compared to PM (Henn, 2009; Lund, 2005). BV-2 cells express NADPH oxidase, which is associated with microglial-induced neuronal damage (Wu, 2006; Yang, 2007). BV-2 cells are currently the most accurate immortal cell line for studying microglia, exhibiting many similarities in behavior to PM, such as cytokine secretion (Lund, 2005).

5.2.2 Functional assays

Nitric oxide production is frequently used as a neuroinflammatory marker in PM and BV-2 clonal cell lines. This is because lipopolysaccharide (LPS) stimulates inducible nitric oxide synthase

(iNOS) to produce NO in these cell lines, resulting in the upregulation of iNOS gene expression and the subsequent production of NO, which marks the inflammatory response.

The upregulation of iNOS gene expression and the subsequent production of NO are well-established markers of neuroinflammation in numerous in vitro and in vivo models. Studies investigating the role of NO in the pathogenesis of diseases such as multiple sclerosis (MS) and Alzheimer's disease have shown increased NO production by microglia and its contribution to the inflammatory response and neuronal damage (Lassmann et al., 2015; Colton CA et al., 2013). Therefore, measuring NO production in PM and BV-2 clonal cell lines in response to inflammatory stimuli such as LPS is a useful tool to evaluate the activation of inflammatory pathways and the potential contribution of NO to the pathogenesis of neuroinflammatory diseases. Other markers such as pro-inflammatory cytokines, chemokines, and reactive oxygen species are also used to broadly evaluate neuroinflammation in different experimental settings.

In this study, functional assays such as the Griess assay, cell viability assays (MTT and LDH assays), and Enzyme-linked immunosorbent assay (ELISA) were used according to the procedures described in Section 2.4-2.5.

Treatment

BV-2 microglial cells were cultured with culture medium containing LPS (0.001-100 ng/mL) and/or Rutin (7.8125 µM-100 µM) for 24 hours. After the 24-hour incubation, two sets of 50 µL were transferred to two fresh 96-well plates to measure nitrate concentration (Griess assay) and to measure cell viability (MTT assay) and cytotoxicity (LDH assay). Each treatment had at least three technical replicates for each experiment, and each experiment was carried out at least three times.

5.3. RESULTS

5.3.1. Effects of LPS on BV2 cells

5.3.1.1 Effects of LPS on BV2 cell viability (MTT assay)

BV-2 cells were treated with LPS at various concentrations (0.03, 0.1, 0.3, 1, 3, 10, 100 ng/mL) for 24 hours. The cell viability in the culture supernatant was evaluated using the MTT assay, as shown in Figure 5.1. The results indicate that there is no significant increase or decrease in cell viability as the dose increases, which suggests the stability of BV2 cells when treated with LPS.
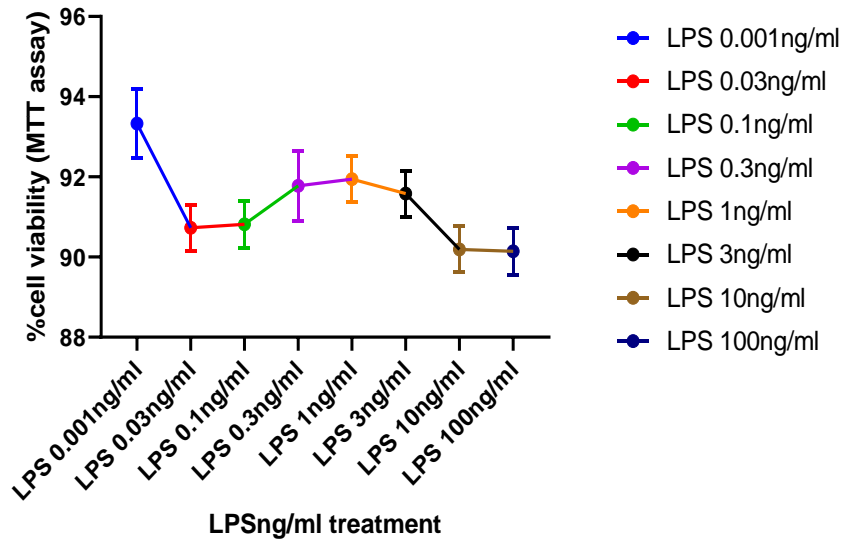
Figure 5.1

Figure 5.1 Effect of LPS dose response on cell viability in BV-2 microglial cells. BV-2 cells were treated with LPS at various concentrations (0.001, 0.03, 0.1, 0.3, 1, 3, 10, 100 ng/mL) for 24 hours. There is no significant increase or decrease in cell viability as the dose increases.

5.3.1.2. Effects of LPS on BV2 cell cytotoxicity (LDH assay)

BV-2 cells were treated with LPS at various concentrations (0.001, 0.03, 0.1, 0.3, 1, 3, 10, 100 ng/mL) for 24 hours. The LDH in the culture supernatant was evaluated using LDH assays. As

shown in Figure 5.2, BV2 cells were exposed to different concentrations of LPS. There was no significant increase or decrease in cell cytotoxicity as the dose increases.
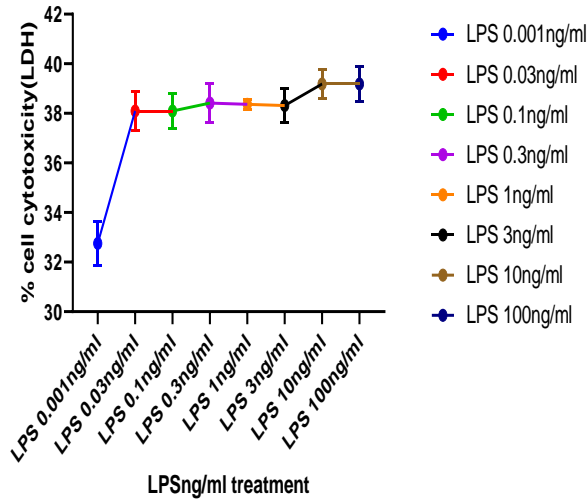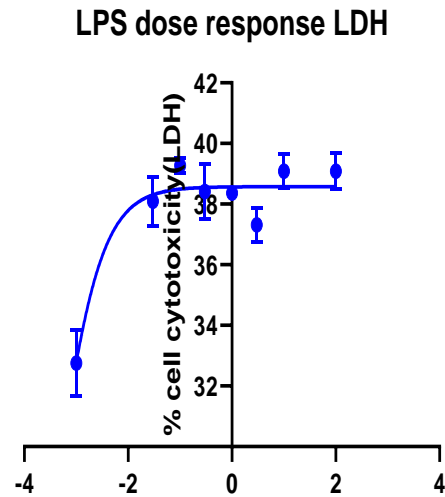
Figure 5.2A   Figure 5.2B

Figure 5.2. Effects of LPS on BV2 cell cytotoxicity. BV2 cells were exposed to different concentrations of LPS, as indicated by LDH release, which induces cytotoxicity. In Figure 5.2A, there was no significant increase or decrease in cell cytotoxicity as the dose increased. The LDH release was quantified on a normalized response curve, and Figure 5.2B shows the mean dose-response curves.

5.3.1.3. Effects of LPS on BV2 cell nitric oxide (NO) production (Griess assay)

To investigate nitric oxide formation, nitrite (NO_2-) is measured, which is one of the two primary, stable, and non-volatile breakdown products of NO. This assay relies on a diazotization reaction originally described by Griess in 1879. The Griess Reagent System is based on a chemical reaction that uses sulfanilamide and N-1-napthylethylenediamine dihydrochloride (NED) under acidic

(phosphoric acid) conditions. This system can detect NO2 – in various biological and experimental liquid matrices such as plasma, serum, or tissue culture medium.

In the assay, nitrite is reduced to nitrogen oxide. Then, nitrogen oxide reacts with Griess Reagent, forming a stable product that can be detected by its absorbance at 540 nm (A540). The assay is simple, fast, and can detect nitrite levels as low as 1 nmol/well. To ensure accurate NO2 – quantitation, a reference (standard) curve is prepared according to the protocol, using the Nitrite Standard for each assay, with the same matrix or buffer used for experimental samples (Figure 5.3A).

BV-2 cells were treated with LPS at various concentrations (0.001, 0.03, 0.1, 0.3, 1, 3, 10, 100 ng/mL) for 24 hours. The nitrite in the culture supernatant was evaluated using Griess reagent. As shown in Figure 5.3B & C, BV2 cells were exposed to different concentrations of LPS. The dose response ranges from 0.001 to 100 ng/mL, as indicated by nitrate production, which induces inflammation and is quantified on a normalized response curve. Cells treated with various LPS concentrations (1, 3, 10, 100 ng/mL) significantly increased the NO levels (*** $p < 0.001$) when compared with the control. The nitrite in the culture supernatant was evaluated using Griess reagent and quantified on a normalized response (mean top value: 1.006, mean EC50: 3.02, mean LogEC50: 0.47).
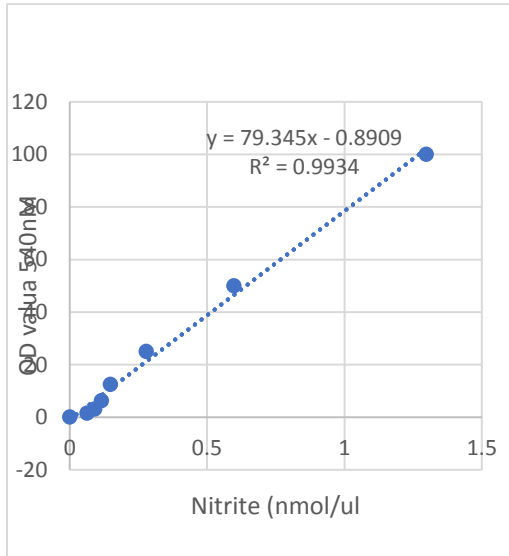
Figure 5.3A
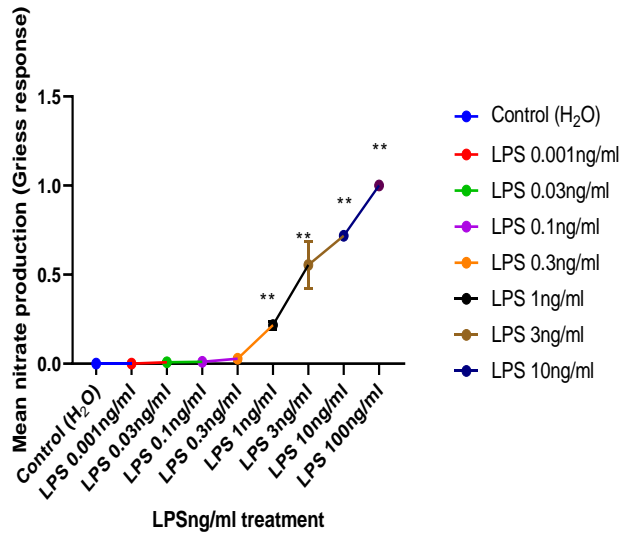
Figure 5.3B

LPS concentration response. Griess
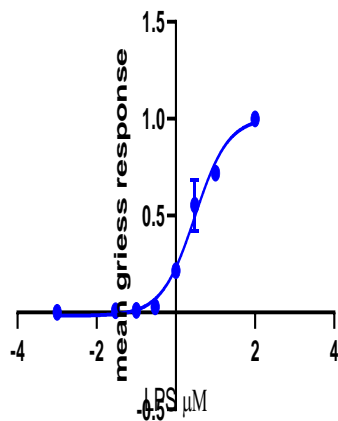
Figure 5.3C

*Figure 5.3 Effect of NO Production in LPS-stimulated BV-2 microglial cells. Figure 5.3A represents a typical nitrite standard curve. In Figure 5.3B, BV-2 cells were treated with LPS at various concentrations (0.03, 0.1, 0.3, 1, 3, 10, 100 ng/mL) for 24 hours. Cells treated with various LPS concentrations (1, 3, 10, 100 ng/mL) significantly increased the NO levels. The ** represents a significant difference (p < 0.001) between the treatment groups (1, 3, 10, 100 ng/mL) when compared with the control. The nitrite in the culture supernatant was evaluated using Griess*

reagent and quantified on a normalized response. Figure 5.3C shows the mean dose-response curves.

5.3.1.4. Effects of LPS (10 ng/mL) on BV2 cell inflammatory cytokine gene and protein expression.

The effect of LPS-induced inflammation in BV-2 microglial cells was evaluated. BV-2 cells were treated with LPS (10 ng/mL) for 24 hours. Data were presented as the mean ± S.E.M. (n = 3) for three independent experiments. In Figure 5.4, LPS induced the production of pro-inflammatory cytokines in microglial cells. The mRNA levels of pro-inflammatory cytokines TNFa and IL-6 were up-regulated by LPS challenge (Figure 5.4A and 5.4B).

In Fig 5.4C, LPS increased NOS2 production in microglial cells. The mRNA levels of NOS2 were up-regulated by LPS challenge. The protein levels of the pro-inflammatory cytokine TNFa were up-regulated by LPS, and this was measured by an ELISA kit (Figure 5.4D).
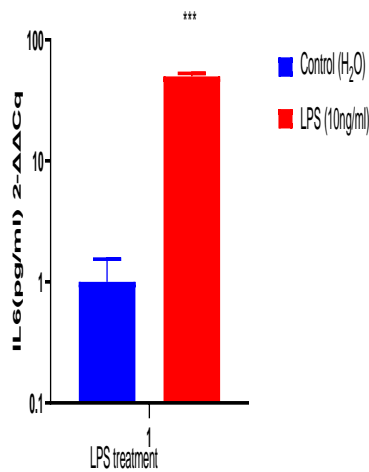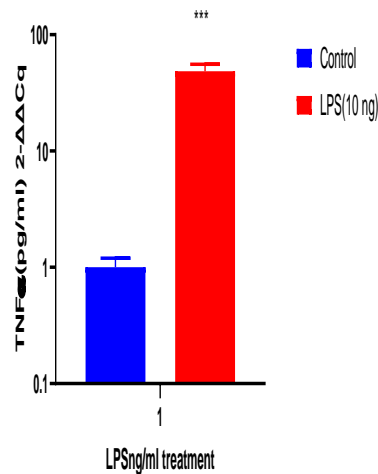
Figure 5.4A   Figure 5.4B
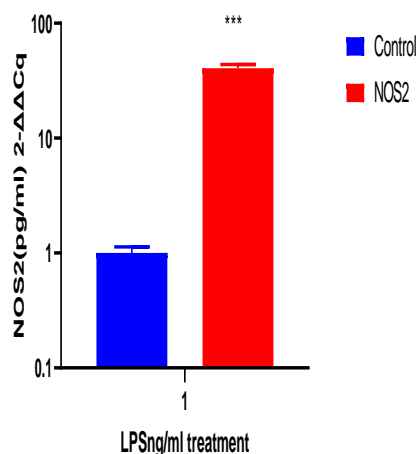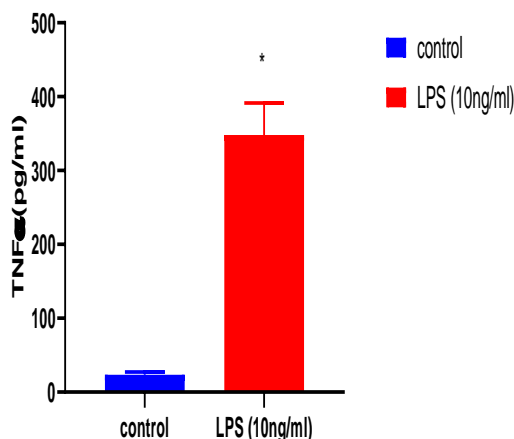
Figure 5.4C   Figure 5.4D

Figure 5.4. RT-qPCR. Effects of LPS on BV2 cell inflammatory gene expression. The mRNA levels of pro-inflammatory cytokines TNFa and IL-6 were up-regulated by LPS (Figure 5.4A and 5.4B). LPS induced a large fold change in TNFa and IL-6 cDNA, with a 48-fold and 50-fold increase compared to the control, respectively (, p < 0.001). The mRNA levels of NOS2 were also up-regulated by LPS, showing a 40-fold increase in NOS2 cDNA compared to the control (, p < 0.001) (Figure 5.4C). The protein levels of the pro-inflammatory cytokine TNFa were up-regulated by LPS, showing a significant difference compared to the control (*, p < 0.001), and this was measured by an ELISA kit (Figure 5.4D).

5.3.2. Rutin on BV2 cells

5.3.2.1. Dose-dependent effect of rutin on BV2 cell viability (MTT assays) and determination of IC50

BV-2 cells were treated with rutin at various concentrations (7.8125, 15.625, 31.25, 62.5, 125, 250, 500, 1000 μM) for 24 hours. The cell viability in the culture supernatant was evaluated using MTT assays. As shown in Figure 5.5, the MTT activity did not show statistically significant changes.
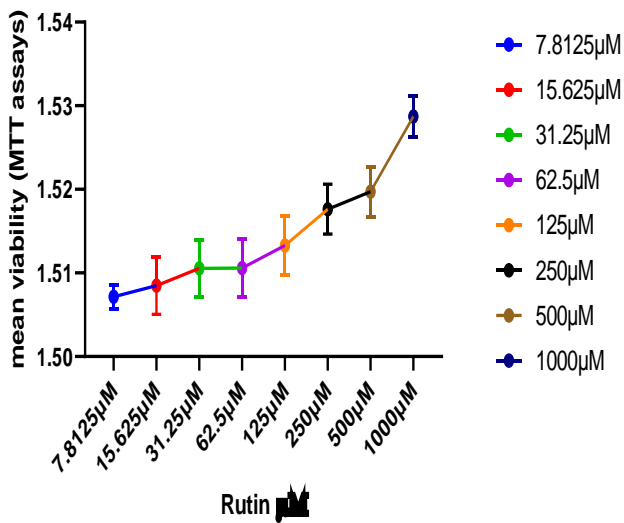
Figure 5.5 . Effect of rutin dose response on cell viability in BV-2 microglial cells. BV-2 cells were treated with rutin at various concentrations (7.8125, 15.625, 31.25, 62.5, 125, 250, 500, 1000 μM) for 24 hours. The figure shows the mean dose response curves and is quantified on a response scale.

5.3.2.2. Effects of rutin on BV2 cell cytotoxicity (LDH assay)

BV-2 cells were treated with rutin at various concentrations (7.8125, 15.625, 31.25, 62.5, 125, 250, 500, 1000 μM) for 24 hours. The LDH in the culture supernatant was evaluated using LDH assays. As shown in Figure 5.6, BV2 cells were exposed to different concentrations of rutin, but no statistically significant difference was observed.
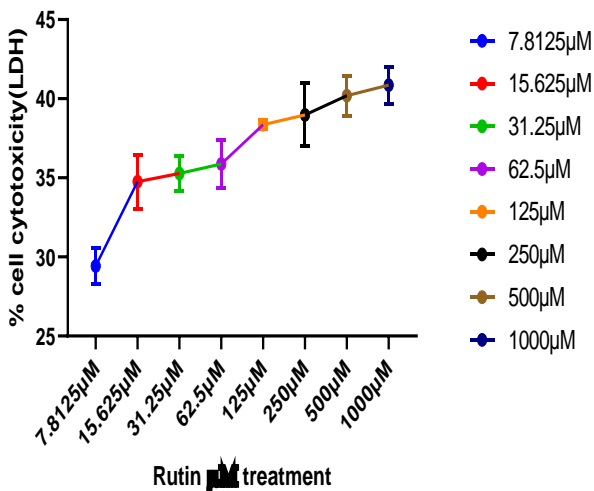
Figure 5.6. Effects of rutin dose on BV2 cell cytotoxicity. BV2 cells exposed to different concentrations of rutin (7.8125, 15.625, 31.25, 62.5, 125, 250, 500, 1000 µM) and evaluated by LDH assays. No statistical significant difference was observed.

5.3.2.3. Effects of rutin on BV2 cells nitric oxide (NO) production (Griess assay)

BV-2 cells were treated with rutin at various concentrations (7.8125, 15.625, 31.25, 62.5, 125, 250, 500, 1000 µM) for 24 hours. The nitrite in the culture supernatant was evaluated using Griess reagent. As shown in Figure 5.7, no significant differences were observed as the dose increased. The EC50 value was calculated and the results are as follows: mean top value: 1.184, mean EC50: 324.1, mean LogEC50: 2.511.

The EC50 (half-maximal effective concentration) value represents the concentration of a drug required to achieve a response halfway between the baseline and maximum level. In this case, since the EC50 of rutin is around 324, it means that half-maximal effect can be achieved at a concentration of 324 units. Based on this information, we chose a range of rutin concentrations around this value (100 to 1000 µM) to test its effect on BV2 cells. Therefore, 100 µM of rutin was chosen for the rest of the experiments in this study.
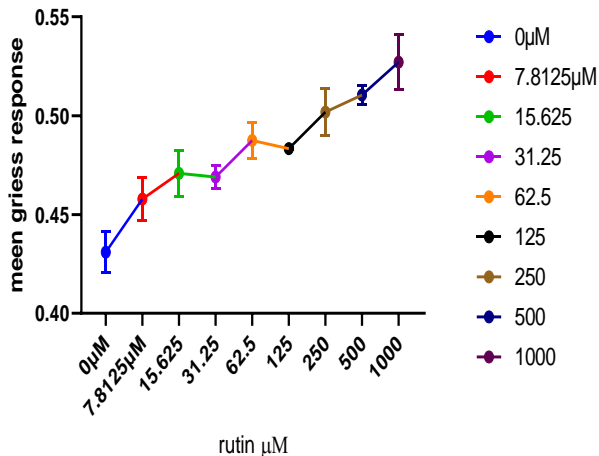
Figure 5.7. Effect of rutin dose response on NO Production in BV-2 microglial cells. BV-2 cells were treated with rutin at various concentrations (7.8125, 15.625, 31.25, 62.5, 125, 250, 500, 1000 mg/mL) for 24 hours and the nitrite was evaluated using Griess assays. There was no statistical significant difference observed.

5.3.3. Rutin plus LPS on BV2 cells

5.3.3.1. Rutin dose response plus LPS (10 ng/mL) on BV2 cells nitric oxide (NO) production (Griess assay) and EC50 Determined

BV-2 cells were treated with rutin at various concentrations (7.8125, 15.625, 31.25, 62.5, 125, 250, 500, 1000 µM) with LPS (10 ng/mL) for 24 hours. The nitrite in the culture supernatant was evaluated using Griess reagent. As shown in Figure 5.8A and 5.8B, BV2 cells stimulated with LPS (10 ng/mL) were exposed to different concentrations of rutin. Cells treated with various rutin concentrations (31.25, 62.5, 125, 250) plus LPS showed a slight reduction in NO levels, while cells treated with (0, 7.8125, 15.625, and 500, 1000 µM) exhibited an increase in NO levels in the presence of LPS. Figure 5.8C shows the EC50 shift of rutin versus rutin + LPS, indicating a rightward shift of the curve.
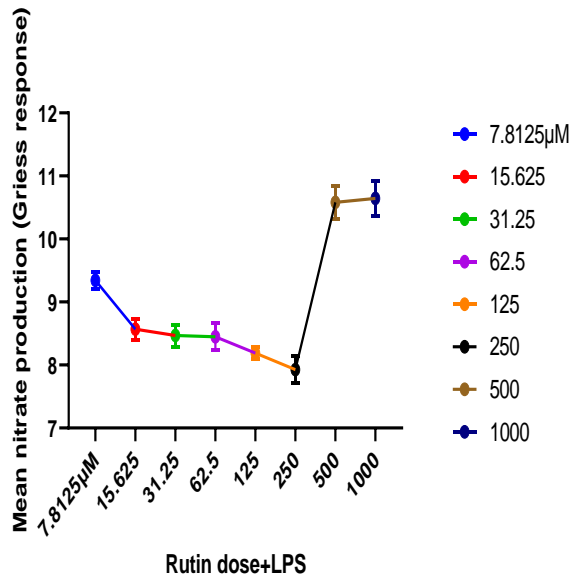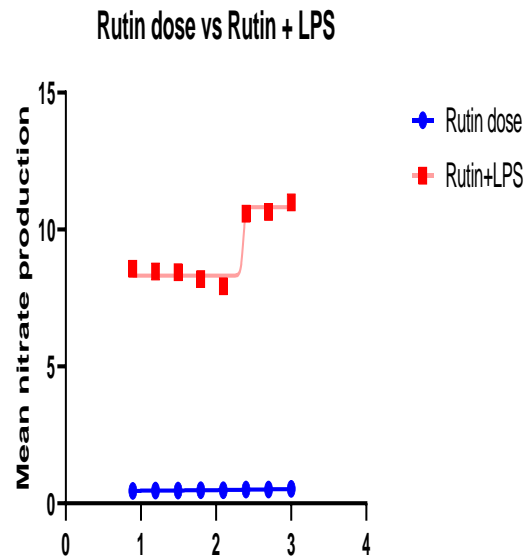
Figure 5.8A   Figure 5.8B

Figure 5.8. Effect of rutin dose + LPS response on NO Production in BV-2 microglial cells. BV-2 cells were treated with rutin at various concentrations (7.8125, 15.625, 31.25, 62.5, 125, 250, 500, 1000 µM) + LPS (100 ng/mL) co-administration for 24 hours. The nitrite in the culture supernatant was evaluated using Griess reagent. Figure 5.8B shows the EC50 shift of rutin vs rutin + LPS, indicating a rightward shift of the curve.

5.3.3.2. LPS dose response plus rutin (100 µM) on BV2 cells NO production

BV-2 cells were treated with LPS at various concentrations (0.03, 0.1, 0.3, 1, 3, 10, 100 ng/mL) with rutin (100 µM) for 24 hours. The nitrite in the culture supernatant was evaluated using Griess reagent. As shown in Figure 5.9A and 5.9B, BV2 cells were exposed to different concentrations of LPS with rutin at 100 µM. Figure 5.9B shows the EC50 shift of LPS vs LPS + rutin, demonstrating a rightward shift of the curve.

LPS dose+ Rutin

LPS+Rutin(EC5O shift)
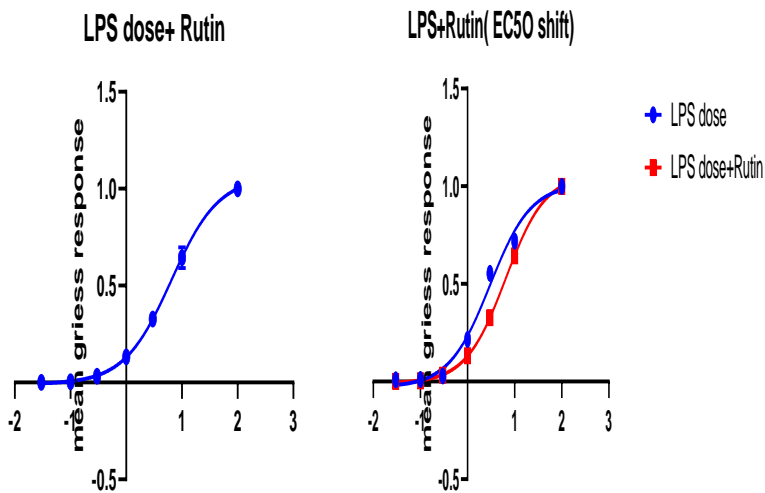
Figure 5.9A   Figure 5.9B

Figure 5.9 Effect of LPS dose + rutin response on NO Production in BV-2 microglial cells. BV-2 cells were treated with LPS at various concentrations (0.03, 0.1, 0.3, 1, 3, 10, 100 ng/mL) + rutin (100 µM) co-administration for 24 hours. The nitrite was evaluated using Griess reagent and quantified on a normalized response curve (mean top value: 1.061, mean EC50: 6.061, mean LogEC50: 0.08100). Figure 5.9A shows the mean dose-response curves. Figure 5.9B shows the EC50 shift of LPS vs LPS + rutin, indicating a rightward shift of the curve.

5.3.3.3. Effects of LPS plus rutin (100 µM) on BV2 cell cytokine gene and protein expression

5.3.3.3.1 Effects of LPS plus rutin (100 µM) on BV2 cell cytokine gene

The effect of inflammatory gene expression of LPS plus rutin on BV-2 microglial cells was evaluated. BV-2 cells were treated with LPS (10 ng/mL) plus rutin (100 µM) co-treatment for 24 hours. In Figure 5.10, rutin downregulates pro-inflammatory cytokine gene expression in LPS-induced microglial cells. The mRNA levels of pro-inflammatory cytokines TNFa and IL-6 were

significantly downregulated by rutin (Figure 5.10A and Figure 5.10B), with a fold change in TNFa

and IL-6 cDNA of 16 and 3, respectively, compared to LPS treatment (***$p < 0.001$).

In Figure 5.10C, rutin (100 µM) decreases NOS2 production in LPS-induced BV2 microglial cells.

The mRNA levels of NOS2 were downregulated by rutin, with a fold change in NOS2 cDNA of

19-fold decrease compared to LPS treatment (***$p < 0.01$).
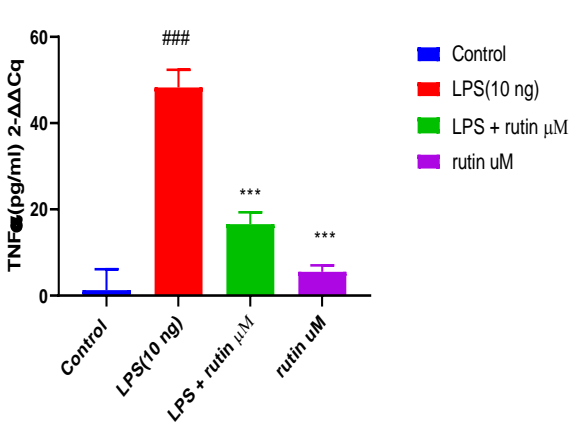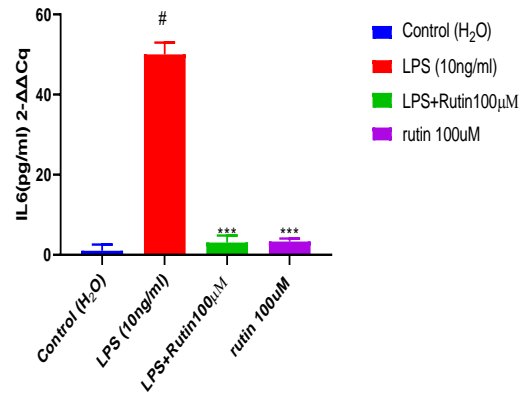
Figure 5.10A   Figure 5.10B
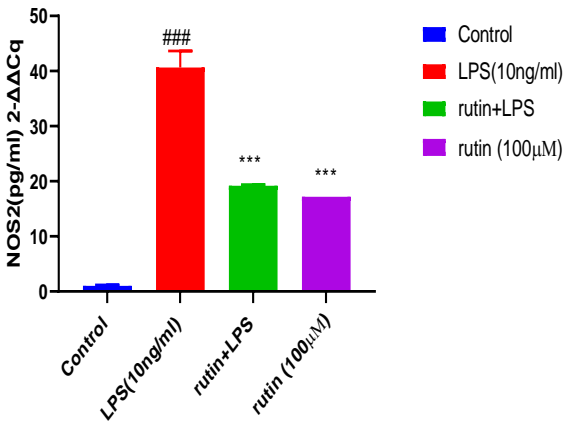
Figure 5.10C

Figure 5.10 . Rutin inhibits the expression of pro-inflammatory cytokines in LPS-induced BV-2

microglial cells. The mRNA levels of pro-inflammatory cytokines TNFa and IL-6 were significantly

downregulated by rutin in (Figure 5.10A and Figure 5.10B). The mRNA levels of NOS2 were also

*downregulated by rutin (Figure 5.10C). Data were presented as the mean ± S.E.M. (n = 3) for three independent experiments. #p < 0.001 when compared with the control group; ***p < 0.001 when compared with the LPS group.*

5.3.3.3.2 Effects of LPS plus rutin (100 μM) on BV2 cell cytokine protein expression

The effect of inflammatory cytokine protein expression, specifically TNF-α, in LPS plus rutin-treated BV-2 microglial cells was evaluated. Protein levels of TNF-α were measured using an ELISA kit. BV-2 cells were treated with LPS (10 ng/mL) plus rutin (100 μM) co-treatment for 24 hours. In Figure 5.11, rutin downregulates the level of inflammatory protein expression in LPS-induced microglial cells. (Figure 5.11).
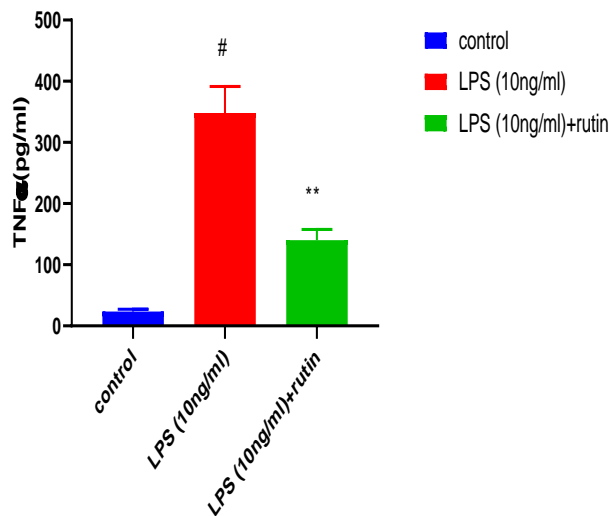
Figure 5.11 : Rutin inhibits the expression of inflammatory cytokine proteins of TNFa in LPS (10ng)-induced BV-2 microglial cells. The levels of TNF-α, an inflammatory protein, were significantly down-regulated by rutin (100μM) (Figure 5.11). The protein levels of TNF-α were measured by ELISA. Data are presented as the mean ± S.E.M. (n = 3) for three independent

*experiments. #p < 0.001, when compared with the control group; **p < 0.001, compared with the LPS group.*

5.4. DISCUSSION

Inflammation is one of the first lines of defense against harmful stimuli (Pereira, 2014). Acute inflammation leads to homeostasis, while uncontrolled inflammation occurs during chronic inflammation, such as allergies, asthma, arthritis, atherosclerosis, multiple sclerosis, metabolic syndromes, and obesity (Mohan and Gupta, 2018).

While convincing evidence shows that AD has a multifactorial etiology (Gong et al., 2018; De Roeck et al., 2019), neuroinflammation plays a central role in its etiopathogenesis (Sala Frigerio et al., 2019), due to its capacity to exacerbate Aβ and tau pathologies (Ising et al., 2019). In vivo positron emission tomography (PET) studies provide direct indication of increased microglia activation (inflammation) in the brains of AD patients (Yao and Zu, 2020). Neuroinflammation is vital in the CNS (Yang, 2016; Mo, 2020). Microglial cells are resident immune cells, which account for 15–20% of cranial nerve gliacytes in the CNS, and are significant in removing injured nerves, cellular fragments, and toxic substances (Schneble, 2017). Microglial cells in the CNS exhibit the first line of defense following infection, inflammation, and other pathophysiological stimuli (Hopp, 2018). Microglial cells are converted from an inactive state into an active state during injury, infection, cerebral trauma, or ischemia (Salvi, 2017; Huang, 2020). Activation of microglia may lead to alterations in cellular phenotypes and functions.

LPS is a prominent cell wall component of gram-negative bacteria that is a strong stimulator of immune cells, including microglia (Xu, 2018). Various in vitro and in vivo studies have revealed that LPS activates glial cells, resulting in neuroinflammation and neurodegeneration (Johansson,

2014; Qin, 2015; Khan, 2017). The synthesis of NO from L-arginine and molecular oxygen is catalyzed by NO synthases (NOS). The iNOS is found to be expressed in macrophages, microglia, astrocytes, and some other cell types in response to inflammatory mediators such as LPS (Pacher, 2007; Silva, 2017).

In this study, the effect of Lipopolysaccharide (LPS) and LPS plus rutin on nitric oxide-induced BV2 cells was evaluated. As expected, LPS-treated BV-2 cells caused an inflammatory response, which was significantly reduced by rutin in terms of nitrate production using the Griess assay. The results showed a decrease from a mean top value of 99.85% to 64.42%, with $P < 0.001$, indicating statistical significance. The mean EC50 was 3.2ng/ml for LPS alone and 6.441 when rutin was added, with $P < 0.001$, showing a statistically significant difference. Therefore, since BV2 microglia were stimulated by LPS, there was an increase in the expression of iNOS, and the combination of LPS and rutin attenuated the induction of these enzymes due to the decrease in LPS. This implies that rutin may have potential therapeutic benefits for the treatment of inflammatory diseases by modulating iNOS expression, and hence it can play a role in inhibiting neuroinflammation in Alzheimer's disease. This agrees with the findings of Kim et al. (2014), which shows that rutin significantly decreased the expression of iNOS in LPS-stimulated macrophages, suggesting that rutin may have anti-inflammatory effects through the inhibition of iNOS expression. This also agrees with the findings of Lv et al. (2016), which revealed that the combination of LPS and rutin significantly decreased the expression of iNOS compared to LPS alone, suggesting that rutin may have potential therapeutic benefits for the treatment of inflammatory diseases by modulating iNOS expression. It also agrees with the findings of Abdel-Hamid et al. (2019), which show that rutin significantly decreased the expression of iNOS and inhibited the production of nitric oxide (NO) in LPS-stimulated liver tissue. Under normal

physiological conditions, NO plays an essential role as a second messenger with a crucial role in intracellular communication and intracellular signaling in the nervous system. However, it can be cytotoxic in large amounts (Gibbons and Dragunow, 2006).

The results of the expression of nitric oxide in BV2 microglial cells treated with rutin somehow remained constant, indicating minimal nitrate production compared to the control cultures. Rutin doses alone showed no significant effect on BV2 microglial NO production. This indicates that rutin on its own has no effect on the microglial cells and does not cause inflammation. However, when LPS was added to variable doses of rutin, at the beginning of low doses of rutin with a constant concentration of LPS in the cell medium, there was high nitrate production, as expected. But as the rutin concentration continued to increase, nitrate production started to decrease, confirming the anti-inflammatory effect of rutin.

In the LDH and MTT assays, rutin revealed its non-cytotoxic effects on BV2 cells at the doses used. The LDH and MTT levels did not change significantly. There was also no significant change in the LPS-treated group. This indicates that there was no increased cell death in the BV2 cells used, as shown by the constant level of LDH found in the cell medium in this assay. These findings agree with the findings of Owona (2013), who found that stimulating the N9 microglial cell line with LPS did not result in cytotoxicity to these cells.

The regulation of the neuroinflammatory response represents a potential therapeutic strategy for the treatment of neurodegeneration. It has been established that activated microglia are major cellular elements of neuroinflammatory responses, affecting specific immune functions to maintain physiological homeostasis (Ransohoff and Perry, 2009; Gemma, 2010; Dhama, 2015; Li, 2018). Microglia can be phenotypically polarized into a classical (pro-inflammatory; M1) or an alternative (anti-inflammatory; M2) phenotype in response to various microenvironmental

disturbances (David and Kroner, 2011; Saijo and Glass, 2011; Joseph and Venero, 2013; Mantovani, 2013; Li, 2018).

The activated microglial cells typically indicate two distinct phenotypes known as M1 and M2. M1 microglial cells can cause neurotoxicity by releasing cytotoxic substances and inflammatory factors, including matrix metalloproteinases, which can destroy the blood-brain barrier, thus aggravating cerebral injury. M1 microglial cells have been found to cause partial or extensive CNS injury, and the M1 phenotype serves as a histopathological marker for neurodegeneration, including AD (Hopp, 2018; Sternberg, 2019). Conversely, M2 microglial cells protect neurons. Macrophages perceive and react to pathogens through pattern-recognition receptors (PRRs) containing toll-like receptors (TLRs) and thus control the inflammatory response (Lee, 2017). Microglia and astrocytes are the first line of defense in the CNS and initiate immune responses to injuries and pathogens (Stephenson, 2018). In the normal brain, microglia play important functions in neuroprotection and also phagocytose cell debris and damaged neurons (Neumann, 2009). However, abnormally activated microglia and astrocytes release a variety of pro-inflammatory cytokines (Zhang and Xu, 2018). Specifically, this abnormally activated microglia produce a variety of inflammatory mediators (COX-2 and iNOS) and inflammatory cytokines (IL-1β, IL-6, and TNF-α). This over-activated microglia, which secrete excessive pro-inflammatory mediators, can lead to neuroinflammation and neurodegenerative diseases such as AD (Akiyama et al., 2000; Teismann et al., 2003; Infante-Duarte et al., 2008; Piirainen et al., 2017).

In general, activated M1 microglia are characterized by an increase in the levels of pro-inflammatory cytokines, including IL-1β, TNF-α, and IL-6, as well as an increase in the levels of iNOS, CD16, CD68, and other markers (David and Kroner, 2011; Saijo and Glass, 2011; Joseph and Venero, 2013; Mantovani, 2013; Li, 2018). On the other hand, M2 microglia are characterized

by an increase in M2 phenotype markers, such as Arg-1, CD206, Ym-1/2, and TGF-β, among others (David and Kroner, 2011; Saijo and Glass, 2011; Mantovani, 2013; Li, 2018). Physiologically, the M1 phenotype worsens neuronal injury and hinders cellular repair during trauma and CNS disorders. In contrast, the M2 microglia is neuroprotective and promotes recovery and remodeling (David and Kroner, 2011; Saijo and Glass, 2011; Mantovani, 2013; Li, 2018). Therefore, inhibiting the M1 phenotype and promoting the M2 stage is considered a better strategy for the treatment of neuroinflammatory disorders compared to solely inhibiting M1 activation (Hu, 2015). However, only a few compounds have been reported to regulate microglia polarization toward the M2 phenotype (Lu, 2010; Zhou, 2014).

Based on the cytokine gene and protein expression analysis of this study, the gene expression of NOS, TNF-α, and IL-6, as well as the protein levels of TNF-α following LPS stimulation was evaluated. Our findings revealed a significant increase in mRNA levels of cytokine genes and protein levels after 24 hours of LPS challenge. This indicates that LPS increased the mRNA levels of TNF-α, IL-1β, IL-6, and iNOS, thereby promoting the production of pro-inflammatory cytokines. This is consistent with a study by Qian et al. (2018), which demonstrated that inflammatory cytokines and chemokines peak after brain injury, while the levels of NO, TNF-α, IL-1β, and IL-6 reach their maximum at 24 hours of LPS stimulation. These results demonstrate that cytokine production was induced by culturing microglia in the presence of LPS. The microglia stimulated with LPS also exhibited an M1 phenotype, characterized by increased levels of TNF-α and IL-6. Pro- and anti-inflammatory cytokines play a key role in protecting against the pathogenesis of various pathologies. Pro-inflammatory cytokines are primarily produced to amplify inflammatory reactions and activate the immune response to the inflammatory stimulus.

Oxidative stress is a significant inducer of inflammation (Yang, 2016). High levels of reactive oxygen species (ROS) can lead to a substantial reduction in antioxidant defense mechanisms, resulting in DNA, protein, and lipid damage (Khurana, 2018). Additionally, ROS regulate intracellular redox-sensitive signaling and nuclear transcription factors, including NF-κB and nuclear factor erythroid 2-related factor 2 (Nrf2), in LPS-challenged macrophage activation (Xu et al., 2015). Nrf2 signaling is widely expressed in various cell types and tissues and constitutes one of the most prominent cellular defense mechanisms against xenobiotic damage and oxidative stress (Chiou et al., 2016). Moreover, Nrf2 is a major transcription factor regulating heme oxygenase-1 (HO-1), an antioxidant enzyme induced by oxidative stress. Overexpression of HO-1 prior to stimulation with LPS has been shown to inhibit the generation of subsequent inflammatory mediators, such as NO, interleukin-6 (IL-6), and monocyte chemoattractant protein-1 (MCP-1) (Jin et al., 2016). Therefore, antioxidants serve as the first line of defense against oxidative damage by scavenging radicals and maintaining optimum wellbeing (Khatua and Acharya, 2018).

Drugs that modulate microglial activation and the release of pro-inflammatory cytokines, effectively inhibiting inflammation, represent a promising therapeutic strategy for neuroinflammation and neurodegeneration-related diseases. Flavonoids are low molecular weight natural chemical compounds that belong to a class of secondary metabolites produced by plants. They are found in fruits, leaves, flowers, and seeds and are widely distributed in the plant kingdom, especially in angiosperms (Lopes, 2013). Studies have demonstrated the antioxidant and anti-inflammatory properties of flavonoids and their significance as dietary supplements (Ruijters, 2014). Flavonoids have been shown to sensitize the microglial response by exerting antioxidant and anti-inflammatory effects on LPS-stimulated microglia (Lee, 2016). Rutin, in particular, has

demonstrated the ability to inhibit beta-amyloid aggregation and cytotoxicity, reduce NO production and pro-inflammatory cytokines, and attenuate oxidative stress in vitro (Wang et al., 2012). Rutin has also been shown to ameliorate damage associated with spinal cord injury (Zhang et al., 2015). Pre-treatment with rutin in chronic dexamethasone-administered mice attenuated cognitive deficits and brain impairment (Tongjaroenbuangam et al., 2011). Numerous studies have indicated that rutin analogues can inhibit β-amyloid aggregation and neurotoxicity, prevent oxidative stress induced by β-amyloid, reduce β-amyloid42 levels in mutant human APP overexpressing cells, and decrease senile plaques in the brains of APP transgenic mice (Lee et al., 2009; Bieschke et al., 2010; Dragicevic et al., 2011; Pocernich et al., 2011; Ansari et al., 2009; Rezai-Zadeh et al., 2005). Rutin has also been shown to inhibit beta-amyloid aggregation and cytotoxicity, inhibit the production of nitric oxide (NO) and pro-inflammatory cytokines, and attenuate oxidative stress in vitro. Furthermore, rutin has been indicated to inhibit damage associated with spinal cord injury (Zhang et al., 2015). However, little is known about the mechanisms of microglial activation by rutin and its effects on the regulation of cytokines and chemokines associated with inflammatory responses in the CNS.

Based on this results, rutin treatment attenuated the mRNA expression of NOS, TNF-α, and IL-6, as well as the secreted protein levels of TNF-α. This suggests that rutin may have potential therapeutic benefits for the treatment of inflammatory diseases by modulating the expression of pro-inflammatory cytokines. These findings are consistent with studies by da Silva et al. (2017) and Sun et al. (2021), which demonstrate that rutin induces a decrease in the mRNA levels of TNF-α, IL-1β, IL-6, and iNOS, thereby reducing the production of IL-6, TNF-α, and NO. These findings also agree with the results of Lv et al. (2016) and Kim et al. (2014), which show that rutin significantly decreases the expression of TNF-α, IL-1β, and IL-6 at both the gene and protein

levels. This implies that rutin may have therapeutic potential for the treatment of inflammatory diseases by modulating the expression of pro-inflammatory cytokines.

In this study, the effect of rutin on resting and LPS-stimulated microglia and characterization of its modulation towards an activated M1 phenotype or an alternatively activated M2 phenotype was evaluated. Results showed that the gene expression levels of NOS were upregulated when BV2 microglial cells were treated with LPS. However, rutin treatment downregulated the upregulation of NOS production, suggesting that rutin may inhibit microglia-mediated neuroinflammation via an NO-dependent mechanism. This study suggests that rutin can facilitate the polarization of microglia from an M1 to an M2 phenotype through a mechanism associated with the downregulation of NO. Furthermore, this results imply that rutin significantly inhibits the activation of TLR4/NF-κB signaling, indicating that NF-κB signaling might be an important target for rutin during this biological process. These findings are in line with the study of de Silva et al. (2017), which indicates that rutin has the ability to induce microglial polarization to the M2 phenotype when cells are stimulated with LPS, suggesting that flavonoids can be an alternative in the treatment or prevention of neurodegenerative disorders.

CONCLUSIONS

In conclusion, this study demonstrated that rutin, in the presence of LPS, effectively reduces neuroinflammation in BV-2 cells by decreasing nitrate production. Furthermore, rutin significantly decreased the LPS-induced elevation of pro-inflammatory cytokine levels in BV2 microglial cells and downregulated NOS expression. These findings indicate that rutin has the ability to shift microglial polarization from the M1 to M2 phenotypes, thereby attenuating microglia-related neuroinflammation. However, to obtain more conclusive results regarding the effects of rutin on neuroinflammation, further investigations are required, including experiments conducted in

primary microglia and animal models. These additional studies will help to better understand the

role of rutin in microglial polarization.

Chapter 6

6.1 Major Findings

Our study established an in vitro AD model using PC12 cells and primary rat neurons to evaluate the effects of rutin, in normoxic or hypoxic conditions as discussed in chapter 2. The aim of the study was to characterize the neuroprotective and anti-inflammatory potentials of rutin in an in vitro model of AD and determine the mechanisms of action. The research investigated whether hypoxia enhances Aβ-induced toxicity and apoptosis in primary neurons and PC12 cells, and evaluated the mechanism of action. The effect of rutin on Aβ$_{25-35}$ induced toxicity and apoptosis on primary neurons and PC12 cells in both normoxia and hypoxia conditions were evaluated as in shown in chapter 2.

Results revealed a dose-related reduction in MTT activity and an increase in LDH release when PC12 cells and primary neurons were exposed to different concentrations of Aβ$_{25-35}$ for 24 hours in both normoxia and hypoxia. The IC50 in normoxia was determined as 30 μM/L. Combined treatment of Aβ and hypoxia further reduced MTT activity and increased LDH release, indicating that both primary neurons and PC12 cells are more vulnerable to Aβ peptide toxicity during hypoxia. This was confirmed by the study of Webster (2006), which states that there is an increased vulnerability of hippocampal neurons to Aβ peptide toxicity during hypoxia and that chronic hypoxia enhances Ca2+ entry and mitochondrial Ca^{2+} content.

In both normoxia and hypoxia, a significant number of cells were undergoing early apoptosis after 24 hours of treatment with 30 μM Aβ$_{25-35}$ in normoxia, and combined treatment with both Aβ and hypoxia for 24 hours further aggravated the effects. Aβ$_{25-35}$ treatment in normoxia increased the levels of reactive oxygen species (ROS) and lipid peroxidation in PC12 cells, and combined

treatment with both Aβ and hypoxia for 24 hours significantly exacerbated the outcomes, possibly due to increased ROS during hypoxia. This implies that Aβ can increase ROS generation, which can stimulate cell death through the mitochondrial pathway or death receptor pathway, and that mitochondria-derived ROS can stabilize and activate HIF-1α during hypoxia.

Furthermore, rutin significantly increased MTT activity of PC12 cells and primary neurons after treatment with 30 μM Aβ$_{25-35}$ for 24 hours in both normoxia and hypoxia. Rutin also significantly reduced LDH release in both normoxic and hypoxic conditions. This implies that rutin can protect PC12 cells and neurons against Aβ$_{25-35}$-induced cytotoxicity by inhibiting cellular damage. Since HIF-1 has been shown to participate in hypoxia-induced adaptive reactions to restore cellular homeostasis (Figure 6.1), rutin may activate HIF in addition to iron chelation, thus having a pharmacological function in HIF stabilization. Additionally, rutin significantly reduced the number of apoptotic/necrotic cells in both normoxia and hypoxia. Moreover, rutin significantly reduced the levels of ROS and lipid peroxidation induced by Aβ$_{25-35}$ in both hypoxia and normoxia conditions. This suggests that rutin can scavenge free radicals, thus protecting neuronal cells from oxidative damage, and it also has the ability to chelate iron and stabilize HIF-1, maintaining the mitochondrial membrane potential and cytosolic accumulation of cytochrome C, thereby inhibiting oxidative stress and preventing neuronal death.

Additionally, an in vitro BV-2 cell model of neuroinflammation was evaluated as detailed in chapter 2. The results revealed that rutin treatment was not toxic to microglial cells. Rutin, in the presence of LPS, was shown to reduce neuroinflammation in BV-2 cells by decreasing nitrate production. Rutin treatment also induced a decrease in the mRNA levels of TNF, IL6, and NOS2, indicating a decrease in the production of pro-inflammatory cytokines. Our studies revealed that the upregulation of NOS genes by LPS was downregulated by rutin treatment, suggesting that rutin

may inhibit microglia-mediated neuroinflammation via an NO-dependent mechanism. These studies suggest that rutin can facilitate the microglial polarization from an M1 to an M2 phenotype through a mechanism associated with the downregulation of NO. Rutin also induced a decrease in the mRNA levels of TNF, IL6, and NOS2 and reduced the production of IL6, TNF, and nitric oxide. This shows that rutin exhibits anti-inflammatory potential and promotes the polarization of microglia towards the M2 phenotype.

6.2 Amyloid β Toxicity

Amyloid β, which is the major component of senile plaques, plays a vital role in Alzheimer's disease progression (Pereira, 2004; Zhi-kun, 2012). Aβ is generated from the intracellular cleavage of the APP by two proteolytic enzymes, β-secretase and γ-secretase, and is a 4.2 kDa short peptide of 40–42 amino acids. The 40- and 42-amino acid residue peptides, Aβ1–40 and Aβ1–42, are the predominant species, with the latter being less abundant but much more toxic (Benilova, 2012). Studies have shown that amyloid beta induces neuronal death through the mechanism of apoptosis (Clementi, 2006). Aβ$_{25-35}$ has been shown to be the shortest fragment of Aβ among the fragments studied and is processed in vivo by brain proteases (Kubo, 2002). This peptide is the functional domain of Aβ required for neurotoxic effects, retaining the toxicity of the full-length peptide. It is highly cytotoxic to neuronal cells (Giunta, 2004) and is widely used in both in vitro and in vivo experiments (Kosuge Y., 2006; Zhi-kun, 2012).

Aβ toxicity has been shown to be mediated by several mechanisms, including oxidative stress, mitochondrial dysfunction, alterations in membrane permeability, inflammation, and synaptic dysfunction (Butterfield, 2007). The progression mechanism of Aβ toxicity in AD is not well understood. Researchers have proposed various hypotheses, including the amyloid hypothesis, oligomer cascade hypothesis, Tau hypothesis, metal ion hypothesis, and oxidative stress

hypothesis (Karran, 2013). Among these, the amyloid hypothesis is the well-known and generally accepted hypothesis, proposing that excess Aβ production, aggregation, and deposition in the brain as plaques are the main causes of AD progression. Conversely, the oligomer cascade hypothesis suggests that Aβ oligomers are highly toxic compared to fully grown fibrils and could be a trigger for AD (Hayden and Teplow, 2013). The metal ion hypothesis is a well-received pathway that contributes considerably to the neuropathogenesis in AD. The presence of high concentrations of metal ions such as Cu^{2+}, Zn^{2+}, and Fe^{2+} matched with the Aβ peptide in senile plaques indicates their robust contribution to Aβ aggregation and its toxicity (Budimir, 2015; Rajasekhar, 2015). Metal binding to Aβ stabilizes the toxic oligomeric form, which is involved in ROS generation and causes synaptic breakdown, leading to neuronal cell death (Savelieff, 2013). Sequestration of physiologically important metal ions by Aβ disturbs metal ion homeostasis in the brain (Rosenberg, 2003). Disturbance of Aβ–metal interactions via metal chelators has been used to decrease neurotoxicity initiated by the Aβ–metal complex and to restore metal ion homeostasis in the brain (Hegde, 2009; Rajasekhar, 2015). Desferrioxamine B was the first metal chelator used to dissolve metal-directed Aβ aggregates and enhance cognitive ability in a mouse model. However, its use was constrained by its poor BBB permeability and rapid in vivo degradation, along with other adverse side effects.

6.2.1. Aβ and Hypoxia Interplay in AD

Recent studies have revealed that a history of stroke can increase the prevalence of AD by 2-fold in elderly patients (White, 2002). Patients with stroke or cerebral infarction exhibit reduced cognitive performance and have a higher severity of clinical dementia (Heyman et al., 1998; Sun et al., 2006). Hypoxia resulting from hypoperfusion is a common vascular component among AD risk factors and may play a significant role in AD pathogenesis. Hypoxia-inducible factor 1 (HIF-

1) is the principal molecule regulating oxygen homeostasis (Huang et al., 1999). HIF-1, a member of the basic helix-loop-helix transcription factor family, binds specifically to the 5RCGTG hypoxia-responsive element (HRE) in gene promoter regions. HIF-1α is rapidly degraded through the ubiquitin-proteasome pathway under normoxic conditions but is quite stable under hypoxic conditions (Huang and Bunn, 2003; Sun et al., 2006). The hypoxia signal transduction pathway plays a major role in vascular development, ischemia, and neurodegeneration (Pugh and Ratcliffe, 2003). When oxygen is in short supply, HIF-1 binds to HRE in promoters or enhancers, thereby activating a broad range of genes involved in angiogenesis, erythropoiesis, cell death, and energy metabolism (Sharp and Bernaudin, 2004; Sun et al., 2006). Activation of the HIF-1 pathway by risk factors such as stroke, age, and cerebral vascular atherosclerosis may contribute to AD pathogenesis by facilitating Aβ deposition.

Sequence analysis and gel shift studies have revealed that HIF-1 binds to the promoter of β-secretase 1 (BACE1), and overexpression of HIF-1α in neuronal cells increases BACE1 mRNA and protein levels, while down-regulation of HIF-1α reduces the levels of BACE1. HIF-1 also binds to the promoter of anterior pharynx-defective phenotype (APH-1), up-regulating its expression and leading to an increase in γ-cleavage of amyloid precursor protein and Notch (Lall et al., 2019).

On the other hand, HIF-1 has been proposed as a neuroprotective factor with the ability to suppress neuronal cell death caused by hypoxia or oxidative stress and to protect against Aβ peptide toxicity (Zheng et al., 2015; Ashok et al., 2017; Merelli et al., 2018). HIF-1 increases glycolysis and the hexose monophosphate shunt, maintains mitochondrial membrane potential and cytosolic accumulation of cytochrome C, thereby inactivating caspase-9 and caspase-3, and preventing neuronal death in the AD brain. Oxidative damage caused by Aβ peptide induces mitochondrial

dysfunction, which is a major characteristic of neuronal apoptosis. HIF-1 is the major transcription factor that increases capillary network density and improves blood circulation in living tissue by regulating protein expression, such as erythropoietin, glucose transporter 1 and 3, and vascular endothelial growth factor. Erythropoietin is able to block Aβ-generated neuronal apoptosis, while glucose transporters 1 and 3 increase glucose transport into brain nerve cells. Therefore, HIF-1 participates in hypoxia-induced adaptive reactions to restore cellular homeostasis and postpone the progression of AD.

A group of agents that can upregulate HIF levels in normoxia are termed hypoxia mimetic agents (Chen et al., 2018). These agents include HIF hydroxylase inhibitors and iron chelators (Figure 6.1).
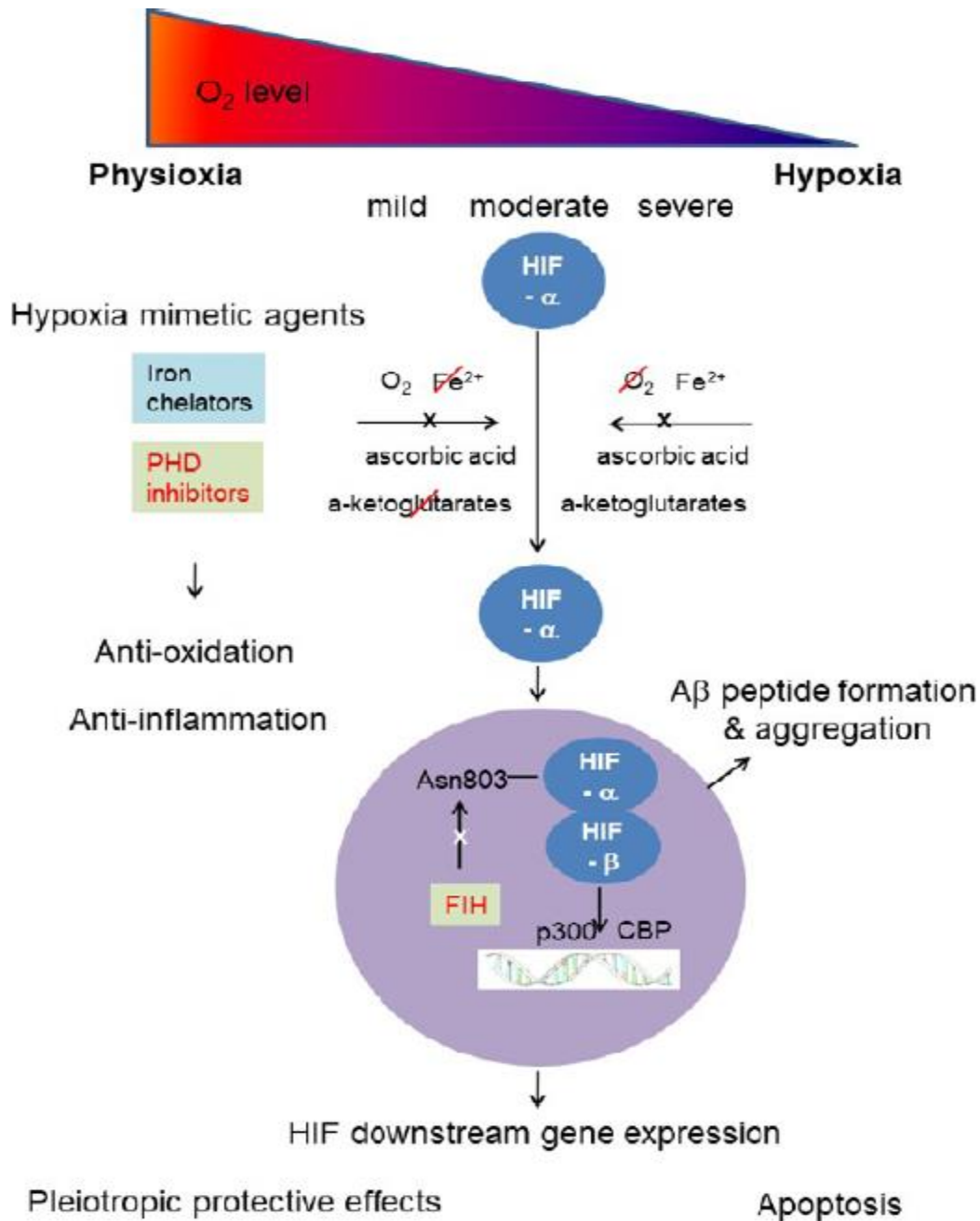
Figure 6.1 Schematic diagram describing the effects of hypoxia and hypoxia mimetic agents on neurons in Alzheimer's disease (AD) process. Hypoxia-inducible factor (HIF), a key mediator of oxygen homeostasis, generates numerous pleiotropic protective effects under hypoxia but also participates in apoptosis. Hypoxia mimetic agents, including iron chelators and HIF prolyl hydroxylase (PHD) inhibitors, can remove reactive oxygen species (ROS) and reduce

neuroinflammation, in addition to activating HIF. Pharmacological stabilization of HIF can be neuroprotective and explored as an adjunctive therapy for chronic ischemic/hypoxic diseases (Lall et al., 2019); (Hassan and Chen, 2021).

Severe and/or chronic hypoxia can lead to amyloid beta (Aβ) peptide formation and aggregation, Ca2+ dyshomeostasis, reactive oxygen species (ROS) formation in neurons, as well as neuroinflammation (Chen, 2018). Mild, moderate, and/or intermittent hypoxia have been found to induce protective adaptations in the brain (Lall, 2019). Hypoxia-inducible factor (HIF), a key mediator of oxygen homeostasis, generates numerous pleiotropic protective effects but also participates in Aβ peptide formation and aggregation. Hypoxia mimetic agents, including iron chelators and HIF prolyl hydroxylase (PHD) inhibitors, can remove ROS and reduce neuroinflammation, in addition to activating HIF. Pharmacological stabilization of HIF can be neuroprotective and could be explored as an adjunctive therapy for AD.

Based on this research findings, the reduction in cell viability and cytotoxicity induced by $Aβ_{25-35}$ under normoxic conditions appeared to be facilitated during hypoxia. This indicates that both primary neurons and PC12 cells are more susceptible to Aβ peptide toxicity during hypoxia. Moreover, during hypoxia, the overexpression of HIF-1α can bind to BACE1 mRNA and increase its expression, which is in line with the studies by Sun et al., 2006, and Zhang et al., 2007. This effect may also be due to an increase in Ca2+ entry into mitochondrial Ca2+ content, leading to the opening of transition pores in the mitochondrial membrane, through which cytochrome C can be released and pro-apoptotic signaling pathways initiated. This finding is consistent with the studies by Green and Peers, 2001, and Webster et al., 2006. Rutin significantly increases cell viability and reduces cell cytotoxicity in $Aβ_{25-35}$-induced PC12 cells and primary neurons under both normoxic and hypoxic conditions. Therefore, since HIF-1 has been shown to participate in

hypoxia-induced adaptive reactions to restore cellular homeostasis, rutin, as an iron chelator, may also activate HIF-1, in addition to its iron chelation properties. This indicates that rutin may have pharmacological functions in HIF stabilization.

Apoptosis (Type I programmed cell death) is a significant mechanism of neurodegeneration in AD pathogenesis, as evidence for apoptotic cell death has been observed in postmortem AD brains (Eckert, 2003). Cultured neurons incubated with Aβ peptides also undergo apoptosis (Yu, 2004). Aβ peptide-triggered neuronal cell death may involve different pathways, including stress kinase activation (Suen, 2003), membrane receptor-mediated response (Li, 2004), calcium imbalance, and oxidative stress, resulting in the activation of caspases (Allen, 2001).

In this studies, $A\beta_{25-35}$-induced primary neurons and PC12 cells in normoxia showed a significant increase in cell apoptosis, which appeared to be augmented during hypoxia. This indicates that $A\beta_{25-35}$ induces cellular apoptosis, which may be due to increased ROS levels. Furthermore, hypoxia may further increase ROS production by affecting the mitochondrial membrane potential, leading to cellular, protein, and DNA oxidative damage. This agrees with the findings of Bell et al., 2007. Additionally, the results revealed that the level of apoptosis was significantly reduced by rutin under both normoxic and hypoxic conditions. This implies that rutin, as an antioxidant, can scavenge free radicals, thereby protecting neuronal cells from oxidative damage and maintaining the mitochondrial membrane potential and cytosolic accumulation of cytochrome C. Rutin also has the ability to chelate iron and may stabilize HIF-1, which plays a role in oxygen homeostasis. Moreover, ROS and lipid peroxidation were significantly increased in $A\beta_{25-35}$-induced PC12 cells under normoxic conditions, and these effects were even more pronounced during hypoxic conditions. This suggests that mitochondria-derived ROS stabilize and activate HIF-1α during hypoxia. Furthermore, the level of ROS and lipid peroxidation was also

significantly reduced by rutin under both normoxic and hypoxic conditions. This implies that rutin may play a role in HIF-1 stabilization and maintain the mitochondrial membrane potential and cytosolic accumulation of cytochrome C.

6.3. Neuroinflammation in AD

Microglia-mediated neuroinflammation, characterized by excessive microglia activation and overproduction of pro-inflammatory cytokines and chemokines, is an important factor in AD. It begins as a defense mechanism against Aβ deposition in the brain but can also lead to neurodegeneration (Giovannini, 2002). Excessive activation of microglia results in the release of inflammatory cytokines, synthesis and release of cytotoxic factors such as nitric oxide and reactive oxygen species, leading to significant neuronal cell damage (Mosher and Wyss-Coray, 2014). Microglia produce both pro-inflammatory and anti-inflammatory cytokines and can exhibit a classically activated M1 phenotype or an alternatively activated M2 phenotype (Geissmann et al., 2008). Therefore, inhibition of the inflammatory responses of microglia can play a prospective therapeutic role in the treatment of AD. However, upon stimulation, these cells can also produce growth factors and chemokines (Butovsky et al., 2005). The production of pro-inflammatory cytokines by microglia is commonly associated with the generation of reactive oxygen species (ROS), nitric oxide-dependent activation, and reactive nitrogen species (RNS) (Taupin, 2010). The brain is particularly vulnerable to excessive generation of ROS and RNS, and microglia have been associated with the pathophysiology of age-related diseases (Harry, 2013), excitotoxicity-induced neurodegeneration (Vinet et al., 2012), glioma (Li and Graeber, 2012), and modulation of their response has been considered a therapeutic strategy (Cartier et al., 2014).

The inhibition of important enzymes involved in inflammation explains the anti-inflammatory effect of rutin. Rutin has been found to alleviate ROS-induced oxidative stress and inflammation

in rats by targeting p38-MAPK, i-NOS, NFκB, COX-2, TNF-α, and IL-6 (Nafees et al., 2015). It has also been shown to decrease brain damage and improve neurological dysfunctions through its anti-inflammatory properties (Hao et al., 2016).

Based on our research, gene expression analysis revealed that rutin significantly reduced the mRNA expression of NOS, TNF-α, and IL-6. This implies that rutin inhibits pro-inflammatory cytokine genes and reduces NO synthesis, indicating its anti-inflammatory role. Moreover, rutin is capable of shifting microglial state from the M1 to M2 phenotype, attenuating microglia-related neuroinflammation. Rutin has been observed to inhibit High Mobility Group Box 1 (HMGB1) release, down-regulate HMGB1-dependent inflammatory responses in human endothelial cells, and inhibit HMGB1-mediated hyperpermeability and leukocyte migration in mice (Yoo, Ku, Baek, and Bae, 2014). HMGB1 protein acts as a late mediator of severe vascular inflammatory conditions. Additionally, treatment with rutin resulted in a reduced cecal ligation and puncture-induced release of HMGB1 and sepsis-related mortality, indicating that rutin could be a candidate therapeutic agent for the treatment of various severe vascular inflammatory diseases through inhibition of the HMGB1 signaling pathway (Yoo, Ku, Baek, and Bae, 2014). Rutin has been shown to reduce the levels of NFκB and its transcriptional activity products, such as TNF-α, in UV-irradiated fibroblasts (Banu et al., 2009). NFκB levels are dependent on prostaglandins, so diminished levels of prostaglandin derivatives, such as F2α isoprostanes, observed after rutin treatment, and may lead to decreased NFκB levels. Decreases in this pro-inflammatory factor were also observed in numerous tissues of rutin-treated rats and were accompanied by secretion of pro-inflammatory cytokines after LPO-induced inflammation (Yeh et al., 2014). Studies have revealed that rutin suppresses phosphorylation of NFκB by inhibiting MAPK in lung tissue, in addition to decreasing the expression and cytoplasmic relocation of NFκB (Yeh et al., 2014). Rutin has been

shown to exert anti-inflammatory effects in UVB-irradiated mouse skin by inhibiting COX-2 and iNOS expression via suppression of p38/MAPK (Choi et al., 2014). Research results also revealed that rutin suppresses p38 levels (Sancho et al., 2003). Inhibition of NFκB activity may also be associated with decreases in fibroblast endocannabinoid levels (Sancho et al., 2003). Rutin also possesses anti-inflammatory properties (Enogieru, Haylett, Hiss, Bardien, & Ekpo, 2018). In a carfilzomib-induced cardiotoxicity model, pretreatment of rutin at 20 and 40 mg/kg in rats led to a significant downregulation of NFκB mRNA expression by increasing its inhibitory protein, IκB-α (Imam et al., 2017), which further reduced the expression of numerous pro-inflammatory cytokines such as interleukin-6 (IL-6), C-reactive protein (CRP), and TNF-α (Dong, Jimi, Zeiss, Hayden, & Ghosh, 2010). Rutin has been shown to potently inhibit pro-inflammatory TNF-α and IL-1β release from monocytes (Yuandani, Jantan, & Husain, 2017). In general, rutin is believed to directly scavenge free radicals by chelating metal iron ions (Huang et al., 2017; Yang, Guo, & Yuan, 2008), thereby reducing oxidative stress and inflammation.

In this research study, rutin in the presence of LPS, was shown to reduce neuroinflammation in BV-2 cells by reducing nitrate production. Additionally, rutin significantly reduced the LPS-mediated increase in pro-inflammatory cytokine levels in BV2 microglial cells and downregulated NOS expression. Therefore, this illustrated that rutin is capable of shifting the microglial state from the M1 to M2 phenotypes, attenuating microglia-related neuroinflammation.

6.4. Pharmacological properties of rutin, with particular attention to its treatment in AD

Rutin exhibits several pharmacological properties, such as reducing oxidative stress, preventing neuroinflammation, possessing anti-diabetic properties, and reducing neurodegeneration. It also has cardio-protective, wound healing, radio-protective, nephron-protective, hepatoprotective, antiplasmodial, anti-arthritic, antiviral, improved endothelial, and anti-nociceptive activities (Riaz,

2018). The established pharmacological effects of rutin are mainly due to its antioxidant and anti-inflammatory properties, as well as its cytoprotective ability connected with anti-aging and anti-cancer properties (La, 2000). Rutin has vaso- and cardio-protective properties (Kim et al., 2005; Riaz et al., 2018). It strengthens the blood vessel walls, diminishes the permeability of capillaries, improves blood concentration, and has antiplatelet functions. By decreasing the cytotoxicity of oxidized low-density lipoprotein cholesterol, it may reduce the risk of atherogenesis (Sheu, 2004).

Rutin decreased oxidative stress and lipid peroxidation via an increase in antioxidant enzyme activities and a decrease in TNF-α and IL-1β in an AD cell model (Wang et al., 2012). It improved memory, decreased oxidative stress and lipid peroxidation, decreased GFAP, increased antioxidant enzyme and acetylcholine esterase activities in a Huntington's disease rat model (Suganya and Sumathi, 2017). Rutin upregulated anti-apoptotic and genes relevant to dopamine biosynthesis, reduced caspase-3 and caspase-9 in a Parkinson's disease cell model (Magalingam et al., 2015). It improved cognitive deficits, reversed β-secretase, p-STAT3, and post-synaptic density protein 95 to normal levels in a high-fat diet rat model (Cheng et al., 2016). Rutin pre-treatment reduces infarct size and neurological deficits in rats after middle cerebral artery occlusion and protects antioxidant enzymes in the brain (Khan et al., 2009). Rutin also protects the brain tissue of Wistar male rats from cerebral ischemia (Abd-El-fatah et al., 2010). It has been revealed that rutin can improve both the cognitive and behavioral symptoms associated with neurodegenerative diseases due to its ability to cross the blood-brain barrier, act as an antioxidant in neuronal cells, and exhibit anti-inflammatory effects. Furthermore, it has effects on Aβ aggregates and processing in AD (Habtemariam, 2016).

Rutin can inhibit aggregation and cytotoxicity of Aβ, inhibit damage to mitochondria, and decrease the production of reactive oxygen species (ROS) (Wang et al., 2012). Several studies have

demonstrated that rutin can interfere with the aggregation and toxicity of Aβ, inhibit oxidative stress induced by Aβ, and reduce Aβ42 levels in mutant human APP-overexpressing cells. It has also been shown to reduce senile plaques in the brains of APP transgenic mice (Jimenez-Aliaga et al., 2011; Xu et al., 2014; Yu et al., 2015). It has been revealed that polyphenol compounds exhibit inhibitory effects on Aβ42 aggregation by binding to hydrophobic β-sheet channels with their aromatic structure, and at the same time, disturb the formation of Aβ hydrogen bonds through the action of hydroxyls as electron donors (Porat, 2006; Porzoor et al., 2015; Velandera et al., 2017; Phan et al., 2019). Rutin is chemically composed of an aromatic core with polyhydroxyl groups and may function through the mechanisms described above (Pu et al., 2007). Rutin also reduces Aβ$_{42}$-induced cytotoxicity by interacting with Aβ to modify the structure of Aβ oligomers and then inhibiting their cytotoxicity. It has been revealed that rutin decreases Aβ$_{25–35}$ fibril formation and accumulation in vitro, thereby decreasing neurotoxicity (Jiménez-Aliaga et al., 2011), as well as decreasing Aβ plaque aggregation, nitric oxide production, pro-inflammatory cytokines, and oxidative stress in vivo (Xu et al., 2014).

Neuroinflammation is a complex response to brain injury involving the activation of glia, release of inflammatory mediators such as cytokines and chemokines, and generation of ROS (DiSabato et al., 2016). Inflammatory responses in the brain are associated with increased levels of prostaglandins (PGs), particularly PGE2. Elevated PGE2 and inflammatory mediators are also characteristic of the aging brain. An increased state of neuroinflammation renders the aged brain more susceptible to the disruptive effects of both intrinsic and extrinsic factors such as infection, diseases, toxicants, or stress (DiSabato et al., 2016). In AD, microglia secrete proinflammatory cytokines, PGs, ROS, and NOS, which result in chronic stress and, over a prolonged period, neuronal death (Calsolaro and Edison, 2016; Rawlinson et al., 2020). Reduction of

"neuroinflammation" in a rat model of AD (Javed et al., 2012) and neuroprotective effects in dexamethasone-treated mice were observed upon rutin administration (Tongjaroenbuangam et al., 2011). Studies have shown that rutin decreased TNF-α and IL-1β generation in microglia (Wang et al., 2012). Additionally, research has reported the inhibition of Aβ aggregation and cytotoxicity by rutin, in addition to the prevention of mitochondrial damage, reduction of pro-inflammatory cytokine production (TNF-α and IL-1), and increase in the levels of catalase (CAT) and superoxide dismutase (SOD) (Wang et al., 2012). Sodium rutin attenuated neuroinflammation, enhanced microglia-mediated Aβ clearance, ameliorated synaptic plasticity impairment, and reversed spatial learning and memory deficits in two mouse models of AD (Pan et al., 2019).

Rutin exerts its neuroprotective potential by interacting with critical protein and lipid kinase signaling cascades, such as PI3K/Akt, protein kinase C, and MAPK, in the brain, resulting in the inhibition of apoptosis triggered by Aβ and promoting neuronal survival and synaptic plasticity. It has beneficial effects on the vascular system, leading to changes in cerebrovascular blood flow through angiogenesis and neurogenesis (Xu et al., 2014). Research has shown that oral rutin administration may protect the CA3 region of the hippocampus in rats and have an impact on their behavior, decreasing the impairment of memory due to trimethyltin toxicity (Koda et al., 2008, 2009). Rutin exerted an antidepressant-like effect partially through a neuroprotective effect on the hippocampus by acting on NMDA receptors (Anjomshoa et al., 2020). Rutin pre-treatment reduces infarct size and neurological deficits in rats after middle cerebral artery occlusion and protects the antioxidant content of enzymes in the brain (Khan et al., 2009; Abd-El-fatah et al., 2010). Rutin protected against the neurodegenerative effects of prion accumulation by increasing the production of neurotrophic factors and inhibiting apoptotic pathway activation (Aldhabi et al., 2015). Rutin

has potential anticonvulsant and antioxidant activities against oxidative stress in kainic acid-induced seizures in mice (Nassiri-Asl et al., 2013).

Rutin attenuates age-related memory deficits in mice (Kishore, 2005). It improves the learning and memory of normal, aged, and experimentally-induced amnesic mice, possibly due to its potent antioxidant action (Kishore and Singh, 2005). Rutin protected against spatial memory impairment induced by trimethyltin and synaptophysin in AD transgenic mice (Xu et al., 2014). Rutin significantly attenuated memory deficits in AD transgenic mice, decreased oligomer Aβ levels, increased SOD activity and GSH/GSSG ratio, reduced GSSG and MDA levels, downregulated microgliosis and astrocytosis, and decreased IL-Iβ and IL-6 levels in the brain (Xu et al., 2014). It improved memory and behavior in open-field tests, elevated plus and Y-mazes tests, probably due to its reduction in neuro-apoptosis (Man et al., 2015). Rutin prevented cognitive deficits and morphological changes in the hippocampus, attenuated lipid peroxidation, COX-2, GFAP, IL-8, iNOS, and NFκB in a rat model of sporadic dementia (Javed et al., 2012). It also prevented memory deficits and ameliorated oxidative stress, apoptosis, and neurite growth in a rat model for cognitive dysfunction (Ramalingayya et al., 2017). Rutin inhibits apoptosis by decreasing oxidative stress, Bax/Bcl-2 ratio, caspase-3 and -9 activation, and c-Jun and p38 phosphorylation in a dopaminergic cell model (Park et al., 2015).

6.5. Pharmaceutical Properties of Rutin

Rutin is poorly absorbed in the small intestine, and it reaches its peak plasma metabolites nine hours after ingestion (Hollman, 1997). This is because the sugar moiety (rutinose) present in rutin needs to be hydrolyzed by colonic microflora before the liberated quercetin can be absorbed from the colon or further degraded to phenolic compounds by gut microorganisms (Olthof et al., 2000). Once absorbed, quercetin undergoes glucuronidation, methylation, and sulfation processes in

enterocytes and hepatocytes before entering the bloodstream for transportation to other tissues (Boyle et al., 2000). Quercetin conjugates in the blood are carried and distributed by albumins, the main blood proteins, to various tissues, including the brain, as quercetin can cross the blood-brain barrier (BBB). Animal studies have shown the presence of quercetin in the colon, liver, kidneys, muscles, lungs, and brain (Deboer et al., 2005). Quercetin and its metabolites are eliminated by the kidneys and excreted through urine (Olthof et al., 2003). The relative bioavailability of rutin is approximately 20% of that of quercetin glucosides (Graefe et al., 2005), and its elimination half-life ranges from 11 to 28 hours for all glycosides (Manach et al., 2005). Accumulation of rutin in plasma requires repetitive intakes. However, quercetin conjugates are not the only beneficial metabolites of rutin. The majority of rutin metabolites, produced by colonic microorganisms, are mainly in the form of phenylacetic acids, which exhibit antioxidative activity similar to that of vitamin E (Olthof et al., 2003).

Although rutin has poor water solubility and low bioavailability, it is capable of crossing the BBB. Studies have reported a peak plasma concentration (Cmax) of rutin to be 262.85 ± 6.15 ng/ml after oral administration of a 35 mg dose of rutin to rabbits (Ramaswamy, 2017), and a serum concentration of approximately 300 ng/ml after 2 hours of oral administration of 100 mg/kg rutin to mice (Pan, 2019). Following intravenous (i.v.) administration of a dose of 10 mg/kg to rats, the Cmax of rutin in plasma and brain homogenate was 1511.24 ± 46.92 ng/ml and 111.57 ± 12.01 ng/ml, respectively (Ahmad, 2016; Xiao-ying, 2021). Various strategies have been developed to enhance the solubility and bioavailability of rutin to extend its clinical application. The sodium salt of rutin, for example, has shown significantly improved water solubility, enhanced bioavailability, and the ability to cross the BBB (Pan, 2019; Xiao-ying, 2021). In AD patients, the concentrations of total-tau in cerebrospinal fluid (CSF) were approximately 700 pg/ml (Karikari,

2020; Xiao-ying, 2021). Rutin has been found to cross the BBB and reach CSF concentrations high enough to neutralize pathological tau, suggesting its potential direct effects on tau pathology in the brain.

Due to its low bioavailability resulting from high metabolism, further studies aimed at improving its bioavailability and investigating its protective activities in additional AD models would provide a solid foundation for its use in clinical trials.

6.6. Bioavailability and Blood-Brain Barrier Penetration of Rutin

Rutin is a flavonoid glycoside that is abundantly found in various fruits, vegetables, and herbs. It has been extensively studied for its potential health benefits, including its anti-inflammatory, antioxidant, and anticancer effects. However, rutin's bioavailability is relatively low due to its poor solubility and absorption in the gastrointestinal tract.

Several studies have investigated the bioavailability of rutin in humans and animals. One study examined the bioavailability of rutin in healthy volunteers who consumed a single dose of 500 mg of rutin in tablet form. The study showed that only 20% of the ingested dose was absorbed and excreted in the urine, indicating low bioavailability (Vennat et al., 1996). Another study conducted on rats revealed that rutin's bioavailability was low due to its rapid metabolism and elimination in the liver and kidneys (Kim et al., 2005). Additionally, a research study evaluated the bioavailability of rutin in rats after oral administration of a rutin-rich extract from tartary buckwheat. The results indicated poor absorption of the compound, with a bioavailability of only 0.13% (Kim et al., 2014).

However, several factors can affect the bioavailability of rutin, such as the form of administration (oral vs. intravenous), co-administration with other compounds, and the presence of enzymes that

can break down rutin in the body. Co-administration of rutin with quercetin has been found to increase its bioavailability in rats (Li et al., 2013).

Various methods can be employed to improve the bioavailability of rutin, including encapsulation, complexation with cyclodextrins, and incorporation into nanoemulsions. Studies have shown that encapsulating rutin in chitosan nanoparticles significantly increased its bioavailability (Zhao et al., 2016). Rutin possesses several pharmacological activities, including antioxidant, anti-inflammatory, and neuroprotective effects, making it potentially useful for treating neurological disorders. However, its ability to cross the blood-brain barrier (BBB) is limited. The BBB is a selective barrier that separates the brain from the systemic circulation, regulating the exchange of nutrients and waste products while preventing the entry of foreign substances. Rutin has been reported to penetrate the BBB through passive diffusion (Gao et al., 2013). Several studies have investigated the BBB penetration of rutin.

In a rat model used to evaluate BBB penetration, rutin was found to cross the BBB and accumulate in the brain, albeit at a low concentration. Conjugating rutin with a peptide derived from apolipoprotein E was shown to enhance BBB penetration and neuroprotective effects in a mouse model of Alzheimer's disease (Wu et al., 2016). Another study loaded rutin into liposomes, which significantly increased its accumulation in the brain and showed promising results in a rat model of traumatic brain injury (Zhang et al., 2018). In vitro BBB models were also used to study the transport of rutin across the BBB, and it was found that rutin was poorly transported, with a permeability coefficient of 1.36×10^{-6} cm/s. However, co-administration of rutin with quercetin significantly increased its transport across the BBB (Ishisaka et al., 2011). In vivo studies using a rat model also demonstrated BBB penetration of rutin after intravenous administration, with a brain-to-plasma concentration ratio of 0.42, indicating moderate BBB penetration. Co-

administration with quercetin further enhanced BBB penetration (Kim et al., 2014). Additionally, a study using liquid chromatography-mass spectrometry (LC-MS) to measure rutin levels in rat brain tissue after oral administration revealed that rutin could cross the BBB and accumulate in the brain, with peak concentration observed around 2 hours after administration (Li et al., 2016). An in vitro model investigating BBB permeability of rutin demonstrated that rutin could pass through the BBB model, with a permeability coefficient of 2.85×10^{-6} cm/s (Liu et al., 2014). Recent studies evaluated the BBB penetration of rutin in a mouse model of cerebral ischemia-reperfusion injury, and it was found that rutin could cross the BBB and accumulate in the brain, with peak concentration observed around 4 hours after oral administration (Guo et al., 2020).

Although rutin can penetrate the BBB, its concentration in the brain remains limited. Therefore, strategies to improve its BBB penetration, such as conjugation with peptides or loading into liposomes, may enhance its therapeutic potential for neurological disorders. Additionally, strategies to improve the solubility and bioavailability of flavonoids could extend their clinical applications, especially for central nervous system diseases. In a recent study, rutin was converted to Sodium rutin (NaR), which exhibited high water solubility and bio-absorption in vivo. NaR, a salt formation of rutin, demonstrated increased water solubility, bioavailability, and BBB penetration. NaR was able to penetrate the BBB in mice, and treatment with NaR significantly reduced Aβ deposits in the brain of AD mice (Pan et al., 2019).

The accumulation and deposition of Aβ in the brain have been postulated as major drivers of the pathogenic cascades of Alzheimer's disease (AD) (Hardy and Selkoe, 2002). Microglia, the resident immune cells of the brain, play a key role in responding to Aβ accumulation and phagocytosis (Fu et al., 2016; Pan et al., 2019). Impairment of Aβ clearance during AD progression is attributed to a decrease in the phagocytic capacity of microglia due to aging (Hickman et al.,

305

2008). NaR treatment increases microglial recruitment around Aβ plaques and enhances CD68+ phagosome expression in AD mice, indicating that NaR treatment restores microglial phagocytic capacity and stimulates Aβ clearance (Pan et al., 2019).

Impairment in the expression or trafficking of different phagocytic receptors can lead to neurodegeneration, as phagocytosis plays a crucial role in maintaining brain homeostasis by removing cellular debris and misfolded proteins (Lucin et al., 2013). Up-regulation of these receptors is significant in the phagocytosis of aggregated proteins like Aβ and can delay neuropathology (Lee et al., 2018). NaR has been shown to enhance microglial Aβ phagocytosis by increasing the expression of microglial phagocytic receptors. Additionally, NaR accelerates the recycling of Trem2 in cultured microglial cells. NaR treatment can rescue microglial phagocytic dysfunction caused by Trem2 knockout or individual knockdown of phagocytic receptors, suggesting that microglial phagocytic receptors are not essential for the NaR-mediated enhancement of Aβ phagocytosis and clearance (Pan et al., 2019).

Microglial phagocytosis requires a large amount of energy for dynamic cytoskeletal reorganization (Kalsbeek et al., 2016). In AD pathology, a metabolic switch from mitochondrial oxidative phosphorylation (OXPHOS) to anaerobic glycolysis occurs in microglia, particularly in cells surrounding Aβ plaques, to increase ATP production for Aβ phagocytosis (Wendeln et al., 2018). However, anaerobic glycolysis only produces two ATP molecules from each glucose molecule and is accompanied by the generation of toxic metabolites like lactate (Kalsbeek et al., 2016). Targeting microglial metabolic reprogramming could be a potential approach for AD treatment. It has been demonstrated that proinflammatory stimulation with lipopolysaccharide (LPS) increases microglial anaerobic glycolysis and inhibits mitochondrial OXPHOS, which can be rescued by NaR treatment. NaR treatment significantly decreases microglial M1-type inflammatory cytokines

(including IL-1β, IL-6, and TNF-α) and increases the expression of microglial M2-type factors (including IL-4 and IL-10) in AD mice (Pan et al., 2019). These findings suggest that NaR treatment can switch the metabolic program from anaerobic glycolysis to mitochondrial OXPHOS, promote microglial M2 polarization, reduce neuroinflammation, and enhance Aβ clearance in the AD brain.

In conclusion, NaR treatment increases the expression and recycling of microglial phagocytosis-related receptors, promotes a metabolic switch from anaerobic glycolysis to mitochondrial OXPHOS, and provides sufficient energy (ATP) through an efficient metabolic pathway. NaR treatment stimulates microglial recruitment to Aβ plaques, enhances Aβ phagocytosis, and alleviates Aβ burden and associated pathological features, including neuroinflammation, synaptic loss, and impairment of plasticity. Therefore, NaR treatment reverses learning and memory deficits in AD mice, suggesting that NaR may be a promising drug candidate for AD treatment.

Why normal rutin was choosen in this studies, rather than more bioavailable formulation

I choosen to use normal rutin rather than bioavailable formulation because of its cost and availability. Normal rutin is usually more readily available and cost-effective compared to bioavailable formulations. Therefore, it is easier to obtain it in sufficient quantities and give greater flexibility in experimental design and replication. Additionally, I choosen standard rutin because of experimental Control. Normal rutin gives better control, because using more bioavailable formulations may contain additional components or modifications that can introduce confounding variables into the study. Thus, by using normal rutin, the effects of rutin itself can be isolated and its mechanisms of action can be well recognised. In addition, using normal rutin in this study, gives easier comparison with previous studies and established literature. This is because, bioavailable formulations may have different pharmacokinetics, bioavailability, or metabolic pathways, which

can make it challenging to directly compare the results with existing research. Thus, standard form of rutin was used, so that it can be easier to build upon previous knowledge and establish a more coherent understanding of its effects.

In general, I choosed normal rutin before progressing to bioavailable formulations, and this have supported me to establish a foundation of knowledge and better understanding of its effects and behavior before moving on to more complex formulations. Therefore, since the basic effects and mechanisms of normal rutin have been established, further studies using bioavailable formulations becomes necessary to explore its therapeutic potential in clinical settings. Bioavailable formulations can enhance its absorption, distribution, and stability, possibly improving its efficacy and bioactivity. Thus, transitioning to bioavailable formulations can be a logical next step in this research studies, particularly when considering future clinical applications.

6.7. General conclusions

In conclusion, this study established an in vitro Alzheimer's disease (AD) model using PC12 cells and primary rat neurons and evaluated the effects of rutin in normoxic or hypoxic conditions. The study revealed that $A\beta_{25-35}$ induced cytotoxicity and apoptosis in PC12 cells and primary neurons, and increased the levels of reactive oxygen species (ROS) and lipid peroxidation. Combined treatment of $A\beta$ with hypoxia for 24 hours significantly ameliorated the effects. Therefore, since HIF-1 is the principal molecule regulating oxygen homeostasis during stroke or cerebral vascular atherosclerosis, activation of the HIF-1 pathway during hypoxia may further contribute to AD pathogenesis by facilitating $A\beta$ deposition and toxicity.

In addition, rutin was found to significantly attenuate the effects in both hypoxic and normoxic conditions. This implies that rutin, as an iron chelator, attenuates or reverses $A\beta_{25-35}$-induced cytotoxicity, apoptosis, ROS, and oxidative damage on primary neurons and PC12 cells. The

possible mechanism can be attributed to its antioxidant effects and a potential role in HIF stabilization. Furthermore, rutin was found to reduce pro-inflammatory cytokine levels in BV2 microglial cells and downregulate NOS expression. It was also revealed that rutin, by reducing nitrate production, can attenuate microglia-related neuroinflammation and shift the microglial state from the M1 to M2 phenotypes. This suggests a possible alternative in the treatment or prevention of neurodegenerative disorders.

Thus, rutin may serve as a novel drug for the treatment of AD due to its ability to scavenge free radicals, inhibit oxidative stress, and its potential role in HIF stabilization. Further experimental research should focus on investigating other molecular targets and signaling pathways of rutin using primary neurons and PC12 cells. Additionally, more investigations on primary microglia and animal models are needed to further understand the role played by rutin in neuroinflammation. Further experimental models are needed to understand AD pathogenesis and conduct preclinical testing of novel therapeutics. Moreover, advanced studies to improve its bioavailability would provide a solid foundation for its use in clinical trials.

6.8. Limitations of the Study

Hypoxia chambers are a standard tool used to induce hypoxia by reducing oxygen levels in the in vitro culture environment. However, the use of hypoxia chambers or incubators has several limitations. One major limitation is that the environmental oxygen concentration does not necessarily correspond to the oxygen concentration at the cellular level (Pavlacky and Polak, 2020; Rinderknecht et al., 2021). Another limitation is the difficulty in accurately measuring pericellular oxygen levels in the chambers during hypoxia, which can make it challenging to determine the oxygen concentration in the control group and lead to result interpretation issues (Chanana et al., 2016; Zhou et al., 2017).

To mitigate this limitation, a slight change in the medium of the control group can be made to achieve a fast onset of hypoxia. It has been observed that partial changes in the medium are required for all hypoxia induction methods, allowing for a rapid onset of hypoxia. Some methods, such as the enzymatic system, can induce hypoxia in less than two minutes, providing an advantage (Baumann et al., 2008). Additionally, there are alternative methods available to induce or mimic hypoxia without reducing environmental oxygen concentrations, which do not require special equipment. For example, the increase of the medium height method reduces the partial oxygen pressure at the cellular site through oxygen consumption by the cells. The CoCl2 method is also recognized as a strong HIF-1 inducer in cellular systems, mimicking the cellular response to hypoxia to some extent. However, all hypoxia induction methods have their drawbacks and limitations, and combining two methods may lead to more promising results in hypoxia induction.

It has been observed in evaluation of apoptosis using annexin V/7-AAD of PC12 cells exposed to control in both normoxia and hypoxia conditions as well as in control group of ROS generations exposed to both normoxia and hypoxia conditions that the effect of hypoxia appears to have no significant change between the control group in hypoxia and normoxia. But during the experiment, a lot of significant difference in the medium of this two-control group was observed, in which the medium of the control in hypoxia appeared to be yellowish at 24 hrs, which indicates a drop in PH, while the medium of control in normoxia conditions is pink. This can be due to lack of oxygen supply to the cells during hypoxic condition, which make the cells to absorb almost all the oxygen within the medium in other to maintain homeostasis. But when 30 µM of Aβ$_{25-35}$ was added to the cells for 24 hrs to the treatment group, toxicity and apoptosis is significantly higher to this group in normoxia, and much significantly higher during hypoxia, and this shows failure of the cells to maintain homeostasis at certain level of increased toxicity. This implies that the toxicity and

apoptosis in hypoxia control group is still higher during hypoxia than in normoxia, due to clear change in colour of the medium between the two conditions, because during the cell culture, if the medium need to be change (after 3-4 days) the medium becomes yellow and this was observed in control hypoxia group in just 24hrs within the chamber. This implies that the toxicity and apoptosis in the hypoxia control group are still higher during hypoxia compared to normoxia, as evidenced by the clear change in the color of the medium between the two conditions. Additionally, significant changes were observed between the normoxia and hypoxia control groups when assessing alterations in cellular morphology using Hoechst 33258 staining and Tuj and DAPI staining of nuclei. In Hoechst 33258 staining, neurons in the normoxia control group showed no nuclei fragmentation, while neurons in the hypoxia control group exhibited some nuclei fragmentation. In the normoxia control group (Tuj and DAPI staining), neurons had numerous long axons and bright nuclei and appeared to have longer axons and brighter nuclei than those in the hypoxia control group.

In the primary neuron studies, there are several limitations in determining neuron purity using Tuj1 immunofluorescence staining, including:

1. Cross-reactivity with non-neuronal cells: Tuj1 can cross-react with non-neuronal cells, such as fibroblasts and endothelial cells, leading to false-positive results and overestimation of neuron purity (Kim et al., 2005).

2. Variable expression of Tuj1: The expression of Tuj1 in neurons can vary depending on the stages of development, differentiation state, and cell type. Therefore, the sensitivity and specificity of Tuj1 staining for identifying neurons can vary depending on the experimental conditions.

3. Co-localization with glial cells: Tuj1 staining can co-localize with glial cells, such as astrocytes and oligodendrocytes, which can lead to inaccurate estimation of neuron purity.

4. Post-translational modifications of Tuj1: Tuj1 is subject to post-translational modifications, such as phosphorylation, acetylation, and glycosylation, which can affect its specificity and sensitivity in detecting neurons.

In future studies, these limitations can be addressed by using additional markers, such as neuronal-specific nuclear protein (NeuN), MAP2, or synaptophysin, to confirm the identity and purity of neurons in immunofluorescence staining experiments.

Another limitation is the use of BV2 cells in the experiment. BV-2 cells are an immortal cell line commonly used as a substitute for primary microglia (PM) in pharmacological studies. They are cheaper and faster to use than PM and originate from raf/myc-immortalized murine neonatal microglia (Henn, 2009; Lund, 2005). BV-2 cells express NADPH oxidase, which is associated with microglial-induced neuronal damage, making them suitable for studying neuroinflammation (Wu, 2006; Yang, 2007). BV-2 cells are currently the most accurate immortal cell line for microglia, exhibiting similarities in behavior to PM, such as cytokine secretion (Lund, 2005). However, a significant limitation of microglial cell lines is their poor proliferation, necessitating fresh isolation for each experiment (Henn, 2009). PM, on the other hand, are mainly obtained from adult mice or neonatal pup brains and are harder to obtain for in vitro studies (Baker, 2002; Giulian & Baker, 1986). PM cells are harvested from neonatal brains (Henn, 2009), which may not fully represent adult microglia and may result in inaccurate responses. Furthermore, PM microglia exhibit heterogeneity within the brain, so they may not represent all microglial cells present (Mahe, 2001; Guilleman & Brew, 2004). PM cell lines are prophylactically treated with antibiotics, which can affect certain experimental results (Kuhlmann, 1993).

Another limitation is the use of rutin in BV2 cells under both normoxia and hypoxia conditions. Initially, the experiment aimed to investigate the anti-inflammatory effect of rutin and its mechanism of action using LPS, which was induced under normoxia conditions. In the second phase of the research, Amyloid β_{25-35} was used to induce inflammation in BV2 cells under both normoxia and hypoxia conditions, and rutin was tested for its anti-inflammatory effect. However, due to the impact of COVID-19, the experiment was interrupted, and the generated data was insufficient for presentation. The viability and toxicity assays, evaluation of nitrate production by the Griess assay, and RNA extraction of Aβ were started but not completed in both normoxia and hypoxia. Future experimental studies can focus on addressing these limitations.

Another limitation is the bioavailability of rutin. Rutin has relatively low bioavailability due to its poor solubility and absorption in the gastrointestinal tract. Several studies have investigated the bioavailability of rutin in humans and animals. For example, a study with healthy volunteers who consumed a single dose of 500 mg of rutin in tablet form showed that only 20% of the ingested dose was absorbed and excreted in the urine, indicating low bioavailability (Vennat et al., 1996). In rats, rutin was found to have low bioavailability due to its rapid metabolism and elimination in the liver and kidneys (Kim et al., 2005). Another study in rats after oral administration of a rutin-rich extract from tartary buckwheat revealed a bioavailability of only 0.13%, indicating poor absorption of rutin (Kim et al., 2014).

However, several factors can affect the bioavailability of rutin, such as the form of administration (i.e., oral vs. intravenous), co-administration with other compounds, and the presence of enzymes that can break down rutin in the body.

Co-administration of rutin with quercetin has been found to increase the bioavailability of rutin in rats (Li et al., 2013). It has been reported that the rapid metabolism of flavonoids can be overcome

by their methoxylation, which also improves their intestinal absorption, bioavailability, and stability (Mostafa et al., 2018). The bioavailability of rutin can be improved through various methods such as encapsulation, complexation with cyclodextrins, and incorporation into nanoemulsions. It has been shown that the bioavailability of rutin was significantly increased when encapsulated in chitosan nanoparticles (Zhao et al., 2016). Additionally, loading rutin onto a novel nanoparticle-lipid polymer hybrid has shown efficacy for targeting rutin delivery to the brain. These nanoparticles were found to be both biocompatible, as tested by a hemolysis test, and bioavailable (Ishak et al., 2017). Moreover, rutin can penetrate the blood-brain barrier (BBB), but its concentration in the brain is limited. Therefore, strategies to improve its BBB penetration, such as conjugation with peptides or loading into liposomes, may enhance its therapeutic potential for neurological disorders. Strategies to improve the solubility and bioavailability of flavonoids could extend their application for clinical use, especially for central nervous system diseases.

Several studies have been conducted to investigate the BBB penetration of rutin. A rat model used to evaluate the BBB penetration of rutin revealed that rutin can cross the BBB and accumulate in the brain, albeit at a low concentration. Research to improve the BBB penetration of rutin by conjugating it with a peptide derived from apolipoprotein E revealed that the conjugate enhanced BBB penetration and neuroprotective effects in a mouse model of Alzheimer's disease (Wu et al., 2016). In another recent study, rutin was converted to sodium rutin (NaR), which gives it high water solubility and bioabsorption in vivo. A salt formation of rutin (NaR) was generated with high water solubility, bioavailability, and BBB penetration. NaR could penetrate the BBB in mice, and NaR treatment markedly reduced Aβ deposits in the brain of AD mice (Pan et al., 2019).

6.9. Future studies

In this study, rutin has shown promising outcomes using an in vitro model of AD. Thus, future studies should be directed towards studying its effect in vivo. In vivo studies would be beneficial to study the overall effect of rutin on AD in both normoxia and hypoxia conditions. Although in vitro cell model systems are cheaper, performed in a controlled environment, simpler to acquire, and the pharmacodynamics of the experiments are easy to evaluate, their major weakness is their failure to capture inherent organ complexity. Additionally, due to the simplicity of this model, reliable pharmacokinetic data cannot be generated, although initial toxicity studies can be carried out (Blaikie et al., 2022). Studying the effect of rutin in vivo addresses these limitations and can evaluate safety and efficacy on organ systems. Transgenic and non-transgenic animal models of AD can be developed to mimic the pathological changes related to the human disease. Generally, mammalian models such as mice and rats are used for AD studies, though non-mammals including C. elegans (Caenorhabditis elegans) and fruit flies (Drosophila melanogaster) can be used and are highly beneficial as they are subject to less strict ethical standards and have lower costs (Alzheimer's Association, 2019). In general, animal models will allow profound studies of the pathogenesis of AD and can reproduce the main hallmarks of the disease (Chierrito et al., 2017; Blaikie et al., 2022). In comparison to the in vitro model, animal models are also essential for safe assessments of novel therapeutics as their multifaceted systems give a better replication of human pharmacokinetics and thus enhanced prediction of toxicity. However, the complexity of animal models leads to a lack of control over experimental conditions (Arantes-Rodrigues et al., 2013), and strict ethical standards and higher costs are also associated with animal models compared to in vitro models. Therefore, models involving clinical studies of individuals with AD and healthy controls can be investigated in the future. Clinical studies of individuals with AD and healthy

controls can be instrumental in identifying risk factors and biomarkers associated with the disease. These studies can also help validate our findings from these cell culture models and investigate the clinical, cognitive, and behavioral changes associated with the disease, as well as the underlying biological mechanisms.

Examples of some human studies that can contribute to a better understanding of AD pathogenesis are as follows:

Neuroimaging studies: These studies use various neuroimaging techniques, such as MRI and PET, to examine brain structure and function in individuals with AD and healthy controls. They have revealed structural and functional changes in the brain associated with AD, such as hippocampal atrophy and increased amyloid and tau deposition (Scheltens et al., 2016).

Longitudinal studies: These studies follow individuals with AD and healthy controls over time and allow researchers to observe changes in cognitive function, behavior, and brain structure and function. They help identify early biomarkers of AD and elucidate the progression of the disease (Jack and Holtzman, 2013).

Genetic studies: These examine the effect of genetic factors in AD pathogenesis. They have identified several genetic risk factors for AD, such as the APOE gene, and provide detailed descriptions of the molecular mechanisms underlying the disease (Guerreiro and Bras, 2015).

Biomarker studies: These studies examine biological markers, such as $A\beta$ and tau levels in CSF. They contribute to the development of diagnostic tools for AD and the evaluation of potential therapies (Blennow et al., 2010).

Clinical trials: These studies evaluate the safety and efficacy of potential therapies for AD in human participants. They have contributed to the approval of several drugs for the treatment of

AD, such as cholinesterase inhibitors and memantine, and continue to be critical for the development of new treatments (Cummings et al., 2020).

All these experimental models can provide valuable insights into the mechanisms underlying AD pathogenesis, but each model has its limitations. Therefore, a combination of different experimental models is often used to gain a more comprehensive understanding of AD pathophysiology.

In the future of this experimental research study, investigation of other molecular targets and signaling pathways of rutin can be implemented. Rutin exerts its neuroprotective and neurotrophic effects on primary neurons and PC12 cells through multiple signaling pathways, including the PI3K/Akt, CREB, ERK, p38 MAPK, and Nrf2 pathways. Rutin has been shown to induce neurite outgrowth and promote differentiation of PC12 cells into a sympathetic neuron-like phenotype through the activation of the extracellular signal-regulated kinase (ERK) and p38 mitogen-activated protein kinase (MAPK) signaling pathways (Fu et al., 2019). Rutin also protects PC12 cells from oxidative stress-induced apoptosis by upregulating antioxidant enzymes such as superoxide dismutase (SOD) and catalase through activation of the nuclear factor erythroid 2-related factor 2 (Nrf2) pathway. Rutin has been shown to modulate several signaling pathways that are involved in AD pathology. For example, rutin activates the Nrf2/ARE signaling pathway, which regulates antioxidant and detoxification enzymes (Jianget al., 2016). Rutin also inhibits the JNK and p38 MAPK pathways, which are involved in neuroinflammation and apoptosis. Hence, rutin has multiple molecular targets and signaling pathways that contribute to its therapeutic effects in Alzheimer's disease, but further research is required to fully understand the mechanisms underlying its effects on the treatment of AD.

In the future, advanced studies are required to improve the bioavailability of rutin for its use in clinical trials. Rutin's low bioavailability has limited its effectiveness in clinical trials. To improve the bioavailability of rutin, several advanced studies can be conducted, including:

Formulation development: This approach involves the development of novel formulations, such as nanoparticles, liposomes, or microemulsions, which can enhance the solubility, stability, and absorption of rutin. These formulations can protect rutin from degradation in the gastrointestinal tract, increase its permeability across the intestinal membrane, and target specific tissues or organs. For example, rutin-loaded polymeric nanoparticles have been shown to increase the bioavailability of rutin by 1.5-fold in rats (Li et al., 2014). Similarly, solid lipid nanoparticles loaded with rutin have been shown to increase the bioavailability of rutin by up to 4.5-fold in rats (Jaiswal et al., 2015).

Complexation with cyclodextrins: Cyclodextrins are cyclic oligosaccharides that can form inclusion complexes with rutin. These complexes have been shown to improve the solubility and bioavailability of rutin. For example, a study showed that the bioavailability of rutin was increased by 2-fold when it was complexed with hydroxypropyl-β-cyclodextrin (Li et al., 2016).

Co-administration with enhancers: In this approach, rutin is co-administered with other substances that can enhance its absorption, such as piperine, quercetin, or vitamin C. These substances can inhibit the enzymes that break down rutin, increase its uptake by the intestinal cells, and improve its transport in the bloodstream (Chang et al., 2017).

Modification of chemical structure: Another approach is to modify the chemical structure of rutin to increase its bioavailability. For example, acylation, glycosylation, or methylation of rutin can change its physicochemical properties, such as lipophilicity or charge, and enhance its absorption

or retention in the body. For example, a study showed that rutin-PEG conjugates had a 3-fold higher bioavailability than free rutin in rats (Patel et al., 2012).

Animal and human studies: Once the advanced studies have been conducted, animal studies can be performed to evaluate the safety and efficacy of the new formulations of rutin. If the results are promising, human studies can be conducted to test the bioavailability, pharmacokinetics, and therapeutic potential of the new rutin products. Even though improving the bioavailability of rutin can be a challenging but important task, it requires interdisciplinary approaches and advanced techniques that can be evaluated. If successful, it can enhance the clinical application of rutin and improve human health outcomes.

There are a few clinical trials that have investigated the use of rutin in AD treatment. For example, a randomized, double-blind, placebo-controlled trial revealed that rutin supplementation (500 mg/day for 12 weeks) improved cognitive function and reduced oxidative stress in AD patients. The study also found that rutin supplementation decreased levels of beta-amyloid in AD patients (Khalatbary et al., 2017). Another study investigated the effects of rutin on brain function and structure in AD patients with mild cognitive impairment (MCI) and found that rutin supplementation (500 mg/day for 6 months) improved cognitive function and increased the thickness of the hippocampus (Mokhtari-Zaer et al., 2020). Additionally, another study revealed that rutin supplementation (1000 mg/day for 12 weeks) improved cognitive function and reduced levels of inflammation in AD patients (Akhondzadeh et al., 2020).

These studies suggest that rutin may have potential therapeutic effects in AD treatment, mainly in improving cognitive function and reducing oxidative stress and inflammation. However, further research is required to confirm these findings and determine optimal dosages and treatment durations.

319

In the future of this research study, investigation on whether hypoxia enhances LPS-induced toxicity and neuroinflammation using BV2 cells can be applied. Further research can investigate if hypoxia enhances Aβ-induced toxicity and neuroinflammation in BV2 cells and primary microglia. Additionally, the effect of rutin on Aβ-induced toxicity and neuroinflammation in BV2 cells and primary neurons in both normoxia and hypoxia conditions can be examined.

Therefore, more research studies are required to fully understand the anti-inflammatory effect of rutin in both normoxia and hypoxia conditions on primary microglia and animal models, to further understand the role played by rutin in neuroinflammation.

References

ABARIKWU, S.O., NJOKU, R.C., LAWRENCE, C.J., CHARLES, I.A., IKEWUCHI, J.C., (2017). Rutin ameliorates oxidative stress and preserves hepatic and renal functions following exposure to cadmium and ethanol. *Pharmaceutical Biology,* **55**, pp. 2161-2169.

ABD-EL-FATTAH, A.A., EL-SAWALHI, M.M., RASHED, E.R. and EL-GHAZALY, M.A., (2010). Possible Role of vitamin E, Coenzyme Q10 and rutin in protection against cerebral ischemia/reperfusion injury in irradiated rats. *International Journal of Radiation Biology*, **86**(12), pp. 1070-1078.

ABDEL-HAMID, N. M., NAZMY, M. H., ABDEL-HAMID, A. Z., & MOUSTAFA, Y. M. (2019). Rutin attenuates lipopolysaccharide-induced inflammation and oxidative stress in rat liver: role of iNOS and COX-2 expression. *Journal of Pharmacy and Pharmacology*, **71**(6), 897-904.

ABE, H., SEMBA, H., & TAKEDA, N. (2017). The roles of hypoxia signaling in the pathogenesis of cardiovascular diseases. *Journal of Atherosclerosis and Thrombosis*, **24**, 884–894.

ADA, T., LUCIA, V., CHIARA, D. and MARCELLA, R., (2014). Cholinergic System Dysfunction and Neurodegenerative Diseases: Cause or Effect? *CNS & Neurological Disorders - Drug Targets,* **13**(7), pp. 1294-1303.

ADAIKKAN, C., MIDDLETON, S.J., MARCO, A., PAO, P.C., MATHYS, H., KIM, D.N., (2019). Gamma entrainment binds higher-order brain regions and offers neuroprotection. *Neuron*. **102**, pp. 929–43.e8

AGHOLME, L., LINDSTRÖM, T., KÅGEDAL, K., MARCUSSON, J., HALLBECK, M., (2010). An in vitro model for neuroscience: differentiation of sh-sy5y cells into cells with morphological and biochemical characteristics of mature neurons. *Journal of Alzheimer's Discovery*. **20**, pp. 069–82.

AHMAD, N., AHMAD, R., NAQVI, A.A., ALAM, M.A., ASHAFAQ, M., SAMIM, M., (2016). Rutin-encapsulated chitosan nanoparticles targeted to the brain in the treatment of Cerebral Ischemia. *International Journal of Biological Macromolecule,* **91**, pp. 640–.

AKHONDZADEH, S., SOLTANI, S., KHORRAM, K., & MOHAMMADI, M. R. (2020). Rutin improves cognitive function in elderly with Alzheimer's disease: An exploratory study. *Psychogeriatrics*, **20**(5), 727-732.

AKSU, E.H.K.F., ÖZKARACA, M., ÖMÜR, A.D., KÜÇÜKLER, S., ÇOMAKLI, S., (2017). Rutin ameliorates cisplatin-induced reproductive damage via suppression of oxidative stress and apoptosis in adult male rats. *Andrologia,* **49**(1), pp. 12593. 36.

ALBERTO, SERRANO-POZO, MATTHEW, P., FROSCH, AND BRADLEY, T., (2011). Hyman Neuropathological Alterations in Alzheimer Disease. *Cold Spring Harbal Perspective Medicine*, **1**, pp. a006189.

ALBERTS, B., JOHNSON, A., LEWIS, J., RAFF, M., ROBERTS, K., WALTER, P., (2002). Programmed cell death (apoptosis) - Molecular biology of the cell. *4th ed. New York: Garland Science.*

AL-DHABI, N.A., ARASU, M.V., PARK C.H. and PARK, S.U., (2015). An up -to-Date Review of rutin and its Biological and Pharmacological Activities'. Experimental and Clinical Sciences, *International Online Journal*, **14**, pp. 59-63.

AL-DHABI, N.A., ARASU, M.V., PARK, C.H., PARK, S.U., (2015). An up -to-Date Review of rutin and its Biological and Pharmacological Activities. *Experimental and Clinical Sciences, International Online Journal*, **14**, pp. 59-63.

AL-ENAZI, M.M., (2014) Protective effects of combined therapy of rutin with silymarin on experimentally-induced diabetic neuropathy in rats. *Pharmacology & Pharmacy* **5** (9), pp. 876–889.

ALHAWARAT, F. M., HAMMAD, H. M., HIJJAWI, M. S., SHARAB, A. S., ABUARQOUB, D. A., AL SHHAB, M. A (2019). The effect of cycling hypoxia on MCF-7 cancer stem cells and the impact of their microenvironment on angiogenesis using human umbilical vein endothelial cells (HUVECs) as a model. *PeerJ*, 7, e5990.

ALHOSHANI, A.R., HAFEZ, M.M., HUSAIN, S., AL-SHEIKH, A.M., ALOTAIBI, M.R., AL REJAIE, S.S., ALSHAMMARI, M.A., ALMUTAIRI, M.M., AL-SHABANAH, O.A., (2017). Protective effect of rutin supplementation against cisplatin-induced nephrotoxicity in rats. *BMC Nephrology* **18**(1), pp. 194.

ALONSO, A.D., GRUNDKE-IQBAL, I., BARRA, H.S., IQBAL, K., (1997). Abnormal phosphorylation of tau and the mechanism of Alzheimer neurofibrillary degeneration: sequestration of microtubule-associated proteins 1 and 2 and the disassembly of microtubules by the abnormal tau. *Proceedings of the National Academy of Sciences of the United States of America,* **94**, pp. 298–303.

ALONSO, A.D., GRUNDKE-IQBAL, I., IQBAL, K., (1996). Alzheimer's disease hyperphosphorylated tau sequesters normal tau into tangles of filaments and disassembles microtubules. *Nat Med*. **2**, pp. 783–787

ALONSO, A.D., LI, B., GRUNDKE-IQBAL, I., IQBAL, K., (2006). Polymerization of hyperphosphorylated tau into filaments eliminates its inhibitory activity. *Proc Natl Acad Sci USA*. **23**, pp. 8864–8869

ALONSO, A.D., ZAIDI, T., GRUNDKE-IQBAL, I., IQBAL, K., (1994). Role of abnormally phosphorylated tau in the breakdown of microtubules in Alzheimer disease. *Proc Natl Acad Sci USA*. **91**, pp. 5562–5566.

ALONSO, A.D., ZAIDI, T., NOVAK, M., GRUNDKE-IQBAL, I., IQBAL, K., (2001). Hyperphosphorylation induces self-assembly of tau into tangles of paired helical filaments/straight filaments. *Proc Natl Acad Sci USA*. **98**, pp. 6923–6928

ALTIERI, M., DI PIERO, V., PASQUINI, M., GASPARINI, M., VANACORE, N., VICENZINI, E., LENZI, G.L., (2004) Neurology 62, pp. 2193–2197.

Alvarez, R., Lee, H.L., Hong, C., & Wang, C.Y. (2015). Single CD271 marker isolates mesenchymal stem cells from human dental pulp. *International Journal of Oral Science,* **7**, 205–212.

ALZHEIMER'S ASSOCIATION, (2018). Alzheimer's disease facts and figures. Alzheimer's Dementia **14**, pp. 367-429

ALZHEIMER'S DISEASE INTERNATIONAL, "WORLD ALZHEIMER REPORT 2015. The Global Impact of Dementia", Alzheimer's disease International.

ALZHEIMER'S ASSOCIATION, (2017). Alzheimer's disease facts and figures. Alzheimer's Dementia **13**, pp. 325-373. *Alzheimer's disease,* **70**(4), 1069–1091.

AN, W.L., COWBURN, R.F., LI, L., BRAAK, H., ALAFUZOFF, I., IQBAL, K., (2003). Up-regulation of phosphorylated/activated p70 S6 kinase and its relationship to neurofibrillary pathology in Alzheimer's disease. *Am J Pathol.* **163**, pp. 591–607.

ANANTHARAMAN, M., TANGPONG, J., KELLER, J.N., MURPHY, M.P., MARKESBERY, W.R., KININGHAM, K.K. (2006). β-amyloid mediated nitration of manganese superoxide dismutase: implication for oxidative stress in a APPNLh/NLh X PS-1 P264L/P264L double knock-in mouse model of Alzheimer's disease. *American Journal of Pathology,* **168**(5), 1608-1618.

ANASTASIO, T. (2011). Data-driven modelling of Alzheimer's disease pathogenesis. *Journal of Theoretical Biology,* **290**, 60–72.

ANDORFER, C., ACKER, C.M., KRESS, Y., HOF, P.R., DUFF, K., DAVIES, P., (2005). Cell-cycle reentry and cell death in transgenic mice expressing non mutant human tau isoforms. *J Neurosci.* **25**, pp. 5446–5454.

ANTANITUS, D.S., (1998). A Theory of Cortical Neuron-Astrocyte Interaction. *The Neuroscientist* **4** (3), pp.154-159.

AOYAGI, A., CONDELLO, C., STOHR, J., YUE, W., RIVERA, B.M., LEE, J.C., (2019). Aβ and tau prion-like activities decline with longevity in the Alzheimer's disease human brain. *Sci Transl Med,* **1**, pp. 11(490)

ARANTES-RODRIGUES, R., COLAÇO, A., PINTO-LEITE, R., and OLIVEIRA, P.A. (2013). In vitro and in vivo experimental models as tools to investigate the efficacy of antineoplastic drugs on urinary bladder cancer. *Anticancer Research*, **33**(4), 1273-1296.

ARENDT, T., STIELER, J., STRIJKSTRA, A.M., HUT, R.A., RUDIGER, J., VAN DER ZEE, E.A., (2003). Reversible paired helical filament-like phosphorylation of tau is an adaptive process associated with neuronal plasticity in hibernating animals. *J Neurosci.* **23**, pp. 6972–6981

ARIMA, H., ASHIDA, H., DANNO, G.I., (2002). Rutin-enhanced antibacterial activities of flavonoids against Bacillus cereus and Salmonella enteritidis. *Bioscience, Biotechnology, and Biochemistry* **66**, pp. 1009e1014.

ARISPE, N., DIAZ, J.C. and SIMAKOVA, O., (2007). Aβ ion channels. Prospects for treating Alzheimer's disease with Aβ channel blockers. *BBA – Biomembranes*, **1768** (8), pp. 1952-1965.

ARRASATE, M., PEREZ, M., ARMAS-PORTELA, R., AVILA, J., (1999). Polymerization of tau peptides into fibrillar structures. The effect of FTDP-17 mutations. *FEBS Lett*. **446**, pp. 199–202.

ASHOK, B.S., AJITH, T.A., SIVANESAN, S., (2017). Hypoxia-inducible factors as neuroprotective agent in Alzheimer's disease. *Clin Exp Pharmacol Physiol* **44**, pp. 327-334.

ASLLANI, I., HABECK, C., SCARMEAS, N., BOROGOVAC, A., BROWN, T.R., STERN, Y., (2008). Multivariate and univariate analysis of continuous arterial spin labelling perfusion MRI in

ATANASSOVA, M. and BAGDASSARIAN, V., (2009). Rutin Content in Plant Products. *University of Chemical Technology and Metallurgy* **44** (2), pp. 203.

ATHIRA, K.V., R.M., MADHANA, M., LAHKAR, (2016). Flavonoids, the emerging dietary supplement against cisplatin-induced nephrotoxicity, *Chem. Biol. Interact* **248**, pp.18-20.

AZARI, H., OSBORNE, G.W., YASUDA, T., GOLMOHAMMADI, M.G., RAHMAN, M., (2011). Purification of immature neuronal cells from neural stem cell progeny. *PLoS ONE*, 6, e20941.

BACHMEIER, C., PARIS, D., BEAULIEU-ABDELAHAD, D., MOUZON, B., MULLAN, M.and CRAWFORD, F., (2012). A Multifaceted Role for APOE in the Clearance of Beta-Amyloid across the Blood-Brain Barrier. *Neurodegenerative Diseases*, **11** (1), pp. 13-21.

BACHMEIER, M., MULLAN, D., and PARIS, D. (2010). Characterization and use of human brain microvascular endothelial cells to examine β-amyloid exchange in the blood-brain barrier. *Cytotechnology,* **62**(6), 519-529.

BAKER, C., MARTIN, D. & MANUELIDIS, L., (2002). Microglia from Creutzfeldt-Jakob disease-infected brains are infectious and show specific mRNA activation profiles. *J. Virol,* **76**, pp. 10905-10913.

BALABAN, R.S., NEMOTO, S., FINKEL, T., (2005). Mitochondria, oxidants, and aging. Cell **120** (4), pp. 483–495.

BALES, K.R., LIU, F., WU, S., LIN, S., KOGER, D., DELONG, C., (2009). Human APOE isoform-dependent effects on brain beta-amyloid levels in PDAPP transgenic mice. *J Neurosci* **29**, pp. 6771–9.

BANCHER, C., BRUNNER, C., LASSMANN, H., BUDKA, H., JELLINGER, K., WICHE, G., (1989). Accumulation of abnormally phosphorylated tau precedes the formation of neurofibrillary tangles in Alzheimer's disease. *Brain Res*. **477**, pp. 90–99

BANCHER, C., GRUNDKE-IQBAL, I., IQBAL, K., FRIED, V.A., SMITH, H.T., WISNIEWSKI, H.M., (1991). Abnormal phosphorylation of tau precedes ubiquitination in neurofibrillary pathology of Alzheimer disease. *Brain Res*. **539**, pp. 11–18.

BANU, S.K., LEE, J., SPEIGHTS, V.O., JR, STARZINSKI-POWITZ, A., AROSH, J.A., (2009). Selective inhibition of prostaglandin E2 receptors EP2 and EP4 induces apoptosis of human endometriotic cells through suppression of ERK1/2, AKT, NFκB, and β-catenin pathways and activation of intrinsic apoptotic mechanisms, *Molecular Endocrinology* **23** (8), pp. 1291–1305.

BARNES, C. (1979). Memory deficits associated with senescence: a neurophysiological and behavioural study in the rat. *Journal of Comparative and Physiological Psychology*, **93**(1), 74-104.

BARNHAM, K.J., BUSH, A.I., (2014). Biological metals and metal-targeting compounds in major neurodegenerative diseases. *Chem. Soc. Rev*, **43**, pp. 6727–6749.

BARRAL, S., ECKLEBE, J., TOMIUK, S., TIVERON, M.C., DESOEUVRE, A., (2013). Efficient neuronal in vitro and in vivo differentiation after immunomagnetic purification of mESC derived neuronal precursors. *Stem Cell Research*, **10**, 133-146.

BARTEN, D.M., FANARA, P., ANDORFER, C., HOQUE, N., WONG, P.Y., HUSTED, K.H., (2012). Hyperdynamic microtubules, cognitive deficits, and pathology are improved in tau transgenic mice with low doses of the microtubule-stabilizing agent BMS-241027. *Journal of Neuroscience*. **32**, pp. 7137–45.

BAUMANN, R.P., PENKETH, P.G., SEOW, H.A., SHYAM, K., & SARTORELLI, A.C. (2008). Generation of Oxygen Deficiency in Cell Culture Using a Two-Enzyme System to Evaluate Agents Targeting Hypoxic Tumor Cells. *Radiation Research*, **170**, 651–660.

BAYER, T.A., CAPPAI, R., MASTERS, C.L., BEYREUTHER, K. and MULTHAUP, G., (1999). It all sticks together-the APP-related family of proteins and Alzheimer's disease. *Molecular Psychiatry*, **4** (6), pp. 524-528.

BEHARRY, K. D., CAI, C. L., VALENCIA, G. B., LAZZARO, D., VALENCIA, A. M., SALOMONE, F. (2018). Human retinal endothelial cells and astrocytes cultured on 3-D scaffolds for ocular drug discovery and development. *Prostaglandins Other Lipid Mediat*, **134**, 93–107.

BERK, C., PAUL, G. and SABBAGH, M., (2014). Investigational drugs in Alzheimer's disease: current progress. *Expert Opinion on Investigational Drugs*, **23** (6), pp. 837-846.

BERNARD, F.X., SABLE, S., CAMERON, B., PROVOST, J., DESNOTTES, J.F., CROUZET, J.F., BLANCHE, F., (1997). Glycosylated flavones as selective inhibitors of topoisomerase IV. Antimicrob. *Agents Chemother*. **41**, pp. 992–998.

BHANDARI, R. K., & DEEM, J. F. (2018). A review of the role of hypoxia in the tumor microenvironment, angiogenesis, and metastasis. *Journal of advanced research*, **13**, 67-75.

BHASKAR, K., YEN, S.H., LEE, G., (2005). Disease-related modifications in tau affect the interaction between Fyn and Tau. *Jornal of Biological Chemistry*. **280**, pp. 35119–35125

BIESCHKE, J., HERBST, M., WIGLENDA, T., FRIEDRICH, R. P., BOEDDRICH, A., SCHIELE, F., EHRNHOEFER, D. E. (2012). Small-molecule conversion of toxic oligomers to nontoxic β-sheet–rich amyloid fibrils. Nature Chemical Biology, **8**(1), 93-101.

BLAIKIE, L., KAY, G., MACIEL, P., KONG THOO LIN, P. (2022). Experimental modelling of Alzheimer's disease for therapeutic screening. *European Journal of Medicinal Chemistry* Reports, 5.

BLENNOW, K., HAMPEL, H., WEINER, M., & ZETTERBERG, H. (2010). Cerebrospinal fluid and plasma biomarkers in Alzheimer disease. *Nature reviews neurology*, **6**(3), 131-144.

Blodgett, H., McCutchan, K. (1947). Place versus response learning in the simple T-maze. *Journal of Experimental Psychology*, **37**(5), 412-422.

BOADA-ROVIRA, M., BRODATY, H., CRAS, P., BALOYANNIS, S., EMRE, M., ZHANG, R., (2004). Efficacy and safety of donepezil in patients with Alzheimer's disease: results of a global, multinational, clinical experience study. *Drugs Aging*. **21**, pp. 43–53.

BOLISETTY, S., JAIMES, E., (2013). Mitochondria and reactive oxygen species: physiology and pathophysiology. *International Journal of Molecular Sciences* **14** (3), pp. 6306–6344.

BOLLAG, D.M., MCQUENEY, P.A., ZHU, J., HENSENS, O., KOUPAL, L., LIESCH, J., (1995). Epothilones, a new class of microtubule-stabilizing agents with a taxol-like mechanism of action. *Cancer Res*. **55**, pp. 2325–33.

BONDI, M.W., EDMONDS, E.C., SALMON, D.P., (2017). Alzheimer's disease: past, present, and future. *J Int Neuropsychol Soc*. **23**, pp. 818–31.

BOOTH, C.A., WITTON, J., NOWACKI, J., TSANEVA-ATANASOVA, K., JONES, M.W., RANDALL, A.D., (2016). Altered intrinsic pyramidal neuron properties and pathway-specific synaptic dysfunction underlie aberrant hippocampal network function in a mouse model of tauopathy. J Neurosci. **36**, pp. 350–63.

BOUKHARY, R.., (2016). Anti-inflammatory and antioxidant activities of salvia fruticosa: an hplc determination of phenolic contents, *Evid Based Complement. Altern Med,* **20**, (16), pp. 7178105.

BOWLES, K.R., T.C.W. J., QIAN, L., JADOW, B.M., & GOATE, A.M. (2019). Reduced variability of neural progenitor cells and improved purity of neuronal cultures using magnetic activated cell sorting. *PLoS ONE*, **14**(3), e0213374.

BOYLE, S.P., DOBSON, V.L., DUTHIE, S.J., HINSELWOOD, D.C., KYLE, J.A. and COLLINS, A.R., (2000). Bioavailability and efficiency of rutin as an antioxidant: a human supplementation study. *European journal of clinical nutrition,* **54** (10), pp. 774-782.

BRAI, E., STUART, S., BADIN, A.S., GREENFIELD, S.A. (2017). A novel ex vivo model to investigate the underlying mechanisms in Alzheimer's disease. *Frontiers in Cellular Neuroscience,* **11**(291), 1–8.

Brambilla, A., Lonati, E., Milani, C., Rizzo, A.M., Farina, F., Botto, L., et al. (2015). Ischemic conditions and β-secretase activation: the impact of membrane cholesterol enrichment as triggering factor in rat brain endothelial cells. *International Journal of Biochemistry and Cell Biology*, 69, 95-104.

BRETON-ROMERO, R., LAMAS, S., (2013). Hydrogen peroxide signalling mediator in the activation of p38 MAPK in vascular endothelial cells. *Methods Enzymol* **528**, pp. 49-59.

BRINES, M.L., (2000). Erythropoietin crosses the blood-brain barrier to protect against experimental brain injury. *Proc Natl Acad Sci USA*. **97**(19), pp. 10526–10531.

BRODBECK, J., MCGUIRE, J., LIU, Z., MEYER-FRANKE, A., BALESTRA, M.E., JEONG, D.E., (2011). Structure-dependent impairment of intracellular apolipoprotein E4 trafficking and its detrimental effects are rescued by small-molecule structure correctors. *J Biol Chem.* **286**, pp. 17217–26

BROOKMEYER, R., ABDALLA, N., KAWAS, C.H. and CORRADA, M.M., (2018). Forecasting the prevalence of preclinical and clinical Alzheimer's disease in the United States. Alzheimer's & Dementia: *The Journal of the Alzheimer's Association*, **14**(2), pp.121-129.

BROOKMEYER, R., GRAY, S., KAWAS, C., (1998). Projections of Alzheimer's disease in the United States and the public health impact of delaying disease onset. Am J Public Health, **88**, pp. 1337–42.

BROOKMEYER, R., JOHNSON, E., ZIEGLER-GRAHAM, K. and ARRIGHI, H.M., (2017). Forecasting the global burden of Alzheimer's disease; Alzheimer's & dementia. *The Journal of the Alzheimer's Association,* **3**(3), pp. 186.

BRUFANI, M., (2014). Acido α-lipoico farmaco o integratore Una panoramica sulla farmacocinetica, le formulazioni disponibili e le evidenze cliniche nelle complicanze del diabete. *Prog Nutr* **16**, pp. 62–74.

BURGOS-RAMOS, E., HERVAS-AGUILAR, A., AGUADO-LLERA, D., PUEBLA-JIMENEZ, L., HERNANDEZ-PINTO, A.M., BARRIOS, V., (2008). Somatostatin and Alzheimer's disease. *Mol Cell Endocrinol*. **286**, pp. 104–11.

BURKHART, A., THOMSEN, L.B., THOMSEN, M.S., LICHOTA, J., FAZAKAS, C., KRIZBAI, I., (2015). Transfection of brain capillary endothelial cells in primary culture with defined blood-brain barrier properties. *Fluids Barriers CNS*, **12**(19), 1-14.

BURNS, J.M., MAYO, M.S., ANDERSON, H.S., SMITH, H.J. and DONNELLY, J.E., (2008). Cardiorespiratory fitness in early-stage Alzheimer disease. *Alzheimer disease and associated disorders,* **22**(1), pp. 39-46.

BURSTEIN, A.H., SABBAGH, M., ANDREWS, R., VALCARCE, C., DUNN, I., ALTSTIEL, L., (2018). Development of azeliragon, an oral small molecule antagonist of the receptor for advanced glycation endproducts, for the potential slowing of loss of cognition in mild Alzheimer's disease. *J Prev Alzheimers Dis*. **5**, pp. 149–54.

Busche, M.A., Wegmann, S., Dujardin, S. (2019). Tau impairs neural circuits, dominating amyloid-β effects, in Alzheimer models in vivo. *Nat Neurosci* **22**, 57–64.

BUTNER, K.A., KIRSCHNER, M.W., (1991). Tau protein binds to microtubules through a flexible array of distributed weak sites. J Cell Biol.115, pp. 717–730.

BUTOVSKY, O., (2005). Activation of microglia by aggregated beta-amyloid or lipopolysaccharide impairs MHC-II expression and renders them cytotoxic whereas IFN-gamma and IL-4 render them protective. *Mol. Cell Neurosci*, **29** (3), pp. 381e393.

BUTTERFIELD, D.A., BOYD-KIMBALL, D., (2018). Oxidative stress, amyloid-β peptide, and altered key molecular pathways in the pathogenesis and progression of Alzheimer's disease. Journal of Alzheimer's Discovery. **62**, pp. 1345–67

BUTTERFIELD, D.A., HALLIWELL, B., (2019). Oxidative stress, dysfunctional glucose metabolism and Alzheimer disease. *Nat Rev Neurosci*. **20**, pp. 148–60.

BUTTERFIELD, D.A., REED, T., NEWMAN, S.F., SULTANA, R., (2007). Roles of amyloid β-peptide-associated oxidative stress and brain protein modifications in the pathogenesis of Alzheimer's disease and mild cognitive impairment. *Free Radical Biology and Medicine*, **43**(5), pp. 658–677

Ca (2019) Increased free prostate specific antigen serum levels in Alzheimer's disease, correlation with cognitive decline. J Neurol Sci 400, pp. 188-193.

CAGLAYAN, C., KANDEMIR, F.M., DARENDELIOĞLU, E., YILDIRIM, S., KUCUKLER, S., DORTBUDAK, M.B.., (2019). Rutin ameliorates mercuric chloride-induced hepatotoxicity in rats via interfering with oxidative stress, inflammation and apoptosis. *Journal of Trace Elements in Medicine and Biology,* **56**, pp. 60-68.

CAJA, L., DITURI, F., CABALLERO-DIAZ, D., MOUSTAKAS, A., GIANNELLI, G., FABREGAT, I., (2018). TGF-β and the tissue microenvironment: Relevance in fibrosis and cancer. *International Journal of Molecular Sciences*, 19, pp. E1294,

CALLAHAN, L.M., VAULES, W.A., COLEMAN, P.D., (1999). Quantitative decrease in synaptophysin message expression and increase in cathepsin D message expression in Alzheimer disease neurons containing neurofibrillary tangles. *J Neuropathol Exp Neurol*. 58, pp. 275–87.

CAMINS, A., VERDAGUER, E., FOLCH, J., CANUDAS, A.M. and PALLÀS, M., (2006). The Role of CDK5/ P25 Formation/Inhibition in Neurodegeneration. *Drug News Prospect*, **19**(8), pp. 453-60.

CAMP, J.P., CAPITANO, A.T. (2007). Induction of Zone-Like Liver Function Gradients in HepG2 Cells by Varying Culture Medium Height. *Biotechnology Progress*, **23**, 1485–1491.

CAO, J., ZHANG, Y., CHEN, W., ZHAO, X., (2010). The relationship between fasting plasma concentrations of selected flavonoids and their ordinary dietary intake. *British Journal of Nutrition*, **103**, pp. 249–55.

CARELLI, S., HEBDA, D.M., TRAVERSA, M.V., MESSAGGIO, F., GIULIANI, G., MARZANI, B., BENEDUSI, A., DI GIULIO, A.M., GORIO, A., (2012). A specific combination of zeaxanthin, spermidine and rutin prevents apoptosis in human dermal papilla cells. *Exp. Dermatol,* **21**(12), pp. 953–955.

CAROLINDAH, M.N., ROSLI, AND NORDIN, N., (2013). An overview of in vitro research models for Alzheimer's disease (AD). *Regenerative Research*, **2**(2), pp. 8-13.

CARPENTER, A.E., JONES, T.R., & LAMPRECHT, M.R. (2006). CellProfiler: image analysis software for identifying and quantifying cell phenotypes. *Genome Biology*, **7**(10), R100.

CARTIER, N., (2014). The role of microglia in human disease: therapeutic tool or target? Acta Neuropathology, 128 (3), pp. 363e380.

CASH, A.D., ALIEV, G., SIEDLAK, S.L., NUNOMURA, A., FUJIOKA, H., ZHU, X., (2003). Microtubule reduction in Alzheimer's disease and aging is independent of tau filament formation. *American Journal of Pathology*. **162**, pp. 1623–1627.

CATO, M.H., YAU, I.W., & RICKERT, R.C. (2011). Magnetic-based purification of untouched mouse germinal center B cells for ex vivo manipulation and biochemical analysis. *Nature Protocols,* **6**, 953-960.

CHAITANYA, G., MINAGAR, A., ALEXANDER, J. S. (2014). Neuronal and astrocytic interactions modulate brain endothelial properties during metabolic stresses of in vitro cerebral ischemia. *Cell Commun Signal*, 12, 7.

CHAN, S. Y., & LOSCALZO, J. (2010). The emerging paradigm of network medicine in the study of human disease. *Circulation research*, **107**(7), 956-967.

CHANANA, V., TUMTURK, A., KINTNER, D., UDHO, E., FERRAZZANO, P., CENGIZ, P. (2016). Sex differences in mouse hippocampal astrocytes after in-vitro ischemia. *J Vis Exp*, 116, 1-9.

CHANG, W., TENG, J. (2015). β-asarone prevents Aβ25-35-induced inflammatory responses and autophagy in SH-SY5Y cells: down expression Beclin-1, LC3B and up

CHANG, W.P., KOELSCH, G., WONG, S., DOWNS, D., DA, H., WEERASENA, V., (2004). In vivo inhibition of Abeta production by memapsin 2. (beta-secretase) inhibitors. *Journal of Neurochemistry*. **89**, pp. 1409–16.

CHANG, Y., XIE, X., ZHANG, L., JIANG, Y., & WU, T. (2017). Co-administration of quercetin and rutin has a synergistic effect on the bioavailability of quercetin in rats. *Journal of Agricultural and Food Chemistry*, **65**(49), 10705-10712.

CHEN, J., NAGAYAMA, T., JIN, K., STETLER, R.A., ZHU R.L., GRAHAM, S.H., SIMON, R.P., (1998*). Journal of Neuroscience*. **18**, pp. 4914–4928.

CHEN, R.L., BALAMI, J., ESIRI, M., CHEN, L.H., BUCHAN, A.M., (2010). Ischaemic stroke in the elderly: an overview of evidence. *Nat Rev Neurol* **6**, pp. 256-265.

CHEN, R.L., LAI U.H., ZHU, L.L., SINGH, A., AHMED, M., FORSYTH, N.R., (2018). Reactive Oxygen Species (ROS) formation in the brain at different oxygen levels: role of hypoxia inducible factors. *Front Cell Dev Biol* 6, pp.132.

CHEN, X., SUN, G., TIAN, E., ZHANG, M., DAVTYAN, H., BEACH, T.G (2021). Modeling sporadic Alzheimer's disease in human brain organoids under serum exposure. *Advanced Science*, **8**(18), 1–16.

CHEN, Z., CAI, Y., ZHANG, W., LIU, X., LIU, S., (2014a). Astragaloside IV inhibits platelet-derived growth factor-BB-stimulated proliferation and migration of vascular smooth muscle cells via the inhibition of p38 MAPK signalling. *Exp Ther Med*. 8, pp. 1253-1258.

CHEN, Z., FU, Q., SHEN, B., HUANG, X., WANG, K., HE, P., LI, F., ZHANG, F., (2014b). Enhanced p62 expression triggers concomitant autophagy and apoptosis in a rat chronic spinal cord compression model. *Mol Med Rep*. 9, pp. 2091-2096.

CHENG, C., FASS, D.M., FOLZ-DONAHUE, K., MACDONALD, M.E., & HAGGARTY, S.J. (2018). Highly Expandable Human iPS Cell-Derived Neural Progenitor Cells (NPC) and Neurons for Central Nervous System Disease Modeling and High-Throughput Screening. *Current Protocols in Human Genetics,* **92**, 1–21.

CHÉRON, N., YU C., KOLAWOLE, A.O., SHAKHNOVICH, E.I., WOBUS, C.E., (2015). Repurposing of rutin for the inhibition of norovirus replication. *Archives of Virology*, 160, pp. 2353–2358.

CHIERRITO, T.P.C., MANTOANI, S.P., ROCA, C., REQUENA, C., SEBASTIAN-PEREZ, V., CASTILLO, W.O (2017). From dual binding site acetylcholinesterase inhibitors to allosteric modulators: a new avenue for disease-modifying drugs in Alzheimer's disease. *European Journal of Medicinal Chemistry*, **139**, 773-791.

CHIOU, Y.S., Q., HUANG, C. T., HO, Y. J., WANG AND M. H., PAN, (2016). "Directly interact with Keap1 and LPS is involved in the anti-inflammatory mechanisms of (-)-epicatechin-3-gallate in LPS-induced macrophages and endotoxemia," *Free Radical Biology & Medicine*. 94, pp. 1–16.

CHO, W.K., WEERATUNGA, P., LEE, B.H., PARK, J.S., KIM, C.J., MA, J.Y., LEE, J.S., (2015). Epimedium koreanum Nakai displays broad spectrum of antiviral activity in vitro and in vivo by inducing cellular antiviral state. *Viruses*, 7(1), pp. 52–377.

CHOI, J.H., KIM, D.W., PARK, S.E., LEE, H.J., KIM, K.M., KIM, K.J., KIM, M.K., KIM, S.J., KIM, S., (2015). Anti-thrombotic effect of rutin isolated from Dendropanax morbifera Leveille. *Journal of Bioscience and Bioengineering*, **120**, pp. 181–186.

CHOI, J.K., KIM, S.H., (2013). Rutin suppresses atopic dermatitis and allergic contact dermatitis. *Exp. Biol. Med (Maywood)*, **238**(4), pp. 410–417.

CHOI, K.S., KUNDU, J.K., CHUN, K.S., NA, H.K., SURH, Y.J., (2014). Rutin inhibits UVB radiation-induced expression of COX-2 and iNOS in hairless mouse skin: p38 MAP kinase and JNK as potential targets. *Arch Biochem Biophys*, **559**, pp. 38-45.

CHOI, S.H., KIM, Y.H., QUINTI, L., TANZI, R.E., KIM, D.Y. (2016). 3D culture models of Alzheimer's disease: a road map to a cure-in-a-dish. *Molecular Neurodegeneration*, **11**(75), 1-11.

CHOI, Y.H., G.-Y., KIM AND H. H., LEE, (2014). "Anti-inflammatory effects of cordycepin in lipopolysaccharide-stimulated RAW 264.7 macrophages through Toll-like receptor 4-mediated suppression of mitogen-activated protein kinases and NF-κB signalling pathways," *Drug Design, Development and Therapy,* 8, pp. 1941–1953.

CHUA, L.S., (2013). A review on plant-based rutin extraction methods and its Pharmacological activities. *Journal of Ethnopharmacology*, **150**(3), pp. 805-817.

CHUANG, J.Y., (2014). Regulatory effects of fisetin on microglial activation, Molecules **19**(7), pp. 8820e8839.

CHUANG, L., CHEN, N., LIN, S.-W., CHANG, Y., LIAO, H., LIN, Y.-S (2014). Increased C-C chemokine receptor 2 gene expression in monocytes of severe obstructive sleep apnea patients and under intermittent hypoxia. *PLOS ONE*, 9, e113304.

CIRRITO, J.R., DEANE, R., FAGAN, A.M., SPINNER, M.L., PARSADANIAN, M., FINN, M.B., JIANG, H., PRIOR, J.L., SAGARE, A., BALES, K.R., PAUL, S.M., ZLOKOVIC, B.V., PIWNICA-WORMS, D. and HOLTZMAN, D.M., (2005). P-glycoprotein deficiency at the blood-brain barrier increases amyloid-beta deposition in an Alzheimer disease mouse model. *The Journal of clinical investigation,* **115**(11), pp. 3285-3290.

COHEN S.I.A., S., LINSE, L. M., LUHESHI , E., HELLSTRAND , D. A., WHITE , L., RAJAH , D. E., OTZEN , M., VENDRUSCOLO , C. M., DOBSON AND T. P. J., KNOWLES, (2013). Proc Natl Acad Sci USA, 110, pp. 9758 —9763

COLE, G.M., TETER, B. and FRAUTSCHY, S.A., (2007). Neuroprotective effects of curcumin. The Molecular Targets and Therapeutic Uses of Curcumin in Health and Disease. Boston, MA: Springer US, pp. 197-212.

COLGIN, L.L., MOSER, E.I., (2010). Gamma oscillations in the hippocampus. Physiology 25, pp. 319–29.

CONDELLO, C., STOEHR, J., (2018). Aβ propagation and strains: Implications for the phenotypic diversity in Alzheimer's disease. Neurobiol Dis. 109(Pt B), pp. 191–200.

CORIC, V., VAN DYCK, C.H., SALLOWAY, S., ANDREASEN, N., BRODY, M., RICHTER, R.W., SOININEN, H., THEIN, S., SHIOVITZ, T., PILCHER, G., COLBY, S., ROLLIN, L.,

DOCKENS, R., PACHAI, C., PORTELIUS, E., ANDREASSON, U., BLENNOW, K., SOARES, H., ALBRIGHT, C., FELDMAN, H.H. and BERMAN, R.M., (2012). Safety and Tolerability of the γ-Secretase Inhibitor Avagacestat in a Phase 2 Study of Mild to Moderate Alzheimer Disease. *Archives of Neurology*, **69**(11), pp. 1430-1440.

CORONEL, R., BERNABEU-ZORNOZA, A., PALMER, C., MUNIZ-MORENO, M., ZAMBRANO, A., CANO, E., (2018). Role of amyloid precursor protein. (APP) and its derivatives in the biology and cell fate specification of neural stem cells. *Mol Neurobiol*, 55, pp. 7107–17.

CORRADIN, S., MAUEL, J., DONINI, S., (1993). Inducible nitric acid oxide synthase activity of cloned murine microglial cells. *Glia*, 7, pp. 255-262

COS P, YING L, CALOMME M (1998) Structure-activity relationship and classification of flavonoids as inhibitors of xanthine oxidase and superoxide scavengers. *Journal of Natural Products*, **61**(1), pp. 71–76.

COSTES, S.V., DAELEMANS, D., & CHO, E.H. (2004). Automatic and quantitative measurement of protein-protein colocalization in live cells. *Biophysical Journal*, **86**(6), 3993–4003.

COTMAN, C.W., POON, W.W., RISSMAN, R.A., BLURTON-JONES, M., (2005). The role of caspase cleavage of tau in Alzheimer disease neuropathology. *J Neuropathol Exp Neurol*. **64**, pp. 104–12.

COTTRELL, D.A., BORTHWICK, G.M., JOHNSON, M.A., INCE, P.G. and TURNBULL, D.M., (2002). The role of cytochrome c oxidase deficient hippocampal neurons in Alzheimer's disease. *Neuropathology and Applied Neurobiology*, **28**(5), pp. 390-396.

CRIPPS, D., THOMAS, S.N., JENG, Y., YANG, F., DAVIES, P., YANG, A.J., (2006). Alzheimer disease-specific conformation of hyperphosphorylated paired helical filament-Tau is polyubiquitinated through Lys-48, Lys-11, and Lys-6 ubiquitin conjugation. *J Biol Chem*. **281**, pp. 10825–10838.

CROES, M., ONER, F.C., KRUYT, M.C., BLOKHUIS, T.J., BASTIAN, O., DHERT, W (2015). Proinflammatory Mediators Enhance the Osteogenesis of Human Mesenchymal Stem Cells after Lineage Commitment. *PLoS ONE*, 10, e0132781.

CROWTHER, D.C., KINGHORN, K.J., MIRANDA, E., PAGE, R., CURRY, J.A., DUTHIE, F.A.I (2005). Intraneuronal Aβ, non-amyloid aggregates and neurodegeneration in a Drosophila model of Alzheimer's disease. *Neuroscience*, **132**(1), 123-135.

CRUZ-VICENTE, P., SILVESTRE, S., GALLARDO, E. (2021). Alzheimer and Parkinson diseases: in-silico approaches. *Molecules*, **26**(2193), 1–28.

CUMMINGS, B.J., SU, J.H., COTMAN, C.W., WHITE, R., RUSSELL, M.J. (1993). β-Amyloid accumulation in aged canine brain: a model of early plaque formation in Alzheimer's disease. *Neurobiology of Aging,* **14**(6), 547-560.

CUMMINGS, J., AISEN, P. S., DUBOIS, B., FRÖLICH, L., JACK JR, C. R., JONES, R. W. AND SCHELTENS, P. (2020). Drug development in Alzheimer's disease: the path to 2025. *Alzheimer's research & therapy,* **12**(1), 1-16.

CUMMINGS, J.L., MORSTORF, T., ZHONG, K., (2014). Alzheimer's disease drug-development pipeline: few candidates, frequent failures. *Alzheimers Res Ther*. 6, pp. 37

CUMMINGS, M.C., WINTERFORD, C.M., WALKER, N.I., (1997). Apoptosis. *Am J Surg Pathol,* **21**(1), pp. 88–101.

CUSHNIE, T.T., LAMB, A.J., (2011). Recent advances in understanding the antibacterial properties of flavonoids. *International Journal of Antimicrobial Agents* 38, pp. 99e107.

D.A., SCHLESINGER, I., MEAD, G., (2017). Post-stroke dementia - a comprehensive review. BMC Med. 15, pp. 11.

DA CRUZ, R.C., AGERTT, V., BOLIGON, A.A., JANOVIK, V., ANRAKU, DE CAMPOS, M.M., GUILLAUME, D., ATHAYDE, M.L., (2012). In vitro antimycobacterial activity and HPLC-DAD screening of phenolics from Ficus benjamina and Ficus luschnathiana. **26**(23), pp. 2251–2254.

DAL PRÀ, I., CHIARINI, A., GUI, L., CHAKRAVARTHY, B., PACCHIANA, R., GARDENAL, E., WHITFIELD, J.F. and ARMATO, U., (2015). Do Astrocytes Collaborate with Neurons in Spreading the "Infectious" Aβ and Tau Drivers of Alzheimer's Disease? *The Neuroscientist,* **21**(1), pp. 9-29.

DE BOER, V., DIHAL, C.J., VAN DER WOUDE, A.A., ARTS, I.C., WOLFFRAM, S., ALINK, G.M., RIETJENS, I., KEIJER, J. and HOLLMAN, P.H., (2005). Tissue distribution of quercetin in rats and pigs. *Journal of nutrition*, **135**(7), pp. 1718-1725.

DE LA TORRE, A., JUNYENT, F., FOLCH, J., PELEGRÍ, C., VILAPLANA, J., AULADELL, C., BEAS-ZARATE, C., PALLÀS, M., VERDAGUER, E. and CAMINS, A., (2012). GSK3β Inhibition is involved in the Neuroprotective Effects of Cyclin-dependent kinase Inhibitors in Neurons. *Pharmacological Research,* **65**(1), pp. 66-73.

DE MEDEIROS, L.M., DE BASTIANI, M.A., RICO, E.P., SCHONHOFEN, P., PFAFFENSELLER, B., WOLLENHAUPT-AGUIAR, B (2019). Cholinergic differentiation of human neuroblastoma SH-SY5Y cell line and its potential use as an in vitro model for Alzheimer's disease studies. *Molecular Neurobiology*, **56**(11), 7355-7367.

DE STROOPER, B., VASSAR, R. and GOLDE, T., (2010). The secretases: enzymes with therapeutic potential in Alzheimer disease. *Nature Reviews Neurology*, **6**(2), pp. 99-107.

DESHPANDE, A., MINA, E., GLABE, C. and BUSCIGLIO, J., (2006). Different Conformations of Amyloid beta Induce Neurotoxicity by Distinct Mechanisms in Human Cortical Neurons. *Journal of Neuroscience*, **26**(22), pp. 6011-6018.

DEVOS, D., CABANTCHIK, Z.I., MOREAU, C., DANEL, V., MAHONEY-SANCHEZ, L., BOUCHAOUI, H., GOUEL, F., ROLLAND, A.S., DUCE, J.A., DEVEDJIAN, J.C.; FAIRPARK-II AND FAIRALSII STUDYGROUPS, (2020). Conservative iron chelation for neurodegenerative diseases such as Parkinson's disease and amyotrophic lateral sclerosis. *Journal of Neural Transmission* (Vienna) **127**, pp. 189-203.

DI CARLO, M., GIACOMAZZA, D., SAN BIAGIO, P.L., (2012). Alzheimer's disease: biological aspects, therapeutic perspectives and diagnostic tools. *J Phys Condens Matter*, 24, pp. 244102

DI SCALA, C., CHAHINIAN, H., YAHI, N., GARMY, N., FANTINI, J (2014). Interaction of Alzheimer's β-amyloid peptides with cholesterol: mechanistic insights into amyloid pore formation. *Biochemistry, pp* 4489–4502.

DIANO, S., FARR, S.A., BENOIT, S.C., MCNAY, E.C., DA SILVA, I., HORVATH, B., (2006). Ghrelin controls hippocampal spine synapse density and memory performance. *Nat Neurosci.* 9, pp. 381–8.

DICKEY, C.A., KAMAL, A., LUNDGREN, K., KLOSAK, N., BAILEY, R.M., DUNMORE, J., (2007). The high-affinity HSP90-CHIP complex recognizes and selectively degrades phosphorylated tau client proteins. *J Clin Invest.* 117, pp. 648–58.

DICKEY, C.A., KOREN, J., ZHANG,Y.J., XU, Y.F., JINWAL, U.K., BIRNBAUM, M.J., (2008). Akt and CHIP coregulate tau degradation through coordinated interactions. Proc Natl Acad Sci USA. **105**, pp. 3622–3627.

DIMITROV, M., ALATTIA, J., LEMMIN, T., LEHAL, R., FLIGIER, A., HOUACINE, J., HUSSAIN, I., RADTKE, F., DAL PERARO, M., BEHER, D. and FRAERING, P.C., (2013). Alzheimer's disease mutations in APP but not γ-secretase modulators affect epsilon-cleavage-dependent AICD production. *Nature communications*, 4, pp. 2246.

DIXIT, R., ROSS, J.L., GOLDMAN, Y.E., HOLZBAUR, E.L., (2008). Differential regulation of dynein and kinesin motor proteins by tau. *Science* **319**, pp. 1086–9.

DIXON, C.E., KOCHANEK, P.M., YAN, H.Q., SCHIDING, J.K., GRIFFITH, R.G., BAUM, E (1999). One-year study of spatial memory performance, brain morphology, and cholinergic markers after moderate controlled cortical impact in rats. *Journal of Neurotrauma,* **16**(2), 109-122.

DMITRIEV, R. I., PAPKOVSKY, D. B. (2015). Multi-parametric O2 imaging in three-dimensional neural cell models with the phosphorescent probes. *Methods Mol Biol*, **1254**, 55–71.

DOERFLER, P., SHEARMAN, M.S., PERLMUTTER, R.M., (2001). Presenilin-dependent gamma-secretase activity modulates thymocyte development. *Proc Natl Acad Sci USA*. **98**, pp. 9312–7

DOI, D., SAMATA, B., KATSUKAWA, M., KIKUCHI, T., MORIZANE, A., ONO, Y., (2014). Isolation of human induced pluripotent stem cell-derived dopaminergic progenitors by cell sorting for successful transplantation. *Stem Cell Reports*, **2**, 337–350.

DOMINY, S.S., LYNCH, C., ERMINI, F., BENEDYK, M., MARCZYK, A., KONRADI, A., (2019). Porphyromonas gingivalis in Alzheimer's disease brains: evidence for disease causation and treatment with small-molecule inhibitors. *Sci Adv*. 5, pp. eaau3333.

DONG, J., JIMI, E., ZEISS, C., HAYDEN, M.S., GHOSH, S., (2010). Constitutively active NFκB triggers systemic TNFα-dependent inflammation and localized TNFα-independent inflammatory disease. *Genes & Development*, **24**(16), pp. 1709–1717.

DOODY, R.S., RAMAN, R., FARLOW, M., IWATSUBO, T., VELLAS, B., JOFFE, S., (2013). A phase 3 trial of semagacestat for treatment of Alzheimer's disease. *N Engl J Med*. 369, pp. 341–50.

DOS SANTOS, A.E., KUSTER, R.M., YAMAMOTO, K.A., SALLES, T.S., CAMPOS, R., DE MENESES, M.D., SOARES, M.R., FERREIRA, D., (2014). Quercetin and quercetin 3-O-glycosides from Bauhinia longifolia (Bong.) Steud show anti-Mayaro virus activity. *Parasit Vectors*, 7, pp. 130.

DRINGEN, R., HIRRLINGER, J., (2003) Glutathione pathways in the brain. *Biological Chemistry,* **384**(4), pp. 505–516.

DU, J.S., ZHAO, Q., ZHANG, Y.L., WANG, Y,, MA, M., (2013). 7,8-dihydroxycoumarin may promote sciatic nerve regeneration by suppressing NF-kappaB expression in mice. *Mol Med Rep.* 8, pp. 1525-1530

DUBEY, S., GANESHPURKAR, A., SHRIVASTAVA, A., BANSAL, D., DUBEY, N., (2013). Rutin exerts antiulcer effect by inhibiting the gastric proton pump. Indian *J. Pharmacol*, **45** (4), pp. 415–417.

DUCE, J.A., TSATSANIS, A., CATER, MA, JAMES, S.A., ROBB, E., WIKHE, K., (2010). Iron-export ferroxidase activity of beta-amyloid precursor protein is inhibited by Zinc in Alzheimer's disease. Cell, **142**, pp. 857–67.

DUNLOP, E.A., TEE, A.R., (2014). mTOR and autophagy: A dynamic relationship governed by nutrients and energy. *Seminars in Cell & Developmental Bioliology*, 36, pp. 121–129.

DUNNETT, S.B., EVENDEN, J.L., IVERSEN, S.D. (1988). Delay-dependent short-term memory deficits in aged rats. *Psychopharmacology*, **96**(2), 174-180.

D'URSI, A.M., (2004). Solution structure of amyloid beta-peptide (25-35) in different media. *J Med Chem*. **47**(17), pp. 4231–4238.

DUVAL, K., GROVER, H., HAN, L., MOU, Y., PEGORARO, A. F., FREDBERG, J (2017). Modeling physiological events in 2D vs. 3D cell culture. *Physiology*, **32**, 266–277.

EDIN, N.J., OLSEN, D.R., SANDVIK, J.A., MALINEN, E., & PETTERSEN, E.O. (2012). Low dose hyper-radiosensitivity is eliminated during exposure to cycling hypoxia but returns after reoxygenation. *International Journal of Radiation Biology*, **88**, 311–319.

EGAN, M. F., KOST, J., TARIOT, P. N., AISEN, P. S., CUMMINGS, J. L., VELLAS, B., (2018). Randomized trial of verubecestat for mild-to-moderate Alzheimer's disease. *North England J Medical*, **378**, pp. 1691–1703.

EGAN, M.F., KOST, J., VOSS, T., MUKAI, Y., AISEN, P.S., CUMMINGS, J.L., (2019). Randomized trial of verubecestat for prodromal Alzheimer's disease. *N Engl J Med*. **380**, pp. 1408–20.

EHRENREICH, H., (2004). Erythropoietin: novel approaches to neuroprotection in human brain disease. *Metabolic Brain Discovery*. **19**(3-4), pp. 195–206.

ELLIOTT, E., TSVETKOV, P., GINZBURG, I., (2007). BAG-1 associates with Hsc70.Tau complex and regulates the proteasomal degradation of Tau protein. *J Biol Chem*. 282, pp. 37276–37284.

EMILIJA, V., WENHAO, X., BLAINE, P., EE TSIN, W., JENNY, H., ALBERTO OVIEDO, C., JULIA, H., MANUAL, P., (2018). Nicotine and other tobacco compounds in neurodegenerative and psychiatric diseases. *Overview of Epidemiological Data on Smoking and Preclinical and*

ENNACEUR, A., DELACOUR, J. (1988). A new one-trial test for neurobiological studies of memory in rats. *Behavioral and Brain Research*, **31**(1), 47-59.

ENOGIERU, A.B., HAYLETT, W., HISS, D.C., BARDIEN, S., EKPO, O.E. (2018). Rutin as a potent antioxidant: implications for neurodegenerative disorders. *Oxidative Medicine and Cellular Longevity.*

ENOGIERU, A.B., HAYLETT, W., HISS, D.C., BARDIEN, S., EKPO, O.E., (2018). Rutin as a potent antioxidant: implications for neurodegenerative disorders. *Oxidative Med. Cell Longev.*

ERASMUS, R., SAVORY, J., WILLS, M., HERMAN, M. (1993). Aluminum neurotoxicity in experimental animals. *Therapeutic Drug Monitoring*, **15**(6), 588-592.

ESKICI, G., AXELSEN, P.H., (2012). Copper and oxidative stress in the pathogenesis of Alzheimer's disease. *Biochemistry* 51, pp. 6289–6311.

ESLAMI, M., SADEGHI, B., GOSHADROU, F., (2018). Chronic ghrelin administration restores hippocampal long-term potentiation and ameliorates memory impairment in rat model of Alzheimer's disease. *Hippocampu*s. 28, pp. 724–34.

ESQUERDA-CANALS, G., RODA, A.R., MARTÍ-CLÚA, J., MONTOLIU-GAYA, L., RIVERA-HERNANDEZ, G., VILLEGAS, S (2019). Treatment with scFv-h3D6 prevented

neuronal loss and improved spatial memory in young 3xTg-AD mice by reducing the intracellular amyloid-β burden. *Journal of*

ESTRADA, L.D., SOTO, C., (2007). Disrupting beta-amyloid aggregation for Alzheimer disease treatment. *Current Top Medical Chemistry*, 7, pp. 115–126.

EVES, E.M., TUCKER, M.S., ROBACKO, J.D., DOWNEN, M., RICH, M., WAINER, B.H., (1992). *Immortal rat hippocampal cell lines. Neurobiology*, 89, pp. 4373–7.

EYO,U.B., M.E., DAILEY, (2013). Microglia: key elements in neural development, plasticity and pathology. *Journal of Neuroimmune Pharmacology* **8** (3), pp. 494e509.

FANSELOW, M. (1980). Conditioned and unconditional components of post-shock freezing. *Pavlovian Journal of Biological Science*, **15**(4), 177-182.

FARIA, A., MEIRELES, M., PESTANA, D., MONTEIRO, R., SANTOS-BUELGA, C., GONZALEZ-MANZANO, S., DUENAS, M., DE FREITAS, V., MATEUS, N., CALHAU, C. (2011). Flavonoid metabolites transport across BBB. *5th International Conference on Polyphenols, Sitges, Barcelona*.

FARIA, A., PESTANA, D., TEIXEIRA, D., AZEVEDO, J., DE FREITAS, V., MATEUS, N., CALHAU, C. (2010). Flavonoid transport across RBE4 cells: A blood-brain barrier model. Cell and *Molecular Biology Letters*, **15**(2), 234-241.

FARIA, A., PESTANA, D., TEIXEIRA, D., COURAUD, P.O., ROMERO, I., WEKSLER, B., DE FREITAS, V., MATEUS, N., CALHAU, C. (2011). Insights into the putative catechin and epicatechin transport across blood-brain barrier. *Food Function*, **2**(1), 39-44.

FERREIRA, S.T., KLEIN, W.L., (2011). The Aβ oligomer hypothesis for synapse failure and memory loss in Alzheimer's disease. Neurobiol Learn Mem. 96, pp. 529–43

FINDEIS, M.A., (2007). The role of amyloid beta peptide 42 in Alzheimer's disease. *Pharmacological Therapeutics*, **116**(2), pp. 266–86.

FLOOD, J.F., CHERKIN, A. (1986). Scopolamine effects on memory retention in mice: a model of dementia? *Behavioral and Neural Biology*, **45**(2), 169-184.

FORMAN, M., TSENG, J., PALCZA, J., LEEMPOELS, J., RAMAEL, S., KRISHNA, G., (2012). The novel BACE inhibitor MK-8931 dramatically lowers CSF Abeta peptides in healthy subjects: results from a rising single dose study. *Neurology* 78, pp. PL02.004-PL02.004.

FRANCIS, P.T., PALMER, A.M., SNAPE, M. and WILCOCK, G.K., (1999). The cholinergic hypothesis of Alzheimer's disease: a review of progress. *Journal of neurology, neurosurgery, and psychiatry*, **66**(2), pp. 137-147.

FROST, B., JACKS, R.L., DIAMOND, M.I., (2019). Propagation of tau misfolding from the outside to the inside of a cell. *J Biol Chem*. **284**, pp. 12845–52.

FU A. K. Y., HUNG K.-W., YUEN M. Y. F., ZHOU X., MAK D. S. Y., CHAN I. C. W., CHEUNG T. H., ZHANG B., FU W.-Y., LIEW F. Y., IP N. Y., (2016). IL-33 ameliorates Alzheimer's disease-like pathology and cognitive decline. *Proc. Natl. Acad. Sci. U.S.A.* **113**, E2705–E2713.

FUNAMOTO, K., ZERVANTONAKIS, I., LIU, Y., OCHS, C.J., KIM, C., & KAMM, R.D. (2012). A novel microfluidic platform for high-resolution imaging of a three-dimensional cell culture under a controlled hypoxic environment. *Lab on a Chip*, **12**, 4855–4863.

GABRIELLE, S., (2008). Keystone Drug News: coMentis BACE Inhibitor Debuts. Available online at: http://www.alzforum.org/new/detail.asp?id=1790

GAGNER, J., LECHPAMMER, M., ZAGZAG, D. (2018). Induction and assessment of hypoxia in glioblastoma cells in vitro. Methods in Molecular Biology. New York, NY: Springer Science+BusinessMedia, pp. 111–123.

GALI, C.C., FANAEE-DANESH, E., ZANDL-LANG, M., ALBRECHER, N.M., TAM-AMERSDORFER, C., STRACKE, A (2019). Amyloid-beta impairs insulin signaling by accelerating autophagy-lysosomal degradation of LRP-1 and IR-β in blood-brain barrier endothelial cells in vitro and in 3XTg-AD mice. *Molecular and Cellular Neuroscience*, **99**(103390), 1-19.

GALLINI, A., SOMMET, A., MONTASTRU, J.L., (2008). Does memantine induce bradycardia? a study in the french pharmacovigilance tabase. Pharmacoepidemiol. *Drug Saf*. 17, pp. 877–81.

GALLUZZI, L., VITALE, I., ABRAMS, J.M., ALNEMRI, E.S., BAEHRECKE, E.H., BLAGOSKLONNY, M.V., (2012) Molecular definitions of cell death subroutines: recommendations of the Nomenclature Committee on Cell Death. *Cell Death Differ* **19**(1), pp. 107–20.

GAMES, D., ADAMS, D., ALESSANDRINI, R., BARBOUR, R., BORTHELETTE, P., BLACKWELL, C., (1995). Alzheimer-type neuropathology in transgenic mice overexpressing V717F β-amyloid precursor protein. *Nature*, **373**, 523-527.

GAMMELLA, E., LEUENBERGER, C., GASSMANN, M., OSTERGAARD, L. (2013). Evidence of synergistic/additive effects of sildenafil and erythropoietin in enhancing survival and migration of hypoxic endothelial cells. *Am J Physiol Cell Mol Physiol*, **304**, L230–L239

GANDHI, S., ABRAMOV A.Y., (2012). Mechanism of oxidative stress in neurodegeneration. *Oxidative Medicine and Cellular Longevity*, 2012, pp. 11.

GANESAN, S., FARIS, A.N., COMSTOCK, A.T., WANG, Q., NANUA, S., HERSHENSON, M.B., SAJJAN, U.S., (2012). Quercetin inhibits rhinovirus replication in vitro and in vivo. *Antiviral Res*. **94**(3), pp. 258–271.

GAO, Y., LI, C., YIN, J., SHEN, J., & WANG, H. (2013). The blood-brain barrier permeability of rutin in an in situ rat brain perfusion model. *Journal of Pharmacy & Pharmaceutical Sciences*, **16**(2), 274–285.

GAUTHIER, S., FELDMAN, H.H., SCHNEIDER, L.S., WILCOCK, G.K., FRISONI, G.B., HARDLUND, J.H., (2016). Efficacy and safety of tau-aggregation inhibitor therapy in patients with mild or moderate Alzheimer's disease: a randomised, controlled, double-blind, parallel-arm, phase 3 trial. *Lancet*. **388**, pp. 2873–84.

GEETHA, R., SATHIYA, PRIYA, C., ANURADHA, C.V., (2017). Troxerutin abrogates mitochondrial oxidative stress and myocardial apoptosis in mice fed calorie-rich diet. *Chemico-Biological Interactions,* **278**, pp. 74–83.

GEGOTEK, A., BIERNACKI, M., AMBROZEWICZ, E., SURAZYŃSKI, A., WROŃSKI, A., SKRZYDLEWSKA, E., (2016). The cross-talk between electrophiles, antioxidant defence and the endocannabinoid system in fibroblasts and keratinocytes after UVA and UVB irradiation. *Journal of Dermatological Science*, **81**(2), pp. 107–117.

GEISERT, E., FRANKFURTER, A., (1989). The neuronal response to injury as visualized by immunostaining of class III beta-tubulin in the rat. Neurosci Lett, 102, pp 137-41.

GEISSMANN, F., (2008). Blood monocytes: distinct subsets, how they relate to dendritic cells, and their possible roles in the regulation of T-cell responses, *Immunol. Cell Biol*. **86** (5), pp. 398e408.

GELING, A., STEINER, H., WILLEM, M., BALLY-CUIF, L., HAASS, C., (2002). A gamma-secretase inhibitor blocks Notch signaling in vivo and causes a severe neurogenic phenotype in zebrafish. *EMBO Rep*. 3, pp. 688–94.

GHIASI, M., AZADNIA, A., ARABIEH, M., ZAHEDI, M., (2012). Protective effect of rutin (vitamin p) against heme oxidation: a quantum mechanical approach. *Computational and Theoretical Chemistry*, 996, pp. 28–36.

GHOSHAL, N., SMILEY, J.F., DEMAGGIO, A.J., HOEKSTRA, M.F., COCHRAN, E.J., BINDER, L.I., (1999). A new molecular link between the fibrillar and granulovacuolar lesions of Alzheimer's disease. *American Journal of Pathol*ogy, 155, pp. 1163–1172

GILLESPIE, A.K., JONES, E.A., LIN, Y.H., KARLSSON, M.P., KAY, K., YOON, S.Y., (2016). Apolipoprotein E4 causes age-dependent disruption of slow gamma oscillations during hippocampal sharp-wave ripples. *Neuron* **90**, pp. 740–51.

GIORGI, C, ROMAGNOLI, A, PINTON, P, RIZZUTO, R., (2008). Ca2+ signalling, mitochondria and cell death. *Current Molecular Medicine*. **8**(2), pp. 119–30.

GIOVANNINI, M.G., SCALI, C., PROSPERI, C., BELLUCCI, A., VANNUCCHI, M.G., ROSI, S., PEPEU, G. AND CASAMENTI, F., (2002). Beta-amyloid-induced inflammation and cholinergic hypofunction in the rat brain in vivo: involvement of the p38MAPK pathway. *Neurobiology Discovery*. **11**, pp. 257-274.

GIRI, M., ZHANG, M., LU, Y., (2016). Genes associated with Alzheimer's disease: an overview and current status. Clin Interv Aging. **11**, pp. 665–81.

GIULIAN, D. & BAKER, T., (1986). Characterization of ameboid microglia isolated from developing mammalian brain. *Journal of Neuroscience*, 6, pp. 2163-2178.

GIULIANI, A.L., SARTI, A.C., FALZONI, S., DI VIRGILIO, D., (2017). The P2X7 receptor-interleukin-1 liaison. *Frontiers in Pharmacology*, 8, pp. 123.

GIUNTA, S., (2004). Transferrin neutralization of amyloid beta 25-35 cytotoxicity. *Clin Chim Acta.* **350**(1-2), pp. 129–136.

GLENNER, G.G., WONG, C.W., (1984). Alzheimer's disease: initial report of the purification and characterization of a novel cerebrovascular amyloid protein. *Biochem Biophys Res Commun*. **120**, pp. 885–90.

GOEDERT, M., JAKES, R., SPILLANTINI, M.G., HASEGAWA, M., SMITH, M.J., CROWTHER, R.A., (1996). Assembly of microtubule-associated protein tau into Alzheimer-like filaments induced by sulphated glycosaminoglycans. *Nature*. **383**, pp. 550–553.

GOLDBAUM, O., RICHTER-LANDSBERG, C., (2004). Proteolytic stress causes heat shock protein induction, tau ubiquitination, and the recruitment of ubiquitin to tau-positive aggregates in oligodendrocytes in culture. J Neurosci. **24**, pp. 5748–5757.

GOLDGABER, D., LERMAN, M.I., MCBRIDE, O.W., SAFFIOTTI, U., GAJDUSEK, D.C., (1987). Characterization and chromosomal localization of a cDNA encoding brain amyloid of Alzheimer's disease. *Science* **235**, pp. 877–880

GÓMEZ-SINTES, R., LEDESMA, M.D., BOYA, P., (2016). Lysosomal cell death mechanisms in aging. *Ageing Research Reviews*, **32**, pp. 150–168.

GONG, C.X., SHAIKH, S., WANG, J.Z., ZAIDI, T., GRUNDKE-IQBAL, I., IQBAL, K., (1995). Phosphatase activity toward abnormally phosphorylated tau: decrease in Alzheimer disease brain. *Journal of Neurochemistry*, **65**, pp. 732–738.

GONG, C.X., SINGH, T.J., GRUNDKE-IQBAL, I., IQBAL, K., (1993). Phosphoprotein phosphatase activities in Alzheimer disease brain. *Journal of Neurochemistry*. **61**, pp. 921–927.

GONG, Y., MEYER, E.M., MEYERS, C.A., KLEIN, R.L., KING, M.A., HUGHES, J.A. (2006). Memory-related deficits following selective hippocampal expression of Swedish mutation amyloid precursor protein in the rat. *Experimental Neurology,* **200**(2), 371-377.

GONZALEZ-MANZANO,S., GONZALEZ-PARAMAS, A., SANTOS-BUELGA, C., DUENAS, M. (2009). Preparation and characterization of catechin sulfates, glucuronides, and methylethers with metabolic interest. *Journal of Agricultural and Food Chemistry*, **57**(4), 1231-1238.

GORLACH, S., FICHNA, J., LEWANDOWSKA, U., (2015). Polyphenols as mitochondria-targeted anticancer drugs. *Cancer Lett*. **366**(2), pp.141–149.

GOUTAGNY, R., GU, N., CAVANAGH, C., JACKSON, J., CHABOT, J.G., QUIRION, R., (2013). Alterations in hippocampal network oscillations and theta-gamma coupling arise before Aβ overproduction in a mouse model of Alzheimer's disease. *European Journal of Neuroscience*. **37**, pp. 1896–902.

GRAEFE, E., WITTIG, J., MUELLER, S., RIETHLING, A., UEHLEKE, B., DREWELOW, B., PFORTE, H., JACOBASCH, G., DERENDORF, H. and VEIT, M., (2001). Pharmacokinetics and Bioavailability of Quercetin Glycosides in Humans. *The Journal of Clinical Pharmacology,* **41**(5), pp. 492-499.

GRAHAM, W.V., BONITO-OLIVA, A., SAKMAR, T.P., (2017). Update on Alzheimer's disease therapy and prevention strategies. *Annu Rev Med*. **68**, pp. 413–30.

GRAY, E.G., PAULA-BARBOSA, M., ROHER, A., (1987). Alzheimer's disease: paired helical filaments and cytomembranes. *Neuropathol Appl Neurobiol*. **13**, pp. 91–110.

GRUNDKE-IQBAL, I., IQBAL, K., TUNG, Y.C., QUINLAN, M., WISNIEWSKI, H.M., BINDER, L.I., (1986). Abnormal phosphorylation of the microtubule-associated protein tau. (tau) in Alzheimer cytoskeletal pathology. *Proc Natl Acad Sci USA*. **83**:4913–7.

GRUNDKE-IQBAL, I., VORBRODT, A.W., IQBAL, K., TUNG, Y.C., WANG, G.P., WISNIEWSKI, H.M., (1988). Microtubule-associated polypeptides tau are altered in Alzheimer paired helical filaments. *Brain Research*. **464**, pp. 43–52

GRUTTER, M.G., (2000). Caspases: key players in programmed cell death. *Curr Opin Struct Biol*. **10**(6), pp. 649–655.

GUARDIA, T., (2001). Anti-inflammatory properties of plant flavonoids. Effects of rutin, quercetin and hesperidin on adjuvant arthritis in rat, *Farmaco* **56**(9), pp. 683e687.

GUERREIRO, R. J., AND BRAS, J. (2015). The age factor in Alzheimer's disease. *Genome medicine,* 7(1), 106.

GUILLEMIN, G. & BREW, B., (2004). Microglia, macrophages, perivascular macrophages, and pericytes: a review of function and identification. *Journal of Leukoc Biol*, **75**, pp. 388-397.

GUILLEMIN, G. & BREW, B., 2004. Microglia, macrophages, perivascular macrophages, and pericytes: a review of function and identification. *J. Leukoc Biol,* **75**, pp. 388-397.

GUNTERT, A., DOBELI, H., & BOHRMANN, B. (2006). High sensitivity analysis of amyloid-beta peptide composition in amyloid deposits from human and PS2APP mouse brain. *Neuroscience,* **143**(2), 461-475.

GUO, C., GAO, Y., YANG, H., CHEN, L., CHEN, Y., (2020). The protective effect of rutin on cerebral ischemia-reperfusion injury through regulation of the Nrf2 pathway. *Journal of Ethnopharmacology,* **249**, 112379.

GUO, C., L., YANG, J., LUO, (2016). "Sophoraflavanone G from Sophora alopecuroides inhibits lipopolysaccharide-induced inflammation in RAW264.7 cells by targeting PI3K/Akt, JAK/STAT and Nrf2/HO-1 pathways. *International Immunopharmacology*, **38**, pp. 349–356.

GUO, M., SONG, L.-P., JIANG, Y., LIU, W., YU, Y., & CHEN, G.-Q. (2006). Hypoxia-mimetic agents desferrioxamine and cobalt chloride induce leukemic cell apoptosis through different hypoxia-inducible factor-1_ independent mechanisms. *Apoptosis,* **11**, 67–77.

GUO, T., NOBLE, W., HANGER, D.P., (2017). Roles of tau protein in health and disease. *Acta Neuropathol.* 133, pp. 665–704.

GUO, Z., RUDOW, G., PLETNIKOVA, O., CODISPOTI, K.E., ORR, B.A., (2012). Striatal neuronal loss correlates with clinical motor impairment in Huntington's disease. *Movement Disorders*, **27**, 1379-1386.

GUTZMANN, H. and HADLER, D., (1998). Sustained efficacy and safety of idebenone in the treatment of Alzheimer's disease: update on a 2-year double-blind multicentre study. Journal of neural transmission Supplementum. **54**, pp. 301-310.

HA, K.Y., CARRAGEE, E., CHENG, I., KWON, S.E., KIM, Y.H., (2011) .Pregabalin as a neuroprotector after spinal cord injury in rats: biochemical analysis and effect on glial cells. J Korean Med Sci **26**, pp. 404-411.

HAASS, C., LEMERE, C.A., CAPELL, A., CITRON, M., SEUBERT, P., SCHENK, D., (1995). The Swedish mutation causes early-onset Alzheimer's disease by beta-secretase cleavage within the secretory pathway. *Nature Medicine*, **1**, pp. 1291–6

HABTEMARIAM, S., (2016). Rutin as a natural therapy for Alzheimer's disease: Insights into its mechanisms of action. *Current Medicinal Chemistry*. **23**, pp. 860-873.

HAKEM, R., HARRINGTON, L., (2005). Cell death. 4th ed. New York: *The McGraw-Hill Companies Inc*;

HALTERMAN, M.W., MILLER, C.C., FEDEROFF, H.J., (1999). *Journal of Neuroscience*. **19**, pp. 6818–6824.

HAMANO, T., GENDRON, T. F., CAUSEVIC, E., YEN, S. H., LIN, W. L., ISIDORO, C., DICKSON, D. W. (2008). Autophagic-lysosomal perturbation enhances tau aggregation in transfectants with induced wild-type tau expression. *European Journal of Neuroscience*, **27**(5), 1119-1130.

HAN, Y., (2009). Rutin has therapeutic effect on septic arthritis caused by Candida albicans. *International Immunopharmacology*, **9**(2), pp. 207–211.

HARAGUCHI, H., TANIMOTO, K., TAMURA, Y., MIZUTANI, K., KINOSHITA, T., (1998). Mode of antibacterial action of retrochalcones from Glycyrrhiza inflata. *Phytochemistry*, 48, pp. 125e129.

HARDY, J., ALLSOP, D., (1991). Amyloid deposition as the central event in the aetiology of Alzheimer's disease. *Trends Pharmacol Sci.* 12, pp. 383–8.

HARDY, J., SELKOE, D.J., (2002). The amyloid hypothesis of Alzheimer's disease: progress and problems on the road to therapeutics. *Science*, **297**, pp. 353–6.26.

HARDY, J.A. and HIGGINS, G.A., (1992). Alzheimer's disease: The Amyloid Cascade Hypothesis. *Science*, **256**(5054), pp. 184-185.

HARRINGTON. C., RICKARD. J.E., HORSLEY, D., HARRINGTON, K.A., HINDLEY, K.P., RIEDEL, G., (2008). Methylthioninium chloride (MTC) acts as a tau aggregation inhibitor (TAI) in a cellular model and reverses tau pathology in transgenic mouse model of Alzheimer's disease. *Alzheimer's & Dementia.* 4, pp. 120

HARRISON, F.E., MAY, J.M. and MCDONALD, M.P., (2010). Vitamin C deficiency increases basal exploratory activity but decreases scopolamine-induced activity in APP/PSEN1 transgenic mice. *Pharmacology, Biochemistry and Behaviour*, **94**(4), pp. 543-552.

HARRY, G.J (2013). Microglia during development and aging, *Pharmacological Therapeutics*. 139 (3), pp. 313e326.

HASEGAWA, M., CROWTHER, R.A., JAKES, R., GOEDERT, M., (1997). Alzheimer-like changes in microtubule-associated protein Tau induced by sulfated glycosaminoglycans. Inhibition of microtubule binding, stimulation of phosphorylation, and filament assembly depend on the degree of sulfation. *J Biol Chem.* 272, pp. 33118–33124.

HASSAN, A., SHARAREH S, ROYA, P.D., JEFF, M.F, MARYAM. R.1., and BRENT A.R (2014). Purifying Immature Neurons from Differentiating Neural Stem Cell. Progeny Using a Simple Shaking Method. *Journal of Stem Cell Research and Therapy*, 4:3

HASSAN, H. and CHEN, R, (2021). Hypoxia in Alzheimer's disease: effects of hypoxia inducible factors. *Neural Regeneration Research*, **16**(2); 310-311.

HASSAN, M., ABBAS, Q., SEO, S.Y., SHAHZADI, S., AL ASHWAL, H., ZAKI, N (2018). Computational modelling and biomarker studies of pharmacological treatment of Alzheimer's disease. *Molecular Medicine Reports*, **18**(1), 639–655. Review.

HAWKES, C.A., DENG, L.H., SHAW, J.E., NITZ, M., MCLAURIN, J., (2010). Small molecule beta-amyloid inhibitors that stabilize protofibrillar structures in vitro improve cognition and pathology in a mouse model of Alzheimer's disease. *European Journal of Neuroscience*. 31, pp. 203–13.

HAWKES, N., (2017). Merck ends trial of potential Alzheimer's drug verubecestat. BMJ. 356, pp. 845.

HAYDEN E.Y., and D. B., TEPLOW, (2013). Alzheimer's Res. Ther., 5, pp. 60

HEGDE, M.L., P., BHARATHI, A., SURAM, C., VENUGOPAL, R., JAGANNATHAN, P., PODDAR, P., SRINIVAS, K., SAMBAMURTI, K. J., RAO, J., SCANCAR, L., MESSORI, L. ZECCA AND P., ZATTA, (2009). J. Alzheimer's Dis., 17, pp. 457 —468

HEIN, A. & O'BANION, M., (2009). Neuroinflammation and memory: the role of prostaglandins. Mol Neurobiol, **40**, pp. 15-32.

HEMMING, M.L., ELIAS, J.E., GYGI, S.P., SELKOE, D.J., (2009). Identification of beta-secretase (BACE1) substrates using quantitative proteomics. PLoS ONE. 4, pp. 8477-47.

HENN, A., LUND S., HEDTJARN M., SCHRATTENHOLZ A., PORZGEN P AND LEIST M, 2009. The suitability of BV2 cells as alternative model system for primary microglia cultures or for animal experiments examining brain inflammation. *ALTEX,* **26**, pp. 83-94.

HEYMAN, A., FILLENBAUM, G.G., WELSH-BOHMER, K.A., GEARING, M., MIRRA, S.S., MOHS, R.C., PETERSON, B.L., PIEPER, C.F., (1998). *Neurology* **51**, pp. 159–162.

HICKMAN S. E., ALLISON E. K., EL KHOURY J., (2008). Microglial dysfunction and defective β-amyloid clearance pathways in aging Alzheimer's disease mice. *J. Neurosci.* **28**, 8354–836.

HIMMLER, A., DRECHSEL, D., KIRSCHNER, M.W., MARTIN, D.W., (1989). Jr Tau consists of a set of proteins with repeated C-terminal microtubule-binding domains and variable N-terminal domains. Mol Cell Biol. **9**, pp. 1381–1388.

HOCHGRÄFE, K., SYDOW, A., MATENIA, D., CADINU, D., KÖNEN, S., PETROVA, O., PICKHARDT, M., GOLL, P., MORELLINI, F., MANDELKOW, E. and MANDELKOW, E., (2015). Preventive methylene blue treatment preserves cognition in mice expressing full-length pro-aggregation human Tau. Acta neuropathologica communications, **3**(1), pp. 25.

HOFF, P., GABER, T., STREHL, C., JAKSTADT, M., HOFF, H., SCHMIDT-BLEEK, K., LANG, A., RÖHNER, E., HUSCHER, D., MATZIOLIS, G (2017). A Pronounced Inflammatory Activity Characterizes the Early Fracture Healing Phase in Immunologically Restricted Patients. *International Journal of Molecular Sciences*, 18, 583.

HOLLMAN, P. C., DE VRIES, J. H., VAN LEEUWEN, S. D., MENGELERS, M. J., & KATAN, M. B. (1997). Absorption of dietary quercetin glycosides and quercetin in healthy ileostomy volunteers. *The American Journal of Clinical Nutrition*, **65**(5), 1444-1450.

HOLLMAN, P.C.H., VAN TRIJP, J.M.P., BUYSMAN, M.N.C.P., V.D. GAAG, M.S., MENGELERS, M.J.B., DE VRIES, J.H.M. and KATAN, M.B., (1997). Relative bioavailability of the antioxidant flavonoid quercetin from various foods in man. *FEBS Letters*, **418**(1-2), pp. 152-156.

HOLTMAAT, A., BONHOEFFER, T., & CHOW, D.K. (2009). Quantitative analysis of spine and synapse morphology and density in neurons. In Imaging in Neuroscience: A Laboratory Manual. *Cold Spring Harbor Laboratory Press*, pp. 387–402

HOLTTA, M., HANSSON, O., ANDREASSON, U., HERTZE, J., MINTHON, L., NAGGA, K., (2013). Evaluating amyloid-β oligomers in cerebrospinal fluid as a biomarker for Alzheimer's disease. PLoS ONE. 8, pp. e66381

HONG-LIANG, S., XIANG, Z., WEN-ZHO, W., RONG-HAN, L., KAI, Z., MING-YUAN, L., WEI-MING, G., BIN, N., (2017). Neuroprotective mechanisms of rutin for spinal cord injury through anti-oxidation and anti-inflammation and inhibition of p38 mitogen activated protein kinase pathway. Neural Regeneration Research, 13(1), pp. 128-134.

HOUCK, A.L., HERNÁNDEZ, F., ÁVILA, J. (2016). A simple model to study tau pathology. *Journal of Experimental Neuroscience,* **10**(1), 31-38.

HSIAO, K., CHAPMAN, P., NILSEN, S., EC, C., HARIGAYA, Y., YOUNKIN, S (1996). Correlative memory deficits, Abeta elevation, and amyloid plaques in transgenic mice. *Science*, **274**(5284), 99-102.

HSIEH, T.J., WANG, J.C., HU, C.Y., LI, C.T., KUO, C.M., HSIEH, S.L., (2008). Effects of rutin from Toona sinensis on the immune and physiological responses of white shrimp (Litopenaeus vannamei) under Vibrio alginolyticus challenge. Fish Shellfish Immunol, **25**(5), pp. 581–588.

HSU, T.M., NOBLE, E.E., REINER, D.J., LIU, C.M., SUAREZ, A.N., KONANUR, V.R., (2018). Hippocampus ghrelin receptor signaling promotes socially-mediated learned food preference. *Neuropharmacology*, **131**, pp. 487–96

HU, B., DAI, F., FAN, Z., MA, G., TANG, Q., ZHANG, X. (2015). Nanotheranostics: Congo red/rutin-MNPs with enhanced magnetic resonance imaging and H2O2-responsive therapy of Alzheimer's disease in APPswe/PS1dE9 transgenic mice. *Advanced Materials*, **27**, 5499-5505.

HUA, Y., WEINA, J., JINPING, L., YAN, Z., CHUN-HUA, W., (2016). Analysis of absorbed components in rat plasma after oral administration of Lianhua Qingwen capsules by UPLC-Q-TOFMS. Tianjin Journal of Traditional Chinese Medicine **33**, pp. 756-17.

HUANG, L.E., BUNN, H.F., (2003). *J Biol Chem,* **278**, pp. 19575–19578.

HUANG, L.E., WILLMORE, W.G., GU, J., GOLDBERG, M.A., BUNN, H.F., (1999) J Biol Chem. **274**, pp. 9038–9044.

HUANG, R., SHI, Z., CHEN, L., ZHANG, Y., LI, J., AN, Y., (2017). Rutin alleviates diabetic cardiomyopathy and improves cardiac function in diabetic ApoE knockout mice. European Journal of Pharmacology **814**, pp. 151–160.

HUDRY, E., DASHKOFF, J., ROE, A.D., TAKEDA, S., KOFFIE, R.M., HASHIMOTO, T., (2013). Gene transfer of human Apoe isoforms results in differential modulation of amyloid deposition and neurotoxicity in mouse brain. Sci Transl Med. **5**, pp. 212ra161

HUNG, P.Y., HO, B.C., LEE, S.Y., CHANG S.Y., KAO, C.L., LEE, S.S., LEE, C.N., (2015). Houttuynia cordata targets the beginning stage of herpes simplex virus infection. PLoS One, **10**(2), pp. e0115475.

HUNT, D.L., CASTILLO, P.E. (2012). Synaptic plasticity of NMDA receptors: mechanisms and functional implications. *Curr Opin Neurobiol*. **22**, pp. 496–508

HUREAU, C. and FALLER, P., (2009). Aβ-mediated ROS production by Cu ions: Structural insights, mechanisms and relevance to Alzheimer's disease. *Biochimie*, **91**(10), pp. 1212-1217. .

HUSS, R., & COUPLAND, S.E. (2020). Software-assisted decision support in digital histopathology. Journal of Pathology, https://doi.org/10.1002/path.5388.

IACCARINO, H.F., SINGER, A.C., MARTORELL, A.J., RUDENKO, A., GAO, F., GILLINGHAM, T.Z., (2016). Gamma frequency entrainment attenuates amyloid load and modifies microglia. *Nature*. **540**, pp. 230–5.

IDE, M., HARRIS, M., STEVENS, A., SUSSAMS, R., HOPKINS, V., CULLIFORD, D., (2016). Periodontitis and cognitive decline in Alzheimer's disease. *PLoS ONE*. 11, pp. e0151081.

IGNEY, F.H., KRAMMER, P.H., (2002). Death and anti-death: tumour resistance to apoptosis. *Nat Rev Cancer*, 2, pp. 277–88.

IKEGAMI, K., KIMURA, T., KATSURAGI, S., ONO, T., YAMAMOTO, H., MIYAMOTO, E., (1996). Immunohistochemical examination of phosphorylated tau in granulovacuolar degeneration granules. *Psychiatry Clin Neurosci*. **50**, pp. 137–140.

IKEN, T., FOUCHIER, R.A., SCHUTTEN, M., RIMMELZWAAN, G.F., VAN AMERONGEN, G., VAN RIEL, D., LAMAN, J.D., DE JONG, T., VAN DOORNUM, G., LIM, W., (2003). Newly discovered coronavirus as the primary cause of severe acute respiratory syndrome. *The Lancet,* 362, pp. 263–270.

IMAM, F., AL-HARBI, N.O., AL-HARBIA, M.M., KORASHY, H.M., ANSARI, M.A., SAYED-AHMED, M.M., (2017). Rutin attenuates carfilzomib-induced cardiotoxicity through inhibition of NF-κB, hypertrophic gene expression and oxidative stress. Cardiovascular. interventional study with aged tau transgenic mice. *The Journal of neuroscience: the official journal of the Society for Neuroscience,* **32**(11), pp. 3601-3611.

IMBIMBO, B., FRIGERIO, E., BREDA, M., FIORENTINI, F., FERNANDEZ, M., SIVILIA, S., GIARDINO, L., CALZÀ, L., NORRIS, D., CASULA, D. and SHENOUDA, M., (2013). Pharmacokinetics and Pharmacodynamics of CHF5074 after Short-term Administration in Healthy Subjects. Alzheimer Disease & Associated Disorders, **27**(3), pp. 278-286.

IQBAL, K., GRUNDKE-IQBAL, I., ZAIDI, T., MERZ, P.A., WEN, G.Y., SHAIKH, S.S., (1986). Defective brain microtubule assembly in Alzheimer's disease. *Lancet*. **2**, pp. 421–426

IQBAL, K., ZAIDI, T., BANCHER, C., GRUNDKE-IQBAL, I., (1994). Alzheimer paired helical filaments. Restoration of the biological activity by dephosphorylation. *FEBS Lett*. **349**, pp. 104–108

ISHAK, R.A.H., MOSTAFA, N.M., KAMEL, A.O. (2017). Stealth lipid polymer hybrid nanoparticles loaded with rutin for effective brain delivery - comparative study with the gold

standard (Tween 80): optimization, characterization and biodistribution. *Drug Delivery*, **24**, 1874-1890.

ISHII, T., KUWAHARA, Y., ICHIYANAGI, T., SATO, M., & SHIBATA, H. (2006). Co-administration of quercetin and rutin, flavonoids with different absorption kinetics, modifies plasma and tissue quercetin levels in rats. *The Journal of Nutrition*, **136**(3), 816-820.

ISHISAKA M, KAKEFUDA K, YAMAUCHI M, TSURUMA K, SHIMAZAWA M, ICHIHARA K, HARA H. (2011). Effect of quercetin and its metabolite on the permeability of a cultured endothelial monolayer. *Biofactors*, **37**(1), 58-65

.IVERSEN, L.L., (1995). The toxicity in vitro of beta-amyloid protein. *Biochem* J. **311**(1), pp. 1–16

IWATSUBO, T., (2004). The gamma-secretase complex: machinery for intramembrane proteolysis. *Curr Opin Neurobiol,* **14**, pp. 379–83.

IWATSUKA, H., SHINO, A., SUZUOKI, Z. (1970). General survey of diabetic features of yellow KK mice. *Endocrinologia Japonica*, **17**(1), 23-35.

JACK CR, J.R., KNOPMAN, D.S., JAGUST, W.J., PETERSEN, R.C., WEINER, M.W., AISEN, P.S., (2013). Tracking pathophysiological processes in Alzheimer's disease: an updated hypothetical model of dynamic biomarkers. *Lancet Neurol*. **12**, pp. 207–16.

JACK JR, C. R., HOLTZMAN, D. M. (2013). Biomarker modelling of Alzheimer's disease. *Neuron*, **80**(6), 1347-1358.

JACOBSEN, K., (2010). Processing of the APP family by the α-secretases ADAM10 and TACE Stockholms universitet, Institutionen för neurokemi.Null, pp. 43-45.

JADHAV, S., KATINA, S., KOVAC, A., KAZMEROVA, Z., NOVAK, M., ZILKA, N., (2015). Truncated tau deregulates synaptic markers in rat model for human tauopathy. Front Cell Neurosci. 9, pp. 24

JAISWAL, M., DUDHE, R., & SHARMA, P. K. (2015). Nanoemulsion: an advanced mode of drug delivery system. *3 Biotech*, **5**(2), 123-127.

JAITOVICH, A., & JOURD'HEUIL, D. (2017). Pulmonary Vasculature Redox Signalling in Health and Disease. In Y.-X. Wang (Ed.), Redox Signalling in Health and Disease Cham *Springer International Publishing,* pp. 135–156.

JANET VAN EERSEL, Y.D., XIN LIU, K.E., FABIEN, D., JILLIAN, J.K., JÜRGEN, G., LARS, M.I. and ETIENNE, E.B., (2010). Sodium selenate mitigates tau pathology, neurodegeneration, and functional deficits in Alzheimer's disease models. *Proceedings of the National Academy of Sciences of the United States of America*, **107** (31), pp. 13888-13893.

JARA, C., ARANGUIZ, A., CERPA, W., TAPIA-ROJAS, C., QUINTANILLA, R.A., (2018). Genetic ablation of tau improves mitochondrial function and cognitive abilities in the hippocampus. Redox Biol. 18, pp. 279–94

JAVED, H., KHAN, M.M., AHMAD, A., VAIBHAV, K., AHMAD, M.E., KHAN, A., ASHAFAQ, M., ISLAM, F., SIDDIQUI, M.S., SAFHI, M.M. and ISLAM, F., (2012). Rutin prevents cognitive impairments by ameliorating oxidative stress and neuroinflammation in rat model of sporadic dementia of Alzheimer type. Neuroscience, 210, pp. 340-352.

JEAN, D.C., BAAS, P.W., (2013). It cuts two ways: microtubule loss during Alzheimer disease. *Embo J*. 32, pp. 2900–2

JEONG, Y.O., SHIN, S.J., PARK, J.Y., KU, B.K., SONG, J.S., KIM, J.J. (2018). MK-0677, a Ghrelin agonist, alleviates amyloid beta-related pathology in 5XFAD mice, an animal model of Alzheimer's disease. *Int J Mol Sci*. 19, pp. 1800.

JIMÉNEZ-ALIAGA, K., BERMEJO-BESCÓS, P., BENEDÍ, J., MARTÍN-ARAGÓN, S., (2011). Quercetin and rutin exhibit antiamyloidogenic and fibril-disaggregating effects in vitro and potent antioxidant activity in APPswe cells. *Life Science*. 89, pp. 939-945.

JIN,C.H., Y. K., SO, S. N., HAN AND J. B., KIM, (2016). Isoegomaketone upregulates heme oxygenase-1 in RAW264.7 cells via ROS/p38 MAPK/Nrf2 pathway. *Biomolecules & Therapeutics,* **24**(50, pp. 510–516.

JO, S., KIM, S., SHIN, D.H., KIM, M.S., (2020). Inhibition of SARS-CoV 3CL protease by flavonoids. *Journal of enzyme inhibition and medicinal chemistry*, **35**, pp. 145–151.

JOHANSSON, S., BOHMAN, S., RADESÄTER, A. C., OBERG, C., AND LUTHMAN, J., (2005). Salmonella lipopolysaccharide (LPS) mediated neurodegeneration in hippocampal slice cultures. *J. Neurotox Res*. **8**, pp. 207–220.

JOLIVALT, C.G., HURFORD, R., LEE, C.A., DUMAOP, W., ROCKENSTEIN, E., MASLIAH, E., (2010). Type 1 diabetes exaggerates features of Alzheimer's disease in APP transgenic mice. *Exp Neurol*. **223**, pp. 422–31.

JONES, B.M., BHATTACHARJEE, S., DUA, P., HILL, J.M., ZHAO, Y. and LUKIW, W.J., (2014). Regulating amyloidogenesis through the natural triggering receptor expressed in myeloid/microglial cells 2 (TREM2). *Frontiers in Cellular Neuroscience*, 8, pp. 94.

JONSSON, T., ATWAL, J.K., STEINBERG, S., SNAEDAL, J., JONSSON, P.V., BJORNSSON, S., STEFANSSON, H., SULEM, P., GUDBJARTSSON, D., MALONEY, J., HOYTE, K., GUSTAFSON, A., LIU, Y., LU, Y., BHANGALE, T., GRAHAM, R.R., HUTTENLOCHER, J., BJORNSDOTTIR, G., ANDREASSEN, O.A., JÖNSSON, E.G., PALOTIE, A., BEHRENS, T.W., MAGNUSSON, O.T., KONG, A., THORSTEINSDOTTIR, U., WATTS, R.J. and STEFANSSON, K., (2012). A mutation in APP protects against Alzheimer's disease and age-related cognitive decline. *Nature*, **488**(7409), pp. 96.

JOSHI, G., WANG, Y., (2015). Golgi defects enhance APP amyloidogenic processing in Alzheimer's disease. *BioEssays*, 37, pp. 240–7. *Journal of Neurochemistry*, **103**(5), pp. pp. 1989–2003.

JUUL, S.E., (1998). Erythropoietin and erythropoietin receptor in the developing human central nervous system. *Pediatric Research*. **43**(1), pp. 40–49.

KACZMAREK, E., BAKKER, J.P., CLARKE, D.N., CSIZMADIA, E., KOCHER, O., VEVES, A., (2013). Molecular biomarkers of vascular dysfunction in obstructive sleep apnea. *PLOS ONE,* 8, e70559.

KAHLE, P.J., DE STROOPER, B., (2004). Attack on amyloid. *EMBO Rep*., **4**, pp. 747–51.

KALARIA, R.N. and BALLARD, C., (1999). Overlap between pathology of Alzheimer disease and vascular dementia. Alzheimer disease and associated disorders, 13 Suppl. 3 (Supplement 3), pp. S123.

Kalsbeek M. J. T., Mulder L., Yi C.-X., (2016). Microglia energy metabolism in metabolic disorder. *Mol. Cell. Endocrinol.* **438**, 27–35.

KAMALAKKANNAN, N. and PRINCE, P.S.M., (2006). Antihyperglycaemic and Antioxidant Effect of Rutin, a Polyphenolic Flavonoid, in Streptozotocin-Induced Diabetic Wistar Rats. Basic & Clinical Pharmacology & Toxicology, **98**(1), pp. 97-103.

KAMER, A.R., PIRRAGLIA, E., TSUI, W., RUSINEK, H., VALLABHAJOSULA, S., MOSCONI, L., (2015). Periodontal disease associates with higher brain amyloid load in normal elderly. *Neurobiol Aging.* **36**, pp. 627–33.

KAMPERS, T., FRIEDHOFF, P., BIERNAT, J., MANDELKOW, E.M., MANDELKOW, E., (1996). RNA stimulates aggregation of microtubule-associated protein tau into Alzheimer-like paired helical filaments. *FEBS Lett*. **399**, 344–349.

KAMPERS, T., PANGALOS, M., GEERTS, H., WIECH, H., MANDELKOW, E., (1999). Assembly of paired helical filaments from mouse tau: implications for the neurofibrillary pathology in transgenic mouse models for Alzheimer's disease. *FEBS Lett*. **451**, pp. 39–44.

KANDEL, N., ZHENG, T., HUO, Q., TATULIAN, S.A (2017). Membrane binding and pore formation by a cytotoxic fragment of amyloid β peptide. *J. Phys. Chem,* **121**, pp 10293–10305.

KANDEMIR, F.M., OZKARACA, M., YILDIRIM, B.A., HANEDAN, B., KIRBAS, A., KILIC, K., AKTAS, E., BENZER, F., (2015). Rutin attenuates gentamicin-induced renal damage by reducing oxidative stress, inflammation, apoptosis, and autophagy in rat. *Renal failure* **37**(3), pp. 518-525.

KANG, J., LEMAIRE, H.G., UNTERBECK, A., SALBAUM, J.M., MASTERS, C.L., GRZESCHIK, K.H., MULTHAUP, G., BEYREUTHER, K., MULLER-HILL, B., (1987). The precursor of Alzheimer's disease amyloid A4 protein resembles a cell-surface receptor. *Nature* 325, pp. 733–736

KANG, N., HAI, Y., YANG, J., LIANG, F., GAO, C.J., (2015). Hyperbaric oxygen intervention reduces secondary spinal cord injury in rats via regulation of HMGB1/TLR4/NF-κB signalling pathway. *Int J Clin Exp Pathol,* **8**, pp. 1141-1153.

KAR, S., STEPHEN, P.M., SLOWIKOWSKI, D.W. and HOWARD, T.J., (2004). Interactions between beta-amyloid and central cholinergic neurons: implications for Alzheimer's disease. *Journal of psychiatry Neuroscience,* **29**(6):427-41.

KARIKARI, T.K., PASCOAL, T.A., ASHTON, N.J., JANELIDZE, S., BENEDET, A.L., RODRIGUEZ, J.L., (2020). Blood phosphorylated tau 181 as a biomarker for Alzheimer's disease: a diagnostic performance and prediction modelling study using data from four prospective cohorts. *Lancet Neurol* **19**(5), pp. 422–33.

KARRAN, E., MERCKEN, M., DE STROOPER, B., (2011). The amyloid cascade hypothesis for Alzheimer's disease: an appraisal for the development of therapeutics. *Nat Rev Drug Discov*. **10**, pp. 698–712.

KATZMAN, R., SAITOH, T, (1991). Advances in Alzheimer's disease. *FASEB*, **1**(5), pp. 86.

KAUR, K., KAUR, R. and KAUR, M., (2015). RECENT ADVANCES IN ALZHEIMER'S DISEASE: CAUSES AND TREATMENT. I*nternational Journal of Pharmacy and Pharmaceutical Science*, **8**(2), pp. 8-15

KAUSHAL, V., DYE, R., PAKAVATHKUMAR, P., FOVEAU, B., FLORES, J., HYMAN, B., (2015). Neuronal NLRP1 inflammasome activation of Caspase-1 coordinately regulates inflammatory interleukin-1-beta production and axonal degeneration-associated Caspase-6 activation. Cell Death Differ. 22, pp. 1676–86.

KAWAII, S., TOMONO, Y., KATASE, E., & OGAWA, K. (1999). Bioavailability of rutin in the rat. *Food and Chemical Toxicology*, **37**(10), 957–962.

KERN, A., MAVRIKAKI, M., ULLRICH, C., ALBARRAN-ZECKLER, R., BRANTLEY, A.F., SMITH, R.G., (2015). Hippocampal dopamine/DRD1 signalling dependent on the ghrelin receptor. *Cell*. **163**, pp. 1176–90.

KHALATBARY, A. R., AHMADVAND, H., AGAH, E. (2017). The effect of rutin on the cognitive impairment in amyloid beta peptide-injected rats: A behavioural study. *Iranian journal of basic medical sciences,* **20**(7), 770-777.

KHAN, M.M., AHMAD, A., ISHRAT, T., (2009). Rutin protects the neural damage induced by transient focal ischemia in rats. *Brain Research,* **1292**, pp. 123–135.

KHAN, S.S., BLOOM, G.S., (2016). Tau: The Center of a Signalling Nexus in Alzheimer's disease. *Front Neurosci*. 10, pp. 31.

KHATOON, S, GRUNDKE-IQBAL, I, IQBAL, K., (1992). Brain levels of microtubule-associated protein tau are elevated in Alzheimer's disease: a radioimmuno-slot-blot assay for nanograms of the protein. *J Neurochem.* 59, pp. 750–753.

KHATOON, S., GRUNDKE-IQBAL, I., IQBAL, K., (1995). Guanosine triphosphate binding to beta-subunit of tubulin in Alzheimer's disease brain: role of microtubule-associated protein tau. *J Neurochem.* **64**, pp. 777–787.

KHATUA, S., AND K., ACHARYA, (2018). "Water soluble antioxidative crude polysaccharide from Russula senecis elicits TLR modulated NF-κB signaling pathway and pro-inflammatory response in murine macrophages, *Frontiers in Pharmacology*, 9.

KHODAPASAND, E., JAFARZADEH, N., FARROKHI, F., KAMALIDEHGHAN, B., HOUSHMAND, M., (2015). Is Bax/Bcl-2 ratio considered as a prognostic marker with age and tumor location in colorectal cancer? *Iranian Biomedical Journal,* **19**(2), pp. 69–75.

KHOYNEZHAD, A., JALALI, Z., TORTOLANI, A.J., (2007). A synopsis of research in cardiac apoptosis and its application to congestive heart failure. *Texas Heart Institute Journal,* **34**(3), pp. 352–359.

KHURANA, N., S.C., SIKKA, (2018). Targeting crosstalk between Nrf-2, NF-kappaB and androgen receptor signalling in prostate cancer, *Cancers*, **10**, pp10.

KIM, D.S., KWON, D.Y., KIM, M.S., KIM, H.K., LEE, Y.C., PARK, S.J., (2010). The involvement of endoplasmic reticulum stress in flavonoid-induced protection on cardiac cell death caused by ischaemia/reperfusion. *Journal of Pharmacy and Pharmacology* **62**(2), pp. 197–204.

KIM, D.S., LEE, M.W., KO, Y.J., PARK, H.J., PARK, Y.J., KIM, D.-I., JUNG, H.L., SUNG, K.W., KOO, H.H., & YOO, K.H. (2016). Application of human mesenchymal stem cells cultured in different oxygen concentrations for treatment of graft-versus-host disease in mice. *Biomedical Research*, **37**, 311–317.

KIM, H. J., OH, Y., KIM, D. H., SHIN, E. J., & RYU, J. H. (2014). Penetration of rutin into the brain and its effect on antioxidant status in rats. *Pharmacology*, **94**(1-2), 11-18.

KIM, I., XU, W., REED, J.C., (2008). Cell death and endoplasmic reticulum stress: disease relevance and therapeutic opportunities. *Nat Rev Drug Discov*. 7, pp. 1013–1030.

KIM, J. H., KIM, H. J., LEE, K. M., KIM, K. H., LEE, D., & LEE, K. T. (2014). Pharmacokinetics and tissue distribution of rutin and its metabolite in rats after oral administration of tartary buckwheat extract. *Journal of Agricultural and Food Chemistry*, **62**(17), 3904-3910.

KIM, J. K., KIM, Y. W., & JIN, Y. R. (2005). Bioavailability and metabolism of rutin in rats. *Archives of Pharmacal Research*, **28**(12), 1391-1396.

KIM, J., KIM, Y., PARK, J., KIM, S., LEE, H., KIM, H., & LEE, Y. (2005). Cross-reactivity of anti-class III beta-tubulin antibody with nonneuronal components in the central nervous system and other tissues. *Journal of Histochemistry & Cytochemistry*, **53**(7), 895-902.

KIM, Y. J., PARK, W. J., LEE, S. K., LEE, S. M., KANG, D. G., LEE, H. S., & LEE, H. S. (2014). Rutin attenuates lipopolysaccharide-induced inflammation and oxidative stress in human umbilical vein endothelial cells. *Journal of Ethnopharmacology*, **153**(1), 435-441.

KIMURA, T., WHITCOMB, D.J., JO, J., REGAN, P., PIERS, T., HEO, S., (2014). Microtubule-associated protein tau is essential for long-term depression in the hippocampus. *Philos Trans R Soc*

Lond B Biol Sci. **369**, pp. 20130144

KISHI, T., MATSUNAGA, S., OYA, K., NOMURA, I., IKUTA, T., IWATA, N., (2017). Memantine for alzheimer's disease: an updated systematic review and meta-analysis. *Journal of Alzheimers Discovery.* **60**, pp. 401–25

KISHORE, K. and SINGH, M., (2005). Rutin, a bioflavonoid antioxidant attenuates age related memory deficit in mice. *Biomedical Research*, **16**(1).

KLICKSTEIN, N., (2019). Tau impairs neural circuits, dominating amyloid-β effects, in Alzheimer models in vivo. *Nat Neurosci.* **22**, pp. 57–64

KNIEWALLNER, K.M., FOIDL, B.M., HUMPEL, C. (2018). Platelets isolated from an Alzheimer mouse damage healthy cortical vessels and cause inflammation in an organotypic ex vivo brain slice model. *Scientific Reports,* **8**(1), 1–16.

KODA, T., KURODA, Y. and MAI, H., (2008). Protective effect of rutin against spatial memory impairment induced by trimethyltin in rats. *Nutrition Research*, **28**(9), pp. 629-634.

KONISHI, Y., (1993).Trophic effect of erythropoietin and other hematopoietic factors on central cholinergic neurons in vitro and in vivo. *Brain Research.* **609**(1-2), pp. 29–35.

KONTUSH, A., BERNDT, C., WEBER, W., AKOPYAN, V., ARLT, S., SCHIPPLING, S. and BEISIEGEL, U., (2001). Amyloid-β is an antioxidant for lipoproteins in cerebrospinal fluid and plasma. Free Radical Biology and Medicine, **30**(1), pp. 119-128.

KOOK, S., LEE, K., KIM, Y., CHA, M., KANG, S., BAIK, S.H., LEE, H., PARK, R. and MOOK-JUNG, I., (2014). High-dose of vitamin C supplementation reduces amyloid plaque burden and ameliorates pathological changes in the brain of 5XFAD mice. *Cell Death and Disease*, 5, pp. e1083.

KOPKE, E, TUNG, YC, SHAIKH, S, ALONSO, AC, IQBAL, K, GRUNDKE-IQBAL, I., (1993). Microtubule-associated protein tau. Abnormal phosphorylation of a non-paired helical filament pool in Alzheimer disease. *J Biol Chem.* **268**, pp. 24374–24384

KORKMAZ, A., KOLANKAYA, D., (2013). Inhibiting inducible nitric oxide synthase with rutin reduces renal ischemia/reperfusion injury. *Canadian Journal of Surgery* **56**, pp. 6-14

KOSTIĆ, D.A., DIMITRIJEVIĆ, D.S., STOJANOVIĆ, G.S., PALIĆ, I.R., ĐORĐEVIĆ, A.S., ICKOVSKI, J.D., (2015). Xanthine oxidase: isolation, assays of activity, and inhibition. *Journal of Chemistry* 2015, p. 8.

KOSUGE, Y., (2006). Comparative study of endoplasmic reticulum stress-induced neuronal death in rat cultured hippocampal and cerebellar granule neurons. *Neurochem Int.* **49**(3), pp. 285–293

KREFT, S., KNAPP, M. and KREFT, I., (1999). Extraction of rutin from buckwheat (Fagopyrum esculentumMoench) seeds and determination by capillary electrophoresis. *Journal of agricultural and food chemistry,* **47**(11), pp. 4649-4652.

KUBO, T., NISHIMURA, S., ODA, T., (2002). Amyloid beta-peptide alters the distribution of early endosomes and inhibits phosphorylation of Akt in the presence of 3-(4,5-dimethylthiazol-2-yl)-2,5-diphenyltetrazolium bromide (MTT). *Brain Res Mol Brain Res*. **106**(1-2), pp. 94–100

KUHLMANN, I., 1993. Zur problematik des prophylaktischen Antibiotikaeinsatzes in Zellkulter (problems of the prophylactic use of antibiotics in cell cultures). *ALTEX,* **10**, pp. 27-49.

KUMAR - SINGH, S., THEUNS, J., VAN BROECK, B., PIRICI, D., VENNEKENS, K., CORSMIT, E., CRUTS, M., DERMAUT, B., WANG, R. and VAN BROECKHOVEN, C., (2006). Mean age - of - onset of familial Aalzheimer's disease caused by presenilin mutations correlates with both increased Aβ42 and decreased Aβ40. *Human Mutation*, **27**(7), pp. 686-695.

KUMAR, A., SINGH, A. and EKAVAL, I., (2015). A Review on Alzheimer's disease pathophysiology and its Management: an update. *Journal of Pharmaceutical Research Experiment*, **67**(2), pp. 195-203.

KUMAR, S., SINGH, S., & KUMAR, V. (2017). Amyloid beta peptide aggregation: a potential target for novel therapeutic strategies for Alzheimer's disease. *Journal of Chemical Neuroanatomy*, **83**, 71-80.

KUO, Y.C., TSAO, C.W. (2017). Neuroprotection against apoptosis of SK-N-MC cells using RMP-7- and lactoferrin-grafted liposomes carrying quercetin. *International Journal of Nanomedicine,* **12**, 2857-2869.

KUPERSTEIN, I., BROERSEN, K., BENILOVA, I., ROZENSKI, J., JONCKHEERE, W., DEBULPAEP, M., VANDERSTEEN, A., SEGERS-NOLTEN, I., VAN DER WERF, K., SUBRAMANIAM, V., (2010). Neurotoxicity of Alzheimer's disease Abeta peptides is induced by small changes in the Abeta42 to Abeta40 ratio. *EMBO J 2*, pp. 3408–3420.

KUZU, M., KANDEMIR, F.M., YILDIRIM, S., KUCUKLER, S., CAGLAYAN, C., TURK, E., (2018). Morin attenuates doxorubicin-induced heart and brain damage by reducing oxidative stress, inflammation and apoptosis. *Biomedicine and Pharmacotherapy* **106**, pp. 443–453.

LAFERLA, F.M., GREEN, K.N. and ODDO, S., (2007). Intracellular amyloid-[beta] in Alzheimer's disease. Nature Reviews Neuroscience, **8**(7), pp. 499.

LAGALWAR, S., BERRY, R.W., BINDER, L.I., (2007). Relation of hippocampal phospho-SAPK/JNK granules in Alzheimer's disease and tauopathies to granulovacuolar degeneration bodies. *Acta Neuropathol.* **113**, pp. 63–73.

LALL, R., MOHAMMED, R., OJHA, U., (2019). What are the links between hypoxia and Alzheimer's disease? *Neuropsychiatr Dis Treat,* 15, pp. 1343-1354.

LAMBERT, J.C., AMOUYEL, P., (2011). Genetics of Alzheimer's disease: new evidences for an old hypothesis? *Curr Opin Genet Dev*. **21**, pp. 295–301.

LANGAN, L. M., DODD, N. J. F., OWEN, S. F., PURCELL, W. M., JACKSON, S. K., JHA, A. N. (2016). Direct measurements of oxygen gradients in spheroid culture system using electron paramagnetic resonance oximetry. *PLoS ONE*, 11, e0149492.

LANI, R., HASSANDARVISH, P., SHU, M.H., PHOON, W.H., CHU, J.J., HIGGS, S., VANLANDINGHAM, D., ABU BAKAR, S., ZANDI, K., (2016). Antiviral activity of selected flavonoids against Chikungunya virus. *Antiviral Res,* **133**, pp. 50–61

LEBLANC, A.C., (2003). Natural cellular inhibitors of caspases. *Prog Neuropsychopharmacol Biol Psychiatry,* **27**(2), pp. 215–29.

LECHPAMMER, M., TRAN, B., SUN, B., CUI, J., DHIR, R., & GULLAPALLI, R. P. (2018). Hypoxia Chamber Systems for Cell Culture and Tissue Engineering. *Advanced healthcare materials*, 7(1), 1700426.

LEE C. Y. D., DAGGETT A., GU X., JIANG L.-L., LANGFELDER P., LI X., WANG N., ZHAO Y., PARK C. S., COOPER Y., FERANDO I., MODY I., COPPOLA G., XU H., YANG X. W.,(2018). Elevated TREM2 gene dosage reprograms microglia responsivity and ameliorates pathological phenotypes in Alzheimer's disease models. *Neuron* **97**, 1032–1048.e5.

LEE, C.T., BENDRIEM, R.M., WU, W.W., SHEN, R.F. (2017). 3D brain Organoids derived from pluripotent stem cells: promising experimental models for brain development and neurodegenerative disorders. *Journal of Biomedical Science*, **24**(1), 1–12.

LEE, H.J., SHIN, J.S., LEE, K.G., (2017). Ethanol extract of Potentilla supina Linne suppresses LPS-induced inflammatory responses through NF-κB and AP-1 inactivation in macrophages and in endotoxic mice. *Phytotherapy Research*, **31**(3), pp. 475–487.

LEE, K.M., JEON, S.M., CHO, H.J., (2010). Interleukin-6 induces microglial CX3CR1 expression in the spinal cord after peripheral nerve injury through the activation of p38 MAPK. *Eur J Pain* 14, pp. 682.e682.e12.

LEE, M., TUTTLE, J., REBHUN, L., CLEVELAND, D., FRANKFURTER, A. (1990). The expression and posttranslational modification of a neuron-specific beta-tubulin isotype during chick embryogenesis. *Cell Motil Cytoskeleton*, **17**, pp. 118-32.

LEE, M.K., (2007). Resveratrol protects SH-SY5Y neuroblastoma cells from apoptosis induced by dopamine. *Exp Mol Med*. **39**(3), pp. 376–384.

LEE, T.K., E. M., DENNY, J. C., SANGHVI, (2009). A noisy paracrine signal determines the cellular NF-kappaB response to lipopolysaccharide. *Science Signalling*, 2, PP.93.

LEE, Y.Y., (2016). Anti-inflammatory and antioxidant mechanism of tangeretin in activated microglia, *J. Neuroimmune Pharmacol* **11**(2), pp. 294e305.

LEHMAN-MCKEEMAN, L. (2008). Absorption, distribution and excretion of toxicants. In - Toxicology, *the basic science of poisons McGraw-Hill*, pp. 131-159.

LESHER-PÉREZ, S. C., KIM, G.-A., KUO, C., LEUNG, B. M., MONG, S., KOJIMA, T., (2017). Dispersible oxygen microsensors map oxygen gradients in three-dimensional cell cultures. *Biomater Sci*, **5**, 2106–2113.

LEVY, E., CARMAN, M.D., FERNANDEZ-MADRID, I.J., POWER, M.D., LIEBERBURG, I., VAN DUINEN, S.G., BOTS, G.T., LUYENDIJK, W. and FRANGIONE, B., (1990). Mutation of the Alzheimer's disease amyloid gene in hereditary cerebral hemorrhage, Dutch type. *Science*, **248**(4959), pp. 1124-1126.

LEVY-LAHAD, E., WASCO, W., POORKAJ, P., ROMANO, D.M., OSHIMA, J., PETTINGELL, W.H., YU, C.E., JONDRO, P.D SCHMIDT, S.D., WANG, K., (1995). Candidate gene for the chromosome 1 familial Alzheimer's disease locus. *Science,* **269**(5226), pp. 973-977.

LEWCZUK, P., (2000). Survival of hippocampal neurons in culture upon hypoxia: effect of erythropoietin. *Neuroreport* **11**(16), pp. 3485–3488.

LEWIS, D. M., BLATCHLEY, M. R., PARK, K. M., GERECHT, S. (2017). O2-controllable hydrogels for studying cellular responses to hypoxic gradients in three dimensions in vitro and in vivo. *Nat Protoc,* **12**, 1620–1638.

LI, B., CHOHAN, M.O., GRUNDKE-IQBAL, I., IQBAL, K., (2007). Disruption of microtubule network by Alzheimer abnormally hyperphosphorylated tau. *Acta Neuropathol (Berl)* **113**, pp. 501–511.

LI, B.Q., FU, T., DONGYAN, Y., MIKOVITS, J.A., RUSCETTI, F.W., WANG, J., (2000). Flavonoid baicalin inhibits HIV-1 infection at the level of viral entry. *Biochem Biophys Res Commun* **276**, pp. 534–538.

LI, C., NI, C., YANG, M., TANG, Y., LI, Z., ZHU, Y (2018). Honokiol protects pancreatic b cell against high glucose and intermittent hypoxia-induced injury by activating Nrf2/ARE pathway in vitro and in vivo. *Biomed Pharmacother*, **97**, 1229–1237.

LI, C., ZHANG, L., WANG, M., & LI, X. (2016). Preparation and evaluation of hydroxypropyl-β-cyclodextrin inclusion complexes of rutin for improved solubility and bioavailability. *Journal of Inclusion Phenomena and Macrocyclic Chemistry*, **84**(3-4), 357-365.

LI, J., ZHANG, B., (2013). Apigenin protects ovalbumin-induced asthma through the regulation of Th17 cells. *Fitoterapia* 91, pp. 298–304.

LI, L., KIM, H.J., ROH, J.H., KIM, M., KOH, W., KIM, Y (2020). Pathological manifestation of the induced pluripotent stem cell-derived cortical neurons from an early-onset Alzheimer's disease patient carrying a presenilin-1 mutation (S170F). *Cell Proliferation*, **53**(4), 1-12.

LI, L., XU, J., HE, L., PENG, L., ZHONG, Q., CHEN, L., (2016). The role of autophagy in HN Siti. Journal of Functional Foods, Acta Biochimica et Biophysica Sinica, **48**(6), pp. 491–500.

LI, M., HONG, H.Y., TAN, N., WANG, Y., (2016). Insights into the role and interdependence of oxidative stress and inflammation in liver diseases. *Oxidative Medicine and Cellular Longevity*, pp. 4234061.

LI, M., WANG, J., (2020). Prospect of ambroxol in the treatment of COVID-2019. The Chinese *Journal of Clinical Pharmacology*, pp. 16.

LI, S., HONG, S., SHEPARDSON, N.E., WALSH, D.M., SHANKAR, G.M. and SELKOE, D., (2009). Soluble Oligomers of Amyloid β Protein Facilitate Hippocampal Long-Term Depression by Disrupting Neuronal Glutamate Uptake. *Neuron*, **62**(6), pp. 788-801.

LI, W., M.B., GRAEBER, (2012). The molecular profile of microglia under the influence of glioma, Neuro Oncology. **14** (8), pp. 958e978.

LI, X., BAO, X., and WANG, R. (2016). Experimental models of Alzheimer's disease for deciphering the pathogenesis and therapeutic screening. *International Journal of Molecular Medicine,* **37**(2), 271-283.

LI, X., CUI, X., CHEN, Y., CHEN, T., XU, H., YIN, H., WU, Y., (2018). Therapeutic potential of a prolyl hydroxylase inhibitor FG-4592 for Parkinson's diseases in vitro and in vivo: regulation of redox biology and mitochondrial function. *Front Aging Neurosci* 10, pp. 121.

LI, X., HU, X., WANG, J., XU, W., YI, C., MA, R., (2018). Inhibition of autophagy via activation of PI3K/Akt/mTOR pathway contributes to the protection of hesperidin against myocardial ischemia/reperfusion injury. *International Journal of Molecular Medicine*, **42**(4), pp. 1917–1924.

LI, X., WANG, Y., XU, X., LI, X., LI, H., (2016). Quantification and Pharmacokinetic Studies of Rutin in Rat Plasma and Brain Tissue after Oral Administration. *Journal of Pharmaceutical and Biomedical Analysis,* **129**, 70-78.

LI, Y., LI, J., LIANG, J., & LI, Z. (2014). Polymeric nanoparticles for increased oral bioavailability of rutin: optimization and characterization. *Journal of Biomaterials Science, Polymer Edition,* **25**(3), 243-255.

LI, Y., LI, S., LIN, S., WANG, X. (2013). Enhancement of the oral bioavailability of rutin by co-administration with quercetin in rats. *Journal of Agricultural and Food Chemistry*, **61**(37), 8780–8785.

LI, Y., XU, M., LAI, M., HUANG, Q., CASTRO, J.L., DIMUZIO-MOWER, J., HARRISON, T., LELLIS, C., NADIN, A., NEDUVELIL, J.G., REGISTER, R.B., SARDANA, M.K., SHEARMAN, M.S., SMITH,

A.L., SHI, X., YIN, K., SHAFER, J.A. and GARDELL, S.J.,(2000). Photoactivated [gamma]-secretase inhibitors directed to the active sitecovalently label presenilin 1. *Nature*, **405**(6787), pp. 689.

LI, Z., ZHANG, Y., QU, C., LV, L., DU, J., XU, Y., LI, S., SUN, C., & SONG, X. (2018). Nanoencapsulation of rutin for improved solubility and bioavailability: Preparation, characterization, and in vitro evaluation. *Journal of Agricultural and Food Chemistry,* **66**(13), 3496-3504.

LIANG, Z., LIU, F., IQBAL, K., GRUNDKE-IQBAL, I., WEGIEL, J., GONG, C.X., (2008). Decrease of protein phosphatase 2A and its association with accumulation and hyperphosphorylation of tau in Down syndrome. *Journal of Alzheimer's Discovery*. **13**, pp. 295–302.

LIAO, Y. and CHEN, Y., (2015). A novel method for expression and purification of authentic amyloid-β with and without 15N label. *Protein Expression and Purification*, **113**, pp. 63-71.

LIAZOGHLI, D., PERREAULT, S., MICHEVA, K.D., DESJARDINS, M., LECLERC, N., (2005). Fragmentation of the Golgi apparatus induced by the overexpression of wild-type and mutant human tau forms in neurons. *America Journal of Pathology.* **166**, pp. 1499–1514.

LICHTENTHALER, S.F., (2011). Alpha-secretase in Alzheimer's disease: molecular identity, regulation and therapeutic potential. *Journal of Neurochemistry*, **116**(1), pp. 10.

LIN, W.L., LEWIS, J., YEN, S.H., HUTTON, M., DICKSON, D.W., (2003). Ultrastructural neuronal pathology in transgenic mice expressing mutant (P301L) human tau. *Journal of Neurocytology*. **32**, pp. 1091–1105.

LIN, Y.J., CHANG, Y.C., HSIAO, N.W., HSIEH, J.L., WANG, C.Y., KUNG, S.H., TSAI, F.J., LAN, Y.C., LIN, C.W., (2012). Fisetin and rutin as 3C protease inhibitors of enterovirus A71. *J Virol Method*s **182**(1–2), pp. 93–98.

LINK, C.D. (1995). Expression of human β-amyloid peptide in transgenic Caenorhabditis elegans. *Proceedings of the National Academy of Sciences of the United States of America,* **92**(20), 9368-9372.

LI-SHUANG, HOU ZHEN-YU, CUI,PENG, SUN,HUI-QING, PIAO, XIN HAN ,JIAN SONG, GE WANG, SHUANG ZHENG, XIU-XIU DONGLU, GAO,YUE ZHU, LI-HUA LIAN, JI-XING NAN, YAN-LING, WU, (2019). Rutin mitigates hepatic fibrogenesis and inflammation

through targeting TLR4 and P2X7 receptor signalling pathway in vitro and in vivo. *Journal of Functional Foods*, pp. 103700.

LIU, K., CHEN, G., LIN, P.-L., HUANG, J., LIN, X., QI, J (2018). Detection and analysis of apoptosis- and autophagy-related miRNAs of mouse vascular endothelial cells in chronic intermittent hypoxia model. *Life Science*, **193**, 194–199.

LIU, M., NING, X., LI, R., YANG, Z., YANG, X., SUN, S (2017). Signalling pathways involved in hypoxia-induced renal fibrosis. *Journal of Cellular and Molecular Medicine*, **21**, 1248–1259.

LIU, Y., LI, X., YU, J., LV, C., & XU, M. M. (2017). Rutin improves spatial memory in Alzheimer's disease transgenic mice by reducing Aβ oligomer level and attenuating oxidative stress and neuroinflammation. *Behavioural Brain Research*, **321**, 291-301.

LIU, Y.H., WEI, W., YIN, J., LIU, G.P., WANG, Q., CAO, F.Y., (2008). Proteasome inhibition increases tau accumulation independent of phosphorylation. *Neurobiol Aging*.

LIU, Z., LI, X., SIMONEAU, A. R., JAFARI, M., ZI, J., (2014). Blood-Brain Barrier Permeability of Rutin and Apigenin in an In Vitro Model of the Neurovascular Unit. *Journal of Agricultural and Food Chemistry*, **62**(49), 12041-12047.

LIU, Z., ZHAO, J., LI, W, SHEN, L., HUANG, S., TANG, J., DUAN, J., FANG, F., HUANG, Y., CHANG, H., CHEN, Z., ZHANG, R., (2016). Computational screen and experimental validation of anti-influenza effects of quercetin and chlorogenic acid from traditional Chinese medicine. Sci *Rep*. 6, pp. 19095.

LOPES, M.B., (2013). Estimation of glomerular filtration rate from serum creatinine and cystatin C in octogenarians and nonagenarians, *BMC Nephrol*. 14, pp. 265.

LOVESTONE, S., BOADA, M., DUBOIS, B., HÜLL, M., RINNE, J.O., HUPPERTZ, H., CALERO, M., ANDRÉS, M.V., GÓMEZ-CARRILLO, B., LEÓN, T. and DEL SER, T.,

LU, D.C., RABIZADEH, S., CHANDRA, S., SHAYYA, R.F., ELLERBY, L.M., YE, X., (2000). A second cytotoxic proteolytic peptide derived from amyloid beta-protein precursor. Nat *Med*. 6, pp. 397–404.

LU, N., KHACHATOORIAN, R., FRENCH, S.W., (2012). Quercetin: bioflavonoids as part of interferon-free hepatitis C therapy? *Expert Rev Anti Infect Ther*. **10**(6), pp. 619–621.

LUCIN K. M., O'BRIEN C. E., BIERI G., CZIRR E., MOSHER K. I., ABBEY R. J., MASTROENI D. F., ROGERS J., SPENCER B., MASLIAH E., WYSS-CORAY T., (2013). Microglial beclin 1 regulates retromer trafficking and phagocytosis and is impaired in Alzheimer's disease. *Neuron* 79, 873–886.

LUNA-MUNOZ, J., GARCIA-SIERRA, F., FALCON, V., MENENDEZ, I., CHAVEZ-MACIAS, L., MENA, R., (2005). Regional conformational change involving phosphorylation of tau protein at the Thr231, precedes the structural change detected by Alz-50 antibody in Alzheimer's disease. *Journal of Alzheimer's Dicovery*. **8**, pp. 29–41.

LUND, S., PORZGEN, P., MORTENSEN, A. SAREN LUND, PETER PORZGEN, ANNE LOUISE M, HENRIK H, DONNA B, SIEGFRIED M, THOMAS H, MARINA B, PIETRO G, MALIKA B, SIPKE D, MARCEL L, (2005). Inhibition of microglial inflammation by the MLK inhibitor CEP-1347. *J. Neurochem,* **92**, pp. 1439-1451.

LUSTBADER, J.W., CIRILLI, M., LIN, C., XU, H.W., TAKUMA, K., WANG, N., (2004). ABAD directly links Abeta to mitochondrial toxicity in Alzheimer's disease. *Science,* **304**, pp. 448–52.

LV, X., YU, Z., FENG, L., MA, S., & ZHANG, X. (2016). Rutin attenuates neuroinflammation in spinal cord injury rats. *International Immunopharmacology*, **40**, 491-497.

LYU, S.Y., RHIM, J.Y., PARK, W.B., (2005). Antiherpetic activities of flavonoids against herpes simplex virus type 1 (HSV-1) and type 2 (HSV-2) in vitro. Arch Pharm Res 28(11):1293–130184.

MANDAL SM, CHAKRABORTY D, DEY S (2010) Phenolic acids act as signalling molecules in plant-microbe symbioses. *Plant Signal Behav*. **5**(4), pp. 359–368

MA, Y., YANG, L., MA, J., LU, L., WANG, X., REN, J., (2017). Rutin attenuates doxorubicin-induced cardiotoxicity via regulating autophagy and apoptosis. *Biochimica et Biophysica Acta: Molecular Basis of Disease*, **1863**(8), pp. 1904–1911.

MAARIT, J., REIN, MATHIEU, R., CRUZ- HERNANDEZ, C., LUCAS, A., GORETTA, S. and MARCIA DA SILVA PINTO, K., (2012). Bioavailability of bioactive food compounds: a challenging journey to bioefficacy. *British Journal of Clinical Pharmacology,* **75**(3), pp. 588-602.

MABLY, A.J., GEREKE, B.J., JONES, D.T., COLGIN, L.L., (2017). Impairments in spatial representations and rhythmic coordination of place cells in the 3xTg mouse model of Alzheimer's disease. *Hippocampus*. **27**, pp. 378–92.

MADHUSOODANAN, S., SHAH, P., BRENNER, R. and GUPTA, S., (2007). Pharmacological Treatment of the Psychosis of Alzheimer's disease: What Is the Best Approach? *CNS Drugs*, **21**(2), pp. 101-115.

MADRASI, K., DAS, R., MOHMMADABDUL, H., LIN, L., HYMAN, B.T., LAUFFENBURGER, D.A (2021). Systematic in silico analysis of clinically tested drugs for reducing amyloid-beta plaque accumulation in Alzheimer's disease. *Alzheimer's & Dementia*, **17**(9), 1487–1498.

MAEDA, S., SAHARA, N., SAITO, Y., MURAYAMA, S., IKAI, A., TAKASHIMA, A., (2006). Increased levels of granular tau oligomers: an early sign of brain aging and Alzheimer's disease. *Neurosci Res*. **54**, pp. 197–201.

MAGALINGAM, K.B., RADHAKRISHNAN, A., HALEAGRAHARA, N., (2013). Rutin, a bioflavonoid antioxidant protects rat pheochromocytoma (PC-12) cells against 6-hydroxydopamine (6-OHDA)-induced neurotoxicity, *International Journal of Molecular Medicine*, **32**(1), pp. 235–240.

MAGDELDIN, T., LÓPEZ-DÁVILA, V., PAPE, J., CAMERON, G. W. W., EMBERTON, M., LOIZIDOU, M., (2017). Engineering a vascularised 3D in vitro model of cancer progression. *Sci Rep*, 7, 44045.

MAGLIONE, E., MARRESE, C., MIGLIARO, E., MARCUCCIO, F., PANICO, C., SALVATI, C., CITRO, G., QUERCIO, M., RONCAGLIOLO, F., TORELLO, C., (2015). Increasing bioavailability of (R)-alpha-lipoic acid to boost antioxidant activity in the treatment of neuropathic pain. *Acta Bio-Medica Atenei Parm.* **86**, pp. 226–233.

MAH, V.H., ESKIN, T.A., KAZEE, A.M., LAPHAM, L., HIGGINS, G.A., (1992). In situ hybridization of calcium/calmodulin dependent protein kinase II and tau mRNAs; species differences and relative preservation in Alzheimer's disease. *Brain Res Mol Brain Res*. 12, pp. 85–94.

MAHE, D., FISSON, S., MONTONI, A.., (2001). Identification and IFNgamma-regulation of differentially expressed mRNAs in murine microglial and CNS-associated macrophage subpopulations. *Moll. Cell Neurosci*, **18**, pp. 363-380

MAHLEY, R.W., APOLIPOPROTEIN, E., (1988). Cholesterol transport protein with expanding role in cell biology. *Science,* **240**, pp. 622–30.

MAN, Y., ZHOU, R. and ZHAO, B., (2015). Efficacy of rutin in inhibiting neuronal apoptosis and cognitive disturbances in sevoflurane or propofol exposed neonatal mice. International journal of clinical and experimental medicine, **8**(8), pp. 14397.

MANACH, C., WILLIAMSON, G., MORAND, C., SCALBERT, A. and RÉMÉSY, C., (2005). Bioavailability and bioefficacy of polyphenols in humans. I. Review of 97 bioavailability studies. The American journal of clinical nutrition, 81(1 Suppl), pp. 230S.

MANNO, M., ROTOLO, C., CASCIO, C., BAVISOTTO, C. C., CORDARO, M., & D'AGATA, R. (2020). Thioflavin T as a fluorescent probe for amyloid fibril detection. *Molecules*, **25**(4), 846.

MANS, L.A., CANO, L.Q., VAN PELT, J., GIARDOGLOU, P., KEUNE, W.J., HARAMIS, A.P.G., (2017). The tumor suppressor LKB1 regulates starvation-induced autophagy under systemic metabolic stress. *Scientific Reports*, **7**(1), pp. 7327.

MARRAZZO, P., ANGELONI, C., HRELIA, S. (2019). Combined treatment with three natural antioxidants enhances neuroprotection in a SH-SY5Y 3D culture model. *Antioxidants,* **8**(10), 1-16.

MARTIN, M.A., (2014). Cocoa flavonoid epicatechin protects pancreatic beta cell viability and function against oxidative stress, *Mol. Nutr. Food Res*. **58**(3), pp. 447e456.

MARTINEZ-ESTRADA, O.M., (2003). Erythropoietin protects the in vitro blood-brain barrier against VEGF-induced permeability. Eur J Neurosci. **18**(9), pp. 2538–2544

MARTINVALET, D., ZHU, P., LIEBERMAN, J., (2005). Granzyme A induces caspase-independent mitochondrial damage, a required first step for apoptosis. *Immunity*, **22**, pp. 355–70.

MARTORELL, A.J., PAULSON, A.L., SUK, H.J., ABDURROB, F., DRUMMOND, G.T., GUAN, W., (2019). Multi-sensory gamma stimulation ameliorates Alzheimer's-associated pathology and improves cognition. *Cell.* **177**, pp. 256–71.e22.

MATHEW, S., FATIMA, K., FATMI, M.Q., ARCHUNAN, G., ILYAS, M., BEGUM, N., AZHAR, E., DAMANHOURI, G., QADRI, I., (2015). Computational docking study of p7 Ion channel from HCV genotype 3 and genotype 4 and its interaction with natural compounds. *PLoS One* **10**(6), pp. e0126510.

MAUGERI, G., D'AMICO, A. G., RASÀ, D. M., LA COGNATA, V., SACCONE, S., FEDERICO, C., (2017). Caffeine prevents blood retinal barrier damage in a model, in vitro, of diabetic macular edema. *J Cell Biochem*, **118**, 2371–2379.

MAURER, K. and MAURER, U., (2003). Alzheimer. New York: Columbia University Press.

Mawuenyega K. G., Sigurdson W., Ovod V., Munsell L., Kasten T., Morris J. C., Yarasheski K. E., Bateman R. J., (2010). Decreased clearance of CNS β-amyloid in Alzheimer's disease. *Science* **330**, 1774.

MAWUENYEGA, K.G., SIGURDSON, W., OVOD, V., MUNSELL, L., KASTEN, T., MORRIS, J.C., YARASHESKI, K.E., BATEMAN, R.J., (2010). Decreased clearance of CNS beta-amyloid in Alzheimer's disease. *Science* **330**, pp. 1774.

MAZZEO, M.F., LIPPOLIS, R., SORRENTINO, A., LIBERTI, S., FRAGNITO, F., SICILIANO, R.A., (2015). Lactobacillus acidophilus-rutin interplay investigated by proteomics. *PLoS One* 10, pp. e0142376.

MCCONLOGUE, L., BUTTINI, M., ANDERSON, J.P., BRIGHAM, E.F., CHEN, K.S., FREEDMAN, S.B., (2007). Partial reduction of BACE1 has dramatic effects on Alzheimer plaque and synaptic pathology in APP Transgenic Mice. *J Biol Chem*, **282**, pp. 26326–34

MCCORD, J.M., (2000). The evaluation of free radicals and oxidative stress. *American Journal of Medicine,* **108**(8), pp. 652-9.

MCGEER, P.L., ROGERS, J., (1992). Anti-inflammatory agents as a therapeutic approach to Alzheimer's disease. *Neurology* 42, pp. 447–9.

MCMURTREY, R. J. (2016). Analytic models of oxygen and nutrient diffusion, metabolism dynamics, and architecture optimization in three-dimensional tissue constructs with applications and insights in cerebral organoids. *Tissue Eng Part C Methods*, **22**, 221–249.

MCNAMARA, P.J., LEGGAS, M. M., BACHMANN, K., (2009). Drug distribution. Pharmacology: Principles and practice. *Academic Press*. pp. 113-131.

MERCK, (2018). Merck Announces Discontinuation of APECS Study Evaluating Verubecestat (MK-8931) for the Treatment of People with Prodromal Alzheimer's disease. Available online at:

https://investors.merck.com/news/press-release-details/2018/Merck-Announces-Discontinuation-of-APECS-Study-Evaluating-Verubecestat-MK-8931-for-the-Treatment-of-People-with-Prodromal-Alzheimers-Disease/default.aspx .

MERELLI, A., RODRÍGUEZ, J.C.G., FOLCH, J., REGUEIRO, M.R., CAMINS, A., LAZAROWSKI, A., (2018). Understanding the role of hypoxia inducible factor during neurodegeneration for new therapeutics opportunities. *Curr Neuropharmacol* 16, pp. 1484-1498.

MESITI, F., CHAVARRIA, D., GASPAR, A., ALCARO, S., BORGES, F. (2019). The chemistry toolbox of multitarget-directed ligands for Alzheimer's disease. *European Journal of Medicinal Chemistry,* **181**, 1-16. microglia. *J Neuroinflammation,* **4**, p. 27.

MIGUEL-ÁLVAREZ, M., SANTOS-LOZANO, A., SANCHIS-GOMAR, F., FIUZA-LUCES, C., PAREJA-GALEANO, H., GARATACHEA, N. and LUCIA, A., (2015). Non-steroidal anti-inflammatory drugs as a treatment for Alzheimer's disease: a systematic review and meta-analysis of treatment effect. *Drugs & aging*, **32**(2), pp. 139.

MIJAJLOVIĆ, M.D., PAVLOVIĆ, A., BRAININ, M., HEISS, W.D., QUINN, T.J., IHLE-HANSEN, H.B., HERMANN, D.M., ASSAYAG, E.B., RICHARD, E., THIEL, A., KLIPER, E., SHIN, Y., KIM, Y.H., CHOI, S., JUNG, S., LEE, Y.B., SINANOVIĆ, O., LEVINE,

MILANO, J., MCKAY, J., DAGENAIS, C., FOSTER-BROWN, L., POGNAN, F., GADIENT, R., (2004). Modulation of notch processing by gamma-secretase inhibitors causes intestinal goblet cell metaplasia and induction of genes known to specify gut secretory lineage differentiation. *Toxicol Sci.* **82**, pp. 341–58

MILLER, A.H., HAROON, E., RAISON, C.L., FELGER, J.C., (2013). Cytokine targets in the brain: impact on neurotransmitters and neurocircuits. *Depress Anxiety,* **30**, pp. 297-306.

MILLER, C.M., N.R., BOULTER, S.J., FULLER, A.M., ZAKRZEWSKI, M.P., LEES, B.M., SAUNDERS, N.C., SMITH, (2011). The role of the P2X7 receptor in infectious diseases. *PLoS Pathogens,* **7** Article, pp. e1002212.

MISITI, F., (2005). Abeta(31-35) peptide induce apoptosis in PC 12 cells: contrast with Abeta(25-35) peptide and examination of underlying mechanisms. *Neurochem Int.* **46**(7), pp. 575–583.

MIYAMOTO, K., TSUJI, A., KAWAI, Y., TERAO, J. (2011). Accumulation of orally administered quercetin in brain tissue and its antioxidative effects in rats. *Free Radical Biology and Medicine,* **51**(7), 1329-1336.

MOCANU, M.M., NISSEN, A., ECKERMANN, K., KHLISTUNOVA, I., BIERNAT, J., DREXLER, D., (2008). The potential for beta-structure in the repeat domain of tau protein determines aggregation, synaptic decay, neuronal loss, and coassembly with endogenous Tau in inducible mouse models of tauopathy. *J Neurosci*. 28, pp. 737–48.

MOHAMED, T., SHAKERI, A. and RAO, P.P.N., (2016). Amyloid cascade in Alzheimer's disease: Recent advances in medicinal chemistry. European Journal of Medicinal Chemistry, 113, pp. 258-272.

MOHAN S., AND D., GUPTA, (2018). Crosstalk of toll-like receptors signaling and Nrf2 pathway for regulation of inflammation. *Biomedicine & Pharmacotherapy*, **108**, pp. 1866–1878

MOHANDAS, E., RAJMOHAN, V. and RAGHUNATH, B., (2009). Neurobiology of Alzheimer's disease. Indian journal of psychiatry, 51(1), pp. 55.

MOKHTARI-ZAER, A., ALIZADEH, A., POURJAFAR, M., & SHARIFIAN, M. (2020). Rutin improves brain function and structure in a mouse model of mild cognitive impairment. *Journal of Alzheimer's Disease,* **73**(3), 1091-1103.

MONTAGNE, A., BARNES, S., SWEENEY, M., HALLIDAY, M., SAGARE, A., ZHAO, Z.,TOGA, A., JACOBS, R., LIU, C., AMEZCUA, L., HARRINGTON, M., CHUI, H., LAW, M. ZLOKOVIC, B., (2015). Blood-Brain Barrier Breakdown in the Aging Human Hippocampus. Neuron, **85**(2), pp. 296-302.

MOON, M., CHA, M.Y., MOOK-JUNG, I., (2014). Impaired hippocampal neurogenesis and its enhancement with ghrelin in 5XFAD mice. *Journal of Alzheimer's Discovery*, **41**, pp. 233–41.

MOREIRA, P., SIEDLAK, S., WANG, X., SANTOS, M., OLIVEIRA, C., TABATON, M., NUNOMURA, A., SZWEDA, L., ALIEV, G., SMITH, M., ZHU, X. and PERRY, G., (2007). Autophagocytosis of Mitochondria Is Prominent in Alzheimer Disease. *Journal of Neuropathology and Experimental Neurology,* **66**(6), pp. 525-532.

MOREIRA, P.L., SIEDLAK, S.L., WANG, X., SANTOS, M.S., OLIVEIRA, C.R. AND TABATON, M., (2007). Increase Autophagic degradation of mitochondria in Alzheimer's disease. *Journal of Neuropathol Exp Neurol,* **3**, pp. 614-5.

MORI, H., KONDO, J., IHARA, Y., (1987). Ubiquitin is a component of paired helical filaments in Alzheimer's disease. *Science*. **235**, pp. 1641–1644.

MORISHIMA-KAWASHIMA, M., HASEGAWA, M., TAKIO, K., SUZUKI, M., TITANI, K., IHARA, Y., (1993). Ubiquitin is conjugated with amino-terminally processed tau in paired helical filaments. *Neuron*. **10**, pp. 1151–1160.

MORRIS, G.P., CLARK, I.A. and VISSEL, B., (2014). Inconsistencies and controversies surrounding the amyloid hypothesis of Alzheimer's disease. *Acta neuropathologica communications,* **2**(1), pp. 135.

MORRIS, R., GARRUD, P., RAWLINS, J., O'KEEFE, J. (1982). Place navigation impaired in rats with hippocampal lesions. *Nature*, **297**(5868), 681-683.

MORSCH, R., SIMON, W., COLEMAN, P.D., (1999). Neurons may live for decades with neurofibrillary tangles. *J Neuropathol Exp Neurol*. **58**, pp. 188–197.

MOSCONI, L., BERTI, V., GLODZIK, L., PUPI, A., DE SANTI, S. and DE LEON, M.J., (2010). Pre-clinical detection of Alzheimer's disease using FDG-PET, with or without amyloid imaging. *Journal of Alzheimer's disease*, **20**(3), pp. 843.

MOSHER, K.I. AND WYSS-CORAY, T., (2014). Microglial dysfunction in brain aging and Alzheimer's disease. *Biochem Pharmacol*. **88**, pp. 594-604.

MOSTAFA, N.M. (2017). Comparative analysis of rutin content in some Egyptian plants: A validated RP-HPLC-DAD approach. *European Journal of Medicinal Plants*, 19, 1-8.

MOSTAFA, N.M. (2017). Rutin: A Potential Therapeutic Agent for Alzheimer Disease. *Pharmaceutica Analytica Acta*, **10**(4), 615.

MOSTAFA, N.M., ABD EL-GHFFAR, E.A., HEGAZY, H.G., ELDAHSHAN, O.A. (2018). New methoxyflavone from Casimiroa sapota and the biological activities of its leaves extract against lead acetate induced hepatotoxicity in rats. *Chemistry & Biodiversity*, 15, e1700528.

MOTAMEDSHARIATY, V.S., AMEL, F.S., NASSIRI-ASL, M., HOSSEINIZADEH, H., (2014). Effects of rutin on acrylamide induced neurotoxicity. *DARU Journal of Pharmaceutical Science* **22**, pp. 27.

MUCKE, L. and PALOP, J.J., (2010). Amyloid-β-induced neuronal dysfunction in Alzheimer's disease: from synapses toward neural networks. *Nature Neuroscience*, **13**(7), pp. 812-818.

MUELLER, S., MILLONIG, G., WAITE, G. (2009). The GOX/CAT system: A novel enzymatic method to independently control hydrogen peroxide and hypoxia in cell culture. *Advances in Medical Sciences,* **54**, 121–135.

MUNIANDY, K., S., GOTHAI, K. M. H., BADRAN, S. S., KUMAR, N. M., ESA AND P., ARULSELVAN, (2018). Suppression of Proinflammatory Cytokines and Mediators in LPS-Induced RAW 264.7 Macrophages by Stem Extract of Alternanthera sessilis via the Inhibition of the NF-κB Pathway. *Journal of Immunology Research*, pp 12.

MUNOZ, D.G. AND FELDMAN, H., (2000). Causes of Alzheimer's disease. *Canadian Medical Association Journal,* 162, pp. 72.

MUÑOZ-SÁNCHEZ, J., & CHÁNEZ-CÁRDENAS, M.E. (2018). The use of cobalt chloride as a chemical hypoxia model. *Journal of Applied Toxicology,* **39**, 556–570.

MURATORE, C.R., SRIKANTH, P., CALLAHAN, D.G., & YOUNG-PEARSE, T.L. (2014). Comparison and optimization of hiPSC forebrain cortical differentiation protocols. *PLoS ONE*, 9.

MYRE, M.A., WASHICOSKY, K., MOIR, R.D., TESCO, G., TANZI, R.E., WASCO, W. (2009). Reduced amyloidogenic processing of the amyloid β-protein precursor by the small molecule Differentiation Inducing Factor-1. *Cellular Signalling*, **21**(4), 567-576.

NA, J.Y., KIM, S., SONG, K., KWON, J., (2014). Rutin alleviates prion peptide-induced cell death through inhibiting apoptotic pathway activation in dopaminergic neuronal cells. *Cell Mol Neurobiol* **34**, pp. 1071-1079.

NABAVI, S. F., BRAIDY, N., GORTZI, O., SOBARZO-SANCHEZ, E., DAGLIA, M., SKALICKA-WOŹNIAK, K., & SHIROOIE, S. (2015). Neuroprotective effects of rutin in neurodegenerative diseases: focus on its mechanisms of action. *Oxidative Medicine and Cellular Longevity*, 1-11.

NAFEES, S., RASHID, S., ALI, N, HASAN, S.K., SULTANA, S., (2015). Rutin ameliorates cyclophosphamide induced oxidative stress and inflammation in Wistar rats: role of NFκB/MAPK pathway. *Chem Biol Interact*, **231**, pp. 98-107.

NAKASHIMA, H., ISHIHARA, T., SUGUIMOTO, P., YOKOTA, O., OSHIMA, E., KUGO, A., (2005). Chronic lithium treatment decreases tau lesions by promoting ubiquitination in a mouse model of tauopathies. Acta Neuropathol. **110**, pp. 547–556.

NARASINGAPA, R.B., JARGAVAL, M.R., PULLABHATLA, S., HTOO, H.H., RAO, J.K.S., HERNANDEZ, J., GOVITRAPONG, P. and VINCENT, B., (2012). Activation of α-secretase by curcumin-amino acid conjugates. Biochemical and Biophysical Research Communications, **424**(4), pp. 691-696.

NASSIRI-ASL, M., FARIVAR, T.N., ABBASI, E., (2013). Effects of rutin on oxidative stress in mice with kainic acid-induced seizure. Journal of Integrative Medicine **11**(5), pp. 337–342.

NECULA, M., CHIRITA, C. N., & KURET, J. (2003). Rapid anionic micelle-mediated α-synuclein fibrillization in vitro. *Journal of Biological Chemistry*, **278**(47), 46674-46680.

NEUMAN, M.G., KATZ, G.G., MALKIEWICZ, I.M., MATHURIN, P., TSUKAMOTO, H., ADACHI, M., (2002). Alcoholic liver injury and apoptosis--synopsis of the symposium held at ESBRA 2001: 8th Congress of the European Society for Biomedical Research on Alcoholism. *Alcohol*, **28**(2), pp. 117–28.

NEVE, R.L., HARRIS, P., KOSIK, K.S., KURNIT, D.M., DONLON, T.A., (1986). Identification of cDNA clones for the human microtubule-associated protein tau and chromosomal localization of the genes for tau and microtubule-associated protein 2. *Brain Res*. **387**, pp. 271–80

NGUYEN, T.L., KIM, C.K., CHO, J.H., LEE, K.H., AHN, J.Y., (2010). Neuroprotection signaling pathway of nerve growth factor and brain-derived neurotrophic factor against staurosporine induced apoptosis in hippocampal H19-7 cells. *Exp Mol Med*. **42**(8), pp. 583.

NODA, Y., ASADA, M., KUBOTA, M., MAESAKO, M., WATANABE, K., UEMURA, M., KIHARA, T., SHIMOHAMA, S., TAKAHASHI, R., KINOSHITA, A., (2013). Copper enhances APP dimerization and promotes Abeta production. *Neurosci. Lett.* **547**, pp. 10–15.

NORTLEY, R., KORTE, N., IZQUIERDO, P., HIRUNPATTARASILP, C, MISHRA, A., JAUNMUKTANE, Z., (2019). Amyloid β oligomers constrict human capillaries in Alzheimer's disease via signaling to pericytes. *Science* 365, pp. eaav9518.

OAKLEY, H., COLE, S.L., LOGAN, S., MAUS, E., SHAO, P., CRAFT, J.,(2006). Intraneuronal β-amyloid aggregates, neurodegeneration, and neuron loss in transgenic mice with five familial

Alzheimer's disease mutations: potential factors in amyloid plaque formation. *Journal of Neuroscience,* **26**(40), 10129-10140.

OBIED, H.K., PRENZLER, P.D., OMAR, S.H., ISMAEL, R., SERVILI, M., ESPOSTO, S., TATICCHI, A., SELVAGGINI, R. and URBANI, S., (2012). Pharmacology of Olive Biophenols. Advances in Molecular Toxicology. Elsevier Science & Technology, pp. 195-242.

O'BRIEN, R.J. AND WONG, P.C., (2011). Amyloid precursor protein processing and Alzheimer's disease. Annual review of neuroscience, **34**(1), pp. 185-204.

ODDO, S. CACCAMO, A., KIM, N., GREEN, K.L., LEVINA, T., YILING, C., FRANCES, M.L., FRANK, ALASZLO, L., (2005). Chronic Nicotine Administration Exacerbates Tau Pathology in a Transgenic Model of Alzheimer's disease. Proceedings of the National Academy of Sciences of the United States of America, **102**(8), pp. 3046-3051.

ODDO, S., CACCAMO, A., SHEPHERD, J.D., MURPHY, M.P., GOLDE, T.E., KAYED, R.(2003). Triple-transgenic model of Alzheimer's Disease with plaques and tangles: intracellular Aβ and synaptic dysfunction. *Neuron*, **39**(3), 409-421.

ODDO, S., VASILEVKO, V., CACCAMO, A., KITAZAWA, M., CRIBBS, D.H., LAFERLA, F.M., (2006). Reduction of soluble Abeta and tau, but not soluble Abeta alone, ameliorates cognitive decline in transgenic mice with plaques and tangles. *J Biol Chem.* 281, pp. 39413–39423.

OH,Y.C., W.-K., CHO, J. H., OH, (2012). Fermentation by Lactobacillus enhances anti-inflammatory effect of Oyaksungisan on LPS-stimulated RAW 264.7 mouse macrophage cells, *BMC Complementary and Alternative Medicine,* 12.

OLA, M.S., AHMED, M.M., AHMAD, R., ABUOHASHISH, H.M., AL-REJAIE, S.S., ALHOMIDA, A.S., (2015). Neuroprotective effects of rutin in streptozotocin-induced diabetic rat retina. *Journal of Molecular Neuroscience*, **56**(2), pp. 440–448.

OLSSON, F., SCHMIDT, S., ALTHOFF, V., MUNTER, L.M., JIN, S., ROSQVIST, S., (2014). Characterization of intermediate steps in amyloid beta (Abeta) production under near-native conditions. *J Biol Chem.*, **289**, 1540–50.

OLTHOF, M.R., HOLLMAN, P.C.H., BUIJSMAN, MICHEL, N. C. P., VAN AMELSVOORT, JOHAN, M. M. and KATAN, M.B., (2003). Chlorogenic acid, quercetin-3-rutinoside and black tea phenols are extensively metabolized in humans. *The Journal of Nutrition*, **133**(6), pp. 1806-1814.

OLTHOF, M.R., HOLLMAN, P.C.H., VREE, T.B and KATAN, M.B., (2000). Bioavailabilies of quercetin-3-glucoside and quercetin-4'- glucoside do not differ in humans. *The Journal of Nutrition*, **130**(5), pp. 1200-1203.

OLTON, D., SAMUELSON, R. (1976). Remembrance of places passed: spatial memory in rats. Journal of Experimental Psychology: *Animal Behaviour Processes*, **2**(2), 97-116.

ORHAN, D.D., OZÇELIK, B., € OZGEN, S., ERGUN, F., (2010). Antibacterial, antifungal, and € antiviral activities of some flavonoids. *Microbiological Research* 165, pp. 496e504.

OSTRAKHOVITCH, E.A., AFANAS'EV, I.B., (2001). Oxidative stress in rheumatoid arthritis leukocytes: suppression by rutin and other antioxidants and chelators. *Biochemical Pharmacology*, **62**(6), pp. 743–746.

OWEGI, H., EGOT-LEMAIRE, S., WAITE, L.R., & WAITE, G.N. (2010). Macrophage activity in response to steady-state oxygen and hydrogen peroxide concentration—Biomed 2010. *Biomedical Science Instruments,* **46**, 57–62.

OYAMA, F., CAIRNS, N.J., SHIMADA, H., OYAMA, R., TITANI, K., IHARA, Y., (1994). Down's syndrome: up-regulation of beta-amyloid protein precursor and tau mRNAs and their defective coordination. *J Neurochem.* **62**, pp. 1062–1066.

OZE, H., HIRAO, M., EBINA, K., SHI, K., KAWATO, Y., KANESHIRO, S., YOSHIKAWA, H., HASHIMOTO, J. (2012). Impact of medium volume and oxygen concentration in the incubator on pericellular oxygen concentration and differentiation of murine chondrogenic cell culture. *In Vitro Cellular & Developmental Biology - Animal*, **48**, 123–130.

PAAVILAINEN, T., PELKONEN, A., MA¨KINEN, M.E.L., PELTOLA, M., HUHTALA, H., FAYUK, D. (2018). Effect of prolonged differentiation on functional maturation of human pluripotent stem cell-derived neuronal cultures. *Stem Cell Research*, **27**, 151–161.

PADURARIU, M., CIOBICA, A., LEFTER, R., SERBAN, I.L., STEFANESCU, C. and CHIRITA, R., (2013). The oxidative stress hypothesis in Alzheimer's disease. Psychiatria Danubina, **25**(4), pp. 401.

PALMER, A.M. (2010). The blood-brain barrier. *Neurobiology of Disease*, **37**(1), 1-2.

PALOP, J.J., MUCKE, L., (2016). Network abnormalities and interneuron dysfunction in Alzheimer disease. *Nat Rev Neurosci.* 17, pp. 777–92.

PAN, P.H., LIN, S.Y., WANG, Y.Y., CHEN, W.Y., CHUANG, Y.H., WU, C.C., CHEN, C.J., (2014). Protective effects of rutin on liver injury induced by biliary obstruction in rats. *Free Radic Biol Med.* 73, pp. 106-116.

PAN, R.Y., MA. J., KONG, X.X., WANG, X.F., LI, S.S., QI, X.L., (2019). Sodium rutin ameliorates Alzheimer's disease-like pathology by enhancing microglial amyloid-beta clearance. *Sci Adv.* 5, pp. eaau6328.

PANCHAL, S.K., POUDYAL, H., ARUMUGAM, T.V., BROWN, L., (2011.) Rutin attenuates metabolic changes, nonalcoholic steatohepatitis, and cardiovascular remodeling in high-carbohydrate, high-fat diet-fed rats. Journal of Nutrition, **141**(6), pp. 1062–1069.

PANDA, D., MILLER, H. P., BANERJEE, A., (2003). Visualization of microtubule growth in cultured neurons via the use of EB3-GFP (end-binding protein 3-green fluorescent protein). *Journal of Neurochemistry Research*, **71**(2), 265-275.

PANEL, M., GHALEH, B., & MORIN, D. (2017). Ca2+ ionophores are not suitable for inducing mPTP opening in murine isolated adult cardiac myocytes. *Scientific Reports*, **7**, 4283.

PANIAGUA-TORIJA, B., AREVALO-MARTIN, A., MOLINA-HOLGADO, E., MOLINA-HOLGADO, F., GARCIA-OVEJERO, D., (2015). Spinal cord injury induces a long-lasting upregulation of interleukin-1β in astrocytes around the central canal. *Neuroscience*, **284**, pp. 283-289.

PANKIEWICZ, J.E., GURIDI, M., KIM, J., ASUNI, A.A., SANCHEZ, S., SULLIVAN, P.M., (2014). Blocking the apoE/Aβ interaction ameliorates Aβ-related pathology in APOE epsilon2 and epsilon4 targeted replacement Alzheimer model mice. Acta Neuropathol Commun. 2, pp. 75

PANZA, F., LOZUPONE, M., LOGROSCINO, G., IMBIMBO, B.P., (2019). A critical appraisal of amyloid-β-targeting therapies for Alzheimer disease. *Nat Rev Neurol*. 15, pp. 73–88.

PAQUET, D., BHAT, R., SYDOW, A., MANDELKOW, E.M., BERG, S., HELLBERG, S (2009). A zebrafish model of tauopathy allows in vivo imaging of neuronal cell death and drug evaluation. *Journal of Clinical Investigation*, **119**(5), 1382-1395.

PARAMESHWARAN, K., DHANASEKARAN, M., SUPPIRAMANIAM, V., (2008). Amyloid beta peptides and glutamatergic synaptic dysregulation. *Experimental Neurology,* **210**(1), pp. 7–13

PARK, J., MIN, J.S., KIM, B., CHAE, U.B., YUN, J.W., CHOI, M.S., KONG, I.K., CHANG, K.T., LEE, D.S., (2015). Mitochondrial ROS govern the LPS-induced pro-inflammatory response in microglia cells by regulating MAPK and NF-κB pathways. *Neurosci Lett* **584**, pp. 191-196.

PARK, S.E., SAPKOTA, K., CHOI, J.H., KIM, M.K., KIM, Y.H., KIM, K.M., KIM, K.J., OH, H.N., KIM, S.J., KIM, S., (2014). Rutin from Dendropanax morbifera Leveille protects human dopaminergic cells against rotenone induced cell injury through inhibiting JNK and p38 MAPK signalling. *Neurochemistry Research,*. 39, pp. 707-718

PAŞCA, A.M., SLOAN, S.A., CLARKE, L.E., TIAN, Y., MAKINSON, C.D., HUBER, N., (2015). Functional cortical neurons and astrocytes from human pluripotent stem cells in 3D culture. *Nature Methods*, **12**, 671–678.

PASQUALETTI, P., BONOMINI, C., DAL FORNO, G (2009). A randomized controlled study on effects of ibuprofen on cognitive progression of Alzheimer's disease. *Aging Clin Exp Res* **21**, 102–110.

PATEL, R. P., PATEL, P. R., KALARIA, D. R., MURTHY, R. S., & GANDHI, T. R. (2012). Development and evaluation of rutin–polyethylene glycol 6000 conjugate for improved solubility, dissolution, and oral bioavailability. *Drug Development and Industrial Pharmacy*, **38**(6), 694-703.

PAVLACKY, J., POLAK, J. (2020). Technical Feasibility and Physiological Relevance of Hypoxic Cell Culture Models. *Frontiers in Endocrinology*, 11, 57.

PEI, J.J., AN, W.L., ZHOU, X.W., NISHIMURA, T., NORBERG, J., BENEDIKZ, E., (2006). P70 S6 kinase mediates tau phosphorylation and synthesis. FEBS Lett. 580, pp. 107–114

PENG, T., & THORN, K. (2017). Improved quantitative image analysis using a nonlinear Bayesian approach: Application to microscopy. *Biophysical Journal*, **112**(1), 42–49.

PENNEY, J., RALVENIUS, W.T., TSAI, L.H. (2020). Modeling Alzheimer's disease with iPSC-derived brain cells. *Molecular Psychiatry*, **25**(1), 148-167.

PEREIRA, D.M., G., CORREIA-DA-SILVA, P., VALENTÃO, N., TEIXEIRA, AND P. B., ANDRADE, (2007). Anti-inflammatory effect of unsaturated fatty acids and Ergosta-(7, 22)-dien-3-ol from Marthasterias glacialis: prevention of CHOP-mediated ER-stress and NF-κB activation. PLoS One, **9**(2).

PEREIRA, L., IGEA, A., CANOVAS, B., DOLADO, I., NEBREDA, A.R., (2013). Inhibition of p38 MAPK sensitizes tumour cells to cisplatin-induced apoptosis mediated by reactive oxygen species and JNK. *EMBO Mol Med*, **5**, pp. 1759-1774.

PEREZ, M., VALPUESTA, J.M., MEDINA, M., MONTEJO DE GARCINI, E., AVILA, J., (1996). Polymerization of tau into filaments in the presence of heparin: the minimal sequence required for tau-tau interaction. *J Neurochem*. **67**, pp. 1183–1190

PERRY, G., FRIEDMAN, R., SHAW, G., CHAU, V., (1987). Ubiquitin is detected in neurofibrillary tangles and senile plaque neurites of Alzheimer disease brains. *Proc Natl Acad Sci USA*. **84**, pp. 3033–3036.

PERRY, G., MULVIHILL, P., FRIED, V.A., SMITH, H.T., GRUNDKE-IQBAL, I., IQBAL, K., (1989). Immunochemical properties of ubiquitin conjugates in the paired helical filaments of Alzheimer disease. *J Neurochem*. **52**, pp. 1523–1528.

PETRUCELLI, L., DICKSON, D., KEHOE, K., TAYLOR, J., SNYDER, H., GROVER, A., (2004). CHIP and Hsp70 regulate tau ubiquitination, degradation and aggregation. *Hum Mol Genet*. **13**, pp. 703–714.

PFEIFFENBERGER, M., BARTSCH, J., HOFF, P., PONOMAREV, I., BARNEWITZ, D., THÖNE-REINEKE, C., (2019). Hypoxia and mesenchymal stromal cells as key drivers of initial fracture healing in an equine in vitro fracture hematoma model. *PLoS ONE*, 14, e0214276.

PFEIFFENBERGER, M., HOFF, P., THÖNE-REINEKE, C., BUTTGEREIT, F., LANG, A., & GABER, T. (2020). The in vitro human fracture hematoma model—A tool for preclinical drug testing. *Altex*, **37**, 561–578.

PIEDRAHITA, J.A., ZHANG, S.H., HAGAMAN, J.R., OLIVER, P.M., MAEDA, N. (1992). Generation of mice carrying a mutant apolipoprotein E gene inactivated by gene targeting in embryonic stem cells. *Proceedings of the National Academy of Sciences of the United States of America*, **89**(10), 4471-4475.

PIKE, C.J., (1995). Structure-activity analyses of beta-amyloid peptides: contributions of the beta 25-35 region to aggregation and neurotoxicity. *J Neurochem*. **64**(1), pp. 253–265

PIKE, C.J., OVERMAN, M.J. and COTMAN, C.W., (1995). Amino-terminal deletions enhance aggregation of beta-amyloid peptides in vitro. *The Journal of biological chemistry*, **270**(41), pp. 23895-23898.

PIMPLIKAR, S.W., (2009). Reassessing the amyloid cascade hypothesis of Alzheimer's disease. *International Journal of Biochemistry and Cell Biology*, **41**(6), pp. 1261-1268.

PIRES, K.M., BUFFOLO, M., SCHAAF, C., SYMONS, J.D., COX, J., ABEL, E.D., (2017). Activation of IGF-1 receptors and Akt signalling by systemic hyperinsulinemia contributes to cardiac hypertrophy but does not regulate cardiac autophagy in obese diabetic mice. *Journal of Molecular and Cellular Cardioogy,* **113**, pp. 39–50.

PLANEL, E., RICHTER, K.E., NOLAN, C.E., FINLEY, J.E., LIU, L., WEN, Y., (2007). Anesthesia leads to tau hyperphosphorylation through inhibition of phosphatase activity by hypothermia. *J Neurosci.* 27, pp. 3090–3097

PLAPER, A., GOLOB, M., HAFNER, I., OBLAK, M., SOLMAJER, T., JERALA, R., (2003) Characterization of quercetin binding site on DNA gyrase. *Biochemical and Biophysical Research Communications* 306, pp. 530e536.

POOLE, S., SINGHRAO, S.K., CHUKKAPALLI, S., RIVERA, M., VELSKO, I., KESAVALU, L., (2015). Active invasion of Porphyromonas gingivalis and infection-induced complement activation in ApoE−□− mice brains. *Journal of Alzheimer's Discovery*. **43**, pp. 67–80.

POPPEK, D., KECK, S., ERMAK, G., JUNG, T., STOLZING, A., ULLRICH, O., (2006). Phosphorylation inhibits turnover of the tau protein by the proteasome: influence of RCAN1 and oxidative stress. *Biochem J.* 400, pp. 511–520.

PRAMANIK, D., C., GHOSH AND S.G., DEY, (2011). *J. Am. Chem. Soc.*, **133**, pp. 15545 — 15552

PRATICÒ, D. and SUNG, S., (2004). Lipid peroxidation and oxidative imbalance: early functional events in Alzheimer's disease. *Journal of Alzheimer's disease*, **6**(2), pp. 171-175.

PRATICÒ, D., (2008). Oxidative stress hypothesis in Alzheimer's disease: a reappraisal. *Trends in pharmacological sciences,* **29**(12), pp. 609.

PRILLER, C., BAUER, T., MITTEREGGER, G., KREBS, B., KRETZSCHMAR, H.A., HERMS, J., (2006). Synapse formation and function is modulated by the amyloid precursor protein. *J Neurosci,* **26**, pp. 7212–21.

PRUSINER, S.B., (2012). Cell Biology: A unifying role for prions in neurodegenerative diseases. *Science* **336**, pp. 1511–3.

PU, F., MISHIMA, K., IRIE, K., MOTOHASHI, K., TANAKA, Y., ORITO, K., EGAWA, T, KITAMURA, Y., EGASHIRA, N., IWASAKI, K., FUJIWARA, M., (2007). Neuroprotective effects of quercetin and rutin on spatial memory impairment in an 8-arm radial maze task and neuronal death induced by repeated cerebral ischemia in rats. *Journal of Pharmacological. Science*, **104**, pp. 329–334.

PULSINELLI, W.A., BRIERLEY, J.B., PLUM, F., (1982). Ann Neurol 11, pp. 491–498.14

QIN, Y., GREENE, V.R., CHATTOPADHYAY, C., EKMEKCIOGLU, S., LIU, C., & GRIMM, E.A. (2013). Induction of hypoxia in 3D human melanoma spheroids leads to c-Met activation and resistance to Vemurafenib. *Cancer Research*, **73**, 2936.

QUAN, J.H., HUANG, R., WANG, Z., HUANG, S., CHOII, W., ZHOU, Y., CHU, P.Z., (2018). P2X7 receptor mediates NLRP3-dependent IL-1β secretion and parasite proliferation in Toxoplasma gondii-infected human small intestinal epithelial cells. *Parasites & Vectors*, 11, pp. 1.

RADOVITS, T., ZOTKINA, J., LIN, L., KARCK, M., SZABÓ, G. (2009). Endothelial dysfunction after hypoxia–reoxygenation: do in vitro models work? *Vascul Pharmacol*, **51**, 37–43.

RAJASEKHARA, K., MALABIKA CHAKRABARTIA AND T., GOVINDARAJU (2015). Function and toxicity of amyloid beta and recent therapeutic interventions targeting amyloid beta in Alzheimer's disease. *Journal of chemical communication*, 7.

RAMALINGAYYA, G.V., NAMPOOTHIRI, M., NAYAK, P.G., KISHORE, A., SHENOY, R.R., MALLIKARJUNA RAO, C.(2016). Naringin and rutin alleviate episodic memory deficits in two differentially challenged object recognition tasks. *Pharmacognosy Magazine*, **12**(2), S63-S70.

RAMAN, B., BAN, T., SAKAI, N., PASTA, S. Y., RAMAKRISHNAN, S., NAIKI, H., & GOTO, Y. (2013). Atomic force microscopy and MD simulations reveal pore-like structures of all-D-enantiomer of Alzheimer's beta-amyloid peptide: relevance to the ion channel mechanism of AD pathology. *Journal of Molecular Biology*, **425**(2), 191-212.

RAMASWAMY, S., DWARAMPUDI, L.P., KADIYALA, M., KUPPUSWAMY, G., (2017). Veera Venkata Satyanarayana Reddy K, Kumar CKA, Paranjothy M: Formulation and characterization of chitosan encapsulated phytoconstituents of curcumin and rutin nanoparticles. Int J Biol Macromol 104(Pt B), pp.1807–

RASOOL, S., MARTINEZ-CORIA, H., WU, J.W., LAFERLA, F., GLABE, C.G., (2013). Systemic vaccination with anti-oligomeric monoclonal antibodies improves cognitive function by reducing Aβ deposition and tau pathology in 3xTg-AD mice. J Neurochem. 126, pp. 473–82.

RAWLINSON, C., JENKINS, S.I., THEI, L., DALLAS, M.L., CHEN, R.L., (2020). Post-ischaemic immunological response in the brain: targeting microglia in ischaemic stroke therapy. *Brain Sci* 10, pp. 159.

RAYGANI, A.V., ZAHRAI, M., RAYGANI, A.V., DOOSTI, M., JAVADI, E., REZAEI, M., (2005). Association between apolipoprotein E polymorphism and Alzheimer disease in Tehran, Iran. *Neurosci Lett.* **375**, pp. 1–6

REGAN, P., WHITCOMB, D.J., CHO, K., (2017). Physiological and pathophysiological implications of synaptic tau. *Neuroscientist*. **23**, pp. 137–51

REITZ, C., (2012). Alzheimer's disease and the Amyloid Cascade Hypothesis: A Critical Review. International Journal of Alzheimer's disease, 2012, pp. 1-11.

REITZ, C., BRAYNE, C. and MAYEUX, R., (2011). Epidemiology of Alzheimer disease. Nature Reviews Neurology, **7**(3), pp. 137-152.

RIAZ, H., RAZA, S., ASLAM, M., AHMAD, M., AHMAD, M. and MARIA, P., (2018). An Updated Review of Pharmacological, Standardization Methods and Formulation Development of Rutin. *Journal of Pure and Applied Microbiology,* **12**(1), pp. 127-132.

RIBER-HANSEN, R., VAINER, B., & STEINICHE, T. (2012). Digital image analysis: A review of reproducibility, stability, and basic requirements for optimal results. APMIS: *Acta Pathologica, Microbiologica, et Immunologica Scandinavica,* **120**, 276–289.

RICHARD J, O' BRIEN AND PHILIP, C WONG, (2011). Amyloid precursor protein processing and Alzheimer's disease. Annual Review in Neuroscience, 34, pp. 185-204.

RICHETTI, S.K., BLANK, M., CAPIOTTI, K.M., PIATO, A.L., BOGO, M.R., VIANNA, M.R., (2011). Quercetin and rutin prevent scopolamine-induced memory impairment in zebrafish. *Behavioural Brain Research*, **217**, 10-15.

RINDERKNECHT, H., EHNERT, S., BRAUN, B., HISTING, T., NUSSLER, A.K., LINNEMANN, C. (2021). The Art of Inducing Hypoxia. *Oxygen*, **1**, 46–61.

ROBERT, D.B., RASHID, D., NIENWEN, C., XIAOCHUN, L., ABHAY, S., ITENDER, S., JEFFREY, W.S., HUANG, G., ANNA, R., WILLIAM, VAN NOSTRAND., JOSEPH, M.M. and BERISLAV, V.Z., (2009). SRF and myocadia regulate LRP-mediated amyloid-[beta] clearance in brain vascular cells. *Nature Cell Biology*, **11**(2), pp. 143.

ROBERT, V., (2001). The beta-secretase, BACE: a prime drug target for Alzheimer's disease. Journal of Molecular Neuroscience, **17**(2):157-70.

RODRIGUEZ, S., HUG, C., TODOROV, P., MORET, N., BOSWELL, S.A., EVANS, K (2021). Machine learning identifies candidates for drug repurposing in Alzheimer's disease. *Nature Communications,* **12**(1), 1–13.

ROMEO, L., INTRIERI, M., D'AGATA, V., MANGANO, N.G., ORIANI, G., ONTARIO, M.L., (2009). The major green tea polyphenol, (-)- epigallocatechin-3-gallate, induces heme oxygenase in rat neurons and acts as an effective neuroprotective agent against oxidative stress. *J Am Coll Nutr*. **28** Suppl, pp. 492S–499S.

ROSENBERG, R.N., (2003). Arch. *Neurol*., **60**, pp. 1678 —1679

ROSS, J., SHARMA, S., WINSTON, J., NUNEZ, M., BOTTINI, G., FRANCESCHI, M., SCARPINI, E., FRIGERIO, E., FIORENTINI, F., FERNANDEZ, M., SIVILIA, S., GIARDINO, L., CALZA, L., NORRIS, D., CICIRELLO, H., CASULA, D. and BRUNO P.I., (2013). CHF5074 Reduces Biomarkers of Neuroinflammation in Patients with Mild Cognitive Impairment: A 12-Week, Double-Blind, Placebo- Controlled Study. *Current Alzheimer Research,* **10**(7), pp. 742-753.

ROSSI, D., (2015). Astrocyte physiopathology: At the crossroads of intercellular networking, inflammation and cell death. *Progress in Neurobiology*, **130**, pp. 86-120.

ROTH, A.D., RAMÍREZ, G., ALARCÓN, R. and VON BERNHARDI, R., (2005). Oligodendrocytes damage in Alzheimer's disease: Beta amyloid toxicity and inflammation. *Biological Research*, **38**(4), pp. 381-387.

ROUX, F., COURAUD, P.O. (2005). Rat brain endothelial cell lines for the study of blood-brain barrier permeability and transport functions. *Cellular and Molecular Neurobiology*, **25**(1), 41-57.

ROZARIO, T., & DESIMONE, D.W. (2010). The extracellular matrix in development and morphogenesis: A dynamic view. *Developmental Biology,* **341**, 126–140.

RUBEN, G.C., IQBAL, K., GRUNDKE-IQBAL, I., WISNIEWSKI, H.M., CIARDELLI, T.L., JOHNSON, J.E., (1991). Jr The microtubule-associated protein tau forms a triple-stranded left-hand helical polymer. *J Biol Chem*. **266**, pp. 22019–22027.

RUIJTERS, E.J., (2014). The cocoa flavanol (-)-epicatechin protects the cortisol response, *Pharmacol. Res.* **79**, pp. 28e33.

RUIJTERS, E.J., (2016).Food-derived bioactives can protect the anti-inflammatory activity of cortisol with antioxidant-dependent and -independent mechanisms, *Int. J. Mol. Sci.* **17**(2), pp. 239.

RUNFENG, L., YUNLONG, H., JICHENG, H., WEIQI, P., QINHAI, M., YONGXIA, S., CHUFANG, L., JIN, Z., ZHENHUA, J., HAIMING, J., (2020). Lianhuaqingwen exerts anti-viral and anti-inflammatory activity against novel coronavirus (SARS-CoV-2). Pharmacological Research, 2020, pp. 104761.

RUSSO-SAVAGE, L., RAO, V.K.S., EIPPER, B.A., MAINS, R.E. (2020). Role of Kalirin and mouse strain in retention of spatial memory training in an Alzheimer's disease model mouse line. *Neurobiology of Aging*, **95**, 69–80.

RYBNIKOVA, E., & SAMOILOV, M. (2015). Current insights into the molecular mechanisms of hypoxic pre- and postconditioning using hypobaric hypoxia. *Frontiers in Neuroscience*, 9, 388.

SADIGH-ETEGHAD, S., SABERMAROUF, B., MAJDI, A., TALEBI, M., FARHOUDI, M. and MAHMOUDI, J., (2015). Amyloid-Beta: A Crucial Factor in Alzheimer's disease. Medical Principles and Practice, **24**(1), pp. 1-10.

SAHARA, N., MURAYAMA, M., MIZOROKI, T., URUSHITANI, M., IMAI, Y., TAKAHASHI, R., (2005). In vivo evidence of CHIP up-regulation attenuating tau aggregation. *J Neurochem*. 94, pp. 1254–1263

SAKLANI, R., GUPTA, S.K., MOHANTY, .I.R, KUMAR, B., SRIVASTAVA, S., MATHUR, R., (2016). Cardioprotective effects of rutin via alteration in TNF-α, CRP, and BNP levels coupled with antioxidant effect in STZ-induced diabetic rats. *Molecular and Cellular Biochemistry*, **420**(1–2), pp. 65–72.

SALKOVIC-PETRISIC, M., TRIBL, F., SCHMIDT, M., HOYER, S., RIEDERER, P. (2006). Alzheimer-like changes in protein kinase B and glycogen synthase kinase-3 in rat frontal cortex and hippocampus after damage to the insulin signalling pathway. *Journal of Neurochemistry*, **96**(4), 1005-1015.

SALVI, V., SOZIO, F., SOZZANI, S., DEL PRETE A (2017). Role of atypical chemokine receptors in microglial activation and polarization. *Front Aging Neurosci* 9, pp. 148.

SAMANTHA, L.R. and IIYAS, M.K., (2014). Late-Onset Alzheimer's Disease Genes and the Potentially Implicated Pathways. *Current Genetic Medicine Reports*, **2** (2), pp. 85-101.

SAMPSON, E.L., JENAGARATNAM, L., MCSHANE, R., (2014). Metal protein attenuating compounds for the treatment of Alzheimer's dementia. Cochrane Database. *Syst Rev*. 2, pp. CD005380.

SANCHO, R., CALZADO, M.A., DI MARZO, V., APPENDINO, G., MUÑOZ, E., (2003). Anandamide inhibits nuclear factor-κB activation through a cannabinoid receptor-independent pathway. *Molecular Pharmacology*, **63**(2), pp. 429–438.

SANTACRUZ, K., LEWIS, J., SPIRES, T., PAULSON, J., KOTILINEK, L., INGELSSON, M., (2005). Tau suppression in a neurodegenerative mouse model improves memory function. *Science*. 309, pp. 476–481.

SAVELIEFF M.G., S., LEE, Y., LIU AND M. H., LIM, (2013). ACS Chem. Biol., 8, pp. 856 — 865

SAYRE, L.M., MOREIRA, P.I., SMITH, M.A., PERRY, G., (2005). Metal ions and oxidative protein modification in neurological disease. *Ann. Ist. Super. Sanita*, **41**, pp. 143–164.

SCHEFF, S.W., PRICE, D.A., SCHMITT, F.A., MUFSON, E.J., (2006). Hippocampal synaptic loss in early Alzheimer's disease and mild cognitive impairment. Neurobiol Aging. 27, pp. 1372–84.

SCHELTENS, P., LEYS, D., BARKHOF, F., HUGLO, D., WEINSTEIN, H. C., VERMERSCH, P. AND WOLTERS, E. C. (2016). Atrophy of medial temporal lobes on MRI in" probable" Alzheimer's disease and normal ageing: diagnostic value and neuropsychological correlates. *Journal of Neurology, Neurosurgery & Psychiatry,* **55**(10), 967-972.

SCHEUNER, D., ECKMAN, C., JENSEN, M., SONG, X., CITRON, M., SUZUKI, N., (1996). Secreted amyloid beta-protein similar to that in the senile plaques of Alzheimer's

SCHINDELIN, J., RUEDEN, C.T., & HINER, M.C. (2015). The ImageJ ecosystem: An open platform for biomedical image analysis. *Molecular Reproduction and Development*, **82**(7-8), 518–529.

SCHIRONE, L., FORTE, M., PALMERIO, S., YEE, D., NOCELLA, C., ANGELINI, F. (2017). A review of the molecular mechanisms underlying the development and progression of cardiac remodeling. *Oxidative Medicine and Cellular Longevity*, pp. 3920195.

SCHMIDT, C., LEPSVERDIZE, E., CHI, S.I., DAS, A.M., PIZZO, S.V., DITYATEV. A. AND SCHACHNER, M., (2008). Amyloid precursor protein and amyloid β-peptide bind to ATP synthase and regulate its activity at the surface of neural cells. *Molecular Psychiatry*, **13**(10), pp. 953-969.

SCHMITT, H., GOZES, I., LITTAUER, U.Z., (1977). Decrease in levels and rates of synthesis of tubulin and actin in developing rat brain. *Brain Res*. **121**, pp. 327–342

SCHNEBLE, N., SCHMIDT, C., BAUER, R., MÜLLER, J.P., MONAJEMBASHI, S., WETZKER, R., (2017). Phosphoinositide 3-kinase γ ties chemoattractant- and adrenergic control of microglial motility. *Mol Cell Neurosci* **78**, pp. 1-8.

SCHNEIDER, A., BIERNAT, J., VON BERGEN, M., MANDELKOW, E., MANDELKOW, E.M., (1999). Phosphorylation that detaches tau protein from microtubules (Ser262, Ser214) also protects it against aggregation into Alzheimer paired helical filaments. *Biochemistry*. 38, pp. 3549–3558

SCHNEIDER, J.A., WILSON, R.S., COCHRAN, E.J., BIENIAS, J.L., ARNOLD, S.E., EVANS, D.A., BENNETT, D.A., (2003). *Neurology* 60, pp. 1082–1088.

SCHNEIDER, L.S., GEFFEN, Y., RABINOWITZ, J., THOMAS, R.G., SCHMIDT, R., ROPELE, S., WEINSTOCK, M., (2019). Ladostigil Study Group. Low-dose ladostigil for mild cognitive impairment: A phase 2 placebo-controlled clinical trial.Neurology. **93**(15), pp. e1474-e1484.

SCHNEIDER, L.S., MANGIALASCHE, F., ANDREASEN, N., FELDMAN, H., GIACOBINI, E., JONES, R., (2014). Clinical trials and late-stage drug development for Alzheimer's disease: an appraisal from 1984 to 2014. *J Intern Med*. **275**, pp. 251–83.

SELKOE D. J., HARDY J., (2016). The amyloid hypothesis of Alzheimer's disease at 25 years. *EMBO Mol. Med.* **8**, 595–608.

SELKOE, D.J. and SCHENK, D., (2003). Alzheimer's disease: molecular understanding predicts amyloid-based therapeutics. *Annual review of pharmacology and Toxicology*, 43, pp. 545.

SELKOE, D.J., (1991). The molecular pathology of Alzheimer's disease. *Neuron*. 6, pp. 87–98.

SELKOE, D.J., (2008). Soluble oligomers of the amyloid beta-protein impair synaptic plasticity and behavior. *Behav Brain Res*. **192**(1), pp.106–13.

SELKOE, D.J., HARDY, J., (2016). The amyloid hypothesis of Alzheimer's disease at 25 years. *EMBO molecular medicine*, **8**(6), pp. 595-608.

SEMINARA, R.S., JEET, C., BISWAS, S., KANWAL, B., IFTIKHAR, W., SAKIBUZZAMAN, M., (2018). The neurocognitive effects of ghrelin-induced signaling on the hippocampus: a promising approach to Alzheimer's disease. *Cureus*. 10, PP. 3285

SENGUPTA, A., GRUNDKE-IQBAL, I., IQBAL, K., (2006). Regulation of phosphorylation of tau by protein kinases in rat brain. *Neurochem Res*. **31**, pp. 1473–1480

SERRANO-POZO, A., QIAN, J., MONSELL, S.E., BETENSKY, R.A., HYMAN, B.T., (2015). APOEepsilon2 is associated with milder clinical and pathological Alzheimer disease. *Ann Neurol*. **77**, pp. 917–29

SHABAB, T., KHANABDALI. R., MOGHADAMTOUSI, S.Z., KADIR, H.A., MOHAN, G., (2017). Neuroinflammation pathways: a general review. *Int J Neurosci* **127**, pp. 624-633.

SHAFIEI, S.S., GUERRERO-MUNOZ, M.J., CASTILLO-CARRANZA, D.L., (2017). Tau oligomers: cytotoxicity, propagation, and mitochondrial damage. *Front Aging Neurosci*. 9, pp. 83

SHAH, H., ALBANESE, E., DUGGAN, C., RUDAN, I., LANGA, K.M., CARRILLO, M.C., CHAN, K.Y., JOANETTE, Y., PRINCE, M., ROSSOR, M., SAXENA, S., SNYDER, H.M.,

SHANKAR, G.M., LI, S., MEHTA, T.H., GARCIA-MUNOZ, A., SHEPARDSON, N.E., SMITH, I., (2008). Amyloid-β protein dimers isolated directly from Alzheimer's brains impair synaptic plasticity and memory. *Nat Med*.**14**, pp. 837–42.

SHARP, F.R., BERNAUDIN, M., (2004). HIF1 and oxygen sensing in the brain. *Nat Rev Neurosci* 5, pp. 437–448.

SHEA, D., HSU, C.C., BI, T.M., PARANJAPYE, N., CHILDERS, M.C., COCHRAN, J., (2019). α-Sheet secondary structure in amyloid β-peptide drives aggregation and toxicity in Alzheimer's disease. *Proc Natl Acad Sci USA*. **116**, pp. 8895–900.

SHEFET-CARASSO, L. AND IT. AI., (2014). Antibody-targeted drugs and drug resistance— Challenges and solutions. *Drug Resistance Updates*, **18**, pp. 36-46.

SHEMESH, O.R., SPIRA, A. MICHA, E., (2011). Rescue of neurons from undergoing hallmark tau-induced Alzheimer's disease cell pathologies by the antimitotic drug paclitaxel. *Neurobiology of Disease,* **43**(1), pp. 163-175.

SHEN, J. and KELLEHER, R.J., (2007). The Presenilin Hypothesis of Alzheimer's disease: Evidence for a Loss-of-Function Pathogenic Mechanism. *Proceedings of the National Academy of Sciences of the United States of America*, **104**(2), pp. 403-409.

SHERRINGTON, R., ROGAEV, E.I., LIANG, Y., ROGAEVA, E.A., LEVESQUE, G., IKEDA,M., CHI, H., LIN, C., LI, G., HOLMAN, K., TSUDA, T., MAR, L., FONCIN, J.-., BRUNI, A.C., MONTESI, M.P., SORBI, S., RAINERO, I., PINESSI, L., NEE, L., CHUMAKOV, I.,POLLEN, D., BROOKES, A., SANSEAU, P., POLINSKY, R.J., WASCO, W., SILVA, H A R DA, HAINES, J.L., PERICAK-VANCE, M.A., TANZI, R.E., ROSES, A.D., FRASER, P.E.,ROMMENS, J.M. and ST GEORGE-HYSLOP, P.H., (1995). Cloning of a gene bearing missense mutations in early-onset familial Alzheimer's disease. *Nature*, **375**(6534), pp. 754.

SHI, J., ZHANG, T., ZHOU, C., CHOHAN, M.O., GU, X., WEGIEL, J., (2008). Increased dosage of Dyrk1A alters alternative splicing factor (ASF)-regulated alternative splicing of tau in Down syndrome. *J Biol Chem*. 283, pp. 28660–28669.

SHIN, J.S., H. T., IM, AND K. T., LEE, (2009). "Saikosaponin B2 Suppresses Inflammatory Responses Through IKK/IκBα/NF-κB Signalling Inactivation in LPS-Induced RAW 264.7 Macrophages. *Inflammation*, **42**, pp. 342–353.

SHIN, J.S., NOH, Y.S., LEE, Y.S., CHO, Y.W., BAEK, N.I., CHOI, M.S., JEONG, T.S., KANG, E., CHUNG, H.G., LEE, K.T., (2011). Arvelexin from Brassica Rapa suppresses NF-kappaB-regulated pro-inflammatory gene expression by inhibiting activation of IkappaB kinase. *British Journal of Pharmacology,* **164**, pp.145-158.

SHOU, Y., LIANG, F., XU, S., LI, X. (2020). The application of brain organoids: from neuronal development to neurological diseases. *Frontiers in Cell and Developmental Biology*, **8**, 1–10.

SIBILLE, N., SILLEN, A., LEROY, A., WIERUSZESKI, J.M., MULLOY, B., LANDRIEU, I., (2006). Structural impact of heparin binding to full-length Tau as studied by NMR spectroscopy. *Biochemistry*. **45**, pp. 12560–12572.

SIERRA-FILARDI, E., NIETO, C., DOMÍNGUEZ-SOTO, Á., BARROSO, R., SÁNCHEZ-MATEOS, P., PUIG-KROGER, A., LÓPEZ-BRAVO, M., JOVEN, J., ARDAVÍN, C., FERNANDEZ, J.L.R. (2014). CCL2 Shapes Macrophage Polarization by GM-CSF and M-CSF: Identification of CCL2/CCR2-Dependent Gene Expression Profile. *Journal of Immunology*, **192**, 3858–3867.

SILVA, O., BUTOVSKY (2017). Activation of microglia by aggregated beta-amyloid or lipopolysaccharide impairs MHC-II expression and renders them cytotoxic whereas IFN-gamma and IL-4 render them protective. *Mol Cell Neurosci,* **29**(3), pp. 381-393.

SIMONYI, A., (2015). Inhibition of microglial activation by elderberry extracts and its phenolic components, *Life Science*. 128, pp. 30e38.

SINGH, A., CHOW, O., JENKINS, S., ZHU, L., ROSE, E., ASTBURY, K. and CHEN, R., (2021). Characterizing Ischaemic Tolerance in Rat Pheochromocytoma (PC12) Cells and Primary Rat Neurons. *Neuroscience,* **453**, pp. 17-31.

SINGH, U., JIALAL, I., (2008). Retracted: Alpha-lipoic acid supplementation and diabetes. *Nutr. Rev*. **66**, pp. 646–657.

SINGH, H., KAUR, P., KAUR, P., MUTHURAMAN, A., SINGH, G., KAUR, M., (2015). Investigation of therapeutic potential and molecular mechanism of vitamin P and digoxin in I/R induced myocardial infarction in rat. *Naunyn-Schmiedeberg's Archives of Pharmacology*, **388**(5), pp. 565–574.

SINGH, M., GOVINDARAJAN, R., RAWAT, A.K., KHARE, P.B., (2008). Antimicrobial flavonoid rutin from Pteris vittata L. against pathogenic gastrointestinal microflora. *American Fern Journal*, 98, pp. 98e103.

SIRK, D., ZHU., Z., WADIA, J.S., (2007). Chronic exposure to sub-lethal beta-amyloid (Aβ) inhibits the import of nuclear-encoded proteins to mitochondria in differentiated PC12 cells. *Journal of Neurochemistry,* **103**(5), pp. 1989–2003.

SJOGREN, T., SJOGREN, H., LINDGREN, A.G., (19520. Morbus Alzheimer and morbus Pick; a genetic, clinical and patho-anatomical study. Acta Psychiatr Neurol Scand Suppl. 82, pp. 1–152.

SMITH, A.K., KLIMOV, D.K (2018) Binding of cytotoxic Aβ25–35 peptide to the dimyristoylphosphatidylcholine lipid bilayer. *J. Chem. Inf. Model,* **58**, pp 1053–1065.

SMITH, R., PUSCHMANN, A., SCHÖLL, M., OHLSSON, T., SWIETEN, J., HONER, M., ENGLUND, E. and HANSSON, O., (2016). 18F-AV-1451 tau PET imaging correlates strongly with tau neuropathology in MAPT mutation carriers. *Brain: a journal of neurology*, **139**(9), pp. 2372-2379.

SNIGDHA, S., SMITH, E.D., PRIETO, G.A., COTMAN, C.W., (2012). Caspase-3 activation as a bifurcation point between plasticity and cell death. *Neuroscience Bulletin* **28**(1), pp. 14–24.

SNOWDON, D.A., GREINER, L.H., MORTIMER, J.A., RILEY, K.P., GREINER, P.A., MARKESBERY, W.R., (1997). *J Am Med Assoc*. *277*, pp. 813–817.

SOFIC, E., COPRA-JANICIJEVIC, A., SALIHOVIC, M., TAHIROVIC, I., KROYER, G., (2010). Screening of medicinal plant extracts for quercetin-3-rutinoside (rutin) in Bosnia and Herzegovina in medicinal plants. *International Journal of Phytomedicines and Related Industries*, **2**(97), pp. 10-59.

SONG, K., KIM, S., NA, J.Y., PARK, J.H., KIM, J.K., KIM, J.H., KWON, J., (2014). Rutin attenuates ethanol-induced neurotoxicity in hippocampal neuronal cells by increasing aldehyde dehydrogenase 2. *Food and Chemical Toxicology* 72, pp. 228-233.

SONG, P., ZOU, M.H., (2015). Atherosclerosis: Risks, Mechanisms, and Therapies. Hoboken, NJ, USA: John Wiley & Sons, Inc Roles of reactive oxygen species in physiology and pathology; pp. 379–392.

SONI, H., MALIK, J., SINGHAI, A.K., SHARMA, S., (2013). Antimicrobial and anti-inflammatory activity of the hydrogels containing rutin delivery. *Asian Journal of Chemistry* 25, pp. 8371e8373.

SORENSEN, E.B. and CONNER, S.D., (2010). Γ-secretase-dependent cleavage initiates notch signaling from the plasma membrane. Traffic (Copenhagen, Denmark), **11**(9), pp.1234-1245.

SPERLING, R., VARGHESE, M., WANG, H., WORTMANN, M. and DUA, T., (2016). Research priorities to reduce the global burden of dementia by 2025. Null, None.

STADELMANN, C., (1999). Activation of caspase-3 in single neurons and autophagic granules of granulovacuolar degeneration in Alzheimer's disease. Evidence for apoptotic cell death. *Am J Pathol*. **155**(5), pp. 1459–1466.

STANIMIROVIC, D.B. and FRIEDMAN, A., (2012). Pathophysiology of the neurovascularunit: disease cause or consequence? Journal of Cerebral Blood Flow & Metabolism, **32**(7), pp. 1207-1221.

STERNBERG, Z., PODOLSKY, R., NIR, A., YU, J., NIR, R., HALVORSEN, S.W., CHADHA, K., QUINN, J.F., KAYE, J., KOLB, HOPP, S.C., LIN, Y., OAKLEY, D., ROE, A.D., DEVOS, HANLON, D., HYMAN, B.T., (2018). The role of microglia in processing and spreading of bioactive tau seeds in Alzheimer's disease. *J Neuroinflammation*, **15**:269

STOHR, J., CONDELLO, C., WATTS, J.C., BLOCH, L., OEHLER, A., NICK, M., (2014). Distinct synthetic Aβ prion strains producing different amyloid deposits in bigenic mice. *Proc Natl Acad Sci USA*. 111, pp. 10329–34.

STOJKOVIC, D., PETROVIC, J., SOKOVIC, M., GLAMOCLIJA, J., KUKIC-MARKOVIC, J., PETROVIC, S., (2013). In situ antioxidant and antimicrobial activities of naturally occurring caffeic acid, p-coumaric acid and rutin, using food systems. *Journal of the Science of Food and Agriculture,* 93, pp. 3205e3208.

STREIT, W.J., (2004). Microglia and Alzheimer's disease pathogenesis, *J. Neurosci. Res*. **77**(1), pp. 1e8.

STRITTMATTER, W.J., SAUNDERS, A.M., SCHMECHEL, D., PERICAK-VANCE, M., ENGHILD J., SALVESEN, G.S., ROSES, A.D., (1993). Apolipoprotein E: High-avidity binding to β-amyloid and increased frequency of type 4 allele in late-onset familial Alzheimer disease. Proc Natl Acad Sci 90, pp. 1977–1981

SU, B., WANG, X., DREW, K.L., PERRY, G., SMITH, M.A., ZHU, X., (2008). Physiological regulation of tau phosphorylation during hibernation. *J Neurochem*. **105**, pp. 2098–2108.

SUCRE, J. M. S., VIJAYARAJ, P., AROS, C. J., WILKINSON, D., PAUL, M., DUNN, B (2017). Posttranslational modification of b-catenin is associated with pathogenic fibroblastic changes in bronchopulmonary dysplasia. *Am J Physiol Cell Mol Physiol*, **312**, L186– L195.

SUN, X., HE, G., QING, H., ZHOU, W., DOBIE, F., CAI, F., (2006). Hypoxia facilitates Alzheimer's disease pathogenesis by up-regulating BACE1 gene expression. *Proc Natl Acad Sci USA*. **103**, pp. 18727–32.

SUO, Z., HUMPHREY, J., KUNDTZ, A., SETHI, F., PLACZEK, A., CRAWFORD, F., (1998). Soluble Alzheimers beta-amyloid constricts the cerebral vasculature in vivo. *Neurosci Lett*. **257**, pp. 77–80.

SWERDLOW, R.H., BURNS, J.M. and KHAN, S.M., (2010). The Alzheimer's disease mitochondrial cascade hypothesis. Journal of Alzheimer's disease, 20 Suppl 2, pp. S265.

SYED, O.H., SCOTT, C.J., HAMLIN, A.S. OBIED, H.K., (2017). The protective role of plant biophenols in mechanisms of Alzheimer's disease. *The Journal of Nutritional Biochemistry*, 47, pp. 1-20.

TABET, N., (2006). Acetylcholinesterase inhibitors for Alzheimer's disease: anti-inflammatories in acetylcholine clothing. Age *and Ageing*, **35** (4), pp. 336-338.

TAFT, D.R. (2009). Drug excretion. In: Hacker, M., Bachmann, K., Messer, W. (Eds.), Pharmacology: Principles and practice. *Academic Press*. pp. 175-199.

TAKAHASHI, S., TAKAHASHI, I., SATO, H., KUBOTA, Y., YOSHIDA, S., MURAMATSU, Y., (2001). Age-related changes in the concentrations of major and trace elements in the brain of rats and mice. *Biological Trace Element Research*, **80**, pp. 145–158.

TAKAMI, M., NAGASHIMA, Y., SANO, Y., ISHIHARA, S., MORISHIMA-KAWASHIMA, M., FUNAMOTO, S., (2009). Gamma-secretase: successive tripeptide and tetrapeptide release from the transmembrane domain of beta-carboxyl terminal fragment. *Journal of Neuroscence,* 29, pp. 13042–52.

TAKEDA, S., WEGMANN, S., CHO, H., DEVOS, S.L., COMMINS, C., ROE, A.D., (2015). Neuronal uptake and propagation of a rare phosphorylated high-molecular-weight tau derived from Alzheimer's disease brain. *Nat Commun*. 6, pp. 8490.

TAKEDA, T., MATSUSHITA, T., KUROZUMI, M., TAKEMURA, K., HIGUCHI, K., HOSOKAWA, M. (1997). Pathobiology of the senescence-accelerated mouse (SAM). *Experimental Gerontology*, **32**(1-2), 117-127.

TAN, H., ADAMS, D., CARR, T., LITTLE, S., SEUBERT, P., ALESSANDRINI, R., CLEMENS, J., HAGOPIAN, S., MCCONLOGUE, L., SCHENK, D., BARBOUR, R., JOHNSON-WOOD, K., BORTHELETTE, P., KHAN, K., PENNIMAN, E., VITALE, J., GUIDO, T., MONTOYA-ZAVALA, M., MUCKE, L., ZHAO, J., POWER, M., BLACKWELL,C., GAMES, D., SORIANO, F., SNYDER, B., WOLOZIN, B., MASLIAH, E.,LIEBERBURG, I., PAGANINI, L., WADSWORTH, S., DONALDSON, T., LEE, M.,GILLESPIE, F. and

LEIBOWITZ, P., (1995). Alzheimer-type neuropathology in transgenicmice overexpressing V717F β-amyloid precursor protein. Nature, **373**(6514), pp. 523-527.

TANG, N., ZHANG, Y.P., YING, W., YAO, X.X., (2013). Interleukin-1β upregulates matrix metalloproteinase-13 gene expression via c-Jun N-terminal kinase and p38 MAPK pathways in rat hepatic stellate cells. *Molecular Medicine Report*, 8, pp. 1861-1865.

TANNER, K., MORI, H., MROUE, R., BRUNI-CARDOSO, A., BISSELL, M. J. (2012). Coherent angular motion in the establishment of multicellular architecture of glandular tissues. *Proceedings of the National Academy of Sciences of the United States of America,* **109**, 1973–1978.

TANZI RE, S.T., GEORGE-HYSLOP, P.H., HAINES, JL, POLINSKY, RJ, NEE, L, FONCIN, J.F., NEVE, R.L., MCCLATCHEY, A.I., CONNEALLY, P.M., GUSELLA, J.F., (1987)b. The genetic defect in familial Alzheimer's disease is not tightly linked to the amyloid β protein gene. *Nature*, **329**: 156–157.

TANZI, R.E., (2012). The genetics of Alzheimer disease. *Cold Spring Harb Perspect Med*. 2, pp. a006296.

TANZI, R.E., GUSELLA, J.F., WATKINS, P.C., BRUNS, G.A., ST GEORGE-HYSLOP, P., VAN KEUREN, M.L., PATTERSON, D., PAGAN, S., KURNIT, D.M., NEVE, R.L., (1987)a. Amyloid β protein gene: cDNA, mRNA distribution, and genetic linkage near the Alzheimer locus. *Science* **235**, pp. 880–884.

TAO, J., HU, Q., YANG, J., LI, R., LI, X., LU, C., CHEN, C., WANG, L., SHATTOCK, R., BEN, K., (2007). In vitro anti-HIV and -HSV activity and safety of sodium rutin sulfate as a microbicide candidate. Antiviral Research, **75**(3), pp. 227–233.

TAUPIN, P., (2010). A dual activity of ROS and oxidative stress on adult neurogenesis and Alzheimer's disease, Central Nerveos System. *Agents Med Chem* **10** (1), pp. 16e21.

TEWARI, D., STANKIEWICZ, A.M., MOCAN, A., SAH, A.N., TZVETKOV, N.T., HUMINIECKI, L (2018). Ethnopharmacological approaches for dementia therapy and significance of natural products and herbal drugs. *Frontiers in Aging Neuroscience*, **10**(3), 1-24.

THIES, E., & MANDELKOW, E. M. (2007). Missorting of Tau in neurons causes degeneration of synapses that can be rescued by the kinase MARK2/Par-1. *Journal of Neuroscience*, **27**(11), 2896-2907.

THILAKARATHNA, S.H. and RUPASINGHE, H.P.V, (2013). Flavonoid bioavailability and attempts for bioavailability enhancement. *Nutrients*, **5**(9), pp. 3367-3387.

THIRUMANGALAKUDI, L., PRAKASAM, A., ZHANG, R., BIMONTE-NELSON, H., SAMBAMURTI, K., KINDY, M.S (2008). High cholesterol-induced neuroinflammation and

amyloid precursor protein processing correlate with loss of working memory in mice. *Journal of Neurochemistry,* **106**(1), 475-485.

TIAN, J., GUO, L., SUI, S., DRISKILL, C., PHENSY, A. Q., (2019). Disrupted hippocampal growth hormone secretagogue receptor 1α interaction with dopamine receptor D1 plays a role in Alzheimer's disease. *Sci Transl Med*. 11, pp. eaav6278.

TIAN, R., (2016). Rutin ameliorates diabetic neuropathy by lowering plasma glucose and decreasing oxidative stress via Nrf2 signaling pathway in rats, European Journal of Pharmacology. 771, pp. 84e92.

TONGJAROENBUANGAM, W., RUKSEE, N., CHANTIRATIKUL, P., PAKDEENARONG, N., KONGBUNTAD, W., GOVITRAPONG, P., (2011). Neuroprotective effects of quercetin, rutin and okra (Abelmoschus esculentus Linn.) in dexamethasone-treated mice. *Neurochemistry international*, 59, pp. 677–685.

TOPOL, A., TRAN, N.N., & BRENNAND, K.J. (2015). A Guide to Generating and Using hiPSC Derived NPCs for the Study of Neurological Diseases. *Journal of Visualized Experiments*, 1–9.

TORRES-REGO, M., FURTADO, A.A., BITENCOURT, M.A., DE SOUZA-LIMA, M.C., DE ANDRADE R.C., DE AZEVEDO, E.P., (2016). Anti-inflammatory activity of aqueous extract and bioactive compounds identified from the fruits of Hancornia speciosa Gomes (Apocynaceae*). BMC Complementary and Alternative Medicine,* **16**, pp. 275.

TSE., J.K.Y., (2017). Gut microbiota, nitric oxide, and microglia as prerequisites for neurodegenerative disorders. *ACS Chem Neurosci* **8**, pp. 1438-1447.

TSUCHIYA, H., IINUMA, M., (2000). Reduction of membrane fluidity by antibacterial sophoraflavanone G isolated from Sophora exigua. *Phytomedicine* 7, pp. 161e165.

TSUJIMOTO, Y., (1998). Role of Bcl-2 family proteins in apoptosis: apoptosomes or mitochondria? *Genes Cells*. **3**(11), pp. 697–707

TUMMERS, M., & THESLEFF, I. (2009). The importance of signal pathway modulation in all aspects of tooth development. *Journal of Experimental Zoolog*y, **312B**, 309–319.

TURNER, P.R., O'CONNOR, K., TATE, W.P., ABRAHAM, W.C., (2003). Roles of amyloid precursor protein and its fragments in regulating neural activity, plasticity and memory. *Prog Neurobiol*, **70**, pp. 1–32

TURNER, R.C., LUCKE-WOLD, B.P., ROBSON, M.J., LEE, J.M. and BAILES, J.E., (2016). Alzheimer's disease and chronic traumatic encephalopathy: Distinct but possiblyoverlapping disease entities. Brain Injury, **30**(11), pp. 1279-1292.

UCHIDA, Y., OHTSUKI, S., KATSUKURA, Y., IKEDA, C., SUZUKI, T., KAMIIE, J., TERASAKI, T. (2011). Quantitative targeted absolute proteomics of human blood-brain barrier transporters and receptors. *Journal of Neurochemistry*, **117**(2), 333-345.

URNOWEY, S., ANSAI, T., BITKO, V., NAKAYAMA, K., TAKEHARA, T., BARIK, S., (2006). Temporal activation of anti- and pro-apoptotic factors in human gingival fibroblasts infected with the periodontal pathogen, Porphyromonas gingivalis: potential role of bacterial proteases in host signalling. *BMC Microbiol*. **6**, pp. 26.

VALKO, M., LEIBFRITZ, D., MONCOL, J., CRONIN, M.T., MAZUR, M., TELSER, J., (2007). Free radicals and antioxidants in normal physiological functions and human disease. International *Journal of Biochemistry & Cell Biology*, **39**, pp. 44–84.

VALKO, M., MORRIS, H., CRONIN, M., (2005). Metals, toxicity and oxidative stress. *Current Medicinal Chemistry,* **12**(10), pp. 1161–1208.

VAN ASSEMA, D M E, LUBBERINK, J.M., BAUER, M.C.R., VAN DER FLIER, W M, SCHUIT, R.C., WINDHORST, A.D., COMANS, E.F.I., HOETJES, N.J., TOLBOOM, N.,LANGER, O., MULLER, M., SCHELTENS, P., LAMMERTSMA, A.A. and VAN BERCKEL,B N M, (2012). Blood-brain barrier P-glycoprotein function in Alzheimer's disease. *Brain*, **135**, pp. 181-189.

VAN DAM, D., DE DEYN, P.P. (2011). Animal models in the drug discovery pipeline for Alzheimer's disease. *British Journal of Pharmacology*, **164**(4), 1285-1300.

VAN DER POEL, A. (1967). Ethological study of the behaviour of the albino rat in a passive-avoidance test. *Acta Physiologica et Pharmacologica Neerlandica*, **14**(4), 503-505.

VAN LEEUWEN, F.W., HOL E.M., FISCHER, D.F., (2006). Frameshift proteins in Alzheimer's disease and in other conformational disorders: time for the ubiquitin-proteasome system. *Journal of Alzheimer's Discovery*. **9**, pp. 319–325.

VANDEBROEK, T., TERWEL, D., VANHELMONT, T., GYSEMANS, M., VAN HAESENDONCK, C., ENGELBORGHS, Y., (2006). Microtubule binding and clustering of human Tau-4R and Tau-P301L proteins isolated from yeast deficient in orthologues of glycogen synthase kinase-3beta or cdk5. *J Biol Chem*. **281**, pp. 25388–25397

VANDEBROEK, T., VANHELMONT, T., TERWEL, D., BORGHGRAEF, P., LEMAIRE, K., SNAUWAERT, J., (2005). Identification and isolation of a hyperphosphorylated, conformationally changed intermediate of human protein tau expressed in yeast. *Biochemistry*, 44, pp. 11466–11475.

VECKENSTEDT, A., GU¨TTNER, J., BE´LA´DI, I., (1987). Synergistic action of quercetin and murine alpha/beta interferon in the treatment of Mengo virus infection in mice. *Antiviral Research*, 7(3), pp. 169–178.

VENNAT, B., POURRAT, A., POURRAT, H., GUIRAUD, H., & WAGNER, H. (1996). Bioavailability of rutin and quercetin in rats. *FEBS Letters*, **388**(1), 167-172.

VERGARA, C., HOUBEN, S., SUAIN, V., YILMAZ, Z., DE DECKER, R., VANDEN DRIES, V., (2019). Amyloid-β pathology enhances pathological fibrillary tau seeding induced by Alzheimer PHF in vivo. *Acta Neuropathol*. **137**, pp. 397–412.

VERMEER, S.E., PRINS N.D., DEN, HEIJER, T., HOFMAN, A., KOUDSTAAL, P.J., BRETELER, M.M., (2003). *N Engl J Med*. **348**, pp. 1215–1222.

VERMES I, HAANEN C, REUTELINGSPERGER C. (2000). Flowcytometry of apoptotic cell death. *Journal of Immunological Methods*, **243**(1–2): 167–90.

VILLALTA, S.A., NGUYEN, H.X., DENG, B., GOTOH, T., TIDBALL, J.G., (2009). Shifts in macrophage phenotypes and macrophage competition for arginine metabolism affect the severity of muscle pathology in muscular dystrophy. *Hum Mol Genet* 18, pp. 482-496.

VINET, J., (2012). Neuroprotective function for ramified microglia in hippocampal excitotoxicity, J. Neuroinflammation, 9, pp. 27.

VON BERGEN, M., FRIEDHOFF, P., BIERNAT, J., HEBERLE, J., MANDELKOW, E.M., MANDELKOW, E., (2000). Assembly of tau protein into Alzheimer paired helical filaments depends on a local sequence motif ((306)VQIVYK(311)) forming beta structure. *Proc Natl Acad Sci USA*. 97, pp. 5129–5134.

WAKE, H., MOORHOUSE, A.J., JINNO, S., KOHSAKA, S. and NABEKURA, J., (2009). Resting Microglia Directly Monitor the Functional State of Synapses In Vivo and Determine the Fate of Ischemic Terminals. Journal of Neuroscience, **29**(13), pp. 3974-3980.

WALLACE, T.L. and BERTRAND, D., (2013). Importance of the nicotinic acetylcholine receptor system in the prefrontal cortex. *Biochemical Pharmacology*, **85**(12), pp. 1713-1720.

WALLE, T., BROWNING, A. M., STEED, L. L., REED, S. G., & WALLE, U. K. (2005). Flavonoid glucosides are hydrolyzed and thus activated in the oral cavity in humans. *Journal of Nutrition,* **135**(1), 48–52.

WAN, L., NIE, G. AND ZHANG, J., (2011). β Amyloid peptide increases levels of iron content and oxidative stress in human cell and Caenorhabditis elegans models of Alzheimer disease. *Free Radical Biology and Medicine,* **50**(1), pp. 122-129.

WAN, L., NIE, G., ZHANG, J., (2011). β Amyloid peptide increases levels of iron content and oxidative stress in human cell and Caenorhabditis elegans models of Alzheimer disease. *Free Radical Biology and Medicine*, **50** (1), pp. 122-129.

WANG, C., WANG, P., CHEN, X., WANG, W., JIN, Y., (2015). Saururus chinensis (Lour.) Baill blocks enterovirus 71 infection by hijacking MEK1-ERK signalling pathway. *Antiviral Res* **119**, pp. 47–56.

WANG, J.Z, GRUNDKE-IQBAL, I., IQBAL, K., (1996). Glycosylation of microtubule-associated protein tau: an abnormal posttranslational modification in Alzheimer's disease. *Nat Med.* 2, pp. 871–875.

WANG, J.Z., GONG, C.X., ZAIDI, T., GRUNDKE-IQBAL, I., IQBAL, K., (1995). Dephosphorylation of Alzheimer paired helical filaments by protein phosphatase-2A and -2B. *J Biol Chem.* **270**, pp. 4854–4860.

WANG, J.Z., GRUNDKE-IQBAL, I., IQBAL, K., (1996). Restoration of biological activity of Alzheimer abnormally phosphorylated tau by dephosphorylation with protein phosphatase-2A, -2B and -1. *Brain Res Mol Brain Res*. **38**, pp. 200–208

WANG, J.Z., GRUNDKE-IQBAL, I., IQBAL, K., (2007). Kinases and phosphatases and tau sites involved in Alzheimer neurofibrillary degeneration. *Eur J Neurosci*.**25**, pp. 59–68

WANG, L., (2015). Sonchus asper extract inhibits LPS-induced oxidative stress and pro-inflammatory cytokine production in RAW264.7 macrophages, *Nutr. Res. Pract*. **9**(6), pp. 579e585.

WANG, L., LIU, W., WANG, Y., WANG, J., TU, Q., LIU, R (2013). Construction of oxygen and chemical concentration gradients in a single microfluidic device for studying tumor cell-drug interactions in a dynamic hypoxia microenvironment. *Lab on a Chip*, **13**, 695–705.

WANG, S., JING, H., YANG, H., LIU, Z., GUO, H., CHAI, L., HU, L., (2015). Tanshinone I selectively suppresses pro-inflammatory genes expression in activated microglia and prevents nigrostriatal dopaminergic neurodegeneration in a mouse model of Parkinson's disease. *J Ethnopharmacol,* **164**, pp. 247-255.

WANG, S.W., WANG, Y.J., SU, Y.J., ZHOU, W.W., YANG, S.G., ZHANG, R., ZHAO, M., LI, Y.N., ZHANG, Z.P., ZHAN, D.W., LIU, R.T., (2012). Rutin inhibits β-amyloid aggregation and cytotoxicity, attenuates oxidative stress, and decreases the production of nitric oxide and proinflammatory cytokines. *Neurotoxicology* **33**, pp. 482-490.

WANG, S.W., WANG, Y.J., SU, Y.J., ZHOU, W.W., YANG, S.G., ZHANG, R., (2012). Rutin inhibits β-amyloid aggregation and cytotoxicity, attenuates oxidative stress, and decreases the production of nitric oxide and proinflammatory cytokines. *Neurotoxicology*, **33**, 482-490.

WANG, X., SU, B., PERRY, G., SMITH, M.A., ZHU, X., (2007). Insights into amyloid-β-induced mitochondrial dysfunction in Alzheimer disease. Free *Radical Biology and Medicine*, **43**(12), pp. 1569-1573.

WANG, X., WANG, W., LI, L., PERRY, G., LEE, H. and ZHU, X., (2014). Oxidative stress and mitochondrial dysfunction in Alzheimer's disease. Biochimica et Biophysica Acta (BBA) - *Molecular Basis of Disease,* **1842**(8), pp. 1240-1247.

WANG, X., WANG, W., WANG, J., YANG, C., LIANG, C. (2018). Effect of apigenin on apoptosis induced by renal ischemia/reperfusion injury in vivo and in vitro. *Ren Fail*, **40**, 498–505.

WANG, X.J., XU, J.X., (2005). Salvianic acid A protects human neuroblastoma SH-SY5Y cells against MPP + -induced cytotoxicity. *Neurosci Res.* **51**(2), pp. 129–138

WANG, Y., LI, M., XU, X., SONG, M., TAO, H., BAI, Y., & LIU, J. (2013). Rutin attenuates Aβ25-35-induced toxicity via the inhibition of oxidative stress and apoptosis in SH-SY5Y cells. *Neurochemistry International,* **62**(7), 912-921.

WANG, Y., WAN, S., SU, Y., ZHOU, W., YANG, S., ZHANG, R., ZHANG, Z., ZHAO, M., LI, Y., ZHAN, LIU, R., (2012). Rutin inhibits β-amyloid aggregation and cytotoxicity, attenuates oxidative stress, and decreases the production of nitric oxide and proinflammatory cytokines. *Neurotoxicology,* **33**(3), pp. 482-490.

WANG, Y., ZHANG, Y., SUN, B., TONG, Q., REN, L., (2017). Rutin protects against pirarubicin-induced cardiotoxicity through TGF-β1-p38 MAPK signaling pathway. Evidence-Based Complementary and Alternative Medicine1759385. *Journal of the American College of Cardiology*, **40**(5), pp. 970–975.

WANG,P., Q. QIAO, J. LI, W. WANG, L. P. YAO, AND Y. J. FU, (2016). "Inhibitory effects of geraniin on LPS-induced inflammation via regulating NF-κB and Nrf2 pathways in RAW 264.7 cells," Chemico-*Biological Interaction*s, **253**, pp. 134–142

WEINREB, O., AMIT, T., BAR-AM, O. and YOUDIM, M.B.H., (2011). A novel anti-Alzheimer's disease drug, ladostigil neuroprotective, multimodal brain-selective monoamine oxidase and cholinesterase inhibitor. *International review of neurobiology*, 100, pp. 191.

WENDELN A.-C., DEGENHARDT K., KAURANI L., GERTIG M., ULAS T., JAIN G., WAGNER J., HÄSLER L. M., WILD K., SKODRAS A., BLANK T., STASZEWSKI O., DATTA M., CENTENO T. P., CAPECE V., ISLAM M. R., KERIMOGLU C., STAUFENBIEL M., SCHULTZE J. L., BEYER M., PRINZ M., JUCKER M., FISCHER A., NEHER J. J., (2018). Innate immune memory in the brain shapes neurological disease hallmarks. *Nature* **556**, 332–338.

WHITE, L., PETROVITCH, H., HARDMAN, J., NELSON, J., DAVIS, D.G., ROSS, G.W., MASAKI, K., LAUNER, L., MARKESBERY, W.R., (2002). Ann NY Acad Sci. 977, pp. 9–23.

WHITEHOUSE, P.J., (2014). The end of Alzheimer's disease from biochemical pharmacology to eco psychosociology: A personal perspective. Biochemical Pharmacology, **88**(4), pp. 677-681.

WILSON, P.G., & STICE, S.S. (2006). Development and differentiation of neural rosettes derived from human embryonic stem cells. *Stem Cell Reviews*, **2**, 67–77.

WINBLAD, B., PROF, A., PHILIPPE, P., SANDRINE, PROF,B.C., PROF,B.H, PROF, C.M, ANGEL, P., DUBOIS,B, PROF, E., DAVID, P., FELDMAN, H., PROF,F., LAURA, P.,FRISONI, G.B, PROF, G.,

WIPPOLD II, N., CAIRNS, K., VO, D.M., HOLTZMAN AND J.C. MORRIS, (2008). Neuropathology for the Neuroradiologist: Plaques and Tangles AJNR. *American Journal of Neuroradiology,* **29**, pp. 18–22.

SERGE, P., GEORGES, J., BA, G., CAROLINE, P., IQBAL,K., PROF, JESSEN., FRANK, P., JOHANSSON, G., LINUS, MD., KIVIPELTO, M., PROF,KNAPP., MARTIN, PROF., MANGIALASCHE, F., MELIS, M.D., RENÉ, P., NORDBERG,A., PROF, R., MARCEL, O., PROF, QIU., CHENGXUAN, M.D., SAKMAR, T.P., PROF,S., PHILIP, P., SCHNEIDER, L.S., PROF, SPERLING., REISA, P., TJERNBERG, L.O.PHD, W., GUNHILD, P., WIMO, A., PROF, Z. and HENRIK, P., (2016). Defeating Alzheimer's disease and other dementias: a priority for European science and society. Lancet Neurology. The, **15**(5), pp. 455-532.

WINSLOW, BRADFORD T., MD|ONYSKO, MARY K., PHARMD|STOB, CHRISTIAN M.,HAZLEWOOD, N.O. and KATHLEEN A.P., (2011). Treatment of Alzheimer Disease. American Family Physician, **83**(12), pp. 1403-1412.

WIRTHS, O., MULTHAUP, G., & BAYER, T. A. (2004). A modified β-amyloid hypothesis: intraneuronal accumulation of the β-amyloid peptide— the first step of a fatal cascade. *Journal of Alzheimer's Disease*, **6**(3), 275-289.

WISCHIK, C.M., BENTHAM, P., WISCHIK, D.J., SENG, K.M., (2008). Tau aggregation inhibitor (TAI) therapy with rember arrests disease progression in mild and moderate Alzheimer's disease over 50 weeks. *Alzheimer's & Dementia*. **4**, pp. 167

WISCHIK, C.M., NOVAK, M., EDWARDS. P.C., KLUG, A., TICHELAAR, W., CROWTHER, R.A., (1988). Structural characterization of the core of the paired helical filament of Alzheimer disease. *Proc Natl Acad Sci USA*. **85**, pp. 4884–8

WISELY, C., WANG, D., HENAO, R., GREWAL, D., THOMPSON, A., ROBBINS, C (2020). Convolutional neural network to identify symptomatic Alzheimer's disease using multimodal retinal imaging. *British Journal of Ophthalmology*, 1–8, 0.

WITTMANN, C.W., WSZOLEK, M.F., SHULMAN, J.M., SALVATERRA, P.M., LEWIS, J., HUTTON, M., (2001). Tauopathy in Drosophila: neurodegeneration without neurofibrillary tangles. *Science*. **293**, pp. 711–714.

WOERMAN, A.L., PATEL, S., KAZMI, S.A., OEHLER, A., FREYMAN, Y., ESPIRITU, L., (2017). Kinetics of human mutant tau prion formation in the brains of 2 transgenic mouse lines. JAMA Neurol. **74**, pp. 1464–72.

WOLTER, K.G., (1997). Movement of Bax from the cytosol to mitochondria during apoptosis. J Cell Biol. **139**(5), pp. 1281–1292.

WONG, G.T., MANFRA, D., POULET, F.M., ZHANG, Q., JOSIEN, H., BARA, T., (2004). Chronic treatment with the gamma-secretase inhibitor LY-411,575 inhibits beta-amyloid peptide production and alters lymphopoiesis and intestinal cell differentiation. J Biol Chem. 279, pp. 12876–82.

WOODHOO, A., & SOMMER, L. (2008). Development of the schwann cell lineage: From the neural crest to the myelinated nerve. *Glia*, **56**, 1481–1490.

WU, D., FU, J., ZHANG, X., ZHANG, J., MAO, J., SHEN, X., & WU, J. (2020). Rutin protects against Aβ25-35-induced neurotoxicity via suppressing oxidative stress and apoptosis in SH-SY5Y cells. *Neurotoxicology and Teratology*, 80, 106876.

WU, D., RE, D., NAGAI, M., ISCHIROPOULOS H., AND PRZEDBORSKI S., 2006. The inflammatory NADPH oxidase enzyme modulates motor neuron degeneration in amyotrophic lateral sclerosis mice. *Pro Natl Acad Sci USA,* **103**, pp. 12132-12137.

WU, W., LI, R., LI, X., HE, J., JIANG, S., LIU, S., YANG, J., (2015). Quercetin as an antiviral agent inhibits Influenza A virus (IAV) Entry. *Viruses*, 10, pp. 3390/v8010006.

WU, Y., DU, S., JOHNSON, J.L., TUNG, H.Y., LANDERS, C.T., LIU, Y., (2019). Microglia and amyloid precursor protein coordinate control of transient Candida cerebritis with memory deficits. *Nat Commun*. **10**, pp. 58.

XI, C., LIANG, X., CHEN, C., BABAZADA, H., LI, T., & LIU, R. (2017). Hypoxia Induces Internalization of k-Opioid Receptor. *Anesthesiology*, **126**, 842–854.

XIANCHU, L., LAN, Z., MING, L., YANZHI, M., (2018). Protective effects of rutin on lipopolysaccharide-induced heart injury in mice. *Journal of Toxicological Sciences*, **43**(5), pp. 329–337.

XIAO, F., LI, X.G., ZHANG, X.Y., HOU, J.D., LIN, L.F., GAO, Q., (2011). Combined administration of D-galactose and aluminium induces Alzheimer-like lesions in brain. *Neuroscience Bulletin*, **27**(3), 143-155.

XIAO-YING, SUN, LING-JIE, LI, QUAN-XIU DONG, JIE ZHU, YA-RU HUANG, SHENG-JIE HOU, XIAO-LIN YU & RUI-TIAN LIU, (2001). Rutin prevents tau pathology and neuroinflammation in a mouse model of Alzheimer's disease. *Journal of Neuroinflammation* **18**, PP. 131.

XIE, Y., SCHUTTE, R.J., NG, N.N., ESS, K.C., SCHWARTZ, P.H., & O'DOWD, D.K. (2018). Reproducible and efficient generation of functionally active neurons from human hiPSCs for preclinical disease modeling. *Stem Cell Research*, **26**, 84–94.

XIE, Y., YANG, W., CHEN, X., XIAO, J., (2014). Inhibition of flavonoids on acetylcholine esterase: binding and structure-activity relationship. *Food and Functions*, **5**(10), pp. 2582–2589.

XIE, Z., SUN, Y., LAM, S., ZHAO, M., LIANG, Z., YU, X., (2014). Extraction and isolation of flavonoid glycosides from Flos Sophorae Immaturus using ultrasonic-assisted extraction followed by high-speed countercurrent chromatography. Journal of Separation Science 37, pp. 957e965.

XU, P., WANG, T., WANG, Y., WANG, S., YU, X., SU, Y., ZHOU, W., ZHANG, H., LIU, R., (2014). Rutin improves spatial memory in Alzheimer's disease transgenic mice by reducing Aβ oligomer level and attenuating oxidative stress and neuroinflammation. Behavioural Brain Research, **264**, pp. 173-180.

XU, X., H., LI, X., HOU, (2015). "Punicalagin Induces Nrf2/HO-1 Expression via Upregulation of PI3K/AKT Pathway and Inhibits LPS-Induced Oxidative Stress in

XUE, F., WU, J., WU, T., WANG, X., & TANG, X. (2018). Endoplasmic reticulum stress and its link to Alzheimer's disease: Review article. *Neural Regeneration Research*, **13**(5), 915.

YAGI, H., KATOH, S., AKIGUCHI, I., TAKEDA, T. (1988). Age-related deterioration of ability of acquisition in memory and learning in senescence accelerated mouse: SAM-P/8 as an animal model of disturbances in recent memory. *Brain Research,* **474**(1), 86-93.

YAMAGATA, K., URAKAMI, K., IKEDA, K., JI, Y., ADACHI, Y., ARAI, H., (2001). High expression of apolipoprotein E mRNA in the brains with sporadic Alzheimer's disease. *Dement Geriatr Cogn Disord* **12**, pp. 57–62.

YANG, C., LEE, H., LEE, J., KIM J., LEE, S., SHIN, D., LEE Y., LEE D., EL- BENNA, J, JO E., (2007). Reactive oxygen species and p47phox activation are essential for the Mycobacterium tuberculosis-induced pro-inflammatory response in murine

YANG, H., SUN, Z., BA, M., XU, J. and XING, Y., (2009). Involvement of protein trafficking in deprenyl-induced [alpha]-secretase activity regulation in PC12 cells. *European Journal of Pharmacology,* **610**(1-3), pp. 37.

YANG, J., (1997). Prevention of apoptosis by Bcl-2: release of cytochrome c from mitochondria blocked. *Science*. **275**(5303), pp. 1129–1132.

YANG, J., GUO, J., YUAN, J., (2008). In vitro antioxidant properties of rutin. LWT Food Science and Technology, **41**(6), pp. 1060–1066.

YANG, J., JU, B., YAN, Y., XU, H., WU, S., ZHU, D., ET AL. (2017). Neuroprotective effects of phenylethanoid glycosides in an in vitro model of Alzheimer's disease. *Experimental and Therapeutic Medicine,* **13**(5), 2423-2428.

YANG, L., KSIEZAK-REDING, H., (1998). Ubiquitin immunoreactivity of paired helical filaments differs in Alzheimer's disease and corticobasal degeneration. *Acta Neuropathol*. **96**, pp. 520–526.

YANG, L.S., KSIEZAK-REDING, H., (1995). Calpain-induced proteolysis of normal human tau and tau associated with paired helical filaments. *Eur J Biochem*. **233**, pp. 9–17.

YANG, X.W., LI, Y.H., ZHANG, H., ZHAO, Y.F., DING, Z.B., YU, J.Z., LIU, C.Y., LIU, J.C., JIANG, W.J., FENG, Q.J., XIAO, B.G., MA, C.G., (2016). Safflower Yellow regulates microglial polarization and inhibits inflammatory response in LPS-stimulated Bv2 cells. *Int J Immunopathol Pharmacol*, **29**, pp. 54-64.

YANG,C., C., ZHANG, Z., WANG, Z., TANG, H., KUANG AND A.-N., KONG, (2016). Corynoline isolated from Corydalis bungeana Turcz exhibits anti-inflammatory effects via modulation of Nfr2 and MAPKs, *Molecules,* 21, pp 8.

YANKNER, B.A., DUFFY, L.K., KIRSCHNER, D.A., (1990). Neurotrophic and neurotoxic effects of amyloid beta protein: reversal by tachykinin neuropeptides. Science, 250(4978), pp.79–282.

YAO, C., XI., C, HU, K., GAO, W., CAI, X., QIN, J., LV., S., DU, C., Wei, Y., (2018). Inhibition of enterovirus 71 replication and viral 3C protease by quercetin. *Virology Journal*, 15, pp. 116.

YE, J. (2009). Emerging role of adipose tissue hypoxia in obesity and insulin resistance. *International Journal of Obesity*, **33**, 54–66.

YE, S., HUANG, Y., MULLENDORFF, K., DONG, L., GIEDT, G., MENG, E.C., (2005). Apolipoprotein. (apo) E4 enhances amyloid beta peptide production in cultured neuronal cells: apoE structure as a potential therapeutic target. *Proc Natl Acad Sci USA. 102*, pp. 18700–5.

YEH, C.H., YANG, J.J., YANG, M.L., LI, Y.C., KUAN, Y.H., (2014). Rutin decreases lipopolysaccharide-induced acute lung injury via inhibition of oxidative stress and the MAPK-NF-jB pathway. *Free Radical Biology and Medicine*, **69**, pp. 249–257.

YIN, D., ZHOU, S., XU, X., GAO, W., LI, F., MA, Y., SUN, D., WU, Y., GUO, Q., LIU, H., HAN, L., WANG, Z., WANG, Y., ZHANG, J., (2018). Dexmedetomidine attenuated early brain injury in rats with subarachnoid haemorrhage by suppressing the inflammatory response: The TLR4/NF- κB pathway and the NLRP3 inflammasome may be involved in the mechanism. *Brain Res*. **1698**, pp. 1-10.

YIN, Y., LI, Y., ZHANG, W., (2014). The growth hormone secretagogue receptor: its intracellular signaling and regulation. *Int J Mol Sci*. **15**, pp. 4837–55.

YOO, G., (2015). Flavonoids isolated from Lespedeza cuneata G. Don and their inhibitory effects on nitric oxide production in lipopolysaccharide-stimulated BV-2 microglia cells, *Pharmacogn. Mag.* **11**(43), pp. 651e656.

YOO, H., KU, S.K., BAEK, Y.D., BAE, J.S., (2014). Anti-inflammatory effects of rutin on HMGB1-induced inflammatory responses in vitro and in vivo. *Inflammation Research*, **63**, pp.197e206.

YOSHIDA, M., (2006). Cellular tau pathology and immunohistochemical study of tau isoforms in sporadic tauopathies. *Neuropathology*. **26**, pp. 457–470.

YOSHIYAMA, Y., HIGUCHI, M., ZHANG, B., HUANG, S.M., IWATA, N., SAIDO, T.C., (2007). Synapse loss and microglial activation precede tangles in a P301S tauopathy mouse model. *Neuron*. 53, pp. 337–351.

YOUDIM, K.A., DOBBIE, M.S., KUHNLE, G., PROTEGGENTE, A.R., ABBOTT, N.J. andRICE - EVANS, C., (2003)a. Interaction between flavonoids and the blood–brain barrier: invitro studies. *Journal of Neurochemistry,* **85**(1), pp. 180-192.

YOUDIM, K.A., DOBBIE, M.S., KUHNLE, G., PROTEGGENTE, A.R., ABBOTT, N.J., RICE-EVANS, C. (2003). Interaction between flavonoids and the blood-brain barrier: In vitro studies. *Journal of Neurochemistry,* **85**(1), 180-192.

YOUDIM, K.A., QAISER, M.Z., BEGLEY, D.J., RICE-EVANS, C.A., ABBOTT, N.J. (2004). Flavonoid permeability across an in situ model of the blood-brain barrier. *Free Radical Biology and Medicine,* **36**(5), 592-604.

YOUNG, K.J. and BENNETT, J.P., (2010). The mitochondrial secret(ase) of Alzheimer's disease. *Journal of Alzheimer's disease JAD*, 20 Suppl 2 (s2), pp. S400.

YUAN, S.H., MARTIN, J., ELIA, J., FLIPPIN, J., PARAMBAN, R.I., HEFFERAN, M.P (2011). Cell-surface marker signatures for the isolation of neural stem cells, glia, and neurons derived from human pluripotent stem cells. *PLoS ONE*, 6.

ZANDI, K., TEOH, B.T., SAM, S.S., WONG, P.F., MUSTAFA, M.R., ABUBAKAR, S., (2011). Antiviral activity of four types of bioflavonoid against dengue virus type-2. Virology Journal 8, pp. 560.

ZENARO, E.P., VITTORINA, D.B., GENNJ, P., LAURA M., SIMONA, B., ERMANNA, T., BARBARA, R., STEFANO, A., SILVIA, D., ALESSIO, M., TOMMASO, C., SARA, N., GABRIELE, T., LUCIA, C., DANIELE, C., GIORGIO, B., BRUNO, B. and GABRIELA C., (2015). Neutrophils promote Alzheimer's disease-like pathology and cognitive decline via LFA-1 integrin. *Nature Medicine*, **21**(8), pp. 880-886

ZENG, K.W., KO, H., YANG, H.O., WANG, X.M., (2010). Icariin attenuates β-amyloid-induced neurotoxicity by inhibition of tau protein hyperphosphorylation in PC12 cells. *Neuropharmacology*; **59**(6), pp. 542–50.

ZHANG, B., CARROLL, J., TROJANOWSKI, J.Q., YAO, Y., IBA, M., POTUZAK, J.S., HOGAN, A.L., XIE, S.X., BALLATORE, C., SMITH, Amos B, LEE, V.M. and BRUNDEN, K.R., (2012). The microtubule-stabilizing agent, epothilone D, reduces axonal dysfunction, neurotoxicity, cognsitive deficits, and Alzheimer-like pathology in an

ZHANG, B., WEI, Y.Z., WANG, G.Q., LI, D.D., SHI, J.S., ZHANG, F., (2018a). Targeting MAPK pathways by naringenin modulates microglia M1/M2 polarization in lipopolysaccharide-stimulated cultures. *Front Cell Neurosci.* 12, pp. 531.

ZHANG, F., ZHONG, R., LI, S., FU, Z., CHENG, C., CAI, H., LE, W., (2017). Acute hypoxia induced an imbalanced M1/M2 activation of microglia through NF-κB signaling in Alzheimer's disease mice and wild-type littermates. *Front Aging Neurosci.* 9, pp. 282.

ZHANG, L., PREVIN, R., LU. L., LIAO, R.F., JIN, Y., WANG, R.K., (2018b). Crocin, a natural product attenuates lipopolysaccharide-induced anxiety and depressive-like behaviors through suppressing NF-kB and NLRP3 signaling pathway. *Brain Res Bull*, 142, pp. 352-359.

ZHANG, L., ZHAO, C., CHEN, C., ZHENG, P.Y., (2014). Synaptophysin and the dopaminergic system in hippocampus are involved in the protective effect of rutin against trimethyltin-induced learning and memory impairment. *Nutritional Neuroscience*, **17**(5), pp. 1179-1476.

ZHANG, P., M.A., X., (2015). Effect of rutin on spinal cord injury through inhibition of the expression of MIP-2 and activation of MMP-9, and downregulation of Akt phosphorylation. *Molecular Medicine Reports*, 12, pp. 7554-7560.

ZHANG, Z., SIMPKINS, J. (2010). An okadaic acid-induced model of tauopathy and cognitive deficiency. *Brain Research*, **1359**(1), 233-246.

ZHANG, Z., SUN, T., NIU, J.G., HE, Z.Q., LIU, Y., WANG, F., (2015). Amentoflavone protects hippocampal neurons: anti-inflammatory, antioxidative, and antiapoptotic effects. Neural *Regenerative Research*, 10, pp. 1125-1133.

ZHAO, H., ZHANG, H., (2020). Coagulopathy and antiphospholipid antibodies in patients with Covid-1. New England Journal of Medicine.

ZHAO, R., YING. M., GU, S., YIN, W., LI, Y., YUAN, H., FANG, S., LI, M., (2019). Cysteinyl leukotriene receptor 2 is involved in inflammation and neuronal damage by mediating microglia M1/M2 polarization through NF-κB pathway. *Neuroscience*, 422, pp. 99-118.

ZHAO, Y., FU, X., ZHANG, L., DONG, P., DU, Y., WANG, W., & WANG, A. (2016). Improved oral bioavailability of rutin by a chitosan–lipid nanocarrier. *Journal of Agricultural and Food Chemistry,* **64**(5), 1263-1270.

ZHENG, H., FRIDKIN, M., YOUDIM, M., (2015). New approaches to treating Alzheimer's disease. *Perspect Medicin Chem* 7, pp. 1-8.

ZHENG, L., ROBERG, K., JERHAMMAR, F., MARCUSSON. J., TERMAN, A., (2006). Autophagy of amyloid beta-protein in differentiated neuroblastoma cells exposed to oxidative stress. *Neurosci Lett*. **394**(3), pp. 184–9.

ZHONG, LT., (1993). Bcl-2 inhibits death of central neural cells induced by multiple agents. *Proc Natl Acad Sci USA*. **90**(10), pp. 4533–4537.

ZHOU, J., PENG, W., XU, M., LI, W. and LIU, Z., (2015). The effectiveness and safety ofacupuncture for patients with Alzheimer disease: a systematic review and meta-analysis of randomized controlled trials. *Medicine*, **94** (22), pp. e933.

ZHOU, K., ZHONG, Q., WANG, Y.C., XIONG, X.Y., MENG, Z.Y., ZHAO, T., ZHU, W.Y., LIAO, M.F., WU, L.R., YANG, Y.R., LIU, J., DUAN, C.M., LI, J., GONG, Q.W., LIU, L., YANG, M.H., XIONG, A., WANG, J., YANG, Q.W., (2017). Regulatory T cells ameliorate

intracerebral hemorrhage-induced inflammatory injury by modulating microglia/macrophage polarization through the IL-10/GSK3β/PTEN axis. *J Cereb Blood Flow Metab*, **37**, pp. 967-979.

ZHOU, Q., WANG, M., DU, Y., ZHANG, W., BAI, M., ZHANG, Z., LI, Z. and MIAO, J., (2015). Inhibition of c - Jun N - terminal kinase activation reverses Alzheimer disease phenotypes in APPswe/PS1dE9 mice. *Annals of Neurology*, 77(4), pp. 637-654.

ZHOU, R., YANG, G., SHI, Y., (2017). Dominant negative effect of the loss-of-function gamma-secretase mutants on the wild-type enzyme through heterooligomerization. Proc Natl Acad Sci USA. 114, pp. 12731–6

ZHOU, Y., RICHARDS, A. M., WANG, P. (2017). Characterization and standardization of cultured cardiac fibroblasts for ex vivo models of heart fibrosis and heart ischemia. *Tissue Eng Part C Methods,* **23**, 422–433.

ZHU, J., LUO, C., WANG, P., H.E., Q., ZHOU, J., PENG, H., (2013). Saikosaponin A mediates the inflammatory response by inhibiting the MAPK and NF-kappaB pathways in LPS-stimulated RAW 264.7 cells. *Experimental and therapeutic medicine* **5**, pp. 1345-1350.

ZHU, X.H., QIAO, H., DU, F., XIONG, Q., LIU, X., ZHANG, X., (2012). Quantitative imaging of energy expenditure in human brain. *Neuroimage* **60**, pp. 2107–17

ZILKA, N., FILIPCIK, P., KOSON, P., FIALOVA, L., SKRABANA, R., ZILKOVA, M., (2006). Truncated tau from sporadic Alzheimer's disease suffices to drive neurofibrillary degeneration in vivo. *FEBS Lett*. **580**, pp. 3582–3588.

ZLOKOVIC, B.V., (2004). Clearing amyloid through the blood–brain barrier. *Journal of Neurochemistry*, **89**(4), pp. 807-811.

ZU, H., LIU, X., YAO, K. (2020). DHCR24 overexpression modulates microglia polarization and inflammatory response via Akt/GSK3β signalling in Aβ25–35 treated BV-2 cells. *Life Sciences*, **260**(1508), 1-7.